Developmental Evolution of the Optic Region in the Cavefish Astyanax mexicanus

Lucie Devos

UNIVERSITÉ PARIS SUD
Comprendre le monde, construire l'avenir

Developmental Evolution of the Optic Region in the Blind Cavefish *Astyanax mexicanus*

Thèse de doctorat de l'Université Paris-Saclay
préparée à Neuroscience Paris Saclay Institute – CNRS UMR9197

École doctorale n°568 BIOSIGNE
Spécialité de doctorat: Sciences de la vie et de la santé

Thèse présentée et soutenue à Gif-sur-Yvette, le 4 juillet 2018, par

Lucie Devos

Composition du Jury :

Anne-Hélène Monsoro-Burq Professeur, Université Paris-Sud (– Institut Curie, UMR3347/U1021)	Présidente
Florencia Cavodeassi Lecturer, St. George's University of London	Rapporteur
Marion Coolen CR2, INSERM (– Institut Pasteur)	Rapporteur
Morgane Locker Maître de Conférences, Université Paris-Sud (– CNRS UMR9197)	Examinateur
Cathy Danesin Maître de Conférences, Université Paul Sabatier (–CNRS UMR5547)	Examinateur
Sylvie Rétaux DR, CNRS (– CNRS UMR9197)	Directrice de thèse

Acknowledgements / Remerciements

I first want to thank all the members of the jury for agreeing to read this thesis. Thank you for taking this time for me. Your opinions and suggestions regarding this work are very important to me.

Au cours de cette thèse, j'ai eu la très grande chance de rencontrer, de discuter et de collaborer avec de nombreuses personnes venant d'équipes et d'horizons très variés. Chacune de ces rencontres et discussions ont participé à rendre cette thèse aussi intéressante et enrichissante. Merci à tous ceux qui y ont contribué !

Je tiens à remercier bien sûr Sylvie de m'avoir accueilli pour cette thèse, merci pour ce projet que tu m'as confié et pour lequel tu m'as fait confiance, il m'a permis d'explorer des techniques et thématiques très variées et cela correspondait parfaitement à ce que j'espérais d'une thèse. Merci de m'avoir donné de l'autonomie et la liberté de collaborer avec d'autres plateformes et équipes, c'est quelque chose que j'ai réellement apprécié. Merci aussi d'avoir réussi à être toujours disponible malgré tes marathons de réunions département / déménagement / direction /… Tu es une chef à la fois humaine, disponible et qui suit scientifiquement chacun des projets très divers de l'équipe ; je mesure vraiment la chance que j'ai eue par rapport à beaucoup d'autres thésards.

Je veux aussi évidemment remercier Alex, mon maître de stage de M2. Je garde un souvenir vraiment incroyable de ce stage et de notre travail à quatre mains, j'ai rarement vu une collaboration aussi évidente (de mon point de vue en tous cas) ! Merci de t'être donné à fond pour mon stage, merci pour ta franchise, je l'apprécie beaucoup. Merci aussi pour ta folie, je me souviens encore de cette explication sur l'ORR pendant que tu dansais le tango au milieu du bureau… magique ! Merci aussi pour ces séances de dissections accompagnées par un duo toi / Francis Cabrel, ce sont finalement de bons souvenirs (même je te maudis parfois quand ses chansons me reviennent en tête et ne veulent plus me quitter !). Le labo est bien silencieux depuis ton départ même si Victor met un point d'honneur à reprendre le flambeau de temps à autres.

Victor, tu sais à quel point ma thèse aurait été différente sans toi ! Merci pour tout, pour ton amitié et pour ton aide au labo, merci pour nos soirées, pour le Mexique et les marchés de Mexico, pour la danse dans la piscine, merci pour Marseille et ton coup de stress avec Ali, merci pour les acrobaties dans l'animalerie à la recherche des fuites de lumière du cubicule et j'en passe. Merci de m'avoir appris tant de choses sur les poissons et l'art de les soigner ; merci d'avoir été là quand j'avais besoin de partager mes frustrations sur les poissons, sur l'animalerie et autres. Merci aussi pour ton aide sur l'établissement de mes lignées, sur le cubicule et même au labo. Amuse-toi bien en Nouvelle-Zélande et j'espère à très bientôt pour de nouvelles aventures !

Un grand merci aussi à Maryline (t'es trop forte, je crois que je ne te l'ai pas assez dit !), merci pour ta gentillesse, ton rire (et tes petits éternuements mignons !), ton coaching et ton aide pour les manips, heureusement que tu étais là pour me montrer comment faire les choses, où les trouver, comment dompter Geslab… merci d'avoir pris le temps pour moi. Merci beaucoup pour le travail que tu fais pour le commun de l'équipe, c'est tellement agréable, heureusement que tu es là ! Merci aussi d'avoir trouvé le temps de m'initier à la microdissection en L3, c'était un grand moment !

Je veux aussi remercier tous les autres membres de l'équipe DECA passés et présents : Carole pour ta gentillesse, ton écoute et tes super bruitages de poissons. François pour tes discussions sur l'enseignement et pour avoir accepté courageusement de reprendre le projet. Yannick pour m'avoir raconté la vie de l'*Astyanax* et son comportement dès la L3 et à nouveau en M2, merci pour nos discussions sur le comportement, les poissons, les stats, excel… j'ai beaucoup appris grâce à toi, merci ! Hélène, la super-thésarde, merci de m'avoir formé à tant de choses : micro-injection, la FIV en nuit blanche, stader les poissons… et merci pour ta pédagogie à toute épreuve, tu es un exemple incroyable ! Merci aussi à Lydvina et Eugène, les stagiaires de L3/M1.5/M2 qui ne veulent pas décrocher de l'*Astyanax* ! Merci pour votre gentillesse, votre motivation et votre intérêt pour tous les sujets de l'équipe, merci pour votre esprit collectif, vous êtes top ! Merci aussi à mes stagiaires, Dominique, Garance, et Florent, merci pour l'intérêt et la motivation dont vous avez fait preuve au labo. Merci particulièrement à Florent pour sa contribution et son efficacité redoutable au cours de son stage de M1. Ton autonomie et ta vivacité d'esprit et ton implication ont été extrêmement agréables, je ne me fais aucun souci pour ton avenir ! Je veux remercier aussi Stéphane, je sais que ton travail à l'animalerie n'est pas facile, merci pour la bonne humeur que tu gardes malgré tout !

Je veux aussi remercier les DECA « par alliance » Julien et Boudjema. Merci Juju pour ta gentillesse, merci pour nos deux trips au Mexique, c'était super de les faire avec toi (merci pour ta patience envers Victor et moi dans les marchés) ! Bravo encore pour ta persévérance face à « l'incrédulité » de certain Astyanaxologues par rapport à tes résultats. Boudjema, merci pour ton humour et ta gentillesse, c'était un plaisir de te rencontrer et de pouvoir t'aider un peu sur tes manips, bon courage pour la fin de ta thèse et à bientôt j'espère !

Je tiens à remercier Franck ; après tout c'est grâce à toi que je suis là, tu es le premier à nous avoir parlé de l'Astyanax en L2. Ton cours était tellement bien que la moitié de la classe a voulu venir au labo voir les poissons et qu'en L3 j'ai voulu venir faire un stage ici ! Merci pour ce cours, pour ce stage et pour tout ce que tu m'as appris sur l'histologie, les microscopes, les médakas et les corneilles, c'était toujours très intéressant de parler avec toi. Les étudiants à qui tu enseignes ont beaucoup de chance!

Merci Aurélie pour ton encadrement en L3, c'était un stage de rêve et tu es une encadrante parfaite : attentive, gentille, intéressante, posée, disponible… et j'en passe ! Tu m'as vraiment donné envie de continué dans la recherche après ce stage ! Merci aussi pour ton soutien lors de la thèse et pour tes conseils, j'ai vraiment apprécié de faire ma thèse en même temps que toi, merci pour tout ! Je veux aussi remercier Ale, pour m'avoir aussi encadré et fait bénéficié de ses connaissances lors de ce stage de L3 et puis bien sûr pour le début de ma thèse. Merci pour ton rire à en flinguer les tympans, il donne le sourire à des km à la ronde ! Merci pour ton humour et ta bonne humeur. Merci aussi à Stéphanie, ma co-thésarde pour sa gentillesse et son courage, à Matthieu pour sa bonne humeur et son humour et à Rosaria pour notre virée ikea et ton partage de la culture Napolitaine. Merci enfin à Jean-Mimi, notre Père Noël préféré, toujours prêt à nous servir du thé et à discuter quand il y a besoin ! Merci à vous tous pour l'ambiance dans laquelle j'ai pu passer au moins une partie de ma thèse, le couloir des fous me manque…

Je tiens aussi à remercier toute l'équipe AMAGEN, ma « deuxième équipe ». Merci à tous pour vos conseils aussi bien BM que poissonnerie et merci à tous d'avoir veillé sur moi tout au long de la thèse (vive AMAGEN sans frontières) ! Merci aussi pour les cafés, pique-niques et barbecues !
Merci à Fred bien sûr, j'adore tes idées « à la con », c'est tellement intéressant et stimulant de parler BM et transgénèse avec toi, j'adore « l'élégance » de tes idées ! Merci de m'avoir fait le cadeau de cette idée de KI, je me suis bien amusée à la réaliser ! Merci pour ton soutien, pour ton humour dont on ne se relève pas, pour ton aide, merci d'avoir partagé tes connaissances (ici et à Marseille), et merci à toi, à Valérie et à Garance pour les apéros, vous êtes géniaux !

Merci aussi à Laurent, qu'est-ce que j'ai pu apprendre sur les poissons grâce à toi ! Quelques nuits blanches à attendre que les poissons se décident enfin à pondre, puis le club du CAES puis le club de Villebon, ta passion pour les bestioles est vraiment contagieuse ! Merci pour ton soutien sans faille, ton amitié, et tes passions étranges pour les poissons et le médiéval…
Merci à Sosthène, merci pour nos pauses café passées à discuter des idées « à la con » du chef et des tiennes, ou encore des façons de faire des zebra-plantes, d'anéantir le monde, ou bien tes idées d'utilisation des poubelles jaunes… Tu serais déçu, personne n'a repris ton rôle de maître des potins, et l'attribution des surnoms est au point mort, bref tu nous manque… Merci aussi pour tous tes conseils BM et clonage, j'ai beaucoup appris au contact du « roi du clonage » !
Merci à ma Nana, merci pour ta gentillesse, ton calme en toutes circonstances et ta bienveillance. Tu arrives à apaiser les esprits en toutes circonstances, ne perds pas ça ! Je t'adore, j'ai eu beaucoup de chance de te rencontrer, merci pour nos cafés, nos discussions, ta bonne humeur en toutes circonstances et ton soutien, merci pour tout !
Joanne, ma Jojo, merci pour tes conseils pratique sur le KI, c'est très largement grâce à toi que j'ai pu y arriver ! Merci pour ton aide, encore maintenant sur la caractérisation, c'est un vrai bonheur de collaborer avec toi, merci pour ton sourire !
Merci aussi aux deux BMistes courageuses qui ont repris le flambeau après le départ de Sosthène et le congé maternité de Joanne : Charlène et Morgan, merci pour votre aide et les pauses café / mots croisés !
Merci à Morgan pour ton cynisme souriant absolument parfait, j'adore ce petit grain de folie chez toi !
Je veux aussi remercier tout le staff poissonnerie d'AMAGEN ! Merci à Marion pour ton soutien, tes coups de main quand l'eau de mes bacs était trouble ou quand j'avais des problèmes de voiture, tu es toujours prête à donner un coup de main, merci beaucoup ! Merci aussi à Axel, que de souvenirs à Marseille (formation/plage/bar/sieste sur les marches/coup de stress avec Ali…). Merci beaucoup à vous deux pour nos soirées, c'était un vrai bol d'air !
Merci aussi à Pascal pour ses conseils bricolage, un vrai génie pratique ! J'adore voir les solutions que tu trouves à tous les problèmes, merci aussi pour les pauses café !
Je veux aussi remercier les membres passé d'AMAGEN : Zlatko qui m'avait fait entrevoir la complexité de la PCR dans toute sa splendeur et la quantité de stress généré par la rédaction d'une thèse. Merci aussi à Noémie grâce à qui j'ai eu l'occasion de faire un superbe voyage au Brésil ! Sans oublier Céline et sa gentillesse, ainsi que son caribou de Ben.

Merci aux membres de bioemergence pour leur aide. Un grand merci à Adeline Rausch pour nos discussions tardives et pour ta bonne humeur constante. Tu m'as vraiment fait peur avec tes malaises mais je suis maintenant rassurée pour toi, la suite paraît s'annoncer plutôt chouette ! Bon courage si tu reprends ta thèse, tu es méritante de bosser sur tes bestioles, elles ne te facilitent pas la vie… Merci aussi à Adeline Boyreau, merci pour ton aide lors de la conception du projet et tes conseils sur les fluorophores, les couleurs, … ça a finalement porté ses fruits ! Merci à Fanny pour son aide au sein de bioemergences, merci d'avoir contribué à plusieurs reprises à l'avancée du projet ! Merci à Thierry pour sa gentillesse, son soutien et ses conseils, merci pour le thermostat-bombe artisanal, belle performance de l'avoir transporté dans le RER, il marche bien en tous cas ! Thank you Mark for your work on adapting the workflow tools to the SPIM and also for the uploader, I only used it once but it worked perfectly !
Merci aussi à Sylvia de m'avoir entrainé au découpage de gâteau en vue de mon pot de thèse depuis le M2, j'espère que tu seras fière ! Malheureusement pour toi, tu seras toujours obligée de partager ta date de naissance, désolée !
Thank you Elena for your great advices on embryo manipulation and low-melting agarose, they were incredibly helpful ! Thanks also for your kindness and your piano playing ! Good luck for your projects here !

Merci aux anciens membres de bioemergences : Ludo et Gaëlle, mais aussi Matthieu, Julien et Dimitri, j'adorais votre folie et vos idées étranges ! And a thank you and good luck to the international Phd students and post-docs of the team : Antonio, Han, Yan, Svetlana, Mageshi.
Merci aussi à Nadine pour son enthousiasme sur des sujets pour le moins variés, j'ai beaucoup apprécié nos discussions, par exemple sur les trichoplax (au hasard), charmantes petites bestioles ! Et merci pour l'autonomie que tu m'as donné sur le SPIM (et pour le futon, lorsque nécessaire !).

Je veux aussi remercier tous les membres du TCF, bien sûr Pierre et Arnim, le duo de choc ! Merci à Pierre pour les discussions sur l'ORR et autres, tu m'auras bien aidé à comprendre tout ça. Merci à Arnim pour tes cours de Linux, nos séances d'escalade, tes vidéos sur les spreadsheets et pour ton intérêt pour tout (surtout les magnets !). Merci à tous les deux aussi pour nos voyages au ski, super souvenirs !
Merci à Johanna, ma Jo, merci pour nos trajets le matin, ils me manquent beaucoup ! Merci pour les vacances au Rayol, merci pour ta gentillesse, pour ton rire, pour ta bonne humeur et pour ton soutien. Je vous adore, toi, Guillaume, Izaak et Loulou (sniff).
Merci aussi à tous les membres du TCF : Laurie, le petit soleil de TEFOR, Lionel, Isabelle (super séances d'escalade !), Elodie, Sylvain, Elodie et Sybille.

Je veux aussi remercier les DEN, Kei, pour ton enthousiasme sur l'ORR et sur mon projet, et puis ta motivation au ski (beaux progrès !). Ingrid, pour nos weekends au ski, merci aussi à Mickaël, Manon, Philippe et Catherine pour votre gentillesse.

Je tiens aussi à remercier de tout cœur les services communs de NeuroPSI qui m'ont permis de travailler dans les meilleures conditions possibles au cours de ma thèse.

Tout d'abord Jocelyne, merci pour ta gentillesse, ton sourire et ta motivation à nous faciliter le travail, merci pour ton courage quand tu étais seule pour nous fournir des quantités astronomiques d'embryo medium. Merci aussi pour ta compréhension lors des problèmes avec cet embryo medium et pour ton aide pour les résoudre. Merci aussi à Natacha, Patricia et Tracy, merci pour votre aide et votre gentillesse !

Merci aussi à l'animalerie centrale pour son formidable travail ! Merci à Diane puis Krystel d'avoir chouchouté nos petits poissons (mes bébés super précieux !), j'ai pu vous les confier les yeux fermés ! Merci pour votre gentillesse ! Merci à Krystel pour ton intérêt pour mon sujet, c'était toujours un plaisir d'en parler avec toi, merci pour ta bonne humeur ! Merci aussi à Valérie pour ton aide et ta gentillesse, merci pour ton caractère et ton humour, tu es formidable, merci! Merci aussi à Aurélien pour nos discussions et pour ton aide. Merci à Christophe, Xavier et Céline pour leur travail et leur gentillesse. Bisous à Jean-Eudes !

Merci à Patrick pour ta gentillesse, ta bonne humeur, ta grande sagesse et ton efficacité ! C'est un tel luxe d'avoir quelqu'un comme toi ici, tu comprends nos besoins et tu y réponds parfaitement, le tout à une vitesse redoutable alors que tu es seul dans cet atelier, bravo et merci ! Merci aussi pour tes explications sur l'atelier et les machines formidables qui y résident, j'aurai beaucoup appris !

Merci au service gestion-RH d'avoir toujours trouvé des solutions à nos problèmes avec le sourire ! Merci à Jeanne, merci pour ton efficacité et pour ta gentillesse et pour ton sourire. Merci pour ton travail et ton aide ! Merci aussi à Angélique, merci pour toutes les solutions que tu m'as trouvé, et toujours avec le sourire. Tu m'as dit un jour que vous faisiez ce boulot pour le contact avec les gens et que votre rôle était de nous permettre de travailler sur la science sans passer notre temps sur les aspects administratifs, Jeanne et toi faisiez ça à la perfection, toujours avec le sourire ! Nous avons perdu un sacré duo ! Merci

aussi à Michèle et Christine qui ont repris le flambeau administratif ! Un grand merci aussi à notre RH préférée Odile, qui répond à toutes nos questions sur les contrats, les thèses et autre !

Merci aussi à Pascal Fangouse pour ses blagues dès le matin, à Alain Pérignon qui réussit à nous retrouver tous les articles même les plus anciens, et également à tous les membres du service informatique Bernard, Nicolas, Maxime et Philippe pour leur aide et leur stock de disques dur que j'aurai bien exploité ces derniers mois.

Je veux aussi à remercier le veilleur de nuit le plus sympa que j'ai pu rencontrer, qui avait toujours un petit mot gentil et un grand sourire même quand les horaires étaient un peu douloureux !

Je remercie aussi toute l'équipe de Phaseview pour leur aide au cours de cette dernière année et demie. Merci à vous pour ce beau module SPIM et pour toutes les améliorations que vous y avez apportées afin que je puisse réaliser mes films malgré toutes les contraintes de mes manips. Merci à Gaël pour ton humour et ta franchise parfois brutale, merci pour les discussions voyage, boulot, SPIM et autres, merci d'avoir partagé un peu de ta grande sagesse (et gratuitement en plus !). Merci pour tes « solutions » originales quand tu me proposais de changer mon sujet pour une étude du rhombencéphale ou de la peau… tu ne m'en voudras pas trop si je ne les ai pas suivies ! Merci à Arthur d'avoir trouvé des solutions à tous mes problèmes logiciel, même quand je poussais QtSPIM à bout ! Très belle version 1.3.4 (je crois), elle a résisté à tous mes assauts, je la déclare donc idiot-proof, très belle performance ! Merci aussi pour ton humour.

Merci à Cyprian, merci pour tes explications sur l'optique et sur les filtres-passoires ! Merci pour les dépannages teamviewer à des heures indues, ton autorité sur le SPIM est incontestable (je te jure que je faisais la même chose mais il ne m'écoutait pas !). Merci pour ton soutien pendant les acquisitions et l'écriture, merci pour ta compréhension, ton aide et ta présence, je ne dirai qu'un mot « plethora ». Merci pour tout, tu es formidable !

Je tiens aussi à remercier les membres de ma super colloc ! Merci à Solal d'avoir lancé cette idée de colloc avec Aurore, c'était génial, une super ambiance malgré une princesse Star Wars un peu relou de temps en temps. Merci Solal pour notre weekend au ski, pour les soirées chez toi depuis la L2 et pour les discussions passionnantes. Tu resteras la seule personne que je connaisse à avoir dressé (dompté devrais-je dire) des zebra pour sa thèse. Merci à Aurore, j'ai adoré cette colloc avec toi, que de bons moments ! On peut dire que Solal avait vu juste, ça a tout de suite très bien collé entre nous ! Continue avec tous tes projets, avec toutes tes idées, tes photos, tes dessins, ton site internet, tes bricolages, tes weekends, la contrebasse, l'escalade… tu es géniale (et très impressionnante) ! Merci aussi à Linda, ma dernière colloc, merci pour ton sourire lumineux, même avant qu'on ne se parle, merci pour ta gentillesse, merci pour les soirées et les discussions ! Tu es un véritable petit soleil ! Merci aussi à mes « collocs par alliance », Max et Sandrine d'avoir contribué à l'ambiance de cet appartement et de ses soirées ! Merci à Max d'être venu passer du temps avec nous ici, à manger des sushis et à discuter voitures, montres, portables, labos, thèses, schizophrénie, médecine, voyage… dommage que ton labo n'ai pas été plus proche, j'aurai vraiment apprécié t'avoir comme colloc plus permanent ! Merci à Sandrine pour sa gentillesse même dans les moments difficiles, tu es adorable, merci d'avoir aussi contribué à la vie de cette colloc pour un temps !

Je veux aussi remercier tous les magistériens, pour leur soutien et pour toutes ces années incroyables de magistère, passées dans une ambiance de folie et avec une motivation sans faille. Merci à tous pour ces soirées, ces TP, ces cours, ces vacances, ces WEI et WEPI, ces parties de frisbee sur les pelouses de la fac et ces révisions de dernière minute au soleil… ces années passées avec vous resteront un souvenir extraordinaire ! Merci à tous, je vous adore !

Je veux évidemment remercier ma famille, qui m'a toujours soutenu dans cette voie et aidé au cours de mes études. Merci à mes parents de m'avoir toujours aidé, toujours accompagné, d'avoir toujours été présents et à l'écoute ! Merci de nous avoir transmis tant de choses, le goût des voyages, de la montagne, de la nature, des sciences… Merci d'avoir cultivé notre curiosité ! Wautier a bien raison, vous êtes des parents formidables ! Merci à mes deux frangins de s'être toujours intéressés à ma thèse malgré nos études différentes. Bravo à vous deux pour vos super parcours respectifs ! Respect à Gabi, qui a maintenu le cap vers la vulcanologie depuis ses 7 ans à peu près, chapeau pour la persévérance ! Et bravo à Vincent pour ses expériences très internationales et son goût du défi !

Merci aussi à Nania, ma grand-mère. Quel exemple tu nous donnes ! Quel dynamisme, quelle détermination ! C'est aussi grâce à toi que j'ai trouvé la force de réaliser cette thèse ! Merci pour tous ces mercredis chez toi, merci pour Saint-Benoist et tous les bons moments passés là-bas avec toi, merci de t'être tellement occupée de nous…

Je te dédie cette thèse.

Table of contents

List of figures

List of abbreviations

5-HT: serotonin

A: anterior

AC: anterior commissure

ACTH: adreno-cortico-trophic hormone

AgRP: agouti-related protein

ANB: anterior neural border

ANP: anterior neural plate

ANR: anterior neural ridge

AVT: arginine-vasotocin

CART: Cocain and Amphetamine related transcript

C-division: crossing division

CF: cavefish

cGMP: cyclic guanosine monophosphate

Ch/CHOR: choroid

CMZ: ciliary marginal zone

CRH: corticotrophin releasing hormone

DA: dopamine

DC dorsal cornea

DD: permanent dark conditions

Di: distal

Do/D: Dorsal

DP: dorsal pupil

dpf: days post fertilization

DR: dorsal retina

ECM: extracellular matrix

Efn: ephrin ligand

Eph: eph receptors

FGF: fibroblast growth factor

GCL: ganglion cell layer

GR: glucocorticoid receptor

H: hyaloid vasculature

Hcrt: hypocretin

HPA: hypothalamic-pituitary-adrenal

hpf: hours post fertilization

HPI: hypothalamic-pituitary-interrenal

hy/Hyp: hypothalamus

INL: inner nuclear layer

IOC: inner optic circle

IPL: inner plexiform layer

Ir: iris

IT: isotocin

L: lens

LD: light/dark photoperiod

LEDGF: lens epithelium-derived growth factor

Lhx: Lim-Homoeobox transcription factor

M: mesencephalon

MAO: monoamine oxydase

MCH: melanin-concentrating hormone

MHB: midbrain-hindbrain boundary

mpf: month post fertilization

MSH: melanin-stimulating hormone

NA: noradrenaline

NPO: neurosecretory preoptic nucleus

NPY: neuropeptide Y

NR: neural retina

ntac: neural tract of the anterior commissure

oc/ch: optic chiasma

OC: optic cup

OE: olfactory epithelium

OF: optic fissure

ON: optic nerve

ONL: outer nuclear layer

OPL: outer plexiform layer

or: optic recess

ORR: optic recess region

OS: optic stalk

OV: optic vesicle

P: pallium

P: posterior

PCP: prechordal plate

PEDF: pigment epithelium-derived factor

PlCP: planar cell polarity pathway

PO: preoptic area

POC: post optic commissure

POM: periocular mesenchymal

POMC: pro-opiomelanocortin

Pr: Proximal

PS: pigmented strip

PVN: paraventricular nucleus

QTL: quantitative trait loci

R: rhombencephalon

RA: retinoic acid

RPE: Retinal Pigmented Epithelium

SF: surface fish

SNP: single nucleotide polymorphism

SP: subpallium

ss: somite stage

SST: Somatostatin

SV: saccus vasculosus

TF: transcription factor

TGF- β: transforming growth factor-β

Th: thalamus

TMZ: tectal marginal zone

UV: ultraviolet

VAB: vibration attraction behaviour

VC: ventral cornea

Ve/V: ventral

VEGF: vascular endothelial growth factor

VP : ventral pupil

VR : ventral retina

WT: wild type

zli: *zona limitans intrathalamica*

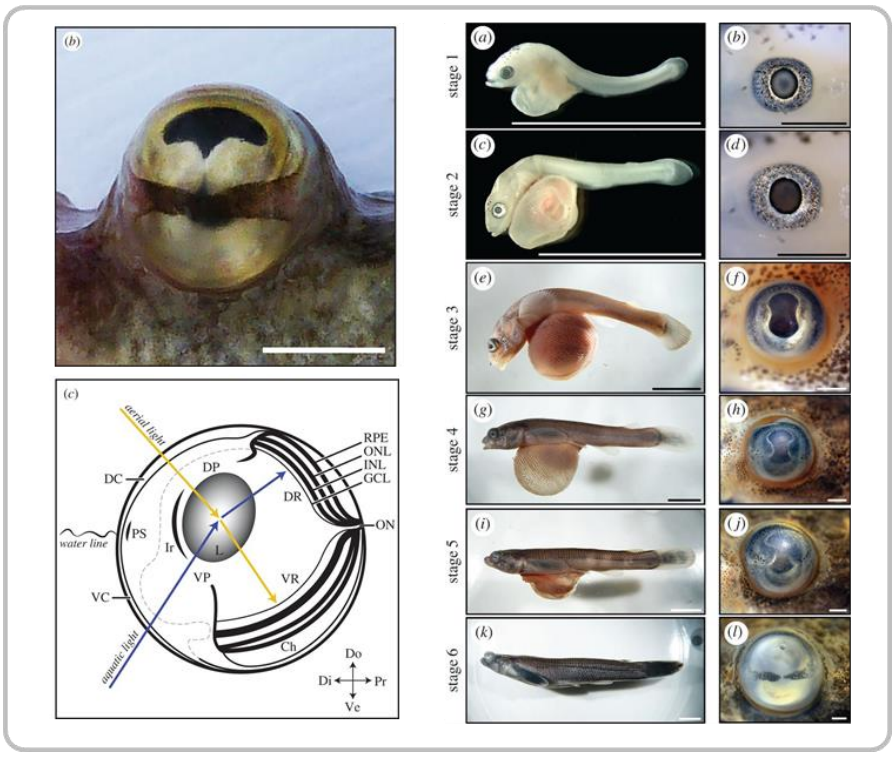

Figure 1 : The eye of *Anableps anableps.*
Top: close-up on the eye of the fish *Anableps anableps.* Bottom: Schematic of the visual aerial and aquatic inputs (sagittal view of the eye). Right : development of the eye in this species with appearance of the pupil separation. RPE, retinal pigmented epithelium; ONL, outer nuclear layer; INL, inner nuclear layer; GCL, ganglion cell layer; ON, optic nerve; DR, dorsal retina; DP, dorsal pupil; VR, ventral retina; VP, ventral pupil; Ch, Choroid; L, lens; Ir, iris; PS, pigmented strip; DC, dorsal cornea; VC, ventral cornea; Do, dorsal; Ve, ventral; Di, distal; Pr, proximal.
From (Perez et al. 2017).

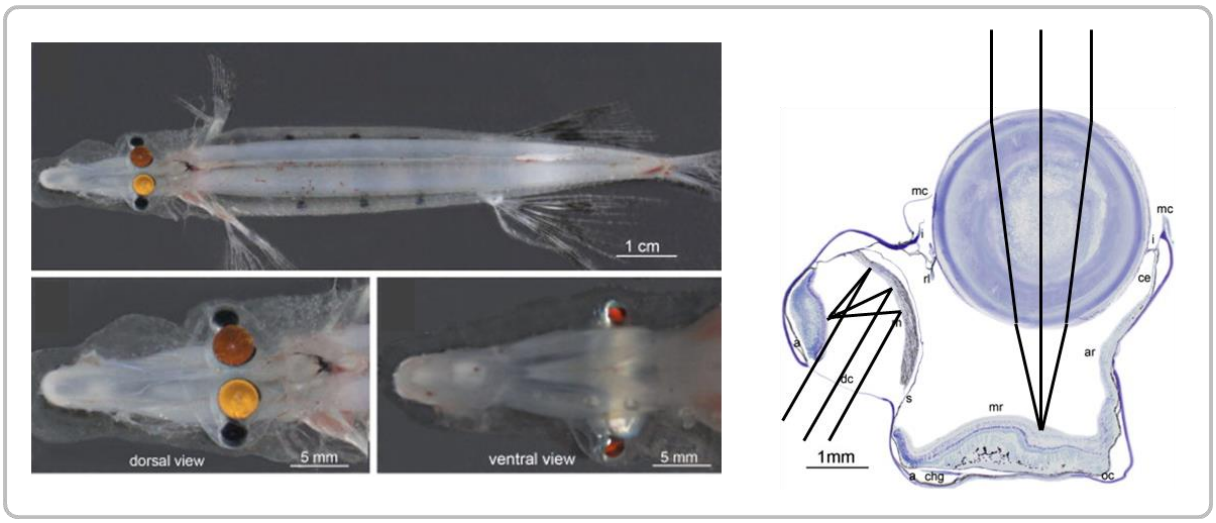

Figure 2 : the eye of the spookfish.
Left panel, top : dorsal view of the spookfish. Bottom left : close-up on the head, the two top eyes display a yellow/brown color. Bottom right : ventral view of the head, the two little orange spheres are the downward-pointing parts of the eye. Right : transverse section of the spookfish eye, the optical paths of light are shown in black
From (Wagner et al. 2009).

General Introduction

Nature is fascinating in many ways and especially in the incredible diversity of adaptations that different species have evolved to thrive in their specific niche. These diverse solutions to the specificities of each environment have allowed the colonization of a vast majority of the existing environments on earth. This occurred by trial and error or rather mutation and selection processes along with other epigenetic processes and generated the amazing diversity that can now admire. Striking example reside in fishes : the annual killifish *Nothobranchius furzeri* lives in ephemeral ponds that dry each year. This fish's eggs are desiccation-resistant and can enter diapause at different stages of development; they can remain in a paused state for up to two years. When the rain season arrives, they hatch and extremely quickly develop to lay eggs (after less than 3 weeks). These fishes age extremely fast and die after a few month even in captivity (Blažek et al. 2013; Furness et al. 2015; Genade et al. 2005). Conversely, other fish species such as the sablefish can live past 100 years. Similarly, behaviour and parental care can be extremely different with some cichlid fish mouth brooding their eggs and larvae to protect them compared to zebrafish which readily eat their own eggs after spawning (Sefc et al. 2012).

Concerning the eye, the diversity is also quite striking. For example the so-called "four-eyed fish" *Anableps anableps* first develops a fairly normal eye, which then elongate and above its head separates in two halves by the growth of a pigmented band in the middle of their cornea creating two distinct pupils. The fish swims at the surface of the water with the top half of its eyes above water and the bottom part immersed. Its ovoid lens simultaneously focuses the aerial and aquatic light on the ventral and dorsal retina, respectively. Moreover, its photoreceptor distribution is different in the ventral and dorsal retina to accommodate the different light wavelengths coming from the two environments (Owens et al. 2012; Perez et al. 2017). Another curious example of eye drastic modification concerns the spookfish *Dolichopteryx longipes* which possesses what could first seem to be 4 eyes, upward-pointing and downward-pointing, but are really just two extremely modified eyes. The upper "eyes" are quite normal with a lens focusing the light on the retina. The second part of these eyes, pointing downwards is much more intriguing as it does not present any lens but still focuses light through a concave mirror (tapedum). This is a quite unique example amongst vertebrates of an ocular image form through a mirror instead of a lens. This adaptation allows this mesopelagic (200m to 100m deep) fish to see both the animals swimming above it in the sunlight and to perceive the bioluminescence or reflection generated by animals swimming beneath it (Wagner et al. 2009). Conversely to these two examples of increased eye complexity to allow enhanced vision in two very different contexts, other fish living in dark environment have regressed their eyes and rely on other senses to find food or mates. This is the case of most cavefish or deep-dwelling fishes such as the Mexican cavefish *Astyanax mexicanus* (Gunter & Meyer 2013; Hinaux et al. 2016). Fishes can of course be used a models for vertebrate studies and biomedical research, but this incredible diversity is also worth studying for itself, simply to be amazed by evolution and how such complex adaptations are generated.

In the model I used for my PhD thesis, the eyeless cavefish *Astyanax mexicanus*, many sensory compensations have been described including an enhanced olfaction, taste and lateral line but this fish adaptations and modifications are not restricted to sensorial modalities and also concern their physiology and behaviour.

Like all cave animals lacking eye at adult stages, the cavefish embryos first form eyes before they degenerate. These eyes display several subtle modifications that can be compared to their conspecific surface fish in an “Evo-Devo” approach. This approach aims at understanding how early and subtle modifications of the development can strongly affect the morphological, sensorial, physiological and behavioural characteristic of the larval and adult fish, potentially modifying its chances of survival in its environment.

During my Phd, I studied the developmental evolution of the optic region (at large) in the Mexican cavefish. I first participated to a project where we analysed the role of early morphogen signalling on neuropeptidergic hypothalamic neurons and larval behaviour. I also worked on the eye phenotype of the embryonic cavefish; indeed, the ventral part of this eye was described as reduced or even lacking. We therefore undertook to better characterize this phenotype by studying the regional and tissue identity of the surface fish eye, always in comparison with the cavefish eye. We also tackled the question of the morphogenetic events leading to this defect by generating transgenic fluorescent reporter lines and performing live imaging.

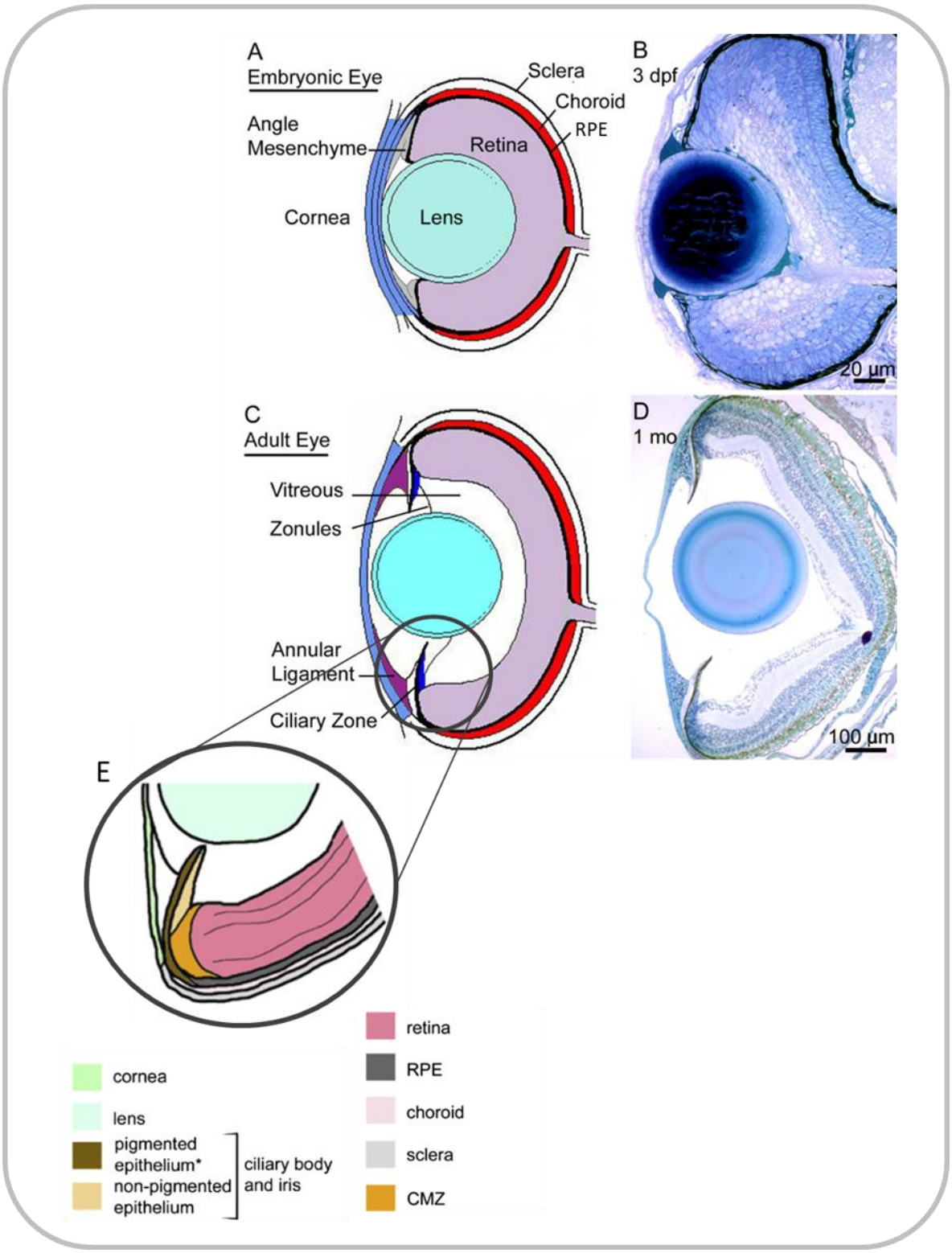

Figure 3 : General anatomy of the embryonic and adult zebrafish eye.
(A) Diagram of the embryonic zebrafish eye at 3 dpf. (B) Transverse section of an embryonic zebrafish eye at 3 dpf.
(C) Diagram of the adult zebrafish eye. (D) Transverse section of an adult zebrafish eye. Note the space for vitreous humour that has appeared. (E) More detailed diagram of the iridocorneal angle of the zebrafish with its own colour legend.
After (Soules & Link 2005; Fischer et al. 2013).

Introduction

1. Eye Anatomy

The eye is the visual sensory organ, it is absolutely essential to many animals in order to escape from predators, to feed and in some cases to choose mates. Indeed, quite a lot of animals rely on the visual modality for these tasks, which includes the zebrafish and its larva, which could explain why its eye becomes functional as early as 72 hours post fertilization (hpf) (Easter, Jr. & Nicola 1996; Gestri et al. 2012). Here I will talk mostly about the fish eye and brain development, and more particularly about the zebrafish, as it is the most studied fish model.

The vertebrate eye is traditionally described in two parts : the anterior segment and the posterior segment, which do not have anything to do with the antero-posterior axis of the animal, at least in the case of animals with lateral eyes like the zebrafish. Indeed, these terms refer to the external and internal parts of the mature eye. The anterior segment comprises the most external parts of the eye including the cornea, lens, iris and ciliary body. The posterior segment includes the neural retina, retinal pigmented epithelium (RPE), vitreous humour and optic nerve (Figure 3)(Soules & Link 2005).

The cornea and the lens are together responsible for the light transmission and focusing. Indeed these two structures are transparent and located in the optic path to the retina, on which they focus the light. In zebrafish, the majority of light refraction is produced by the lens. Of note, in fish the lens does not change shape to accommodate focus, instead, the entire lens is moved backward or forward to achieve same result (Gestri et al. 2012).

1.1. The cornea

The cornea is the outermost part of the eye, and is therefore the first line of defence against the external lesions, especially in animals without eyelids like fishes. It is continuous with the more “posterior” opaque sclera that forms the outer layer of the adult eye. The cornea is composed by several layers : the epithelium, Bowman’s layer, the stroma, Descemet’s membrane and the endothelium, from the most external to the most internal.

The corneal epithelium is 3-6 cells-thick, and sits on a thin basal membrane, the Bowman’s layer, that separates it from the stroma. The stroma is mostly composed of extracellular matrix with thin layers of collagen fibrils, all running parallel to the lamina but orthogonal to each other. This particular organization allows for a good transparency of the cornea. Just beneath the stroma, lies another basal lamina : Descemet’s membrane, which covers the last single-cell layer : the corneal endothelium, which plays a role in metabolic homeostasis and stromal collagen organization maintenance.

The corneal epithelium develops from the surface ectoderm, from which it detaches around 1 month post fertilization (mpf). The stroma and corneal endothelium on the other hand, are both derived from the periocular mesenchyme (POM) (Soules & Link 2005).

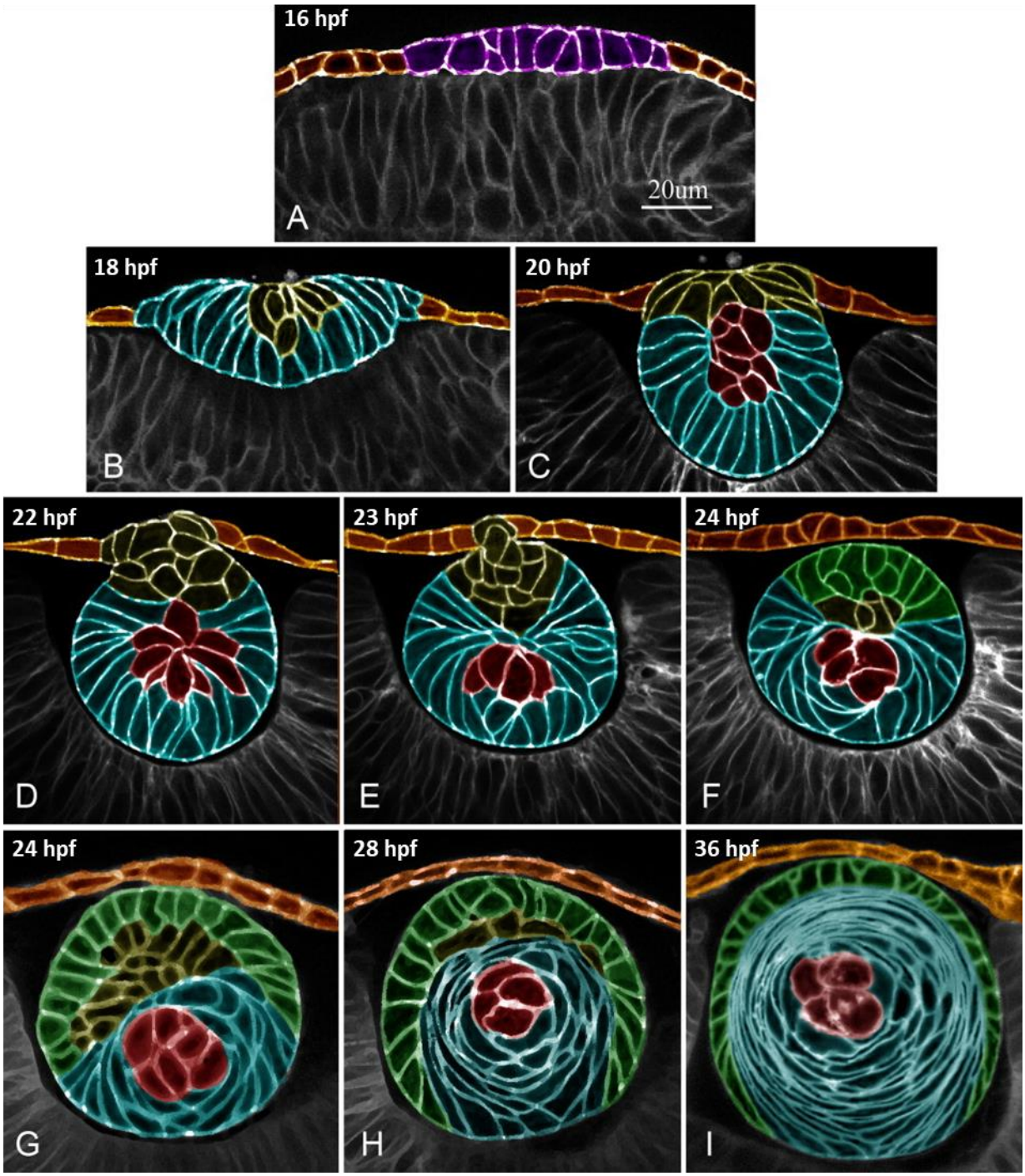

Figure 4 : Lens development, from a flat placode to the spherical lens.
Live imaging of the lens development, cell membranes have been pseudo-coloured. (A) Approximately 16 hpf, the cells in the surface ectoderm are orange and the cells in the lens placode are purple. (B) 18 hpf, elongating fiber cells are blue. (C) 20 hpf, center cells (red) of the delaminating lens mass are surrounded by columnar primary fiber cells (blue). (D–F) 22 hpf, 23 hpf, and 24 hpf, delamination completes the separation of the spherical lens from the developing cornea (orange). Morphologically undifferentiated cells at the external surface of the lens mass (yellow) lose adhesion contacts with the surface ectoderm. (G) After delamination, at approximately 24 hpf, the external epithelium (green) began to form. (H,I) 28 and 36 hpf, circular elongation and compaction of the fiber cells. All images have the same scale.
From (Greiling & Clark 2009)

1.2. The lens

The lens is located just beneath the cornea and its role lies in focusing the light onto the retina. It is composed of lens fiber cells that are covered by lens epithelial cells. The fiber cells are known to accumulate large amounts of crystallin proteins -which give the lens its refractive properties - and to degrade their nuclei and organelles, which allows for a better transparency (Dahm et al. 2007).
Most epithelial cells are in a quiescent state but some remain in a proliferative state, giving rise to new epithelial cells as well as fiber cells.

The lens derives from a placode, with a non-neural ectoderm origin. The establishment of the lens proper begins around 16 hpf in zebrafish with a thickening of the lens placode upon contacting the optic vesicle. Placodal cells then delaminate to give rise to a solid spherical lens that will detach from the surface ectoderm around 24 hpf (Greiling & Clark 2009). The central fiber cells then elongate in a circular fashion and progressively lose their organelles and establish ball-and-socket joints with each other. The differentiation then progresses outwards and the compaction of these fiber cells continues until 1 mpf (Figure 4) (Gestri et al. 2012).

1.3. The iridocorneal angle

The region where the cornea meets the iris is termed iridocorneal angle. The iris and ciliary zone derive from the margin of the retina but the iris stroma derives from the POM. The iris stroma contains layers of pigment appearing between 3 days post-fertilization (dpf) and 7 dpf with a layer of black melanosomes, a layer of silver iridophores and one of golden xanthophores (Soules & Link 2005). The ciliary epithelia cells are located just posterior to the iris, and they produce the aqueous humour (Figure 3) (Gestri et al. 2012).

The iridocorneal angle plays an important role in the maintenance of intraocular pressure through the balance between aqueous humour production and clearance. In zebrafish, the dorsal quadrant of the ciliary epithelium seems to have an enhanced production of aqueous humour, which then flows above the lens and below the cornea towards the ventral quadrant where it can be evacuated both at the iridocorneal angle and through a break in the ciliary epithelium (Figure 5) (Gestri et al. 2012).

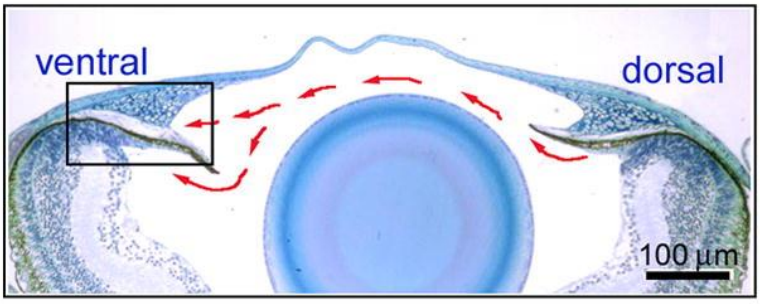

Figure 5 : Iridocorneal angle of the zebrafish eye.
Transverse section of the adult zebrafish “anterior segment”, red arrows show the general flow of aqueous humour.
From (Gestri et al. 2012)

The inner/posterior segment of the eye, which is the part I focused on during my Phd, is the part of the eye that allows the translation of the received light into nervous output and sends this information to the midbrain visual processing center, the optic tectum.

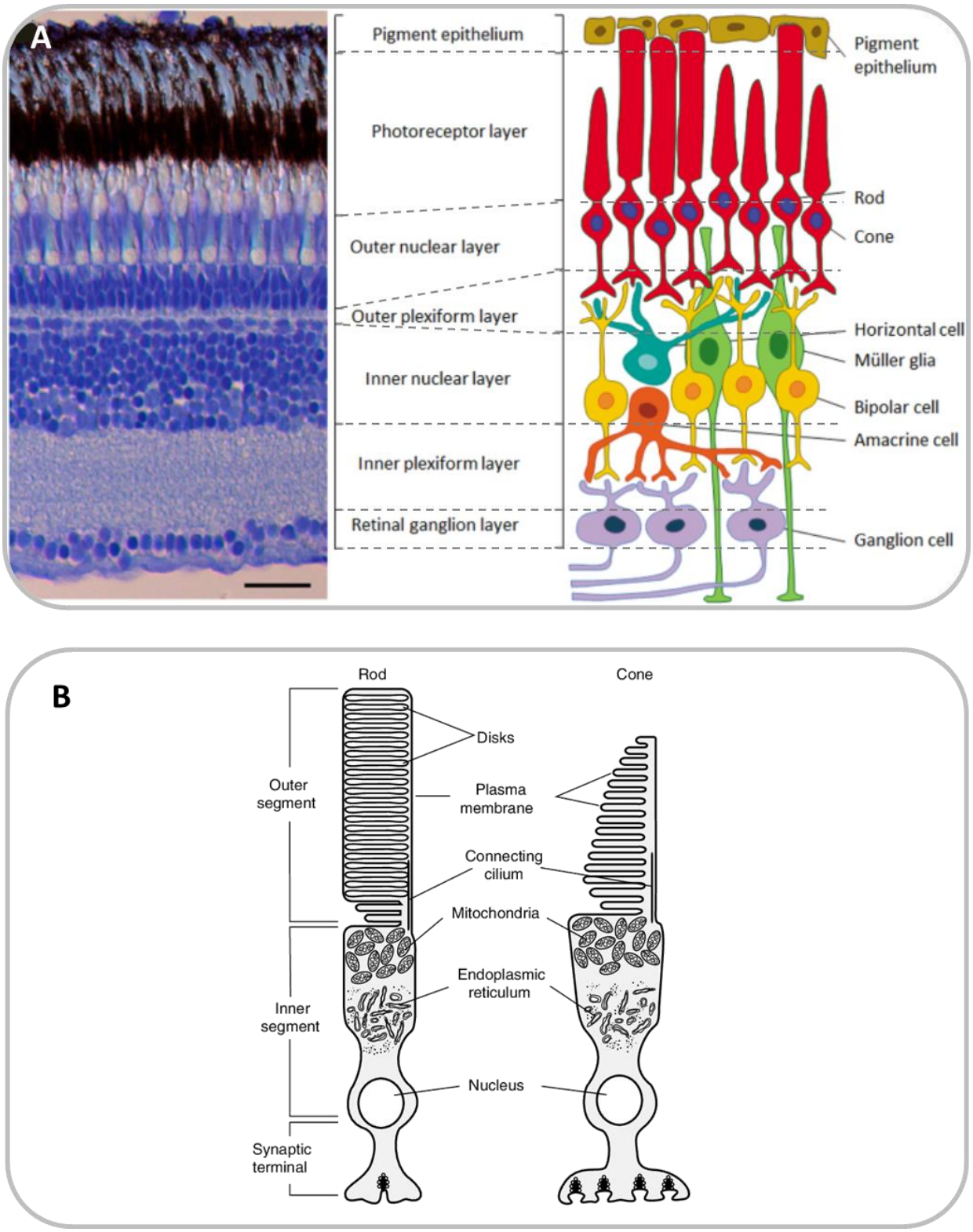

Figure 6 : Structure of the retina and morphology of photoreceptors
(A) The different layer of the adult zebrafish retina. The outer part is on the top, inner part on the bottom.
(B) Structure of the photoreceptors.
From (Gramage et al. 2014; Cote 2006)

1.4. The Neural Retina

The vertebrate retina is the primary information-processing visual organ whose role is to detect and enhance luminance and colour contrast before projecting to central processing centres (Stenkamp 2007).

Embryonically, the neural retina derives from the neuroepithelium of the anterior neural plate. As such, it is part of the central nervous system.

The zebrafish neural retina (NR) possesses 6 different types of neurons and one type of glial cells. They are organized in 3 nuclear layers separated by 2 synaptic –or plexiform- layers that are already visible by 3 dpf (Figure 6A).

1.4.1. The outer nuclear layer

The most external layer, that contacts the retinal pigmented epithelium (RPE) is called the outer nuclear layer (ONL) and contains the photoreceptors. These cells receive the light stimulus and convert it into nervous output. They can be divided into 2 main types : the rods, that are able to detect very dim light but do not discriminate colours ; and the cones which require more intense light input to be activated but that can differentiate colours. Cone cells can be further split into 4 types according to the wavelength they can detect : red, green, blue and ultraviolet (UV). Indeed, in contrast to humans who only have 3 cone types, zebrafish can see UV light (Gestri et al. 2012).

Photoreceptors morphology and function

All photoreceptors share a common morphology with some variations according on the precise type. They contain an outer segment which is the part closest to the RPE; it is actually a modified cilium which is composed of piled discs. These discs are filled with opsin-retinal complexes, the molecules reacting to photon absorption. New discs are regularly added while the external-most ones are shed. Connected to the outer segment via a connecting cilium stands the inner segment of the photoreceptor which is enriched in mitochondria. Finally comes the cell body, containing the nucleus and other organelles, and finally, the axon (Figure 6B).

The photoreceptors establish glutamatergic synapses which are active in the dark and inactivated upon detection of light. The first step of light reception takes place in the outer segment of the photoreceptor containing opsins. Opsins are large membrane-bound proteins that differ according to the photoreceptor type; they are bound to a small molecule, the 11-cis-retinal. Upon light absorption, the 11-cis-retinal is transformed into all-trans-retinal which indirectly causes the cGMP-gated sodium channels to close. This results in the hyperpolarization of the photoreceptor and therefore, to an inhibition of the synaptic release of glutamate.

1.4.2. The inner nuclear layer

The inner nuclear layer contains the cell bodies of 3 other neuronal types of the retina : the bipolar, horizontal and amacrine cells as well as the somata of the glial cells of the retina : the Müller cells. The bipolar neurons are interneurons that connect the photoreceptors to the retinal ganglion cells (RGC), therefore transducing the signal. Horizontal cells establish connections with several photoreceptors; they modulate the signal relative to the neighbouring photoreceptor inputs, resulting in increased perceived contrast, therefore allowing for a better detection of edges. The synapses between these 2 types of neurons and the photoreceptors are established in the outer plexiform layer.

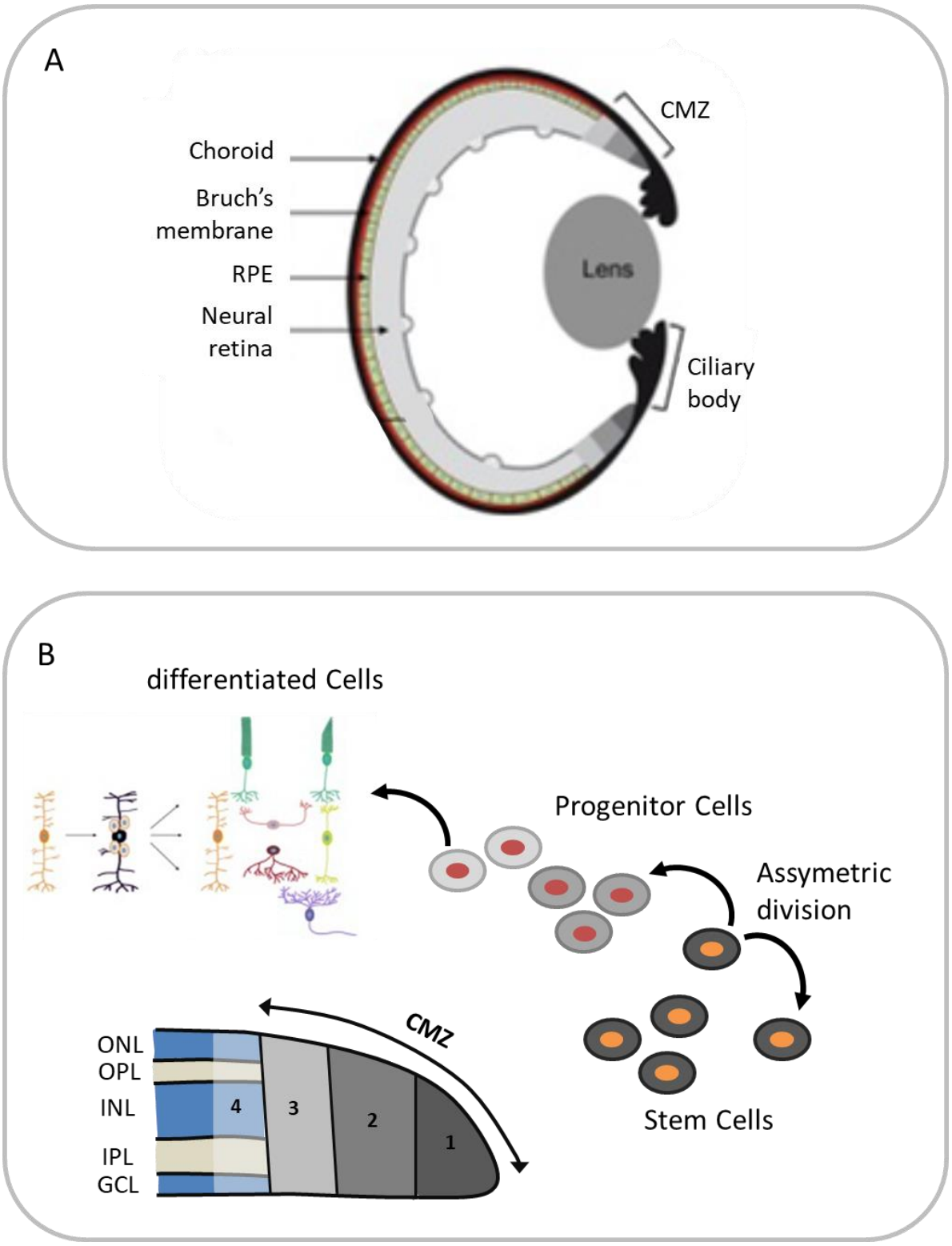

Figure 7 : Structure of the retina and ciliary marginal zone.
(A) Schematic representation of a transverse section of a zebrafish or *Xenopus* eye showing the ciliary marginal zone (CMZ), retinal pigment epithelium (RPE), neural retina, choroid and Bruch's membrane. (B) The different zones of the CMZ. Zone I, the most peripheral part is the stem cell niche; zone II contains rapidly proliferating progenitors. Zone III is composed by less proliferative and more fate-restricted retinoblasts, and zone IV consists in the differentiating neurons. ONL, outer nuclear layer; OPL outer plexiform layer; INL, inner nuclear layer; IPL, inner plexiform layer; GCL, ganglionic cell layer.
From and modified from (Ail & Perron 2017)

1.4.3. The ganglion cell layer

The amacrine cells establish synapses with several retinal ganglion cells (RGC) which lie in the ganglionic layer. The RGCs connections to the amacrine and bipolar cells are established in the inner plexiform layer. RGCs send very long axons that constitute the optic nerve to cross the midline ventrally at the level of the optic chiasm before reaching contra-laterally the dorsal optic tectum, for the vast majority of them (Gestri et al. 2012).

1.5. The Ciliary Marginal Zone

The Ciliary marginal zone or CMZ is a circular region located at the periphery of the neural retina, around the lens. It is a niche of retinal stem cells and progenitors that exists in larval and adult fishes but also in other vertebrates such as larval frogs and birds (Figure 7A). This niche allows the continual addition of new cells at the periphery of the retina so that the central-most cells of the retina are the oldest neurons and the most peripheral cells close to the CMZ are the youngest-born neurons. Indeed, fishes are continuously-growing animals even if their growth slows down with time, which means that their eyes but also optic tectum and brain also continuously grow.

The CMZ is organized in four zones; from peripheral to central, the self-renewing retinal stem cells are at the rim of the neural retina (zone I), they give rise to the slightly more central pluripotent retinoblasts (zone II). These retinoblasts will proliferate extensively and give rise to the central retinoblasts which have a more restricted fate and less proliferative capacities (zone III). From these central retinoblasts, the last category of cells of the CMZ will emerge : these are differentiating precursors (zone IV) that have stopped dividing and are adopting the neural retinal layered organization (Figure 7B)(Perron & Harris 2000; Fischer et al. 2013).

1.6. The Retinal Pigmented Epithelium

1.6.1. General presentation

The retinal pigmented epithelium (RPE) is a monolayer of large and flat pigmented cells that lies just behind and in contact with the photoreceptors of the ONL. The apical pole of this epithelium displays long microvilli that surround the photoreceptor outer segments; each RPE cell faces several photoreceptors (between 20 and 45 photoreceptors per RPE cell in rhesus monkey). The basal part of the RPE sits on Bruch's membrane, a basal lamina associated to a fibrous and collagenous membrane, separating the RPE from the choroid layer (Figure 7A).

The RPE derives from the embryonic neuroepithelium and the later medial optic vesicle and plays many essential roles to ensure the eye homeostasis, immunity and correct function.

1.6.2. Roles of the RPE in vertebrates

Photoprotection

The first role of the pigmented epithelium is to absorb the scattered light after its passage through neural retina, thus limiting photo-oxidation and therefore oxidative stress. Indeed, photo-oxidation occurs in presence of light and oxygen which are both present in large amounts in the retina, it is therefore essential to absorb light after it has been detected in order to reduce the damages caused by this phenomenon (Figure 8)(Strauss 2005).

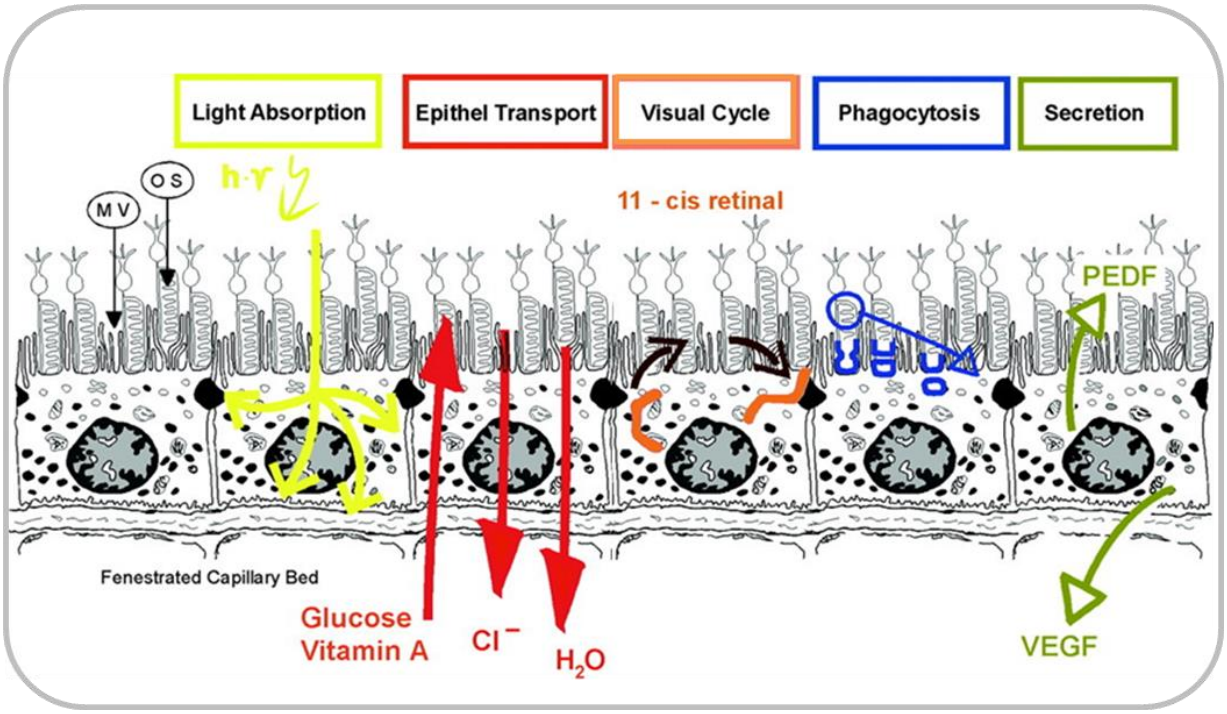

Figure 8 : roles of the retinal pigmented epithelium.
OS, outer segment of the retinal epithelium; MV, microvilli.
The RPE scatters light, transports nutrients and metabolites, recycles retinal, phagocytes the shedding disks of the photoreceptors and secretes growth factors.
From (Strauss 2005)

Blood-brain barrier

The RPE takes part in the blood-brain barrier. Indeed, the retina being part of the brain, it is therefore protected by the blood-brain barrier in the same way. The nutrients and diverse molecules have to transit from the choroid capillary network to the retina and vice-versa; as the RPE cells establish tight junctions with each other these molecules have to be transported through the RPE cells. This includes water, ions, nutrients…

Water is produced in large quantities in the retina mainly because of the metabolic activity of the neurons and photoreceptors but also because the intraocular pressure forces the water from the vitreous humour to pass into the retina. This water is then transported from the retina to the sub-retinal space by Müller glia. The RPE contains aquaporins on both its apico-basal sides which then allows the water to go from the sub-retinal space to the choroid vascular network (Strauss 2005).

Ions are also transported actively or passively through the RPE. Overall, Cl^- ions are driven out of the retina and toward the vascular system along with water and lactic acid which is a metabolic product from the photoreceptor's activity.

On the other hand, nutrients are transported from the choroid system to the retina. Indeed, the RPE contains many glucose transporters in both its apico and basal membranes that allow it to efficiently provide energy to the retina according to its needs.

Vitamin A (all-trans-retinol) is also imported from the blood to the RPE to help supply the needs of photoreceptors for all-trans-retinal (Figure 8)(Strauss 2005).

Retinal recycling

One of the very crucial functions of the RPE is to provide the photoreceptors with all-trans-retinal so that they can function and achieve their light detection role. Indeed, upon reception of light, photoreceptors convert 11-cis-retinal into all-trans-retinal but they are unable to recycle the all-trans-retinal into 11-cis-retinal. To achieve that, the RPE functions as a recycling unit that uptakes the all-trans-retinal coming from the photoreceptor and recycles it into 11-cis-retinal which is then transported back to the photoreceptor where it is re-associated to an opsin. This cycle of retinal between photoreceptors and RPE is termed visual cycle. Rod cells rely only on this visual cycle while cone cells can regenerate part of their retinal in another visual cycle occurring in Müller cells (Figure 8)(Strauss 2005).

Phagocytosis of Shed Photoreceptor discs

As mentioned earlier, the photoreceptors are exposed to high levels of light and oxygen, leading to photo-oxidation and oxidative stress which is increased by retinal metabolism. Furthermore, light damages proteins and lipids; all of these add-up and concentrate toxic reactive species in the discs. In order to maintain the integrity and the functionality of the photoreceptors, the external-most discs are shed and replaced by addition of new discs at the base of the outer segment. The shed discs are phagocytosed by the RPE and the important molecules, such as retinal, are recycled and exported back to the photoreceptor. The shedding and the phagocytosis processes are tightly regulated and coordinated to ensure a sufficient turnover but a constant length of outer segment. These processes are also controlled in a circadian manner with a peak of phagocytosis of rod outer segment occurring at the onset of light. This circadian regulation however seems to differ between cones and rods and across species (Figure 8Figure 7)(Strauss 2005).

Secretion of growth factors

The RPE secrete growth factors that are necessary for retina and choroid vessels integrity. Indeed, the RPE is able to secrete a variety of immunosuppressive factors and growth factors such as fibroblast growth

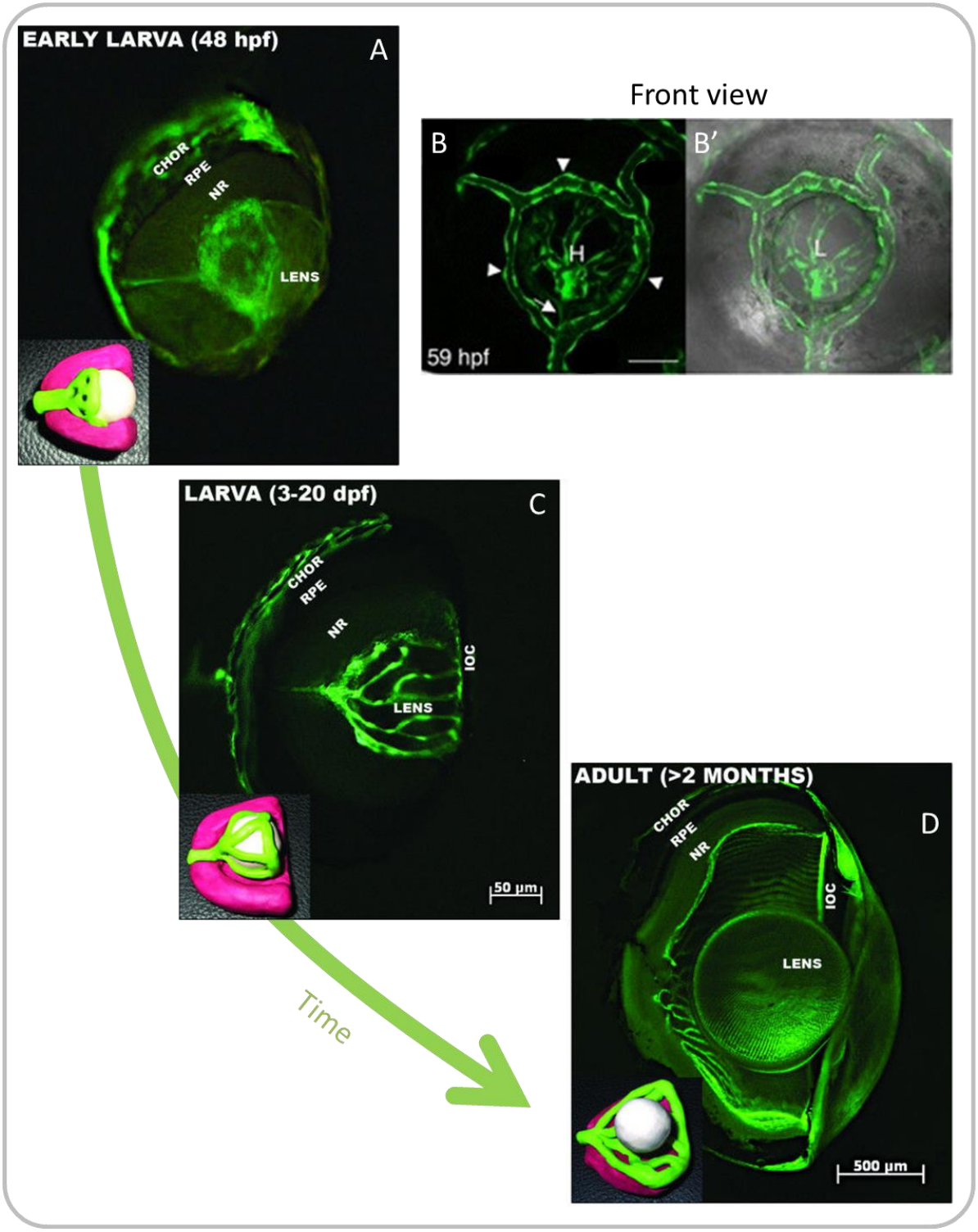

Figure 9 : Hyaloid to retinal vascular system transition.
Stages of retinal vasculature development in zebrafish. (C, C, D) partially dissected eyes from transgenic fish labelling the vascular system, including the hyaloid and retinal vasculature in larvae and adult. (A) Hyaloid vessels first appear attached to the back of the lens at 48 hpf and grow rapidly to reach the front of the lens at 3 dpf (C). (B-B') front views of the eye of a similar 59 hph transgenic zebrafish that llustrate of the inner optic circle (arrowheads). (D) In the adult, vessels are found associated with the inner surface of the retina. Insets are 3D models of this process where vessels have been coloured in green, retinas in pink and lens in white. CHOR: choroidal vasculature; RPE: retinal pigmented epithelium; NR: neuro-retina; IOC: inner optic circle, H hyaloid vasculature; L, lens.
Modified from (Alvarez et al. 2007; Kaufman et al. 2015)

factors (FGF), transforming growth factor-β (TGF- β), vascular endothelial growth factor (VEGF), lens epithelium-derived growth factor (LEDGF), pigment epithelium-derived factor (PEDF) …

For example PEDF, which is secreted on the photoreceptor side (apical), has a neuroprotective effect by inhibiting glutamate-induced or hypoxia-induced apoptosis, it also stabilizes the choroid endothelium by inhibiting its proliferation. VEGF is secreted on the basal side of the RPE at low concentration and prevents apoptosis in the choroid capillaries and maintains their fenestration.

The secretion of these different growth factors changes in response to damages to the retina to better protect the photoreceptors (Figure 8)(Strauss 2005).

1.7. Vascular systems of the eye

The eye is a highly oxygen-consuming tissue, indeed, the retina has an even higher rate of oxygen consumption than the brain and therefore needs an efficient vascular network (Alvarez et al. 2007). This vascular system is composed of 2 networks: the hyaloid vessels which then become the retinal system, and the choroid system. These 2 networks anastomose at the level of the inner optic circle (Figure 9).

All of these systems are believed to derive from the mesodermal part of the periocular mesenchyme.

1.7.1. Hyaloid and retinal system

The hyaloid system appears between 2.5 dpf and 5 dpf in the embryonic zebrafish. It forms a vascular hemispherical basket that surrounds the back of the lens entering the eye close to the exit point of the optic nerve : the optic fissure and then the optic disc. These vessels are formed by angiogenesis and create an arterial network attached to the lens. This network needs to connect to the venous system and does so by fusing with the superficial annular vessel also called inner optic circle which makes a ring around the rim of the retina, at the CMZ level. It connects to the optic vein that exits from the eye first ventrally and later on close to the optic nerve, at the optic disc (Figure 9)(Kaufman et al. 2015; Alvarez et al. 2007; Hartsock et al. 2014; Hashiura et al. 2017).

After 15dpf, this vascular system starts attaching rather to the retina and slowly detaches from the lens to become the retinal vasculature which is in contact with the RGC layer. This differs from the mammal case where the hyaloid network is strictly transient and regresses while the retinal vasculature forms by angiogenesis (Figure 9).

Like the hyaloid network, this retinal network still enters the eye via the optic disc before branching to form a highly ramified network that will still connect to the choroid system at the annular vessel around the CMZ.

This vascular system is wrapped by pericytes that participate in the blood-brain barrier and seem to actively deliver nutrients to the RGC through vesicle trafficking from the endothelium (Alvarez et al. 2007; Hartsock et al. 2014; Kaufman et al. 2015; Saint-Geniez & D'Amore 2004).

1.7.2. Choroid system

The choroidal system surrounds the optic cup and future retina; indeed, this vascular network develops just next to the RPE, only separated from it by Bruch's membrane. The capillaries from this system join at the rim of the optic cup, close to the lens to form the annular vessel. The choroid system allows the irrigation of the more superficial layers of the retina such as the RPE, the photoreceptor. Its endothelium is highly fenestrated, unlike the retinal system. Indeed, the blood-brain barrier is maintained by the RPE (Saint-Geniez & D'Amore 2004).

1.7.3. The sclera

The sclera is the most external envelop of the eye. This tissue is very rigid and fibrous; indeed, it is composed of various extracellular matrix proteins such as collagen and serves a protective function. It even has a cartilaginous part shaped as a ring and called the scleral ossicle. The sclera is also the attachment point of the extraocular muscles allowing the fish to move its eyes (Gestri et al. 2012). It derives from the neural crest cells (Stenkamp 2007).

1.8. The optic nerve

The optic nerve is composed of the RGC axons that run on top of the ganglionic layer before gathering and exiting through the central part of the retina in a region called the optic disc. Along with the optic nerve, the optic artery and vein that irrigate both the choroid and retinal system also exit through the optic disc. The optic nerve then crosses the midline ventrally and reaches the optic tectum.

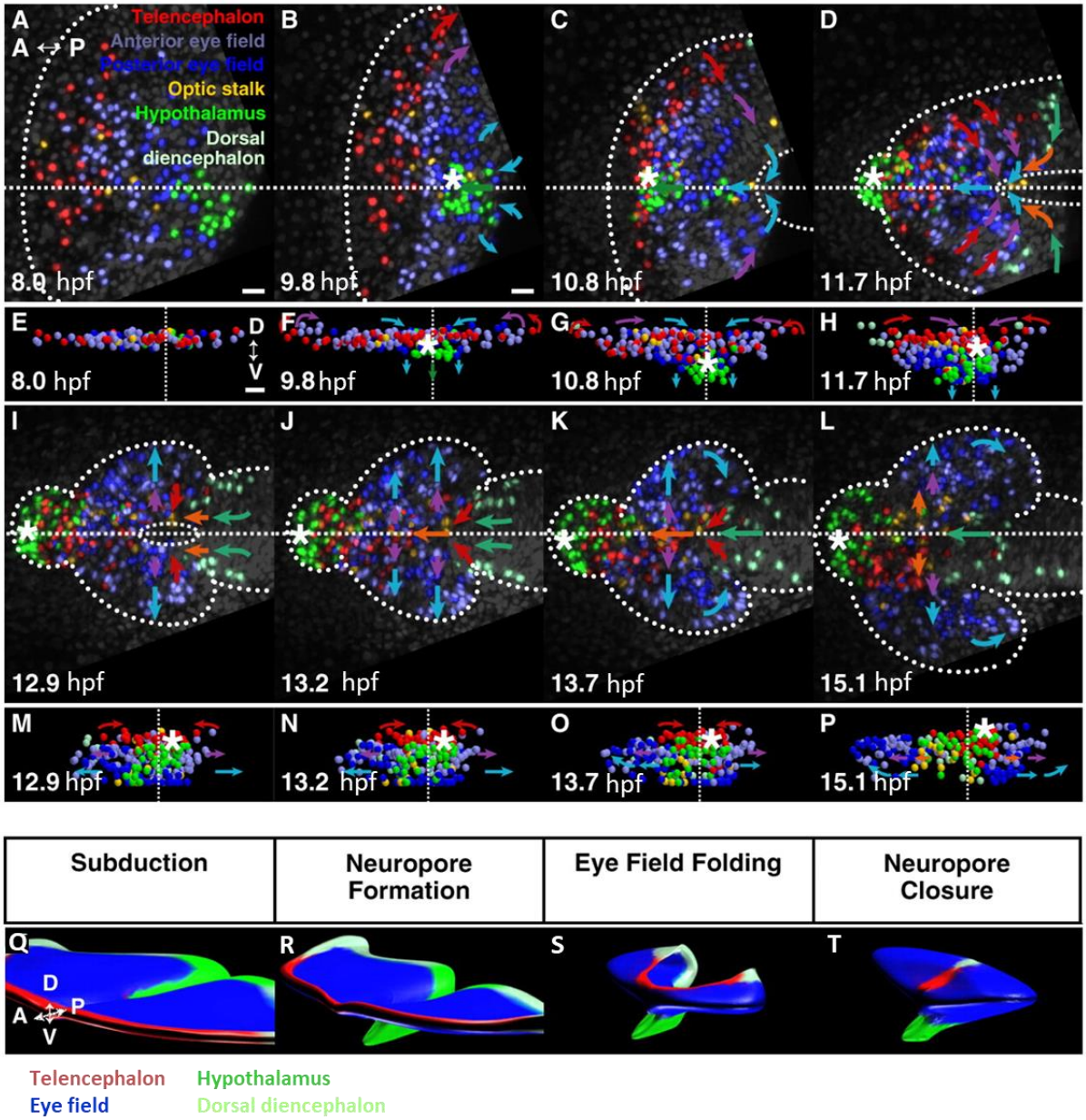

Figure 10 : Forebrain morphogenesis during neurulation.
(A-D,I-L) Projections of nuclei from a time-lapse acquisition. Dorsal projection, anterior is left. (E-H,M-P) Frontal projection, dorsal is up. (A,E) neural plate stage (midline, broken line). (B,F) Anterior neural plate contracts posteriorly towards the hypothalamic tip, where neural keel formation starts (asterisk). (C,G) Subducting hypothalamus moves anteriorly beneath the medial eye field. Convergence narrows the neural plate, which begins to fold lateral to medial, forming a neuropore (broken line). Posterior eye field moves anteriorly. (D,H) Hypothalamus emerges anterior and ventral, eye field remains contiguous across midline. (I,M) Eye evagination begins with cells moving into vesicles as diencephalon converges and moves anteriorwards. (J,N) Medial eye field continues to enter the eye vesicles. (K,O) migrating telencephalic cells meet at the midline to close the neuropore; anterior eye-field splitting is complete (arrows). Posterior optic stalk arrives beneath anterior stalk precursors. (L,P) End of evagination, beginning of elongation of the OV. Asterisks indicate anterior tip of hypothalamus. Arrows indicate the direction of movement of the cells. Time (bottom left-hand corner) in hpf. A, anterior; P, posterior. Scale bars: 25µ m.
(Q-T) Illustrated summary of the forebrain early morphogenesis. Note the folding of the telencephalon and the subduction of the hypothalamus.
From (England et al. 2006)

2. Eye development

2.1. Eye Morphogenesis

The eye morphogenesis is a sophisticated process that includes many different successive movements that radically transform this structure and its axes during development. Because of these shape and axis changes, it is quite complicated to describe eye development with the usual antero-posterior nomenclature. For that reason, I will rather use nasal-temporal references after neurulation since the olfactory epithelium keeps a rather stable localization in the eye referential. This will correspond to the final antero-posterior axis of the developed eye.

The main eye morphogenetic movements are the evagination of the optic vesicles, their elongation, the invagination of the optic cup, the anterior rotation of the eye and the optic fissure (Figure 11).

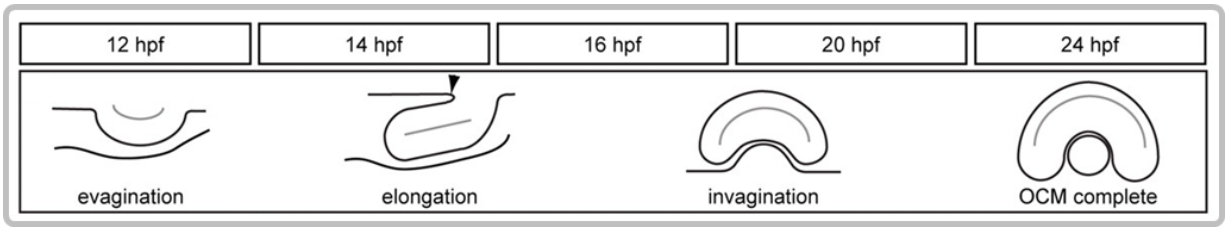

Figure 11 : the main steps of eye morphogenesis, from optic vesicles evagination to optic cup formation. Diagram of the eye morphogenesis steps, arrowhead indicates the formation of a furrow between the optic vesicle and the neural keel. Dorsal view, medial to the top, lateral to the bottom.
From (Kwan et al. 2012)

2.1.1. From neural plate to the onset of optic vesicle (OV) evagination

The whole central nervous system derives from an early structure called the neural plate which is a flat epithelium that arises during late gastrulation and is ectodermal in nature.
The anterior part of the neural plate, that will give rise to the brain, is multi-layered, from three to six cells deep. The more posterior part of the neural plate is much thinner, only one cell thick, and will give rise to the spinal cord. The neural plate is not a conventional epithelium as it doesn't show any obvious apico-basal polarity, although resting on a basal lamina (Clarke 2009).

This neuroepithelium undergoes extensive morphogenetic rearrangement to give rise to the brain - including retina- and the spinal cord. During neurulation, the posterior neural plate / future spinal cord undergoes converging movements where the neuroepithelial cells move toward the midline and divide there. During this particular division, the daughter cells acquire apico-basal polarity in a symmetrical manner, and one of them crosses the midline to be integrated on the contra-lateral side while the other one remains on the ipsi-lateral side. This type of division is termed midline-crossing division or C-division (Tawk et al. 2007).

The prospective telencephalon is composed by the lateral and rostral-most cells of the anterior neural plate (ANP). During neurulation, these cells move dorsally and posteriorly to converge towards the midline, progressively closing up the neural plate and covering the eye field, the region of the neural plate fated to become the neural retina and RPE (Figure 10) (England et al. 2006). They then form a keel where they undergo C-division and subsequently acquire apico-basal polarity at around 12 somites stage (12 ss) in zebrafish (Ivanovitch et al. 2013).

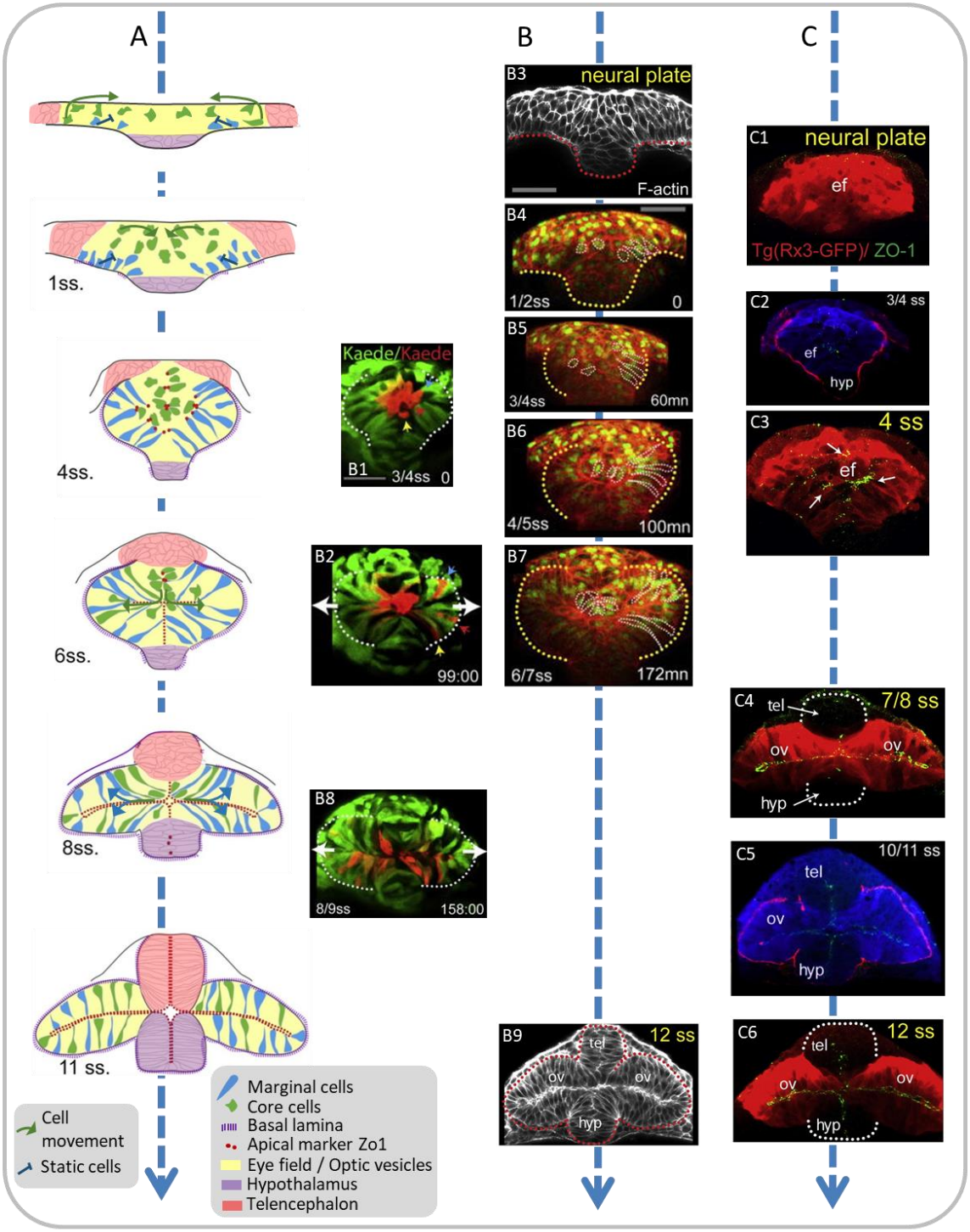

Figure 12 : Eye morphogenesis, from neural plate to optic vesicles.
(A) Summary diagram of the optic vesicle morphogenesis in frontal view. First step is hypothesized from (Rembold et al. 2006)(B) Two populations of cells : the core cells and the marginal cells compose the eye field / optic vesicle. The core cells intercalate between the epithelial marginal cells. (B4-7) Time-lapse movie of a zebrafish embryo with RFP-labelled membranes (Red) and GFP-labelled nuclei. Examples of marginal and core cells are outlined in white. (B3, B9) Zebrafish embryos with stained membranes. (B1, B2, B8) Photoconversion in red of the originally green core cells at 3/4 ss, showing the intercalation of these cells. (C) Acquisition of the apico-basal polarity in the eye field. In green, the apical marker Zo1. (C1, C3, C4, C6) Rx3:GFP transgenics, labelling of the eye field in Red. (C2, C5) The basal lamina is labelled in red. (A-C) Frontal optic sections.
Modified from (Ivanovitch et al. 2013)

The eye field is located medially in the ANP and undergoes morphogenetic movements quite distinct from the rest of the neural plate, with in particular, a reduced convergence. During these early stages, two cell populations with different behaviours have been described.

Indeed, Rembold et al. showed in medaka fish that ventromedial cells of the very early (late gastrula stage, st 16) eye field do not exhibit any convergence. These cells maintain the eye field wide throughout neurulation and may correspond to the "marginal cells" described at slightly later stages in zebrafish (onset of neurulation, 3 ss) by Ivanovitch et al. At this point, these cells are located at the ventral margin of the eye field. They start to elongate radially and progressively acquire apico-basal polarity and start coordinating length with their neighbours. Marginal cells are attached to the basal surface of the eye field and, as they divide, their nucleus moves apically and the daughter cells are integrated into the marginal layer (Figure 12A,B) (Rembold et al. 2006; Ivanovitch et al. 2013; Martinez-Morales et al. 2017).

The other cell population identified by Rembold et al. are located laterally in the very precocious eye field. By contrast to the marginal cells, they move posteriorly and converge medially, along with the telencephalic cells (England et al. 2006; Rembold et al. 2006). Upon reaching the midline, they dive ventrally before migrating laterally again and into the early evaginating optic vesicles (OV). During these processes, they adopt various shapes and extend filopodia and lamellipodia.
This population may correspond to the "core cells" described at slightly later stages by Ivanovitch et al. in zebrafish. Indeed, they describe a population of round cells, with mesenchymal morphology, located in the middle of the eye field during early neurulation (4-5 ss), which could fit the position and morphology of these previous diving cells. Despite not having any contact with the basal lamina at this point, the core cells are able to coordinate polarization with their neighbours, marginal or core cells. They then progressively intercalate between the marginal cells throughout OV evagination. During this process, they keep their apical domain bound to the midline while extending their cell body and sending basal processes between the marginal cells to reach the basal lamina. They then integrate in between marginal cells and become indistinguishable from them. As they keep intercalating randomly during the OV evagination, the first core cells to integrate the OV are more likely to end up in the most distal parts of the OV, being passively moved by the evagination process while the latest ones will remain more medial (Rembold et al. 2006; Ivanovitch et al. 2013; Martinez-Morales et al. 2005).
None of the eye cell population undergoes C-division : each side of the neural plate only contribute to the ipsi-lateral OV. This also means that the apico-basal polarity is established via other mechanisms. The apico-basal polarity is actually established much earlier in the OV, starting around 4 ss and being clearly established by 7-8 ss, than in the neighbouring brain tissues (Figure 12A,B) (Ivanovitch et al. 2013).

More posteriorly in the neural plate, behind the eye field, lies the prospective hypothalamus. During neurulation, this structure quickly compacts, dives ventrally and start moving anteriorly beneath the eye field until emerging anterior and ventral to the telencephalon. This movement is called the hypothalamus subduction (Figure 10)(England et al. 2006). Hypothalamic cells undergo C-divisions and subsequently acquire apico-basal polarity at around 12ss (Ivanovitch et al. 2013).

The establishment of apico-basal polarity in the developing brain is essential and allows for the formation of the different ventricles and recesses of the prosencephalon. In particular, the third ventricle that crosses the neural tube in an antero-posterior and dorso-ventral fashion is formed, along with the optic recess that crosses orthogonally to the third ventricle and both eyes (Figure 12A, C) (Ivanovitch et al. 2013).

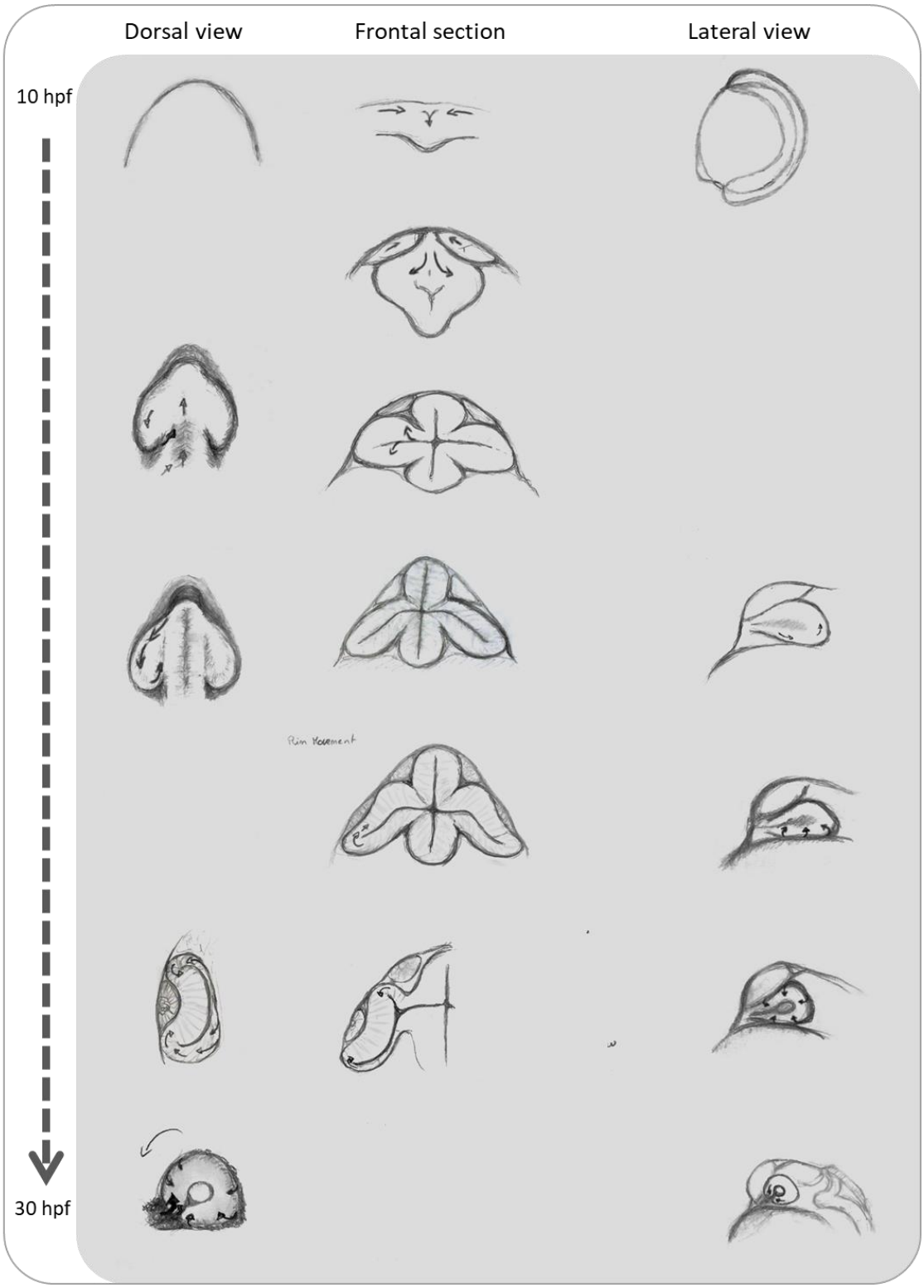

Figure 13 : different views of eye morphogenesis.
Schematic representation of the different morphogenetic movements occurring during eye development. On the left, dorsal views at neural plate stage, early optic vesicle, late optic vesicle, early optic cup (anterior to the top) and lateral view of the optic cup around 30 hpf (bottom). In the middle; frontal sections through the developing neural plate/ optic vesicle/cup. On the right, lateral views of the corresponding stages. Left and middle drawings are from the literature data on medaka fish and zebrafish, the right drawing represent Astyanax matching stages. Arrows describe the morphogenetic movements happening at each stage.

2.1.2. Optic vesicle evagination and elongation

The process of optic vesicle evagination starts with the mechanisms described above, keeping the eye field wide and starting a lateral movement which results in the formation of a pouch. The subduction of the hypothalamus pulls the posterior eye field cells ventrally and anteriorly which results in an initial folding of the posterior eye field (England et al. 2006).

The general posterior to anterior movement of the posterior ANP contributes to the optic vesicle elongation. Indeed, the dorsal diencephalon -that is originally posterior and lateral to the hypothalamus- converges and moves forward towards the telencephalon, therefore displacing the posterior eye cells forward and pushing them out into the forming optic vesicle. This also results in the separation of the posterior OV from the neural keel, creating a furrow that progresses anteriorly to leave only a stalk connecting the OC to the forming brain (Figure 10, Figure 11)(England et al. 2006; Kwan et al. 2012). Cells enter the optic vesicle mostly in its anterior part. They keep evaginating and entering the OV through the optic stalk until 14 ss in the zebrafish, contributing mostly to the nasal retina after 6 ss (Kwan et al. 2012). The more medial cells that will not have evaginated to contribute to the eye or the optic stalk will become optic recess region (ORR) which is a brain region, organized around the optic recess and conserved through development and adulthood (Affaticati et al. 2015).

The OV elongation has been described as a movement where the whole OV undergoes a "pinwheel movement". This is a morphogenetic movement where the anterior-most cells –the ones that entered the OV last- move laterally and posteriorly in the OV. The cells that occupy a more posterior position –which will give rise to the RPE- move around the optic recess and toward a more anterior and medial position (Figure 13). This is a quite rapid movement that spans from 6 ss to 10 ss in zebrafish (Kwan et al. 2012).

2.1.3. Optic cup invagination

As elongation progresses, the OV and the optic recess bend toward the yolk. The most ventral part of the OV becomes more medial due to that movement and starts to thin down, while the previous dorsal part becomes rather lateral, facing the presumptive lens ectoderm. The OV then starts to invaginate to give rise to the optic cup (OC).

This morphogenetic movement is crucial as it allows for the correct positioning of the main different eye tissues with an inner / lateral / lens-facing neural retina and an outer / medial RPE surrounding it.

This invagination is initiated by a basal constriction of the lens-facing epithelium before being continued by the "rim movement" that starts between 15 ss and 18 ss and lasts until 24hpf (Kwan et al. 2012; Picker et al. 2009; Heermann et al. 2015; Nicolás-Pérez et al. 2016).

This movement starts by seemingly reversing the cell flow that was proceeding during OV elongation. Indeed, the posterior cells of the eye that had a lateral to medial movement now adopt a medial to lateral flow around the optic recess at the rim of the optic vesicle.

A similar movement, where cells move around the edge of the OV and toward the lens-facing epithelium, is observable throughout almost the whole OV, especially in the ventral parts and including at the nasal and temporal edges between the OS and the OV, resulting in the formation of the optic fissure (OF). This movement is quite similar to the gastrulation process and will ultimately result in a hemispherical eyeball (Kwan et al. 2012; Heermann et al. 2015). The small part of the outer OC in the prospective dorsal position of the eye, which does not undergo such movement, exhibits a quite different behaviour as it is fated to become the RPE. Indeed, this originally small region of the posterior/distal OV has enlarged during OV elongation through recruitment of new cells acquiring RPE identity and has started to move slowly towards more proximal/prospective ventral regions. During OC invagination, this domain exhibits rapid

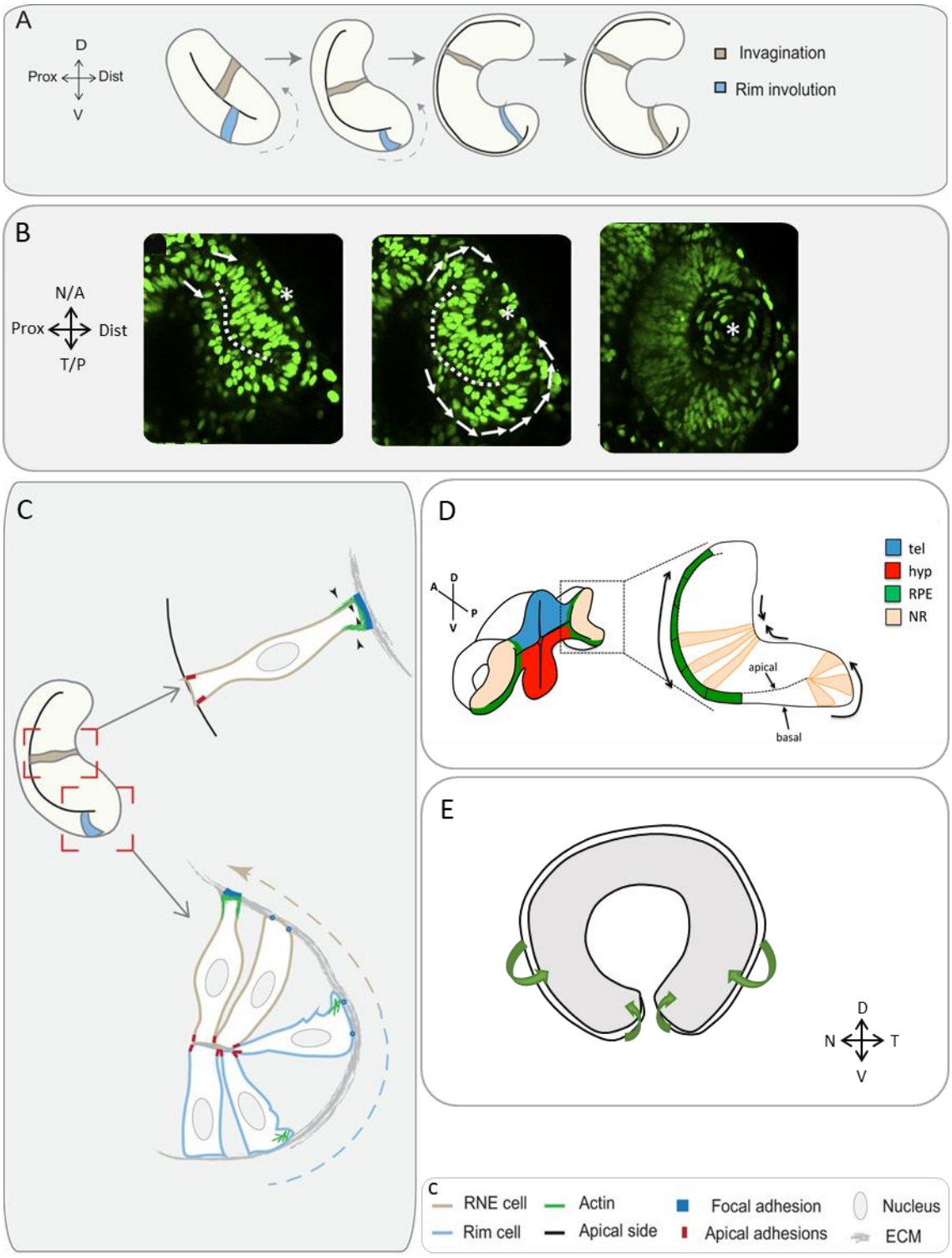

Figure 14 : Optic cup invagination and rim movement.
(A) Diagram of the optic cup invagination in time. Cells from the outer optic cup flow and migrate around the rim. Dotted arrows represent the cell migration. (B) Dorsal view of the optic cup invagination from 16.5hpf, optical sections of a live embryo. Dotted line represents the optic recess; arrows show the flow of cells migrating around the rim; asterisk, lens. (C,c) Schematic representation of the different mechanisms leading to the optic cup invagination. The invagination is driven by basal contraction; rim involution is driven by collective, active migration of the epithelium at the rim of the developing optic cup. Cells display protrusions. (D) Diagram of the optic cup invagination, note the expansion of the RPE. (E) The RPE comes to engulf the neural retina.
From (Cavodeassi 2018; Sidhaye & Norden 2017; Heermann et al. 2015)

movements within the outer OC, towards the prospective temporal and nasal domains and in a lesser extent towards the prospective dorsal domain (from which it is originally closer); these movements slow down upon approaching the rim of the OC where they stop. During this period, RPE cells flatten and enlarge to ultimately occupy the whole outer OC layer, surrounding the neural retina until contacting the lens (Figure 14)(Heermann et al. 2015; Cechmanek & McFarlane 2017).

The rim movement is led by an active and collective migration of the cells coming from the medial / outer OV/OC. Upon reaching the edge of the OV/OC, these neuroepithelial cells acquire some characteristics of a rather mesenchymal nature, displaying at the same time apico-basal polarity and cell-cell adhesion –that are typical features of an epithelium- but also lamellipodia and dynamic cell-matrix contacts that are more associated to a mesenchymal state. They possess a very stable, anchored apical domain with adherens junctions, this domain constricts when cells reach the rim. On the other hand, they display a highly dynamic basal side, where protrusions expand in the direction of the movement only and create dynamic focal adhesions, leading to the assumption that they generate a pulling force driving this rim migration (Sidhaye & Norden 2017). The mesenchymal features of these cells are essential for their migration since disruption of the extracellular matrix (ECM) – cell adhesion leads to defects of the OC due to a delayed migration, but the epithelial features are also important. Indeed, cells with perturbed ECM attachment that are transplanted in a WT OC are able to follow the rim movement, probably pulled by their neighbours through cell-cell adhesions, highlighting the collective aspect of this movement (Figure 14).

Once reaching the lens-facing, lateral / inner OC layer, cells shift back to a more canonical epithelial state, with stable basal ECM adhesion and no protrusion. They then undergo a basal constriction around 20-22 ss, followed by an apical expansion around 22-24 ss. These two modifications of cell shape participate in the bending of the OC (Nicolás-Pérez et al. 2016; Martinez-Morales & Wittbrodt 2009).
Another factor contributing to this bending may be cell divisions as the inhibition of proliferation results in a slightly more open OC. This highlights a small role for neural retina proliferation in the OC curvature, probably due to physical compaction of the increasing number of cells in the lens-facing epithelium (Figure 14)(Sidhaye & Norden 2017).

The correct completion of the invagination is paramount since the retinal cells are already specified by this stage and a delay in this movement will result in ectopic retinal cells in place of the RPE. The last cells to go around the rim will give rise to the ciliary marginal zone (CMZ), the stem cell niche of the retina.

2.1.4. Anterior rotation

From 6 ss to 24hpf, the whole developing eye rotates in a counter clock-wise manner from a left lateral view so that the optic stalk and the choroid fissure come to a ventral position. Concomitantly, the forebrain also undergoes a similar rotation so that the telencephalon, that originally lies dorsally, adopts a rostral position and the Optic Recess that is originally almost parallel to the yolk surface, ends up almost perpendicular to it (Figure 15)(Kwan et al. 2012).

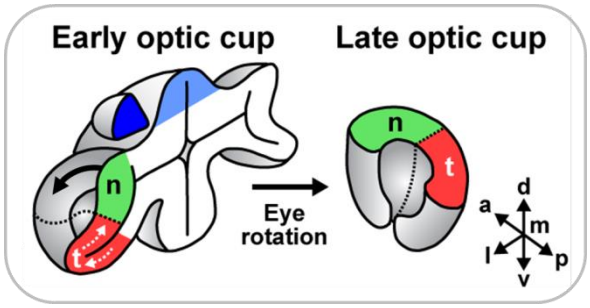

Figure 15 : Eye rotation. From (Picker et al. 2009)

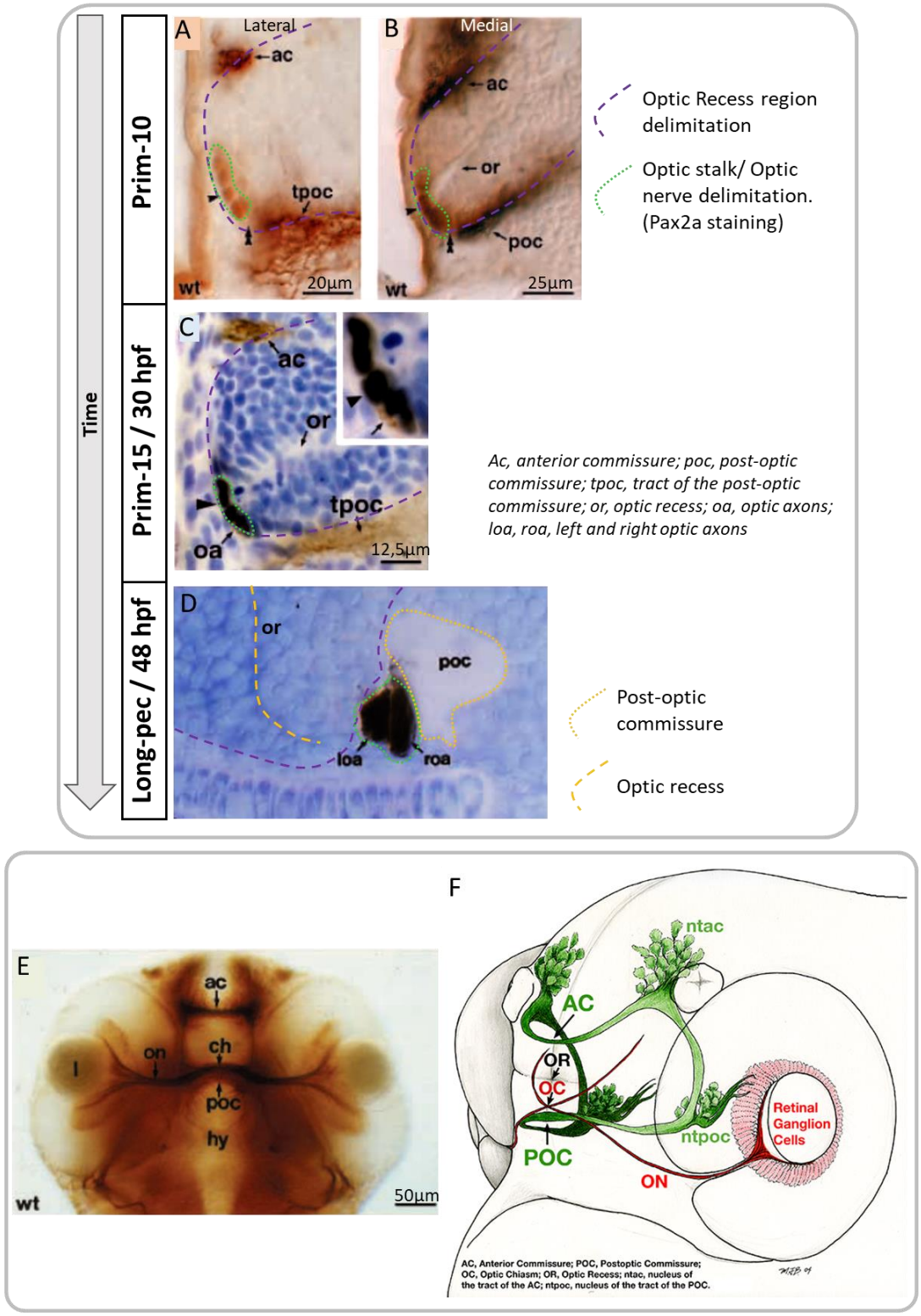

Figure 16 : The optic stalk and the Optic Recess region.
(A-D) The optic stalk (OS) position throughout development. Immuno-labelling of the optic stalk marker Pax2a and of the axons in A,B,C by acetylated-tubulin, parasagittal sections. Arrowheads indicate the OS cells. Note the first axons coming beneath the OS cells in (C, inset). (D) Optic chiasma, the two axon bundles (left and right) are just in front of the POC. (E) Axonal labelling on a 48 hpf embryo, note the position of the optic nerves and optic chiasma, just next to the POC. Ventral view. (F) Diagram of the tracts of the forming forebrain. On, optic nerve; oc, ch, optic chiasma; ntac, neural tract of the anterior commissure; hy, hypothalamus.
From (Macdonald et al. 1997), drawing from Barresi lab.

2.1.5. Eye cells differentiation

Once morphogenesis is achieved, around 24hpf, retinal cells start differentiating in waves : first the RGC, then cells from the inner nuclear layer : amacrine, bipolar and horizontal cells, then cone photoreceptors, rod photoreceptors and finally Müller glia.

Moreover, differentiation does not occur simultaneously throughout the whole retina. In zebrafish, neurogenesis starts ventrally, close to the optic stalk and proceeds in a fan-shape manner: it continues nasally, then dorsally and finally temporally (Stenkamp 2007; Stenkamp 2015).

2.1.6. Optic stalk, optic nerve.

When RGCs start differentiating around 24-28hpf, they project their axons through the optic stalk. The optic stalk is a transient *Pax2a*-expressing structure that connects the developing eye to the brain. It serves as a scaffold that is invaded by the retinal axons which will form the optic nerve. The first RGC axons exit the retina around 30hpf via the optic fissure and follow the optic stalk. As development proceeds, the originally very ventral optic nerve gathers the RGC axons in a tight bundle and moves towards the centre of the retina, at the level of the lens, where the final exit point of the RGC axons, the optic disk, will remain. The optic nerve trajectory dives ventrally to cross the whole brain ventrally and slightly anterior to the post-optic commissure (POC); there, the two optic nerves cross, forming the optic chiasma around 34-36 hpf. They then navigate towards the optic tectum on the contra-lateral side around 48hpf (Figure 16) (Masai et al. 2003; Macdonald et al. 1997; Poulain et al. 2010). The optic stalk cells prevent the RGC axons from mixing with the adjacent POC axons or with the other contralateral optic nerve. These stalk cells will ultimately become glial cells : reticular astrocytes that will remain in the optic nerve (Macdonald et al. 1997).

In most fishes, RGC project strictly to the contra-lateral tectum. The tectal regions where the RGC axons connect are dependent on their position of origin in the eye. Indeed, these connections are retinotopic which means that the positional information is conserved in the tectum, with neighbouring cells in the eye projecting to neighbouring cells in the tectum (Sperry 1963; Retaux & Harris 1996). For example, the nasal RGC will project to the posterior tectum while temporal RGC will project to the anterior tectum.

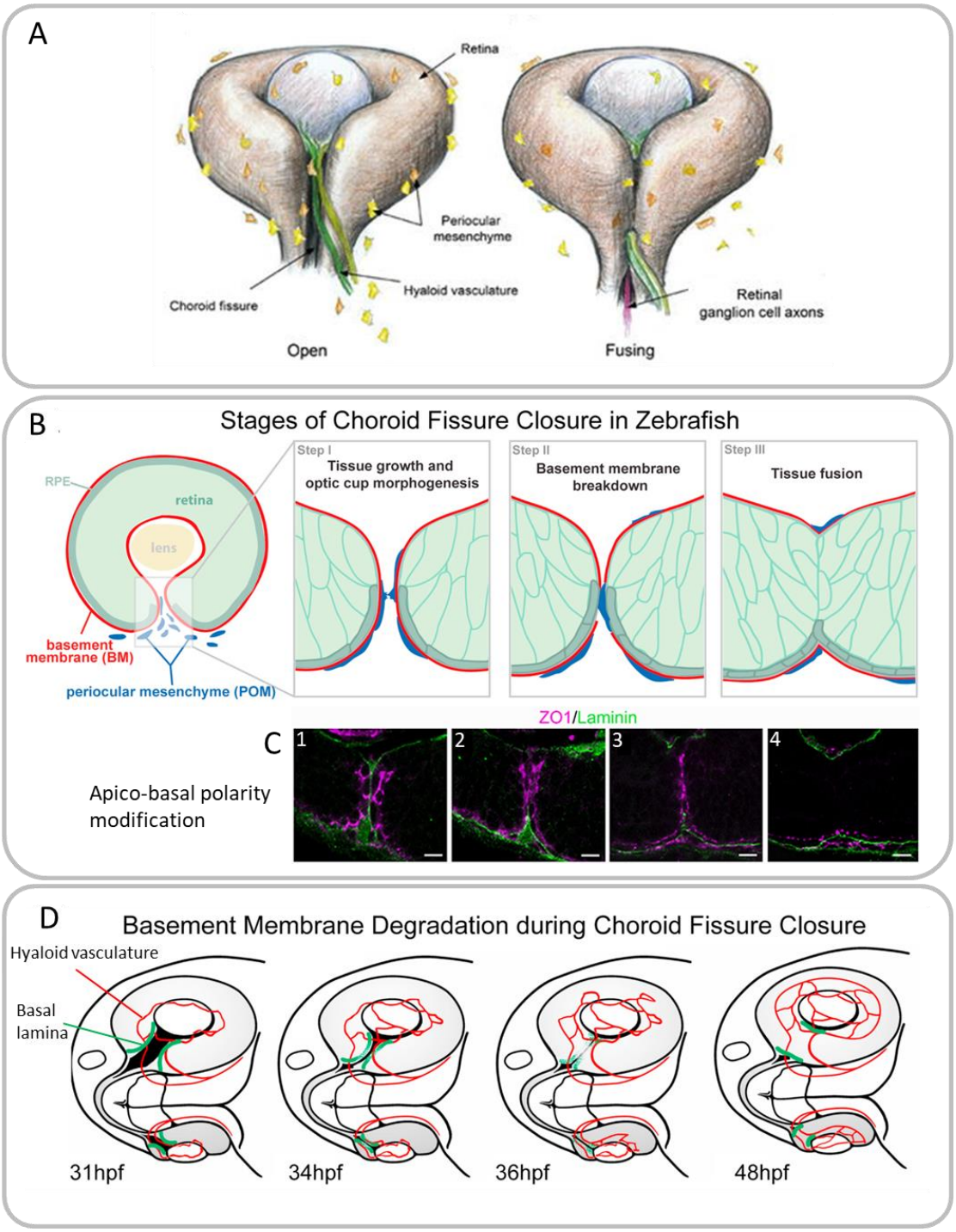

Figure 17 : Optic fissure closure.
(A) Schematics of the forming eye (ventral view) showing the ventrally positioned choroid fissure before and during closure (drawing by Clarissa Scholes). (B) Stages of the choroid fissure closure, (I) the two margins of the optic fissure come in contact; (II) the basal membrane breaks down and the apical side of the margin cells come in contact. (III) The tissue of the two margins fuse. (C) Cell polarity during optic fissure closure. ZO1 labels the apical side of the cells, Laminin labels the basal lamina. (C1) The two margins are juxtaposed at the basal membrane. (C2) The basal membrane breaks down and the apical sides come in contact. (C3) The apical sides of the margin cells are in contact. (C4) The tissue has fused; no apico-basal maker is seen at this level except close to the RPE, around the optic recess. (D) Diagram of the dynamics of choroid fissure closure, note the initial fusion starts halfway in the OF and the zipper-like bidirectional progression of the basal membrane breakdown and tissue fusion. Tilted ventral view.
From (Gestri et al. 2012; Gestri et al. 2018; James et al. 2016)

2.1.7. The optic fissure and its resolution

The optic fissure, also called choroid fissure or ventral fissure, which is created at the edge between the optic stalk and the optic cup during OC evagination, serves as an entry point for cells of the periocular mesenchyme (POM) that come to vascularize the eye. These cells give rise to the hyaloid vessels which form a basket-shaped network of blood vessels behind the lens. After this invasion, the optic fissure (OF) will close around the hyaloid vein and artery, leaving a rounded-shaped eye (Figure 17) (Hartsock et al. 2014; James et al. 2016).

The optic fissure is fully closed at 3 days post fertilization (dpf) in zebrafish. Failure to close the optic fissure is called a coloboma (from the greek, *koloboma*, mutilated) and, depending on the severity of the phenotype, can be a cause for blindness. A coloboma is a phenotype that can result from a wide variety of developmental alterations, from abnormal dorso-ventral specification to rim movement defects and problems in angiogenesis (Heermann et al. 2015; Weiss et al. 2012).

The epithelial cells lining the OF display a particular, cuboidal shape that is different from both the columnar morphology of the neural retina and the flat squamous shape of the RPE cells, evidencing a special identity of these OF lips cells (Gestri et al. 2018).

The mechanisms leading to the correct closure of the OF are just starting to be understood. One of the early steps seems to be the break-down of the basal membrane of the optic cup at the site of the OF. This degradation of the basal membrane starts around 34hpf in the centro-proximal OF and then proceeds bi-directionally towards more proximal and more distal regions. The basal lamina has disappeared at 48 hpf in most embryos apart in the distal-most OF; and is completely gone in all zebrafish embryos by 60 hpf. This degradation of the basal lamina is accompanied by the retraction of basal polarity markers and apposition of apical markers at the point of fusion. After that step, the OF starts closing and fusing by establishing adherens junctions in its centro-proximal domain around 44 hpf. The fusion is followed by a retraction of the apical markers such as Zo-1 that come to be only apparent close to the outer border of the eye, around the position of the optic recess that separates the RPE from the neural retina. This probably reflects the correct fusion or the nasal and temporal RPE layers and neural retina layers. The bi-directional fusion continues with adherens junctions visible at 47 hpf in the central and proximal domains and at 49hpf in the centro-distal region. The most distal part of the OF closes last, as late as 72 hpf (Figure 17)(James et al. 2016; Gestri et al. 2018).

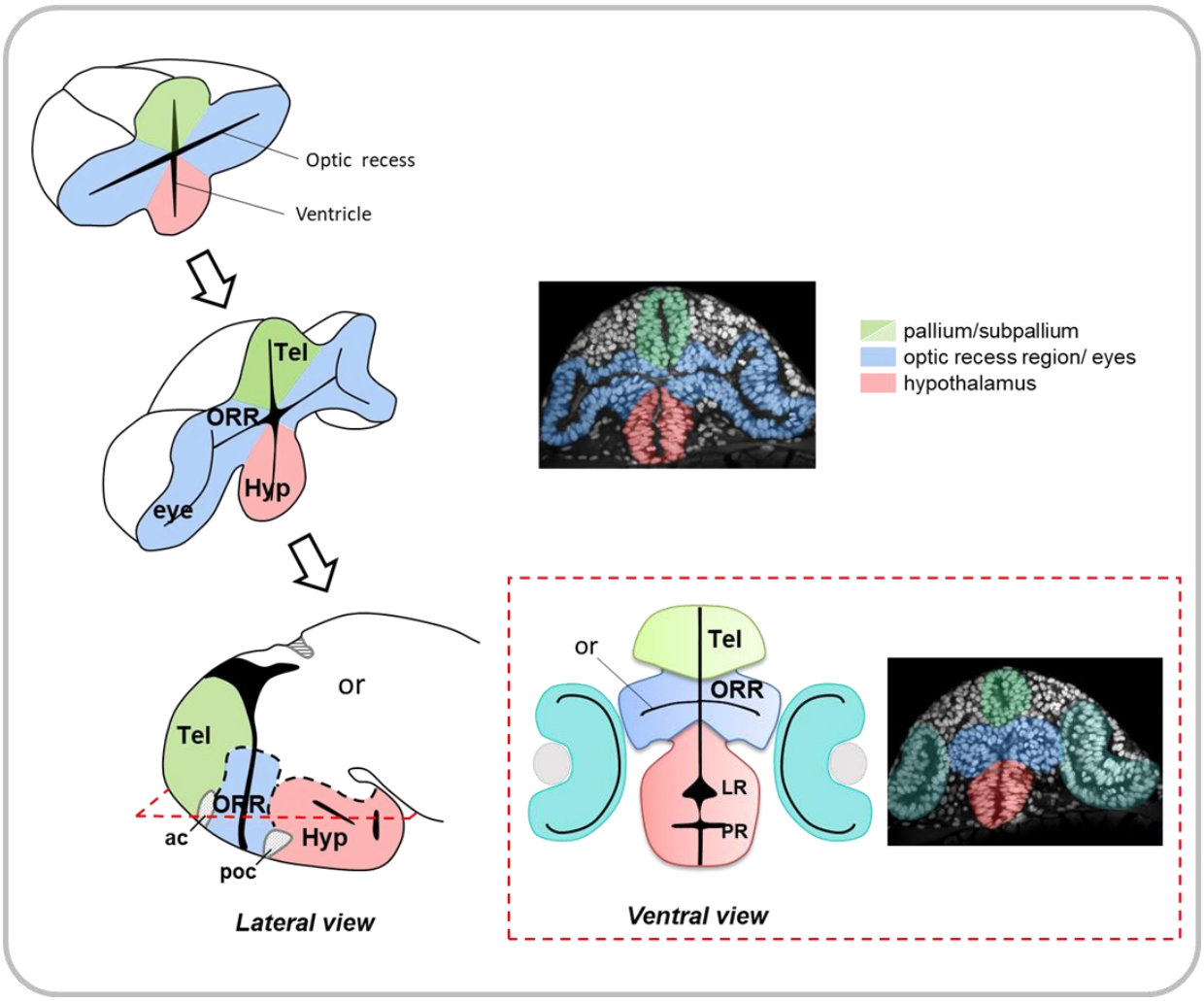

Figure 18 : Optic Recess Region.
The optic recess region (ORR) derives from the medial part of the optic vesicles. Diagram of the ORR morphogenesis and optical sections of the forebrain. Top picture is a frontal section, bottom picture is a horizontal section at the level indicated by the red dotted line.
Modified from (Yamamoto et al. 2017; Picker et al. 2009)

2.1.8. The optic Recess and Optic Recess Region

During eye morphogenesis, the optic recess closes up and stops being visible. The optic recess stands between the RPE and the neural retina so its disappearance could be due to the close interactions between the photoreceptors outer segment and the RPE cells microvilli, the latest surrounding the first. The recess would therefore no longer be visible as an empty space.

On the contrary, in more medial regions such as the optic recess region (ORR), cells on each side of the recess do not exhibit such interactions and the recess stays visible until adulthood but is no longer connected to the eye. Indeed, the optic recess region loses its connection to the retina via the optic stalk and becomes a differentiated brain region which is delimitated by two commissures or axonal tracks. The anterior commissure defines the dorsal border of the ORR with the telencephalon; while the post-optic commissure separates it ventrally from the hypothalamus (Figure 18)(Affaticati et al. 2015; Yamamoto et al. 2017).

The ORR limits have been defined by these two commissures. The neurogenesis pattern being centrifugal, progenitors line the optic recess and differentiated neurons stand close to the commissures and above them (Affaticati et al. 2015).

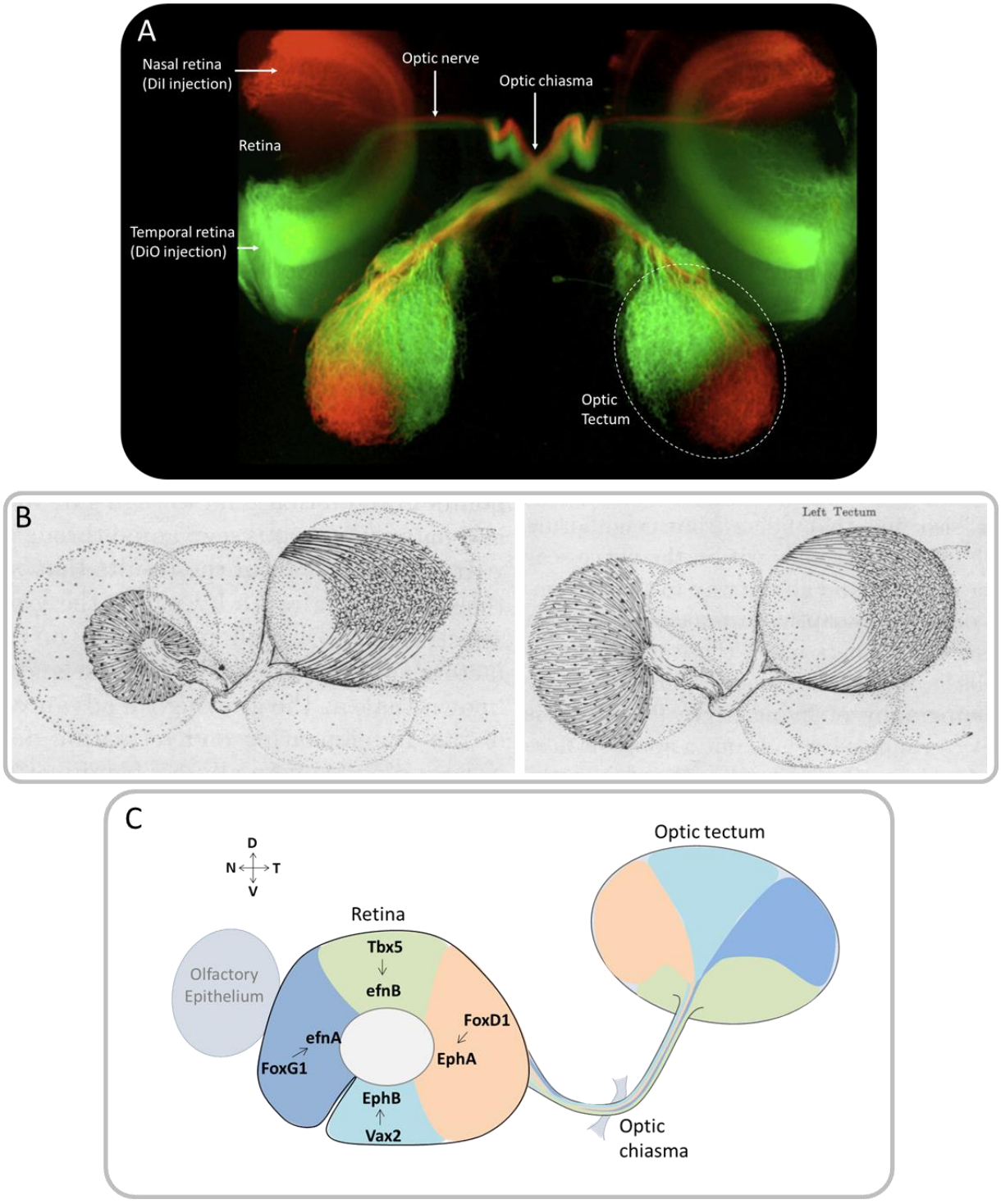

Figure 19 : retinotopic mapping of the optic tectum.
Injection of lipophilic dyes (DiI, DiO) into the nasal and temporal quadrants of the retina allows tracing the retinal projections to the tectum. Note the mirror inversion of the retinal mapping in the tectum. (B) Original drawings from Sperry showing the retinotopic mapping of the tectum observed from regeneration experiments. (C) Diagram of the Retina, showing the transcription factors expressed on the different quadrants and the type of Ephrin or Eph Receptor they induce.
Picture from Chi-Bin Chien, drawings from (Sperry 1963).

2.2. Eye regionalization

2.2.1. Role and significance

As previously mentioned, the retinal ganglion cells project to the tectum in a topographic manner, with some kind of symmetry in all directions : axons from the nasal retina project to the posterior tectum while those from the temporal retina reach the anterior tectum and RGCs from the ventral retina project to the medial tectum while those of the dorsal retina target the lateral tectum. This inversion is actually already present to some extent at the level of the optic nerve, where dorsal axons run through the ventral part of the tract, and ventral axon through the dorsal part of the nerve (Figure 19)(Poulain et al. 2010; Sperry 1963).

Such an organization implies a regionalization of both the retina and the tectum, allowing for a correct addressing of RGC axons. Indeed, many genes have a regionalized expression in the retina as in the tectum such as Eph Receptors (eph) and Ephrin ligands (efn).

These molecules are involved in cell-cell interactions and usually function in the establishment of boundaries between regions with different identities but are also involved in axon guidance. Indeed, Ephs and Ephrins are membrane-bound proteins that can both transduce signal upon binding with each other. These interactions are often repulsive but can also be attractive, thus creating compartments and boundaries. Ephs and ephrins can each be divided in two classes : EphA / EphB and ephrinA / ephrinB respectively. Eph receptors of one class bind preferentially to the corresponding class of ephrins.

In vertebrates, misexpression of *Ephrins* in the retina or tectum lead to errors in the retinotopic mapping of the tectum. These molecules are therefore important for a proper topography establishment (Brennan et al. 1997; Kita et al. 2015).

In the retina, different quadrants can be described with these genes expression : in zebrafish, the ventral quadrant expresses two Eph B receptors : *ephB2* and the more restricted *ephb3a*, while the dorsal quadrant expresses an Ephrin B ligand : *efnB2a*. Similarly, the temporal quadrant expresses an Eph A receptor : *ephA4b* while the nasal quadrant expresses an Ephrin A ligand : *efna5a* (Gosse & Baier 2009; French et al. 2009; Holly et al. 2014; Picker & Brand 2005). Therefore, the A subtype of Eph/ephrins seems to handle the temporo-nasal identity while the B subtype seems to account for the dorso-ventral identity of the retina (Figure 19C).

***On a side note**: fishes are continuously-growing organisms for most of them, which means that their eyes and optic tectum also continue to grow, even after the initial retinotectal map is established. New cells are added to the entire circumference of the retina from the CMZ and to the caudal rim of the tectum by its own stem cell niche : the Tectal Marginal Zone (TMZ). These two stem cells niches do not match in term of retinotopy, which means that the newly formed RGCs cannot target directly the newly born tectal neurons without disturbing the retinotopic map. In order to preserve it, all RGC axonal terminations are constantly shifting on the tectum to maintain an undistorted map* (Simpson et al. 2013; Becker et al. 2000).

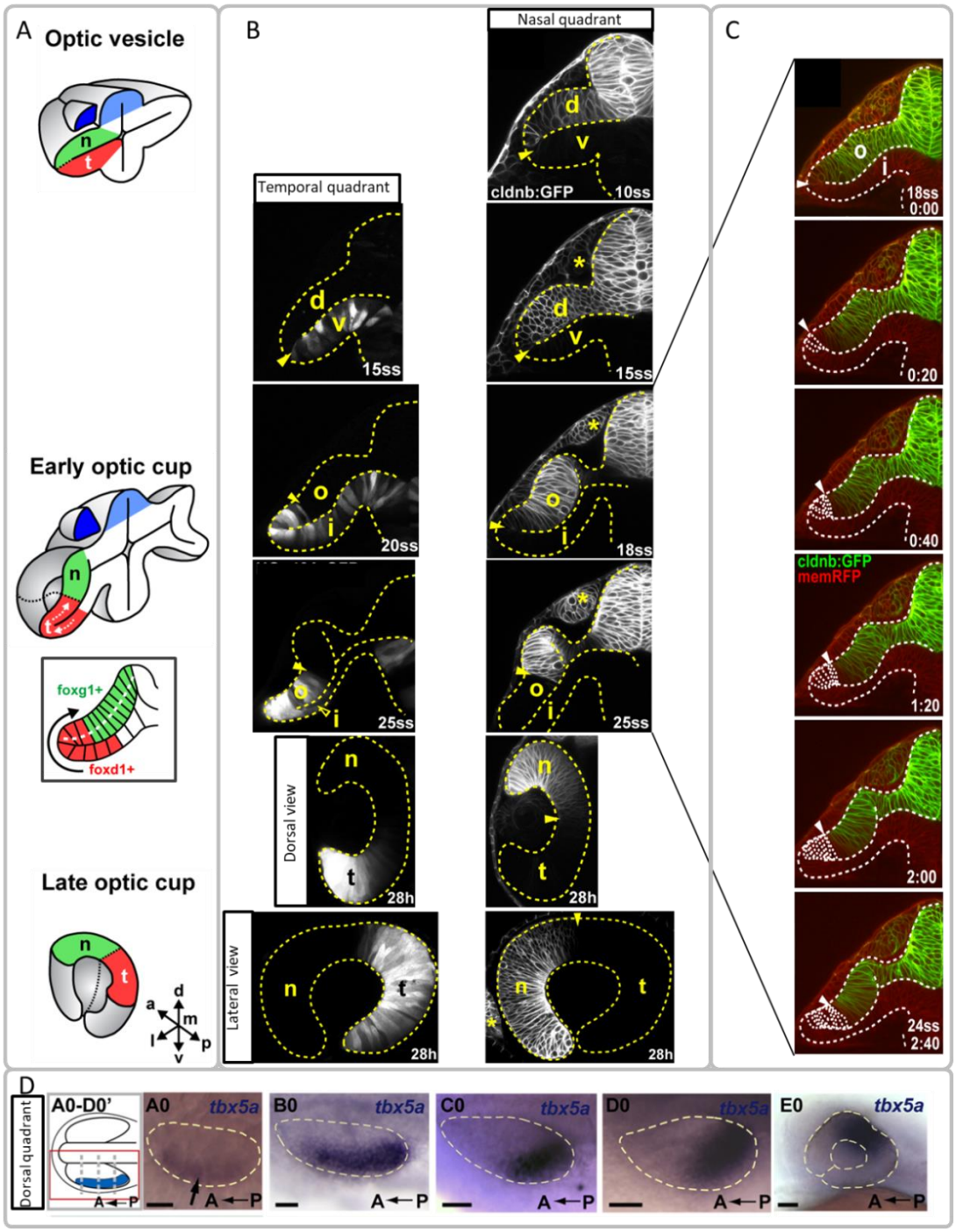

Figure 20 : Origin of the eye quadrants.
(A) Diagram of the eye development and the movement of the different quadrants over time. Nasal quadrant is in green, temporal quadrant is in red. Olfactory epithelium is in dark blue. The inset shows the movement of the cells during optic cup morphogenesis, bringing the temporal cells in the lens-facing epithelium. Then the anterior rotation brings the quadrants in their final position. (B) Time-lapse imaging of the temporal (on the left) and nasal (on the right) quadrant development, using zebrafish transgenic lines *HGn42A* enhancer-trap (downstream of FoxD1) and *Tg(-8.0cldnb:lynGFP)zf106.* Note the progressive ventral-wards bending of the OV before the optic cup invagination starts. (C) Details of the progression of the temporal cells into the lens-facing epithelium. White dotted lines show the migrating cells, arrowheads show the progressive displacement of the two presumptive quadrants.(B, C) Frontal view when not specified otherwise. (D) The origin of the dorsal (distal) quadrant. Dorsal views from 12 to 18 hpf, lateral view at 24 hpf.
From (Kruse-Bend et al. 2012; Picker et al. 2009)

2.2.2. Molecular mechanisms

Transcription factors

Ephs and Ephrins are under the control of different transcription factors that are also regionalized in the retina.

Indeed, *Vax2*, which is expressed in the ORR, optic stalk and ventral retina has been shown in mice and chicks to regulate positively the expression of *EphB3* and *EphB2* and negatively that of *efnB2* (Schulte et al. 1999). Reciprocally, *Tbx5* is expressed in the dorsal retina and promotes the expression of *efnB2a* while reducing that of *EphB2* in zebrafish (French et al. 2009).

Concerning the naso-temporal axis, studies in chicks have shown that *FoxG1* is expressed in the nasal retina and induces *EphrinA5*, while *FoxD1* is expressed in the temporal retina where it promotes *EphA3* and represses *EphrinA5* expression (Sakuta et al. 2006). *FoxG1* and *FoxD1* expressions are mutually exclusive due to reciprocal repression, as shown in the zebrafish and chick retina (Hernández-Bejarano et al. 2015; Takahashi et al. 2009).

All of the above-mentioned transcription factors have been evidenced as necessary to achieve correct retinotopic mapping of the tectum in various species (Schulte et al. 1999; Barbieri et al. 2002; Yuasa et al. 1996; Koshiba-Takeuchi et al. 2000). The control of their expression is under the influence of morphogens from various signalling centres around the eye during all stages of eye development; this will be discussed later on.

Origin of the eye quadrants

The different quadrants of the eye are specified quite early in development, as evidenced by the expression of *Tbx5a*, already detectable at 6 ss; and the expression of *FoxG1*, *FoxD1* and *Vax2* which are present at 10 ss in zebrafish embryos (French et al. 2009; Picker et al. 2009). By the optic vesicle stage, the regionalisation has already taken place or is still occurring; we can therefore observe their origins, which is what was done by Picker et al. for the temporal and nasal regions.

The nasal retina originates from the dorsal leaflet of the optic vesicle which becomes the lens-facing epithelium while the temporal retina is first visible as the ventral leaflet of the optic vesicle. After the ventral-wards bending of the OV, the temporal retina stands in the medial OV/outer OC which is the final position of the RPE while the nasal retina is already in the lens-facing epithelium, where the neural retina will stand. A massive rearrangement must then occur to allow the temporal retina to reach a lens-facing position. This is achieved by the rim movement from 15-18 ss to 25 ss which leads the temporal retina to migrate around the ventral rim of the OV and seemingly “push” the nasal retina so that they each stand in the lens facing epithelium, but in complementary regions along the naso-temporal axis (Figure 20A-C)(Picker et al. 2009).

The final dorsal quadrant of the retina originates from the lateral part of the dorsal leaflet of the OV at 6 ss. It then moves posteriorly in the OV and upwards in its caudal-most part, curling up at the distal margin of the OV at 10 ss. This upwards movement towards the nasal part of the OV continues, together with the acquisition of a more medial position in the OV dorsal leaflet at 12 ss. This movement is associated with a compaction of the *Tbx5* domain. At 18 ss, during optic cup invagination, the *Tbx5*-positive domain is located in the middle of the lens-facing epithelium at the level of the lens but has a much more medial localization in the posterior-most part of the OC. Finally, at 24 hpf, *Tbx5* is expressed in a dorsal domain located opposite from the optic fissure and extending behind the lens until the middle of the retina (Figure 20D, see also Figure 29B)(Kruse-Bend et al. 2012).

Neuropeptides and their potential cleavage products	Roles in fishes	Regulation
CART (Cocain and Amphetamine related transcript)	- Reduces food intake (Volkoff et al. 2005) - Reproduction (Barsagade et al. 2010)	- decreases during starvation (Volkoff 2014)
POMC-a et POMC-b Pro-OpioMelanoCortin) Cleavage products : - MSH - ACTH - β-endorphin	- α-MSH reduces food intake (Volkoff et al. 2005) - Increase in pigmentation (Cerdá-Reverter et al. 2011) - Cortisol synthesis and stress (Cerdá-Reverter et al. 2011) - Energy expenditure (Cerdá-Reverter et al. 2011) - Body fat storage (Cerdá-Reverter et al. 2011)	
AVT (Arginin-Vasotocin, Arginin-Vasopressin homolog)	- Reduces food intake (Gesto et al. 2014) - Osmotic balance - Blood pressure - Increases aggressiveness (Kagawa 2013) - Stress response (Gesto et al. 2014) - Elicits courtship behaviour (Hasunuma et al. 2013)(Kagawa 2013)	- Dependant on the social rank (Kagawa 2013) - In response to stress (Gesto et al. 2014) - Circadian rhythmicity (Eaton et al. 2008; Rodríguez-Illamola et al. 2011)
Isotocine (IT, Oxytocin homolog)	- Decreases food intake (Mennigen et al. 2017) - Osmoregulation (Martos-Sitcha et al. 2013) - Social behaviour (Mennigen et al. 2017; Weitekamp et al. 2017) - Reproduction (Mennigen et al. 2017) - Parental care (DeAngelis et al. 2017)	
Orexin / Hypocretin (Hcrt) Cleavage products : - orexin A - orexin B	- Increases food intake (Volkoff et al. 2005) - Sleep consolidation (Prober et al. 2006) - Increases locomotor activity (Nakamachi et al. 2006; Volkoff et al. 2005)	- Stress response (Sakurai 2014)
NPY (NeuroPeptide Y)	- Increases fod intake (Lin et al. 2000)(Volkoff et al. 2005). - Decerases locmotor activity (Matsuda et al. 2012) - Promotes sleep (Singh et al. 2017)	
AgRP (Agouti-Related Protein)	- POMC receptor antagonist (Cerdá-Reverter et al. 2011) - Increases body weight (Cerdá-Reverter et al. 2011) - Growth (Zhang et al. 2012)	- increased during fasting (Cerdá-Reverter et al. 2011)
MCH (Melanin-Concentrating Hormone)	- Decrease in pigmentation (Lin et al. 2000) - Increases food intake (Lin et al. 2000)	
CRH (Corticotrophin Releasing Hormone)	- Stress response including : - decrease of food intake (Volkoff et al. 2005) - increase of locomotor activity (Lowry & Moore 2006)	- Stress Response (Volkoff et al. 2005)
SST (Somatostatin)	- Phototaxic swimming (Horstick et al. 2017) - Inhibits the release of GH by the pituitary (Sheridan & Hagemeister 2010)	

Table 1 : Neuropeptides and their roles.

3. Hypothalamus and Optic Recess Region Functions

The hypothalamus and optic recess region (ORR) are regions of the forebrain that regulate many physiological and behavioural processes such as energy expenditure, food intake, sleep, locomotor activity, stress, osmotic balance, sexual differentiation, social interactions, reproductive behaviour…

3.1. Modes of action of the Hypothalamus/ORR and neuropeptides

The hypothalamus/ORR can act via two different modes of action: either direct innervation, by releasing a neurotransmitter into a synapse with another neuron; or by secretion of neuro-hormones in the blood which allow for a long distance and systemic action. This endocrine function can be achieved in two ways, the first is through direct release of the neuro-hormone by the hypothalamic/ORR neuron in the blood at the level of the neurohypophysis; the second is indirect, via an innervation of the adenohypophysis that will in turn release neuro-hormones in the blood.

The hypothalamus/ORR uses both classical neurotransmitters such as glutamate and GABA, but also neuromodulators like dopamine, histamine or serotonin, and many neuropeptides. These neuropeptides are small peptides, often the cleavage products of larger precursors, which have the capacity to signal either as neurotransmitters or as neuro-hormones. Another difference between the neuropeptides and the more classical neurotransmitters lies in their clearance from the synaptic cleft: while the classical neurotransmitters are quickly removed from the synapse through diverse mechanisms (degradation, re-uptake…), the neuropeptides released in the synapse are slowly degraded by peptidases, thus allowing for a long-lasting signalling.
Of note, the hypothalamus/ORR are not the only brain regions containing neuropeptidergic neurons, but they are over-represented there, in link with the neuro-endocrine function of the hypothalamus/ORR in the control of many aspects of body homeostasis.

Indeed, neuropeptides are involved in the control of many functions, as illustrated in Table 1 where some examples of neuropeptides expressed at least in part in the hypothalamus or the ORR are given, together with their known functions in teleosts.

Basic organisation and functions of the hypothalamus/ORR

The hypothalamus and ORR are organized in nuclei or groups of several neuron types controlling diverse functions. Let's take the example of the neurosecretory preoptic nucleus (NPO). This nucleus is located in the dorsal ORR and contains isotocin (the homolog of mammalian oxytocin), arginine-vasotocin (AVT, homologous to the mammalian arginine-vasopressin), somatostatin (SST) and corticotropin-releasing hormone (CRH) neurons (Machluf et al. 2011; Pogoda & Hammerschmidt 2007; Herget & Ryu 2015).

One example of functional role is given by "the stress axis" or hypothalamic-pituitary-inter-renal axis (HPI, homologous to the HPA or hypothalamic-pituitary-adrenal axis in mammals) which controls the cortisol levels. Cortisol allows a return to normal homeostatic parameters after a stressful episode.
In this axis, like in many others the hypothalamus/ORR are the first players. Indeed, they receive inputs from both the central and peripheral nervous system, which allows them to detect and integrate stress

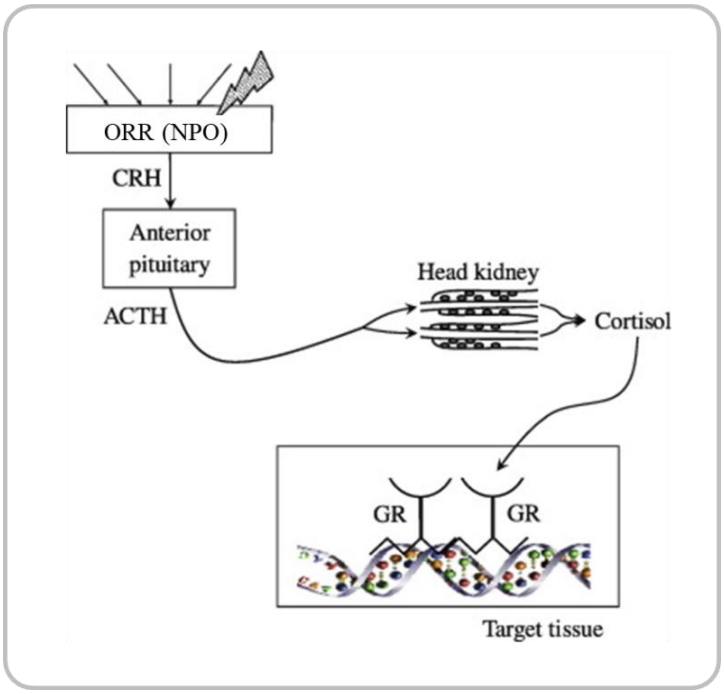

Figure 21 : The stress axis.
The NPO in the optic recess region (ORR) integrates stress signals and releases CRH in the corticotrophic area of the adenohypophysis. In turn, corticotropic cells release ACTH in the blood. This hormone provokes the synthesis and release of cortisol in the blood. Cortisol can then activate the glucocorticoid receptor of its target cells, which act as a transcription factor and activate specific gene expression.
CRH, corticotropin-releasing hormone; ACTH, adrenocorticotropic hormone; GR, glucocorticoid receptor.
From (Alsop & Vijayan 2009)

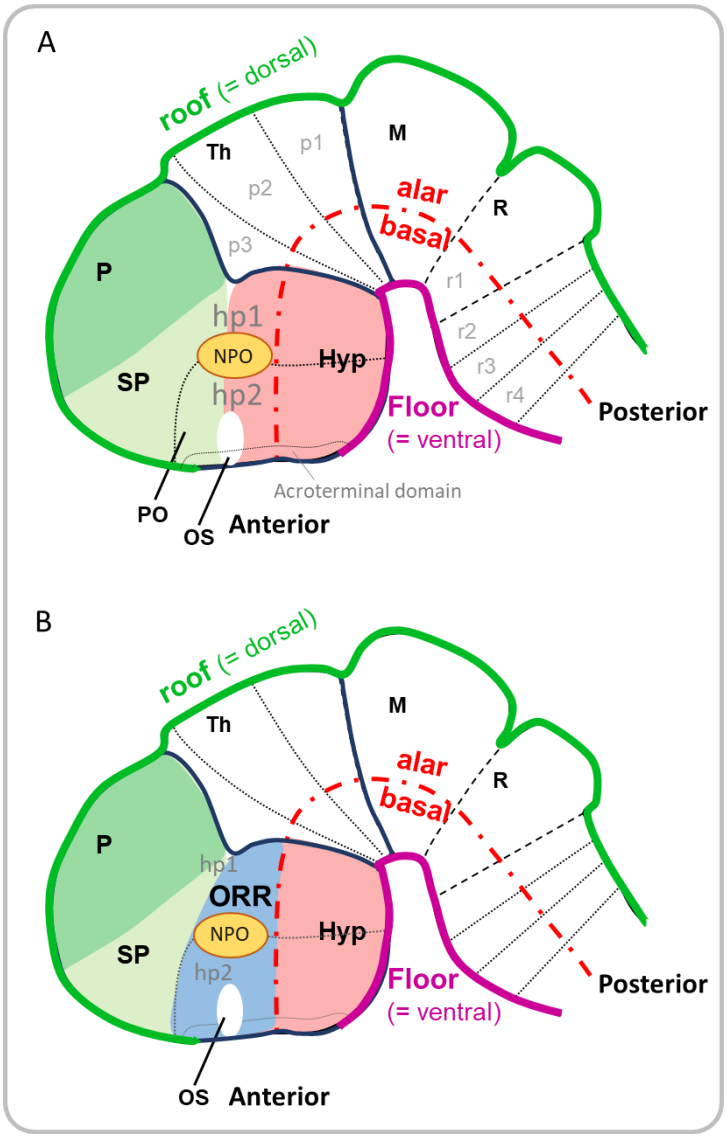

Figure 22 : Axes and regions of the brain.
(A) the prosomeric model, defining the antero-posterior axis of the brain and the alar-basal boundary. Note the separation of the hypothalamus and telencephalon at the level of the optic stalk and the optic recess.
(B) The addition of the optic recess region in the forebrain partition.
P, pallium; SP, subpallium; PO, preoptic area; Hyp, hypothalamus; Th, thalamus; M, mesencephalon; R, rhombencephalon. Green line is the roof plate, magenta line is the floor plate, red dotted line is the alar basal boundary.
From (Yamamoto et al. 2017)

signals. Upon detection of such signals, the CRH cells of the NPO nucleus (in the ORR) are activated and start releasing CRH at their axonal ending which is located in the adenohypophysis, in the area of corticotropic cells. These cells in turn secrete adrenocorticotropic hormone (ACTH) in the blood stream. When ACTH reaches the inter-renal cells of the head kidney (adrenal gland homolog), it triggers cortisol synthesis and release in the blood. Cortisol acts by binding the glucocorticoid receptor (GR) which is a ligand-activated transcription factor which then regulates specific gene transcription. Amongst its targets are genes controlling glucose metabolism, iono-regulation, immune response and behaviour (Figure 21)(Alsop & Vijayan 2009).

Other circuits involving the hypothalamus in a broad sense (including the ORR) exist such as the hypothalamic-pituitary-gonadal axis, controlling reproductive function; or the hypothalamic-pituitary-thyroid axis controlling thyroid hormones levels and therefore mechanisms such as growth, energy balance and metabolism.

3.2. Development and anatomy of the hypothalamus and ORR

3.2.1. Defining axes and regions in the brain

Neuroanatomy and the description of brain regions is a complicated exercise because of the complexity of the brain within a species. Adding to this first complexity, the diversity of brain shapes across vertebrates renders comparisons across species not always straightforward. In order to gain understanding on brain evolution and to be able to accurately compare brain regions across taxa, it is important to establish regional homologies between different species; and for that purpose, to segment the brain into meaningful units. I will here focus on the anatomical interpretations of the hypothalamus/ORR.

Since 1993 (Bulfone et al. 1993), the prosomeric model has been proposed and set forward. This model redefined the axes of the brain in order to segment it in different transversal “rings” called prosomeres, each containing from ventral to dorsal, a floor plate, basal plate, alar plate and roof plate component. More recently, the emphasis was put on the signalling centers to help and give causal explanations to the definition of brain axes. Indeed, these centers are responsible for patterning the brain, and the strongly patterned expression of some genes is used as a read-out of the relative influence of these signalling centers and serves to define “natural” regions.
In this model, the longitudinal axis is defined by the expression of *Shh* and *Nkx2.2*; these genes expression also defines, along with others, the alar-basal boundary. Indeed, *Shh* is interpreted as being expressed in the floor and basal plates and therefore to be a “ventral” marker. This alar-basal boundary terminates at the level of the post-optic commissure. The roof plate terminates at the level of the anterior commissure and the floor plate at the level of the “mamillary” hypothalamus. These axes actually match the axes observed during early development, when the optic vesicles elongate and the hypothalamus emerges ventrally to the OV (just above the yolk), while the dorsal (alar) telencephalon is visible above the OV.
In the updated prosomeric model, the forebrain is divided in diencephalon posteriorly and secondary prosencephalon anteriorly. The secondary prosencephalon contains the telencephalon and the hypothalamus which, together, are divided in 3 prosomeres : the posterior hp1, the hp2 and the anterior-most acroterminal domain which is a small band spanning from the anterior limit of the roof plate (anterior commissure) to the anterior limit of the floor plate (mamillary hypothalamus).The strength of this model is that, by examining conserved axes, signalling centers and their influence, this segmentation of the brain should be applicable to all vertebrates and provide a better support to understand mutant phenotypes, developmental diseases and evolution (Figure 22)(Puelles & Rubenstein 2015).

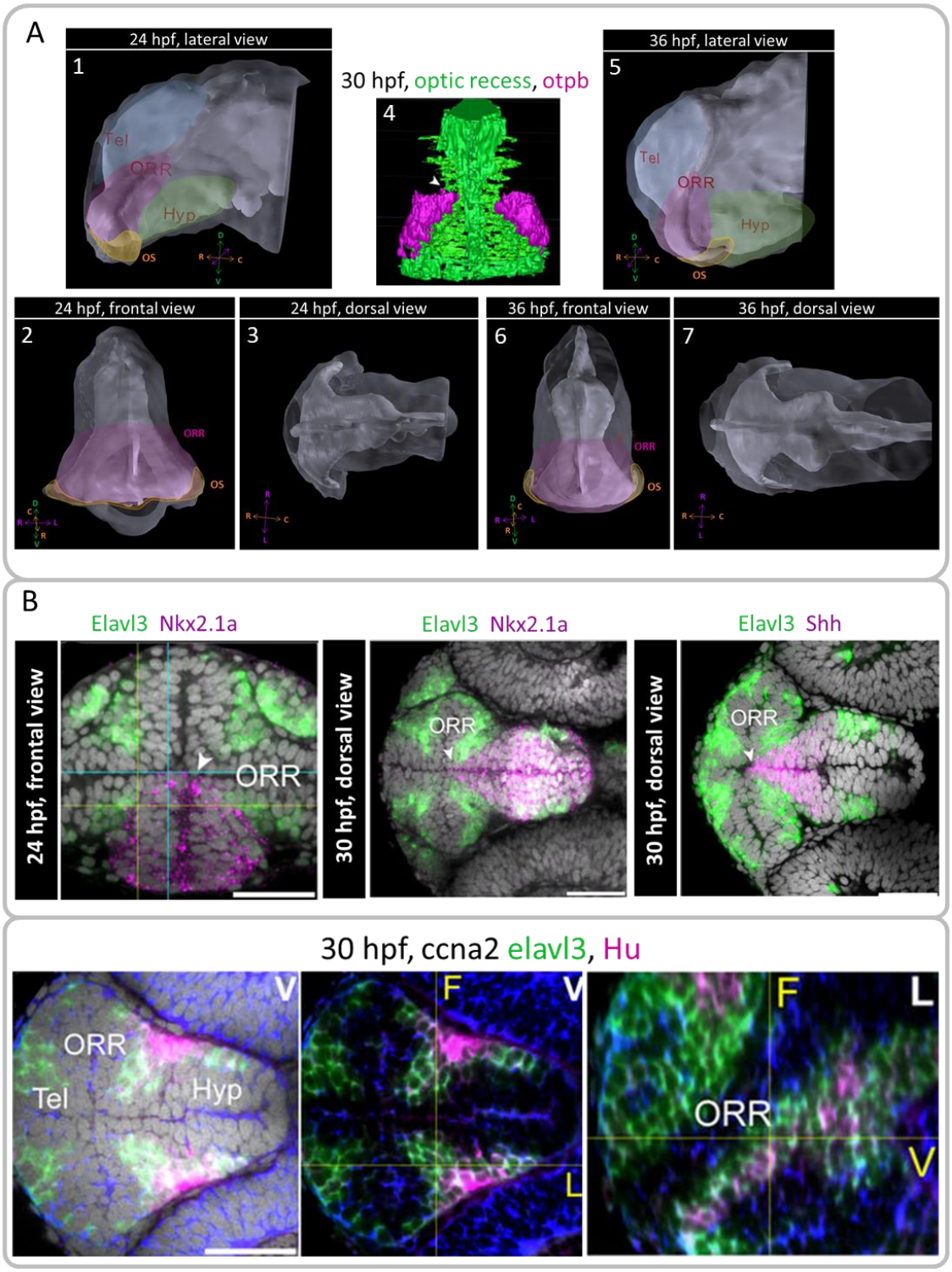

Figure 23 : The optic recess region.
(A) Segmentation of the ventricles of the forebrain, including the optic recess. The different regions of the secondary prosencephalon are highlighted in colors, (from literature), telencephalon is blue, ORR is magenta, the optic stalk (*Pax2a*-positive region) is yellow, hypothalamus is green. (A4) Frontal view, optic recess is green from a segmentation, *Otp*-positive cells are in magenta, delaminating the dorsal ORR. (B) The hypothalamus and ORR boundaries as showed by *Nkx2.1a* (Hypothalamus). The alar-basal boundary, defined by *Shh* expression. (C) ORR an hypothalamus boundaries, defined by the differentiation gradient. *ccna2* : cell cycle marker; *elalv3* marks the differentiating neurons and *Hu* labels the differentiated neurons. From (Affaticati et al. 2015)

As previously mentioned, the hypothalamus is organized in nuclei containing different types of neurons expressing neuropeptides and other neurotransmitters. These nuclei have been studied extensively in mammals but their homologous counterparts in other species have not always clearly been identified.

Some researchers undertook to find in zebrafish the structures homologous to some of these nuclei such as the paraventricular nucleus (PVN) of rodents. The PVN contains a set of neurons expressing various neuropeptides; their approach was to analyse the expression of the same neuropeptides in zebrafish, together with the expression of conserved transcription factors. That way, they managed to define the neurosecretory preoptic nucleus (NPO) that I already mentioned, as the homologous structure to the mammalian PVN (Herget et al. 2014; Herget & Ryu 2015).

The mammalian PVN belongs to the hypothalamus (alar hypothalamus in the prosomeric model), while the NPO is located in the teleost "preoptic area". The preoptic area of fishes is a structure that results from the evagination of the eyes and spans from the anterior commissure to the post-optic commissure so that, according to the prosomeric model, it is part of both the telencephalic subpallium and the alar hypothalamus. The fact that a single morphogenetic unit is considered part of two different structures was somewhat confusing. Adding to this confusion, a region called the preoptic area also exists in mammals but is only part of the telencephalic subpallium and does not include any part of the hypothalamus. To resolve these inconsistencies of naming and partitioning, Affaticati, Yamamoto and colleagues proposed to define a new region of the secondary prosencephalon : the optic recess region, that would be essentially identical to the teleost preoptic area (Affaticati et al. 2015; Yamamoto et al. 2017). This new way of partitioning the secondary prosencephalon is not in contradiction with the prosomeric model as it does not question its axis definition or even the prosomere boundaries but simply proposes to redefine the telencephalon/ hypothalamus division into three distinct regions: the telencephalon, the ORR and hypothalamus in order to better fit the development and morphogenesis of this region. Even from the prosomeric point of view, this partition makes more sense: the telencephalon was already a strictly roof/alar structure but the hypothalamus had a dual identity with an alar part and a basal/floor part; with this new partition, the telencephalon keeps its roof/alar identity, the ORR is strictly alar and the hypothalamus becomes strictly basal/floor (Figure 22).

This new division of the secondary prosencephalon also allows locating both the mammalian PVN and the teleost PVO into the ORR without reference to the confusing name of preoptic area.

3.2.2. The Optic Recess Region (ORR)

As mentioned previously (see section Eye development), the ORR results from the evagination/elongation of the optic vesicles and develops around the optic recess, between the anterior commissure dorsally (according to the prosomeric model axes) and the post-optic commissure ventrally. At the examined stages of the ORR study (24-48hpf)(Affaticati et al. 2015), the optic recess displays an hourglass-like shape in frontal view, with a narrowing located roughly in the middle of the recess and which is accompanied by an inversion of its curvature in a lateral view. Indeed, the ventral part is bent rostrally while the dorsal part is rather bent caudally. This inversion of the recess curvature coincides with a boundary of gene expression: the two transcription factors *sim1* and *otpb* are expressed anteriorly (ventrally in the whole body axis) and *pax6* is expressed posteriorly (dorsally in the whole body axis). This inversion of curvature can be considered the dorsal boundary of the optic recess region (Figure 23A)(Affaticati et al. 2015).

The ORR was identified as a region because of the centrifugal neurogenic gradient present at these stages throughout the secondary prosencephalon. Indeed, in this whole region, elongated progenitors line the

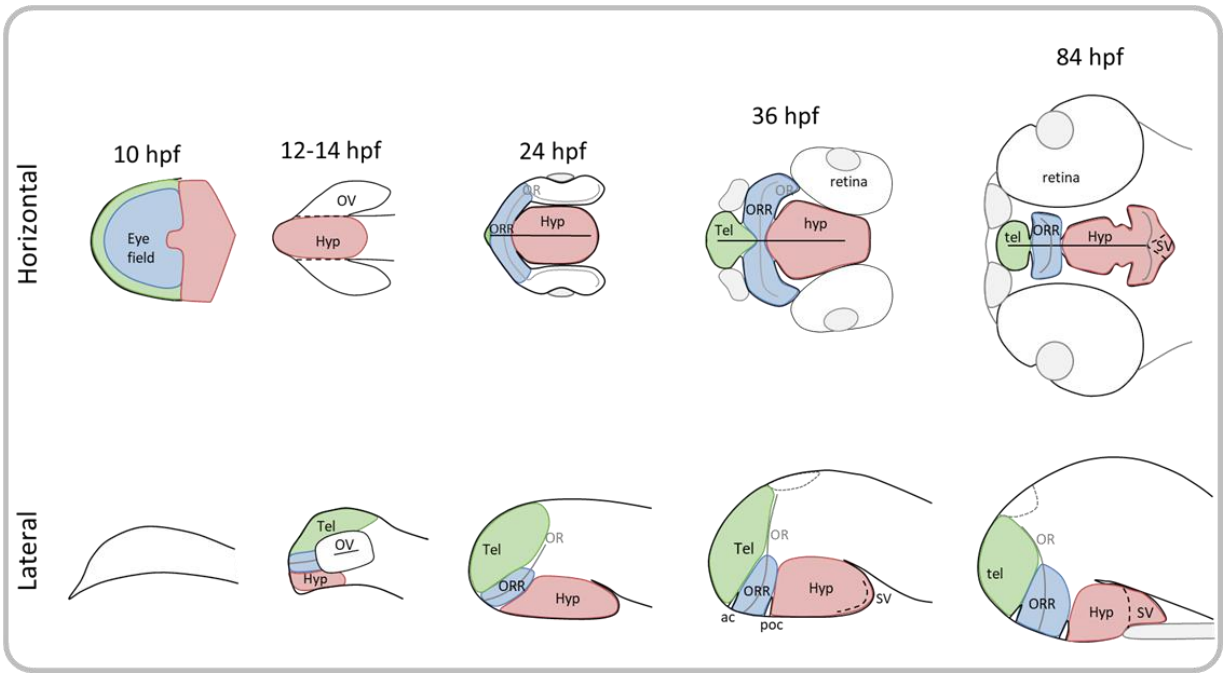

Figure 24 : Summary of the secondary prosencephalon development.
The hypothalamus shape is modified trough time with the appearance of new recesses. The horizontal planes are ventral. Note the formation of the *saccus vasculosus* (SV). Tel, telencephalon; Hyp, hypothalamus; OR, optic recess. Anterior is to the left.

recess and the ventricle while differentiating and mature neurons with a rounder nucleus are located further away. A consequence of this neurogenic gradient is to bring neurons originating from distinct regions in contact with each other; for example above the post-optic commissure, neurons of a hypothalamic origin and neurons from an ORR origin are juxtaposed. The hypothalamus and the telencephalon actually come to abut the optic recess medially as evidenced by the neurogenic patterns and the expression of *Nkx2.1a* and *Shh* (Figure 23)(Affaticati et al. 2015).

While development proceeds, the originally laterally elongated ORR will compact more and more between increasingly growing axon bundles running laterally between the eyes and the ORR, as well as rostrally and caudally in the commissures; nevertheless, the ORR will persist until adulthood.

3.2.3. The Hypothalamus

As previously described (see section Eye development), the hypothalamic cells are originally located posterior to the eye field in the neural plate before undergoing a subduction movement, that leads them in a very anterior and ventral position, “in front” of the telencephalon.

The progressive bending and rotation of the forebrain then progressively brings it closer to the yolk, under the diencephalon and abutting the notochord. As development progresses, the originally simple shape of the hypothalamus complexifies with the formation of two new ventricles : the lateral recess, around which the inferior lobe of the hypothalamus forms, and the teleost and gar-specific posterior recess (Yamamoto et al. 2017).

At the caudal-most extremity of the hypothalamus (along body axis), lies the *saccus vasculosus*, a circumventricular organ that is only present in some fishes which do not include the zebrafish nor the medaka fish. This poorly studied organ is involved in the osmoregulation of the cerebro-spinal fluid and has been hypothesized to control seasonal variations in some fishes (Figure 24) (Maeda et al. 2015; Nakane et al. 2013).

Ventrally to the hypothalamus are located the neurohypophysis and adenohypophysis. The neurohypophysis has a neural origin while the adenohypophysis derives from the placodal ectoderm.

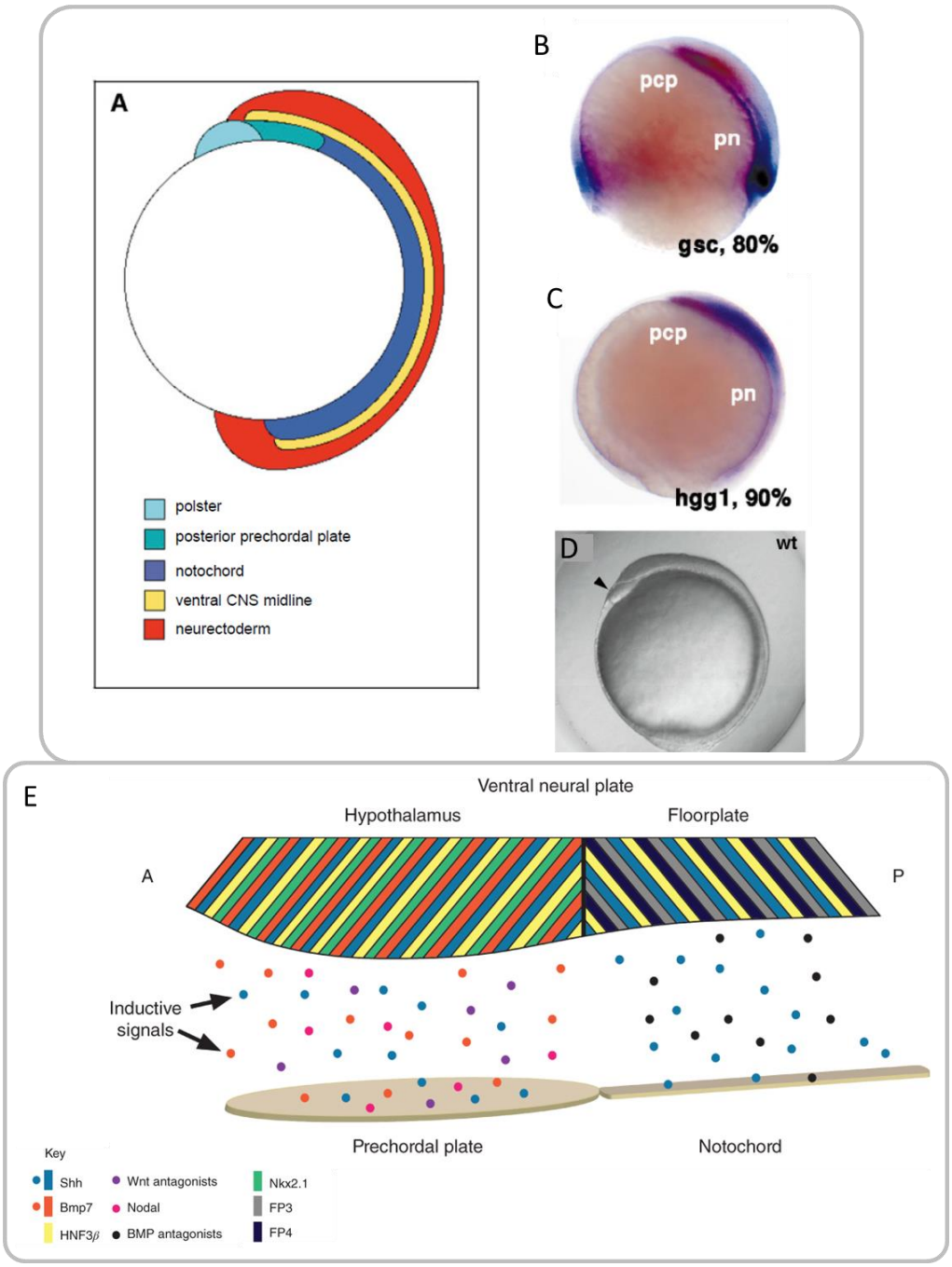

Figure 25 : the prechordal plate.
(A) Diagram of a bud-stage zebrafish embryo showing the prechordal plate (PCP) with its anterior polster and posterior part, followed by the notochord. (B) *Goosecoid* expression (in red) labels the PCP at 80% epiboly. (C) *Hgg1* expression labels the PCP at 90% epiboly. (D) Zebrafish embryo at bud-stage, the arrowhead indicates the polster. (E) Diagram showing the inductive signals that act on the ventral neural plate. The posterior neural plate receives signals from the notochord to become floor plate, whereas the more anterior neural plate receives signals from the PCP to become the hypothalamus. Dots represent signaling from the PCP/notochord, diagonal bars in the neural plate represent local gene expression. Note that this configuration is only transient as the PCP continues its migration to reaches its final anterior position further away from the presumptive hypothalamus (at neural plate stage). The hypothalamus then undergoes subduction and passes rostrally past the PCP. Thus by the time the floor plate and the hypothalamic neural plate are specified, the prechordal plate actually resides caudal to the hypothalamic neural plate. Lateral view, anterior to the left.
From(Bedont et al. 2015; Chan et al. 2001; Heisenberg & Nüsslein-Volhard 1997)

4. Signalling centers, morphogens and the development of the optic region

The coordinated development of the embryo is orchestrated by several organizing centers or signalling centers that secrete morphogens. These molecules diffuse throughout the tissue, creating gradients that will determine the fate of the recipient cells. This fate choice will be modulated according to the cell competence and to the combinations and relative concentrations of morphogens it receives. Many factors can influence these gradients such as the physical properties of the tissue (dense, loose…), the degradation of the morphogen, or the presence of antagonists.

The development of the forebrain is directed by signalling centers successively located in different regions in the embryo, and producing various combinations of morphogens and antagonists, resulting in the amazing complexity of morphogenetic movements, brain regions and neuronal fates of the forebrain. I will hereafter give a first overview of the main signalling centers involved in the forebrain patterning and their role in the general forebrain development. In a second part, I will focus more specifically on the effect of these different signalling centers on eye regionalization and tissue specification.

4.1. The signalling centers and their role during forebrain development

In vertebrates, the neural fate of cells from the ectoderm is acquired during gastrulation due to the secretion of Fgf ligands by the organizer (the “shield” in fishes) and underlying endoderm that initiate the acquisition of neural fate. This decision is further maintained and confirmed by BMP antagonists -such as chordin and noggin- released by the organizer, which counteract the effect of BMPs secreted by the surrounding non-neural ectoderm.

Once the neural identity of the neural plate ectoderm has been acquired, it is necessary to specify the dorso-ventral (or lateral-medial at this stage) and antero-posterior axes so that the positional identity of the territories can be set.
The posterior identity is defined in part by the organizer which is becoming more and more distant from the anterior tip of the neural plate and starts secreting posteriorizing factors such as Wnts. Meanwhile, the prechordal plate (PCP) and the notochord, which are essential midline signalling centers of mesodermal origin, migrate anteriorly beneath the neural plate. In turn, new signalling centers are induced such as the anterior neural border (ANB) and subsequently the anterior neural ridge (ANR).
The signals released from these centers will result in the acquisition of regional identities such as eye field, hypothalamus or telencephalon. Subsequently, new signalling centers, such as the zli *(zona limitans intrathalamica* in the diencephalon) or the MHB (mid-hindbrain boundary) will be induced and contribute to further refine this patterning (Beccari et al. 2013).

4.1.1. Prechordal plate

The prechordal plate is the anterior-most part of the axial mesoderm, and is a direct derivative of the shield organiser. The prechordal cells are the first axial cells to be internalized during gastrulation. After that, this small sheet of cohesive cells undergoes anteriorwards collective migration (followed by the notochord) until it passes the tip of the ANP. This structure is a major signalling center which expresses a number of signalling molecules and morphogens such as :

- Nodal protein Cyclops (Cyc)
- Hedgehog proteins Sonic Hedgehog (Shh) and Tiggy winkle Hh (TwHh)

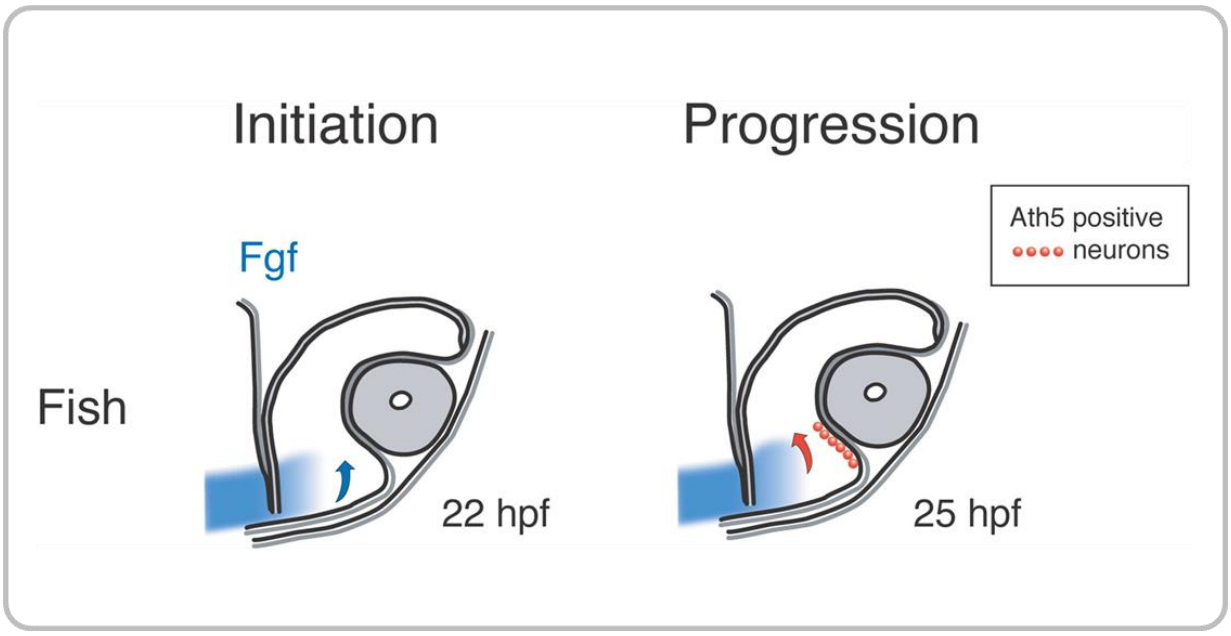

Figure 26 : the optic stalk acts as an organizing center
After induction by the prechordal plate, the optic stalk secretes Fgfs that in turn induce neuronal differentiation. Drawn as a transverse section.
From (Martinez-Morales et al. 2005)

- Bone morphogenetic proteins BMP4, BMP7, and the anti-dorsalizing morphogenetic protein (ADMP)
- Wnt antagonists dickkopf (Dkk)

(Wu et al. 2011; Beccari et al. 2013; Bedont et al. 2015; Mathieu et al. 2002).

The PCP is strongly involved in eye and hypothalamus development. Indeed, the PCP, through its secretion of Wnt inhibitors, is necessary for the specification of the hypothalamic field anteriorly, while the more posterior medial neural plate adopts a floorplate identity (Kapsimali et al. 2004).
In terms of morphogenesis, the absence of prechordal nodal signalling leads to a failure of the presumptive hypothalamus to undergo subduction and the eye field does not separate bilaterally; more generally, the lack of PCP results in a dorsalized forebrain, highlighting its role as a ventral inducer (Figure 25)(Chuang & Raymond 2002; García-Calero et al. 2008).
The cooperation of PCP-derived Nodal, BMP7 and HH are also necessary for the expression of early hypothalamus markers such as *Nkx2.1* (Bedont et al. 2015). The PCP also plays a role in the subsequent patterning of the hypothalamus as nodal and Hh signallings are necessary for the specification of the posterior-ventral and the antero-dorsal hypothalamic regions, respectively (Mathieu et al. 2002).
The PCP migrates anteriorly under the neuroepithelium and its anterior part, called the polster, finally gives rise to the hatching gland.

The prechordal plate induces the optic stalk organizing center

It also seems that PCP-derived nodal signalling is indirectly involved in retinal differentiation. Indeed, nodal would modulate the optic stalk fate and its secretion of a signalling factor that would, in turn, promote *Atho5* expression and the subsequent retinal differentiation (Masai et al. 2000).
In *Xenopus* as in chicks and zebrafish, *Atho5* has been shown to be regulated by Fgfs (Willardsen et al. 2009; Martinez-Morales et al. 2005). Three *fgfs* are known to be expressed in the zebrafish optic stalk : *fgf8a*, *fgf3* and *fgf17*, although removal of both *fgf8a* and *fgf3* are sufficient to prevent retinal differentiation (Martinez-Morales et al. 2005; Thisse & Thisse 2005). This fgf signalling has also been shown to trigger the expression of *Shh* in the RGC and amacrine cells, which is necessary for their differentiation (Figure 26)(Martinez-Morales et al. 2005).

4.1.2. Notochord

The notochord is part of the axial mesoderm; upon involution, this structure undergoes convergence and extension movements to form a rod-like structure that follows the PCP migration until abutting the developing hypothalamus. This transient structure is a very important ventral midline signalling center that expresses Hh and BMP antagonists. It is necessary for floor plate induction.

The expression of Hh ligands by both the PCP and the notochord induces the expression of *Shh* in the ventral forebrain (hypothalamus mainly) and the floor plate, respectively (Bedont et al. 2015)

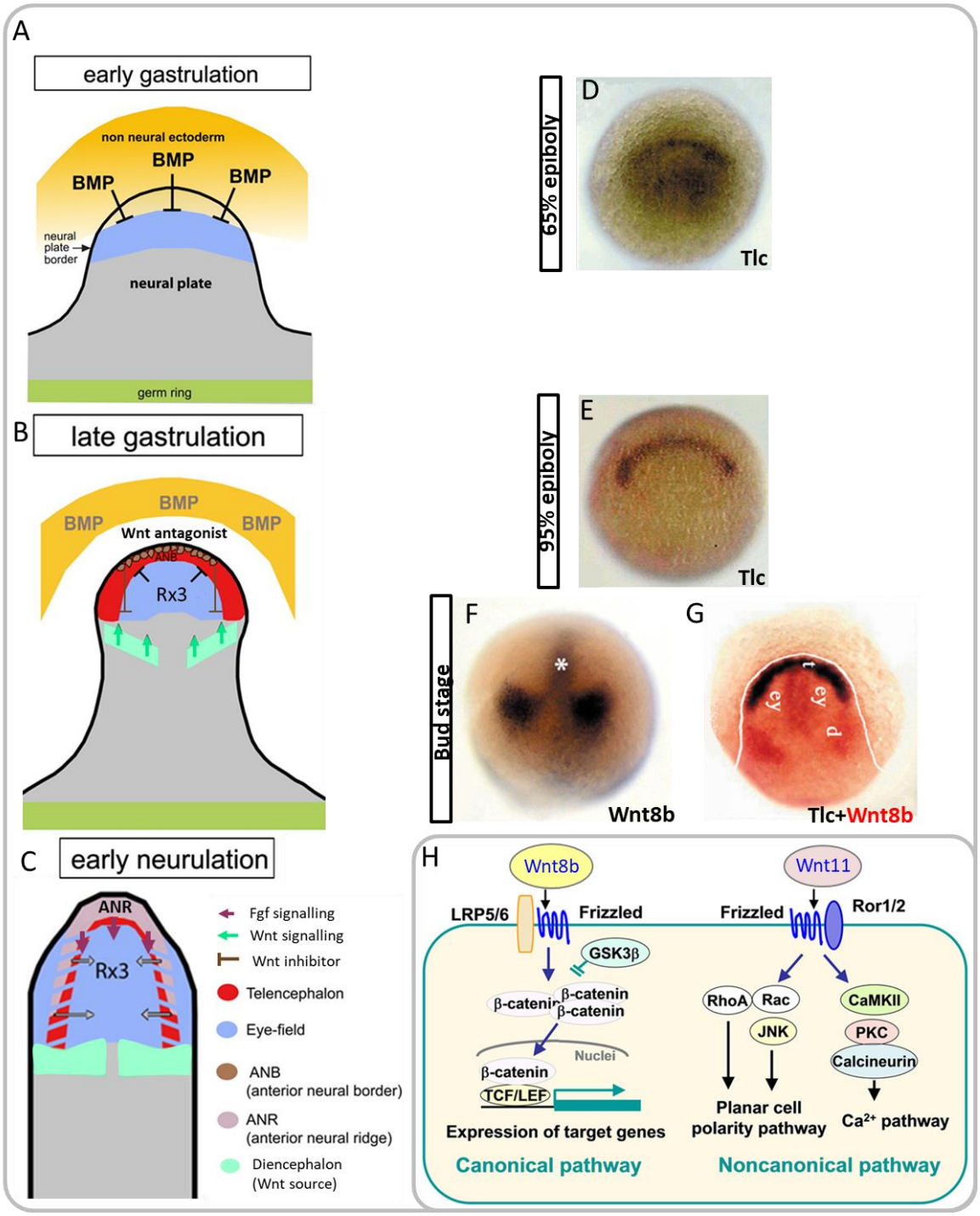

Figure 27 : The anterior neural border and anterior neural ridge signalling centers.
(A) BMP is secreted from the non-neural ectoderm, and counteracted by the BMP inhibitors secreted by the organizer. (B) Intermediate levels of BMP induce the anterior neural border (ANB) that secretes Wnt antagonists such as Tlc that counteract the posteriorizing effect of the Wnt (β-catenin pathway) signals from the diencephalon. (C) The anterior neural ridge secretes Fgf ligands that influence Hh proteins expression but also forebrain patterning, grey arrows indicate morphogenetic converging movements (D) Early *Tlc* expression throughout the anterior neural plate. (E) *Tlc* expression is then restricted to the ANB. (F) *Wnt8b* expression in the diencephalon and PCP (asterisk). (G) *Tlc* (blue) and *Wnt8b* (red) expression in the anterior neural plate. Ey, eye field; t, telencephalon; d, diencephalon. (A-G) Dorsal views, anterior to the top.
(H) Diagram of the Wnt pathways, canonical β-catenin pathway and non-canonical Planar cell polarity pathway and calcium pathway.
Adapted from (Cavodeassi et al. 2005; Bielen & Houart 2012; Takahashi et al. 2011)

4.1.3. Anterior neural border VS posterior Wnt signalling

The anterior neural border (ANB) is a small group of cells located at the anterior margin of the ANP. This signalling center is active around mid-gastrulation and is necessary for the induction and maintenance of the telencephalon (Houart et al. 1998). Indeed, the ANB secretes a Frizzled-related Wnt antagonist : *Tlc*, which is expressed from early gastrulation in the whole ANP before being restricted to the ANB at late gastrulation (Figure 27A, B, D, E)(Houart et al. 2002). The expression of this Wnt antagonist is induced by intermediate levels of BMP signalling from the non-neural ectoderm. In the absence of *Tlc*, the telencephalon is lacking, demonstrating the role of the ANB/ANR in antero-posterior patterning of the neural tissue.

Wnt signalling can act via two different pathways : the canonical β-catenin-dependent pathway, and two non-canonical β-catenin-independent pathways : the planar cell polarity pathway (PlCP) and the Ca^{2+} pathway. In all of these pathways, a Wnt ligand binds to a Frizzled receptor (Figure 27H).

Tlc inhibits the action of Wnt8b and probably Wnt1, which both act via the β-catenin pathway and are expressed by cells from the prospective diencephalon and midbrain, a few cell rows away and posteriorly from the eye field. Wnt8b has been shown to act as a posteriorizing factor and an antagonist of telencephalic and eye fate, and Wnt1 is known to inhibit eye development. More generally, activation (by pharmacological treatments or via mutations) of the Wnt/β-catenin pathway during mid-gastrulation – before the eye field specification- results in a shift from eye fate to diencephalic fate. Therefore, the Wnt/β-catenin pathway inhibits the eye fate (Houart et al. 2002; Cavodeassi et al. 2005).
On the other hand, another Wnt family member, *Wnt 11,* is also expressed in the posterior ANP, abutting the *Rx3*-expressing eye field. This Wnt ligand acts via the PlCP non-canonical pathway and promotes eye fate but also the cohesion of the eye field cells, therefore probably contributing to the subsequent morphogenesis of the eye. Moreover Wnt11 seems to act as a repressor of the Wnt/β-catenin pathway and therefore also contributes to the repression of posteriorizing Wnt signals (Cavodeassi et al. 2005).

To summarize, telencephalic specification requires low levels of Wnt/β-catenin activity (Wnt8b/Wnt1), which is permitted by the expression of the Wnt antagonist *Tlc* in the ANB, while the diencephalon require high levels of Wnt/β-catenin activity which are present in the caudal ANP. Between these two territories, the eye fate is inhibited by Wnt/ β-catenin activity but is promoted by the non-canonical Wnt/PlCP pathway (Wnt11) activity (Figure 27F, G)(Cavodeassi et al. 2005; Houart et al. 2002).

4.1.4. Anterior Neural Ridge and Fgf signalling: an interplay with ventral Hh to pattern the anterior forebrain

The anterior neural ridge (ANR) seems to originate from or close to the ANB, around bud stage (10hpf in zebrafish). It is an anterior source of Fgf ligands such as Fgf8a and Fgf3 (Danesin & Houart 2012; Walshe & Mason 2003).

The ANR formation requires ANB activity, indeed, early expression of *Tlc* is required for the induction of *Fgf8a* expression, by preventing its repression by Wnt signalling (Figure 27C)(Houart et al. 2002; Shanmugalingam et al. 2000).

An important interplay between Fgfs -secreted from the ANR- and Hh factors -secreted from the PCP and later on from the ventral forebrain- has been demonstrated, even though some studies seem to find contradictory results.
There seems to be a consensus regarding the fact that Hh signalling from the ventral midline promotes *Fgf8* and *Fgf3* expression in the ANR, as several teams have shown by cyclopamine (Hh signalling

inhibitor) treatments at slightly different stages and on different fish species. Miyake and colleagues performed this treatment on zebrafish embryos from 40-50% epiboly onwards and detected a reduction in ANR/telencephalic expression of both *Fgf8* and *Fgf3*. Similarly, Hernández-Bejarano and colleagues applied cyclopamine on zebrafish from 1-3 ss onwards and analysed *Fgf8* and the Fgf pathway target *sprouty* expressions at 12 ss. Both were down-regulated in the ANR/telencephalon at this stage. Finally, Pottin et al performed the Hh inhibition on *Astyanax mexicanus* cavefish from 80% epiboly until 5/6 ss at which point they analysed *Fgf8* expression which was missing in the ANR/telencephalon. Therefore, the Hh pathway seems to promote the expression of *Fgf8* and *3* at the ANR (Hernández-Bejarano et al. 2015; Pottin et al. 2011; Miyake et al. 2005).

On the other hand, the influence or not of Fgf signalling on *Shh* expression seems more controverted. Indeed, Walshe and Mason showed a decrease of *Shh* hypothalamic expression at 30hpf in *Fgf3/8* zebrafish morphants, but also a decrease in *Twhh* in the posterior ORR at the same stage (Walshe & Mason 2003). The use of such morpholino treatment does not allow for the temporal resolution of the window at which Fgf signalling is important for *Shh* expression. Our team also tackled the question of the influence of Fgf signalling on *Shh* expression by treating *Astyanax mexicanus* cavefish with SU5402 -an inhibitor of Fgf receptor 1- both from 80% epiboly to 5/6 ss and from shield stage to 5/6 ss with several concentrations. The analysis of *Shh* expression was performed at 5/6 ss and showed a dose-dependent decrease in *Shh* rostral expression, which was more prominent with the shield-stage treatment (Pottin et al. 2011). Conversely, Hernández-Bejarano and colleagues evidenced the absence of effect of SU5402 treatment on both *Shh* expression and on the Hh pathway downstream effector *Ptch2* expression. In this case, the Fgf pathway inhibition was performed from 1/2 ss zebrafish embryos onwards (i.e., much later than in the previous examples) and analysed at 10/12 ss.

One explanation for this apparent discrepancy of results is that Fgf induction of *Shh* might occur earlier than 1/2 ss since *Fgf3* is expressed as early as 80% epiboly and *Fgf8* from bud stage. This timing of expression and action could explain why Walshe and Mason observed almost no effect on *Shh* expression in *Fgf8* single morphant, as the time window between its expression and the 1/2 ss at which it does not influence Shh anymore, is very short. This is consistent with the stronger reduction of Shh observed in *Fgf3* morphants by the same authors and with the stronger effect of the shield stage treatment on the cavefish, which would account for a longer time of action of *Fgf3* before the stage 1/2 ss. This could also explain why their double *Fgf8/3* morphants display the strongest reduction : the early and long-lasting effect of *Fgf3* combined with a shorter but nevertheless existing action of *Fgf8* would add-up to promote *Shh* expression before the onset of somitogenesis (Walshe & Mason 2003; Pottin et al. 2011; Hernández-Bejarano et al. 2015).

In conclusion, it seems that *Fgf3/8* promote anterior *Shh* and *Twhh* expression before somitogenesis and that reciprocally, Shh promotes *Fgf3/8* expression, even though *Shh* and *Fgf8* expression domains are mutually exclusive, at least during bud-stage/somitogenesis. In other words, *Shh* expression does not cross the optic recess and stays ventral/posterior to it, while *Fgf8* stays dorsal/anterior to the recess, without overlapping (Figure 28).

These two morphogen signals then promote the expression of different transcription factor (TF) that specify different regions of the forebrain (Walshe & Mason 2003; Pottin et al. 2011; Miyake et al. 2005). Some of these important TFs are FoxG1 and FoxD1.

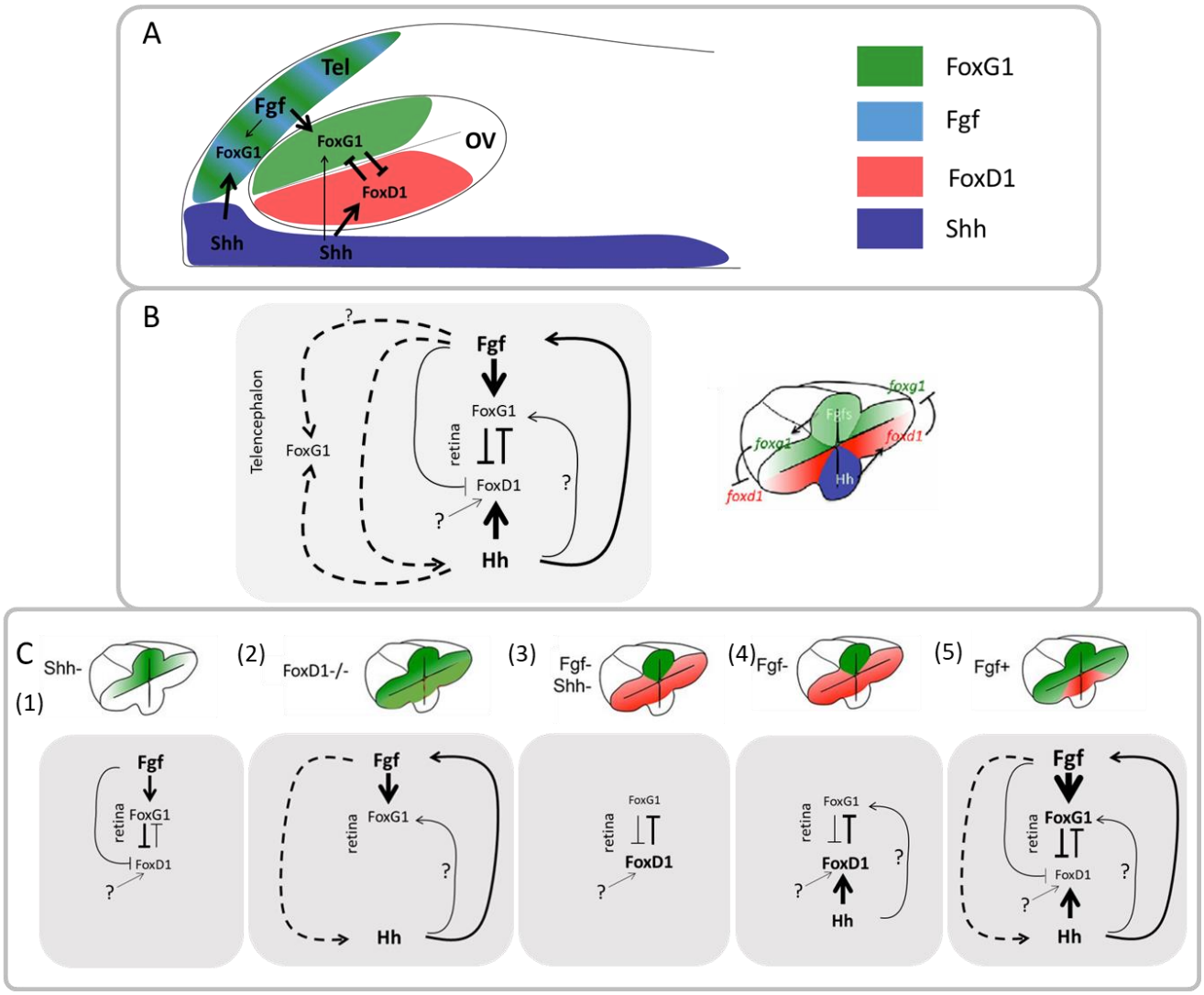

Figure 28 : Morphogen influence on the naso-temporal quadrants.
(A) Distribution of the morphogens and naso-temporal markers at the OV stage. *Shh* is expressed at the midline. *Fgfs* are expressed in the ANR. Lateral view, anterior to the left. (B) Interactions between morphogens and naso-temporal markers in a wild-type condition. Dotted lines indicate timing-specific interactions, question marks indicate hypothesized relationships. (C) Different cases of morphogen signaling modification. (1) Fgf signalling is sufficient to prevent *FoxD1* from being expressed. Indeed, as *FoxG1* is not invading the ventral retina, it cannot be reponsible for *FoxD1* inhibition. (2) In the chick, *FoxG1* becomes able to invade the ventral retina upon loss of *FoxD1*. This result, taken together with the previous Hh inhibition, results seem to indicate a promotion of *FoxG1* expression by Hh which is usually hidden by the promotion of *FoxD1.* (3) In the absence of both Hh and Fgf signalling, *FoxD1* seems to be induced by another independent factor since it is expressed throughout the OV. (4) In the absence of Fgf, Hh signalling induces *FoxD1* which invades the whole OV. (5) Ectopic Fgf signalling in the ventral retina leads to its invasion by *FoxG1* expression.
From (Hernández-Bejarano et al. 2015)

FoxG1

FoxG1 is expressed very early (tailbud stage) in the prospective telencephalon, while later on, around 10 ss, it becomes expressed in the dorsal OV : in the prospective anterior ORR and nasal retina where it stays expressed later on.

FoxG1 and Hh signalling

A publication focusing mostly on the telencephalic aspects reported that *FoxG1* expression was promoted by Hh signalling (Danesin et al. 2009) while another study, focusing rather on the retina reported no influence of Hh on *FoxG1* expression in this region (Hernández-Bejarano et al. 2015). In the first study, cyclopamine was applied on zebrafish embryos from bud stage onwards and analysis at 5 ss showed a clear reduction of *FoxG1* expression. In the second article, the treatment was performed from 1/3 ss onwards and analysed at 10/12 ss where no obvious reduction of *FoxG1* expression domain either in the telencephalon or in the nasal retina could be observed. Again, this could be due to time-dependent interaction between Shh and *FoxG1*, where Hh signalling could play an important role during the initiation of *FoxG1* expression in the telencephalon. Of note, in the same article, supplementary data are provided showing that a mosaic overexpression of *Shh* throughout the brain seems to increase *FoxG1* expression in the telencephalon but not in the retina. This could also suggest a different effect of *Shh* on *FoxG1* depending on the regional identity of the cells (Figure 28).

FoxG1 and Fgf signalling

The role of Fgf factors in the regulation of *FoxG1* expression has also been evidenced. Several articles in zebrafish demonstrate the induction of *FoxG1* in the nasal retina by Fgf signalling, either through SU5402 treatments or by analysis of simple *Fgf8* mutant (Ace) or triple knock-out/knock-down of Fgf3/8/24. The treatments were performed either between 1/2 ss and 10/12 ss or between 5 and 10 ss; both resulted in a reduction of *FoxG1* expression in the retina visible at 10/12 ss and at 28 hpf respectively. Similarly, expression knock-out or knock-down resulted in a smaller domain of *FoxG1* expression at 28 hpf. In mice, Fgf8 also seems to play a role in *FoxG1* telencephalic expression (Hernández-Bejarano et al. 2015; Picker & Brand 2005; Storm et al. 2006; Picker et al. 2009) .
FoxG1 expression is therefore under the influence of Fgf signalling, at least in the zebrafish retina but also possibly in its telencephalon.
Of note, and in turn, *FoxG1* seems to directly or indirectly downregulate *Fgf8* expression in the ANR/telencephalon as *FoxG1* morphants display an increase in *Fgf8* expression (Danesin et al. 2009).

To my knowledge, the question of which pathway(s) is/are directly activating *FoxG1* expression has not been answered. These effects of Hh and Fgf on *FoxG1* expression could either be the result of the mutual activation of these two morphogens, with only one of these pathways directly activating *FoxG1* expression, or alternatively they could both cooperate in activating the expression of this TF. Another possibility is that Hh signalling in the PCP, very close to the telencephalic anlage during neural plate stage, could influence *FoxG1* expression there; but after the morphogenesis of the optic vesicles, the PCP seems too far to actually influence the dorsal OV and promote *FoxG1* expression.

FoxD1

FoxD1 is expressed in the temporal retina and in the optic stalk. Its expression starts around 10 ss. Hernández-Bejarano and colleagues demonstrated that this *FoxD1* expression is dependent on Hh signalling but only in the presence of Fgf signalling, as the double inhibition of these two pathways results in a normal expression of *FoxD1* (Figure 28C)(Hernández-Bejarano et al. 2015).

FoxG1 and FoxD1 expressions are mutually exclusive

In the retina, the dorsal/nasal *FoxG1* and the ventral/temporal *FoxD1* repress each other to establish a clear boundary between them, originally approximatively at the recess.

As *FoxD1* expression is promoted by Hh, this could also explain why a possible effect of Hh on the retinal *FoxG1* is not seen. It is possible that this effect is still present but that the inhibition of *FoxG1* by *FoxD1* prevents us from seeing it. Indeed, when Hh signalling is absent, there is no *FoxD1* but *FoxG1* does not invade the ventral/ temporal retina while in chicks, the removal of *FoxD1* without altering Hh signalling leads to the invasion of the temporal retina by *FoxG1* (Hernández-Bejarano et al. 2015; Herrera et al. 2004).

In the next paragraphs, I will detail the influence of these morphogens on the forebrain.

Fgfs and the telencephalon

Both Fgf8 and Fgf3 are not required for the establishment of telencephalic fate but rather, they contribute to its regionalization by specifying the subpallial telencephalon (Walshe & Mason 2003). Both Fgf8 and Shh are required for the induction of *FoxG1* throughout the telencephalon and anterior ORR, with high-ventral to low-dorsal gradient, with an absence of expression at the roof plate. The telencephalon roof is another signalling center of the brain, secreting both Wnt and BMP ligands which could repress *FoxG1*. *FoxG1* has been proven to inhibit *Wnt* expression and to restrict it to the telencephalon roof which is responsible for the induction of the pallial fate. *FoxG1* is involved in the development of the ventral telencephalon and is essential for the specification of the subpallium. This TF is integrating several signals (Hh, Wnt, Fgf) and that way, allows to regulate the proportions between pallial and subpallial identities (Danesin & Houart 2012; Sylvester et al. 2013).

Fgfs and the ORR

In *Fgf8* (Ace) mutants the ORR is extremely reduced, the optic recess is more closed in its ventral part and adopts a different shape with no caudal-wards bending of its ventral-most part. The anterior and post-optic commissures are not correctly established and *Pax2a*, a marker of the optic stalk, is disrupted at the midline. This could either be a direct effect of Fgf8 absence, or an indirect one, through the reduction of Shh and Twhh signaling in the posterior ORR (Shanmugalingam et al. 2000). A combination of *Fgf8* and *Fgf3* morpholinos was also shown to be more efficient at reducing Twhh than either one alone; in parallel, each of these morpholino resulted in a reduction of the size of the ORR (Walshe & Mason 2003). These studies indicate a role for both Fgf3 and Fgf8 signalling for the correct development of the ORR.

4.2. Morphogens, signalling centers and eye development

4.2.1. Eye regionalization

During eye regionalization, several signalling centers and morphogens come into play. As previously discussed, Fgfs from the ANR and Hhs from the midline are involved in regulation of *FoxG1* and *FoxD1*, respectively and therefore in the nasal/temporal patterning of the retina. These two signalling centers are also involved in the patterning of other quadrants. In addition to the ANR and the midline signalling, the olfactory placode, the extraocular ectoderm, dorsal retina, ventral and RPE also participate in the delimitation of the quadrants.

In a simplified way, one could describe the patterning of the eye as follow :

- The ANR specifies the nasal quadrant

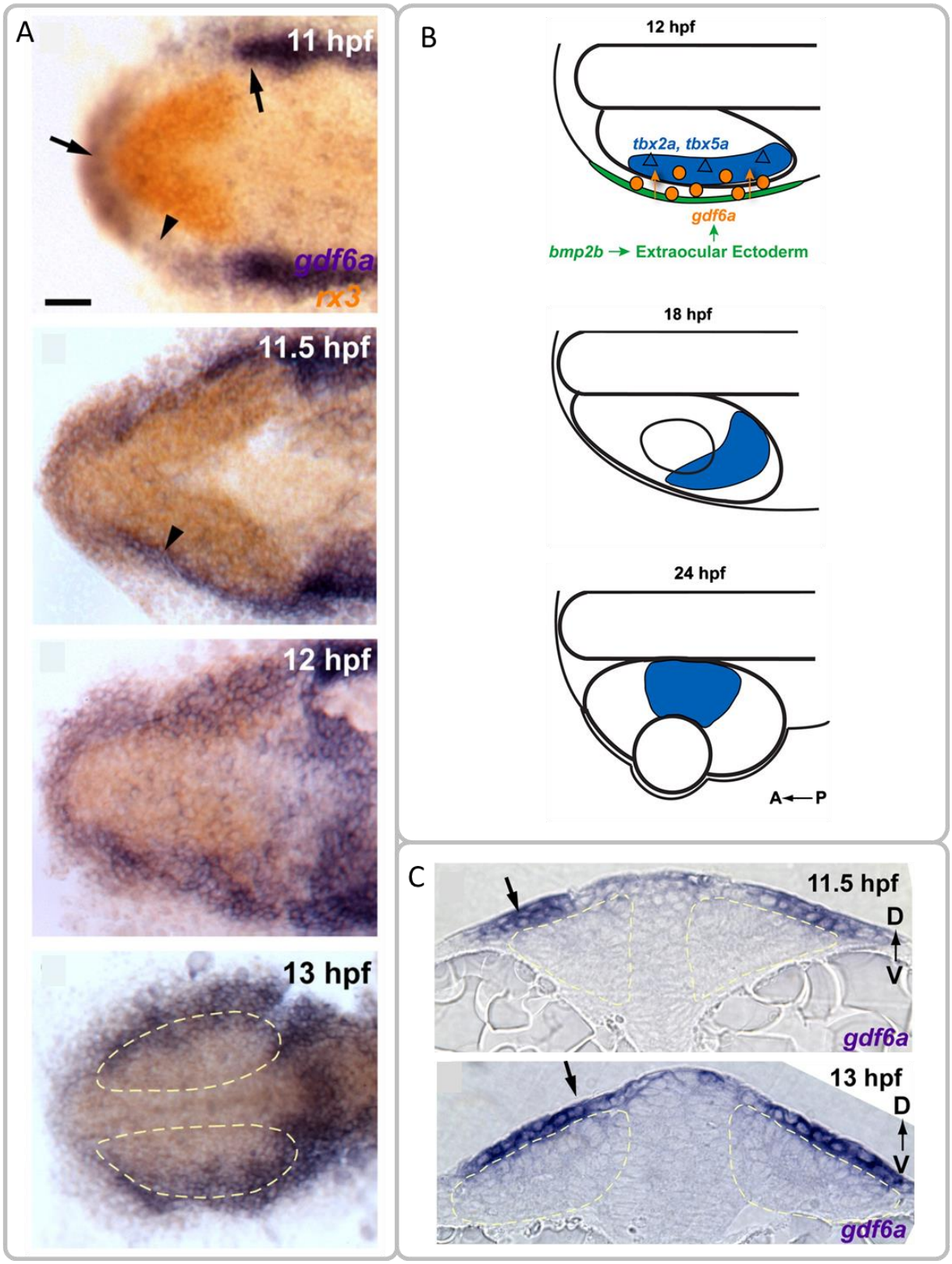

Figure 29 : Induction of the dorsal quadrant.
(A) Expression of *Gdf6a* and the early eye-field marker *Rx3*. *Gdf6a* is expressed very early in the non-neural ectoderm, at 11 hpf, its expression is stronger anterior and posterior to the eye field/young optic vesicle(OV). Quickly after, at 11.5 hpf, its expression strengthens around the OV and covers the lateral portion of the dorsal OV leaflet (see C). *Gdf6a* then continues to expand to cover the whole dorsal leaflet of the OV (C). (B) Diagram showing the inductive effect of the extraocular ectoderm on the specification of the dorsal retina. Blue indicate the dorsal retina. (A, B) Dorsal views, anterior to the left. (C) Transverse sections.
From (Kruse-Bend et al. 2012)

- The extraocular ectoderm specifies the dorsal quadrant
- The ventral midline signals pattern the ventral quadrant and in a lesser extent, the temporal quadrant

Of course, this process is more complicated and involves many interactions between the different morphogens and the TFs.

The nasal quadrant

The nasal fate of the eye is promoted by *Fgf8* and *Fgf3* which are both expressed in the ANR/telencephalon, but also by *Fgf24* which is expressed in the olfactory placode. The effect of these different Fgf is additive as the loss of nasal identity and gain of temporal identity increases when their loss of function are combined (Picker et al. 2009). Of note, the loss or gain or nasal/temporal identities always involves a shift at the level of the dorsal retina/distal OV. This probably reflects the impossibility for the morphogen ligands to cross the optic recess so that they have to reach the distal rim of the OV before diffusing in the opposite leaflet.

Gdf6a, a BMP-family ligand expressed dorsally is also responsible for the dorsal restriction of *FoxG1* expression, as *Gdf6a* morphants show dorsally-expanded *FoxG1* expression (Asai-Coakwell et al. 2007).

The dorsal eye

The dorsal quadrant of the eye can be labelled by *Tbx5* as early as 12hpf, but other *Tbx* factors are also expressed there (Veien et al. 2008).

The dorsal identity of the eye is largely controlled by BMP signals but also by Wnt signalling. The initiation of dorsal identity acquisition seems to be due to Gdf6a signalling, emanating from the extraocular ectoderm ; this tissue being itself specified by *Bmp2b*. *Gdf6a* is first expressed lateral to the OV, in contact with the dorsal leaflet of the OV, where the future dorsal retina is induced, at 4-5 ss. Gdf6a then induces the expression of various dorsal markers in the retina such as itself and *Bmp2b* (which are also expressed within the dorsal retina) but also *Tbx5a*, *Tbx2a* or *BMP4* (Figure 29) (Kruse-Bend et al. 2012; Asai-Coakwell et al. 2007; French et al. 2009; Gosse & Baier 2009).

If BMP signalling is responsible for the acquisition of dorsal fate, Wnt is necessary for the maintenance of this identity.

Wnt2 and *Wnt8b* are both expressed in the dorsal RPE from 10-14 ss. This Wnt signalling from the RPE starts after the initial acquisition of the dorsal identity but is required for the maintenance of several dorsal retina makers such as *BMP4, Gdf6a* and *Bmp2b*. Conversely, inhibition of Wnt pathway, even after 18 ss, triggers an important expansion of the ventral marker *Vax2* both on the nasal and temporal quadrants (Veien et al. 2008).

The action of BMPs and Wnts in the eye is also modulated by Sfrps (Secreted frizzled-related protein), which are soluble modulators of Wnt primarily but also of BMP signalling. *Sfrp1a* and *Sfrp5* are both expressed from 6 ss in the ventral eye, with a wider expression domain for *Sfrp1a*. It was proposed that the high ventral to low dorsal gradient of these factors could help the establishment of dorso-ventral boundaries. Indeed, they function as Wnt and BMP inhibitors at high concentration but they enable them and act as facilitators of their signalling at low concentration. They would therefore allow the repression of dorsal fate in the ventral retina but facilitate its acquisition and maintenance dorsally (Figure 30)(Holly et al. 2014).

Hh is also an important player in the dorso-ventral patterning. Regarding the dorsal fate, its effect is only very precocious as shown in *Xenopus.* Indeed, treatment with a Hh agonist (purmorphamine) starting at blastula or early neurula stages leads to a decrease in the dorsal *Tbx3* expression, while later treatment does not affect *Tbx3* anymore (Wang et al. 2015).

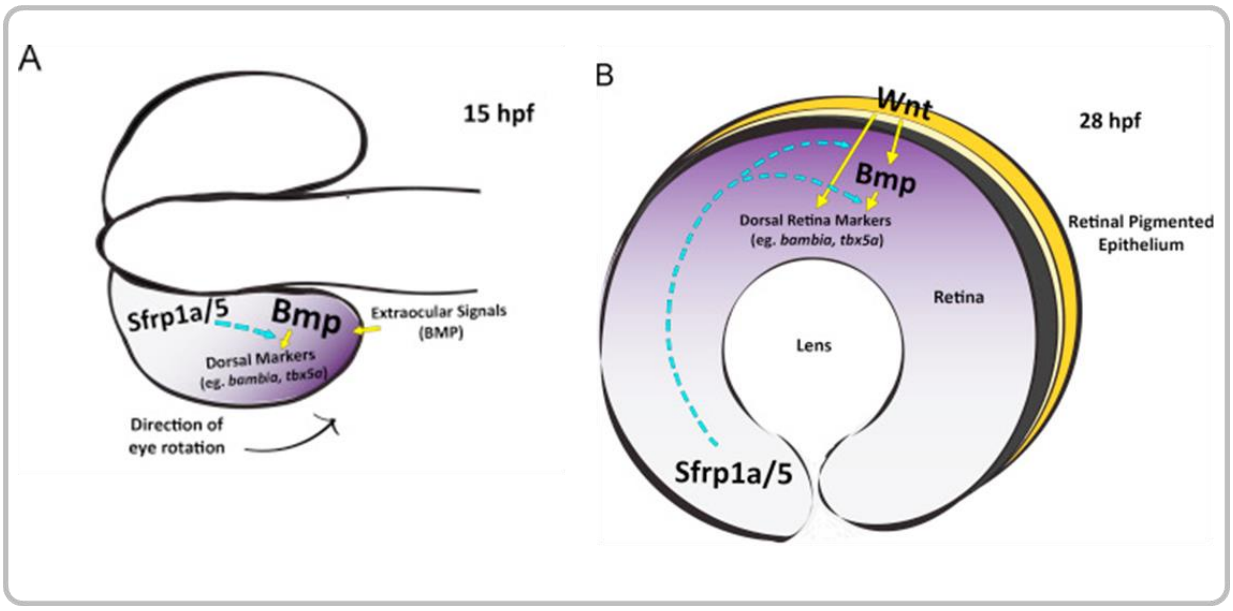

Figure 30 : Roles of the Sfrps in the maintenance of dorso-ventral patterning.
Sfrps secreted ventrally counteract BMP and Wnt at high concentrations (ventrally) but enable them at low concentration (dorsally).Wnts are secreted from the dorsal RPE and BMP from the extraocular ectoderm precociously and in the dorsal retina. (A) Dorsal view, anterior to the left, (B) lateral view.
From (Holly et al. 2014)

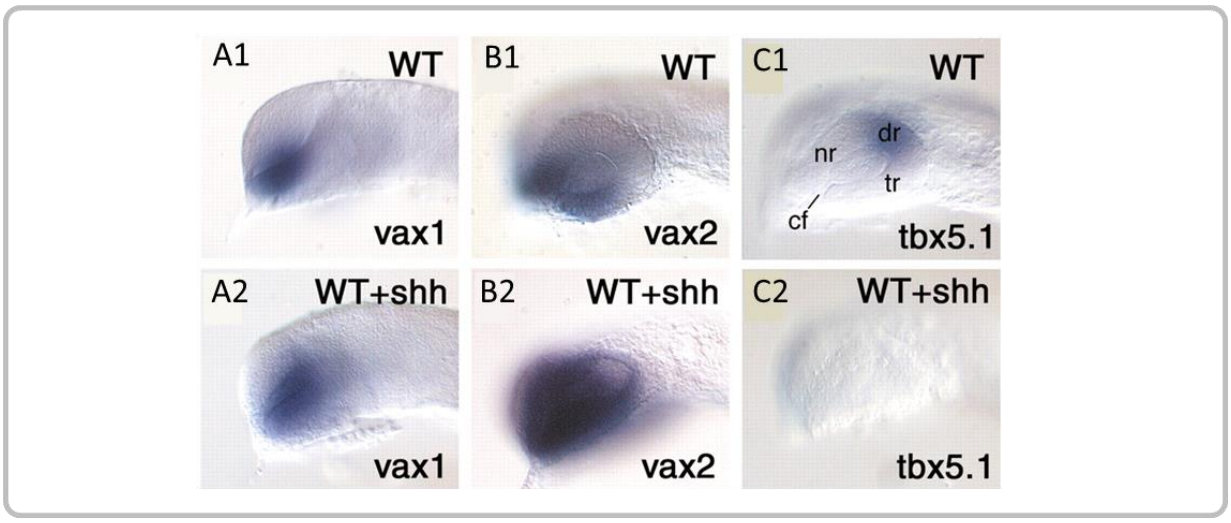

Figure 31 : Shh and the dorso-ventral patterning.
Shh promotes the ventral fate and represses the dorsal fate. Lateral views, anterior to the left. (A1, B1, C1) Wild type expression of *Vax1, Vax2* and *Tbx5.1*. (A2, B2, C2) Embryos injected with Shh mRNA, expression of *Vax1, Vax2* and *Tbx5.1*. cf, choroid fissure; nr, nasal retina; tr, temporal retina; dr, dorsal retina.
(Take-uchi et al. 2003)

Fgf signalling is also able to modify dorsal fate by modulating its span and position. Fgf inhibition between 5 ss and 10 ss leads to a nasal-wards shift of *Tbx5* expression domain without modifying its span. *Ace* mutants on the other hand, display a reduction of *Tbx5* domain without altering its position (Picker & Brand 2005).

Similarly to the nasal/temporal patterning, where these two opposite fates are mutually exclusive, a similar mechanism seems to be at play in the dorso/ventral patterning of the retina, even though the dorsal and ventral boundaries seem further away from each other. This is the case at least in chicks where *cVax* overexpression inhibits *Tbx5* expression (Schulte et al. 1999) and conversely *Tbx5* overexpression leads to a decrease in *cVax* (Koshiba-Takeuchi et al. 2000). I am not aware of any similar experiments in fishes.

The ventral eye

Vax2 is often used as a marker of the ventral eye, although its expression is not strictly restricted to the ventral retina but also encompasses the optic stalk and the ORR. *Vax1* presents a more restricted pattern with an expression in the OS and the ORR but not in the ventral retina. To my knowledge, there are no identified transcription factor whose expression is strictly restricted to the ventral retina and excluded from both the OS and ORR. This illustrates how much the dorso-ventral patterning corresponds in fact to the proximo-distal patterning of the whole optic region, comprising the retina, the optic stalk and the optic recess region; hence the utility of considering this entire optic region as a morphogenetic unit.

The Hh pathway is involved in the acquisition of the ventral identity. Hh has a clear role in promoting the ventral/ proximal fate; indeed, Shh overexpression leads to a shift in identity towards a more proximal fate with an expansion of *Vax2* expression into the dorsal retina and an expansion of *Vax1* into the ventral retina, showing not only a modification of the retinal regionalization but also a modification of the identity of the tissue (Figure 31)(Take-uchi et al. 2003). In *Xenopus*, time-specific treatments with a Hh agonist showed that Hh pathway can influence the proximo-distal fate of the OV at early stages and that *Vax1* window of activation is earlier than that of *Vax2*. *Vax1* expression was increased when the treatment was active between early gastrula and early neurula stages; any later treatment had little effect. On the other hand, *Vax2* expression was increased in treatments performed between blastula and late neurula stages (Wang et al. 2015).

Fgf signalling does not affect *Vax2* expression in the ventral retina, specifically (Take-uchi et al. 2003; Picker & Brand 2005).

The BMP pathway represses the ventral fate. In *Gdf6a* mutants, *Vax2* expression is expanded dorsally, sometimes even invading the whole eye (Kruse-Bend et al. 2012; Gosse & Baier 2009; French et al. 2009)

The retinoic acid (RA) pathway has also been involved in the control of the ventral identity of the eye, in *Xenopus,* as the *Vax2* expression domain is increased upon RA treatment (Lupo et al. 2005).

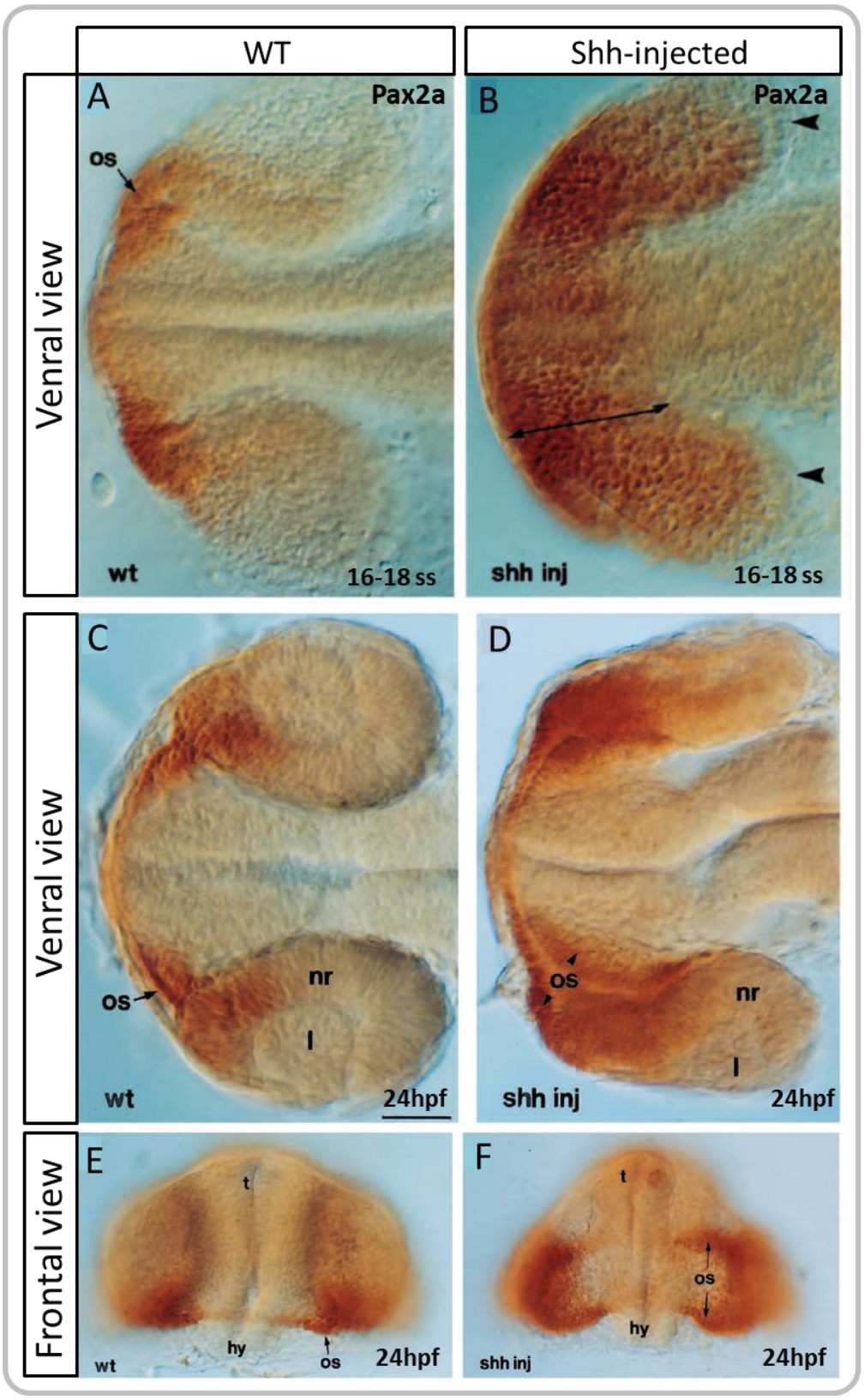

Figure 32 : Shh and the optic stalk.
(A, B) Shh signalling expands Pax2a expression in the ventral retina and enlarges the optic stalk at 16-18 ss. (C, D) The optic stalk is still enlarged with a persisting connection to the retina, whose shape is altered ventrally. Also; the optic recess stays wider. Anterior is to the left. (E, F) Frontal view of the same phenotype. From (Macdonald et al. 1995)

4.2.2. Morphogens, optic stalk and coloboma

The stalk identity and Pax2 regulation

The acquisition of optic stalk identity is also regulated by different morphogens. The most classical marker to label this structure is *Pax2a*. This structure is under the control of ventral midline signalling as evidenced by the study of *Cyclops* (Nodal pathway) mutants or by *Shh* injections. In the case of *cyclops* mutant where *Shh* expression at the midline is lacking, cells located in the region of the presumptive optic stalk finally adopt a neural retina identity. These embryos display a cyclopic phenotype with the two retinae fused at the position that MacDonald et al. describe as "ly[ing] ventral to the telencephalon and occupy[ing] the position of cells that normally form the optic stalks and ventral/anterior hypothalamus" (Macdonald et al. 1995). This position corresponds to the region that Affaticati and colleagues describe as the ORR (Affaticati et al. 2015) and was shown to express the neural retinal/RPE marker *Pax6* (Figure 32)(Macdonald et al. 1995). This means that midline signalling is necessary for the acquisition of ORR and OS identity and for the subsequent morphogenetic events associated with these regions, such as separation of the OV from the ORR.

Conversely, zebrafish injected with *Shh* mRNA exhibit several defects : their OV are smaller, the optic stalk/ medial region of the OV are hypertrophied and the OV do not manage to separate from the medial ORR and they display a strong expansion of *Pax2a* expression throughout the retina (Figure 32).
The OV connections to the medial brain are extremely thick and persist at 24 hpf in the *Shh*-injected embryos while the RPE separates the neural retina from the OS. Also, the optic recess stays connected between the two eyes. Indeed, MacDonald and colleagues describe that the optic stalk is expanded at the expense of the RPE, which could explain the persistence of the continuous optic recess (Macdonald et al. 1995).
Hh signalling from the midline is therefore essential for the correct specification of the optic stalks.

Of note, a pharmacological inhibition of Fgf signalling results in a down-regulation of *Pax2a* in the OS and OF margins of zebrafish (Sanek *et al.*, 2009, supp data), and similar results were obtained in *FgfR* mutant mice (Cai et al. 2013).

The optic recess region and Vax genes

Vax genes (*Vax1* and *Vax2*) are both expressed in the OS and ORR, *Vax* 2 is also expressed in the ventral retina. As I already mentioned both *Vax1* and *Vax2* expression in the ORR is controlled by Shh but also by Fgf signalling as treatments with an Fgf inhibitor from 70% epiboly to 24hpf are able to suppress *Vax1* and *Vax2* expression specifically in the ORR and medial OS but not in the distal OS or in the retina (Take-uchi et al. 2003). The correct expression of *Vax* genes in the ORR but also of *Fgf8* in the OS and ORR requires *Lhx2* expression. Indeed, *Lhx2* mutants (bel) display a specific loss of *Vax* genes and *fgf8* expression in these regions associated with a strong reduction in the proliferation of these regions. *Lhx2* itself is under the control of Fgf signalling (Take-uchi et al. 2003; Seth et al. 2006), also in *Astyanax* (Pottin et al. 2011). *Vax1* and *Vax2* are required to limit retinal specification/ development to the OC, and knock-down of these TFs leads to the invasion of the presumptive ORR/OS by retinal neurons that can go as far as reaching the optic chiasm (Take-uchi et al. 2003).

The Optic Fissure closure and coloboma

The completion of OF closure depends on a series of steps including the correct proximo-distal patterning of the optic region and the correct specification of the OS and the OF lips, a correct morphogenesis that brings the OF lips in contact and a correct fusion of the nasal and temporal lips.

The effect of incorrect proximo-distal patterning on the OF closure has been evidenced in many studies. Indeed, if a shift towards distal fates can result in cyclopic phenotypes, it can also, in milder cases, result in defective OF closure (coloboma) (Gregory-Evans et al. 2004). Surprisingly, a shift towards proximal fate can also result in coloboma (Lee et al. 2008; Take-uchi et al. 2003). Of course, Shh and midline signalling play a major role in this patterning and therefore in these phenotype but Gdf6a and dorsal signalling are also logically involved.

The importance of proximo-distal patterning in this phenotype is probably due to the role of *Vax1*, *Vax2* and *Pax2a* genes which have all been implicated in coloboma-related defects. First, let us consider the shift towards a proximal/ventral fate : *Vax2* overexpression in *Xenopus* leads to coloboma (Barbieri et al. 1999), this is also the case for *Pax2* overexpression in chicks (Sehgal et al. 2008) which is consistent with the fact either Hh pathway hyperactivation (Lee et al. 2008) or *Gdf6a* knock-down (Asai-Coakwell et al. 2007) in zebrafish lead to such phenotype. If, on the contrary, we now consider the shift towards a distal fate : *Vax1* and/or *Vax2* knock-down leads to defect in the OF closure in zebrafish as in mice (Take-uchi et al. 2003; Hallonet et al. 1999), which is also the case in *Pax2a* mutants (Viringipurampeer et al. 2012; Macdonald et al. 1997) and in heterozygous Shh human mutants (in which holoprosencephaly includes a coloboma) (Gregory-Evans et al. 2004).

Vax2 and *Pax2a* roles in OF closure start to be deciphered. Indeed, *Pax2* seems to be necessary for contact-dependent degradation of the basal lamina on the lips of the OF fissure (Gregory-Evans et al. 2004). *Pax2a* also cooperates with *Vax2* to activate the expression of the *fas-associated death domain (fadd)* gene. Fadd is involved in promoting apoptosis and inhibiting the programmed necrosis (necroptosis), in the eye, it also seems to be responsible for limiting the proliferation. Viringipurampeer and colleagues showed that both *Fadd* mRNA injection and pharmacological inhibition of necroptosis are able to rescue the coloboma phenotype of *pax2a* zebrafish mutants; and that conversely, *Fadd* knock-down in wild-type (WT) fishes prevents the OF closure. Additionnaly, *Pax2a* mutants exhibit abnormally high levels of necroptosis at the margin of the OF, and conversely, in WT fish, no cell death was detected specifically in the vicinity of the OF (Viringipurampeer et al. 2012; Gestri et al. 2018). This highlights a role of *Vax* and *Pax* genes in the regulation of cell death through Fadd activation (Viringipurampeer et al. 2012).

Several other genes involved in the control of either *Hh* genes or *Vax*/*Pax2* genes have also been implicated in coloboma phenotypes such as *Sox4* and *Sox11* or *Zic2* genes which repress Hh signalling and whose morphants or mutants display coloboma (Wen et al. 2015; Pillai-Kastoori et al. 2014; Sedykh et al. 2017). Also in mice, Fgf signaling alteration leads -independantly of Hh or BMP signalling- to defects of OF closure through down-regulation of *Pax2* (Cai et al. 2013).

Retinoic acid (RA) also plays a role both in the induction of ventral retina/OS and in the induction of periocular mesenchyme (POM) genes. Lupo and colleagues showed that knock-down of some of the RA-induced POM genes resulted in a coloboma, highlighting a role for this tissue, along with RA signalling in the closure of OF (Lupo et al. 2011).

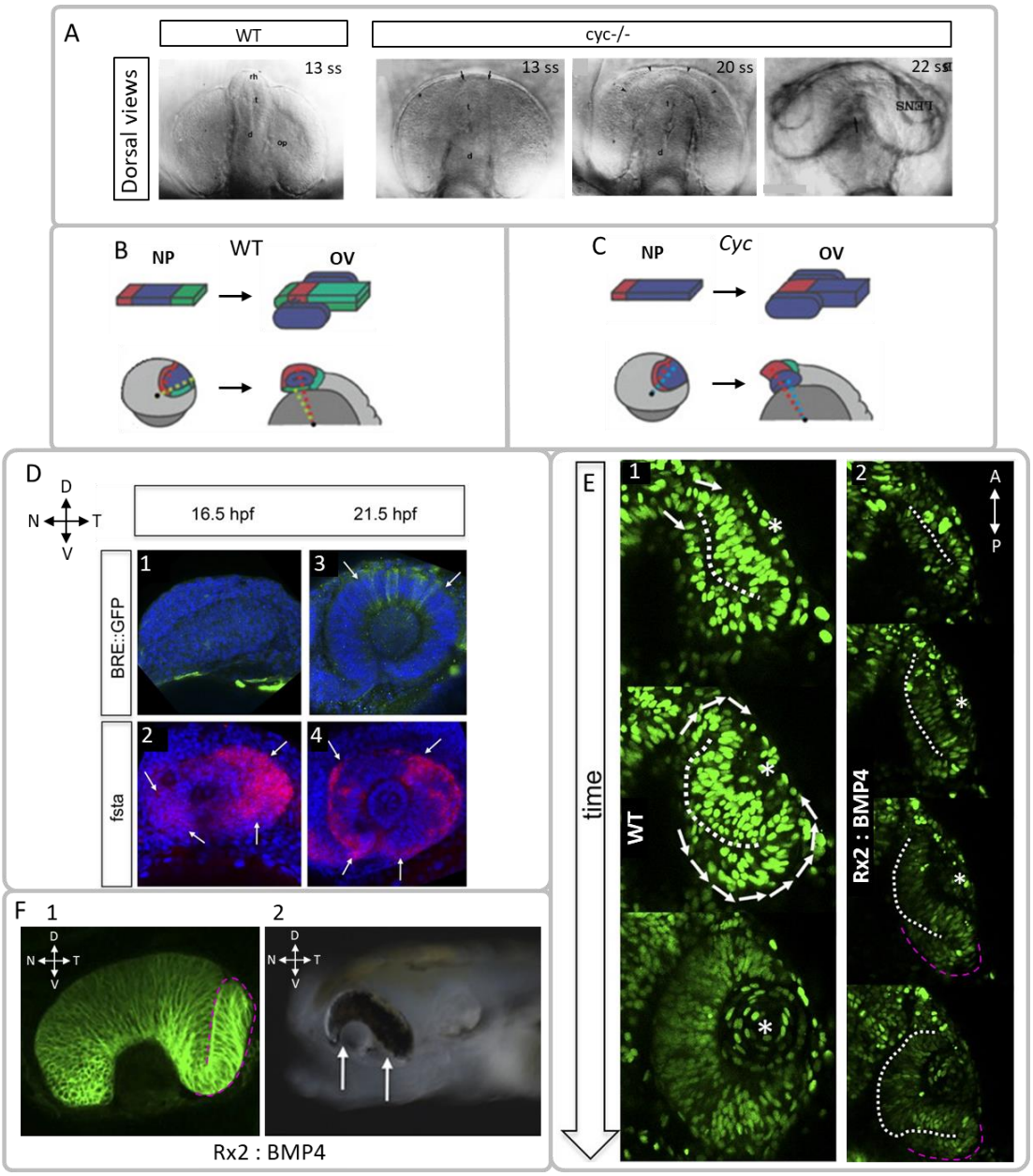

Figure 33 : Impact of morphogens on morphogenesis.
(A-E) Morphogens and neurulation. (A) *Cyclops* (*cyc*) mutant phenotype, anterior to the top. Note the bridge of fused retinas at the anterior pole of the neural keel (arrows) and the slight invagination in this bridge at 20 ss. (B,C) Schematic representations of the secondary prosencephalon development from neural plate (NP) to optic vesicle (OV) stage. Green: hypothalamus and diencephalon, blue: eye field, red: telencephalon. (C) Wild type, the 3 territories are present, the hypothalamus undergoes subduction and becomes anterior to the telencephalon (see the relative position of the dotted lines at NP and OV stages). (D) *Cyc* mutants, the hypothalamus is missing, the medial eye field subducts but does not pass before the telencephalon. (D-F) BMPs and optic cup (OC) invagination. (D) BMP signalling in the OC. (D1,3) BMP activity, visualized by GFP expression under the control of a BMP-responsive element. (D2,4) Expression of the BMP antagonist follistatin. (E) Invagination of the optic cup in the WT context (1) or in the case of BMP4 misexpression throughout the retina (2), dorsal views. Note the persisting bulge of cells in the outer OC that does not complete rim movement (magenta outline). Arrows in G1 indicate cell movement, asterisk: lens. (F) Coloboma phenotype resulting from BMP4 retinal misexpression, note the persisting temporal bulge and the lack of OF margin apposition. Lateral views.
From (Macdonald et al. 1995; Fulwiler et al. 1997; England et al. 2006; Heermann et al. 2015)

4.3. Morphogens, morphogenesis

The recent advances in the field of live microscopy have allowed to better study the morphogenetic movements underlying the correct acquisition of various shapes in the embryos but to this day, very few publications have studied these movements in relationship to morphogen signalling.

4.3.1. Neurulation

The morphogenetic events leading to a correct rearrangement of the forebrain territories are controlled by several pathways. The effects of nodal signalling impairment in *cyclops* (*cyc*) mutants have been studied by England and colleagues.

In *cyc* mutants, the hypothalamus is not induced and the initiation of the neural keel formation takes place not at the tip of the hypothalamus as in WT, but within the eye field. The medial eye field then undergoes a mild subduction beneath the remaining eye field and telencephalon that is reduced in amplitude compared to WT hypothalamic subduction. Consequently, the neural keel never manages to emerge "anterior" to the eye field and telencephalon. In this mutant, the eye field never fully splits; a portion remains medially and anteriorly, creating a band of tissue connecting the two eyes. Thus the lack of nodal signal, maybe through the lack of hypothalamic identity, results in a defect in the subduction movement, both in the initial point of migration and in the amplitude of the movement (Figure 33 A-C).

4.3.2. morphogens and optic cup morphogenesis

BMPs

Heermann and colleagues sought to study the role of BMP signalling in the optic cup morphogenesis. To this end, they expressed *BMP4* (which is normally restricted to the dorsal retina) throughout the eye with an *Rx2:BMP4* line. They then performed live 3D imaging on these fishes and compared them to WT. They observed a strong reduction in the epithelial flow toward the lens-facing epithelium during the optic cup invagination/rim movement (Figure 33G). This eventually resulted in a large portion of the temporal but also a small portion of the nasal outer OC layer remaining in the presumptive RPE domain but still differentiating into neural retina. This reduction of cell flow seriously impaired the ability of the temporal OF margin to converge towards its nasal counterpart and to juxtapose, therefore resulting in a coloboma (Figure 33 H). In this study, they find that in WT embryos, the epithelial flow is less important in the dorsal/distal retina, which correlates with BMP activity there, and with a dorsal gap of expression of the BMP antagonist Follistatin-a (Figure 33F). They therefore propose that repression of BMP activity – potentially mediated by *Follistatin-a*- is necessary for the flow of outer OC epithelium into the lens-facing epithelium during rim movement, in order for the neural retina to be correctly located and to achieve proper OF margins juxtaposition and OF closure (Heermann et al. 2015). The dorsal activity of BMP could prevent the nearby presumptive RPE from flowing into the lens-facing epithelium; indeed, the RPE domain adopts a different movement within the outer OC towards more proximal/prospective ventral regions before starting to engulf the neural retina (Cechmanek & McFarlane 2017).

FGFs

Picker and colleagues showed the implication of Fgf signalling in the rim movement bringing prospective temporal retina cells into the lens-facing epithelium. Indeed, upon inhibition of the Fgf receptor 1, they observe an enhanced movement of the prospective temporal cells into the lens-facing epithelium, conversely, when they implanted Fgf8 beads beneath the ventral optic vesicle (prospective temporal), they observed a delay in this movement but not an abolition as the temporal cells finally manage to reach their correct final position at 36 hpf. Their results suggest that Fgf signalling regulates the kinetics of but not in the extent of the rim movement (Picker et al. 2009).

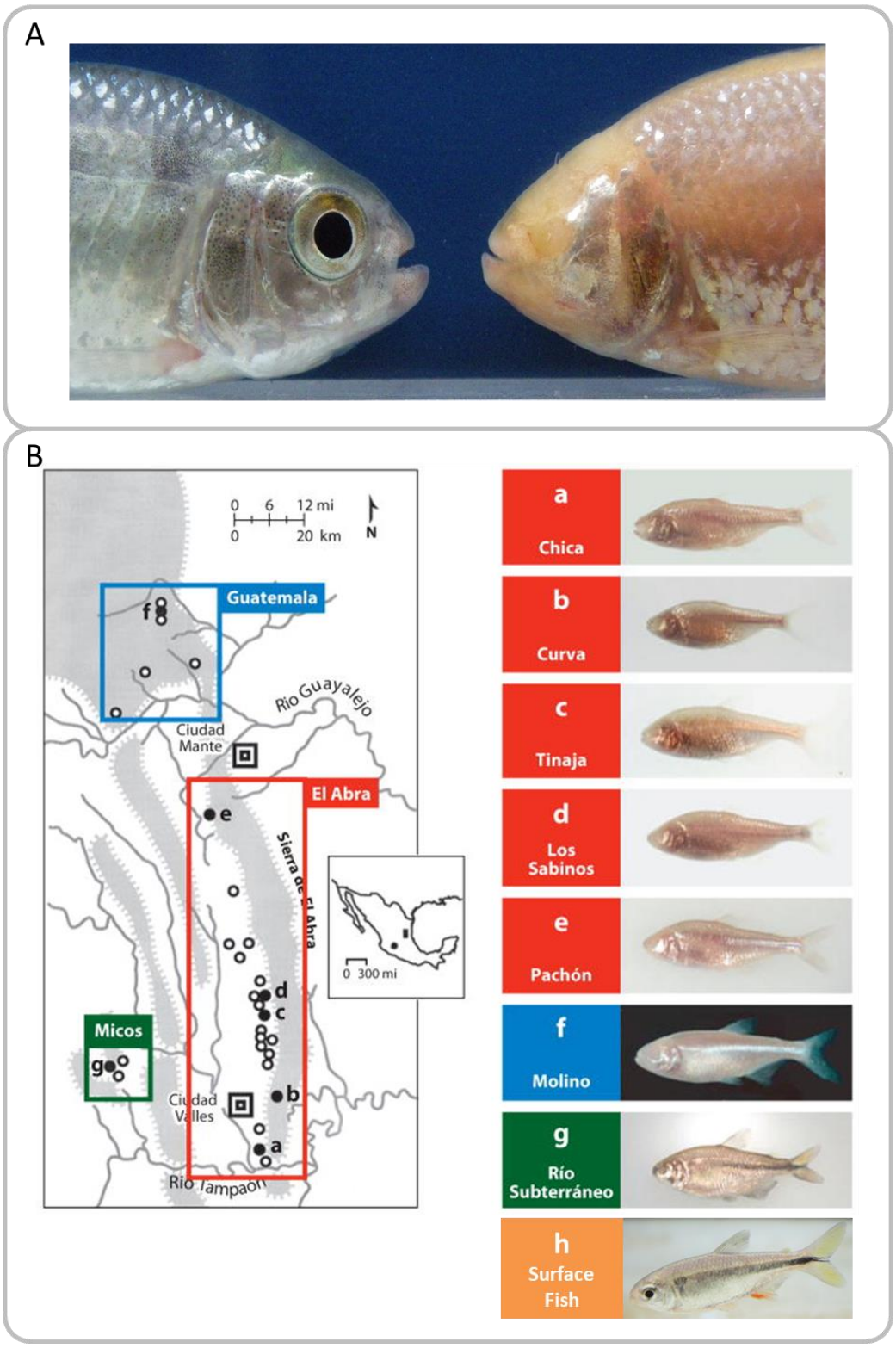

Figure 34 : *Astyanax mexicanus* : cavefish, surface fish.
(A) Astyanax mexicanus surface fish (left) and Pachón cavefish, picture by Y. Elipot and S. Rétaux. (B) *Astyanax mexicanus* populations, an example of convergent evolution. On the left, a map of the Mexican region containing the 30 known *A. mexicanus* cavefish populations. Colour squares indicate the three different regions representing 3 independent invasions. Dots indicate the cave locations; black dots associated with a letter match the individuals presented on the right panel, apart from the surface fish which is found in virtually every river of the region.
Modified from (Yamamoto et al. 2009)

5. The Astyanax cavefish

5.1. General introduction

During my Phd, I used the Mexican tetra model : *Astyanax mexicanus*. In this term we regroup both the cave-dwelling forms (CF, cavefish) which are blind and depigmented at adult stage (they develop eyes during embryogenesis that subsequently degenerate), and the surface forms (SF, surface fish) which inhabit Central American rivers and are sighted and pigmented (Figure 34A). There are actually 30 known cave populations that all seem to be interfertile with the surface population and with each other (for the tested crosses); for that reason, they are often considered a same species. However, species are a human-designed concept that finds its limits in a context of micro-evolution such as ours, where surface and cave populations but also different cave populations could probably be described as different species. In this context of small-scale evolution, I will consider all of the above mentioned fishes to be different populations of the same *A. mexicanus* species.

As mentioned, 30 caves containing *Astyanax mexicanus* species have been discovered in the Huasteca region of Mexico but many more definitely must exist and are simply less accessible or less conspicuous (as evidenced by the discovery of the "Chiquitita" cave by Luís Espinasa during our 2016 field trip, which is a simple hole under a tree in someone's garden but that contains cavefishes). These caves belong to different "Sierras" (mountain range): Sierra de El Abra, Sierra de Guatemala and the Micos area. Genetic analyses of these different populations point to two to five independent origins of the cave populations, correlated with these regions (Bradic et al. 2012). The extremely similar phenotype acquired by cave populations originating from independent invasions give a very good example of convergence (Figure 34B). One striking example is albinism : in two independent populations, Pachón from the El Abra group and Molino from the Guatemala group, the albino phenotype is linked to the loss of function of the Oca2 gene but the mutations in the two populations are different : the 24th exon is lost in the Pachón population and a few SNPs have appeared while in Molino population, the 21st exon is deleted (Protas et al. 2006).

For the rest of this manuscript, I will mostly focus on the Pachón population since this is the one we study in the team.

5.2. Origins

It is believed that an ancestral from of surface *A. mexicanus* got trapped in caves during some flooding events and managed to survive there and adapt. However, the age of the cavefish populations has been a very controversial topic in the community. Looking at the literature, dates between 10,000 and 1-2 million years are mentioned, with references to an "old" and a "new" lineage of cavefish. The approximate time after divergence between the cave and river populations has been estimated to be 525,000–710,000 years after examination of a small number of nuclear loci (Avise & Selander 1972; Chakraborty & Nei 1974), but with a very large standard error bringing the confidence interval from a few thousand years to more than a million years ago. The hypothesis of very old cave populations has been set forward by studies on mitochondrial DNA that dated the divergence to several million years ago (Strecker et al. 2004).

However recent studies by Fumey et al. (2018), on both microsatellite polymorphisms and SNPs in transcriptome sequences in cave and surface populations show a much more recent separation of the

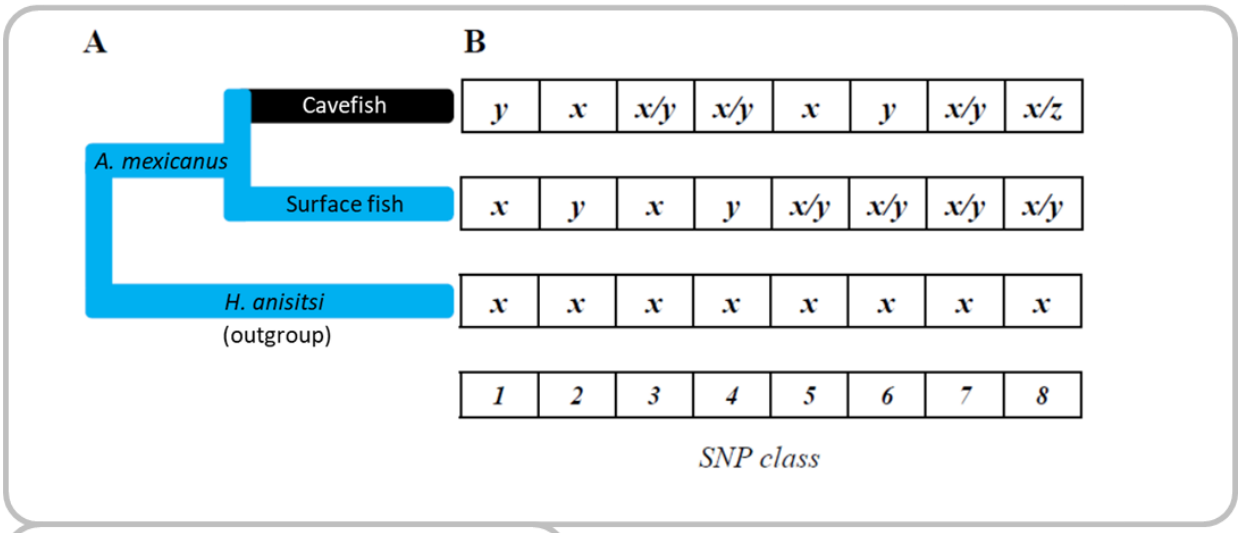

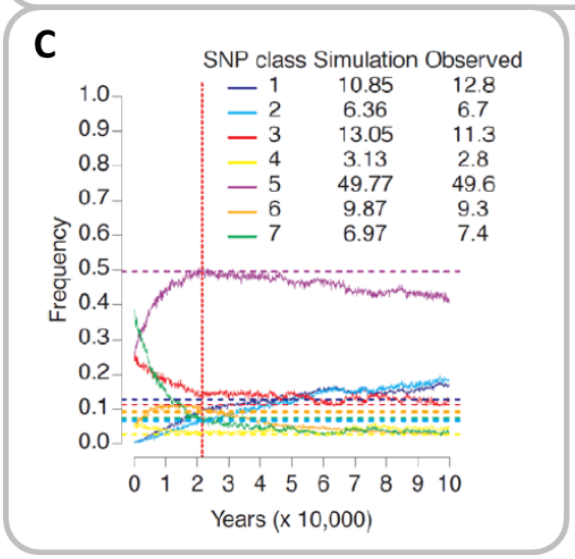

Figure 35: Population genetic through SNP analysis.
(A) Diagram of the evolutionary history of *A. mexicanus*. (B) the different classes of SNP, x, y, z are different alleles, x is assumed to be the ancestral allele, shared with the outgroup. x/y or x/z indicate a polymorphism present within a population. (C) Plot of the simulated evolution of frequency of the different SNP classes over time. Horizontal dotted lines indicate the observed frequencies. The vertical red dotted line represents the best fitting divergence time, around 20 000 years.
From(Fumey et al. 2018)

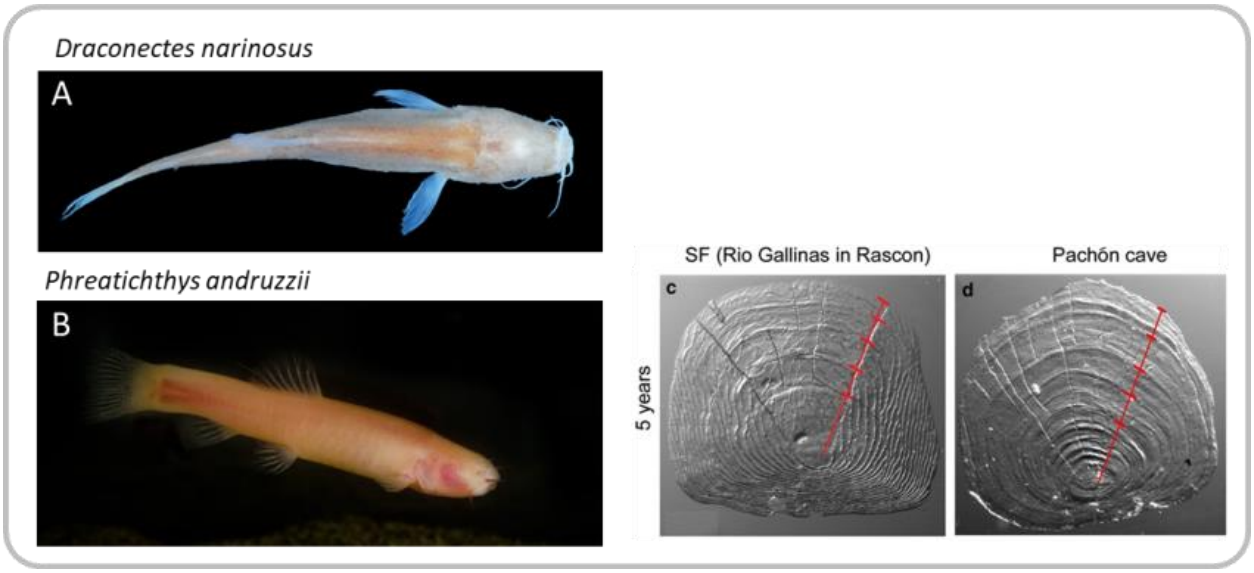

Figure 36 : Cavefishes and scales.
(A, B) Two examples of scale-less cavefishes. (C, D*) A.mexicanus* scales, comparison between surface fish and cavefish.
(Simon et al. 2017; Kottelat 2012; Fumey et al. 2018), Phreactichthys picture from Luca scapoli.

surface and cave populations, ranging from 1,000 to 30,000 years. Indeed, in their microsatellite study, they used a simulation program that allows the estimation of effective population sizes (ie, the number of individuals in a population who contribute offspring to the next generation), migration rates and divergence times from the dataset, depending on the mutation rate assumed. The effective population size estimated was 150 for Pachón cavefish and around 11,000 for surface fish, the migration rate was very low and the divergence time was estimated around 5,000 years. Similar divergence times were found with this method for 6 caves, ranging from 1,000 to 10,000 years.
They confirmed this analysis for the Pachón cave by looking at SNPs from cave fish and surface fish transcriptomes. Indeed, in this second approach, they simulated genetic drift in time for two separated populations and an outgroup with different parameters of migration and population size; from these simulations, they retrieved the frequencies of diverse "situations" (8 different in total) across time, such as "derived allele fixed in CF, ancestral allele fixed in SF"(SNP class 1, Figure 35B), "polymorphism in CF, fixed derived allele in SF" (SNP class 4), or "shared polymorphism between CF and SF" (SNP class 7). They then examined the correspondence between the observed frequencies from the transcriptome dataset and the simulated values obtained at each time point and for each set of parameters. The best fits they obtained were around 20,000 years (Figure 35 C) and the fit was decreasing with increased time of divergence, confirming their previous analysis on microsatellites and the idea that the cave colonization by surface *A. mexicanus* is very recent (Fumey et al. 2018).

These findings are in rupture with the previous assumption of an old and new lineage since Pachón, which was supposed to belong to the "old" lineage, seems to have a very recent origin. This seems consistent with the moderate degree of troglomorphism of the *A. mexicanus* cavefish, which for example still possesses scales even if slightly smaller (10% smaller than surface fish)(Figure 36 C, D), while many other cave fishes such as the Somalian cavefish (*Preatichtys andruzzii*) or the Halong bay cavefish (*Draconectes narinosus*) have lost theirs, potentially due to lower predation in caves(Figure 36 A, B) (Simon et al. 2017; Kottelat 2012; Wilkens & Strecker 2017). Similarly, Pachón cavefish do not exhibit many loss-of-function mutations of eye-specific genes such as crystallins or opsins, which would be expected in old cave population since these genes are probably not under selection anymore in the absence of light and vision (Hinaux et al. 2015; Fumey et al. 2018).

5.3. Cave environment

The cave environment is primarily characterized by total and permanent darkness so that the main challenges of the cavefishes are probably to find food and mates in the dark. Indeed, if food is readily available at the surface with smaller fishes, insects or animal and vegetal debris falling in the water, the darkness of the caves implies no photosynthesis and no primary production there. This has strong consequences in terms of food availability, so that cave organisms depend on organic material transported inside the caves by animals or water, making different caves probably very different environments, offering very different types of resources to the cavefish living there. As a matter of fact, different caves can harbour very differently-sized bat colonies, if any; for example Subterráneo cave barely hosts any bats, while Pachón cave has a few and Chica cave possesses a very large colony, hence a very different amount of guano available for the fish. Also, the topological situation of caves can have a strong impact in terms of organic material input; for example Subterráneo's entrance is a hole, located between flat fields of sugar cane so that floods during the rainy season can bring vegetal and other organic debris along with other fishes, therefore providing an important but sporadic food source. Of note, the flooding of the Subterráneo cave also bring surface fish that breed with the residing cavefish there, resulting a various mix of phenotypes due to repetitive hybridization. On the contrary, Pachón is a

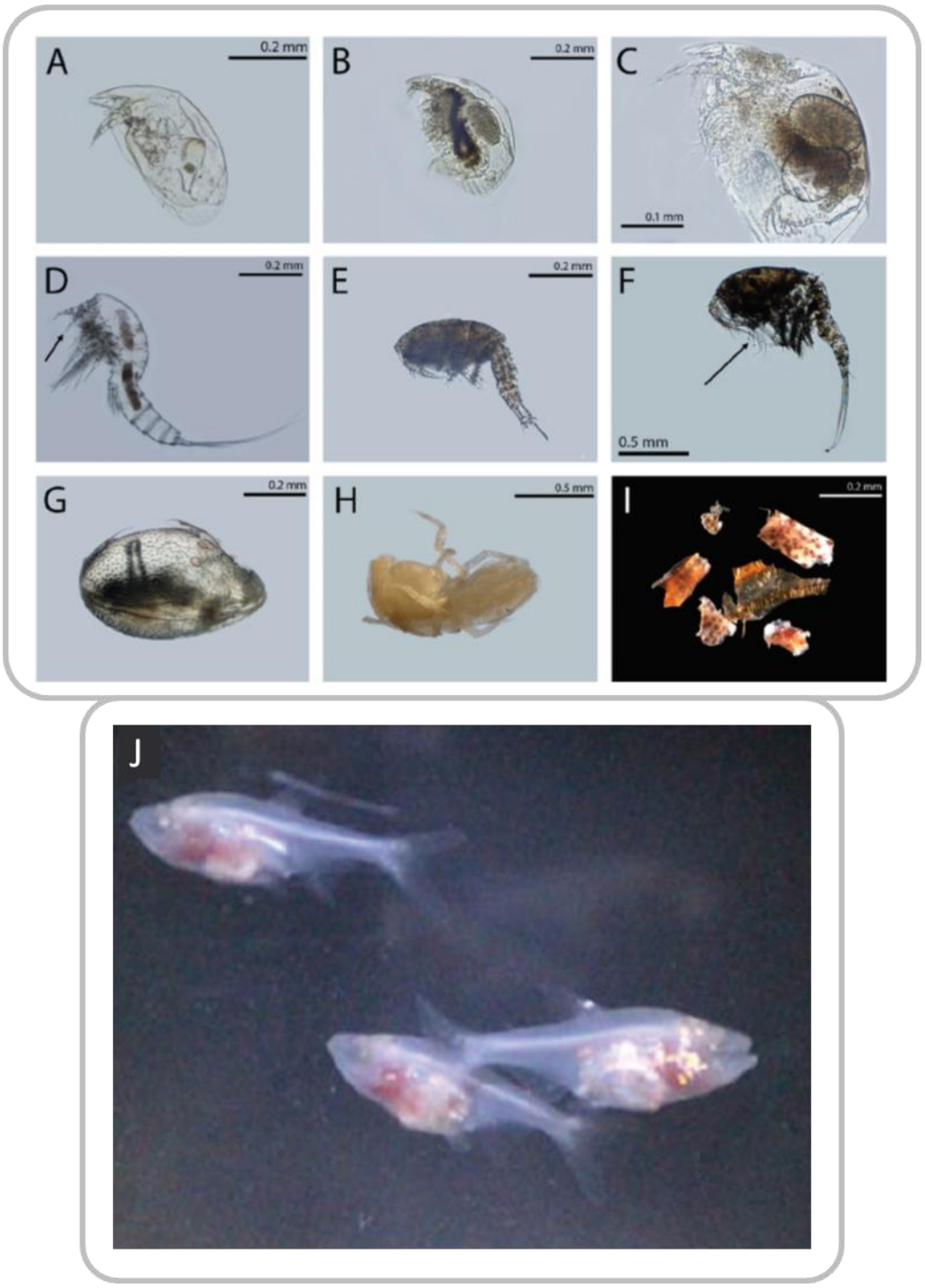

Figure 37 : Cavefish meal, what's on the menu in the cave ?
(A-I) Gut content of young Pachón fry. (A-C) Water fleas, (D-F) copepods, (G) ostracod, (H) isopod, (I) pieces of arthropods. (J) Young Pachón cavefish, note their visibly full stomachs.
(Espinasa et al. 2017)

perched cave where probably very little organic debris are brought by the rainy season suggesting a possibly less important but more stable food source relying mostly on bats and arthropods entering or living in the cave (Elliott 2016; Espinasa et al. 2017). Also, the isolation of Pachón prevents surface fish from entering and mixing with this cave population.

The question of what cavefish eat is paramount in order to make well-grounded hypotheses on the adaptive value of traits examined; therefore, several studies tackled that question. It was found that adult cavefish from Chica cave fed mostly on bat guano but also on parasites from the guano, insects and various arthropods, flood debris, other fishes and dead bats (Elliott 2016). In Pachón, the stomach content of adult fishes was mostly composed of "gunk" and debris of insects, consistent with feeding on insectivorous bat guano; their stomach content also consisted in soil detritus and a few insects. In this study, the gut content of juvenile cavefish fry was also analysed; it was mostly composed of arthropods and especially water flies that were still identifiable, suggesting that they were hunted and ingested alive rather than scavenged while already dead (Figure 37)(Espinasa et al. 2017).

Other parameters strongly differ between the surface and the cave environments such as the presence of predators and, the temperature or the conductivity of the water. Indeed, in most caves, no predators of fish were found, although we have personally witnessed crayfishes in Subterráneo cave. As a general rule, the temperature in caves is relatively stable and often corresponds to the average annual temperature of the region, while some little ponds where surface *Astyanax* fishes are found can exhibit drastic variations in temperature across the year. In terms of conductivity, which reflects to some extent the ionic concentration of water, the conductivity in rivers is often very high (around 1200µS) while that of ponds and caves is often much lower (around 500µS) during the dry season. During the rainy season, the conductivity of rivers is supposed to drop due to the nearly null conductivity of the rain, triggering large variation of conductivity.

All these parameters contribute to make the change in environmental conditions sustained by surface fishes falling into the caves very drastic. It is therefore very interesting to note that despite the large variety of fishes living in the nearby rivers (cichlids, cyprinids, swortails…), only *Astyanax mexicanus* are found living in the caves, suggesting a possible advantage of this species in dealing with such a drastic change.

5.4. Mechanisms of evolution and loss of the eye

5.4.1. Initial settlement

Why did *Astyanax* outmatch other fish species in colonizing the caves ? We do not have the answer to that question but it is worth noting that *Astyanax mexicanus* are very robust and generalist fishes that are found in various environments from large flowing rivers to puddles with a pH of 9.7, and that have a quite omnivorous diet. Also, *Astyanax* surface fish naturally reproduce at night, indicating that the presence of light is not necessary for their courtship and mating behaviour, which could allow them to reproduce in the cave while species relying on a visually-driven courtship/mating behaviour would not. Plasticity could also play a role in a quick adaptation at the level of the individual, so that fish displaying a stronger phenotypic plasticity at the first or second generation could gain advantage on their competitors; for example, *Astyanax* surface fish raised in the dark are able to smell at least 10 times less concentrated food odours than their counterparts raised in normal light/dark conditions (Blin et al. 2018); if this is not the case in other fishes, it could be a remarkable advantage for *Astyanax*.

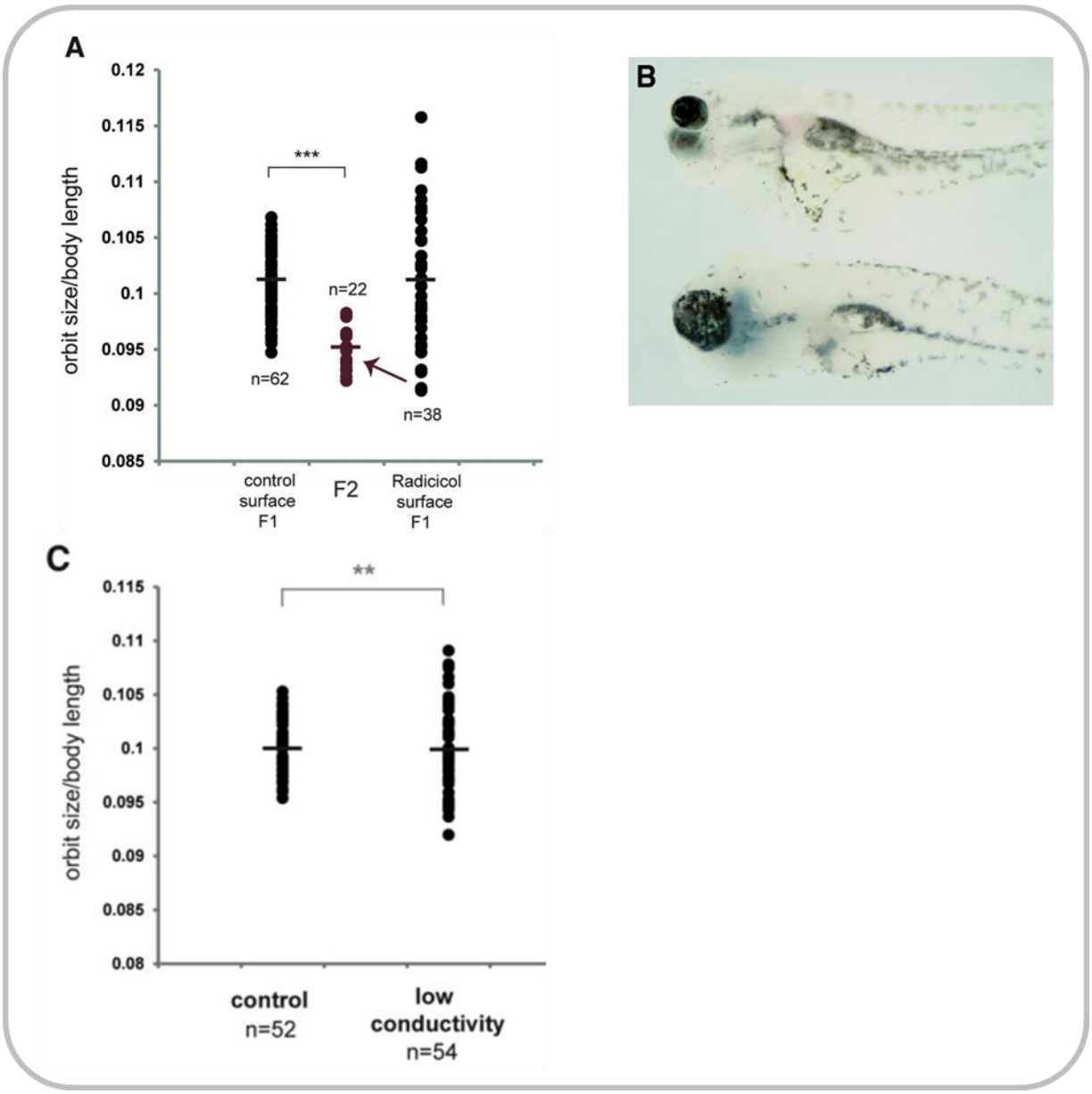

Figure 38 : decanalization, revealing the cryptic variation.
(A) Normalized orbit size. Left, WT surface fish (control surface F1). Right, surface fish treated with the HSP90 inhibitor (radicicol), observe the identical average size but the increased variation. Middle, offspring of radicicol-treated SF that were selected for their small eyes and bred. Note the decrease in average orbit size. (B) Radicicol-treated surface fish embryos displaying a strong variation of eye size. (C) Normalized orbit size of WT surface fish or SF raised in low-conductivity water. Fishes raised in low conductivity conditions display more important variations of eye size.
From (Rohner et al. 2013)

5.4.2. Evolution in the caves

The very recent origin of the *Astyanax* cavefish suggests that very few *de novo* mutations had time to appear and be selected for, pointing to a rather important role of selection from the standing genetic variation. By standing genetic variation, we refer to the mutations and polymorphisms that were already present in the ancestral surface population, before they got trapped in the caves. Selection through standing genetic variation can be achieved in two ways, either by selecting alleles that readily produced a phenotype even before entering the caves, or by selecting alleles from "cryptic variation" after decanalization.

"Canalization" describes a process that stabilizes or buffers a phenotype against genetic variation, meaning that the effect of a particular mutation could be silenced. For example, a mutation causing an alteration in protein folding could be silenced if chaperones forced the mutated protein to fold normally. Therefore, while canalization is active, these mutations could not be selected for or against and would constitute a pool of cryptic genetic variation. Upon exposure to a new environment or a stress, these mutations would become visible and be subjected to selection. These ideas were formulated and evidenced by Waddington; he found a *Drosophila* strain that had normal wing vein patterns when raised in normal conditions, but this same strain would produce a proportion (about 1/3rd) of adult flies with a defect in wing vein pattern if submitted to a heat shock during development. He selected for this defect over a few generations raised with a heat shock and managed to reach almost 100% of flies presenting the wing vein phenotype; but the most surprising is that when he raised these selected flies in normal conditions again (i.e., without the heat shock), the vein phenotype remained. It had been "genetically assimilated" (Waddington 1953). Heat shock proteins such as HSP90 play a role as chaperone proteins and were shown to be involved in the canalization process by experiments on flies where inactivation of this protein increased the phenotypic variation observed. Similarly to the previously described experiment, these phenotypes could subsequently be selected for (Rutherford & Lindquist 1998).

Recently the same mechanism was investigated in *Astyanax* by Rohner and colleagues, who wanted to see if cryptic genetic variation could play a role in cave adaptation and if surface fish possessed indeed a pool of cryptic alleles.
They raised *Astyanax* surface fish with an inhibitor of HSP90 and obtained an increased variability in some phenotypes. In their study, they focused on the eye size for which they used orbit size as a proxy. The average normalized eye size was similar in treated and in control surface fish but the variation was much more important in treated fishes, indicating that both larger and smaller eyes had appeared (Figure 38 A, B). They selected fishes with smaller eyes and bred them; the offspring were raised in normal conditions, without inhibition of HSP90, yet they still displayed a reduced eye size (Figure 38C). To my knowledge the question of how the phenotype is then expressed in the following generations without the need for HSP90 inactivation has not been solved yet. Anyway, these data show that there is indeed a pool of cryptic alleles whose effects are revealed when HSP90 is inactivated. They then sought to find what could trigger such decanalization upon switching to cave environment. Different stressors are supposed to be able to trigger the titration of the HSP90 pool because of stress-induced damage caused to many proteins. In the caves, the parameter that appeared to them as a potential stressor was the low conductivity; they therefore raised surface fishes in low-conductivity conditions. In these fishes, heat-shock response genes were up-regulated and a similar increase in eye size variability was present. Thus it was suggested that the new cave environment in which ancestral surface fish got trapped could have generated a stress sufficient to trigger decanalization, therefore revealing the standing cryptic genetic variation and allowing natural selection to act on these new and various phenotypes. Upon this scenario, advantageous alleles could quickly be selected for and allow for a faster adaptation to the new environment than "waiting for" *de novo* mutations (Rohner 2016; Rohner et al. 2013).

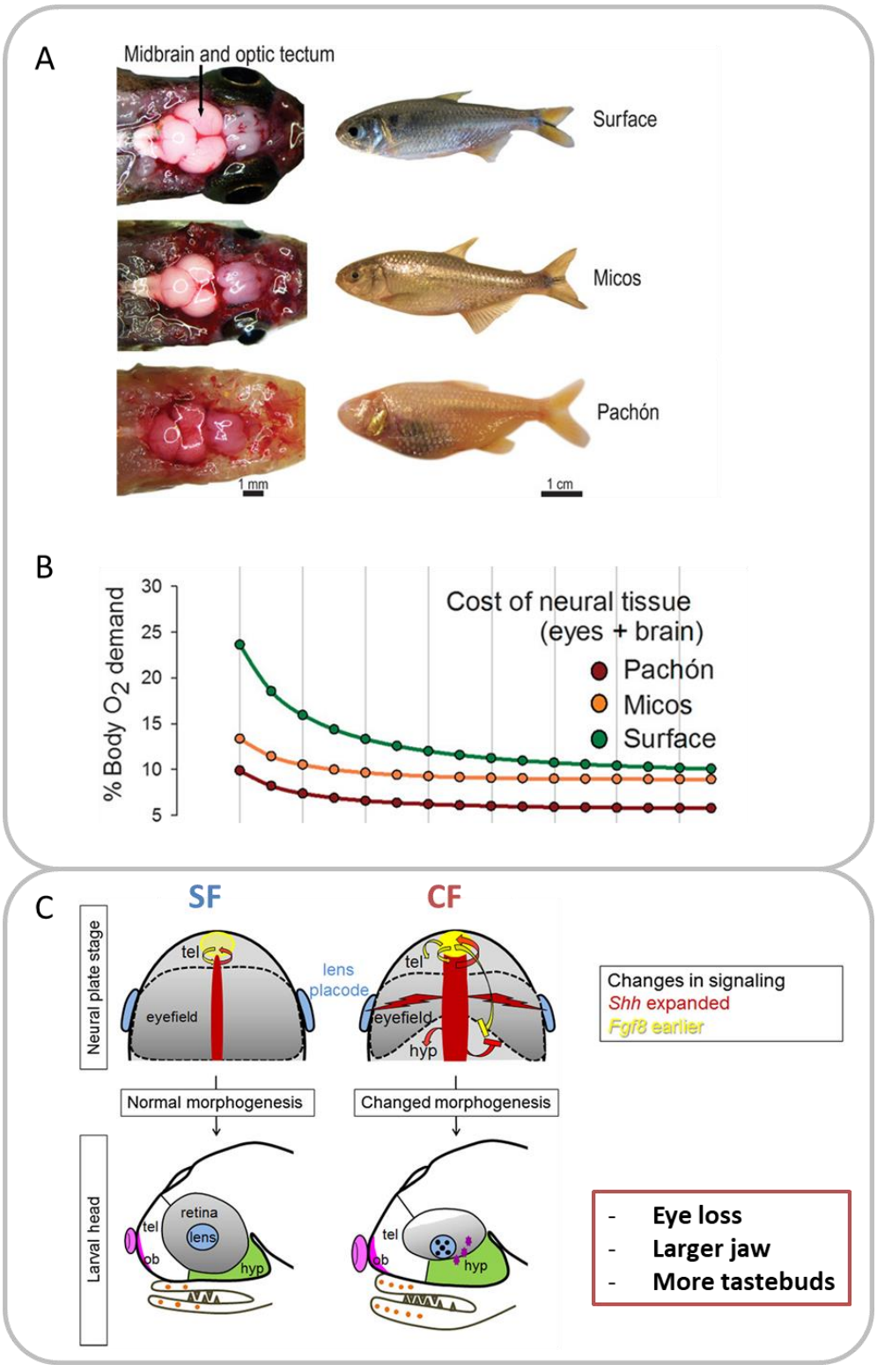

Figure 39 : Eye loss and evolutionary mechanisms.
(A) Brain anatomy of the surface and 2 cave populations : Micos and Pachón. The surface fish has large eyes and a large optic tectum; Micos cavefish have small eyes and an intermediate size of tectum; Pachón cavefish have no eyes and a small tectum. (B) Energetic cost of the neural tissue of these populations, the O_2 consumption decreases with the eye and tectum size allowing cavefis to save energy. (C) Diagram summarizing the pleiotropic effects of the increase of Shh signalling.
From (Rétaux & Casane 2013; Moran et al. 2015)

5.4.3. Why did cavefish lose their eyes ?

The eye loss is one of the most obvious phenotype of the *Astyanax* cavefish but also of many other cavefishes and animals. Several hypotheses can explain this phenotype : 1) the disuse of the eye in the dark could result in a relaxed selection compared to surface environment where eyes are indispensable. Such absence of selection would allow for a slow accumulation of random mutations, including loss-of-functions mutations, in eye genes that would ultimately result in the loss of visual function. 2) The presence or size of the eye could be under direct negative selection. Indeed, eyes are very energy-consuming organs, especially in the dark, and one could easily imagine that lower energy consumption could be advantageous in cave where the nutrient availability is reduced compared to surface environment. 3) Another possibility is an indirect selection of the eye loss through pleiotropy, meaning that the set of genes responsible for the eye loss could be responsible at the same time for a different phenotype that would provide a selective advantage in caves. These different possibilities are not mutually exclusive and the complete loss of eyes could be due to a combination of these (Rétaux & Casane 2013).

If the eye size was simply neutral, one would expect various mutations accumulated in the cave, to influence the eye size in both ways, towards bigger size and smaller size. Some quantitative trait loci (QTL) analyses have demonstrated that it was not the case and that all cavefish loci associated with eye size tended to decrease it (Protas et al. 2007).This indicates that the reduction in eye is probably under some kind of selection; on the other hand, eye-specific genes that are necessary only for the eye function are probably not under selection anymore.

Concerning direct negative selection, the loss of eyes and reduction in optic tectum size in the cavefish has been proven to reduce the amount of resource used for neural tissue. Indeed, the energetic cost of neural tissue (retina plus brain) for 1g fishes represent 23% of the resting metabolism of a surface fish but only 10% for the Pachón cavefish. Furthermore, the authors of this study calculated the global cost of vision to be equivalent to 15% of the resting metabolism for 1g fishes, evidencing a clear freeing of resources through the loss of eyes (since the energetic cost of neural tissue/weight of neural tissue stays the same across populations) (Figure 39 A, B)(Moran et al. 2015).

The eye degeneration has been linked to an increase in Shh signalling which also triggers an increase in tastebud number and jaw size (Yamamoto et al. 2009) and olfactory organ (Hinaux et al. 2016), therefore, the eye loss could also be indirectly selected for because of pleiotropic effects (Figure 39C).

5.5. Eye development and loss

If the adult cavefish does not have eyes, the embryo first develops them. Cavefish eyes develop relatively normally until 25hpf when the lens starts entering apoptosis (Jeffery & Martasian 1998). The lens then induces retinal apoptosis at 2 dpf (Langecker et al. 1993; Yamamoto & Jeffery 2000) which results in eye degeneration so that only a tiny eye cyst remains at adult stages. This eye degeneration was shown to result at least in part from an increase in Hh signalling at the midline (Yamamoto et al. 2004).

5.5.1. Morphogens

Very early in development, the cavefish already displays subtle modifications of morphogens expression that were shown to have strong developmental effects. Indeed, it was shown that from early neural plate stage onwards, midline signalling is enhanced in the cavefish population as *Twhh* and *Shh* expressions are expanded laterally and anteriorly (Figure 40 A-E). This modification has dramatic effects on the eye and

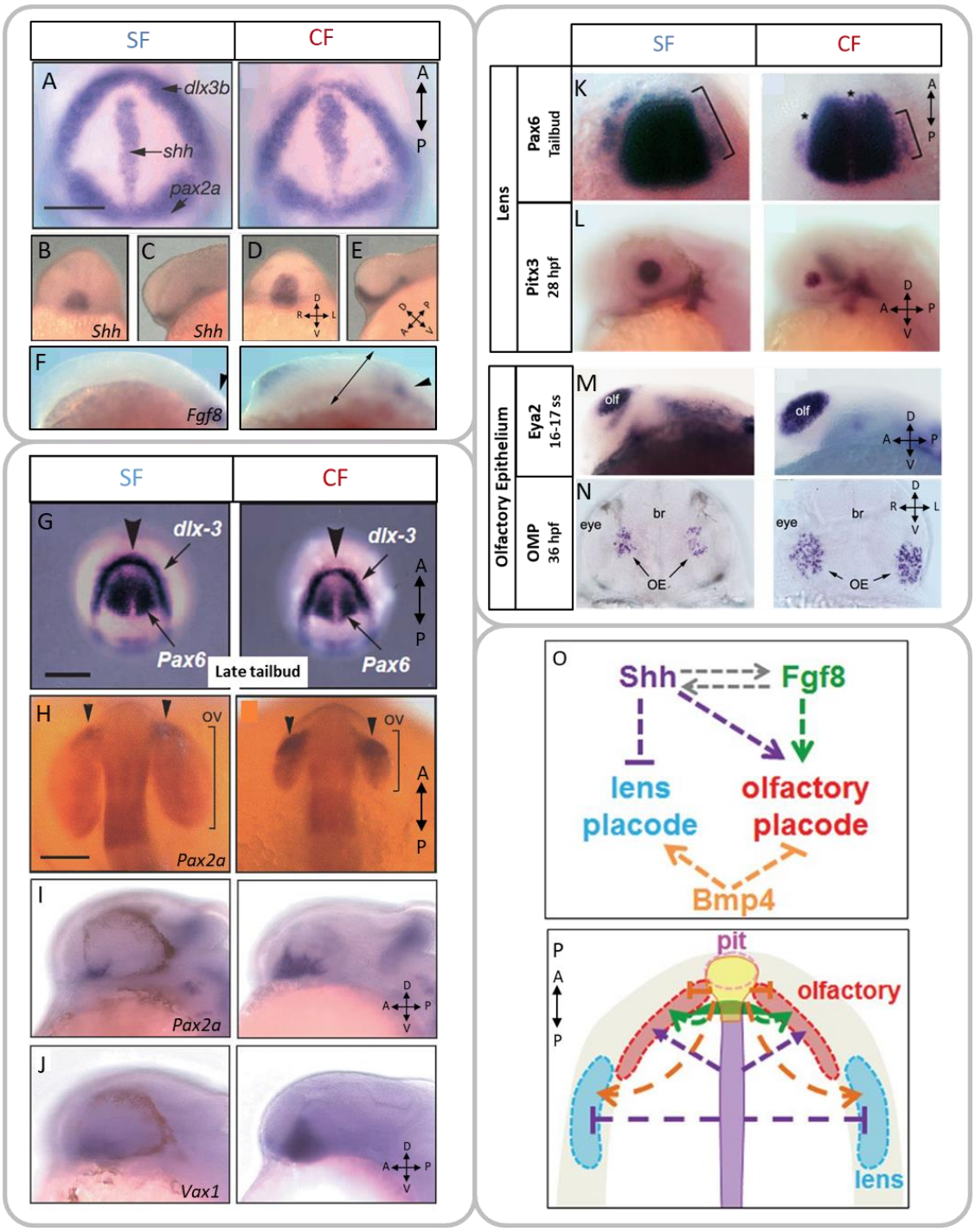

Figure 40 : Signalling modifications and their effects during optic vesicle/optic cup stages.
(A-F) *Shh* expression is enlarged at the midline (see A) and anteriorly (see B-E) in the CF. *Dlx3b* delimitates the anterior neural plate, *Pax2a* is expressed in the midbrain-hindbrain boundary. (F) At 10 hpf, *Fgf8* is expressed in the CF but not in the SF.(G-J) Modifications of OV patterning in the CF. (G) *Pax6* expression is lacking anteriorly in the CF. (H, I) The OV size is reduced, *Pax2a* expression is enlarged. (J) *Vax1* expression is enlarged. (K-N) Modification of placodal patterning. (K) The light peripheral *Pax6* staining labels the presumptive lens (brackets) which is smaller in the CF, consequently, the lens stays smaller at later stages (L). Conversely, the olfactory placode (olf) (M) and the later olfactory epithelium (oe) (see N) are larger in the CF. (O) Summary diagram of the impact of various morphogens on the placodal patterning. (P) Same interactions represented in a schematic neural plate.
From (Yamamoto et al. 2004; Hinaux et al. 2016; Strickler et al. 2001; Pottin et al. 2011)

brain development (Yamamoto et al. 2004). Fgf8 signalling in the anterior neural ridge was also shown to differ between the two populations as its expression starts two hours earlier in the cavefish ANR (at 10hpf - tailbud) than in the surface fish (12hpf – 5/6 ss)(Figure 40F). This last modification was proposed to be due to the previous Hh enhancement as Hh inhibition inhibits *Fgf8* expression in the ANR of the cavefish. Reciprocally, Shh anterior expansion is dependent on Fgf signalling as FgfR inhibitor treatment between 8hpf (80% epiboly) and 12 hpf (5-6 ss) in order to mimic the surface fish signalling produced a SF-like reduction of *Shh* expression anteriorly. This effect was even stronger if the treatment was applied from 6hpf (shield stage) suggesting an additional role for another Fgf such as Fgf3 (Pottin et al. 2011). One last morphogen expression has been shown to differ slightly between CF and SF : *BMP4* seems to be expressed more posteriorly within the prechordal plate in the cavefish (Figure 40 O, P)(Pottin et al. 2011; Hinaux et al. 2016).
It is worth noting that, if the *Fgf8* and BMP4 phenotypes have only been investigated in the Pachón CF population, the *Hh* phenotype was found also in Los Sabinos and Chica populations, which live in the same Sierra than Pachón.

5.5.2. Neural plate patterning and early eye development

If we compare the early anterior neural plate patterning between surface and cavefish embryos, some modifications are already visible. In the ANP of surface fish embryos, the eye-specific gene *Pax6* is expressed bilaterally in the eye field and extends across the midline anteriorly, but in the cavefish, Pax6 domains are reduced and leave an anterior gap of expression so that they are not joined at the midline (Figure 40G). Later on, the OS marker *Pax2a* and the OS and ORR marker *Vax1* expressions are both expanded in the optic vesicle and later optic cup, evidencing a shift towards proximal fate in the OV (Figure 40 H-J). Strikingly, the *Pax6* phenotype is similar in Los Sabinos and Curva cavefishes. These early patterning modification seem to be linked to the Hh midline signalling modification (Strickler et al. 2001; Yamamoto et al. 2004).

If we now focus on the placodes at early stages (tailbud-early OV), it has been shown that in the cavefish, the lens placode is shortened while the adjacent and anterior olfactory placode that will give rise to the olfactory epithelium is enlarged. These modifications persist later on and at 36hpf it is still possible to observe a larger olfactory epithelium primordium and a smaller lens in the cavefish (Figure 40 K-N). These modifications have been linked to several morphogens such as Shh, Fgf8 and BMP4. Shh and Fgf8 were proposed to promote olfactory fate in the placodal field while Shh would repress the lens fate. Conversely, it was suggested that BMP4 promotes the lens fate while repressing the olfactory fate (Hinaux et al. 2016). However, the small size of the CF lens is not responsible for its degeneration as evidence by partial laser ablation of the lens in a surface fish, which does not trigger lens apoptosis (Hinaux et al. 2017).

5.5.3. Optic cup and late eye development

The cavefish eye begins by forming quite normally, despite evaginating shorter optic vesicle and forming smaller lens, but as development proceeds differences become more obvious. Indeed, when the optic cup is formed, a reduction of its ventral part and/or an enlarged optic fissure (coloboma) is seen in most cavefish of Pachón but also of Tinaja and Curva populations (all from El Abra group). This defect can be rescued by inhibiting Fgf signalling from 8 to 12 hpf in CF, thereby mimicking the surface fish signalling. On the contrary, a similar ventral reduction can be obtained in SF injected with *Shh* mRNA, which simultaneously produces an expansion of *Vax1* expression and a shorter OV (Jeffery et al. 2003; Pottin et al. 2011; Yamamoto et al. 2004).

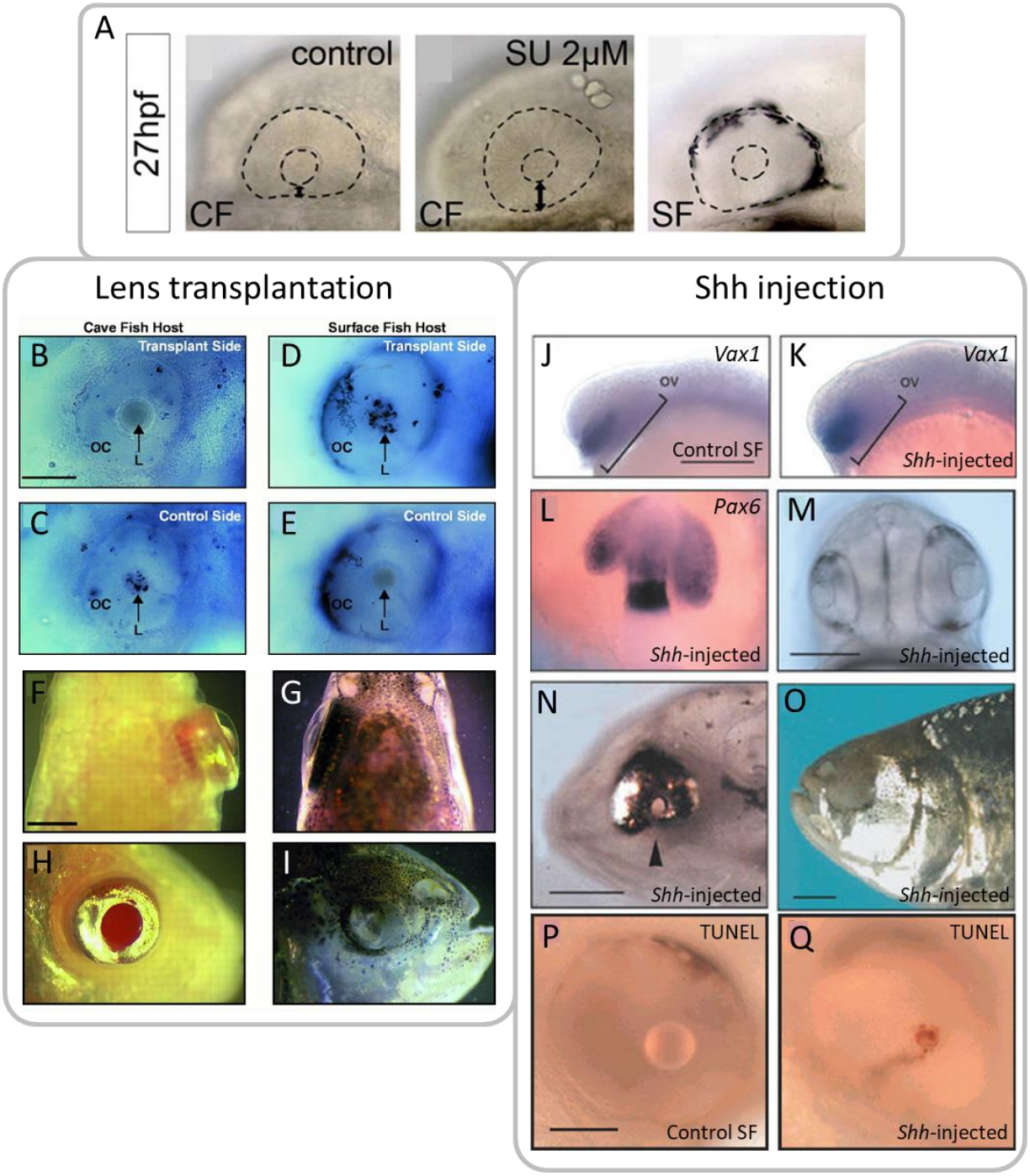

Figure 41 : Coloboma and eye degeneration.
(A) The CF displays a severe reduction of the ventral quadrant of the retina compared to the SF. Upon Fgf8 inhibition from 8hpf to 12 hpf (SU 2µM), the ventral retina is restored. (B-I) The lens is responsible for the eye degeneration. Lens grafts from a SF into a CF optic cup (B, F, H) and from a CF into a SF optic cup (D, G, I). (B-E) are TUNEL labelling, showing apoptosis, the transplanted SF lens survives in the CF eye (B) while the CF lens in the SF eye still undergoes apoptosis (D). (C, E) Non transplanted control from the same embryos. (F, G) Dorsal views of the resulting adult fishes, transplanted side on the right, the cavefish eye is restored while the SF eye is regressed after lens graft. (H, I) Lateral view of the transplanted side. (J-Q) Shh injections in SF mimic the CF eye phenotype. (J, K), Shh-injected SF have a larger expression of Vax1. (L, M) Reduce OV and OC sizes. (N) Reduction of the ventral retina. (O) Some injected fishes lose their eyes. (P, Q) Shh mRNA injection triggers apoptosis in the lens of a SF.
From (Yamamoto et al. 2004; Yamamoto & Jeffery 2000; Pottin et al. 2011)

Other defects have been noted in the cavefish eye : although the proliferation and formation of retinal layers occurs close to normal (which suggests that the retinal tissue is quite healthy in CF), the retinal differentiation is delayed and only a few rods appear; the lamination of the retina is disorganized and the cornea and iris are not induced or enter apoptosis and never form (Figure 42) (Jeffery et al. 2003; Strickler et al. 2007; Jeffery & Martasian 1998; Alunni et al. 2007).

Regarding the lens, its degeneration was proposed to be triggered by the expansion of Hh midline signalling, as *Shh* mRNA injection in a surface fish embryo results in an apoptotic lens (Figure 41 J-Q) (Yamamoto et al. 2004). The lens is then responsible for the retinal degeneration, as evidenced by graft experiments where the lens of a 22 hpf SF was transplanted in the optic cup of a CF. This transplanted lens did not undergo apoptosis and was able to rescue the eye in the cavefish until adult stages (Figure 41 B-I). Furthermore, it rescued the lamination of the retina, induced the formation of the cornea and iris and provoked an increased growth of the contralateral optic tectum (Yamamoto & Jeffery 2000; Jeffery et al. 2003; Strickler et al. 2007). Yet, this eye was suggested to be non-functional as rescued CF did not show any place preference in a tank split into light and dark compartments (Romero et al. 2003). This absence of vision could be due to mutations in genes involved in eye function.
In the reciprocal case of a CF lens transplanted in a SF eye, the CF lens still enters apoptosis, showing that the apoptosis induction takes place earlier. Furthermore, this graft leads to a small and disorganized retina without iris, cornea or pupil. The fact that there is no retinal apoptosis when a CF lens is grafted in a SF optic cup was interpreted as follows: in order for the retina to survive, it must receive two different survival signals, one from the lens and one from another signalling center, possibly the RPE (Figure 41 B-I) (Strickler et al. 2007; Jeffery et al. 2003).

Langecker described eye development in Piedras cavefish (El Abra group) in 1993; he wrote that the growth and differentiation of the retina is similar to that of a surface fish until 65 hpf, when the eye diameter stops growing. This is associated with a delayed differentiation and retinal cell death which was also shown to occur along the optic stalk (Langecker et al. 1993; Alunni et al. 2007). An interesting fact is that in 3 month-old (young adult) Pachón fishes, the CMZ is still present and functional so that new cells are produced there; however, they fail to survive and undergo apoptosis so that there is not net growth of the eye (Figure 42)(Strickler et al. 2007).

5.5.4. Sensory compensations

In many animals, when a sensory system is lost or diminished, it is compensated for by other senses so that the animal can still find food, mates and avoid predators. In the case of the cavefish, several sensory compensations to the lack of visual modality have been found that make the cavefish more efficient at finding food in the dark compared to surface fish. Indeed, surface fish rely mostly on their sight to hunt or forage, and in a dark environment, their efficiency is much reduced. A food-finding competition experiment was performed, where 6 CF and 6 SF where put in the same tank, in a dark room. One after the other, pieces of beef heart were put in the tank and Kathrin Hüppop watched with infrared night-sight apparatus which fish would find the meat. She observed that in 80% of the cases, CF caught the meat, while SF would only manage to get the remaining 20%. This shows that cavefish are better adapted to find food in the dark, either due to improved sensory modalities or to a better foraging technique, or both (Hüppop 1987).

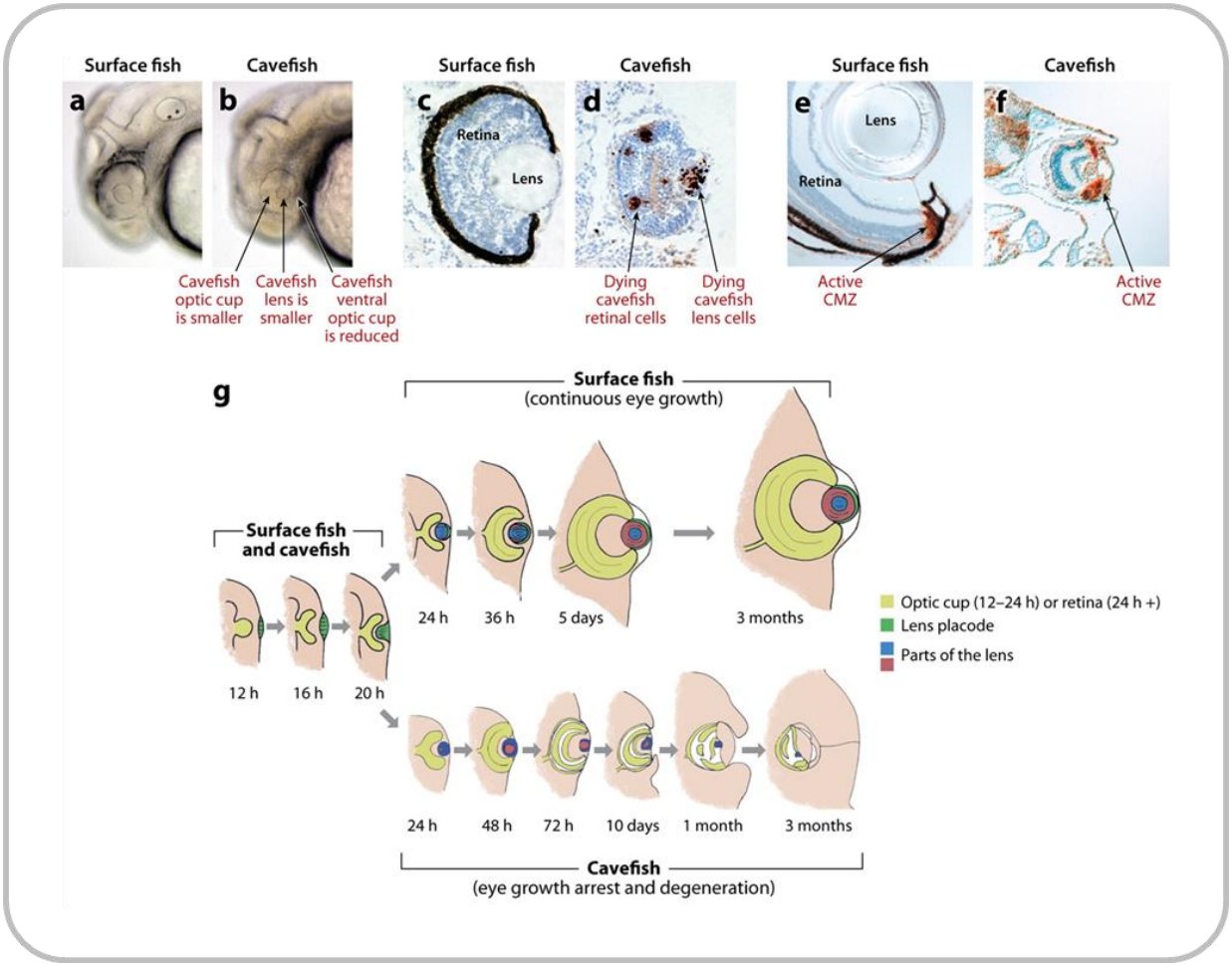

Figure 42 : Summary of eye development and differences between cavefish and surface fish.
(a, b) The lens and optic cup of the CF are smaller; the ventral quadrant of the OC is reduced. (c, d) TUNEL assay showing apoptosis in the CF lens and retina at 2 dpf. PCNA labelling showing the actively cycling cells in the CLZ of both the SF and CF at 10 dpf. (g) Diagram showing the events of *Astyanax* eye development and degeneration. Left, early development of the eye primordium seems similar in SF and CF until approximately 1 dpf. Top, in SF, the eye differentiates and the eye grows. Bottom, in CF the eye primordium grows for a while, then arrests, degenerates, and is internalized by overgrowth of the body.
From (Jeffery 2009)

In the cavefish, several sensory modalities have been found to be enhanced. A first example is the increased number of tastebuds present on the face and lips of the cavefish. This increase was linked to the increased Hh signalling in the cavefish (Yamamoto et al. 2009).

5.5.5. Olfaction

The olfactory modality has also been shown to be enhanced in the cavefish. Indeed, behavioural experiment on 1 month-old fishes showed that CF larvae are able to smell 100,000 times more diluted food-related odours than SF larvae. This tremendous improvement of the CF olfactory capacities is certainly not solely due to plasticity, even if SF raised in dark conditions smell at least 10 times more diluted odours (their precise detection threshold still needs to be established). As I mentioned earlier, the olfactory placode of the cavefish is larger than that of the surface fish and this difference is maintained throughout development so that 1 month-old CF possess larger nostrils than SF (Hinaux et al. 2016). But a larger nose does not necessarily mean a better olfaction, as proven by experiments with fishes presenting a larger olfactory epithelium such as older (2 mpf) surface fishes or F1 hybrids. Indeed older fishes have a larger olfactory epithelium, both in absolute size and in relative size normalized to their body length, but none of these fishes with larger noses were able to smell better than the regular 1 mpf surface fish (Blin et al. 2018).

In order to better understand the cause for CF enhanced olfaction, further studies on the neuronal composition of the cavefish olfactory epithelia were performed by our team. Indeed, there are several different neuronal types in the olfactory epithelium and each is specialized in the detection of one type of odour such as social cues, food-related odours or sexual pheromones. They found that in the cavefish, the microvillus cells that are responsible for detecting alimentary odours are present in a higher density in the CF olfactory epithelium while the ciliated cells that respond to social cues are in a lower density compared to SF (Blin et al. 2018). This increase in density, associated with an increased size of the olfactory epithelium results in a much more important pool of food-smelling neurons, which could activate more efficiently the central integrating centers, therefore eliciting a stronger response even in the case of lower concentrations.

5.5.6. Vibration attraction behaviour and neuromasts

Another sensory modality that is specific to some aquatic vertebrates such as fishes or frogs is the lateral line and neuromast system. It is a sensory system that allows the perception of water movements and pressure changes in the water. The neuromasts are the sensory structure of this system and are composed of several mechano-sensory hair cells, whose hair bundles protrude out of the skin and are covered by a gelatinous case that forms the cupula (Figure 43A). This system is composed of two different types of neuromasts, those present either directly on the skin, called the superficial neuromasts, and those standing in fluid-filled canals that are open to the environment through series of pores, which are called the canal neuromasts. In the superficial neuromasts, the cupula is elongated and bends with the water flow; this bending is due to the drag generated by the cupula and increases with the length of this structure so that a longer cupula give a greater sensitivity to the neuromast (Bleckmann & Zelick 2009).

In the cavefish, several modifications of the superficial neuromast system have occurred. Indeed, CF possess twice as much superficial neuromasts than the SF and their cupula is 7 times longer so that they are more sensitive (Figure 43 B, C)(Teyke 1990; Yoshizawa et al. 2010). This enhancement of this sensory system is furthermore accompanied by a behavioural modification. Indeed, cavefish tend to be attracted by vibrations between 10 and 50Hz which corresponds to the frequency perceived by the superficial neuromasts, as both canal neuromasts and inner ear perceive higher frequencies. This particular

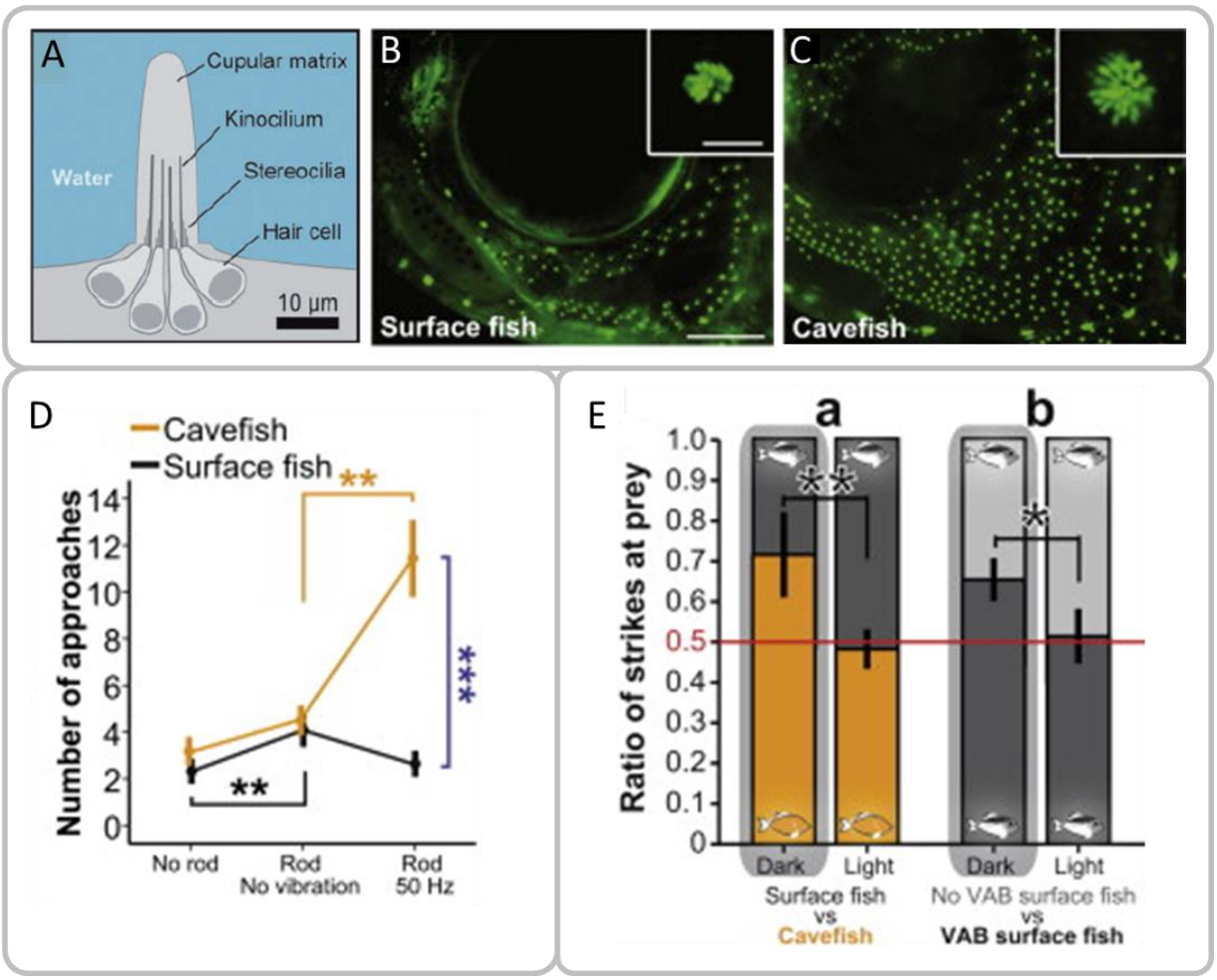

Figure 43 : Neuromasts and the vibration attraction behaviour.
(A) Schematic representation of a neuromast. (B,C) DASPEI staining, showing the superficial neuromasts in a surface fish (B) and a Pachón cavefish (C). Insets show a higher magnification of a superficial neuromast, which are also wider in the Pachón CF.(D) VAB. Number of times fishes approached the center of the tank when there was nothing, when a still rod was placed there, or when the rod was vibrating. (E) Prey catching duels in dark and light condition between VAB-positive CF and VAB-negative SF and between VAB-positive SF and VAB-negative SF. Note that in both cases, the VAB-positive fish does better than the VAB-negative fish in the dark but that the difference is abolished in light conditions.
From (Yoshizawa et al. 2010; Windsor & McHenry 2009)

behaviour is called vibration attraction behaviour (VAB) and is found in some cavefish populations but not all. The Pachón population presents this behaviour as demonstrated with a vibrating rod placed in a circular tank: in the absence of rod, CF tend to swim along the walls, they occasionally come towards the rod when it is not vibrating but increase strongly their approaches when the rod vibrates, which is not the case for SF (Figure 43D). Yet, Yoshizawa and colleagues found some cavefish which did not exhibit this behaviour and some surface fish that did.

To assess the potential adaptive value of the VAB, they tested its impact in prey-capture experiment where artemia nauplii were distributed in a tank containing two fishes and the strikes at preys in the dark and in the light were counted.

In VAB-positive cavefish *vs* VAB-negative SF duel, cavefish struck more in dark conditions but both had the same number of strikes in light conditions. This suggests that VAB could help cavefish in capturing small preys in the dark, but other differences between CF and SF could also explain such difference. In order to sort out the role of VAB in this higher prey strikes, they performed the same experiments between VAB-positive and VAB-negative surface fish and cavefish. In VAB-positive surface fish *vs* VAB-negative SF duels, the VAB-positive SF struck more than the VAB-negative one, while the number of strikes was equal under light conditions. This shows that VAB brings an advantage in prey hunting in the dark, within the same population and same genetic background (Figure 43E).

Overall these findings argue towards an adaptive value of the VAB in the dark by enhancing prey capture abilities. On the other hand, a strong VAB could be disadvantageous in an environment presenting predators, such as surface rivers. Upon entering the caves, VAB-positive surface fish could have been selected for as they had better hunting capacities and this trait could have been further enhanced without being deleterious in absence of predators (Yoshizawa et al. 2010; Yoshizawa 2016; Yoshizawa et al. 2014).

5.6. Behavioral evolution: social behaviors

Several behavioural changes have occurred between cavefish and surface fish, I already mentioned the cavefish attraction towards vibrations and I will briefly describe a few others such as schooling, aggressiveness or feeding behaviours.

5.6.1. Schooling

Schooling is the tendency of some fishes to synchronize their behaviour so that they all swim in the same direction. This behaviour can be advantageous for predator avoidance and is exhibited by *Astyanax* surface fish. On the contrary, cavefish from different origins (Pachón, Tinaja and Molino) have lost this behaviour (Figure 44A). The ability to school was shown in some species to rely on both sight and neuromasts, however, in *Astyanax* surface fish, chemical ablation of neuromasts did not modify schooling. On the other hand, loss of vision, either by enucleation or by conducting the experiment in the dark resulted in a loss of schooling, evidencing a clear need for visual modality in that behaviour. Yet, the loss of sight in CF was not the only factor involved in the evolution of schooling, as shown by Tinaja cavefish X surface fish crosses. The F1 hybrids resulting from these crosses possess eyes and do school like SF, but F2 hybrids present various phenotypes. Kowalko and colleagues selected F2 that were capable of seeing light in order to remove the sight factor of the question; they observed that some of these fishes still did not school, indicating an additional genetic factor in this equation. They performed a quantitative trait loci (QTL) analysis on the F2 and were able to find 3 loci linked with schooling; however surprisingly, in one of these loci, the cavefish allele was associated with increased schooling. This could suggest that schooling is under relaxed selection in the caves, as cave alleles do not seem to always promote a decrease of this behaviour (Kowalko, Rohner, Rompani, et al. 2013).

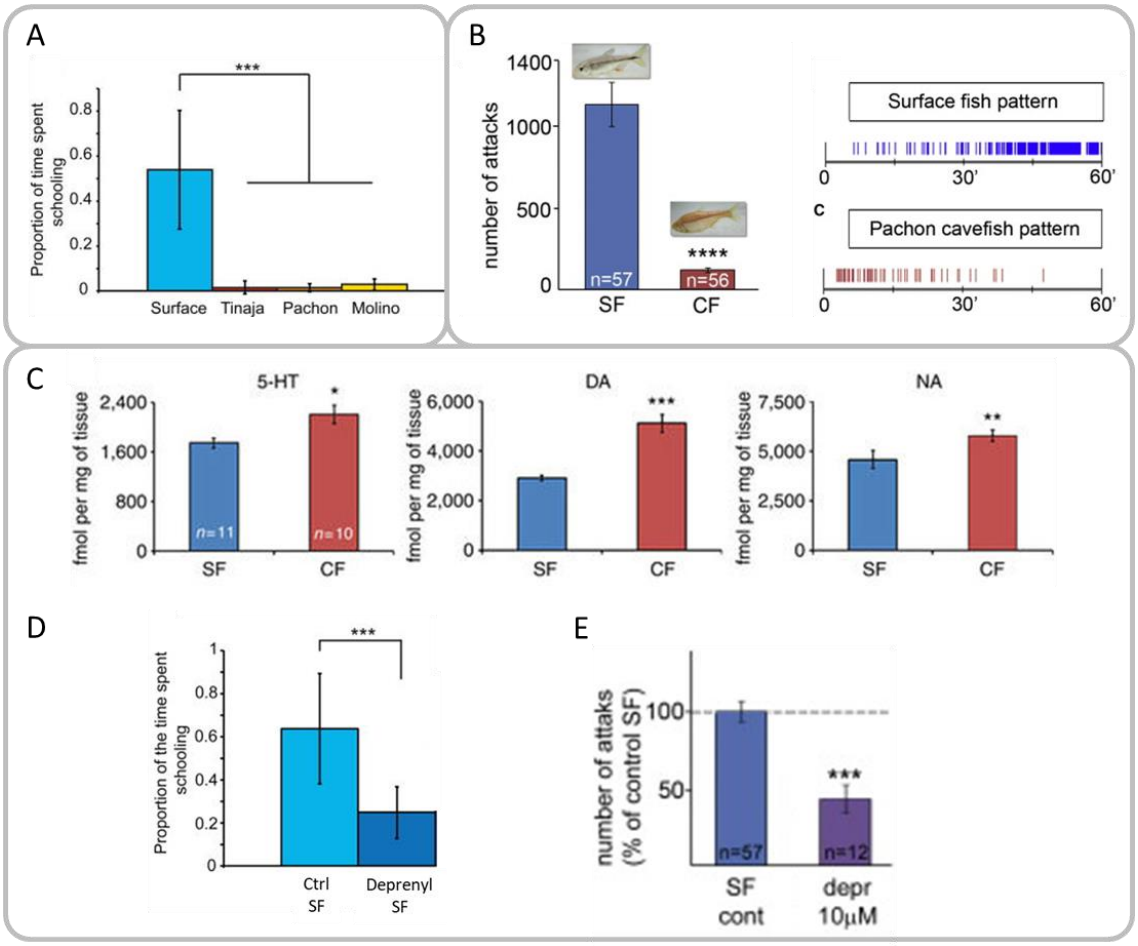

Figure 44 : Social behaviour and monoamine-oxidase (MAO).
(A) Schooling in surface and cave populations, cavefish do not school. (B) Aggressive behaviour. Total number (left) and pattern of attacks during an resident-intruder test for SF and CF. (C) Increased amounts of serotonin (5-HT), dopamine (DA) and noradrenaline (NA) in Pachón CF, due to a mutation of the MAO. (D, E) Time spent schooling (D) and number of attacks (E) after treatment with Deprenyl, a MAO inhibitor. From (Kowalko, Rohner, Rompani, et al. 2013; Elipot et al. 2013)

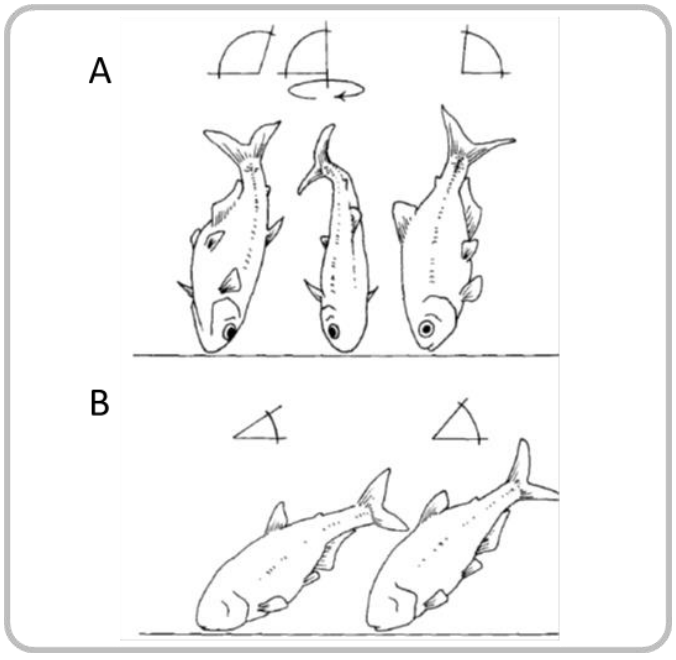

Figure 45 : Feeding position in the dark.
(A) Surface fish adopt a vertical position and a slight twirling movement. (B) The cavefish adopt a 40-55° angle and scan the floor.
From (Schemmel 1980)

5.6.2. Aggressiveness and hierarchy

Another striking difference between cavefish and surface fish is the quasi absence of aggressive behaviour of the Pachón population. Indeed, it was shown in several studies that SF are highly aggressive towards each other and in a resident-intruder test, the frequency of attacks increases with time. This was interpreted as being related to hierarchy establishment, as dominant and subordinate fishes can be identified in SF groups, both on the basis of behaviour and by analysis of their raphe serotonin levels. On the contrary, Pachón CF exhibit very low aggressiveness, which decrease over time in a resident-intruder assay (Figure 44B). The few bites observed were interpreted as being related to food-search, rather than hierarchy as CF do not seem to establish any; moreover, starved CF exhibited higher aggressiveness. It is also worth noting that blinded SF still exhibited high aggressiveness (Elipot et al. 2013; Espinasa et al. 2005).

5.6.3. Serotonin and MAO

The levels of three neurotransmitters : serotonin, dopamine and noradrenaline have been shown to be increased in Pachón cavefish (Figure 44C). These neurotransmitters are involved in many processes, such as stress, reward, appetite or energy expenditure, amongst many others. The increase in these neurotransmitters levels is due to a mutation in the monoamine-oxidase (MAO) which degrades all of these transmitters; this mutation decreases strongly the MAO catalytic activity (Elipot et al. 2014). The effects of this mutation are very important to understand the cavefish behaviour, indeed, surface fishes treated with deprenyl -a MAO inhibitor- reduce drastically their schooling behaviour but also their aggressiveness (Figure 44 D,E)(Kowalko, Rohner, Rompani, et al. 2013; Elipot et al. 2013). This mutated allele is present at high frequency but is not fixed in the Pachón population; it is also found in other cave populations of El Abra group but not in the other regions suggesting either that this allele was present in the surface population that colonized these caves and/or that there has been connections between these caves at some point, allowing fishes to colonize them or to mix with an existing population (C. Pierre, S. Rétaux, unpublished). The potential adaptive value of this mutation is not self-evident, especially because of the multiple effects it has or could have; indeed, it is worth noting that serotonin is known to be a potent appetite-inhibitor in fishes (Pérez Maceira et al. 2014; De Pedro et al. 1998; Mennigen et al. 2010; Mancebo et al. 2013).

5.6.4. Feeding position

Surface fish find food mostly relying on sight; when they see a prey or food falling on the surface of the water or in the water column, they quickly and accurately strike to catch it. However, when they are put in the dark, they try to catch food off the ground by adopting a close-to-vertical angle (74° on average), head on the ground and pivoting slightly, a posture than is not very efficient for catching food. On the contrary, Pachón CF adopt a “scanning” position that has been described with an angle between 38° and 55° depending on the study (Figure 45)(Kowalko, Rohner, Linden, et al. 2013; Schemmel 1980). This posture allows them to sweep the substrate in a continuous manner, head down, meaning that their tastebuds are in contact with the ground and potentially the food. This posture could definitely help them to forage more efficiently -although this is not the only food searching behaviour they exhibit, Pachón cavefishes are also seen swimming frenetically at the surface of the water, when stimulated with odorants or vibrations (personal observations in the lab and in the field, together with other team members). It is worth mentioning that if several cave populations possess this type of low-angle “scanning” behaviour (Los Sabinos, Piedras, Tinaja), others have kept a steep angle such as Molino (66°) (Kowalko, Rohner, Linden, et al. 2013; Schemmel 1980).

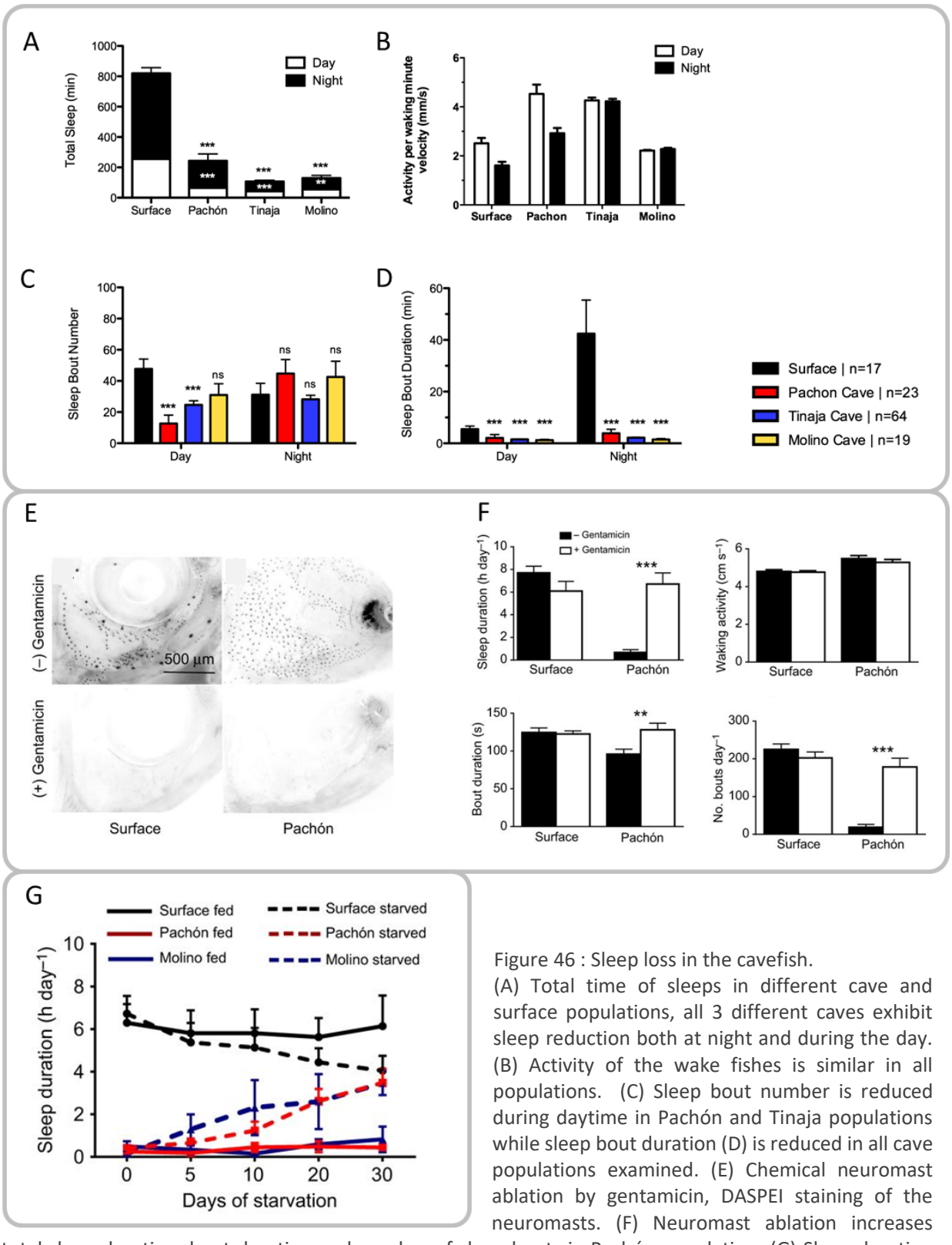

Figure 46 : Sleep loss in the cavefish.
(A) Total time of sleeps in different cave and surface populations, all 3 different caves exhibit sleep reduction both at night and during the day. (B) Activity of the wake fishes is similar in all populations. (C) Sleep bout number is reduced during daytime in Pachón and Tinaja populations while sleep bout duration (D) is reduced in all cave populations examined. (E) Chemical neuromast ablation by gentamicin, DASPEI staining of the neuromasts. (F) Neuromast ablation increases total sleep duration, bout duration and number of sleep bouts in Pachón population. (G) Sleep duration increases upon starvation in the different cavefish populations.
From (Duboué et al. 2011; Jaggard et al. 2017)

5.7. Behavioral and physiological evolution: energy management

Cave environment poses the challenge of correctly managing resources so that you can survive prolonged periods of food scarcity. In order to thrive in this environment, several strategies can come useful: eating more, storing more fat, consuming less… Energy intake, storage and consumption have evolved in cavefish, in close relationship with its behavioural evolution.

5.7.1. Sleep and activity

Sleep has been characterized as a period of behavioural quiescence that correlates with a reduced responsiveness to sensory stimuli. In *Astyanax* cavefish, total sleep duration is drastically reduced in several independently evolved populations. Juvenile CF from Pachón, Tinaja and Molino sleep less than 5 hours a day while SF sleep almost 15 hours; interestingly, this reduction of sleep persists to adulthood in Pachón and Molino populations but not in Tinaja, where adults sleep as much as SF. For CF juveniles, both the number of sleep bouts and their duration was decreased, except for Molino where only the bout duration was decreased, indicating a poor sleep consolidation (Figure 46 A-D). These findings highlight a difference in sleep regulation between juvenile and adults fish but also a convergence of sleep loss in independently-evolved cave populations, indicating a possible advantage to this phenotype (Yoshizawa et al. 2015; Duboué & Keene 2016; Duboué et al. 2011).

Recently, Jaggard and colleagues showed that ablation of the neuromasts resulted in an increase in sleep duration in Pachón CF but not in Tinaja, Molino or surface fish, further evidencing the different mechanisms of sleep loss in these different populations. Following the ablation, both the number of sleep bouts and the bout duration was increased in Pachón. These interesting findings suggest that the higher number and higher sensitivity of the CF neuromasts could overstimulate the CF so that it cannot sleep much, representing a sort of sensory gating on the expression of sleep (Figure 46 E, F).
Another very interesting finding of this study is that sleep is increased following starvation in both Pachón and Molino populations, while it is not the case for SF. Moreover, neuromast ablation after starvation did not increase sleep duration in Pachón. The authors suggest that when food is available, presumably during rainy season, cavefish will decrease their sleep and intensively forage, while when food becomes scarce, they will increase their sleep and potentially save more energy that way (Figure 46)(Jaggard et al. 2017).

Of note, many studies concerning sleep in the cavefish looked at the waking activity and described that this activity was exactly the same between CF and SF, so that overall, the cavefish display a higher locomotor activity but that is solely due to the increased waking time (Figure 46B)(Yoshizawa et al. 2015; Jaggard et al. 2017; Duboué et al. 2011).

5.7.2. Circadian rhythm

The circadian clocks are internal mechanisms providing an organism with an approximate 24h rhythmicity. This clock needs to be set by external cues such as light-dark cycles. These mechanisms help the organism to adapt many physiological, metabolic or behavioural processes to the external rhythmicity. Cave are a very stable environment, where much less rhythmicity is observed (bat-rich cave can present some rhythmicity due to the bats movements at dusk and dawn), so a commonly asked question is whether CF have conserved a circadian rhythm or not.

Beale and colleagues compared various parameters between Pachón CF and SF in different conditions. In agreement with our own observations in the lab, they note that CF like SF are able to be entrained by light

in light-dark (LD) conditions, both in terms of activity and in terms of circadian clock gene expression. Yet, they observed that CF clock gene (*per1*) expression was reduced and shifted toward later time (6 hours shift) and that the day-night rhythmicity in terms of locomotor activity was less contrasted in CF. Upon switching to constant dark conditions (DD), cavefish immediately lost rhythmicity in activity while SF conserved it a bit longer, both where able to retain per1 rhythmicity. They also tested light-inducible genes and reported that the response to light was decreased in amplitude in CF, in part due to higher basal levels. They conclude that CF still possess a functional circadian clock but that is less robust than in SF, they also suggest that CF experience "constant light conditions" rather than constant dark (Beale et al. 2013; Beale & Whitmore 2016).

5.7.3. Food intake

Depending on the cave, some CF populations are probably exposed to high food supply during some seasons (rainy season), before enduring long starvation periods. It could be advantageous to eat as much as possible during the rainy season in order to better survive the dry season.

One first probable advantage of the CF (Pachón) is that their intestine does not seem to suffer from prolonged starvation as its length remains constant after 3 months and even 6 months of starvation. On the contrary, SF's intestine length reduced from 74% of the fish's standard length to 50% after 3 months of starvation, suggesting that reabsorption of nutrients would probably be harder for them (Hüppop 2001).

Aspiras and colleagues investigated the question of cavefish appetite. They showed that in lab conditions, Tinaja but not Pachón CF ate more than SF. They then investigated a gene that is known to control appetite in fish in an anorexigenic fashion : the melanocortin receptor MC_4R (Cerdá-Reverter et al. 2011; Aspiras et al. 2015). They detected hypomorphic mutations of MC_4R in Tinaja CF, in wild-caught Pachón CF and several other cave populations but not in their Pachón laboratory strain. They then assayed homozygous mutant Pachón CF versus heterozygous Pachón CF and observed that in young 3 mpf fishes, homozygous mutants ate more than heterozygotes but not to the extent of Tinaja CF. Moreover, homozygote mutants were larger. Interestingly, the appetite difference between the two Pachón genotypes disappeared when older fish (over 1 year-old) were assayed. This indicates that MC_4R mutations only affect juvenile fishes, and that other modifications must have taken place in Tinaja population to explain their appetite increase at adult stages. Nevertheless, eating more at early stages can constitute a real advantage, in order to quickly accumulate fat and be able ready to cope with starvation periods (Aspiras et al. 2015).

5.7.4. Fat storage

Several independent studies have shown that cavefish raised in lab conditions are fatter than surface fish raised in the same fashion. Indeed, Hüppop reported that Pachón CF had a fat content of 71% of their dry body mass, while in SF it only represented 27% (Hüppop 2001). Similarly, Aspiras et al reported that the triglyceride content of Pachón CF was significantly higher than that of SF and that Tinaja's was even higher (Aspiras et al. 2015). The same group investigated the blood glucose levels of CF and found that they were more elevated for Pachón and Tinaja caves compared to SF, although after 3 weeks of fasting, glucose levels were similar between the two morphs. Indeed, both cave population have an impaired glucose clearance due to a mutation in the insulin receptor, rendering them insulin-resistant. They showed the importance of this mutation in weight gain by generating SF X Tinaja CF second generation hybrids and weighing them. F2 carrying at least one mutated allele and fed *ad libitum* weighed 27% more than sibling carrying only the WT allele. In order to remove appetite difference from the equation, they individually housed and fed these F2 fish along with CF and SF. Homozygous mutant F2 gained more weight than F2 homozygous for the WT allele, similarly, CF gained more weight than SF; therefore, the insulin receptor mutation increases the weight gain independently from appetite regulation. They also

showed that this insulin receptor mutation was not the only factor influencing blood glucose levels and that other factors were necessary to explain the difference observed between CF and SF. Interestingly, they note that despite their diabetic-like phenotype, both CF populations are extremely healthy and do not show any sign of senescence even above 14 years-old, contrarily to SF, and that they do not display excess glycation of their proteins, as seen in diabetic patients (Riddle et al. 2018).

5.7.5. Metabolism

We have seen that CF tend to eat more and to store more fat than SF but how about their metabolism ? Moran and colleague investigated this important question using long experiments (7 days of measurements) in a "flume respirometer", which is a small chamber in which they apply some constant water current in order to impose a stable activity to the fish. They performed their tests in two sets of conditions, light-dark (LD) cycles of complete darkness (DD). They noted that both SF and CF had the same value of minimum metabolism under their respective natural photoperiod (LD for SF and DD for CF), meaning that there is no intrinsic difference in their O_2 consumption. On the other hand, when tested in DD conditions, SF increased of their minimal metabolism. In LD cycle, SF had an elevated metabolism during daylight and upon switching to DD conditions, they maintained a 20% increase of consumption during subjective daytime.

Overall, they show that CF and SF share a same minimal metabolism in their respective natural photoperiod but the average consumption of the SF is 27% more elevated than that of Pachón. They associated this increased expenditure to the circadian rhythmicity of the SF that elevates its metabolism during daytime while CF always keep their metabolism low. Overall, given the increase of O_2 consumption of the SF in DD conditions, and the lower average metabolism of the CF, they show that in cave conditions, SF would consume 38% more O_2 than Pachón CF. Such an elimination of rhythmicity in cavefish metabolism allows them to save energy.

5.7.6. Starvation resistance

Up to now we had seen that CF are able to increase their sleep duration upon starving, but that when food is available, they will decrease it, which should allow them to spend more time foraging. Moreover, they are able to eat more than SF and to gain more weight than them, even from the same amount of food. Therefore, they will have increased fat storage that they will probably consume more slowly given their decreased metabolism. The logical question is now : are CF indeed more resistant to starvation than SF ?

CF from Pachón, Tinaja or Molino that are submitted to 2 months of starvation lose 15% of their weight; in comparison, SF lose twice as much: 30% of their initial weight. Pachón CF that are homozygous for the mutated MC_4R allele lose less weight than their heterozygous siblings (Aspiras et al. 2015). An older study starved Pachón and surface fishes for 3 months and showed that SF decreased their fat content from 27% of their dry body mass to 8% while CF started with 71% and still had a fat content of 63% of dry body mass after starvation. The test continued until 6 month of starvation for CF, after which their fat content was 62% which is still higher than the initial one of SF. In this study, Hüppop also describes the progressive atrophy of the SF intestine which was not visible in the CF even after 6 months. Moreover, she describes that during starvation, some SF died, concluding that SF do not seem adapted to starvation at all. Assuming that the fish will die when its initial weight is decreased by half, she calculated that Pachón CF should be able to sustain approximately 1 year of starvation (Hüppop 2001). In the case of an insufficient food supply during rainy season, we can imagine that the cavefish could hold until the next one and even if this one is delayed, one could imagine that should the weakest cavefish die, cannibalism would allow the others to survive.

Results

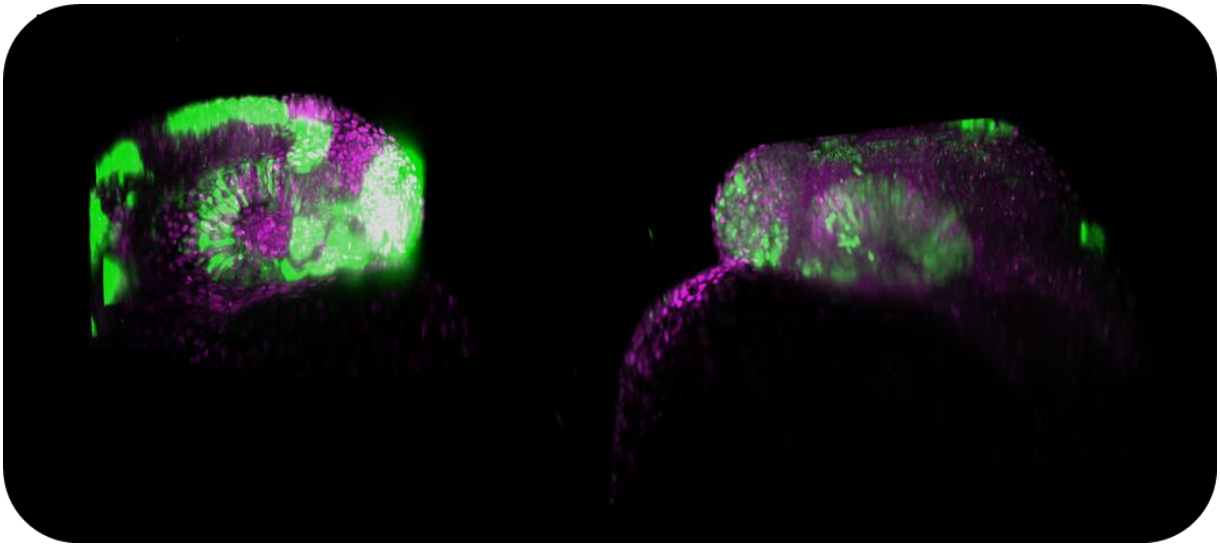

1. Peptidergic neurons in the cavefish : from early morphogen modifications to larval behaviour.

1.1. Foreword

Cavefish present many behavioural and physiological differences compared to their surface counterpart, including quasi loss of sleep, increased fat storage and lower energy expenditure which are –at least in part- controlled by the hypothalamus and its neuropeptidergic neurons. This led us to examine more specifically this brain region, which was already known to be modified, with an expansion of the hypothalamic marker *Nkx2.1* in the cavefish and an increased proliferation both in the hypothalamus and in the ORR (Menuet et al. 2007). More specifically, we focused on appetite-related neuropeptides since this aspect had not yet been studied (it has been done since, see Introduction 5.7.3 Food intake).

We mapped and quantified peptidergic clusters for 9 appetite-related neuropeptides. We chose 3 orexigenic (promoting food intake): Hypocretin (Hcrt, also called orexin), neuropeptide Y (NPY) and agouti-related protein (AgRP); and 6 anorexigenic neuropeptides: the proopiomelanocortins A and B (POMCa, POMCb), melanin-concentrating hormone (MCH), cocaine and amphetamine-regulated transcript (CART), arginine vasotocin (AVT) and isotocin (IT). Importantly, although we originally chose these neuropeptides based on their roles in feeding, all of them also take part in the control of other processes (see Table 1 in Introduction 3.1 Modes of action of the Hypothalamus/ORR and neuropeptides).

This study of peptidergic clusters brought to light several quantitative differences between cavefish and surface fish. However, since it had now been shown that Pachón cavefish do not eat more than surface fish (a finding that we confirmed ourselves), we focused on one other behaviour controlled by some of these neuropeptides: sleep.

We also sought to link the peptidergic clusters modification to a causal developmental explanation and therefore examined both the role of Lim-Homeobox transcription factors (Lhx) -known to be involved in the acquisition of neuronal identity- and the more precocious effect of the morphogens.

This study is an excellent example of the interest of the cavefish model: behavioural or physiological differences between the two morphs prompt us to examine the modifications at the level of the organ or the neurons, which in turn drive us to study the developmental mechanisms underlying these latter differences. This way, we can piece up a whole story: starting from early developmental difference and leading to late behavioural or physiological modifications that can have (or not) an adaptive value in the cave context. Moreover, contrarily to model organism mutant collections that often display strong phenotypes due to one strong genetic alteration (loss of function for example), the cavefish model, a natural mutant, provides us with subtle changes in gene expression, like a wider *Shh* expression or a 2 hours-heterochrony of *Fgf8* onset of expression, in an overall viable organism. This allows for a better understanding of how such modifications impact the brain shape, function and consequently modifies the abilities of an animal.

Developmental evolution of the forebrain in cavefish, from natural variations in neuropeptides to behaviour

eLIFE elifesciences.org

RESEARCH ARTICLE

Developmental evolution of the forebrain in cavefish, from natural variations in neuropeptides to behavior

Alexandre Alié†, Lucie Devos†, Jorge Torres-Paz†, Lise Prunier, Fanny Boulet, Maryline Blin, Yannick Elipot, Sylvie Retaux*

Paris-Saclay Institute of Neuroscience, Université Paris Sud, CNRS UMR9197, Université Paris-Saclay, Avenue de la terrasse, Gif-sur-Yvette, France

Abstract The fish *Astyanax mexicanus* comes in two forms: the normal surface-dwelling and the blind depigmented cave-adapted morphs. Comparing the development of their basal forebrain, we found quantitative differences in numbers of cells in specific clusters for six out of nine studied neuropeptidergic cell types. Investigating the origins of these differences, we showed that early Shh and Fgf signaling impact on the development of NPY and Hypocretin clusters, via effect on Lhx7 and Lhx9 transcription factors, respectively. Finally, we demonstrated that such neurodevelopmental evolution underlies behavioral evolution, linking a higher number of Hypocretin cells with hyperactivity in cavefish. Early embryonic modifications in signaling/patterning at neural plate stage therefore impact neuronal development and later larval behavior, bridging developmental evolution of a neuronal system and the adaptive behavior it governs. This work uncovers novel variations underlying the evolution and adaptation of cavefish to their extreme environment.

DOI: https://doi.org/10.7554/eLife.32808.001

***For correspondence:** retaux@inaf.cnrs-gif.fr

†These authors contributed equally to this work

Competing interests: The authors declare that no competing interests exist.

Funding: See page 21

Received: 13 October 2017
Accepted: 12 January 2018
Published: 06 February 2018

Reviewing editor: Marianne Bronner, California Institute of Technology, United States

Introduction

The secondary prosencephalon of the vertebrate forebrain, comprising the telencephalon, the optic/preoptic region and the hypothalamus, develops from the anterior neural plate. By the end of gastrulation, the neural plate is already patterned and the regional fate of its antero-posterior and medio-lateral domains is specified, as a result of the concerted action of diffusible morphogen molecules that emanate from secondary organizers (reviewed in [***Cavodeassi and Houart, 2012***]). Endo-mesodermal tissues (prechordal plate and notochord) located ventral to the neural plate secrete Nodal/TGFβ and Sonic Hedgehog (Shh) molecules necessary for induction of ventral forebrain and maintenance of hypothalamic fate (***Chiang et al., 1996***; ***Kiecker and Niehrs, 2001***; ***Mathieu et al., 2002***). The anterior-most neural plate border, named ANB then ANR (anterior neural border and ridge) secrete Wnt inhibitors and Fibroblast Growth Factors that are required for the establishment of telencephalic fate (***Houart et al., 2002***; ***Houart et al., 1998***) and its patterning (***Miyake et al., 2005***; ***Shanmugalingam et al., 2000***; ***Shimogori et al., 2004***; ***Walshe and Mason, 2003***), respectively. Thus, the elaboration of the vertebrate forebrain depends on the tight spatial and temporal regulation of relatively few morphogenetic signals. Changes in these early events have the potential to modulate brain organization, notably the relative size of different brain regions (***Hinaux et al., 2016***; ***Sylvester et al., 2010***; ***Sylvester et al., 2013***) (reviewed in [***Rétaux et al., 2013***]).

The evolution of brain development and its behavioral consequences is a major topic to understand how vertebrates colonize novel environments. *Astyanax mexicanus* is a model of choice to tackle this question (***Jeffery, 2008***; ***Jeffery, 2009***; ***Rétaux et al., 2016***). This teleost fish exhibits two morphotypes: a surface-dwelling form (thereafter designated as SF) that inhabits South and

Central America rivers, and a cave-dwelling form (CF) that consists in multiple populations living in the total and permanent darkness of Mexican caves (**Mitchell et al., 1977**). These two forms have split from a surface fish-like ancestor less than 30,000 years ago (**Fumey et al., 2017**). During this time, cavefish have evolved regressive traits - the most spectacular being the loss of eyes and pigmentation - but they also evolved several constructive traits such as a larger jaw, more taste buds and neuromasts, or larger olfactory epithelia (reviewed in [**Rétaux et al., 2016**]).

Inside the cavefish brain, patterning modifications have been described as well and are the consequences of subtle modifications in the early expression of morphogens during evolution. Enlarged ventral midline Shh expression during gastrulation and neurulation (**Yamamoto et al., 2004**) results in a larger hypothalamic region, presumably via extension of *Nkx2.1a*, *Lhx6* and *Lhx7* transcription factor expression domains and increased cell proliferation (**Menuet et al., 2007**; **Rétaux et al., 2008**). Early expansion of Shh is also responsible for a heterochrony in the onset of *Fgf8* expression in the ANR (**Pottin et al., 2011**). Fgf8 is turned on at 10hpf in CF ANR, while its expression starts 2 hrs later in SF. In turn, Fgf8 maintains *Shh* expansion in the CF developing forebrain basal plate, with consequences on neural plate patterning at the onset of neurulation: the expression domains of transcription factors (TFs) such as *Lhx2*, *Lhx9*, *Pax6*, or *Zic1* are different in SF and CF at neural plate stage and related differences in fate maps have been reported (**Hinaux et al., 2016**; **Pottin et al., 2011**; **Strickler et al., 2001**). In particular, cell populations that give rise to the ventral quadrant of the retina in SF seem to be allocated to the dorsal retina or to the hypothalamus in CF. Accordingly, early manipulation of Fgf signaling in CF (thus mimicking the SF situation) is able to restore the ventral quadrant of the retina (**Pottin et al., 2011**). Taken together, these studies highlight the morphogenetic consequences of small spatio-temporal changes in early Shh and Fgf signaling in cavefish. Similar variations in early Wnt signaling in distinct ecotypes of cichlid fish result in the development of brains with large or small telencephalon, thalamus and tectum (**Sylvester et al., 2010**; **Sylvester et al., 2013**). Thus, natural variations of forebrain patterning by signaling modulations may be a widespread mechanism for forebrain evolution.

The hypothalamus is a hub that integrates central and peripheral signals and elicits multiple neuroendocrine and homeostatic responses. Hypothalamic circuits control behaviors such as locomotor activity, sleep/wake cycles and food intake, but also responds to metabolic state of the body (level of adiposity and blood glucose) by directly acting on peripheral organs to control energy expenditure ([**Loh et al., 2015**; **Myers and Olson, 2012**; **Tsujino and Sakurai, 2013**] for recent reviews). *Astyanax* cavefish has evolved multiple behaviors of putative adaptive value to live in cave environment where survival challenges reside in finding food and interacting with congeners in permanent darkness. Several of these behaviors are typically controlled by the hypothalamus: CF show enhanced foraging traits and increased locomotor activity (**Elipot et al., 2013**; **Yoshizawa et al., 2015**), sleep loss (**Duboué et al., 2011**) and, for some populations, enhanced food intake and high fat content (**Aspiras et al., 2015**) when compared to their surface conspecifics.

The behaviors described above are under the control of different, but neighboring neuronal populations in the hypothalamus of vertebrates, including fish (**Herget et al., 2014**; **Löhr and Hammerschmidt, 2011**; **Machluf et al., 2011**; **Matsuda et al., 2012a2012**; **Matsuda et al., 2012b**). Here, we have first compared and interpreted in details the developmental neuroanatomy of nine neuropeptidergic cell types in the hypothalamus and preoptic region of SF and CF embryos and larvae, highlighting specific differences in neuron numbers between the two morphs. We then established causal relationships between early signaling modifications, regional patterning and cell specification processes in cavefish. We further showed that Lhx9 and Lhx7 transcription factors serve as 'relays' and are involved in the observed changes in Hypocretin and NPY neurons in cavefish, respectively. Finally we provide evidence that such developmental evolution in hypothalamic neuronal networks affects the behavior of cavefish larvae.

Results

Anatomical interpretation

The morphogenetic movements of the early neural plate and tube are complex. Recently several novel interpretations of the developmental neuroanatomy of the vertebrate secondary prosencephalon have been put forward (***Figure 1—figure supplement 1***). In tetrapods, the updated prosomeric

model aims at proposing causal explanations of the hypothalamic and preoptic area structures, by the effects of antero-posterior and dorso-ventral signaling (***Puelles and Rubenstein, 2015***). Two transverse hypothalamo-telencephalic prosomeres, hp1 and hp2, encompassing the four dorso-ventral domains of the neuroepithelium (roof, alar, basal, and floor plates) have been proposed, supported by genoarchitecture and embryological data (***Figure 1—figure supplement 1A***). In zebrafish, a morphogenetic interpretation of the development of the optic/pre-optic region suggests the existence of three morphogenetic units based on centrifugal neurogenesis patterns rather than on gene expression boundaries –the telencephalon, the optic recess region (ORR) and the hypothalamus-, which helps to resolve some inconsistencies between tetrapod and teleost basal forebrain (***Affaticati et al., 2015***)(***Figure 1—figure supplement 1B***). Finally in zebrafish also, a homology relationship was proposed between the teleost 'neurosecretory pre-optic area' or NPO (located in the ORR as defined by Affaticati and colleagues, or in the preoptic region/PO according to the classical nomenclature) and the mammalian paraventricular nucleus (PVN), which belongs to the mammalian alar hypothalamus (***Herget et al., 2014***; ***Herget and Ryu, 2015***)(***Figure 1—figure supplement 1C***). Here, our analyses take into account both the crucial interpretation along the neural axis and according to the alar or basal plate nature of the neuroepithelium, and the peculiarities of the teleost forebrain.

With the aim to precisely document cavefish basal forebrain developmental evolution, we have first compared the ontogenesis of neuropeptidergic cell groups, their organization and their size, between SF and CF embryos and larvae originating from the Pachón cave, at three critical stages of forebrain development (see Materials and methods, ***Figure 1—figure supplement 3*** and ***Figure 1—videos 1–4***).

More NPY, Hypocretin and AgRP neurons in developing cavefish

Among the nine studied neuropeptides, NPY, Hcrt and AgRP are expressed by more neurons in CF than SF in our regions of interest (***Figure 1***). The results are summarized in ***Figure 1U***, and the raw cell counts are provided as ***Supplementary file 1***.

Neuropeptide Y (NPY) is expressed from 24 hpf in a medial and superficial hypothalamic cell group, which progressively shifts posteriorly (36 hpf) and clusters in the mammillary region of the hypothalamus (ventral along the neural axis) at 84 hpf (***Figure 1A–F' and U***). We interpret this cell group as part of the *saccus vasculosus* (see discussion). It is located in the hypothalamic basal plate and may belong to the newly proposed acroterminal domain of the secondary prosencephalon (***Puelles and Rubenstein, 2015***)(***Figure 1—figure supplement 1A***). This group of NPY neurons is significantly more numerous in CF than in SF at all investigated stages (***Figure 1G and U***). From 36 hpf, then 84 hpf, NPY is expressed in many additional brain regions (***Figure 1C–F'***). This includes two symmetrical and large cell groups located in the hypothalamus (basal plate) extending dorsally to the region around the post-optic commissure (poc) at the border of the ORR (***Figure 1E–F'***). In this region as well, CF possess about twice more NPY neurons than SF (***Figure 1H and U***). In contrast to these basal regions, the NPY population located in the telencephalon (alar plate) from 36 hpf onwards was similar in the two morphs and a cluster located in the medial part of the dorsal ORR, around the anterior commissure, contained more cells in SF (***Figure 1C–F' and U***). The NPY cells in the optic tectum (alar mesencephalon) were more numerous in SF than in CF (***Figure 1E'F' and U***; cell counts were not performed, but the difference is obvious).

Hypocretin is expressed as two symmetrical groups in the hypothalamus basal plate (Shh-positive, see below and Figure 5H), in a posterior and dorsal position along the brain axis that may topographically correspond to the peduncular (posterior) hypothalamus (***Puelles and Rubenstein, 2015***). Hcrt expression is turned on at 18hpf (***Figure 1—figure supplement 2***) and remains similar in pattern at later stages (***Figure 1I–N'***). Surprisingly, the number of Hcrt neurons raises and is maximal at 24 hpf (average 27 neurons in CF, 17 neurons in SF) and slightly decreases thereafter. At all stages between 18 hpf and 84 hpf, more Hcrt neurons were found in CF than in SF (***Figure 1O and U***, ***Figure 1—figure supplement 3*** and ***Figure 1—videos 1–4***.

AgRP onset of expression is later than NPY and Hcrt: it is first expressed at 36 hpf in cell clusters located in the tuberal hypothalamus, and then becomes distributed in two lateral elongated patches (***Figure 1P–S'***). No differences are detected regarding AgRP neuron abundance between the two *Astyanax* morphs at 24 hpf and 36 hpf, but at 84 hpf CF possess slightly but significantly more AgRP neurons than SF (***Figure 1T and U***).

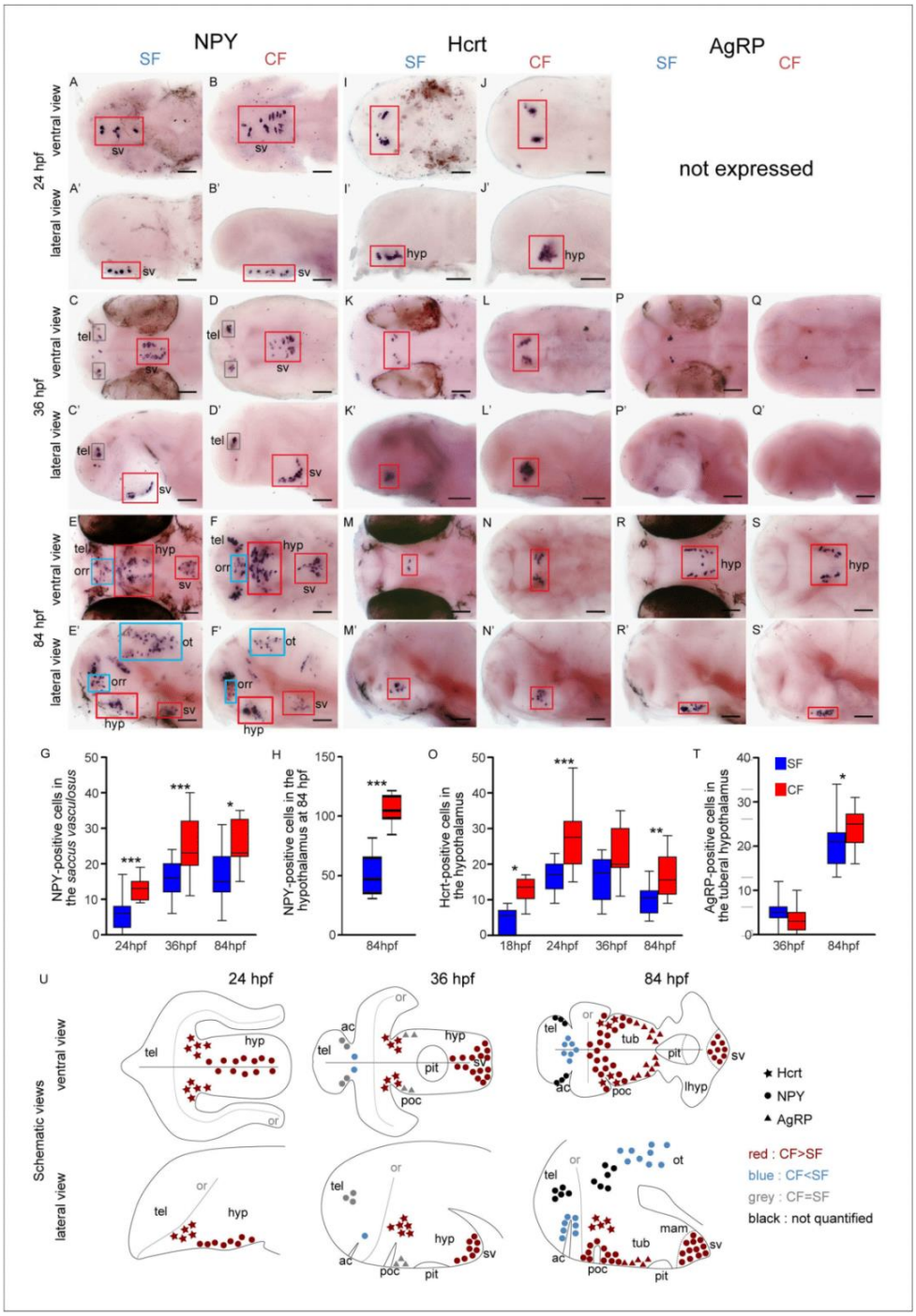

Figure 1. Comparative development of NPY, Hypocretin and AgRP neurons in SF and CF. (A–S') Photographs of embryonic brains after in situ hybridization for NPY, Hypocretin and AgRP at 24, 36, and 84 hpf. The stages, the lateral or ventral orientations, and the probes are indicated. Red squares and blue squares indicate peptidergic clusters with higher numbers of neurons in CF or in SF, respectively. For this and the following figures, raw data including the number of embryos examined are given in ***Supplementary file 1***. (G, H, O, T) Quantification and time-course of cell numbers in

Figure 1 continued on next page

Figure 1 continued

specific clusters. Mann-Whitney tests. (**U**) Anatomical interpretation of peptidergic patterns and time-course of appearance. Hcrt (stars), NPY (circles) and AgRP (triangles) neurons are reported on schematic embryonic brains, in ventral or lateral views. A color code indicates higher numbers of neurons in CF (red) or in SF (blue), or equivalent numbers (grey). Black clusters were not counted. ac, anterior commissure; hyp, hypothalamus; mam; mamilary hypothalamus; or, optic recess; orr, optic recess region; ot, optic tectum; pit, pituitary; poc, post-optic commissure; tel, telencephalon; tub, tuberal hypothalamus; sv, *saccus vasculosus*.

DOI: https://doi.org/10.7554/eLife.32808.002

The following video and figure supplements are available for figure 1:

Figure supplement 1. Models and interpretations of prosencephalic development.

DOI: https://doi.org/10.7554/eLife.32808.003

Figure supplement 2. Onset of expression of Hcrt and POMCb around 18hpf.

DOI: https://doi.org/10.7554/eLife.32808.004

Figure supplement 3. Comparison of colorimetric versus fluorescent in situ hybridization results.

DOI: https://doi.org/10.7554/eLife.32808.005

Figure 1—video 1. Comparison of colorimetric *versus* fluorescent in situ hybridization results.

DOI: https://doi.org/10.7554/eLife.32808.006

Figure 1—video 2. Comparison of colorimetric versus fluorescent in situ hybridization results.

DOI: https://doi.org/10.7554/eLife.32808.007

Figure 1—video 3. Comparison of colorimetric versus fluorescent in situ hybridization results.

DOI: https://doi.org/10.7554/eLife.32808.008

Figure 1—video 4. Comparison of colorimetric *versus* fluorescent in situ hybridization results.

DOI: https://doi.org/10.7554/eLife.32808.009

Less POMCa, POMCb and AVT neurons in developing cavefish

Three of the studied neuropeptides are expressed by less neuron in CF than SF: POMCa, POMCb, and AVT (***Figure 2***). The results are summarized in ***Figure 2V*** and the raw cell counts are provided as ***Supplementary file 1***.

POMCa is first expressed at 36 hpf in a few cells at the dorsal border of the hypothalamus basal plate. The POMCa pattern then takes the shape of two elongated stripes in the tuberal part of the terminal (or anterior) hypothalamus at 84 hpf (***Figure 2A–D'***), similar to the above-described AgRP neurons. At both 36 hpf and 84 hpf, POMCa is also expressed in the pituitary gland, which is apposed onto to the hypothalamus midline and clearly recognizable at 84 hpf as a single structure with closely condensed cells (***Figure 2A–D'***). At 36 hpf, we count significantly more POMCa neurons in SF than in CF (***Figure 2E***; of note at this stage hypothalamic and pituitary neurons were very difficult to distinguish and were therefore pooled). At 84 hpf, SF display more POMCa neurons than CF in the pituitary (now well identifiable; ***Figure 2F***) but not in the hypothalamus (***Figure 2E and V***).

POMCb is first expressed at 18 hpf at the rostral tip of the developing hypothalamus (***Figure 1—figure supplement 2***). At 24 hpf, a cluster of POMCb neurons is located at the dorsal limit of the hypothalamus basal plate, bordering the ORR (***Figure 2G–H'***). At 36 hpf, POMCb and POMCa are partially co-expressed in the anterior hypothalamus (***Figure 2I–J' and W***), with POMCb extending more dorsally close to the ORR, and POMCa more ventrally. At 84 hpf, POMCb neurons form two elongated stripes in the tuberal hypothalamus, but unlike POMCa, many POMCb neurons lie along the poc close to the hypothalamus/ORR border (***Figure 2K–L'***). Some of these POMCb neurons extend posteriorly, so that Hcrt and POMCb cells are very close to each other (compare ***Figure 1M'***-N' and ***Figure 2K'***-L'), but the two peptides are never co-expressed (***Figure 2W***). POMCb is also detected in the pituitary from 36 hpf onwards (***Figure 2I–L'***). From 36 hpf, POMCb neurons become more abundant in both the pituitary and the hypothalamus of SF, reaching about twice more cells at 84 hpf than in CF (***Figure 2M–N***).

Another neuropeptide expressed in this same region is AVT. It is expressed from 24 hpf in a very similar pattern to POMCb, and the two peptides indeed partially co-localize in some cells (***Figure 2O–T', W***). Between 36 hpf and 84 hpf, the number of AVT neurons in the hypothalamus keeps increasing in SF but not in CF so that AVT neurons are more abundant in SF (***Figure 2U***). In addition, two symmetrical clusters appear in the lateral and posterior ORR at 84 hpf (***Figure 2S–T'***), which we propose to belong to the teleost-specific NPO (***Herget et al., 2014***) (***Figure 1—figure***

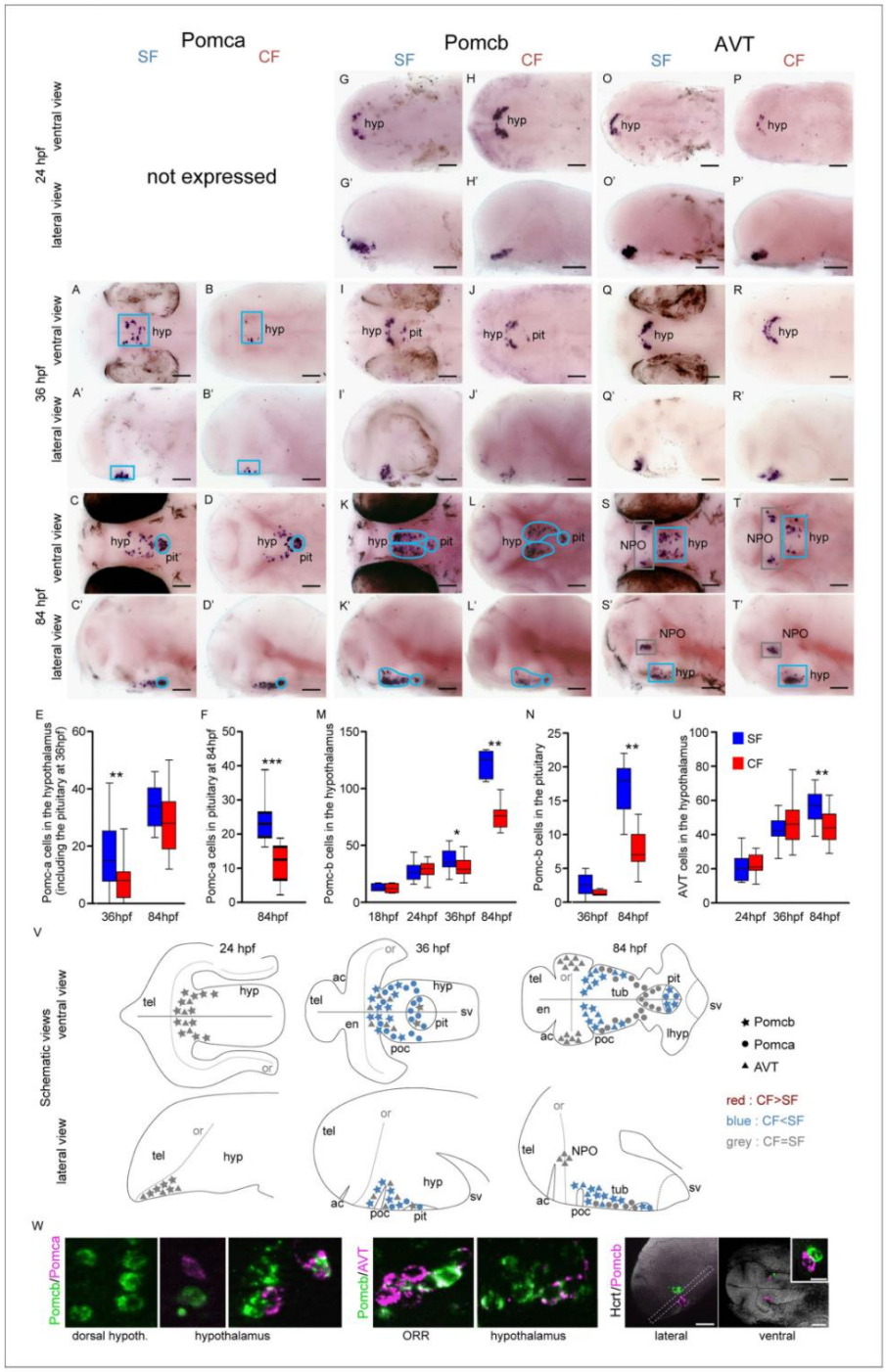

Figure 2. Comparative development of POMCa, POMCb and AVT neurons in SF and CF. (**A–T'**) Photographs of embryonic brains after in situ hybridization for POMCa, POMCb and AVT at 24, 36, and 84 hpf. The stages, the lateral or ventral orientations, and the probes are indicated. Blue squares indicate peptidergic clusters with higher numbers of neurons in SF. (**E, F, M, N, U**) Quantification and time-course of cell numbers in specific clusters. Mann-Whitney tests. (**V**) Anatomical interpretation of peptidergic patterns and time-course of appearance. POMCb (stars), POMCa (circles) and

Figure 2 continued on next page

Figure 2 continued

AVT (triangles) neurons are reported on schematic embryonic brains, in ventral or lateral views. A color code indicates higher numbers of neurons in CF (red) or in SF (blue), or equivalent numbers (grey). ac, anterior commissure; hyp, hypothalamus; NPO, neurosecretory preoptic nucleus; or, optic recess; orr, optic recess region; pit, pituitary; poc, post-optic commissure; tel, telencephalon; tub, tuberal hypothalamus; sv, *saccus vasculosus*. (**W**) Confocal pictures after double fluorescence in situ hybridization for POMCa/POMCb (left), POMCb/AVT (middle) and Hcrt/POMCb (right), showing colocalisation or lack of colocalisation of the indicated neuropeptides.

DOI: https://doi.org/10.7554/eLife.32808.010

The following figure supplements are available for figure 2:

Figure supplement 1. Comparative development of IT, CART and MCH neurons in SF and CF.

DOI: https://doi.org/10.7554/eLife.32808.011

Figure supplement 2. Comparative expression of *otpb* between 14 hpf and 36 hpf in SF and CF.

DOI: https://doi.org/10.7554/eLife.32808.012

supplement 1C). By contrast to the hypothalamus, the number of AVT cells in the NPO of SF and CF was not different (SF: 30.3 ± 2.7, n = 14; CF: 31 ± 3, n = 16).

Similar numbers of IT, CART3 and MCH neurons in developing cavefish and surface fish

The three other neuropeptides we studied are CART3, IT, and MCH (***Figure 2—figure supplement 1***). The results are summarized in panel T and the raw cell counts are provided as ***Supplementary file 1***. IT is expressed in two symmetrical groups in the lateral and posterior ORR, corresponding to the NPO as demonstrated by *Otpb* co-expression, and starting between 24 hpf and 36 hpf (***Figure 2-figure supplement 1A–E',U***). IT neurons counts were remarkably identical in the NPO of the two morphs at all stages examined (***Figure 2—figure supplement 1G,T***). CART3 is transiently expressed by more neurons in the SF telencephalon at 24 hpf and in the CF NPO at 36 hpf but none of these differences are maintained at 84 hpf (***Figure 2—figure supplement 1H–M',N,T***). Finally, MCH onset of expression is around 36 hpf, a stage where more MCH neurons are observed in a very discrete cell cluster of the posterior tuberal hypothalamus in CF (***Figure 2—figure supplement 1O–R',S***). At 84 hpf, the difference is not maintained, and a few MCH cells also appear in the mammillary region of the hypothalamus (***Figure 2—figure supplement 1Q–R',S,T***).

In sum, the comparative developmental maps of neuropeptidergic cell clusters presented above demonstrate region-specific, neuropeptide-specific, and time-specific differences in peptidergic neuron development in the two *Astyanax* morphs. There is a general trend for cavefish to possess more NPY, Hcrt, AgRP and less POMCa, POMCb, AVT neurons, even though these different types of neurons develop from the same or very close neuroepithelial zones in the hypothalamus basal plate, at the border of the ORR/PO region (examples: Hcrt/POMCb or AgRP/AVT). In line with this observation, these two categories of neuropeptides are never co-expressed. Interestingly, all peptidergic cell types showing quantitative variations in numbers between SF and CF were located in the basal plate of the hypothalamus. By contrast, neuropeptidergic cells located in the alar plate, in the NPO, displayed no difference between the two morphs. Finally, the data also show that in *Astyanax*, neuropeptidergic neurons show terminal differentiation signs (expression of their peptide transmitter) very early in embryogenesis, and therefore must be born equally early. The earliest expressed neuropeptides are Hcrt and POMCb (18hpf), followed by NPY, AVT, IT, CART3 (24hpf) and finally AgRP, POMCa, MCH (36hpf). The earliest differentiated neuropeptidergic cells are located in the dorsal hypothalamus at the frontier with the ORR, in a zone around the poc (***Figures 1U*** and ***2V***; ***Figure 1—figure supplement 1***).

Lhx7 and Lhx9 delineate NPY and Hcrt neuron territories and specify their peptidergic phenotypes

We next sought to define some of the causal molecular determinism for the above-described differences, taking advantage of the cavefish 'natural mutant' to pinpoint developmental mechanisms that can participate in the evolution of the hypothalamic networks in natural populations.

Previous analyses in zebrafish have defined the posterior half of the *otpa* (*orthopedia a*) domain as the larval NPO and as the homologous region to the mammalian PVN (***Herget et al., 2014***; ***Herget and Ryu, 2015***). In *Astyanax* embryos, *otpb* (and *otpa*, not shown) were also strongly

expressed in the region of the ORR corresponding to the NPO, and indeed co-localized with IT (***Figure 2—figure supplement 2*** and ***Figure 2—figure supplement 1U***). In line with the lack of difference of peptidergic populations in the NPO between SF and CF embryos, there was no difference in *otpb* (or *otpa*, not shown) expression patterns between the two morphs, between 14 hpf and 36 hpf (***Figure 2—figure supplement 2***).

For neuronal populations which vary between the two morphs and are located in the hypothalamic basal plate close to the ORR, we used a candidate approach focusing on two LIM-homeodomain TFs. We first built a co-expression map between *Lhx7* and *Lhx9,* and NPY, Hcrt and POMCb, at 24 hpf. The results described below apply for both SF and CF, as we did not observe qualitative differences between the two morphotypes (***Figure 3*** and ***Figure 3—figure supplement 1***).

Lhx7 and *Lhx9* are both expressed in the region of interest around the poc and they are not co-expressed (***Figure 3A***). *Lhx9* is seen in the hypothalamus, and *Lhx7* is expressed at the ORR/hypothalamic border (i.e. more dorsal than *Lhx9* according to the axis). In a lateral confocal plan, the two genes form diagonal domains parallel to the optic recess (***Figure 3A***). As neuronal differentiation occurs in a centrifuge fashion, from the progenitors lining the ventricular surface to the post-mitotic neurons at a distance from them in the mantle (Arrows in ***Figure 1—figure supplement 1B***) (***Affaticati et al., 2015***), the *Lhx7* and *Lhx9* patterns suggest that the 2 TFs are expressed in post-mitotic neurons.

All Hcrt neurons express *Lhx9* (***Figure 3B***). *Lhx9+/Hcrt-* cells are also visible around the Hcrt population. To further assess the functional role of *Lhx9* in Hcrt specification, we performed *Lhx9* morpholino (MO) knock-down and counted Hcrt neurons at 24hpf. Three different MOs were used: AUG MO, 5'UTR MO, and splice blocking MO. The latter was controlled for effective *Lhx9* knock-down by RT-PCR (***Figure 3—figure supplement 2A***). All 3 *Lhx9* CF morphants types had reduced numbers of Hcrt neurons in the hypothalamus when compared to mismatch (mm) control MO (***Figure 3CD*** and ***Figure 3—figure supplement 3A***). Moreover, co-injection of *Lhx9* mRNA with the splice blocking MO rescued the phenotype (***Figure 3D***). Conversely, embryos injected with *Lhx9* mRNA had more Hcrt neurons (***Figure 3CD***). Thus, *Lhx9* has a conserved role in Hcrt neurons specification in *Astyanax* when compared to mouse or zebrafish (***Dalal et al., 2013***; ***Liu et al., 2015***).

All NPY neurons express *Lhx7* (***Figure 3E,H***). At 24hpf and 84hpf (not shown), all NPY cells identified as the future *saccus vasculosus* express *Lhx7* - but only a subset of *Lhx7+* cells express *NPY* (***Figure 3E***). At 84 hpf, NPY cells located at the ORR/hypothalamic border also express *Lhx7* (***Figure 3H***). In addition, while some Hcrt neurons fall into the *Lhx7* domain and *Hcrt+* and *Lhx7* + cells were clearly intermingled, we could not detect any cell co-expressing the two genes (***Figure 3I***). Thus, *Lhx7* is a good novel candidate to play a role in NPY-ergic specification, a hypothesis which was tested through morpholino knock-down. *Lhx7* morphant CF (either AUG MO or 5'UTR MO or splice blocking MO; ***Figure 3—figure supplement 2B*** for controls) had less NPY neurons in the presumptive *saccus vasculosus* at 24 hpf (***Figure 3FG*** and ***Figure 3—figure supplement 3B***). Co-injection of *Lhx7* mRNA with the splice blocking MO rescued the phenotype (***Figure 3G***). Conversely, embryos injected with *Lhx7* mRNA showed more NPY neurons (***Figure 3FG***). These data demonstrate a novel role for *Lhx7*, which is necessary and sufficient for NPY neurons specification.

In contrast to NPY and Hcrt neuropeptides, we could not find any expression of the two LIM-hd TFs in POMCb neurons. In fact, POMCb neurons are located within the *Lhx9* and *Lhx7* domains, but they are intermingled in a salt-and-paper fashion among cells expressing the two TFs (***Figure 3JK***). POMCb cells are also excluded from the superficial acroterminal *Lhx7* domain (***Figure 3K***). In summary, POMCb neurons (less abundant in CF) are surrounded by NPY and Hcrt neurons (more abundant in CF) that express distinct TFs. In line with these expression data, the number of POMCb cells at 24 hpf was unaffected after *Lhx9* or *Lhx7* MO knock-down (***Figure 3—figure supplement 4A–C***). These results also confirm the specificity of Lhx9 and Lhx7 TFs functions toward Hcrt and NPY fates, respectively. These data are summarized in the schematic ***Figure 3L***.

Finally, we noticed that although non-statistically significant, POMCb cell numbers had a tendency to be slightly higher in CF *Lhx7* morphants than in their controls (***Figure 3—figure supplement 4C***). Given the anatomical organization of POMCb cells relatively to *Lhx9*/Hcrt cells and *Lhx7*/NPY cells, we next tested the possibility of a balance between POMCb versus Hcrt/NPY specification at progenitor level by double *Lhx9/Lhx7* knock-down in CF. However, the number of POMCb cells were unchanged in the double morphants (***Figure 3—figure supplement 4D***).

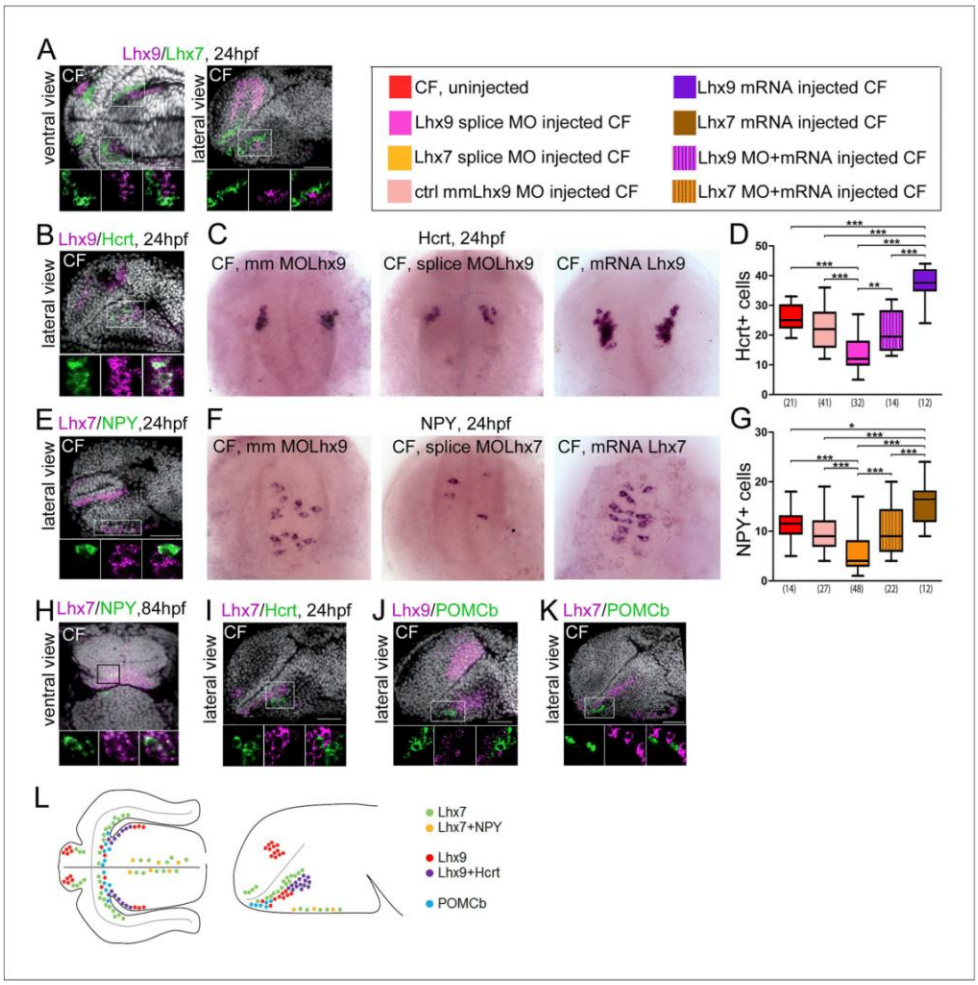

Figure 3. Expression and roles of Lhx7 and Lhx9 in NPY and Hypocretin neurons development. (**A, B, E** and **H–K**) Confocal pictures after double fluorescence in situ hybridization in CF (one probe in magenta, the other in green, as indicated) with DAPI counterstain (grey nuclei). On all panels, the orientation, the stage, and the probes are indicated. The top photos show low magnification pictures of the whole forebrain, and the bottom photos show high power views for assessment of co-localization. (**C**) Photographs of control mismatch (mm), *Lhx9* e1-i1 splice MO and *Lhx9* mRNA-injected CF embryos after Hcrt in situ hybridization at 24 hpf. (**D**) Quantification of the number of Hcrt cells in control mismatch (pale red, 0.48 mM), *Lhx9* splice MO-injected (pink, 0.48 mM), *Lhx9* mRNA (purple, 200 ng/µl) or *Lhx9* splice MO + *Lhx9* mRNA (striped) injected CF. Un-injected CF are in red. See color code. ANOVA tests. In this and the following figures, numbers under boxplots indicate the numbers of embryos examined. (**H**) Photographs of control mismatch (mm), *Lhx7* e4-i4 splice MO and *Lhx7* mRNA-injected CF embryos after NPY in situ hybridization at 24hpf. (**I,**) Quantification of the number of NPY cells in control mismatch (pale red, 0.96 mM), *Lhx7* splice MO-injected (orange, 0.96 mM), *Lhx7* mRNA (brown, 200 ng/µl) or *Lhx9* splice MO + *Lhx7* mRNA (striped) injected CF. Un-injected CF are in red. See color code. ANOVA tests. (**L**) Summary of Lhx7/Lhx9/NPY/Hcrt/POMCb expression. A color code indicates the presence or absence of co-localization.

DOI: https://doi.org/10.7554/eLife.32808.013

The following figure supplements are available for figure 3:

Figure supplement 1. Expression of *Lhx7*, *Lhx9*, *Hcrt* and *NPY* in SF.

DOI: https://doi.org/10.7554/eLife.32808.014

Figure supplement 2. Controlling *Lhx9* and *Lhx7* splice-blocking morpholinos knock-down efficiency.

DOI: https://doi.org/10.7554/eLife.32808.015

Figure supplement 3. Effects of *Lhx9* or *Lhx7* ATG and 5'UTR morpholinos knock-down on Hcrt and NPY neurons numbers, respectively.

DOI: https://doi.org/10.7554/eLife.32808.016

Figure supplement 4. Effects of *Lhx9* or/and *Lhx7* morpholino knock-down on POMCb neurons numbers.

DOI: https://doi.org/10.7554/eLife.32808.017

Expansion of Lhx7 and Lhx9 domains precedes the onset of Hcrt and NPY expression

We next reasoned that if *Lhx7* and *Lhx9* are involved in NPY and Hcrt specification, respectively, then their expression should precede neuropeptide expression, and may be spatially or temporally different between CF and SF embryos.

At 14-15 hpf, 4 hrs prior to the onset of Hcrt expression, *Lhx9* is expressed in the optic vesicles, but also in a stripe of cells adjacent to it (***Figure 4A***). This latter *Lhx9* domain topologically corresponds to the future Hcrt expression site. All CF but not all SF embryos present this stripe of cells at 14 hpf, suggesting that in this domain *Lhx9* expression is turned on slightly earlier in CF than in SF (***Figure 4—figure supplement 1***). We have then quantified the length of the *Lhx9* domain at 15 hpf and found that it is expanded in CF (***Figure 4A***). Indeed, while in CF these *Lhx9*+ cells extend all along the entire optic vesicle in SF they are restricted to the anterior half of the optic vesicle.

At 22 hpf, 2 hr prior to the onset of *NPY* expression in the acroterminal floor, *Lhx7* expression is already similar to that described above at 24 hpf (***Figure 4B***). Its expression is expanded in the superficial floor of the forming hypothalamus in CF (***Figure 4B***), where we found a higher number of NPY neurons 2 hr later as compared to SF. In ventral view the area covered by *Lhx7* +cells and the number of *Lhx7* +cells is higher in CF than SF and in lateral view the *Lhx7* +domain is extended in CF (***Figure 4B***). Moreover, in the dorsal hypothalamus, where we observed an increased number of NPY neurons at 84hpf in CF, we found an expanded *Lhx7* expression spot at 60 hpf, that is, 24 hr before the appearance of these neurons (***Figure 4C***), and in line with previous findings from the group (***Menuet et al., 2007***).

Taken together, these results show that the increased numbers of differentiating NPY and Hcrt neurons in the CF basal forebrain are preceded by a parallel expansion of their co-expressed *Lhx* genes. Although the functional analyses and the spatio-temporal co-expression data we provide cannot strictly be taken as an indication on the lineage of NPY and Hcrt neurons, they strongly suggest that the differences in hypothalamic peptidergic neuron patterning between SF and CF originate in the early embryonic neuroepithelium (e.g. before 14 hpf for *Lhx9*/Hcrt). Thus, we next decided to investigate whether the changes in neuropeptidergic cell numbers observed in CF are the consequence of the same embryonic signaling events that affect its neural tube and eye morphogenesis.

Fgf and Shh signaling during gastrulation control the future numbers of specific peptidergic neuronal populations

We reasoned that neuronal populations which vary between the two morphs are located in the basal hypothalamus, so that their progenitors are subjected to the influence of ventral midline, prechordal plate and basal plate Shh signaling, as well as anterior neural ridge/acroterminal domain Fgf signaling. In cavefish, heterotopic (larger) expression of *Shh* at the ventral midline and heterochronic (earlier) expression of *Fgf8* at the ANR impact the anterior neural plate fate map and lead to morphogenetic defects (***Yamamoto et al., 2004***; ***Pottin et al., 2011***). We hypothesized that in cavefish, the increased numbers of NPY and Hcrt neurons and the decreased numbers of POMCb neurons may result from changes in above signaling systems in the early neuroepithelium.

NPY neurons

To test this hypothesis, we performed cyclopamine treatments (50 µM; Shh signaling inhibitor) between 8 and 12 hpf in CF to mimic the SF condition. This resulted in a massive reduction of *Lhx7* expression in the prosencephalon, but without affecting at all the *Lhx7* acroterminal/putative *saccus vasculosus* domain at 24hpf (***Figure 5AB***), showing that the acroterminal and the hypothalamic NPY cell groups are controlled through distinct signaling mechanisms. Accordingly, the same cyclopamine treatment did not affect the number of NPY cells in the acroterminal region at 24 hpf (***Figure 5B***). As NPY hypothalamic cells arise later, around 84 hpf (***Figure 1***), and cyclopamine treatments affect later larval survival, we did not assess cyclopamine effect on 84 hpf larvae. We used instead a treatment with the FgfR signaling inhibitor SU5402 (5 µM; between 8 hpf and 12 hpf), which results in a decrease of *Shh* expression in CF, therefore also indirectly mimicking the SF phenotype (***Hinaux et al., 2016***; ***Pottin et al., 2011***), but with less deleterious effects on larval development. In line with the effect of cyclopamine on the hypothalamic *Lhx7* domain at 24 hpf, and with the role of *Lhx7* in NPY specification shown above, SU5402 treatment on CF caused a reduction of

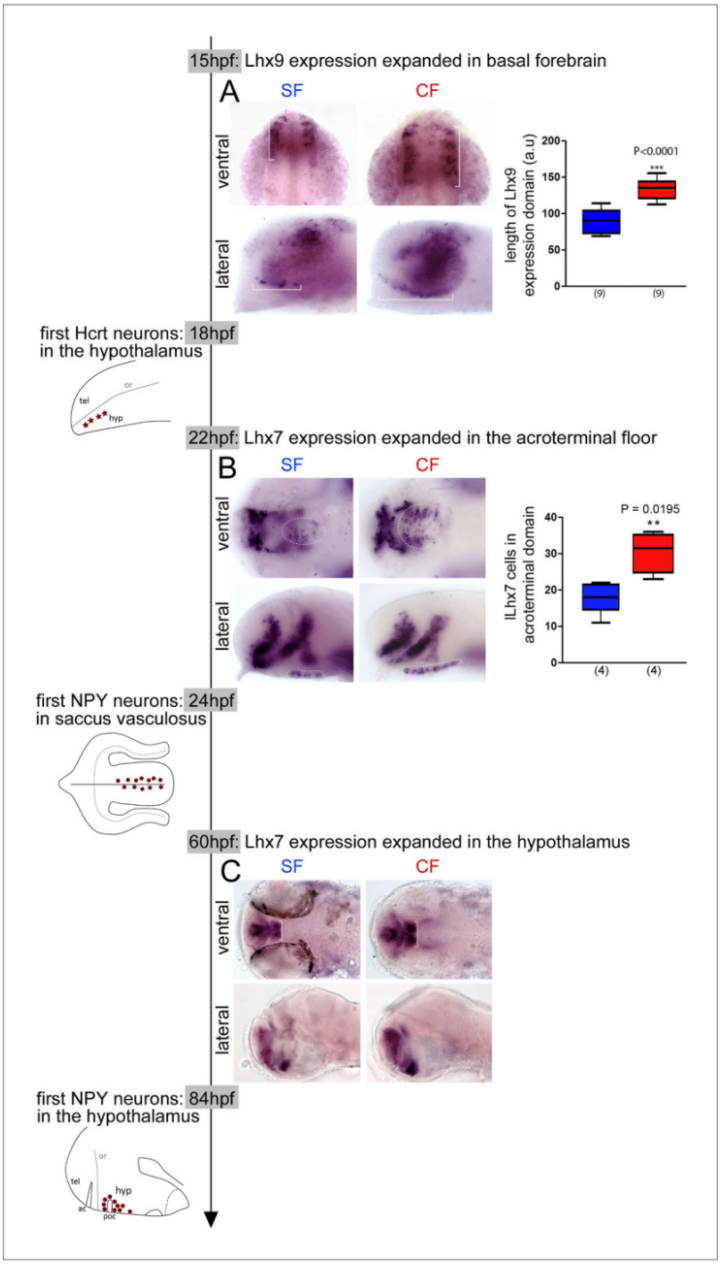

Figure 4. Time-line of expression of *Lhx9* and *Lhx7* relative to Hcrt and NPY neuron differentiation between 15 hpf and 84 hpf in SF and CF. (**A**) Photographs of embryonic brains after in situ hybridization for *Lhx9* at 15 hpf in SF and CF, in lateral and ventral views, and quantification of the hypothalamic expression domain (in brackets on the pictures). SF in blue, CF in red. (**B**) Photographs of embryonic brains after in situ hybridization for *Lhx7* at 22 hpf in SF and CF, in lateral and ventral views, and quantification of the acroterminal expression domain (in dotted lines on the pictures). SF in blue, CF in red. (**C**) Photographs of larval brains after in situ hybridization for *Lhx7* at 60 hpf in SF and CF, in lateral and ventral views.

DOI: https://doi.org/10.7554/eLife.32808.018

The following figure supplement is available for figure 4:

Figure supplement 1. A slight heterochrony in the onset of *Lhx9* expression between SF and CF.

DOI: https://doi.org/10.7554/eLife.32808.019

hypothalamic NPY cell numbers at 84 hpf (***Figure 5C***). Conversely, SU5402 had no effect on *Lhx7* expression or NPY neuron numbers in the acroterminal domain at 24 hpf or 84 hpf, confirming that Shh and Fgf signaling are not involved in the control of the size of this group of NPY cells (***Figure 5D***). As the acroterminal domain is a source of Fgf signaling according to the prosomeric model (***Puelles and Rubenstein, 2015***), and is also very close to Shh signaling sources in the hypothalamic basal plate, we sought to test the possibility that at later stages these signaling systems could affect the development of the future *saccus vasculosus* NPY cells. To this aim, CF embryos were treated with cyclopamine or SU5402 between 20 and 24 hpf, that is, during the time window when these NPY cells differentiate. However, neither of these treatments changed the number of acroterminal NPY cells assessed at 24 hpf (***Figure 5—figure supplement 1A***).

Hcrt neurons

Neither cyclopamine (50 µM, 8-12 hpf) nor SU5402 (5 µM, 8 hpf-12 hpf) treatment affected *Lhx9* expression at 15 hpf (***Figure 5EF***). Cyclopamine did not change the numbers of Hcrt neurons at 24 hpf either (***Figure 5G***) suggesting that Hcrt progenitors are not under the control of these signaling systems. We considered this result surprising as Hcrt cells (contrarily to NPY cells; ***Figure 5—figure supplement 1B***) clearly belong to the basal hypothalamus *Shh+* lineage (***Figure 5H***; see also [***Alvarez-Bolado et al., 2012***]). We thus performed the cyclopamine treatment slightly later, between 16 and 20 hpf. Such a treatment done during the differentiation of the first Hcrt neurons resulted in a decrease in Hcrt neurons numbers (***Figure 5IJ***), suggesting a positive control by Shh signaling on Hcrt differentiation (but not early specification). Of note, the same type of treatment with cyclopamine (16-20 hpf) or SU (16-20 hpf) did not affect POMCb cell numbers (***Figure 5—figure supplement 1C***), demonstrating further the specificity of Shh and FgfR signaling toward neuropeptidergic neurons development. Surprisingly, SU5402 (5 µM, 8 hpf-12 hpf) treatment on the other hand systematically resulted in a reduction of Hcrt cell numbers at 18 hpf or 36 hpf, persisting at 84 hpf (***Figure 5K***). This suggests that in this case, (1) the effect of early FgfR signaling is not mediated through a reduction of Shh signaling – as early cyclopamine treatment does not affect Hcrt cell numbers, and (2) FgfR signaling may be necessary or permissive to allow Lhx9 TF effect on Hcrt fate – as SU5402 diminishes Hcrt but not Lhx9 cell numbers.

In summary, this series of experiments provide evidence that Shh and FgfR signaling at the end of gastrulation and during neurulation influence later hypothalamic neuroanatomy, and thus are, at least in part, responsible for the developmental variation in neuropeptidergic patterning in the cavefish brain.

Behavioral consequences of the developmental evolution of neuropeptidergic patterning in cavefish

Finally, we sought to assess the functional outcomes of the above described variations in peptidergic neurons development in CF.

There is a striking general trend for cavefish to possess more orexigenic NPY, Hcrt and AgRP neurons (which stimulate food intake) and less anorexigenic POMCa, POMCb and VP neurons (which inhibit food intake; as shown above these two categories of neuropeptides are never co-expressed). Therefore, we first compared food intake between CF and SF larvae. We set up a test in which individual larvae were given an excess of *Artemia* nauplii, and the number of *Artemia* eaten over a period of 5 hr were counted. The test was performed on larval stages from 5.5 dpf (days post-fertilization, i.e. after mouth opening) to 26 dpf. At all ages studied, CF and SF larvae eat consistently the same amounts of food (***Figure 6A***). The results were identical after normalization to the size of the larvae, which may slightly vary between individuals after 10 dpf (not shown). This result is in line with recently published data showing that adult Pachón cavefish and their surface conspecifics have a comparable appetite (***Aspiras et al., 2015***), and further shows that larval food intake is also identical between the two morphs.

This result prompted us to examine alternative potential consequences for CF of having more of certain neuropeptidergic types. We focused on Hcrt, because this neuropeptide is also well known for its role in locomotion and sleep regulation, and CF larvae and adults show a dramatic change in these traits when compared to SF (***Yoshizawa et al., 2015***; ***Duboué et al., 2011***). We thus compared locomotor activity in 1-week-old *Lhx9* morphants, their controls, and SF. Importantly, 7 dpf

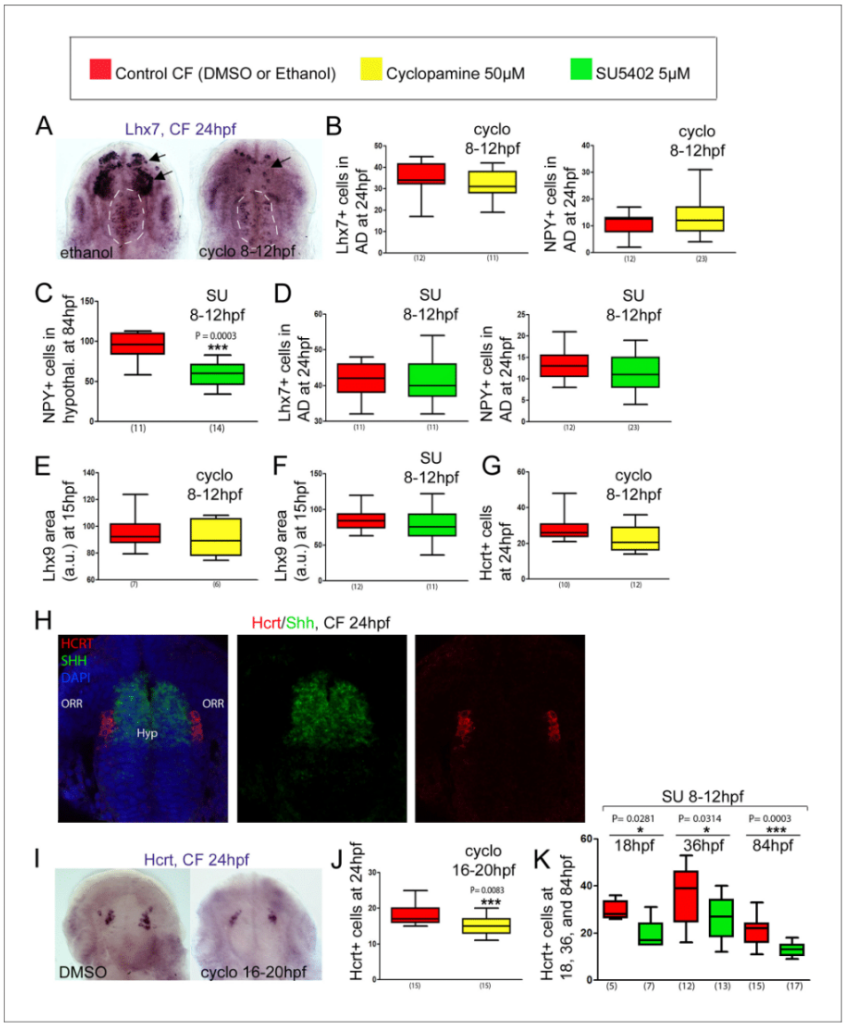

Figure 5. Effect of early or late inhibition of Shh and Fgf signaling on Lhx7, Lhx9, NPY, Hcrt and POMCb expression. (**A**) Photographs of embryonic brains after in situ hybridization for *Lhx7* at 24 hpf in control and cyclopamine-treated CF, in ventral views. The treatment was performed between 8 and 12 hpf. The presumptive *saccus vasculosus* (unaffected by the treatment) is delineated by a white dotted line, whereas the other, affected, expression domains are indicated by black arrows. (**B**) Quantification of the number of Lhx7 cells (left) and NPY cells (right) in the acroterminal domain (AD) of control CF (red) and cyclopamine-treated CF (yellow) at 24 hpf after an 8-12 hpf treatment. (**C**) Quantification of the number of NPY cells in the hypothalamus of control CF (red) and SU-treated CF (green) at 84 hpf after an 8-12 hpf treatment. Mann-Whitney tests. (**D**) Quantification of the number of Lhx7 cells (left) and NPY cells (right) in the AD of control CF (red) and SU-treated CF (green) at 24 hpf after a 8-12 hpf treatment. (**E, F**) Quantification of the Lhx9-expressing area in the hypothalamus of control CF (red) versus cyclopamine-treated (yellow)(**E**) or SU-treated CF (green)(**F**) at 15 hpf, after an 8-12 hpf treatment. (**G**) Quantification of the number of Hcrt cells in the hypothalamus of control CF (red) and cyclopamine-treated CF (yellow) at 24 hpf after an 8-12 hpf treatment. (**H**) Confocal pictures after double fluorescence in situ hybridization (Hcrt in red, Shh in green, as indicated) with DAPI counterstain (blue nuclei) at 24 hpf, in ventral view. (**I**) Photographs of embryonic brains after in situ hybridization for *Hcrt* at 24 hpf in control and cyclopamine-treated CF, in ventral views. The treatment was performed between 16 and 20 hpf. (**J**) Quantification of the number of Hcrt cells of control CF (red) and cyclopamine-treated CF (yellow) at 24 hpf after a 16-20 hpf treatment. Mann-Whitney tests. (**K**) Quantification of the number of Hcrt cells of control CF (red) and SU-treated CF (green) at 18, 36, and 84 hpf, after an 8-12 hpf treatment. Mann-Whitney tests.

DOI: https://doi.org/10.7554/eLife.32808.020

The following figure supplement is available for figure 5:

Figure supplement 1. Late inhibition of Shh or Fgf signaling has no effect on acroterminal NPY or POMCb differentiation.

DOI: https://doi.org/10.7554/eLife.32808.021

Lhx9 CF morphants still had less Hcrt neurons in their hypothalamus than controls, thereby mimicking the SF situation (***Figure 6B***), and showing that the effect of *Lhx9* knock-down has not been compensated. Behavioral recordings were then performed on 24 hr cycles. Seven dpf CF larvae are about 30–50% more active than SF (***Figure 6CD***), hence the difference in locomotor activity in the 7 dpf larvae of the two morphs is similar to that observed in older fish (***Yoshizawa et al., 2015***; ***Duboué et al., 2011***) or younger fish (***Pottin et al., 2010***). Of note, the locomotion did not vary significantly according to the day/night periods, although some level of diurnal rhythms has been reported in 3-week-old fish and in adults (***Yoshizawa et al., 2015***; ***Duboué et al., 2011***). This may relate to the developmental establishment of rhythmicity. Importantly, the distances swam by the 7 dpf *Lhx9* morphant CF with reduced numbers of Hcrt neurons was identical to SF, both during day and night (***Figure 6CD*** and ***Figure 6—figure supplement 1A***), suggesting a role for the CF supernumerary Hcrt neurons in the control of this behavior. *Lhx9* CF morphants behave like SF, while mm*Lhx9* MO-injected CF behave like un-injected CF (***Figure 6D***), showing that the injection by itself does not affect swimming behavior. We also quantified the time spent by the larvae in a state of low activity (***Kalueff et al., 2013***; ***Mathuru et al., 2012***). SF and *Lhx9* CF morphants spent 2 and 2.2 more time, respectively, in a hypoactive state than control CF (***Figure 6—figure supplement 1BC***). Therefore, the developmental control of hypothalamic peptidergic circuits that we have uncovered in CF has important behavioral consequences.

Discussion

In this paper, we provide evidence for developmental evolution of hypothalamic neuropeptidergic clusters that accompany adaptation of cavefish to life in the dark. We uncover some of the underlying developmental mechanisms, and we pinpoint behavioral consequences of such anatomical developmental variations. In our interpretations, we always consider SF as the 'wildtype controls' and CF as the 'natural mutants'.

Comparative developmental neuroanatomy

The anatomical interpretation of the results was crucial to draw hypotheses on the causal mechanisms of neuropeptidergic variations between the two *Astyanax* morphs. In particular, reasoning in terms of brain axes in the frame of the updated prosomeric model (***Puelles and Rubenstein, 2015***), and taking into account the particularities of the teleost brain (***Herget et al., 2014***; ***Affaticati et al., 2015***) was instrumental to understand that the most affected peptidergic populations in cavefish were located in the hypothalamic basal plate, while alar plate populations including those of the NPO were unchanged. In fact, the developmental origin of the neuropeptides we have studied is very similar in *Astyanax* fish and in mouse (***Díaz et al., 2014***) in terms of D/V and A/P coordinates (***Figure 7A***). For example, NPY, Hcrt, POMC and AgRP have basal progenitor sources while IT comes from alar sources and CART have alar +basal sources in both species. The only difference we observed in this regard is a double alar +basal origin of AVT cells in fish. The A/P organization seems also conserved with for example the fish Hcrt cluster in a posterior position that corresponds well to its origin in the peduncular hypothalamo-telencephalic prosomere (Hp1, tuberal part) in the mouse, or the AgRP fish cluster located in an anterior position that fits well with its acroterminal origin (tuberal part, arcuate nucleus) in the mouse (***Díaz et al., 2014***). We propose that early born fish NPY cells also belong to the acroterminal domain. In mouse, a population of NPY cells born in the tuberal (dorsal) part of the acroterminal domain migrates tangentially and ventrally inside the acroterminal domain to populate the arcuate nucleus (***Díaz et al., 2014***). In fish, acroterminal NPY cells also seem to migrate ventrally to end up in the position of the fish-specific *saccus vasculosus*, a circumventricular organ with poorly studied neurosecretory functions and that may serve as a sensor of seasonal changes in day length (***Castro et al., 1999***; ***Nakane et al., 2013***; ***Tsuneki, 1986***). These acroterminal NPY cells of fishes and mammals thus have a shared developmental origin but distinct final fates and functions. Finally and interestingly, early-born acroterminal and later-born hypothalamic NPY cells behaved strikingly differently with regards to their response to signaling influences emanating from the borders of the neural plate and tube, further emphasizing the importance of interpreting anatomical data according to models of brain development.

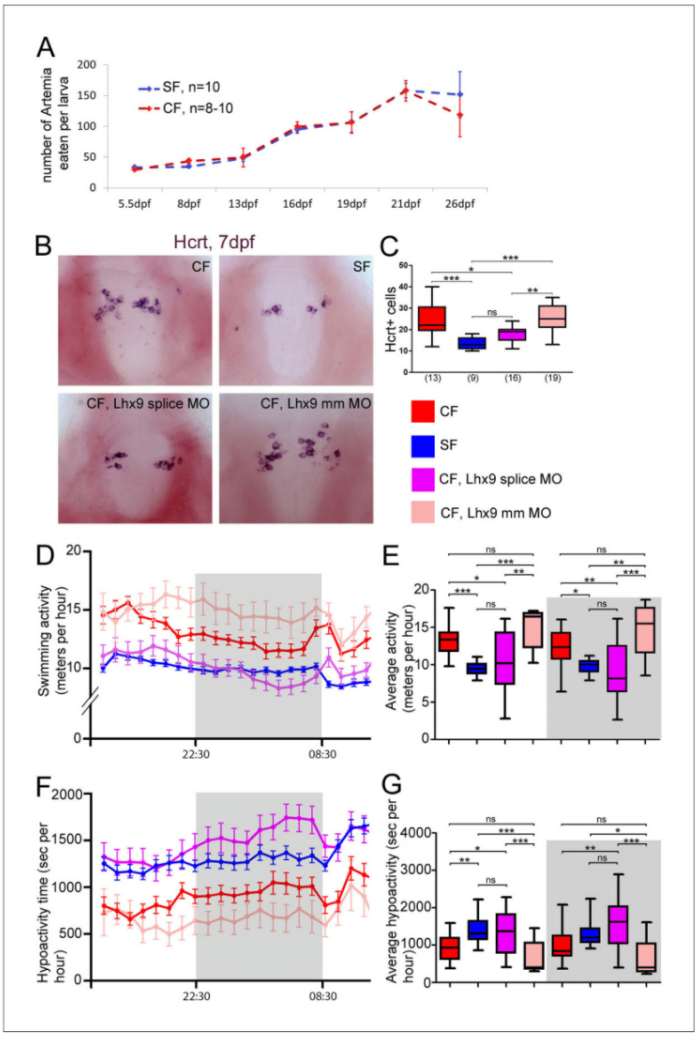

Figure 6. Neuropeptidergic evolution and cavefish larval behavior. (**A**) Comparison of food intake during larval and juvenile stages in SF (blue) and CF (red). (**B, C**) Photographs of brains after in situ hybridization for Hcrt, in ventral views, in 7 dpf juveniles, in the indicated condition (**B**) and quantification of Hcrt cell numbers at 7 dpf in CF (red), SF (blue), *Lhx9* splice MO-injected (purple) and mm*Lhx9* injected CF (pale red). (**C**). ANOVA test. (**D, E**) 24 hr plots of locomotor activity, and histogram showing average activity in the four conditions (see color code). The dark/night time is shaded in grey. In these and following graphs, the numbers of tested larvae are: CF, n = 23; SF, n = 21; *Lhx9* splice MO-injected CF, n = 33; mm*Lhx9* injected CF, n = 11. ANOVA test. (**F, G**) 24 hr plots of time spent in hypoactivity, and histogram showing average time spent in hypoactivity in the four conditions (see color code). The dark/night time is shaded in grey. ANOVA test.

DOI: https://doi.org/10.7554/eLife.32808.022

The following figure supplement is available for figure 6:

Figure supplement 1. Statistics on locomotion data on 24 hr.

DOI: https://doi.org/10.7554/eLife.32808.023

Factors influencing the development of neuropeptidergic clusters

Neuropeptidergic clusters showing cell number differences between SF and CF are all located in the dorsal part of the hypothalamic basal plate, in a region topologically corresponding to the tuberal hypothalamus in mouse. Conversely, NPO clusters do not vary between the two morphs. Even more so, in the case of AVT which displays alar and basal clusters in *Astyanax*, the alar NPO cluster is

identical in SF and CF but the basal hypothalamic cluster is larger in SF. This strongly suggests that the neuroepithelial region giving rise to the 'tuberal' hypothalamus in CF is specifically subjected to patterning variations. Interestingly, in their new interpretation of prosencephalic development, Puelles et al. ascribe the induction of the hypothalamic basal plate in its ventrodorsal axis to the action of the migrating prechordal plate (**Puelles and Rubenstein, 2015**; **García-Calero et al., 2008**), rather than to the notochord. In cavefish, there is evidence for stronger Shh and dynamically modified Bmp4 signaling from the prechordal plate at the end of gastrulation (**Hinaux et al., 2016**; **Yamamoto et al., 2004**). On the other hand, Fgf8 secreted from the ANR potentially influences neuroepithelial regions topographically related to the anterior commissure, the rostral-most point of the neural tube, and also interacts with the Shh-secreting prechordal plate (**Hinaux et al., 2016**; **Pottin et al., 2011**). There, Fgf8 is expressed earlier in CF than in SF. Moreover, Fgf8/10/18 are also expressed at later stages in the acroterminal domain itself from embryonic day 11.5 in the mouse (**Ferran et al., 2015**) and from 15 hpf in zebrafish ([**Sbrogna et al., 2003**] and ZFIN), representing another potential source of signaling molecules.

Focusing on NPY, Hcrt and POMCb neurons, and using early (8-12 hpf) or later (16-20 hpf) pharmacological manipulations, we found that early Shh and FgfR signaling at neural plate stage positively regulate the size of a Lhx7/NPY cluster which differentiates in the hypothalamus at 84 hpf (**Figure 7B**). Conversely, the Lhx7/NPY cells of the acroterminal *saccus vasculosus* are insensitive to these signaling systems, and more investigations are needed to understand why they are more numerous in CF. Concerning the Lhx9/Hcrt cells, while an unknown mechanism must be responsible for the initial enlargement of the *Lhx9* expression domain at early stage, we uncovered a positive role of Shh/FgfR signaling during their differentiation but not their initial specification at neural plate stage, together with a putative 'priming' role of FgfR signaling for future Hcrt development (**Figure 7B**). Taken together, these data show that signaling variations at the end of gastrulation (i.e. unexpectedly very early) and during neurulation influence later hypothalamic progenitor dynamics and/or neuronal differentiation, and thus are, at least in part, responsible for the developmental variation in neuropeptidergic patterning in the cavefish brain. These data also add to the emerging knowledge on the role of signaling molecules on the successive steps of development of hypothalamic cell types (examples: [**Bosco et al., 2013**; **Muthu et al., 2016**; **Peng et al., 2012**; **Russek-Blum et al., 2008**]).

In addition, we provide evidence for a novel role of Lhx7, necessary and sufficient for the specification of NPY neurons. In the past years, several factors controlling specification and differentiation within specific nuclei or regions of the developing hypothalamus have been found (for review [**Bedont et al., 2015**]), among which LIM-homeodomain TFs are well represented. Indeed, Lhx9 is necessary and sufficient for Hcrt neuron specification in zebrafish and mouse (**Dalal et al., 2013**; **Liu et al., 2015**), a role that we also find conserved in *Astyanax*. Islet1 controls hypothalamic (but not pituitary) POMC/POMCa development in mouse and zebrafish, respectively (**Nasif et al., 2015**), and Lhx1 controls differentiation of several peptidergic types including VIP or Enk in the suprachiasmatic nucleus (**Bedont et al., 2014**). The present finding of the Lhx7/NPY link suggests the possibility of an emerging 'LIM code' for hypothalamic cell type development (**Bachy et al., 2002**; **Shirasaki and Pfaff, 2002**).

From developmental evolution of neuronal clusters to behavior

The developing hypothalamus is larger in *Astyanax* CF than SF (**Menuet et al., 2007**; **Rétaux et al., 2008**). We reasoned that if all the hypothalamic neuronal populations of *Astyanax* CF were homothetically changed, then the net resulting behavioral and metabolic consequences should not be modified. But it is not the case. Some peptidergic clusters are larger, some are smaller, and some are unchanged. This prompted us to investigate potential functional behavioral consequences of these variations.

Within the arcuate nucleus of the mouse hypothalamus, neurons directly act on food intake and energy balance, with sometimes antagonist effects. Neurons that co-express NPY and AgRP, together with Orexin/Hcrt neurons, act to increase appetite (orexigenic). On the contrary, neurons that co-express CART and POMC decrease appetite (anorexigenic) (for reviews [**Loh et al., 2015**; **Larsen and Hunter, 2006**; **Millington, 2007**]). These systems are functionally conserved in fish (**Cerdá-Reverter et al., 2011**; **Volkoff and Peter, 2006**), including *Astyanax* cavefish (**Penney and Volkoff, 2014**; **Wall and Volkoff, 2013**). Here, we found that increased numbers of orexinergic

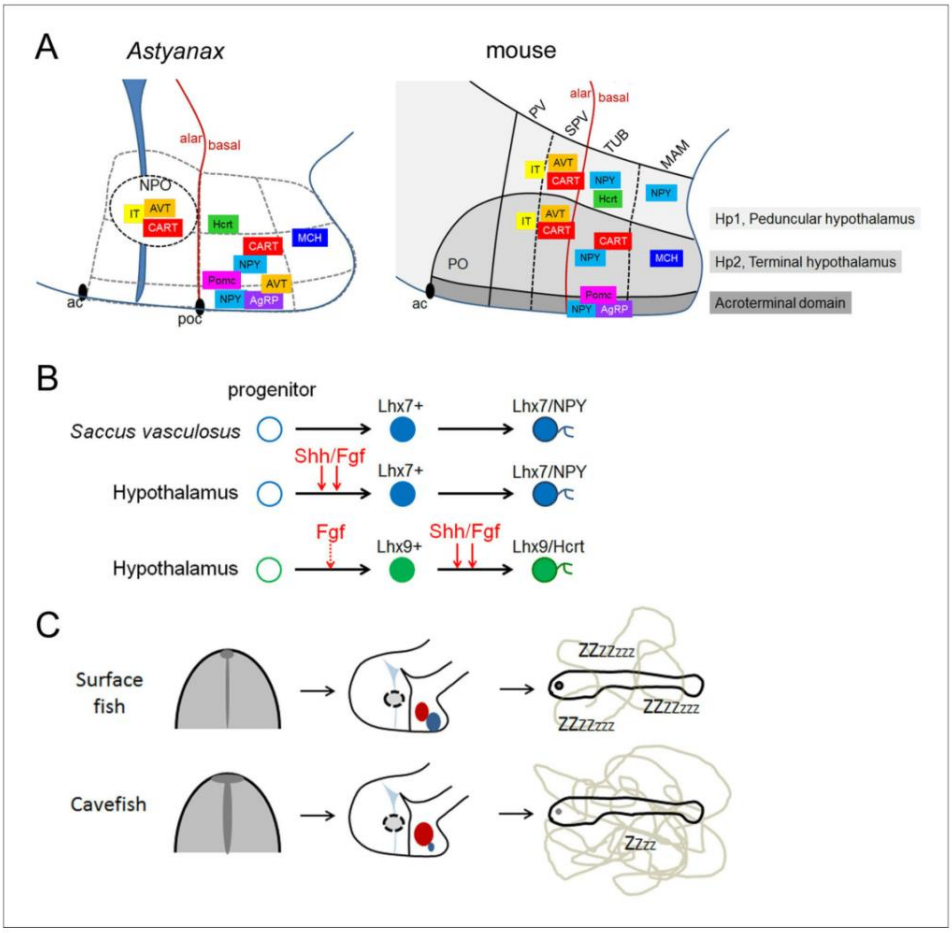

Figure 7. Summary schemes. (**A**) Comparative developmental maps of neuropeptidergic cell types between *Astyanax* and mouse. For mouse, data were taken from (***Díaz et al., 2014***). For *Astyanax mexicanus*, boundaries between putative hypothalamic subdivisions are grey dotted lines because we did not assess the position of the neuropeptidergic clusters within molecularly distinct cytoarchitectonic domains as it was done in the mouse (***Ferran et al., 2015***). Their relative positions are indicated, according to the brain axes and to the double labeling we have performed. Their localization in the mouse-like subdivisions is only tentative. (**B**) Signaling and transcription factors involved in NPY and Hcrt neurons development. Shh/Fgf signaling acts at different steps for the two neuropeptidergic types of neurons. The 'priming' effect of Fgf signaling on Hcrt fate without affecting *Lhx9* expression is indicated by a dotted line. (**C**) From early developmental evolution to behavioral consequences in cavefish. The SF/CF comparison is schematized at neural plate stage (left, with modified midline signaling in CF), at embryonic stage (middle, with modified hypothalamic peptidergic cluster sizes in CF), and in terms of larval behavior (right, with increased locomotion in CF).

DOI: https://doi.org/10.7554/eLife.32808.024

neurons (NPY, Hcrt, AgRP) and decreased numbers of anorexigenic neurons (POMCa/b, AVT) do not have a direct effect on food intake in Pachón CF larvae and juveniles. This is in contrast to adults and juveniles of other CF populations such as Tinaja or Molino, who carry a mutation in the coding sequence of the melanocortin four receptor (mc4r) (***Aspiras et al., 2015***), a constitutively-activated receptor on which AgRP acts as an antagonist, including in fish (***Cerdá-Reverter et al., 2011***). In the Pachón CF, who do not carry this mutation, compensatory mechanisms to the disequilibrium in orexigenic/anorexigenic neurons might exist. This may include modulations by other neurotransmitter systems which are also modified in CF, such as the serotonergic system (***Elipot et al., 2013***; ***Elipot et al., 2014a***), well known as a negative appetite-regulating system through its action on the melanocortin system (***Lam et al., 2010***).

Hcrt in the hypothalamus has a conserved role in the regulation of locomotion and sleep (**Sakurai et al., 2010**). Here, we have developmentally manipulated the number of Hcrt neurons in CF through *Lhx9* MO knock-down. We found that 7dpf CF with reduced numbers of Hcrt neurons show decreased locomotion and increased hypoactivity state at larval stage, and are indistinguishable from the SF behavior. Therefore we propose that high locomotor activity in CF is due to developmental evolution of their Hcrt system (**Figure 7C**).

Mice with reduced numbers of orexin neurons are narcoleptic (**Hara et al., 2001**) and zebrafish overexpressing Hcrt are hyperactive and display an insomnia-like phenotype (**Prober et al., 2006**) (in fish, sleep-like states can be identified behaviorally as periods of inactivity associated with increased arousal thresholds). Moreover, in zebrafish, Hcrt seems to control the transitions from states of no or low activity into a high activity state (**Prober et al., 2006**). In *A. mexicanus*, high locomotor activity and reduction of sleep are described in 3 weeks old and adult CF (**Yoshizawa et al., 2015**; **Duboué et al., 2011**), and genetic or pharmacological inhibition of Hcrt signaling increases sleep duration in adult CF (**Jaggard et al., 2017a**). Although we have not directly measured sleep in the present study, it is tempting to speculate that developmental evolution of the Hcrt cluster in CF plays a role in sleep loss. Other neurotransmitters might play a role as well: noradrenalin, whose brain levels are higher in Pachón CF than in SF (**Elipot et al., 2014a**), also regulates sleep in CF (**Duboué et al., 2012**).

In conclusion, we provide a developmental origin to the evolution of behavior in cavefish. Juveniles and adults of Pachón CF show vibration-attraction behavior mediated by their more sensitive lateral line neuromasts (**Yoshizawa et al., 2010**), and ablation of the lateral line enhances sleep in the Pachón cavefish population (**Jaggard et al., 2017b**), suggesting that heightened sensory input participates to evolutionarily derived sleep loss in adults. QTL studies have recently demonstrated that increased locomotion/sleep loss and enhanced sensory responsiveness have a different genetic determinism (**Yoshizawa et al., 2015**). No loci linked to the CF locomotor activity phenotype have been identified so far, but they may well correspond to early embryonic signaling pathways which determine the numbers of neurons in the Hcrt hypothalamic cluster.

Materials and methods

Fish samples

Laboratory stocks of *A. mexicanus* surface fish and cavefish (Pachón population) were obtained in 2004 from the Jeffery laboratory at the University of Maryland, College Park, MD. Fish are maintained at 23–26°C on a 12:12 hr light:dark cycle. Embryos were collected after spawning and fixed at various stages in 4% paraformaldehyde (PFA), overnight at 4°C. Embryos younger than 24hpf that had not hatched were de-chorionated manually then fixed again for 12 hr at 4°C. After progressive dehydration in methanol, they were stored at −20°C. For morpholino injection experiments, eggs were obtained by in vitro fertilization. *A. mexicanus* development is highly similar to zebrafish in the first 20 hr post-fertilization (hpf) and, importantly, there is no difference in early developmental timing between the cave and surface forms (**Hinaux et al., 2011**). Animals were treated according to the French and European regulations for handling of animals in research. SR's authorization for use of animals in research including *Astyanax mexicanus* is 91–116 and Paris Centre-Sud Ethic Committee authorization numbers are 2012–0052, −0053, and −0054.

Phylogenetic analyses

Astyanax mexicanus sequences similar to Pomcb, Pomca, AgRP, IT, CART3, NPY, AVT and Hcrt were obtained by TBlastN searches using *Danio rerio* sequences on the *A. mexicanus* EST assembly or developmental transcriptome contig sequences [available at http://genotoul-contigbrowser.toulouse.inra.fr:9099/index.html, (**Hinaux et al., 2013**)]. Alignments were constructed using available sequences retrieved by blast searches on public databases for a representative set of chordates. Sequences were aligned using Mafft (**Katoh and Standley, 2013**). Alignments were slightly corrected manually to eliminate major mistakes. Ambiguous regions were identified by visual inspection and removed manually. Maximum-likelihood (ML) analyses were performed using the PhyML program (**Guindon et al., 2003**), with the LG model of amino-acid substitution and a BioNJ tree as the input tree. A gamma distribution with four discrete categories was used in these ML analyses. The

gamma shape parameter and the proportion of invariant sites were optimized during the searches. The statistical significance of the nodes was assessed by bootstrapping (100 replicates). Resulting phylogenetic trees are not shown and are available upon request.

cDNA cloning and data availability

Total RNA from cavefish embryos at multiple stages was reverse transcribed with random primers using AMV reverse transcriptase (Promega). Sequence for Hcrt transcript was obtained from our own next-generation sequencing data, and partial 750 bp sequence was amplified by PCR using specific primers. PCR products were subcloned in TOPO-PCR II vector (Invitrogen, Carlsbad, CA, USA) and sequenced. They corresponded to XM_007287820.3 (Hcrt precursor mRNA predicted from the genome). Pomcb, Pomca, AgRP, IT, AVT, CART3 and NPY cDNAs were obtained from our in house clonal library of ESTs (accession numbers FO375681, FO257910, FO289826, FO221370, FO234678, FO230154, FO263072). PCR products were sequenced by Sanger method before probe synthesis. Lhx9 (NM001291259.1) and Lhx7 cDNA were previously cloned by our group and by David Stock, respectively. These two LIM-homeodomain factors were chosen for analysis because unpublished work in the group had mapped their expression domains in the exact territories where Hcrt and NPY cells (modified in numbers in cavefish) are located.

Whole-mount in situ hybridization

The expression patterns of nine neuropeptides (Agouti-related protein/AgRP, Arginine-Vasotocin/AVT, Cocaine and Amphetamine related transcript/CART3, Oxytocin-Isotocin/IT, Melanin-Concentrating Hormone/MCH, Neuropeptide Y/NPY, Hypocretin/Hcrt (also called orexin), and Pro-opiomelanocortin a and b/POMCa and POMCb) were systematically studied at three embryonic and larval stages: 24 hpf (hatching), 36 hpf (swimming larva), and 84 hpf (before first feeding) (***Hinaux et al., 2011***), which correspond to important steps in the morphogenesis and development of the secondary prosencephalon where most peptidergic neurons are located. These nine neuropeptides were chosen to cover the whole neuroendocrine territory in the basal forebrain (NPO, optic region, hypothalamus), and with respect to their known physiological roles in relation with known behavioral modifications in cavefish. The nine neuropeptides all show increasingly complex expression patterns as development proceeds. In some cases, earlier stages were also studied to determine the onset of neuropeptide expression.

cDNAs were amplified by PCR, and digoxygenin- or fluorescein-labelled riboprobes were synthesized from PCR templates. Embryos were rehydrated by graded series of EtOH/PBS, then for embryos older than 24 hpf, proteinase-K permeabilization at 37°C was performed (36hpf: 10 µg/ml, 15 min; 84 hpf: 40 µg/ml, 30 min; 7 dpf: 100 µg/ml, 45 min) followed by a post-fixation step. Riboprobes were hybridized for 16 hr at 65°C and embryos were incubated with anti-DIG-AP (Roche, dilution 1/4000) overnight at 4°C. Colorimetric detection with BCIP/NBT (Roche) was used. Mounted embryos were imaged on a Nikon Eclipse E800 microscope equipped with a Nikon DXM 1200 camera running under Nikon ACT-1 software. For fluorescent in situ hybridization, Cy3- and FITC-tyramides were prepared as described (***Zhou and Vize, 2004***). Embryos were incubated with anti-FITC-POD antibody (Roche, 1/400), washed in PBS/Tween 0.1% (PBST) and incubated for 20 min at room temperature with FITC-tyramide at 1/100. Tyramides were activated by H2O2 (Sigma, 0.003%) for 1 hr and washed again in PBST. The first peroxidase conjugate was inactivated by incubation in 3% H2O2 for 30 min at room temperature. Embryos were washed in PBST and incubated with the second antibody (anti-digoxygenin-POD, Roche, 1/200). The same protocol was applied for the Cy3-tyramide revelation. Then embryos were stained with Dapi at a final concentration of 1 µg/ml, overnight at 4°C, and washed in PBS before mounting. Fluorescent in situ hybridizations were imaged on a Leica-SP8 confocal microscope combined to Leica Application Suite software.

Neuron quantification and statistical treatment

Neuron counting and delineation of expression domains were performed by eye on colorimetric in situ hybridizations, on dissected and mounted fish brains. Counts were performed under the microscope (not on pictures) while progressively changing the plane of focus and ticking each counted cell on the camera software. We found that this method was reliable and gave highly reproducible results (***Figure 1—figure supplement 3***). Investigators were not blinded to fish groups (CF vs SF or

control vs morphants) and animals were not randomly allocated to experimental groups because pigmentation renders SF and CF immediately distinguishable. In the absence of existing pilot studies, no effect size was pre-specified and therefore no sample size was predetermined. For pair-wise comparisons, and when the distribution of the data was not normal, we used Mann-Whitney non-parametric tests. For multiple comparisons, and when the distribution was normal, ANOVA analyses were performed, with Bonferroni's post-test. Statistical significance was set at $p<0.05$ (*$p<0.05$; **$p<0.01$; ***$p<0.001$). Values represent the results of at least two independent experimental replicates.

Pharmacological treatments

Manually or chemically (Pronase 417 µg/mL; 3 min) de-chorionated CF embryos were incubated in 50 µM cyclopamine (C-8700, LC Laboratories) or 5 µM SU5402 (215543-92-3, Calbiochem) diluted in HBSS (55037C, Sigma) at developmental stages indicated in the main text. Controls were incubated in an equivalent concentration of ethanol or DMSO, respectively. They were washed in HBSS, raised in HBSS/methyl cellulose (M0387, Sigma)/Penicillin Streptomycin 1X (P4333, Sigma) and fixed at stages of interest. To define and ascertain the effect of cyclopamine and SU5402, we checked that hatched larvae have a typical 'comma shape' or tail bud defects, respectively.

Morpholino and mRNA injections

FITC-labeled Morpholino oligos (MOs) were designed and produced by Gene Tools, complementary to the 5'UTR, AUG and exon-intron (e-i) junctions containing sequences in the *Lhx7* and *Lhx9* mRNA. The sequences were as follows:

Lhx7 AUG MO, 5'-GTTCATCTCTCCAGAACATGAGGGT-3';
Lhx7 5'UTR MO, 5'- ACTCAGGCTGAGCAACAGGAGAACC-3';
Lhx7 e4-i4 splice blocking MO, 5'-GTAAGTAATTCTGACCGTTCTTCCAT-3';
Lhx9 AUG MO, 5'-CCTTGCACCCCACCACTTCCATAC-3';
Lhx9 5'UTR MO, 5'-CTCCGCAGCCTCAGACCATCCGAAA-3';
Lhx9 e1-i1 splice blocking MO, 5'- GAAGTTAAAGATCTCACCGTCTCCC-3'.

MOs were re-suspended in distilled water to prepare stock solutions at a final concentration of 1 mM. Different dilutions of stock solutions were tested for each MO (working solutions, containing 0.05% Phenol red) to avoid abnormal phenotypes due to toxicity. Embryos were injected with 5–10 nL of working solutions using borosilicate glass pipettes (GC100F15, Harvard Apparatus LTD) pulled in a Narishige PN-30 Puller (Japan). For each experimental condition, the same concentration of a MO, with a similar sequence to the *Lhx9* 5'UTR MO, but containing five mismatches (5'-CgTTcCACCgCACCAgTTCgATAC-3', i.e. mm*Lhx9* MO), was injected as control. Injected embryos positive for FITC were screened under fluorescence.

Full length *Lhx7* and *Lhx9* cDNA were amplified (AccuPrime Pfx DNA Polymerase, ThermoFisher) and cloned into the pCS2 +vector using BamHI and XbaI restriction sites.

Primers used were as follows:

Lhx7 forward, 5'-GGTGGTGGATCCACCATGTTCTGGAGAGATGAACAAACGG-3';
Lhx7 reverse, 5'-ACCACCTCTAGACTAAAAATGCTCTGATAGGTTTGGGCT-3';
Lhx9 forward, 5'-GGTGGTGGATCCACCATGGAAGTGGTGGGGTGCAA-3';
Lhx9 reverse, 5'-ACCACCTCTAGATTAGAAAAGATTTGTCAAGGTAGTTTGTGGG-3'; mRNAs were prepared in vitro with the mMessage mMachine kit (ThermoFisher) using the SP6 RNA polymerase. 5 µL of *Lhx7* or *Lhx9* mRNA were injected per embryo at a final concentration of 100–150 ng/µL and 150–200 ng/µL, respectively.

To test the efficiency of the splice blocking MOs, the E4E5 junction of *Lhx7* mRNA and E1E2 junction of *Lhx9* mRNA were amplified from cDNA samples and PCR products were visualized in an agarose gel (1%) to determine the sizes of the amplicons. As controls of size, genomic DNA was also included as template. The primers used were:

*Lhx7_* e4-e5 forward, 5'-AAGGAAACACCTACCACCTCG-3';
*Lhx7_* e4-e5 reverse, 5'-TGGTTCGTGCTCTTTTGGCT-3';
*Lhx9*_e1-e2 forward, 5'-CTGGCCAAAACGGTCCAGAT-3';
*Lhx9_* e1-e2 reverse, 5'-CGACTCCAAGGCCAGTTTACA-3'.

As control, levels of *β-actin* and *gapdh* mRNAs were also assessed through semi-quantitative RT-PCR. The primers used were: *gapdh* forward, 5′-GTTGGCATCAACGGATTTGG-3′; *gapdh* reverse, 5′-CCAGGTCAATGAAGGGGTCA-3′;

β-actin forward, 5′-GGATTCGCTGGAGATGATGCTC-3′;

β-actin reverse, 5′-CGTCACCTTCACCGTTCCAGT-3′.

Behavioral analyses

For the feeding assays, 10 CF and 10 SF larvae were individually raised in 60 mm diameter Petri dishes containing 15 mL of blue water (***Elipot et al., 2014***) from 2.5 dpf onwards, in ambient light conditions. Twice a week, at noon, starting from 5.5dpf (when the mouth is opened) and until 1mpf, a precise excess amount of 2-day-old artemia nauplii was manually counted and added to each Petri dish (1st week: 100 nauplii, 2nd week: 120 nauplii, 3rd week: 200 nauplii and 4th week: 300 nauplii). Water volume was constant during 1 month including during the feeding test (water volume added with nauplii was removed immediately). Fish were allowed to feed for 5 hr. The amount of leftover nauplii was then removed and counted to deduce the number of nauplii eaten. On all other days, larvae were fed once a day with an excess of artemia nauplii and the medium was changed twice a day.

For the locomotion/activity assays, 6 dpf fish were individually placed in one well of a 24-well plate the day before starting the experiment, for habituation during 18–24 hr. For automatic tracking (ViewPoint imaging software), animals were illuminated from below with an infra-red light source and recorded with a Dragonfly2 camera (ViewPoint) during 26 hr. In order to simulate circadian conditions, lights were turned on from 8:30 (AM) to 22:30 (14:10 hr light:dark cycle). Average and minimum speed (mm/s) were calculated on 10 min bouts in CF to set a threshold speed (two times the minimum speed). Values under this threshold were considered as states of low-activity. After the recordings, animals were sacrificed and fixed for ISH processing and counting of Hcrt neurons.

Acknowledgements

We thank Stéphane Père and Victor Simon for care of our *Astyanax* breeding colony, and Cynthia Froc of the Amatrace platform for help with behavior experiments. Work supported by an ANR (Agence Nationale pour la Recherche) grant [BLINDTEST] and an « Equipe FRM » grant [DEQ20150331745] from the Fondation pour la Recherche Médicale to SR.

Additional information

Funding

Funder	Grant reference number	Author
Agence Nationale de la Recherche	Blindtest	Sylvie Retaux
Fondation pour la Recherche Médicale	DEQ20150331745 RETAUX	Sylvie Retaux

The funders had no role in study design, data collection and interpretation, or the decision to submit the work for publication.

Author contributions

Alexandre Alié, Conceptualization, Investigation, Writing—original draft; Lucie Devos, Conceptualization, Investigation; Jorge Torres-Paz, Conceptualization, Investigation, Methodology, Writing—original draft; Lise Prunier, Fanny Boulet, Maryline Blin, Yannick Elipot, Investigation; Sylvie Retaux, Conceptualization, Supervision, Funding acquisition, Investigation, Writing—original draft, Project administration, Writing—review and editing

Author ORCIDs

Sylvie Retaux http://orcid.org/0000-0003-0981-1478

Ethics

Animal experimentation: Animals were treated according to the French and European regulations for handling of animals in research. SR's authorization for use of animals in research including Astyanax mexicanus is 91-116 and Paris Centre-Sud Ethic Committee authorization numbers are 2012-0052, -0053, and -0054.

Decision letter and Author response

Decision letter https://doi.org/10.7554/eLife.32808.044
Author response https://doi.org/10.7554/eLife.32808.045

Additional files

Supplementary files

- Supplementary file 1. Cell counts. Table showing raw data for cell counts for the nine studied neuropeptides in CF and SF at three different developmental stages.

DOI: https://doi.org/10.7554/eLife.32808.025

- Transparent reporting form

DOI: https://doi.org/10.7554/eLife.32808.026

Major datasets

The following previously published datasets were used:

Author(s)	Year	Dataset title	Dataset URL	Database, license, and accessibility information
Hinaux H, Poulain J, Da Silva C, Noirot C, Jeffery W.R, Casane D, Retaux S	2012	FO375681 Astyanax mexicanus whole embryos and larvae neurula to swimming larvae Astyanax mexicanus cDNA clone ARA0AHA20YB20, mRNA sequence	https://www.ncbi.nlm.nih.gov/nucest/FO375681	Publicly available at NCBI (accession no: FO375681).
Hinaux H, Poulain J, Da Silva C, Noirot C, Jeffery W.R, Casane D, Retaux S	2012	FO257910 Astyanax mexicanus whole embryos and larvae neurula to swimming larvae Astyanax mexicanus cDNA clone ARA0ABA19YH22, mRNA sequence	https://www.ncbi.nlm.nih.gov/nucest/FO257910	Publicly available at NCBI (accession no: FO257910).
Hinaux H, Poulain J, Da Silva C, Noirot C, Jeffery W.R, Casane D, Retaux S	2012	FO289826 Astyanax mexicanus whole embryos and larvae neurula to swimming larvae Astyanax mexicanus cDNA clone ARA0ABA97YN12, mRNA sequence	https://www.ncbi.nlm.nih.gov/nucest/FO289826	Publicly available at NCBI (accession no: FO289826).
Hinaux H, Poulain J, Da Silva C, Noirot C, Jeffery W.R, Casane D, Retaux S	2012	FO221370 Astyanax mexicanus whole embryos and larvae neurula to swimming larvae Astyanax mexicanus cDNA clone ARA0AAA24YM17, mRNA sequence	https://www.ncbi.nlm.nih.gov/nucest/FO221370	Publicly available at NCBI (accession no: FO221370).
Hinaux H, Poulain J, Da Silva C, Noirot C, Jeffery W.R, Casane D, Retaux S	2012	FO234678 Astyanax mexicanus whole embryos and larvae neurula to swimming larvae Astyanax mexicanus cDNA clone ARA0AAA59YC09, mRNA sequence	https://www.ncbi.nlm.nih.gov/nucest/FO234678	Publicly available at NCBI (accession no: FO234678).
Hinaux H, Poulain J, Da Silva C, Noirot C, Jeffery W.R, Casane D, Retaux S	2012	FO230154 Astyanax mexicanus whole embryos and larvae neurula to swimming larvae Astyanax mexicanus cDNA clone ARA0AAA6YH03, mRNA sequence	https://www.ncbi.nlm.nih.gov/nucest/FO230154	Publicly available at NCBI (accession no: FO230154).
Hinaux H, Poulain J, Da Silva C, Noirot C, Jeffery W.R, Casane D, Retaux S	2012	FO263072 Astyanax mexicanus whole embryos and larvae neurula to swimming larvae Astyanax mexicanus cDNA clone ARA0ABA37YE05, mRNA sequence	https://www.ncbi.nlm.nih.gov/nucest/FO263072	Publicly available at NCBI (accession no: FO263072).

Wes Warren, Suzanne McCaugh	2017	PREDICTED: Astyanax mexicanus hypocretin neuropeptide precursor (hcrt), mRNA	https://www.ncbi.nlm.nih.gov/nucleotide/XM_007287820	Publicly available at NCBI (accession no: XM_007287820.3).

References

Affaticati P, Yamamoto K, Rizzi B, Bureau C, Peyriéras N, Pasqualini C, Demarque M, Vernier P. 2015. Identification of the optic recess region as a morphogenetic entity in the zebrafish forebrain. *Scientific Reports* **5**:8738. DOI: https://doi.org/10.1038/srep08738, PMID: 25736911

Alvarez-Bolado G, Paul FA, Blaess S. 2012. Sonic hedgehog lineage in the mouse hypothalamus: from progenitor domains to hypothalamic regions. *Neural Development* **7**:4. DOI: https://doi.org/10.1186/1749-8104-7-4, PMID: 22264356

Aspiras AC, Rohner N, Martineau B, Borowsky RL, Tabin CJ. 2015. Melanocortin 4 receptor mutations contribute to the adaptation of cavefish to nutrient-poor conditions. *PNAS* **112**:9668–9673. DOI: https://doi.org/10.1073/pnas.1510802112, PMID: 26170297

Bachy I, Failli V, Rétaux S. 2002. A LIM-homeodomain code for development and evolution of forebrain connectivity. *Neuroreport* **13**:A23–A27. DOI: https://doi.org/10.1097/00001756-200202110-00002, PMID: 11893924

Bedont JL, LeGates TA, Slat EA, Byerly MS, Wang H, Hu J, Rupp AC, Qian J, Wong GW, Herzog ED, Hattar S, Blackshaw S. 2014. Lhx1 controls terminal differentiation and circadian function of the suprachiasmatic nucleus. *Cell Reports* **7**:609–622. DOI: https://doi.org/10.1016/j.celrep.2014.03.060, PMID: 24767996

Bedont JL, Newman EA, Blackshaw S, Patterning BS. 2015. Patterning, specification, and differentiation in the developing hypothalamus. *Wiley Interdisciplinary Reviews: Developmental Biology* **4**:445–468. DOI: https://doi.org/10.1002/wdev.187, PMID: 25820448

Bosco A, Bureau C, Affaticati P, Gaspar P, Bally-Cuif L, Lillesaar C. 2013. Development of hypothalamic serotoninergic neurons requires Fgf signalling via the ETS-domain transcription factor Etv5b. *Development* **140**:372–384. DOI: https://doi.org/10.1242/dev.089094, PMID: 23250211

Castro A, Becerra M, Manso MJ, Anadón R. 1999. Development of immunoreactivity to neuropeptide Y in the brain of brown trout (Salmo trutta fario). *The Journal of Comparative Neurology* **414**:13–32. DOI: https://doi.org/10.1002/(SICI)1096-9861(19991108)414:1<13::AID-CNE2>3.0.CO;2-R, PMID: 10494075

Cavodeassi F, Houart C. 2012. Brain regionalization: of signaling centers and boundaries. *Developmental Neurobiology* **72**:218–233. DOI: https://doi.org/10.1002/dneu.20938, PMID: 21692189

Cerdá-Reverter JM, Agulleiro MJ, R RG, Sánchez E, Ceinos R, Rotllant J. 2011. Fish melanocortin system. *European Journal of Pharmacology* **660**:53–60. DOI: https://doi.org/10.1016/j.ejphar.2010.10.108, PMID: 21208603

Chiang C, Litingtung Y, Lee E, Young KE, Corden JL, Westphal H, Beachy PA. 1996. Cyclopia and defective axial patterning in mice lacking Sonic hedgehog gene function. *Nature* **383**:407–413. DOI: https://doi.org/10.1038/383407a0, PMID: 8837770

Díaz C, Morales-Delgado N, Puelles L. 2014. Ontogenesis of peptidergic neurons within the genoarchitectonic map of the mouse hypothalamus. *Frontiers in Neuroanatomy* **8**:162. DOI: https://doi.org/10.3389/fnana.2014.00162, PMID: 25628541

Dalal J, Roh JH, Maloney SE, Akuffo A, Shah S, Yuan H, Wamsley B, Jones WB, de Guzman Strong C, Gray PA, Holtzman DM, Heintz N, Dougherty JD. 2013. Translational profiling of hypocretin neurons identifies candidate molecules for sleep regulation. *Genes & Development* **27**:565–578. DOI: https://doi.org/10.1101/gad.207654.112, PMID: 23431030

Duboué ER, Borowsky RL, Keene AC. 2012. β-adrenergic signaling regulates evolutionarily derived sleep loss in the Mexican cavefish. *Brain, Behavior and Evolution* **80**:233–243. DOI: https://doi.org/10.1159/000341403, PMID: 22922609

Duboué ER, Keene AC, Borowsky RL. 2011. Evolutionary convergence on sleep loss in cavefish populations. *Current Biology* **21**:671–676. DOI: https://doi.org/10.1016/j.cub.2011.03.020, PMID: 21474315

Elipot Y, Hinaux H, Callebert J, Launay JM, Blin M, Rétaux S. 2014a. A mutation in the enzyme monoamine oxidase explains part of the Astyanax cavefish behavioural syndrome. *Nature Communications* **5**:3647. DOI: https://doi.org/10.1038/ncomms4647, PMID: 24717983

Elipot Y, Hinaux H, Callebert J, Rétaux S. 2013. Evolutionary shift from fighting to foraging in blind cavefish through changes in the serotonin network. *Current Biology* **23**:1–10. DOI: https://doi.org/10.1016/j.cub.2012.10.044, PMID: 23159600

Elipot Y, Legendre L, Père S, Sohm F, Rétaux S. 2014. Astyanax transgenesis and husbandry: how cavefish enters the laboratory. *Zebrafish* **11**:291–299. DOI: https://doi.org/10.1089/zeb.2014.1005, PMID: 25004161

Ferran JL, Puelles L, Rubenstein JL. 2015. Molecular codes defining rostrocaudal domains in the embryonic mouse hypothalamus. *Frontiers in Neuroanatomy* **9**:46. DOI: https://doi.org/10.3389/fnana.2015.00046, PMID: 25941476

Fumey J, Hinaux H, Noirot C, Thermes C, Rétaux S, Casane D. 2017. Evidence for Late Pleistocene origin of Astyanax mexicanus cavefish. *bioRxiv*. DOI: https://doi.org/10.1101/094748

García-Calero E, Fernández-Garre P, Martínez S, Puelles L. 2008. Early mammillary pouch specification in the course of prechordal ventralization of the forebrain tegmentum. *Developmental Biology* **320**:366–377. DOI: https://doi.org/10.1016/j.ydbio.2008.05.545, PMID: 18597750

Guindon S, Gascuel O, A simple GO. 2003. A simple, fast, and accurate algorithm to estimate large phylogenies by maximum likelihood. *Systematic Biology* **52**:696–704. DOI: https://doi.org/10.1080/10635150390235520, PMID: 14530136

Hara J, Beuckmann CT, Nambu T, Willie JT, Chemelli RM, Sinton CM, Sugiyama F, Yagami K, Goto K, Yanagisawa M, Sakurai T. 2001. Genetic ablation of orexin neurons in mice results in narcolepsy, hypophagia, and obesity. *Neuron* **30**:345–354. DOI: https://doi.org/10.1016/S0896-6273(01)00293-8, PMID: 11394998

Herget U, Ryu S. 2015. Coexpression analysis of nine neuropeptides in the neurosecretory preoptic area of larval zebrafish. *Frontiers in Neuroanatomy* **9**:2. DOI: https://doi.org/10.3389/fnana.2015.00002, PMID: 25729355

Herget U, Wolf A, Wullimann MF, Ryu S. 2014. Molecular neuroanatomy and chemoarchitecture of the neurosecretory preoptic-hypothalamic area in zebrafish larvae. *Journal of Comparative Neurology* **522**:1542–1564. DOI: https://doi.org/10.1002/cne.23480, PMID: 24127437

Hinaux H, Devos L, Blin M, Elipot Y, Bibliowicz J, Alié A, Rétaux S. 2016. Sensory evolution in blind cavefish is driven by early embryonic events during gastrulation and neurulation. *Development* **143**:4521–4532. DOI: https://doi.org/10.1242/dev.141291, PMID: 27899509

Hinaux H, Pottin K, Chalhoub H, Père S, Elipot Y, Legendre L, Rétaux S. 2011. A developmental staging table for Astyanax mexicanus surface fish and Pachón cavefish. *Zebrafish* **8**:155–165. DOI: https://doi.org/10.1089/zeb.2011.0713, PMID: 22181659

Hinaux H, Poulain J, Da Silva C, Noirot C, Jeffery WR, Casane D, Rétaux S. 2013. De novo sequencing of Astyanax mexicanus surface fish and Pachón cavefish transcriptomes reveals enrichment of mutations in cavefish putative eye genes. *PLoS ONE* **8**:e53553. DOI: https://doi.org/10.1371/journal.pone.0053553, PMID: 23326453

Houart C, Caneparo L, Heisenberg C, Barth K, Take-Uchi M, Wilson S. 2002. Establishment of the telencephalon during gastrulation by local antagonism of Wnt signaling. *Neuron* **35**:255–265. DOI: https://doi.org/10.1016/S0896-6273(02)00751-1, PMID: 12160744

Houart C, Westerfield M, Wilson SW. 1998. A small population of anterior cells patterns the forebrain during zebrafish gastrulation. *Nature* **391**:788–792. DOI: https://doi.org/10.1038/35853, PMID: 9486648

Jaggard J, Robinson BG, Stahl BA, Oh I, Masek P, Yoshizawa M, Keene AC. 2017b. The lateral line confers evolutionarily derived sleep loss in the Mexican cavefish. *The Journal of Experimental Biology* **220**:284–293. DOI: https://doi.org/10.1242/jeb.145128, PMID: 28100806

Jaggard J, Stahl BA, Lloyd E, Prober DA, Duboue ER, Keene AC. 2017a. Hypocretin underlies the evolution of sleep loss in the 1 Mexican cavefish. *BioRxiv*.

Jeffery WR. 2008. Emerging model systems in evo-devo: cavefish and microevolution of development. *Evolution & Development* **10**:265–272. DOI: https://doi.org/10.1111/j.1525-142X.2008.00235.x, PMID: 18460088

Jeffery WR. 2009. Chapter 8. Evolution and development in the cavefish Astyanax. *Current Topics in Developmental Biology* **86**:191–221. DOI: https://doi.org/10.1016/S0070-2153(09)01008-4, PMID: 19361694

Kalueff AV, Gebhardt M, Stewart AM, Cachat JM, Brimmer M, Chawla JS, Craddock C, Kyzar EJ, Roth A, Landsman S, Gaikwad S, Robinson K, Baatrup E, Tierney K, Shamchuk A, Norton W, Miller N, Nicolson T, Braubach O, Gilman CP, et al. 2013. Towards a comprehensive catalog of zebrafish behavior 1.0 and beyond. *Zebrafish* **10**:70–86. DOI: https://doi.org/10.1089/zeb.2012.0861, PMID: 23590400

Katoh K, Standley DM. 2013. MAFFT multiple sequence alignment software version 7: improvements in performance and usability. *Molecular Biology and Evolution* **30**:772–780. DOI: https://doi.org/10.1093/molbev/mst010, PMID: 23329690

Kiecker C, Niehrs C. 2001. The role of prechordal mesendoderm in neural patterning. *Current Opinion in Neurobiology* **11**:27–33. DOI: https://doi.org/10.1016/S0959-4388(00)00170-7, PMID: 11179869

Lam DD, Garfield AS, Marston OJ, Shaw J, Heisler LK. 2010. Brain serotonin system in the coordination of food intake and body weight. *Pharmacology Biochemistry and Behavior* **97**:84–91. DOI: https://doi.org/10.1016/j.pbb.2010.09.003, PMID: 20837046

Larsen PJ, Hunter RG. 2006. The role of CART in body weight homeostasis. *Peptides* **27**:1981–1986. DOI: https://doi.org/10.1016/j.peptides.2005.11.027, PMID: 16762453

Liu J, Merkle FT, Gandhi AV, Gagnon JA, Woods IG, Chiu CN, Shimogori T, Schier AF, Prober DA. 2015. Evolutionarily conserved regulation of hypocretin neuron specification by Lhx9. *Development* **142**:1113–1124. DOI: https://doi.org/10.1242/dev.117424, PMID: 25725064

Loh K, Herzog H, Shi YC. 2015. Regulation of energy homeostasis by the NPY system. *Trends in Endocrinology & Metabolism* **26**:125–135. DOI: https://doi.org/10.1016/j.tem.2015.01.003, PMID: 25662369

Löhr H, Hammerschmidt M. 2011. Zebrafish in endocrine systems: recent advances and implications for human disease. *Annual Review of Physiology* **73**:183–211. DOI: https://doi.org/10.1146/annurev-physiol-012110-142320, PMID: 21314433

Machluf Y, Gutnick A, Levkowitz G. 2011. Development of the zebrafish hypothalamus. *Annals of the New York Academy of Sciences* **1220**:93–105. DOI: https://doi.org/10.1111/j.1749-6632.2010.05945.x, PMID: 21388407

Mathieu J, Barth A, Rosa FM, Wilson SW, Peyriéras N. 2002. Distinct and cooperative roles for nodal and hedgehog signals during hypothalamic development. *Development* **129**:3055–3065. PMID: 12070082

Mathuru AS, Kibat C, Cheong WF, Shui G, Wenk MR, Friedrich RW, Jesuthasan S. 2012. Chondroitin fragments are odorants that trigger fear behavior in fish. *Current Biology* **22**:538–544. DOI: https://doi.org/10.1016/j.cub.2012.01.061, PMID: 22365850

Matsuda K, Azuma M, Kang KS. 2012. Orexin system in teleost fish. *Vitamins and Hormones* **89**:341–361. DOI: https://doi.org/10.1016/B978-0-12-394623-2.00018-4, PMID: 22640622

Matsuda K, Sakashita A, Yokobori E, Azuma M. 2012b. Neuroendocrine control of feeding behavior and psychomotor activity by neuropeptideY in fish. *Neuropeptides* **46**:275–283. DOI: https://doi.org/10.1016/j.npep.2012.09.006, PMID: 23122775

Menuet A, Alunni A, Joly JS, Jeffery WR, Rétaux S. 2007. Expanded expression of sonic hedgehog in astyanax cavefish: multiple consequences on forebrain development and evolution. *Development* **134**:845–855. DOI: https://doi.org/10.1242/dev.02780, PMID: 17251267

Millington GW. 2007. The role of proopiomelanocortin (POMC) neurones in feeding behaviour. *Nutrition & Metabolism* **4**:18. DOI: https://doi.org/10.1186/1743-7075-4-18, PMID: 17764572

Mitchell RW, Russell WH, Elliott WR. 1977. Mexican eyeless characin fishes, genus Astyanax: environment, distribution, and evolution. *Spec Publ Mus Texas Tech Univ* **12**:1–89.

Miyake A, Nakayama Y, Konishi M, Itoh N. 2005. Fgf19 regulated by Hh signaling is required for zebrafish forebrain development. *Developmental Biology* **288**:259–275. DOI: https://doi.org/10.1016/j.ydbio.2005.09.042, PMID: 16256099

Muthu V, Eachus H, Ellis P, Brown S, Placzek M. 2016. Rx3 and Shh direct anisotropic growth and specification in the zebrafish tuberal/anterior hypothalamus. *Development* **143**:2651–2663. DOI: https://doi.org/10.1242/dev.138305, PMID: 27317806

Myers MG, Olson DP. 2012. Central nervous system control of metabolism. *Nature* **491**:357–363. DOI: https://doi.org/10.1038/nature11705, PMID: 23151578

Nakane Y, Ikegami K, Iigo M, Ono H, Takeda K, Takahashi D, Uesaka M, Kimijima M, Hashimoto R, Arai N, Suga T, Kosuge K, Abe T, Maeda R, Senga T, Amiya N, Azuma T, Amano M, Abe H, Yamamoto N, et al. 2013. The saccus vasculosus of fish is a sensor of seasonal changes in day length. *Nature Communications* **4**:2108. DOI: https://doi.org/10.1038/ncomms3108, PMID: 23820554

Nasif S, de Souza FS, González LE, Yamashita M, Orquera DP, Low MJ, Rubinstein M. 2015. Islet 1 specifies the identity of hypothalamic melanocortin neurons and is critical for normal food intake and adiposity in adulthood. *PNAS* **112**:E1861–E1870. DOI: https://doi.org/10.1073/pnas.1500672112, PMID: 25825735

Peng CY, Mukhopadhyay A, Jarrett JC, Yoshikawa K, Kessler JA. 2012. BMP receptor 1A regulates development of hypothalamic circuits critical for feeding behavior. *Journal of Neuroscience* **32**:17211–17224. DOI: https://doi.org/10.1523/JNEUROSCI.2484-12.2012, PMID: 23197713

Penney CC, Volkoff H. 2014. Peripheral injections of cholecystokinin, apelin, ghrelin and orexin in cavefish (Astyanax fasciatus mexicanus): effects on feeding and on the brain expression levels of tyrosine hydroxylase, mechanistic target of rapamycin and appetite-related hormones. *General and Comparative Endocrinology* **196**:34–40. DOI: https://doi.org/10.1016/j.ygcen.2013.11.015, PMID: 24287340

Pottin K, Hinaux H, Rétaux S. 2011. Restoring eye size in Astyanax mexicanus blind cavefish embryos through modulation of the Shh and Fgf8 forebrain organising centres. *Development* **138**:2467–2476. DOI: https://doi.org/10.1242/dev.054106, PMID: 21610028

Pottin K, Hyacinthe C, Rétaux S, Conservation RS. 2010. Conservation, development, and function of a cement gland-like structure in the fish Astyanax mexicanus. *PNAS* **107**:17256–17261. DOI: https://doi.org/10.1073/pnas.1005035107, PMID: 20855623

Prober DA, Rihel J, Onah AA, Sung RJ, Schier AF. 2006. Hypocretin/orexin overexpression induces an insomnia-like phenotype in zebrafish. *Journal of Neuroscience* **26**:13400–13410. DOI: https://doi.org/10.1523/JNEUROSCI.4332-06.2006, PMID: 17182791

Puelles L, Rubenstein JL. 2015. A new scenario of hypothalamic organization: rationale of new hypotheses introduced in the updated prosomeric model. *Frontiers in Neuroanatomy* **9**:27. DOI: https://doi.org/10.3389/fnana.2015.00027, PMID: 25852489

Rétaux S, Alié A, Blin M, Devos L, Elipot Y, Hinaux H. 2016. Neural development and evolution in Astyanax mexicanus: comparing cavefish and surface fish brains. Keen A. C, Yoshizawa M, McGaugh S. E *Biology and Evolution of the Mexican Cavefish*. Elsevier, Academic Press. 223–240 . DOI: https://doi.org/10.1016/B978-0-12-802148-4.00012-8

Rétaux S, Bourrat F, Joly J, Hinaux H. 2013. Perspectives in Evo-Devo of the vertebrate brain. In: Todd Streelman J (Ed). *Advances in Evolutionary Developmental Biology*. John Wiley & Sons, Inc. p. 151–172 . DOI: https://doi.org/10.1002/9781118707449.ch8

Rétaux S, Pottin K, Alunni A. 2008. Shh and forebrain evolution in the blind cavefish Astyanax mexicanus. *Biology of the Cell* **100**:139–147. DOI: https://doi.org/10.1042/BC20070084, PMID: 18271755

Russek-Blum N, Gutnick A, Nabel-Rosen H, Blechman J, Staudt N, Dorsky RI, Houart C, Levkowitz G. 2008. Dopaminergic neuronal cluster size is determined during early forebrain patterning. *Development* **135**:3401–3413. DOI: https://doi.org/10.1242/dev.024232, PMID: 18799544

Sakurai T, Mieda M, Tsujino N. 2010. The orexin system: roles in sleep/wake regulation. *Annals of the New York Academy of Sciences* **1200**:149–161. DOI: https://doi.org/10.1111/j.1749-6632.2010.05513.x, PMID: 20633143

Sbrogna JL, Barresi MJ, Karlstrom RO. 2003. Multiple roles for Hedgehog signaling in zebrafish pituitary development. *Developmental Biology* **254**:19–35. DOI: https://doi.org/10.1016/S0012-1606(02)00027-1, PMID: 12606279

Shanmugalingam S, Houart C, Picker A, Reifers F, Macdonald R, Barth A, Griffin K, Brand M, Wilson SW. 2000. Ace/Fgf8 is required for forebrain commissure formation and patterning of the telencephalon. *Development* **127**:2549–2561. PMID: 10821754

Shimogori T, Banuchi V, Ng HY, Strauss JB, Grove EA. 2004. Embryonic signaling centers expressing BMP, WNT and FGF proteins interact to pattern the cerebral cortex. *Development* **131**:5639–5647. DOI: https://doi.org/10.1242/dev.01428, PMID: 15509764

Shirasaki R, Pfaff SL. 2002. Transcriptional codes and the control of neuronal identity. *Annual Review of Neuroscience* **25**:251–281. DOI: https://doi.org/10.1146/annurev.neuro.25.112701.142916, PMID: 12052910

Strickler AG, Yamamoto Y, Jeffery WR. 2001. Early and late changes in Pax6 expression accompany eye degeneration during cavefish development. *Development Genes and Evolution* **211**:138–144. DOI: https://doi.org/10.1007/s004270000123, PMID: 11455425

Sylvester JB, Rich CA, Loh YH, van Staaden MJ, Fraser GJ, Streelman JT. 2010. Brain diversity evolves via differences in patterning. *PNAS* **107**:9718–9723. DOI: https://doi.org/10.1073/pnas.1000395107, PMID: 20439726

Sylvester JB, Rich CA, Yi C, Peres JN, Houart C, Streelman JT. 2013. Competing signals drive telencephalon diversity. *Nature Communications* **4**:1745. DOI: https://doi.org/10.1038/ncomms2753, PMID: 23612286

Tsujino N, Sakurai T. 2013. Role of orexin in modulating arousal, feeding, and motivation. *Frontiers in Behavioral Neuroscience* **7**:28. DOI: https://doi.org/10.3389/fnbeh.2013.00028, PMID: 23616752

Tsuneki K. 1986. A survey of occurrence of about seventeen circumventricular organs in brains of various vertebrates with special reference to lower groups. *Journal fur Hirnforschung* **27**:441–470. PMID: 3760554

Volkoff H, Peter RE. 2006. Feeding behavior of fish and its control. *Zebrafish* **3**:131–140. DOI: https://doi.org/10.1089/zeb.2006.3.131, PMID: 18248256

Wall A, Volkoff H. 2013. Effects of fasting and feeding on the brain mRNA expressions of orexin, tyrosine hydroxylase (TH), PYY and CCK in the Mexican blind cavefish (Astyanax fasciatus mexicanus). *General and Comparative Endocrinology* **183**:44–52. DOI: https://doi.org/10.1016/j.ygcen.2012.12.011, PMID: 23305930

Walshe J, Mason I. 2003. Unique and combinatorial functions of Fgf3 and Fgf8 during zebrafish forebrain development. *Development* **130**:4337–4349. DOI: https://doi.org/10.1242/dev.00660, PMID: 12900450

Yamamoto Y, Stock DW, Jeffery WR. 2004. Hedgehog signalling controls eye degeneration in blind cavefish. *Nature* **431**:844–847. DOI: https://doi.org/10.1038/nature02864, PMID: 15483612

Yoshizawa M, Goricki S, Soares D, Jeffery WR. 2010. Evolution of a behavioral shift mediated by superficial neuromasts helps cavefish find food in darkness. *Current Biology* **20**:1631–1636. DOI: https://doi.org/10.1016/j.cub.2010.07.017, PMID: 20705469

Yoshizawa M, Robinson BG, Duboué ER, Masek P, Jaggard JB, O'Quin KE, Borowsky RL, Jeffery WR, Keene AC. 2015. Distinct genetic architecture underlies the emergence of sleep loss and prey-seeking behavior in the Mexican cavefish. *BMC Biology* **13**:15. DOI: https://doi.org/10.1186/s12915-015-0119-3, PMID: 25761998

Zhou X, Vize PD. 2004. Proximo-distal specialization of epithelial transport processes within the Xenopus pronephric kidney tubules. *Developmental Biology* **271**:322–338. DOI: https://doi.org/10.1016/j.ydbio.2004.03.036, PMID: 15223337

Figure supplements

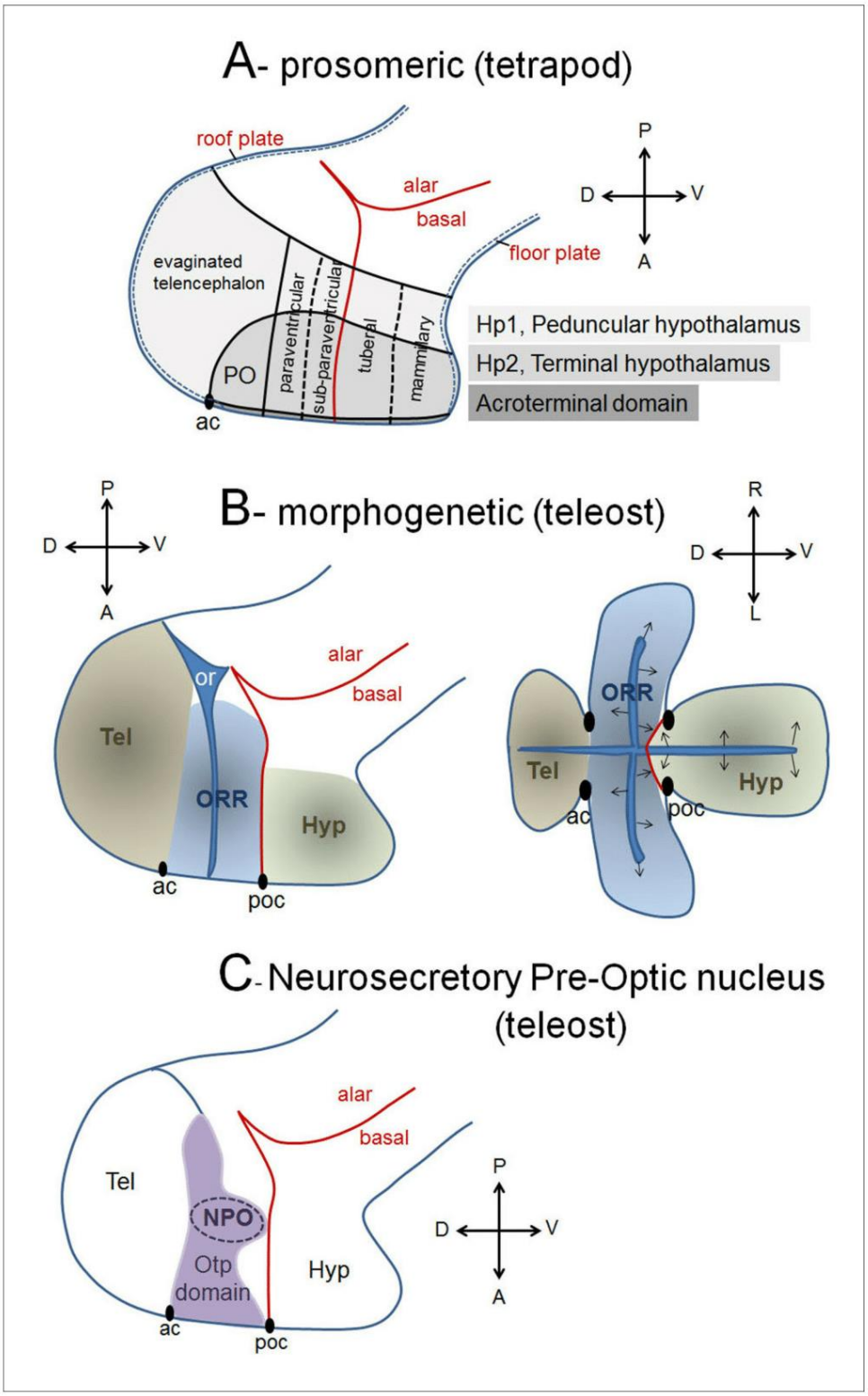

Figure 1—figure supplement 1. Models and interpretations of prosencephalic development. (**A**) The updated prosomeric model interprets neuroepithelial domains with transverse and longitudinal boundaries according to the neuraxes (antero-posterior given by the alar/basal boundary; dorso-ventral orthogonal to the former, between the roof and the floor plates). The two hypothalamo-telencephalic prosomeres (light and medium grey) and their subdivisions are indicated, as well as the newly proposed acroterminal domain (dark grey). PO, preoptic area; ac,

Figure 1—figure supplement 1 continued on next page

Figure 1—figure supplement 1 continued

anterior commissure. (**B**) In teleosts, a morphogenetic interpretation of forebrain regionalization suggests that morphogenesis (and neurogenesis) follows the ventricular organization and forms three masses: the telencephalon (tel), the optic recess region (ORR) and the hypothalamus (hyp). Arrows illustrate the centrifuge pattern of neurogenesis, from the ventricular surface to the mantle. ac, anterior commissure; poc, postoptic commissure. (**C**) The teleost NPO is a dense clustering of neuropeptidergic neurons (AVT, IT, CRH, CCK, enk, VIP, neurotensin, somatostatin) located inside the *Otp* transcription factor expression domain (purple). A homology relationship is proposed between the NPO and the mammalian PVN (paraventricular nucleus in the alar hypothalamus, see A).

DOI: https://doi.org/10.7554/eLife.32808.003

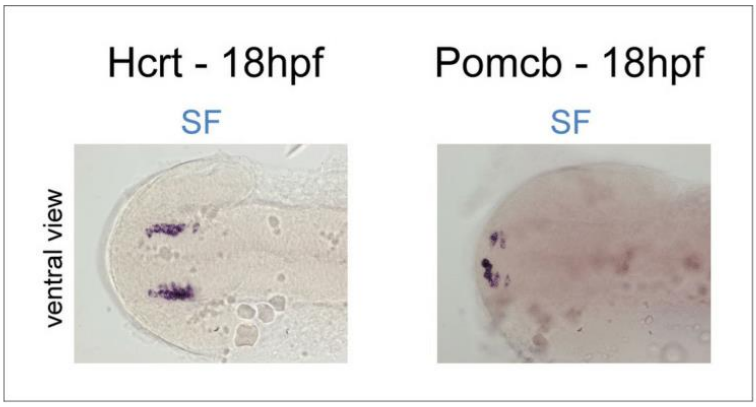

Figure 1—figure supplement 2. Onset of expression of Hcrt and POMCb around 18hpf. Photographs of embryonic brains after in situ hybridization for *Hcrt* or *POMCb* at 18hpf in SF, in ventral views.

DOI: https://doi.org/10.7554/eLife.32808.004

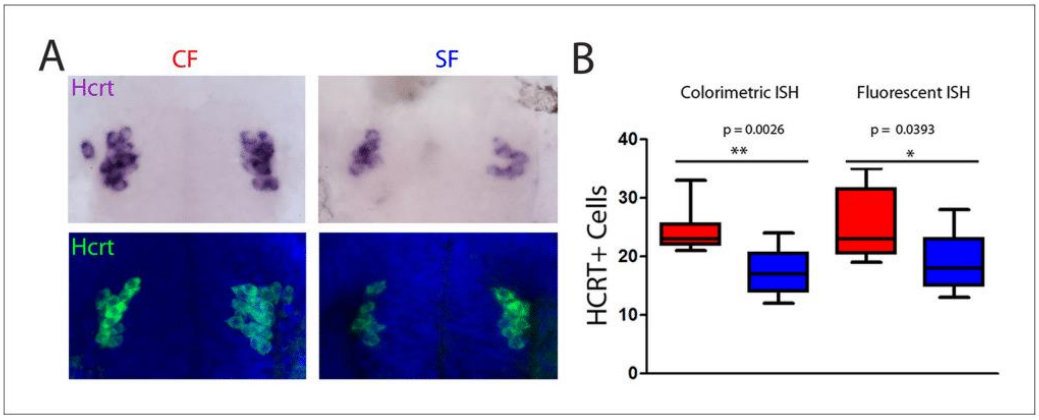

Figure 1—figure supplement 3. Comparison of colorimetric versus fluorescent in situ hybridization results. (**A**) Photographs of embryonic brains after in situ hybridization for *Hcrt* at 24hpf in CF (left) and SF (right), after colorimetric (top) or fluorescent (bottom) in situ hybridization, in ventral views. (**B**) Quantification of cell numbers, compared between the two methods. The cell counts are identical and the difference between the two morphs is the same with the two types of revelations. Mann-Whitney tests.

DOI: https://doi.org/10.7554/eLife.32808.005

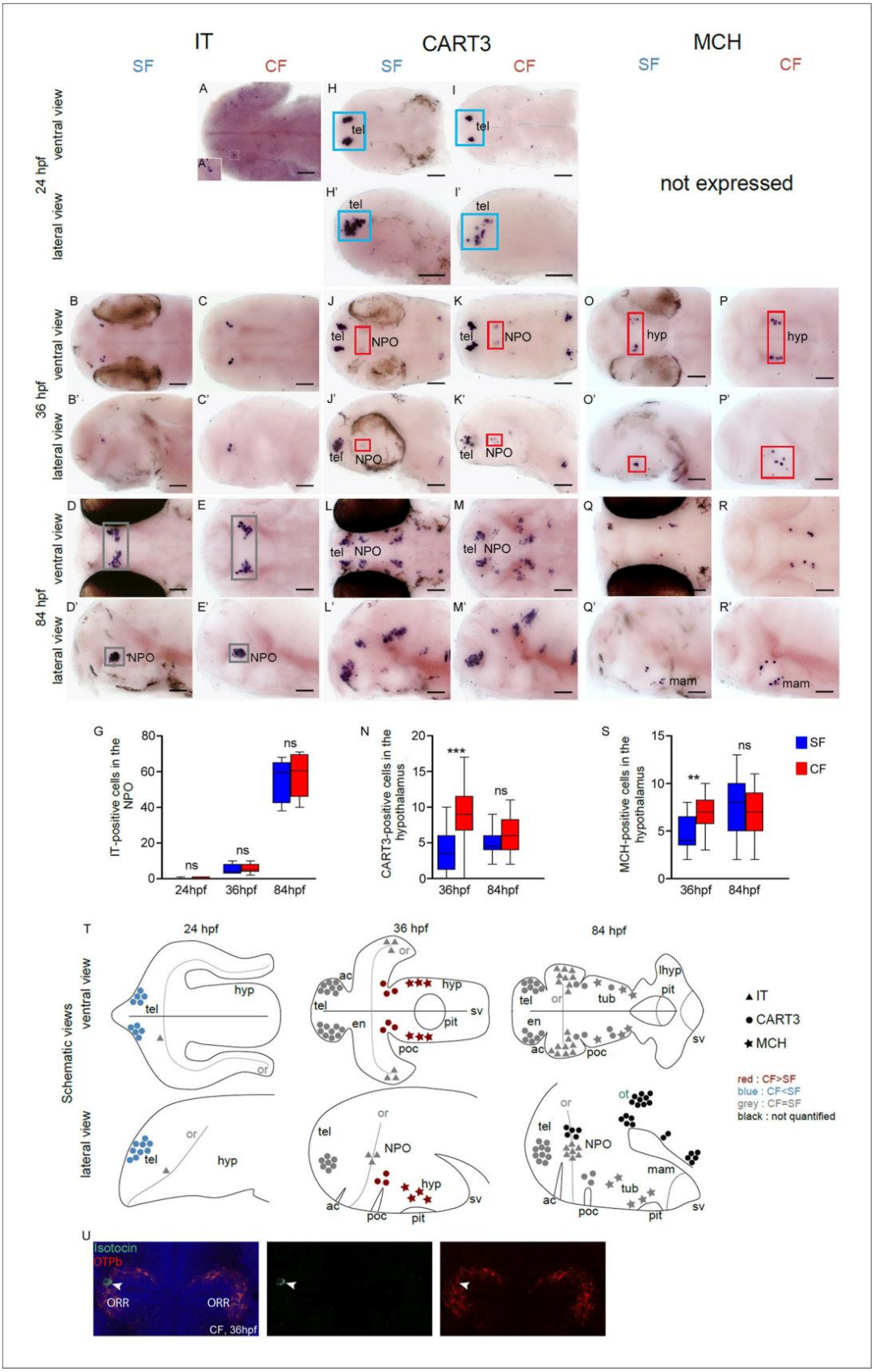

Figure 2—figure supplement 1. Comparative development of IT, CART and MCH neurons in SF and CF. (**A–R'**) Photographs of embryonic brains after in situ hybridization for IT, CART and MCH at 24, 36, and 84 hpf. The

Figure 2—figure supplement 1 continued on next page

Figure 2—figure supplement 1 continued

stages, the lateral or ventral orientations, and the probes are indicated. Red squares and blue squares indicate peptidergic clusters with higher numbers of neurons in CF or in SF, respectively. Grey squares indicate equal numbers. (**G, N, S**) Quantification and time-course of cell numbers in specific clusters. Mann-Whitney tests. (**T**) Anatomical interpretation of peptidergic patterns and time-course of appearance. MCH (stars), CART3 (circles) and IT (triangles) neurons are reported on schematic embryonic brains, in ventral or lateral views. A color code indicates higher numbers of neurons in CF (red) or in SF (blue), or equivalent numbers (grey). Black clusters were not counted. ac, anterior commissure; hyp, hypothalamus; mam, mamilary hypothalamus; NPO, neurosecretory preoptic nucleus; or, optic recess; orr, optic recess region; ot, optic tectum; pit, pituitary; poc, post-optic commissure; tel, telencephalon; tub, tuberal hypothalamus; sv, *saccus vasculosus*. (**U**) Confocal pictures after double fluorescence in situ hybridization for IT (green) and Otpb (red), showing that IT neurons are located in the *Otpb*-expressing NPO. DAPI counterstain appears in blue.

DOI: https://doi.org/10.7554/eLife.32808.011

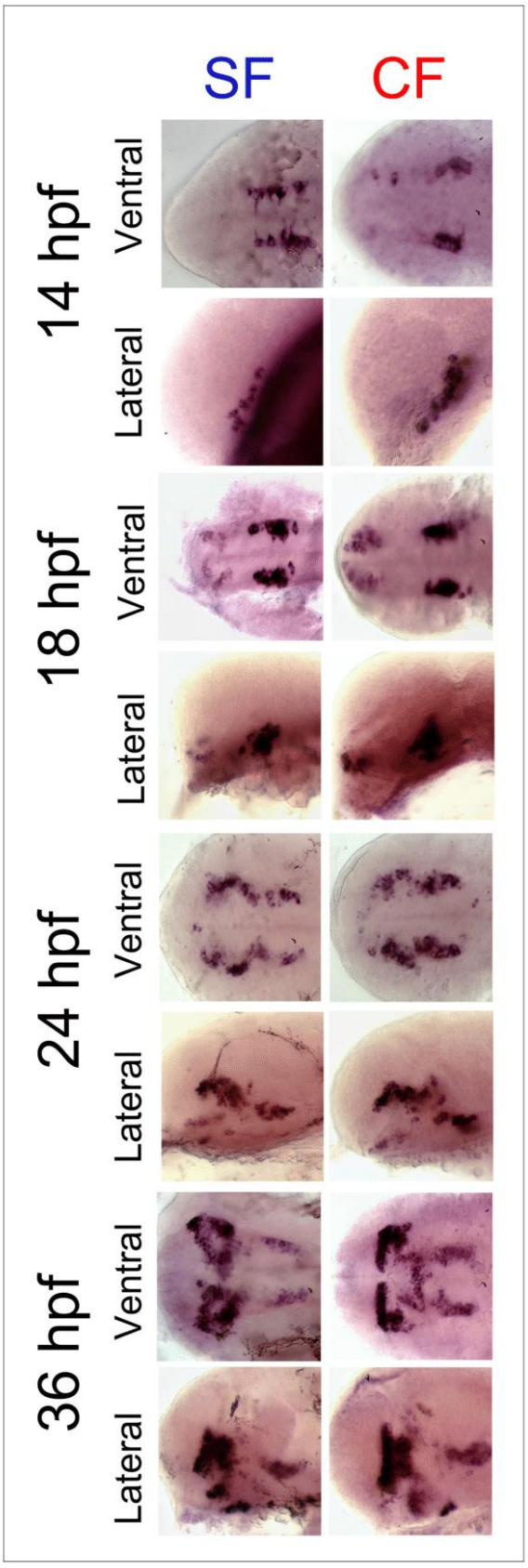

Figure 2—figure supplement 2. Comparative expression of *otpb* between 14 hpf and 36 hpf in SF and CF. Photographs of embryonic brains after in situ hybridization for *otpb* at 14, 18, 24, and 36 hpf. The stages, the morph and the lateral or ventral orientations are indicated. Anterior is left.

DOI: https://doi.org/10.7554/eLife.32808.012

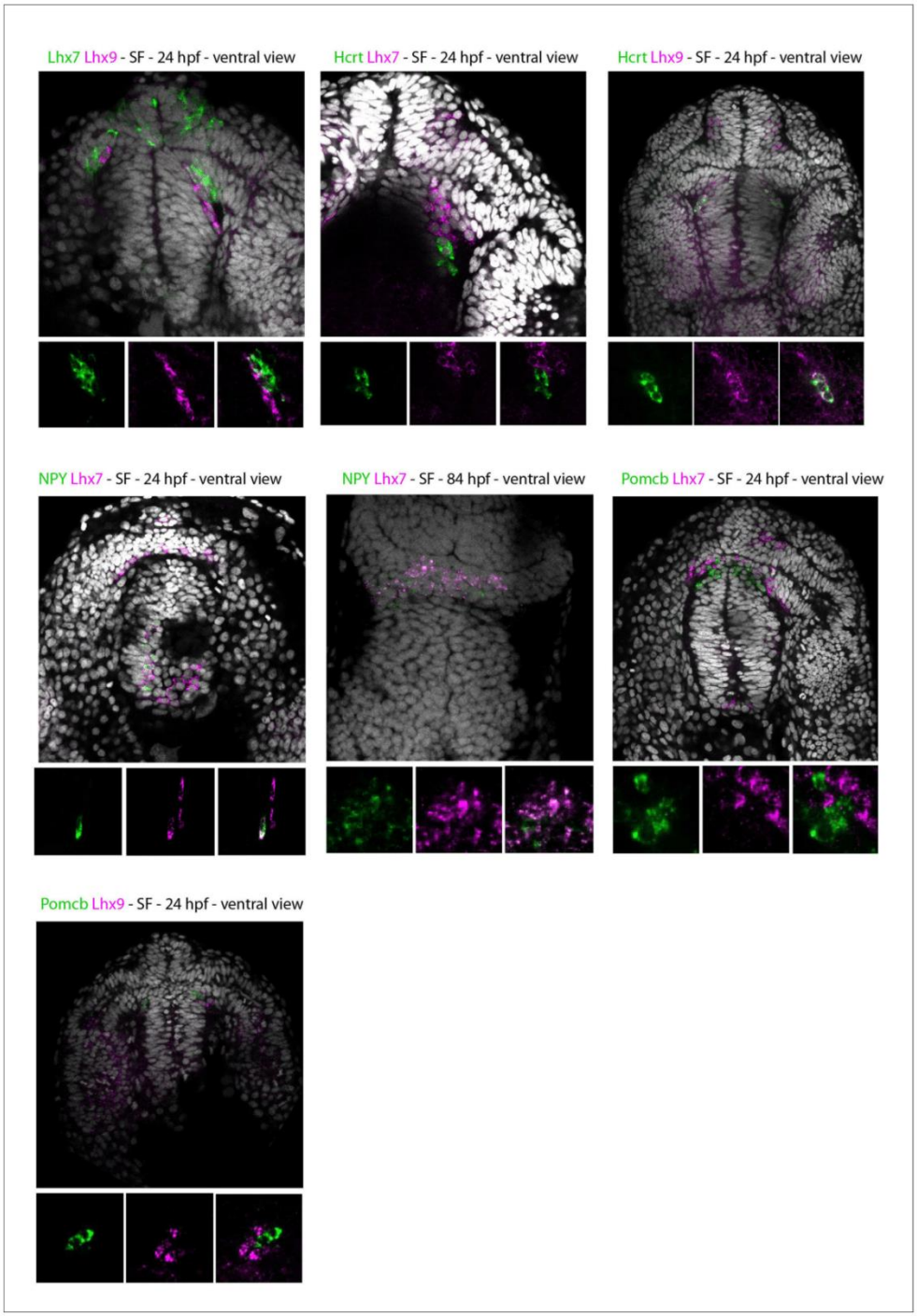

Figure 3—figure supplement 1. Expression of *Lhx7*, *Lhx9*, *Hcrt* and *NPY* in SF. Confocal pictures after double fluorescence in situ hybridization (one probe in magenta, the other in green, as indicated) with DAPI counterstain (grey nuclei). All panels show SF, for comparison with CF shown on main

Figure 3—figure supplement 1 continued on next page

Figure 3—figure supplement 1 continued

Figure 3. The top photos show low-magnification pictures of the whole forebrain, and the bottom photos show high-power views for assessment of co-localization.

DOI: https://doi.org/10.7554/eLife.32808.014

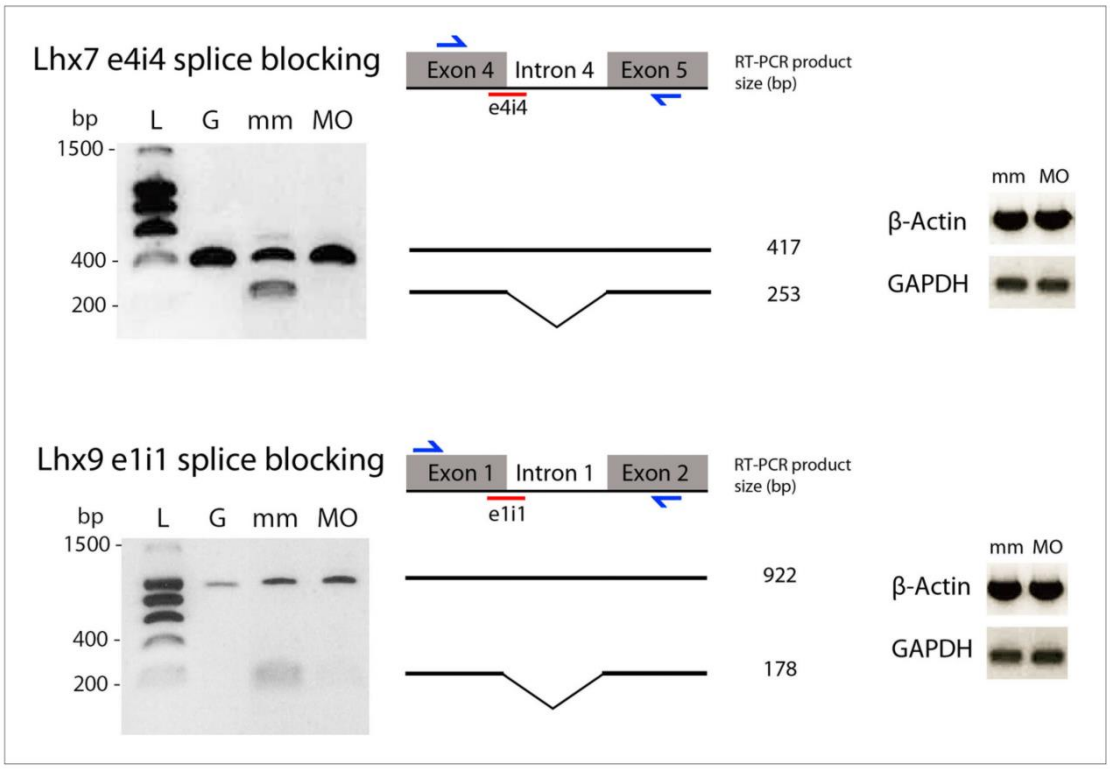

Figure 3—figure supplement 2. Controlling *Lhx9* and *Lhx7* splice-blocking morpholinos knock-down efficiency. **Left**: agarose gels of PCR products. L: ladder; G: PCR on genomic DNA template; mm and MO: RT-PCR on RNA extracted from embryos injected with the indicated mismatch and splice blocking morpholinos. **Middle**: scheme of the targeted intron/exon region of *Lhx7* and *Lhx9*, respectively. The exon-intron junction targeted by the splice blocking morpholino is indicated in red, and the PCR primers are depicted in blue. Expected sizes of PCR products, with or without splicing, are indicated. **Right**: gel loading controls showing amplification of control housekeeping genes by semi-quantitative RT-PCR.

DOI: https://doi.org/10.7554/eLife.32808.015

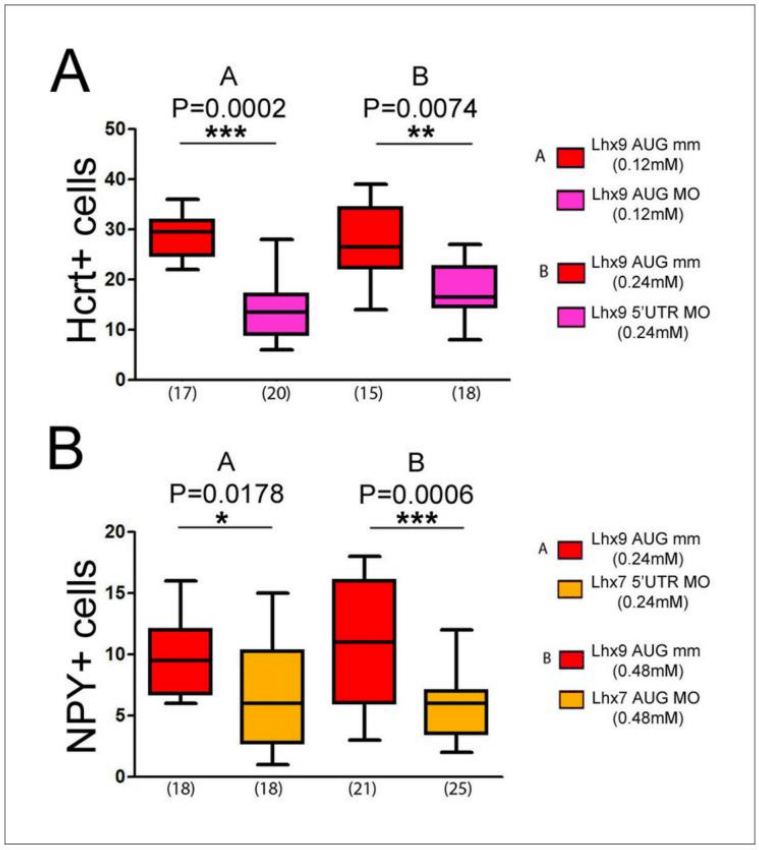

Figure 3—figure supplement 3. Effects of *Lhx9* or *Lhx7* ATG and 5'UTR morpholinos knock-down on Hcrt and NPY neurons numbers, respectively. (**A**) Quantification of the number of Hcrt cells in control mismatch (red) and *Lhx9* MO-injected (pink) CF embryos. The concentrations and types of MO used for mismatch control and knock-down are indicated. The effect is the same as for the *Lhx9* splice MO. Mann-Whitney tests. (**B**) Quantification of the number of NPY cells in control mismatch (red) and *Lhx7* MO-injected (orange) CF embryos. The concentrations and types of MO used for mismatch control and knock-down are indicated. The effect is the same as for the *Lhx7* splice MO. Mann-Whitney tests.

DOI: https://doi.org/10.7554/eLife.32808.016

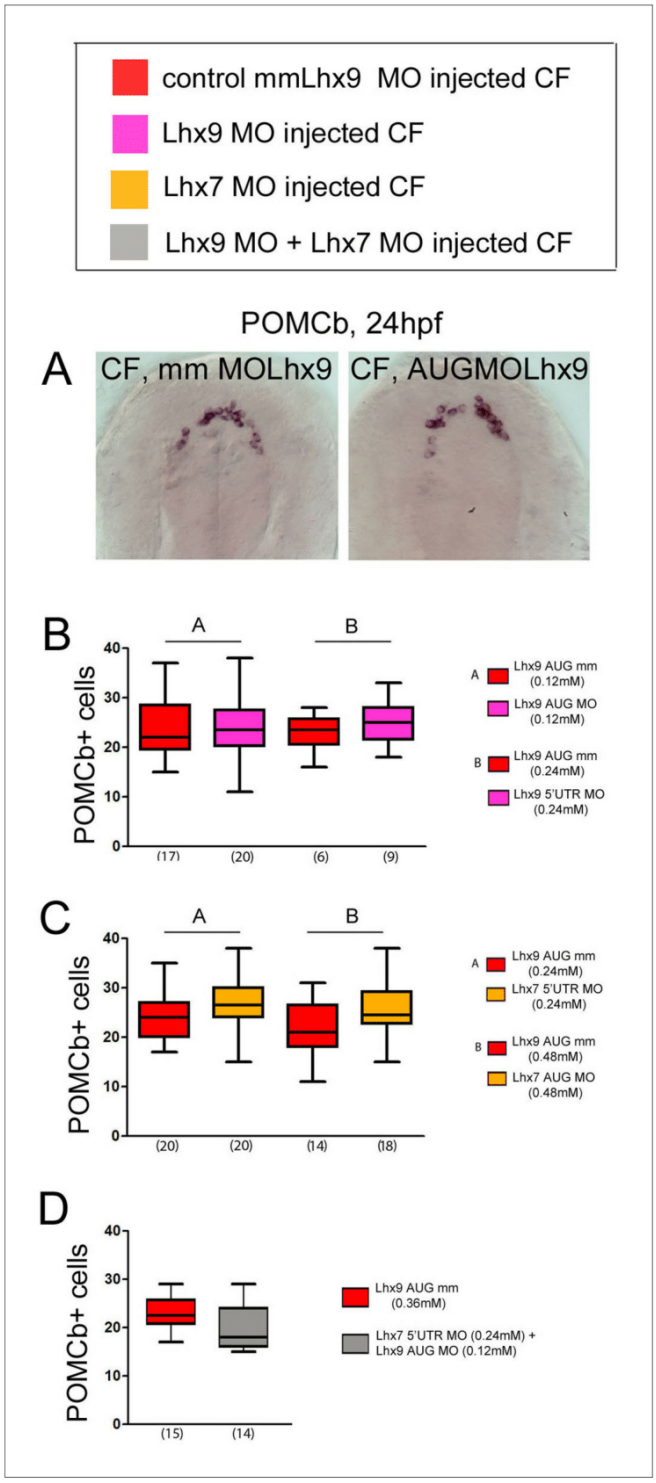

Figure 3—figure supplement 4. Effects of *Lhx9* or/and *Lhx7* morpholino knock-down on POMCb neurons numbers. (**A**) Photographs of control mismatch (mm) and *Lhx9* MO-injected CF embryos after POMCb in situ hybridization at 24 hpf. (**B, C**) Quantification of the number of POMCb cells in control mismatch (red), *Lhx9* MO-

Figure 3—figure supplement 4 continued on next page

Figure 3—figure supplement 4 continued

injected (pink), and *Lhx7* MO-injected (orange) CF embryos. The concentrations and type of MO used are indicated. Mann-Whitney tests. (**D**) Quantification of the number of POMCb cells in control mismatch (red) and *Lhx7*MO + *Lhx9* MO-injected (grey) CF embryos. The concentrations and type of MO used are indicated. Mann-Whitney tests.

DOI: https://doi.org/10.7554/eLife.32808.017

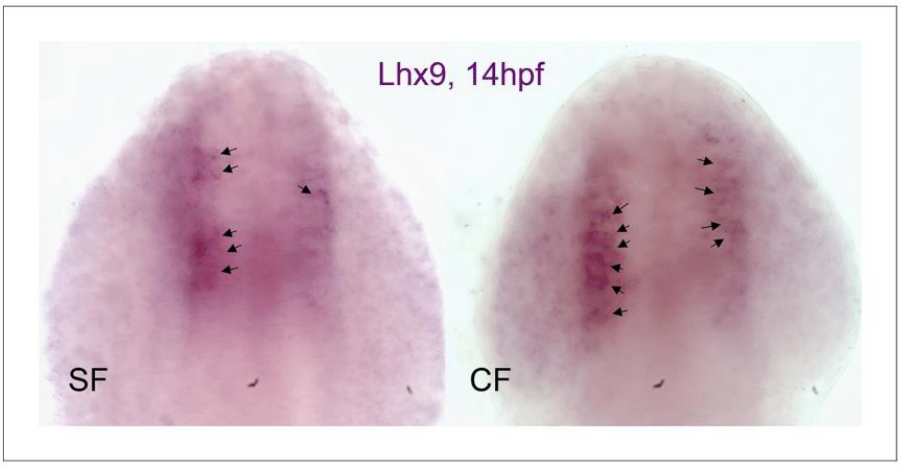

Figure 4—figure supplement 1. A slight heterochrony in the onset of *Lhx9* expression between SF and CF. Photographs of representative embryonic brains after in situ hybridization for *Lhx9* at 14 hpf in SF and CF. In CF, all embryos show expression at 14 hpf, while in SF some do not or only show a few cells turning on *Lhx9* expression in the region of interest. Arrows point to Lhx9-positive cells.

DOI: https://doi.org/10.7554/eLife.32808.019

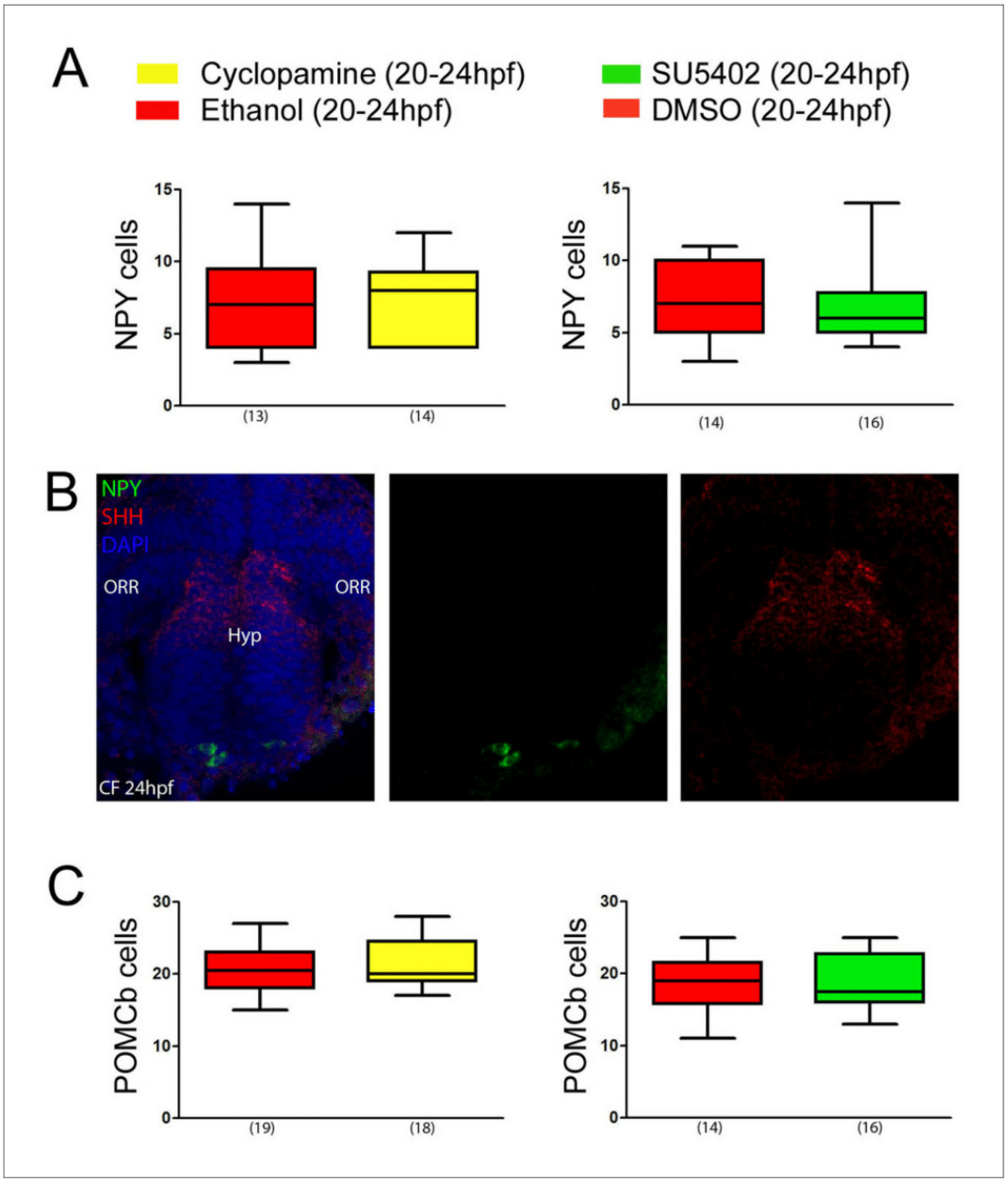

Figure 5—figure supplement 1. Late inhibition of Shh or Fgf signaling has no effect on acroterminal NPY or POMCb differentiation. (**A**) Absence of effect of a cyclopamine (yellow) or a SU5402 (green) treatment between 20-24 hpf on the number of NPY neurons in the acroterminal region at 24 hpf, when compared to vehicle treated CF embryos (red). The numbers of embryos treated and analyzed are indicated in parentheses under the box plots. (**B**) Confocal photographs of double fluorescence in situ hybridization for NPY (green) and Shh (red) in a ventral view on a 24 hpf CF embryo. DAPI counterstain appears in blue. (**C**) Absence of effect of a cyclopamine (yellow) or a SU5402 (green) treatment between 20 and 24 hpf on the number of POMCb neurons at 24 hpf, when compared to vehicle-treated CF embryos (red). Same color code as in A. The numbers of embryos treated and analyzed are indicated in parentheses under the box plots.

DOI: https://doi.org/10.7554/eLife.32808.021

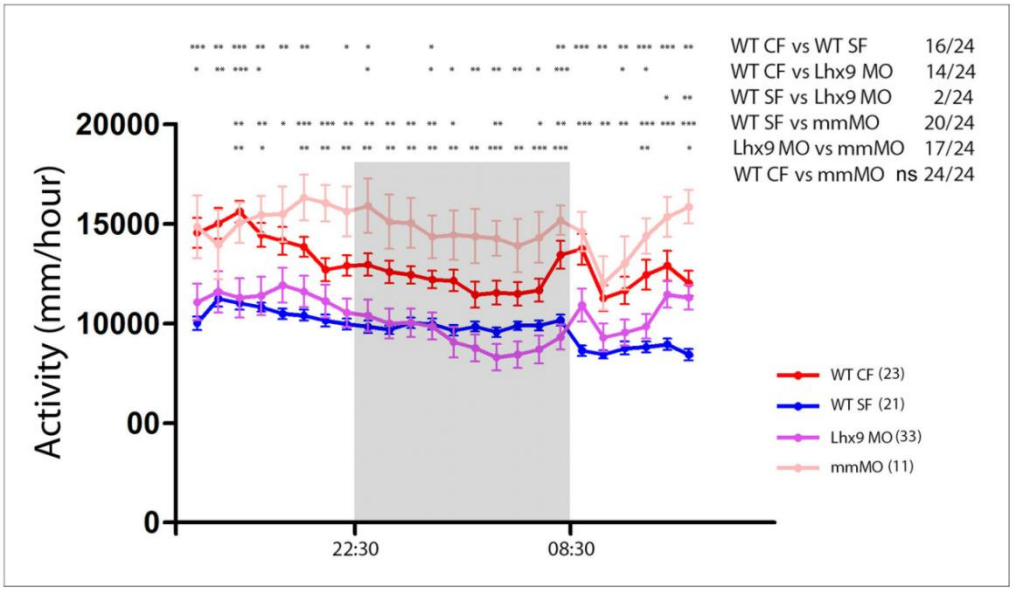

Figure 6—figure supplement 1. Statistics on locomotion data on 24 hr. Same plot as in ***Figure 6D***, with statistical significance between the four curves for everytime point (Mann-Whitney). Numbers in parentheses indicate the number of larvae tested.

DOI: https://doi.org/10.7554/eLife.32808.023

1.2. Discussion

With this study, we exemplify how very early morphogen modifications can impact larval -and most probably later adult- behaviour. Indeed, we show that early inhibition of Hh signalling during neurulation results in a region-specific decrease of *Lhx7* in the ORR/hypothalamic boundary. Moreover, we showed that *Lhx7* is necessary and sufficient for NPY neuronal specification. Consequently, we propose a scenario where in the cavefish, the increase in midline Hh signalling leads to an increased expression domain of *Lhx7* that in turn leads to an increased number of NPY neurons in the ORR/hypothalamic boundary.

We also show that *Lhx9* is necessary and sufficient for *Hcrt* neuronal specification and that its expression domain is enlarged in the cavefish; however *Lhx9* expression is not modified by early Hh or Fgf signalling alterations. Nevertheless, early Fgf inhibition leads to a decrease in *Hcrt*-positive population so that Fgf signalling seems to increase or allow *Hcrt* specification in the presence of *Lhx9*. Later Hh inhibition during *Hcrt* neuron differentiation time window also leads to a decrease of *Hcrt* neurons, suggesting that Hh promotes or allows *Hcrt* neurons differentiation. Moreover, we show that diminution of *Hcrt* cluster size leads to a decrease of time spent in a hypoactive state (similar to sleep) in the 7dpf larva. In other words, the more Hcrt neurons they have, the more active they are and the less they sleep.

This latter behavioural modification is further supported by a concurrent article from Jaggard and colleagues where they find that in adult Pachón cavefish, the number of *Hcrt* neurons is doubled compared to SF (around 100 cells in the SF versus almost 200 in the CF). They also find that the total *Hcrt* mRNA level is three times that of the surface fish, showing that the *Hcrt* neurons also express stronger levels of *Hcrt*.

They also show by pharmacological and genetic inhibition of Hcrt signalling that this neuropeptide promotes sleep in the cavefish but not in the surface fish (or not at detectable levels) while treatment with an agonist of the Hcrt receptor triggers a decrease of sleep in the SF but not in the CF. Some of their treatments affect both sleep bout number and sleep bout duration but never the waking activity, while several other, including the agonist treatment and a blockade of *Hcrt*-neurons signalling (via specific Botulinum toxin expression) modify the total sleep time by changing either sleep bout number or bout duration. We find that an *Lhx9* knock-down-induced decrease of Hcrt neuron number triggered an increase in both sleep bout number and sleep bout length (Figure 47). This suggests that Hcrt is involved both the decrease in sleep bout number and sleep consolidation in the case of the CF (Jaggard et al. 2018).

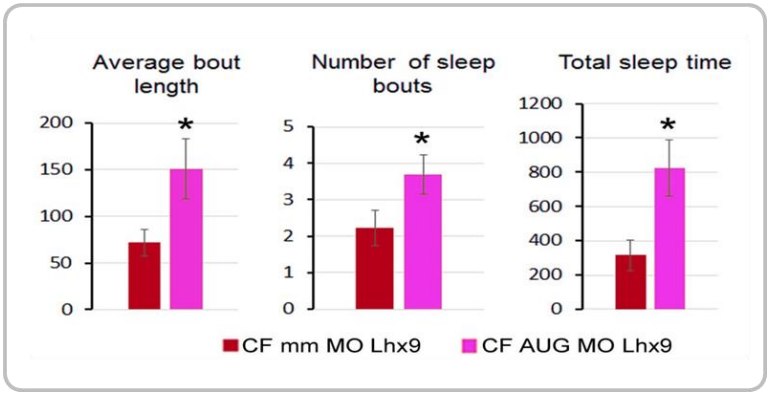

Figure 47 : Lhx9 knock-down effect on sleep (through Hcrt neurons reduction)
Quantification of sleep parameters in control mismatch (mm, red, n=35) and Lhx9MO-injected (pink, n=39) CF embryos, during a 60 minutes period.

Furthermore, they link the effect of Hcrt on sleep to the lateral line effect on sleep. Indeed, upon chemical ablation of the neuromasts, cavefish exhibit *Hcrt* mRNA levels similar to the surface fish, while the latter is

not impacted by the treatment. Quite logically, when they checked the number of *Hcrt* neurons after the treatment, it was unaltered in both morphs. Similarly, starved CF levels of *Hcrt* mRNA decreased to reach SF levels, further linking Hcrt to their previous findings that both starvation and lateral line ablation promote sleep in the CF but not in the SF (Jaggard et al. 2018; Jaggard et al. 2017).

Taken together, their article and ours suggest that in the cavefish, an early expansion of *Lhx9* expression domain allows for an increased specification of *Hcrt*-neurons, which is further promoted by Fgf8 earlier signalling. Later on, *Hcrt* neuronal differentiation is also increased by Hh expansion at the midline so that throughout development CF possess more *Hcrt*-neurons than SF and ultimately twice as much *Hcrt*-neurons than the surface fish adult. Additionally, CF express higher levels of *Hcrt*-mRNA than the SF, which seems to be linked to their "improved" neuromast sensory system when the fish is well-fed. Indeed, Hcrt has already been linked to sensory responsiveness and sleep-wake behaviour (Elbaz et al. 2012; Woods et al. 2014) so that when food is available, the lateral line sensitivity could promote wakefulness and foraging through Hcrt-signalling in the CF (Hcrt is orexigenic), while in times of food scarcity lower levels of Hcrt would decrease the responsiveness to external stimuli and allow the cavefish to sleep more.

It is also interesting to note that the neuropeptides for which we found a persistent increase (at 84hpf) in neuronal cluster size in the hypothalamus all belonged to the orexigenic group (Hcrt, NPY and AgRP), while those for which we found a decrease (POMCb and AVT) or transient differences (MCH, CART) belong to the anorexigenic group. Even though Pachón cavefish have an appetite similar to surface fish, they also have a prevalent *MAO* mutation that increases serotonin levels, which is a known anorexigen. Therefore it is possible to imagine a compensation between these two signallings that allow the cavefish to maintain its appetite. Nevertheless, these neuropeptides are involved in many processes and these cluster size modification could have various effects that could have been selected for; alternatively, they may also very well be side-effects of other pleiotropic modifications that confer other selective advantages to the cavefish in its environment, or even not be under selection in this environment.

As a perspective, it would be interesting to look at the other behaviours controlled by these neuropeptides but also to further investigate the developmental mechanisms involved in these modifications. In particular, we have not found the cause of the increased size of *Lhx9* expression domain in the cavefish hypothalamus.

2. Studying eye development in the cavefish

2.1. Foreword

The eye of the cavefish is quite clearly not under positive selection anymore, yet, it still develops roughly normally during embryogenesis. Looking closely however, one can detect many subtle differences between this embryonic structure and that of its surface conspecific; some examples are smaller optic vesicles, smaller lens, open optic fissure, reduced ventral retina… each of these differences offers a chance to better decipher the eye development and the mechanisms at play. One example would be the role for Fgf signalling in the development of the ventral eye. Indeed, it was shown by Pottin and colleagues that inhibiting Fgf signalling in the cavefish at neural plate stage to compensate for the earlier onset of *Fgf8* expression could restore the ventral quadrant of the eye (Pottin et al. 2011).

Here we sought to follow-up on this study of the ventral retina phenotype. We set out to better characterize this phenotype by studying the regionalization of the cavefish embryonic retina, which could help us glean insights on the mechanisms underlying this phenotype. We also decided to examine the tissue identity of two optic vesicle derivatives: the optic stalk and the RPE. Indeed optic stalk marker *Pax2a* expansion had already been reported but no RPE marker expression had been studied in the cavefish. This study brought to light several previously unknown modifications of the cavefish eye: a temporal shift of regional fate with larger nasal territories but reduced temporal parts in the eye of the cavefish. We therefore refine the previously described ventral reduction into a temporal and ventro-temporal reduction. We also confirmed the enlargement of *Pax2a* expression into the retina; moreover, we show a delay in RPE engulfment of the retina compared to the surface fish.

We also tackled the question of the morphogenetic events leading to the ventral position of the lens and the ventral/temporal reduction of the cavefish eye. To that end, we created *Zic1:GFP* reporter transgenic lines of cavefish and surface fish by a CRISPR-Cas9 mediated knock-in. We then performed live-imaging on these lines on a light-sheet microscope. Our preliminary analyses of these acquisitions reveal a defect in the rim movement in the cavefish and allow for a better understanding of the lens ventral position in the cavefish eye.

Manuscript in preparation

Eye morphogenesis in the Mexican cavefish: first hints of an impaired optic cup invagination.

Lucie Devos[1], Joanne Edouard[2], Victor Simon[1,2], Laurent Legendre[2], Naima Elkhallouki[2], Dominic Nappez[1], Fréderic Sohm[2] and Sylvie Rétaux[1].

[1] DECA group, NeuroPSI, CNRS UMR 9197, Université Paris-Saclay
[2] UMS AMAGEN, CNRS UMS 3504, UMS 1374 INRA

Key words: *Zic1*; CRISPR/Cas9 knock-in; *Astyanax mexicanus*; live imaging

1. Introduction

The eye morphogenesis is a complex choreography of cell movements starting from a flat neural plate and leading to the formation of a spherical multi-layered eye. Owing to the technological improvement of mostly microscopy and transgenesis, this process has been increasingly investigated in the last decade, especially on teleost models which are very amenable to live imaging due to their external development and transparency (Rembold et al. 2006; Kwan et al. 2012; Martinez-Morales et al. 2009; Picker et al. 2009; England et al. 2006; Sidhaye & Norden 2017; Ivanovitch et al. 2013). This focus on morphogenesis led to the description of several movements during eye development in teleost fishes.

Very early on, the eye field is specified in the anterior and medial neural plate, surrounded anteriorly and laterally by the prospective telencephalon, and posteriorly by the future hypothalamus and diencephalon. During neurulation, some eye-fated cells behave like the nearby telencephalic cells and converge toward the midline to close the neural keel while others seem to lag behind and keep the eye field wide (Rembold et al. 2006). These lagging cells could correspond to the population of “marginal cells” described by Ivanovitch and colleagues, which are located rather ventrally and quickly acquire epithelial characteristics.The converging cells intercalate themselves in between these epithelial cells, leading to the optic vesicles evagination (Ivanovitch et al. 2013). The eye vesicles then elongate due to a flow of cells entering mostly the anterior/nasal optic vesicle (Kwan et al. 2012); simultaneously, they separate from the neural keel by the anterior-wards progression of a furrow between the diencephalon and the optic vesicles, leaving only a connection at the level of the optic stalk (England et al. 2006). Cells from the medial part of the optic vesicle then migrate all around the rim of the eye ventricle (called the optic recess) and into the lens facing part of the optic cup, leading to its invagination. At the end of this movement, lens-facing cells will give rise to the neural retina, while cells in the outer layer of the optic cup have adopted a flat shape and will give rise to the retinal pigmented epithelium (Heermann et al. 2015; Cechmanek & McFarlane 2017). This last invagination movement leads to the formation of a fissure at the level of the connection of the eye with the optic stalk, which is called the optic fissure. This fissure allows bloods vessels to invade the eye and leads the way of retinal axons out of the eye and towards the neural tube midline and optic chiasm. However this fissure needs to close in order to have a functional round eye. Failure to correctly complete any of these steps can lead to defects in vision, for example, failure to properly close the optic fissure is termed coloboma and can lead to congenital blindness.

Astyanax mexicanus is a teleost fish that comes in two morphs: the classical river-dwelling eyed morph and the cave-dwelling blind morph. Although eyes are absent in the adult cavefish, they first develop in embryos before degenerating during larval stages. The early eyes developed by the cavefish already presents several abnormalities of morphogenesis : the optic vesicles are shorter (Alunni et al. 2007), the optic cup and lens are smaller (Yamamoto & Jeffery 2000; Hinaux et al. 2015; Hinaux et al. 2016) and the ventral part of the optic cup is severely reduced or even lacking, leaving the optic fissure wide open (coloboma) (Yamamoto et al. 2004; Pottin et al. 2011). Additionally, several modifications of morphogen expression have been evidenced in the cavefish such as an expansion of *Shh* at the midline and anteriorly, a heterochrony of Fgf8 onset of expression in the anterior neural ridge and a modification of BMP4 expression in the prechordal plate. All three modifications have been linked to eye development in the cavefish and most interestingly here, overexpression of *Shh* in a surface fish shortens its optic vesicles, optic cup and triggers the apoptosis of the lens while inhibition of Fgf signalling in the cavefish compensates the heterochrony and restores the ventral retina (Pottin et al. 2011; Hinaux et al. 2016; Yamamoto et al. 2004). Comparison of eye morphogenesis between the cavefish and the surface fish should allow for a better understanding of the defects of the cavefish embryonic eye and should help understanding the role of these different signalling molecules in eye morphogenesis in general.

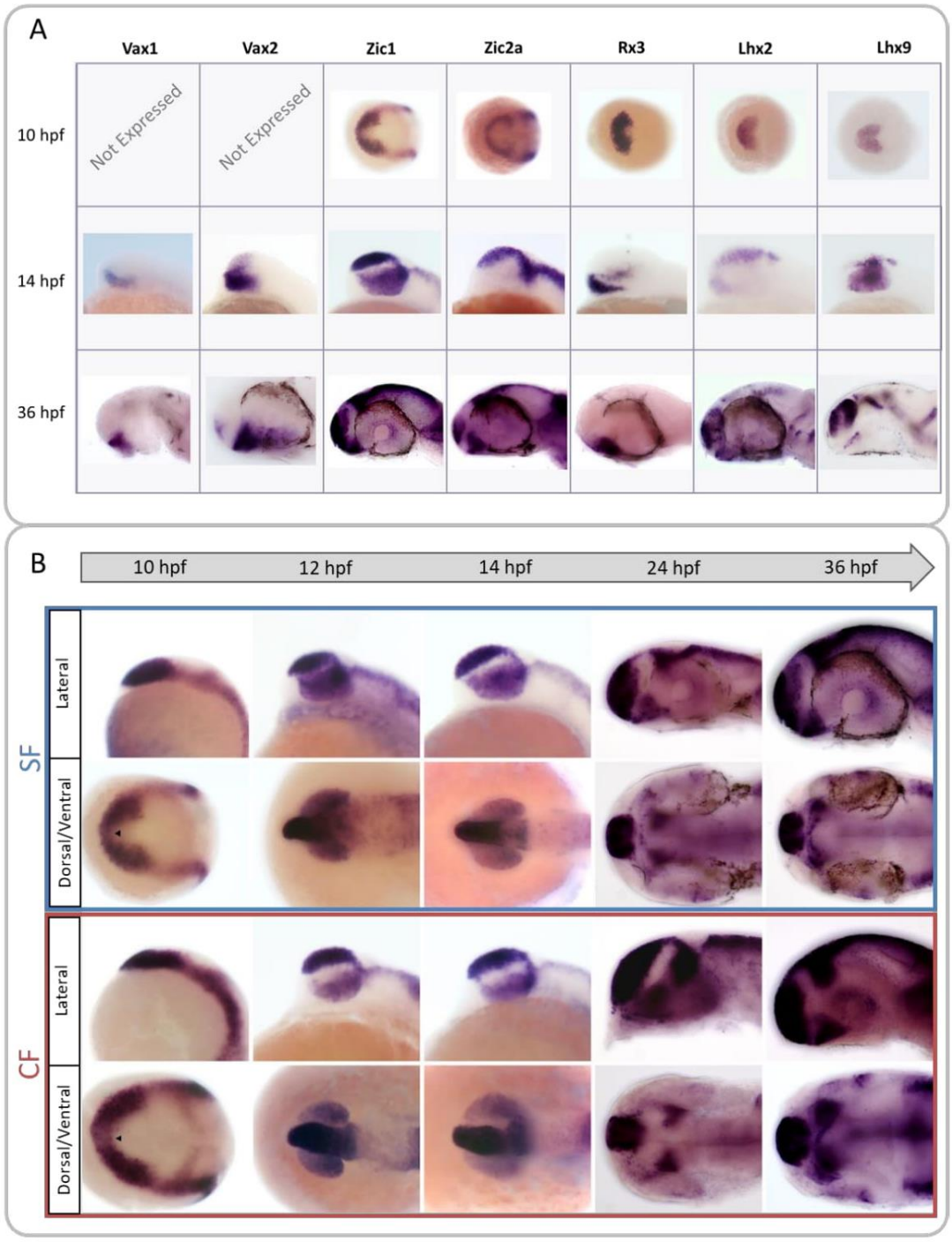

Figure 1: choosing a gene for transgenesis.
(A) Mini-screen of candidate genes by *in situ* hybridization at different stages of interest on surface fish embryos (anterior is to the left). Dorsal views at 10 hpf; lateral views at 14 hpf and 36 hpf. The eyes were dissected out for *Vax1* and *Lhx9* (as no eye expression was detected for either of them) to allow better visibility of the inner tissue.
(B) Detailled analysis of the expression pattern of our candidate gene for transgenesis: *Zic1*, at 5 different stages in surface (SF) and cavefish (CF). Anterior is to the left, at 10, 12 and 14 hpf, bottom pictures are taken in dorsal view; at 24 and 36 hpf, bottom picture are taken in ventral views. Arrowheads indicate an indentation in the eye field.

In order to compare the eye morphogenesis of the two *A. mexicanus* morphs, we set out to label our regions of interest, i.e., the whole eye field, optic vesicles and their resulting regions : the retina and the more medial optic stalk and optic recess region (Affaticati et al. 2015; Yamamoto et al. 2017). To that end, we performed a CRISPR-Cas9 mediated targeted enhancer trap, and generated cavefish and surface fish *Zic1:hsp70:GFP* lines, recapitulating with GFP the expression pattern of *Zic1*. Comparative live imaging on developing embryos from the two knock-in lines on a light sheet microscope revealed modifications of the optic vesicle and optic cup morphogenesis that shed some light on the mechanisms leading to the reduced ventral quadrant of the cavefish. Notably, we propose a prolonged elongation of the optic vesicle/ optic cup that occurs simultaneously with the invagination of the optic cup and leads to an abnormal final position of the lens.

2. Results

2.1. Screening candidate genes for transgenesis

In order to label regions of interest, i.e., the entire optic region, we sought to find a gene that would be expressed in the eye field from the neural plate stage (10 hpf) until at least 24 or 36 hpf, when optic recess region (ORR) and retina are clearly separated. We were also interested in labelling the ventral retina and the ORR more specifically in order to focus on the morphogenesis of this region, which seems defective in cavefish. An *in situ* hybridization mini-screen for candidate genes selected from publications or ZFIN zebrafish expression database was performed. Chosen candidates were *Vax1*, *Vax2* (Take-uchi et al. 2003), *Zic1* (Hinaux et al. 2016), *Zic2a* (Sanek et al. 2009), *Rx3* (Rembold et al. 2006), *Lhx2* and *Lhx9* (Pottin et al. 2011). For these 7 genes, we performed *in situ* hybridization on both cavefish (CF) and surface fish (SF) embryos at 5 different stages (10, 12, 14, 24 and 36 hpf) in order to get a comparative overview of their expression.

Of the 7 genes, 5 were already expressed in the anterior neural plate at 10 hpf while 2 were not: *Vax1* and *Vax2*, whose expressions were detectable from 12 hpf only (Figure 1A). Five of them were expressed at least partially in the optic vesicle per se (excluding ORR and optic stalk): *Vax2*, *Zic1*, *Rx3*, *Lhx9* and *Zic2a* (extremely faintly). At 36 hpf, only 4 of them were expressed in the optic cup: *Zic2a* and *Zic1* (around the lens), *Lhx2* (faintly) and *Vax2* (in the ventral retina). Overall, subtle differences between cave and surface fish patterns of expression were observed (see below).

Vax1 expression was detectable from 12 hpf in the presumptive ORR (between the optic vesicles) and additionally in the dorsal hypothalamus (according to brain axis (Puelles & Rubenstein 2015), closest to the ORR) and quite faintly in the ventral telencephalon. *Vax2* expression was very similar to *Vax1* both in terms of onset of expression and pattern, with the addition of the ventral quadrant of the eye. Although *Vax2* had a very interesting ventral pattern, we discarded it as a candidate for transgenesis for its expression onset was very late. Moreover, in *Vax2* enhancer trap zebrafish line (Kawakami Laboratory), the GFP fluorescence is only visible at 18 hpf (personal observation, data not shown).

Rx3 showed a typical eye field expression pattern at 10hpf but which progressively faded away during optic vesicle stages and was finally not expressed anymore at 24 hpf. Conversely, an anterior and ventral expression in the presumptive hypothalamus was detectable from 12 hpf and remained throughout the stages examined. At 36 hpf, it was clear that only the dorsal half of the hypothalamus, closest to the ORR, was labelled. Due to the rapid fading of its optic vesicle expression, we did not consider *Rx3* as a valid candidate for our project.

Lhx2 and *Lhx9* were both already known to be expressed in the eye field at neural plate stages in *Astyanax* (Pottin et al. 2011). *Lhx2* expression was very dim, if any, in the optic vesicles at 12 and 14 hpf but was expressed both in the prospective telencephalon and more faintly in the prospective hypothalamus. Later on at 36 hpf, *Lhx2* was expressed strongly in the telencephalon and the olfactory epithelia; lighter expression was also visible in the ORR, hypothalamus and sometimes eyes. Additional expression in the pineal, optic tectum and in the hindbrain was also present.

Lhx9 staining was strong in the optic vesicles at 12 hpf (during evagination) and slightly lighter at 14hpf. Moreover dorsal and ventral lateral labelling at the border of the neural keel and the optic vesicles appeared, possibly prefiguring respectively the strong telencephalic staining visible at 24 and 36 hpf and the hypothalamic cluster at the limit of the ORR already described in our previous publication (Alié et al. 2018). At these late stages, we could not detect *Lhx9* expression in the eye anymore. Salt and pepper staining was visible in the olfactory epithelia; a band of expression outlining the optic tectum and lateral discrete marks in the hindbrain were present. We did not choose any of these genes because of the rapid decay of their eye expression.

At 10 hpf, *Zic2a* was expressed at the border of the neural plate and almost entirely surrounding the eye field except for a medial posterior gap. Faint staining in the bilateral eye field could also be seen on some embryos. At 12 and 14 hpf, there was a strong *Zic2a* expression in the telencephalon and a faint staining in the eye or distal part of the eye could often be seen. Strong staining was generally visible throughout the dorsal-most brain. At 24hpf, *Zic2a* expression remained strong in the telencephalon and was also now strongly visible at the border of the eye, in the ORR or optic stalk but without reaching the midline. Faint staining in the eye remained. At 36 hpf, the expression pattern was similar, with the ORR/optic stalk staining reaching much closer to the midline. The eye expression was now more focused around the lens, probably in the CMZ. Roof plate staining persisted throughout development. Because *Zic2a* was never strongly expressed in the eye, we did not favour it as a candidate for transgenesis.

Zic1 was strongly expressed at 10 hpf in the neural plate border and in the anterior neural plate, at the level of the eye field. At 12 and 14 hpf, *Zic1* expression was consistently found in the optic vesicles and between them (prospective ORR and optic stalk). A strong staining was also present throughout the telencephalon. More posteriorly, in the midbrain and hindbrain, the roof plate was stained. The somites were also labelled. The staining was very similar at 24 and 36 hpf with a strong telencephalic expression and a milder ORR (mainly laterally and posterior to the optic recess)/optic stalk and eye staining (widely around the lens). Roof plate and somites expression remained. Even though its pattern of expression was complex and encompassed a region wider than the optic region of interest, *Zic1* was chosen as our best candidate for transgenesis due to its early and persistent expression throughout the eye and the ORR/optic stalk regions.

Overall, only one of the candidate genes was consistently expressed in the eye from neural plate to 36 hpf: *Zic1* (Figure 1A).

2.2. Comparative expression of *Zic1* in surface fish and cavefish embryos

A closer examination of *Zic1* expression pattern highlighted some patterning and morphological differences between cave and surface fish. A difference of the expression pattern in the anterior neural plate was observed as early as 10 hpf: in the surface fish, the staining was wide in the bilateral eye field with a medial indentation reaching the neural border (Figure 1B, asterisk); on the other hand in the

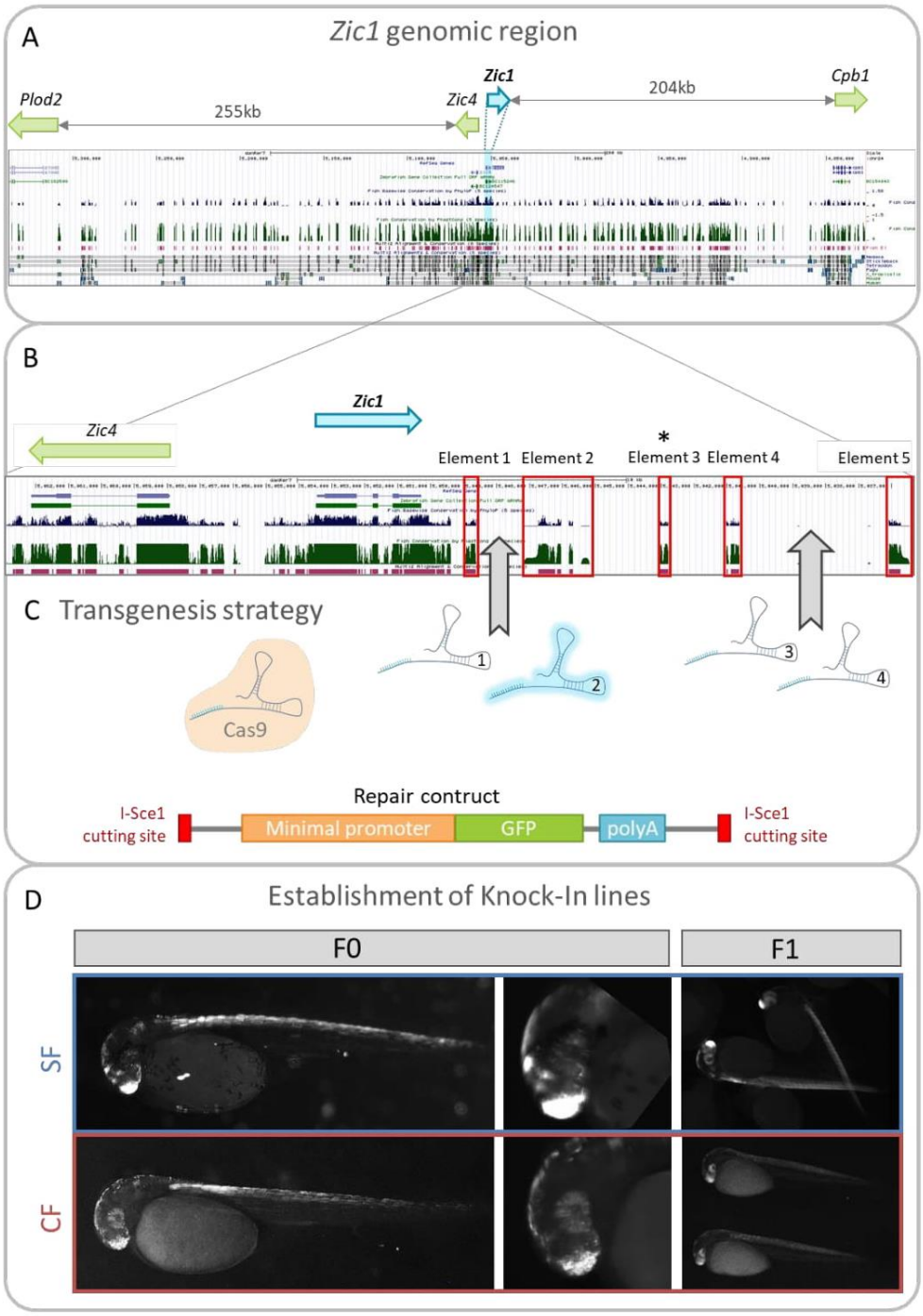

Figure 2: Transgenesis strategy, a targeted enhancer-trap.
(A) Zebrafish genomic region around *Zic1* in UCSC genome browser (2010 assembly). Green blue peaks as well as magenta and black elements correspond to high conservation (see UCSC genome browser), showing the high complexity of this large region. (B) Close-up on *Zic1*'s immediate environment. Red boxes highlight conserved elements; note that element 3 is not conserved in *Astyanax*. (C) sgRNA were designed to target the low-conservation regions between elements 1 and 2 and between elements 3 and 4. Two sgRNA were designed per region and the first one to efficiently generate cuts was the sgNRA 2 (highlighted in pale blue). We injected it together with the Cas9 protein and the linear repair construct containing a minimal HSP70 promoter and the GFP. (D) These injections produced some very encouraging GFP patterns in F0, strikingly resembling that of *Zic1*. These embryos were screened and raised before individual screening for transmission. On the right side are two examples of transgenic lines established that way, for SF and CF.

cavefish, *Zic1* was expressed in narrower lateral bands in the eye field, with a wider staining present anteriorly (Figure 1). At 12 hpf, *Zic1 in situ* hybridization confirmed that the cavefish optic vesicles were shorter than those of the surface fish but they also looked more "plump". Indeed, from a dorsal view the surface fish optic vesicles looked more elongated, slender and pointier in the distal/posterior part while the cavefish optic vesicles look rounder both proximally/anteriorly and distally/posteriorly. On a lateral view, the surface fish optic vesicles appeared more angular with a shape reminding more of a rectangle or a trapezium while the cavefish optic vesicles had a rather oval shape. At 36 hpf the optic recess *Zic1*-expressing region was much larger in the cavefish, and rather thin in the surface fish. The fact that *Zic1* expression allowed us to visualize such differences allowed us to confirm our choice for transgenesis.

2.3. Establishing *Zic1:hsp70:GFP* surface fish and cavefish lines

The genomic region around *Zic1* was examined in order to find conserved elements that might point toward putative regulatory elements. The region was large (approx. 500 kb in zebrafish) and complex (Figure 2A). In the zebrafish genome which has a much better quality and annotation than the *Astyanax* genome (McGaugh et al. 2014), *Zic1* and *Zic4* were very close to each other in a head to tail configuration, and located in the middle of a gene desert (approximately 200kb downstream of *Zic1* and 220kb downstream of *Zic4* in the zebrafish, and approximately 275kb downstream of *Zic1* and 235kb downstream of *Zic4* in *Astyanax)*. As shown in Figure 2A, this gene desert contained many elements conserved amongst fishes (also conserved with tetrapods and mammals for some of them). Such a regulatory landscape suggested that the regulatory elements driving *Zic1* expression are probably modular and difficult to identify. We therefore decided to adopt a directed enhancer-trap approach, by inserting a minimal promoter *hsp70:GFP* construct into the *Zic1* putative regulatory region (Figure 2C). This option also had the advantage that the insertion would be similar in cave and surface fish lines.

We chose to target two regions located between *Zic1* conserved putative regulatory sequences and designed 2 sgRNA per sequence (Figure 2B) (Note that element 3 (Figure 2B) was not present in *Astyanax*). First the efficiency of the sgRNA s was tested, since this technique had not been used in *Astyanax* yet (it has since been used for knock-out purposes (Klaassen et al. 2018)). At the concentration of 50ng/µL, none of the four sgRNA co-injected with *Cas9* mRNA efficiently cut genomic DNA. When concentration was increased to 100ng/µL, the sgRNA2 was found to cut efficiently (Figure S 1). Similarly, the use of Cas9 protein instead on mRNA was found to be much more efficient. We therefore injected the linearised repair construct with sgRNA2 and Cas9 protein. Injected embryos were screened at 30 hpf for fluorescence patterns consistent with Zic1 expression pattern. Excellent *Zic1* pattern recapitulation in F0 was observed at low frequency (usually between 1 and 2% of the injected embryos); while other more partial or approximate patterns were also seen at higher frequencies (Figure 2D). All potential founder embryos were sorted and raised until males were sexually mature (around 5-6 month post fertilization) and could be screened by individual *in vitro* fertilization (as *Astyanax* do not breed in pairs). We detected 3 founder fish for surface fish (out of 15 F0 males screened) and 5 founders for cavefish (out of 9 F0 males screened) with various rates of transmission : 4%, 7% and 30% for the surface fish founders and 4%, 45%, 48%, 50% and 54% for cavefish founders, respectively. The fish were screened based on their GFP pattern, matching *Zic1* pattern (Figure 2D). In both morphs some variations in relative intensities of fluorescence were observed, with some lines exhibiting more homogeneous levels of expression and others having an extremely strong GFP fluorescence in the telencephalon and a dimer fluorescence in the eye. We focused on the most homogeneous lines for imaging purposes. Of note, genomic analyses could confirm the proper insertion at the exact targeted site for one surface fish line and one cavefish line (Figure S 2).

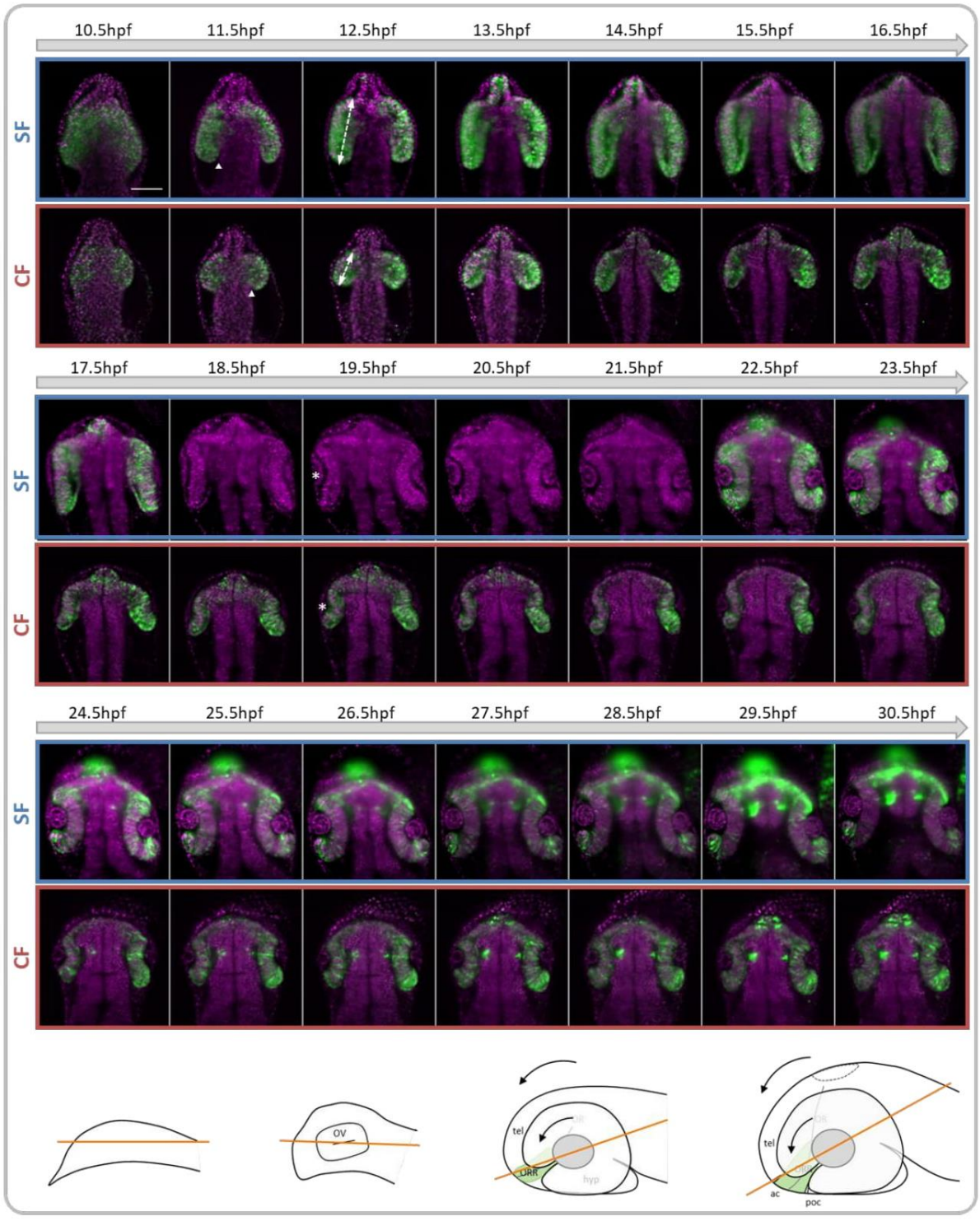

Figure 3 : Eye morphogenesis

Illustration of the time-lapse acquisitions realized from 10.5 hpf to 30.5 hpf on both cavefish and surface fish *Zic1:HSP70:GFP* transgenic lines. Optical section planes are illustrated as orange line on the bottom diagrams, they follow an optic stalk to lens centre axis and accompany the anterior rotation illustrated by the arrows. Measures were realized on these planes. The optic vesicle length measure is illustrated by the arrows at 12.5 hpf; the appearance of the furrow is shown by the arrowhead at 11.5 hpf; the lens is indicated at 19.5 hpf by an asterisk. Dorsal view, anterior to the top, the absence of green labelling in the SF between 18.5 and 21.5 hpf is due to a manipulation error.

2.4. Comparative morphogenesis

Live imaging was performed on both lines from approximately 10.5 hpf and until 24-30 hpf depending on the acquisitions. The planes used for analysis were chosen to always cross the middle of the lens and the optic stalk (, bottom diagrams), in order to follow the anterior rotation of the eye. Overall, eye morphogenesis in surface fish recapitulates step by step all the events described in zebrafish, while in cavefish the previously described morphogenetic movements are conserved but their relative timing and extent seem different: elongation seems to last longer in the cavefish while invagination of the optic cup seems impaired. At the time of writing this manuscript, the quantifications described below have been performed on a single embryo of each morph, but the qualitative observations have been confirmed on two embryos of each morph.

2.4.1. Evagination and elongation

The optic vesicle is much shorter in the cavefish from the beginning of evagination onward and span half the length of the surface-fish optic vesicles at the same stage (135 µm compared to 261 µm). The elongation then proceeds at approximately the same pace than in the surface fish until 17.5 hpf (Figure 4 A,B). However, while the size of the eye primordium decreases between 17.5 hpf and 25.5 hpf approximately in the surface fish, due to the invagination movement, the elongation continued until 31.5 hpf in the cavefish. Hence, the increase in length from 11.5 hpf (beginning of the furrow progression to separate the optic vesicles from the neural tube) until 31.5 hpf is more important in the cavefish than in the surface fish (Figure 4B). It is also interesting to note that the final size of the surface fish optic cups is very similar to that of its early evaginating eye field (252 µm at 31.5 hpf compared to 261 µm at 10.5 hpf) while in the cavefish a net increase in the optic primordium size is visible (184 µm at 31.5 hpf compared to 135 µm at 10.5 hpf).
In addition, while the surface fish optic vesicles stay very close to the neural tube, the cavefish optic vesicle starts by growing away from the neural tube before getting back closer between 18.5 and 21.5 hpf.
Finally the width of the optic stalk throughout development proved to be highly similar between the two morphs despite an initially smaller size in the cavefish due to the smaller optic vesicles (here the term optic stalk is used in the wide meaning of connection between the optic vesicle/ cup and the neural tube) (Figure S 3).

2.4.2. Optic cup formation and lens position

The posterior end of the optic vesicles starts curling back in both cavefish and surface fish around 15.5hpf, probably due to basal constriction. The lens starts being identifiable at 17.5 hpf in both morphs. At this point, the lens is centred in regard to the retina (slightly posteriorly located in the cavefish). In the surface fish, the invagination/rim movement quickly brings closer the edges of the optic cup, in contact with the lens. In contrast, despite originally harbouring a curvature typical of an invaginating optic cup, the edges of the cavefish optic cup do not move much closer than they already are and stay “flat” (Figure 4C). In fact, the cavefish optic vesicles continue to elongate while the lens remains static, therefore increasing the posterior optic cup size and seemingly shifting the lens position in front of the anterior optic cup (Figure 4D). During this prolonged elongation period, the posterior part of the optic cup seems to have a very slow rim movement with a slow and reduced curling, which leads in some embryos to a separation of the posterior optic vesicle from the lens. Nevertheless, the posterior/ prospective dorsal optic cup seems to finally reach the lens (see progression, especially on the right eye from 22.5hpf to 30.5hpf). It however seems that the cavefish optic cup remains shallower as its lens, albeit smaller, always bulges out of the optic cup while in the surface fish the lens seems contained inside of the optic cup curvature.

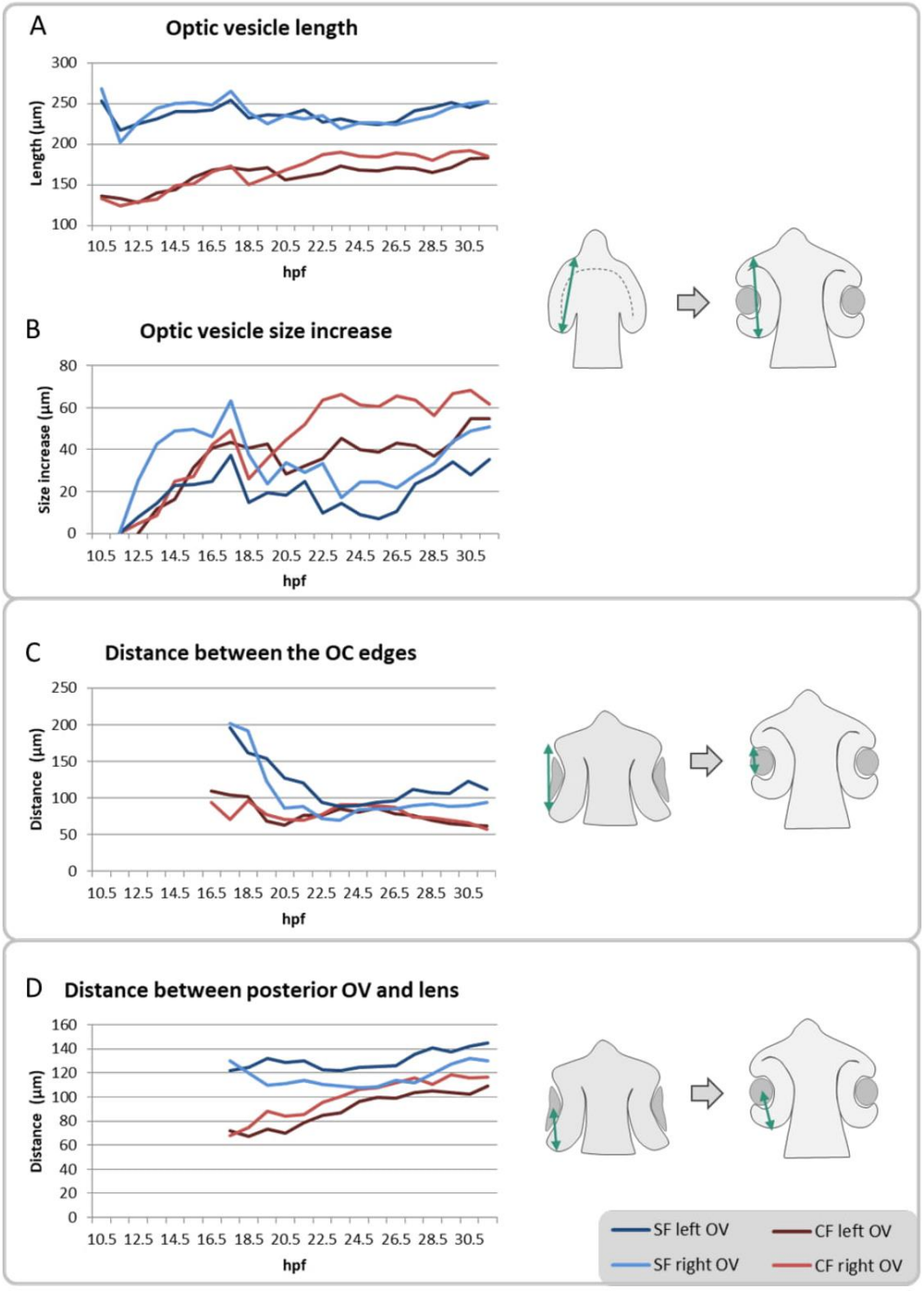

Figure 4 : Morphological quantification of the eye morphogenesis.
(A) Quantification of the optic vesicle (OV) length. The length difference is particularly marked during early OV formation and then tends to decrease. (B) OV size increase was calculated by subtracting the OV length at the onset of furrow formation to the current OV length. It shows a similar size evolution in CF and SF until approximately 18.5-19.5 hpf. Then the cavefish optic cup (OC) continues to grow while the surface fish OC length decreases due to the invagination. (C) Distance between the OC edges through time. The surface fish OC margins undergo a more important movement to come closer to the each other compared to the cavefish. (D) Distance between the lens centre and the most distant part of the posterior OV/OC. Measures are illustrated by the green arrows on the diagrams on the right.

3. Discussion

3.1. Methodological discussion

3.1.1. transgenesis

Several transgenesis techniques are available in zebrafish and several have already been shown to be adaptable to *Astyanax*: a classical approach consists in cloning a promoter or regulatory element driving the desired pattern of expression with a reporter or an effector gene under its control, and flanking this construct with either transposons or meganuclease cutting sites. This construct is then injected with the appropriate enzyme, transposase or meganuclease (in protein or mRNA form), in the 1st cell of the embryo. The construct will be randomly inserted one or several times in the genome. This method is technically simple and has been proved to be efficient in *Astyanax* (Elipot et al., 2014). It has however several drawbacks: the correct identification of most if not all the regulatory sequences driving expression is necessary and often difficult; the insertion of the transgene is random and its expression is dependent on the site of insertion. Indeed, it is possible that a strong transcriptional enhancer or repressor in the insertion region would influence the expression pattern of the reporter gene; conversely, it is also possible that the insertion of the construct would influence the surrounding genes by adding a regulatory element that could alter their expression or even disrupt the coding sequence.

In the recent years, Zinc finger nucleases (ZFN) and TALENs opened the way to targeted mutagenesis and transgenesis by coupling a specifiable DNA-binding domain to the DNA cleavage domain of a nuclease, therefore allowing for a precise cut in the genome. These technologies are now being replaced by the more flexible CRISPR-Cas9 technique which allows for an easy RNA-mediated targeting. However, if performing a targeted knock-out by cutting into a gene and relying on the imprecise non-homologous end joining (NHEJ) DNA repair mechanism to generate indels and frameshifts has proven quite efficient, more precise repair and insertions are still difficult to obtain, at least in zebrafish. The more precise methods require homology-directed repair and therefore involve homology arms flanking a repair construct. Although different methods to increase homology-directed repair efficiency have been tested, it is still a very challenging method.

For our purpose, we were originally considering the classical approach, using the Tol2 transposon technique (Kawakami, Shima and Kawakami, 2000); however, the difficulty of identifying *Zic1* enhancers and regulatory elements with comparative genomics led us to adopt a different strategy: a targeted enhancer-trap, using the non-homologous end-joining DNA repair mechanism. This option also had the advantage that the insertion would be identical in cave and surface fish lines, which is crucial for comparative purposes. Enhancer traps were originally performed by random insertions in a two-step process, the first step being the selection of the expression pattern of interest, the second the identification of the region in which the transgene was inserted.This allowed the generation of transgenic lines with various patterns of expression, reflecting the activity of one or more enhancers and regulatory elements. Here, we “addressed” our enhancer-trap construct to *Zic1* downstream genomic region using CRISPR-Cas9 methodology, similarly to what was performed by Kimura and colleagues (Kimura et al. 2014). This method yielded good results but with a limited efficiency, which was compensated by the possibility of a fluorescence-based screening of the F0 embryos. Due to the possibility of selecting F0, we obtained an excellent ratio of founder fish in our pool of selected F0 embryos (more than 50% in cavefish). The method made use of NHEJ repair mechanism which is the preferred repair mechanism in fish embryo. Finally, for both morphs the different *Zic1:hsp70:GFP* lines, although recapitulating the *Zic1* expression pattern, showed slight variations in the relative intensities of reporter fluorescence in the

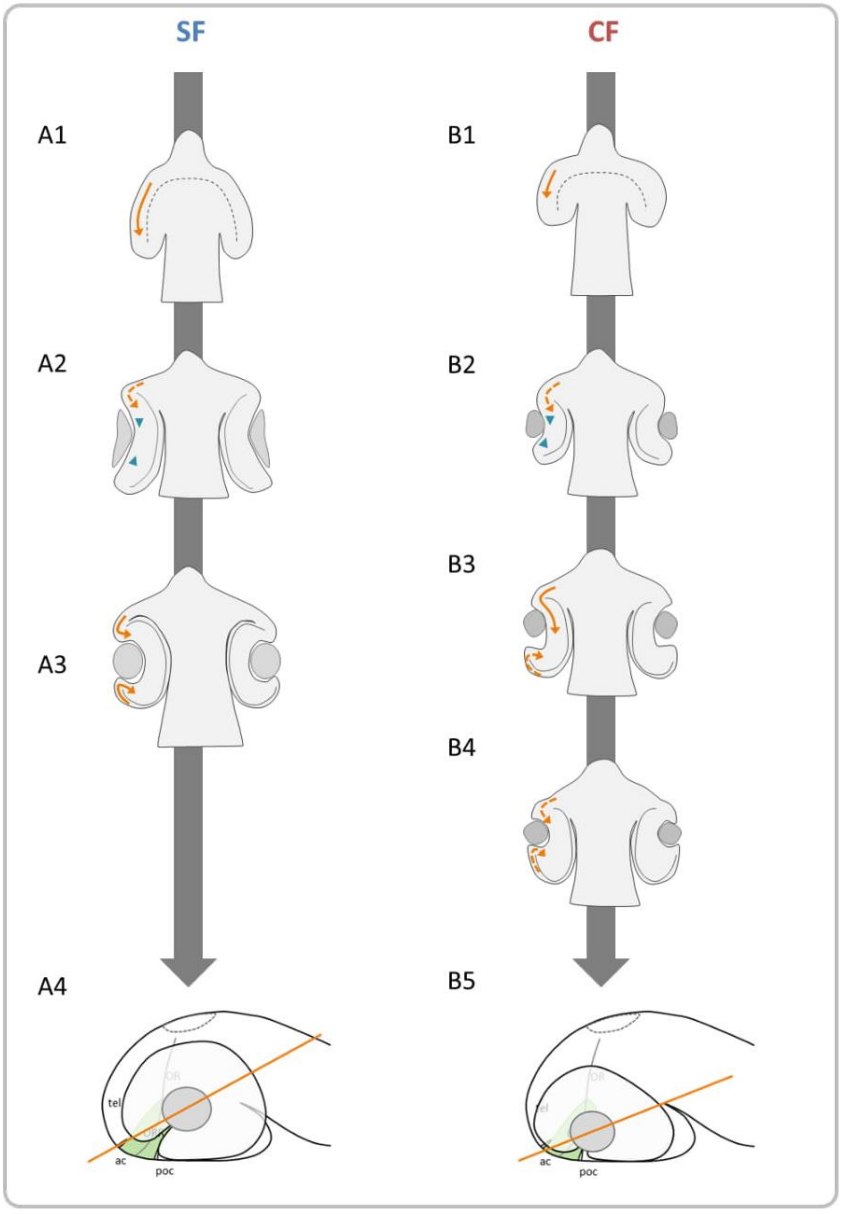

Figure 5 : Summary of the morphogenesis differences and hypotheses about their origin.
(A1, B1) The eye field and the optic vesicles of the cavefish are smaller but the movements of evagination and elongation seem to proceed quite normally. (A2, B2) In both morphs, the lens is correctly located in the centre of the optic cup, which starts invaginating correctly, probably due to basal constriction of the lens-facing cells. (A3-B3) Cells keep entering the optic cup via the optic stalk, possibly to a greater extent in the cavefish. The rim movement of the posterior optic cup is slower in the cavefish, probably due to an impaired migration, creating a gap between the lens and the posterior optic cup. (B4) The slow but persistent rim movement at the posterior optic cup brings the OC margin in contact with the lens again. (A4, B5) lateral views of the final morphology of the surface and cavefish around 30 hpf, the orange line represents the optical section. Orange arrows indicate cell movement; blue-green arrowhead indicate the basal constriction initiating the optic cup invagination.

telencephalon and in the eye. It is possible that the *hsp70:GFP* construct insertion generated indels during the DNA repair event at the site of insertion, which may have affected the nearby regulatory sequences.

3.1.2. Live imaging

The choice of live imaging microscopy technique was directed by several parameters, from the intensity of the labelling to temporal-spatial resolution trade-off. Indeed, light-sheet microscopy offered several advantages such as wide dynamic range of the camera, allowing to detect both the very strong labelling of the telencephalon and the fainter labelling of the eye and early neural plate. In comparison, some detectors found in confocal microscopy (hybrid detectors or GaAsP (Galium Arsenic Photocathods)) tend to be fragile and to shut-down if the fluorescence intensity becomes too important (in order to preserve themselves from damage) which would have been a problem for this study. Moreover, the goal of this study is to perform a tracking of the cells participating in the optic region formation, i.e. eye, optic stalk, optic recess region. Cells in these regions undergo fast movements during early morphogenesis so that a good temporal resolution is necessary. However, these cells are also very densely packed in some of these regions and therefore require a good spatial resolution. In addition, live embryos are quite fragile and laser power needs to be kept minimal in order to avoid bleaching of the fluorescence and photo-damage. The use of SPIM (single plane illumination microscopy) allowed fast imaging due to the plane acquisition in contrast to the point acquisition of a confocal microscope with a sufficient spatial resolution. Moreover, the orthogonal illumination allows for a minimal photo-damage and embryos developing for more than 20 hours under the microscope usually recovered very well and were alive with a normal head shape at 48-60hpf (even though the tail was usually twisted due to the mechanical constraint in the low-melting agarose).

3.2. Morphology and morphogenesis

Rapid analysis through time of the live imaging performed on the *zic1:hsp70:GFP* transgenic lines allowed us to reveal some differences in eye morphology and morphogenesis between the cavefish and the surface fish. First, the shorter size of the cavefish optic vesicles already described by Strickler and colleagues (Strickler et al. 2001) seems to be principally due to the shorter eye field since elongation proceeds similarly in the cavefish and surface fish until 17.5hpf (Figure 5, A1, B1).

Secondly, the lens is formed in the middle of the optic vesicle of both the cavefish and the surface fish and is at the centre of the initial invagination of the optic cup (Figure 5, A2, B2); it is only at later stages that it appears more anterior/ ventral in the cavefish. However the apparent displacement of the lens in regard to the optic cup is not due to a movement of the lens -which remains static throughout eye morphogenesis as it is attached to the overlying ectoderm from which it delaminates around 22hpf in Astyanax ((Hinaux et al. 2017); see also)- but to a persistent elongation of the optic vesicle (Figure 5, B3). This suggests normal interactions between the optic vesicle and the lens to correctly adjust their relative position and initiate the optic cup invagination. Indeed, in chicks, the pre-lens ectoderm is required for normal optic cup invagination while the lens placode itself is dispensable (Hyer et al. 2003). This suggests that in the cavefish such mechanisms could exist and correctly initiate the optic cup folding.

Thirdly, if the invagination of the optic vesicle seems to start normally between 15.5 and 19.5 hpf, it only progresses very little afterwards so that the optic cup remains shallow and elongated. This timing is very reminiscent of the 2 steps of optic cup invagination already described : a basal constriction initiating the primary folding between 18 and 20 hpf in zebrafish (18 ss to 22 ss) followed by the rim movement with cells flowing toward the lens-facing epithelium between 20 and 24 hpf (Nicolás-Pérez et al. 2016; Heermann et al. 2015; Sidhaye & Norden 2017). In *Astyanax*, 18 ss corresponds to approximately 16.5 hpf, suggesting that the initial basal constriction leading to the onset of optic cup invagination is well conserved in the cavefish. In contrast, the prolonged extension of the optic cup and the fact that the curvature of the retina remains shallow with the lens bulging out of the eye suggests that the rim movement might be impaired in the cavefish. The continuous flow of cells entering the retina would lead to its elongation, counteracting the weak rim movement of the cavefish (Figure 5,B3). This movement does seem weaker but not absent in the cavefish as the posterior part of its optic cup still manages to contact the lens at later stages (Figure 5,B4).

This difference of rim movement could be due to various causes such as defects in the basal membrane or failure to establish proper focal adhesion as seen in the *ojoplano* medaka mutant (Martinez-Morales et al. 2009; Sidhaye & Norden 2017; Nicolás-Pérez et al. 2016). Alternatively, the active migration described by Sidhaye and Norden could be altered by extrinsic signals, as in BMP overexpression experiments where the cell flow toward the lens-facing epithelium is reduced (Heermann et al. 2015). The various morphogen modifications in the cavefish and the fact that the ventral quadrant can be restored by delaying the onset of the Fgf signalling in the cavefish to match the surface fish scenario seem to point in this direction.

Overall, the small initial optic vesicle interacting probably with the lens so that it appears in its centre, followed by a continuous extension of the optic cup with only very little rim movement allows explaining several phenotypes observed in the cavefish. Indeed, the ventral quadrant is much reduced and this explains why the lens seems so ventral in the cavefish eye (as the anterior rotation brings the anterior lens in a ventral position). Furthermore, the lens of the cavefish often appears to be “floating” in the eye cup, without much contact with the edges of the retina. Moreover grooves / folds in the retina (typically between the dorsal and temporal quadrants) can be sometimes seen (personal observations, Figure S 4). Both phenotypes can be explained by the prolonged elongation of the optic cup without the matching rim movement, resulting in a gap between the posterior retina and the lens and a very shallow cup that does not encompass the lens as seen in the surface fish or zebrafish case.

These preliminary results have already allowed us to draw some conclusions regarding the cavefish eye morphogenesis but more precise analyses including more individuals will be necessary in order to characterize and compare the cell movements occurring in both morphs. For example the extent of the rim movement, the curvature of the optic cup and the amount of cells entering the optic vesicle through time would be extremely informative. These data also pave the way for functional experiments aiming at understanding the defective molecular or signaling mechanisms in cavefish eye morphogenesis, using the *Zic1:hsp70:GFP* knock-in lines.

4. Material and methods

4.1. Animals

Laboratory stocks of *A. mexicanus* surface fish and cavefish were obtained in 2004 from the Jeffery laboratory at the University of Maryland. The surface fish were originally collected from San Solomon Spring, Texas and the cavefish are from the Pachón cave in Mexico. Surface fish are kept at 26°C and cavefish at 22°C. Natural spawns are induced after a cold shock (22°C over weekend) and a return to normal temperature for surface fish; cavefish spawns are induced by raising the temperature to 26°C. Embryos destined for *in situ* hybridization were collected after natural spawning, grown at 24°C and staged according to the developmental staging table (Hinaux et al. 2011) and fixed in 4% paraformaldehyde. After progressive dehydration in methanol, they were stored at -20°C. Embryos destined to transgenesis or live imaging were obtained by *in vitro* fertilization. Embryos were raised in an incubator until 1 month post fertilization for the surface fishes and two month post fertilization for the cavefishes. They were kept at low density (15/20 per litre maximum) in embryo medium, in 1 litre plastic tanks with a soft bubbling behind the strainer. Larvae were fed from day 5 with paramecium and transitioned to artemia nauplii from day 10-15. Artemia were given twice a day except for the weekends (once a day) and carefully removed afterward to avoid polluting the medium. At least two thirds of the medium were changed every day and dead larvae removed. After one month for the surface fish and two months for the cavefish, juveniles were taken to the fish facility where they were fed zebrafish food (Skretting Gemma wean 0.3) and quickly moved to bigger tanks in order to allow their fast growth.

Animals were treated according to French and European regulations of animals in research. SR' authorization for use of animals in research is 91-116, and Paris Centre-Sud Ethic committee authorization numbers are 2012-52 and 2012-56.

4.2. *In situ* hybridization

The expression patterns of 7 transcription factors selected for their expression pattern in zebrafish (ZFIN database) were studied in both surface and cavefish at 5 stages embryonic stages: (10 hpf (neural plate), 12 hpf, 14 hpf (optic vesicle stages), 24 hpf (optic cup stage, hatching) and 36 hpf (separation of the optic recess region from the optic cup, optic fissure closure, approximatively) (Hinaux et al., 2011). These genes were candidates for transgenesis, with the following criteria: expression in the ORR and eye or ventral eye, from neural plate stage to 36 hpf.

Some cDNAs were available from our cDNA library : *Zic1* (FO290256), *Zic2a* (FO320762) and *Rx3* (FO289986); others were already cloned in the lab : *Lhx2* (EF175737) and *Lhx9* (EF175738) (Alunni et al. 2007); obtained from other labs (*Vax1* : Jeffery lab, University of Maryland,(Yamamoto et al. 2004)); or cloned for the purpose of this work in pGEMT-Easy (Promega) : *Vax2* (Forward primer :GGGCAAAACATGCGCGTTA, Reverse primer : CAGTAATCCGGGTCCACTCC).

cDNAs were amplified by PCR, and digoxygenin-labelled riboprobes were synthesized from PCR templates. Embryos were rehydrated by graded series of EtOH/PBS, then for embryos older than 24 hpf, proteinase-K permeabilization at 37°C was performed for 36hpf embryos only (10 µg/ml, 15 min) followed by a post-fixation step. Riboprobes were hybridized for 16 hr at 65°C and embryos were incubated with anti-DIG-AP (Roche, dilution 1/4000) overnight at 4°C. Colorimetric detection with BCIP/NBT (Roche) was used. Mounted embryos were imaged on a Nikon Eclipse E800 microscope equipped with a Nikon DXM 1200 camera running under Nikon ACT-1 software.

4.3. In vitro fertilization (IVF) and injections

Surface and cavefish were maintained in a room with shifted photoperiod (light: 4pm – 7am, L:D 15:11) in order to obtain spawns during the working day (Astyanax spawn during the night period). Fish activity was monitored after induction and upon visible excitation or when first eggs were found at the bottom of the tank, fish were fished. Females were processed first to obtain eggs: they were quickly blotted on a moist paper towel and laid on their side in a petri dish. They were gently but firmly (to avoid a fall) maintained there while their flank was gently stroked. If eggs were not released immediately, the female was put back in the tank. Once eggs were collected, a male was quickly processed similarly to females, on the lid of the petri dish to collect sperm. The sperm was then washed on the eggs with 10-20mL of tank water (conductivity ~500µS) and left for a few moments (30s to 2 min approximatively), after which embryo medium was added in the petri dish. Fertilised eggs were quickly laid on a zebrafish injection dish containing agarose grooves. They were injected with a Picospritzer III (Parker Hannifin) pressure injector.

4.4. CRISPR injections and Knock-In lines

The mix contained Cas9 protein generously provided by TACGENE and sgRNA2 with the following targeting sequence: CCCAATTCACCAGTATACGT (synthesized with AMBION T7 MEGAshortscript™ T7 transcription kit). Concentrations were kept with a 1:1.5 Cas9 to sgRNA molar ratio and varied between 0.71µM (25ng/µL) and 5.67µM (200ng/µL) of sgRNA 2, mostly 2.84 and 1.42µM were used. The donor construct contained a HSP70 promoter used as a minimal promoter, a GFP cDNA and SV40 poly-adenylation signal, flanked by I-SceI meganuclease cutting sites. I-SceI was used to generate sticky ends and was either detached by 7 min at 96°C or injected with the construct. Concentrations of the repair construct varied between 3.33 and 10.92nM but were mostly used at 10.71nM.

4.5. mRNA injection

Embryos were injected in the cell or yolk at 1 cell stage with a H2B-mCherry fusion mRNA at a concentration of 50ng/µL.

4.6. Imaging

Transgenic embryos were obtained by IVF with wild-type eggs and transgenic sperm and were immediately injected with H2B-mCherry mRNA for nuclear labelling. Injected embryos were screened for GFP and mCherry fluorescence under a Leica M165C stereomicroscope around 10-11hpf, when GFP reporter fluorescence first becomes detectable.

Selected embryos were immediately mounted in a phytagel tube (SIGMA, CAS Number: 71010-52-1) molded with Phaseview Teflon mold (1.5mm of diameter) and maintained in position with 0.4% low melting point agarose (Invitrogen UltraPure™ Low Melting Point Agarose). The tube containing the embryo was placed horizontally into the chamber containing 0.04% Tricaine in embryo medium (Sigma, CAS Number: 886-86-2). The tube was rotated under the microscope so that the embryo would face the objective.

Live imaging was performed approximately from 11hpf to 24hpf every 2.5min-3min, using a Phaseview Alpha ^{3} light sheet apparatus, coupled with an Olympus BX43 microscope and using either a 20X/NA 0.5 Leica HCX APO objective or a 20X/NA 0.5 Olympus objective. Images were acquired using QtSPIM software (Phaseview), which controlled a Hamamatsu ORCA-Flash4.0 Digital sCMOS camera.

Room temperature was maintained around 24°C by air conditioning and the chamber temperature was further controlled by a BIOEMERGENCES-made thermostat. Medium level was maintained by a home-made perfusion system and an overflow to renew the medium.

1.1. Imaging analysis

Images obtained for 1 surface fish and 1 cavefish were visualized with Arivis Vision4D software and reoriented to adopt a similar optical section plane, cutting through the middle of the lens and the optic stalk at all time steps. On one time step per hour, measurements were performed on the reoriented image: optic vesicle/ optic cup length (at the widest), optic stalk width, distance between the anterior optic cup and the lens, distance between the posterior optic cup and the lens, distance between the optic cup edges.

Cutting efficiency of sgRNA2 with either Cas9 mRNA or protein, assessed by HMA

Cas9 mRNA / sg2 (200ng/µL = 5,6µM)

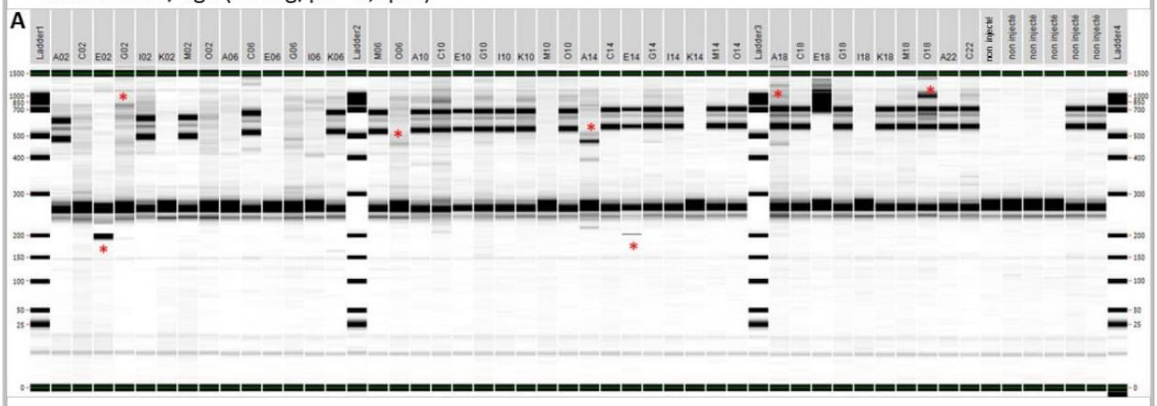

Cas9 Protein (1,87µM) / sg2 (100ng/µL = 2,8µM)

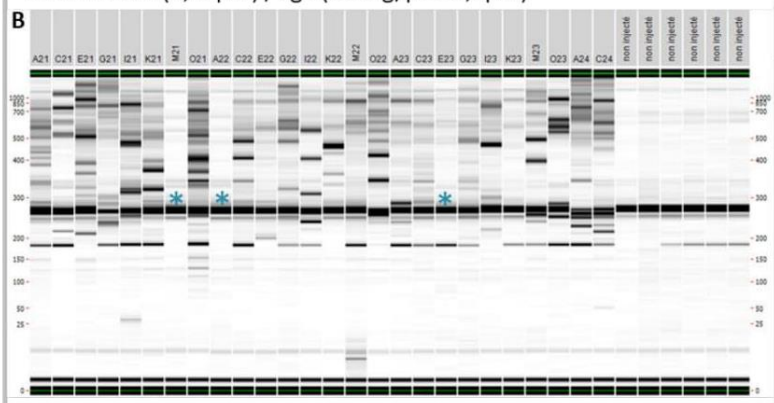

C HMA principle

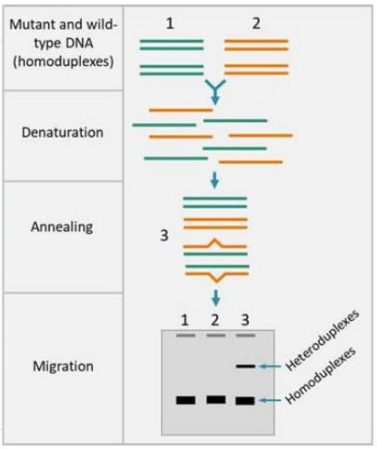

D *Confirmation of correct cutting by F0 embryo sequencing*

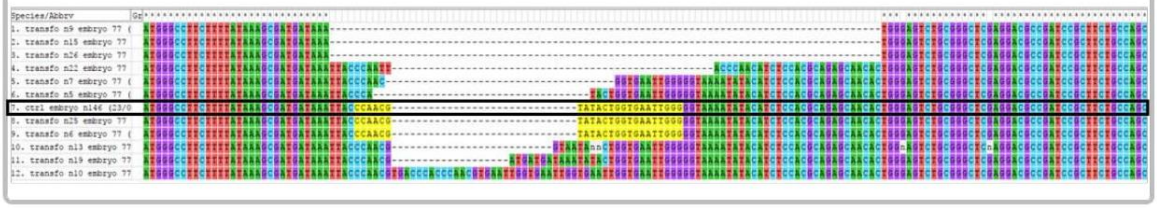

Figure S 1 : cutting efficiency of sgRNA 2

(A) Assessment of sgRNA 2 cutting efficiency when injected with Cas9 mRNA by heteroduplex mobility assay (explained in (C)). Each column is an individual F0 embryo. Embryos with strong additional bands are labelled with a red asterisk; additional light bands can be seen in several fishes indicating cuts and imprecise repairs. Note that the 2 heavy bands seen on many embryos are also present in some of the uninjected controls (the 6 right hand columns) indicating a polymorphism in this region in the wild-type fish (not on the sgRNA target sequence). (B) Assessment of sgRNA 2 cutting efficiency when injected with Cas 9 protein, note the strong presence of additional band compared to the 6 control embryos on the right. Embryos without any visible cuts are labelled with a blue asterisk. Additional bands are seen much more frequently and are much more important than with the mRNA, probably indicating more frequent but also more precocious cut and repair events in the embryo so that many cells share the same sequence. (C) Principle of the heteroduplex mobility assay: in an electrophoresis, heteroduplexes are slowed down compared to homoduplexes so that they form additional bands that can be seen even if the polymorphism is only a substitution. The DNA fragments are therefore denatured and renatured to form heteroduplexes. An electrophoresis is then performed (here with a LabChip, PerkinElmer) to detect the presence of polymorphism.

(D) Different cutting and repair events in a single injected embryo. A PCR was performed on one injected embryo (100ng/µL sgRNA2, Cas9mRNA) around sg2 target site and the product was cloned into pGEM-T Esay (Promega) and transformed into One shot TOP10 competent bacteria (Thermo Fischer). Plasmidic preparations from individual colonies were then sequenced. Various sequences were obtained, evidencing different cut and repair events in one single embryo. sgRNA2 target sequence is highlighted in yellow whenever intact. This F0 fish harbours both insertions and deletions around the cutting site of sgRNA2. A non-injected control fish sequence is included, outlined in black.

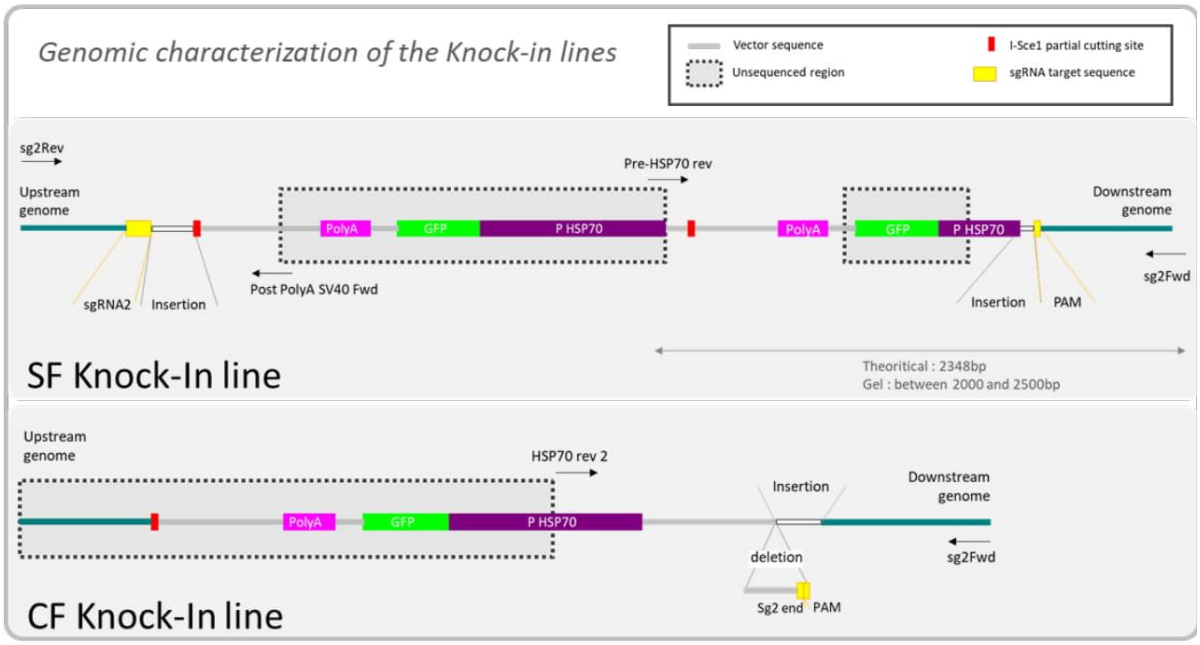

Figure S 2: genomic characterization of the Knock-in lines.
Knock-In insertions, based on partial sequencing. Dotted boxes indicate unsequenced regions, leaving uncertainties. For example, in the surface fish line, there is at least a partial insertion of the repair construct, containing a truncated HSP70 promoter and at least another insert in the same direction (but potentially several).
The conclusion is that for both lines the transgenes are inserted at the correct targeted site.
More precise characterization of the Knock-in lines is still in process. Indeed, the surrounding genomic region is very rich in T and A (GC content around 35%) with many repeats, making PCRs sometimes challenging.

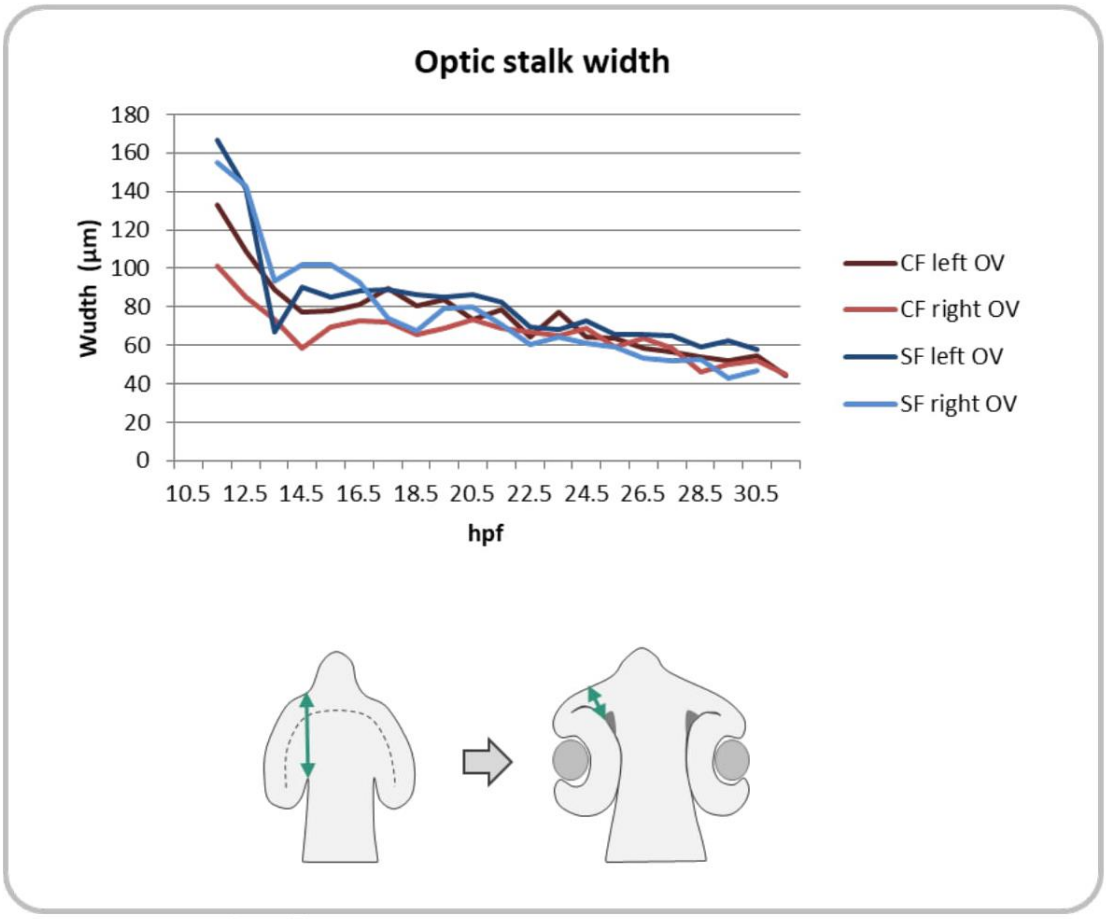

Figure S 3 : optic stalk width.

The size of the optic stalk (in a wide meaning: the connection between the optic vesicle and the neural tube) is smaller in cavefish during early development due to the smaller size of the optic vesicles but rapidly becomes indistinguishable from the optic stalk of the surface fish.

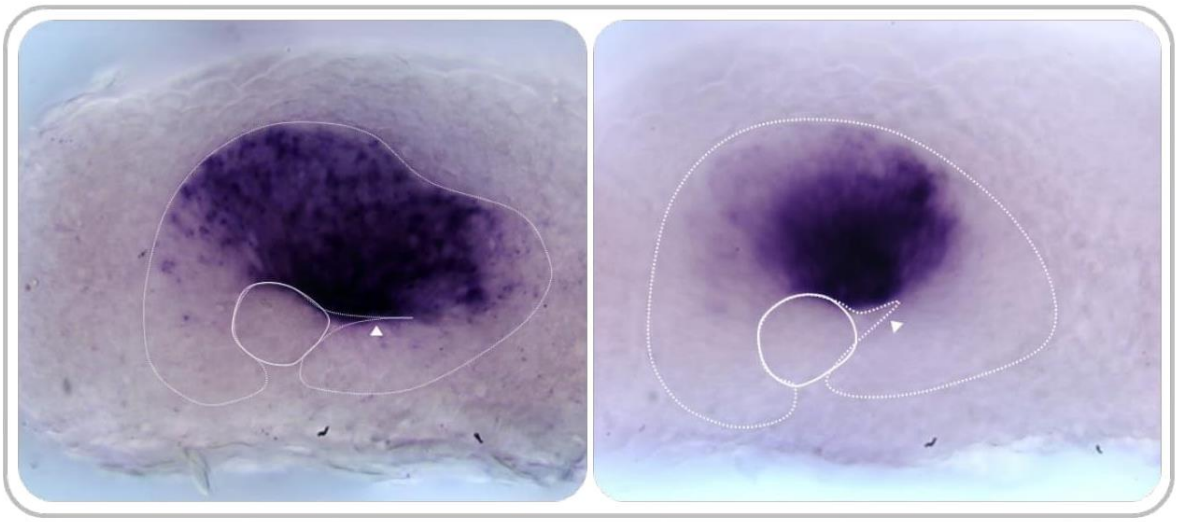

Figure S 4 : Retinal fold

Illustration of the retina folds sometimes observed in cavefish: an “extreme case” on the left and a more classical case on the right. 36 hpf cavefish embryos, mounted laterally, anterior is to the left.

Manuscript in preparation

Regionalization and specification defects in the Mexican cavefish retina.

Lucie Devos, Florent Klee, Maryline Blin and Sylvie Rétaux.

DECA group, NeuroPSI, CNRS UMR 9197, Université Paris-Saclay

Key words : *FoxG1*, *FoxD1*, *Vax2*,*Tbx5a*, *Pax2a*, *Bhlhe40*, retina quadrants, retinal pigmented epithelium, optic stalk.

1. Introduction

We perceive our environment through several sensory modalities, including vision. This sense requires a topographic perception of the light stimuli and a topographic processing of the signal. Indeed we do not just perceive a global colour or light intensity but we are able to pinpoint the different origins of the visual stimuli and assemble them into a complex image. This contrasts with olfaction for example that does not allow for a direct localization of the stimulus source and does not form a map of the stimuli sources. The topographic feature of the visual system is reflected by its structure: a dense grid of photoreceptors distributed on the retina, each of them connected to a bipolar cell, in turn linked to a ganglion cell. The retinal ganglion cells then project their axons through the optic nerve and to the visual processing centres, the lateral geniculate nucleus in the diencephalon in mammals and the optic tectum in the mesencephalon in fish and amphibians. In the case of fishes, the neuronal map of the retina is replicated onto the contralateral tectum, in a symmetrical manner so that the nasal retina projects to the posterior optic tectum, while the temporal retinal ganglion cells project to the anterior optic tectum. This reproduction of the retinal map is called retinotopy and requires a precise regional identity of both the retina and the tectum for a proper matching. In the retina, several genes have been clearly identified that possess a strong regional localization and define several quadrants. Amongst them, *Eph* receptors and *ephrins* but also transcription factors acting upstream of the previous genes.

Astyanax mexicanus is a Mexican freshwater fish species comprising two morphs : the “surface” fish, an eyed and pigmented fish inhabiting a large variety of rivers and ponds in central America; and the cavefish, eyeless and depigmented, living in Mexican caves. If the adult cavefish does not possess eyes, they still develop during embryogenesis before slowly degenerating. This embryonic eye displays several defects such as a smaller size (already present at the eye field stage during neural plate patterning) and a much reduced ventral quadrant and quite often a failure to close the ventral fissure (coloboma phenotype) (for review, see (Jeffery, 2009; Keene, Yoshizawa and McGaugh, 2016)). Several morphogen expressions are modified in the cavefish, including an earlier onset of *Fgf8* expression in the anterior neural ridge (2 hours earlier than in the surface fish) which has been shown to be responsible for the reduction of the ventral quadrant (Pottin, Hinaux and Rétaux, 2011). Another important morphogen modification is the anterior enlargement of *Shh* expression together with a widened midline expression. These changes in morphogen expression trigger modifications of the eye field and the subsequent eye as evidenced by the expression of *Lhx9/2* or *Pax6* (Yamamoto, Stock and Jeffery, 2004; Pottin, Hinaux and Rétaux, 2011).
Because of these various modifications of the embryonic eye and of morphogen signalling, the cavefish is an interesting natural mutant model to study the development of the eye. Moreover, these morphogens have been shown to influence the regionalization of the retina : *Shh* is involved in the regulation of the ventral and temporal fates while *Fgfs* secreted at the anterior neural ridge seem to be rather involved in the nasal specification (Take-uchi, Clarke and Wilson, 2003; Picker and Brand, 2005; Picker *et al.*, 2009; Hernández-Bejarano *et al.*, 2015). We therefore undertook to study the regionalization of the cavefish eye, in comparison with the surface fish.
Additionally, we explored the identity specification of the eye tissues .The retina is divided in three tissues: the neural retina, facing the lens and composed of various neuronal types; the retinal pigmented epithelium (RPE) which during development comes to encompass the back of the neural retina. It then nurtures it by recycling the retinal used by photoreceptors, phagocyting their shed disks and transporting nutrients from the blood to the photoreceptors amongst other functions. The third tissue composes a transient structure that connects the retina to the neural tube: the optic stalk. This thin ventral structure is invaded by the ganglionic cells and guides them to cross the midline on their way to the tectum. These cells then differentiate into reticular astrocytes surrounding the optic nerve. All of these structures derive from the

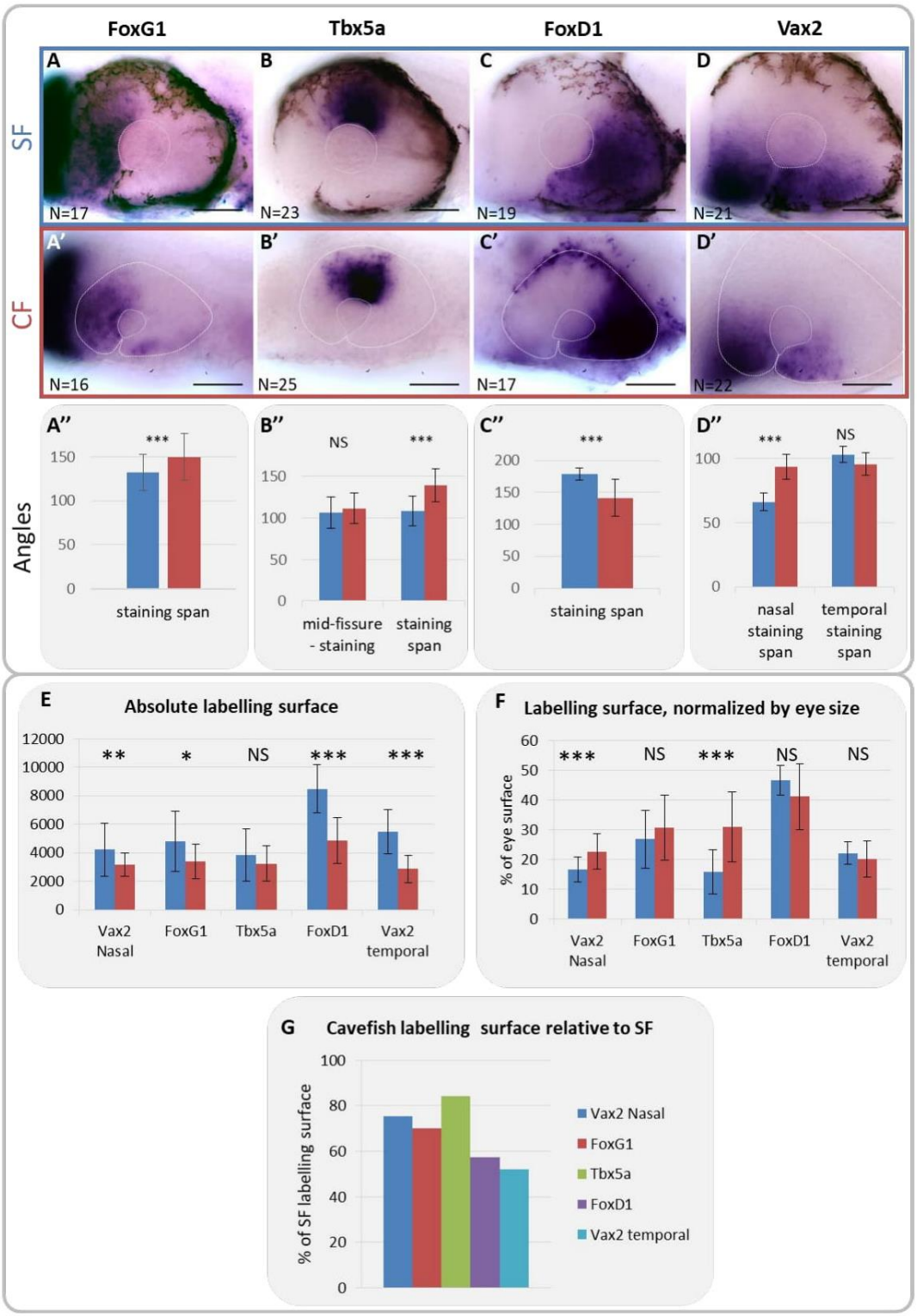

Figure 1 : regionalization of the cavefish eye.
(A-D') *in situ* hybridization of the quadrant markers on surface fish (SF) and cavefish (CF) embryos of 36 hpf. (A''-D'') Quantification of angles of expression span and localization with regards to the middle of the choroid fissure. (E) Absolute surface of the *in situ* hybridization labelling in µm^2. (F) Surface of the *in situ* hybridization normalized by eye size, expressed in percentage of the eye surface. (G) Surface of the *in situ* hybridization labelling of the cavefish expressed as a percentage of the surface of surface fish staining. Surface fish measures are represented in blue, cavefish's in red. Sample sizes are indicated in (A-D'). Statistical test : Mann-Whitney; * p<0.05; ** p<0.01; *** p<0.001.

optic vesicles and have neural origin. We show here that the cavefish eye display modifications of the span of the different quadrants with a tendency to preserve or increase the importance of the nasal and dorsal quadrants while diminishing strikingly the temporal quadrant. Moreover, the optic stalk fate is widely increased throughout the retina while conversely the RPE encompassing of the neural retina is delayed in the cavefish.

2. Results

2.1. Regionalisation: a shift from temporal to nasal fate?

In order to label the different quadrants of the eye, several classical markers were chosen: *FoxG1* for the nasal quadrant, *Tbx5a* for the dorsal quadrant, *FoxD1* as a temporal marker and *Vax2* as a ventral marker, spanning both the nasal and temporal sides of the optic fissure.

The difficulty of comparing these quadrants between cavefish (CF) and surface fish (SF) resided in the difference of morphology and of size of their eyes so that there was no obvious or perfect method to compare them. It was therefore decided to measure different parameters such as the angles of expression, taking as a reference the center of the lens and the middle of the optic fissure if a positional information was necessary (angles measured are presented in Figure 3). The expression surface area was expressed either as an absolute value or as a relative value normalized to the eye size. Below the expression patterns of the four markers are described in a clock-wise manner starting at the optic fissure.

The nasal marker *FoxG1* presented a larger angle of expression in the cavefish compared to the surface fish (CF : 149°, SF :132°) due to a dorsal expansion of the staining (Figure 1 A-A''). In cavefish the dorsal marker *Tbx5a* had an expression beginning at the same angle from to the middle of the optic fissure but spanning an increased angle towards the temporal part of the retina (angle to mid-fissure, 106° for the SF and 111° for the CF; span, 108° for the SF and 139 for the CF)(Figure 1 B-B''). Reciprocally to these two increases in expression spans in the clock-wise direction, the temporal marker *FoxD1* span was reduced in its dorsal part of the cavefish eye (179° in the SF, 141° in the CF)(Figure 1 C-C''). Finally the ventral marker *Vax2* had different features on the nasal and the temporal margins of the optic fissure. Its span was increased in the ventro-nasal quadrant, indicating a dorsal-wards or clock-wise progression (66° in the SF, 94° in the CF) while it was unchanged in the temporal quadrant when compared to surface fish (Figure 1 D-D'').

All of the markers examined presented a modification of expression in a fan-opening fashion, from nasal toward temporal, overall increasing the nasal and dorsal fate at the expense of the temporal quadrant.

The smaller size of the cavefish eye was reflected by the absolute values of marker expression surfaces (Figure 1E). Indeed, all of them but one were decreased in size, including nasal *Vax2* and *FoxG1* expression domains which were slightly but significantly reduced. *Tbx5a* was the only gene showing the same surface of expression in the cavefish and the surface fish eye. The two temporal genes, *FoxD1* and *Vax2*, exhibited a strong reduction of expression surface. This seemed to hint at a temporal reduction in the cavefish eye, which is further visible when the gene expression surfaces were expressed in relative values (normalized to eye size)(Figure 1F) or in percentage of the surface fish labelling (Figure 1G). Indeed, the most strongly reduced quadrant was the temporal quadrant, labelled by *FoxD1* and the temporal aspect of *Vax2* domain.

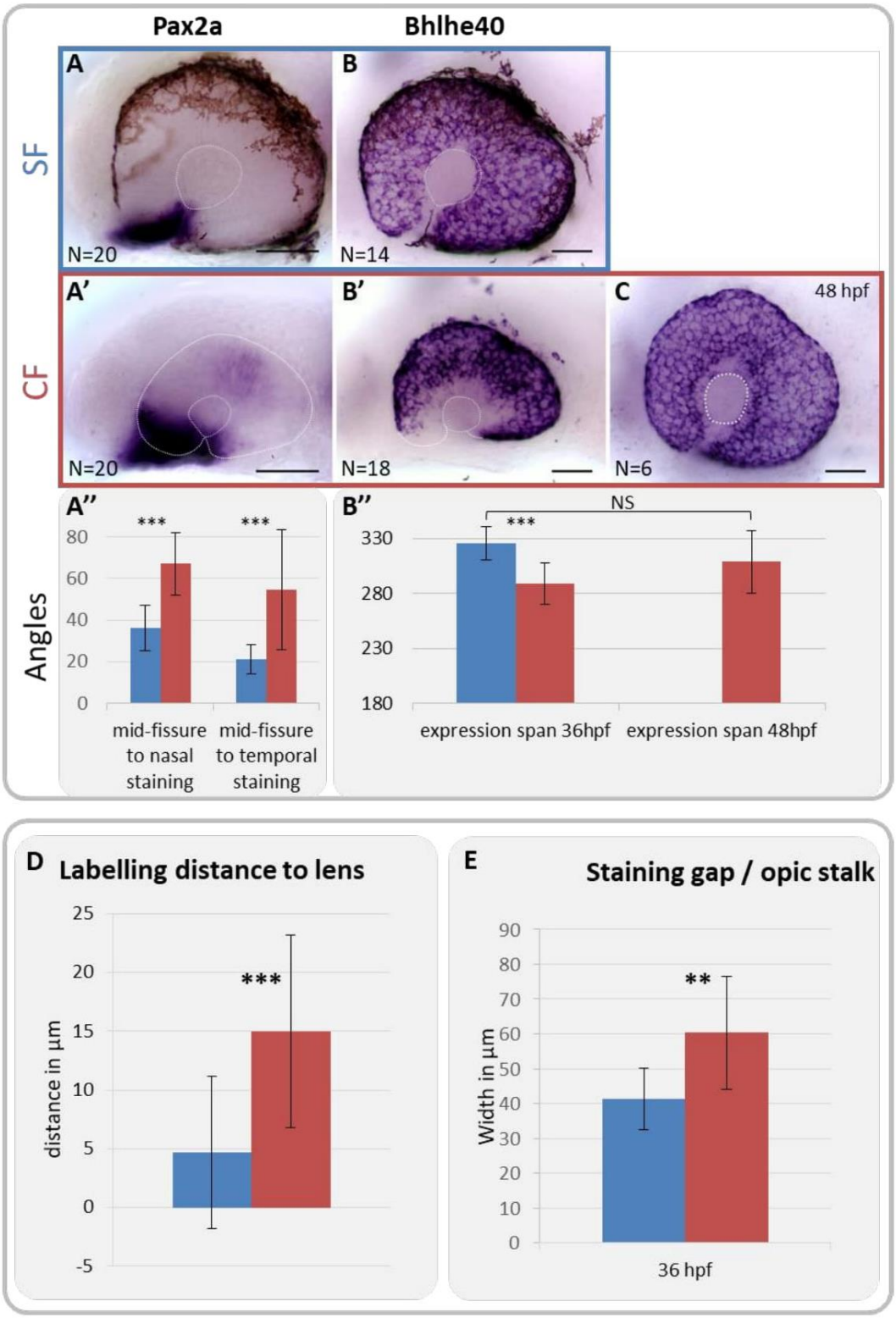

Figure 2: tissue identity.
(A-C) *in situ* hybridization of the tissue identity marker on surface fish (SF) and cavefish (CF) embryos of 36 hpf. (C) *in situ* hybridization of Bhlhe40 on 48 hpf cavefish (CF) embryo. (A'') Angle between the middle of the optic fissure and the limit of the staining. (B'') Angle of Bhlhe40 expression span at 36 hpf and 48 hpf. (D) Distance between Bhlhe40 staining and the lens at 36 hpf. (E) Width of the gap of Bhlhe40 at the back of the eye. Surface fish measures are represented in blue, cavefish's in red. Sample sizes are indicated in (A-C). Statistical test : Mann-Whitney; * $p<0.05$; ** $p<0.01$; *** $p<0.001$.

Normalizing the expression surface by the eye size evidenced a strong increase in dorsal proportion of the cavefish eye, which was expected given the previously known ventral reduction of the cavefish eye. However, until now, the embryonic cavefish eye phenotype was rather described as a ventral reduction. The present results suggest that proportionally, the naso-ventral quadrant is rather increased, while the reduction seems to be exclusively ventro-temporal. This is consistent with our observations that in terms of morphology, the ventro-temporal margin of the optic fissure corresponds to a reduced/thin piece of tissue, while the naso-ventral margin seems more preserved in the cavefish compared to the surface fish embryo (compare Figure 1 A-D to A'-D').

2.2. Tissue specification and morphogenesis

In order to assess tissue identity, *Pax2a* was used as a marker for optic stalk and optic fissure margin identity (Macdonald *et al.*, 1997) and Bhlhe40 (Cechmanek and McFarlane, 2017) was used as an RPE identity marker. The tissue identity was assessed the same way than the quadrants identity, by measuring expression angles but also other parameters such as the distance between the RPE cells and the lens that we took as an indicator of the correct engulfment of the retina by the RPE.

Pax2a was expressed in a much wider fashion in the cavefish compared to the surface fish. Indeed, the expression was expanded beyond the restricted optic fissure margins and occupied a large part of the ventral quadrants both nasally (angles from mid-optic fissure to nasal staining, SF: 36°, CF: 67) and temporally (angles from mid-optic fissure to temporal staining, SF : 21°, CF: 55°) (Figure 2 A-A''). Surprisingly, *Pax2a* expression in the cavefish eye sometimes expanded throughout the whole retina (with a lighter, although very specific, expression intensity; Figure 2A'). Staining was even sometimes present in the dorsal quadrant, opposite to the optic stalk or optic fissure margins without obvious staining between the dorsal and the ventral quadrant (see Figure 2A'). These "dorsal" phenotypes were observed in 60% of the cavefish embryos compared to 0% in the surface fish.

The RPE marker *Bhlhe40* was expressed all around the eye often contacting or extremely near the lens in 36 hpf surface fish embryos (4.7 µm away in average) (Figure 2B, B', D). The extreme edges of the optic fissure margins sometimes lacked staining but overall the expression spanned 326° around the eye (Figure 2B''). Conversely, in the cavefish, *Bhlhe40* staining was reduced, with usually a wider ventral gap, probably resulting from the wider optic fissure opening and a diminished covering of the retina by the RPE (289° around the eye). *Bhlhe40* staining was also found further away from the lens (15 µm away), reinforcing the idea of a reduced retina covering by the RPE at this stage; at 48hpf however, the staining span seemed increased and was no longer significantly different from the level of the 36 hpf surface fish (CF 48 hpf: 309°, SF 36 hpf: 326°)(Figure 2 B, C, B''), although this absence of significance could come from the low number of 48 hpf fish analysed (6 embryos only). Altogether, these results suggested that both the RPE engulfment movement and the optic fissure margins juxtaposition are slowed but still occur in the cavefish.

Additionally, we measured and analysed in *Bhlhe40*-stained embryos the "gap" of ventral staining at the back of the retina. Indeed, the back of the retina was usually well covered with *Bhlhe40* staining but a ventral gap was always observed which was very well delimited by strongly stained, sharp edges (see Figure S 1Figure S 1). We interpreted this gap as the "exit point" of the optic stalk and therefore used it as a proxy for optic stalk width. This gap was wider in the cavefish than in the surface fish (SF: 41 µm, CF: 60 µm) (Figure 2E). This is consistent with the above reported increase in *Pax2a* expression and points towards an increased optic stalk size in the cavefish.

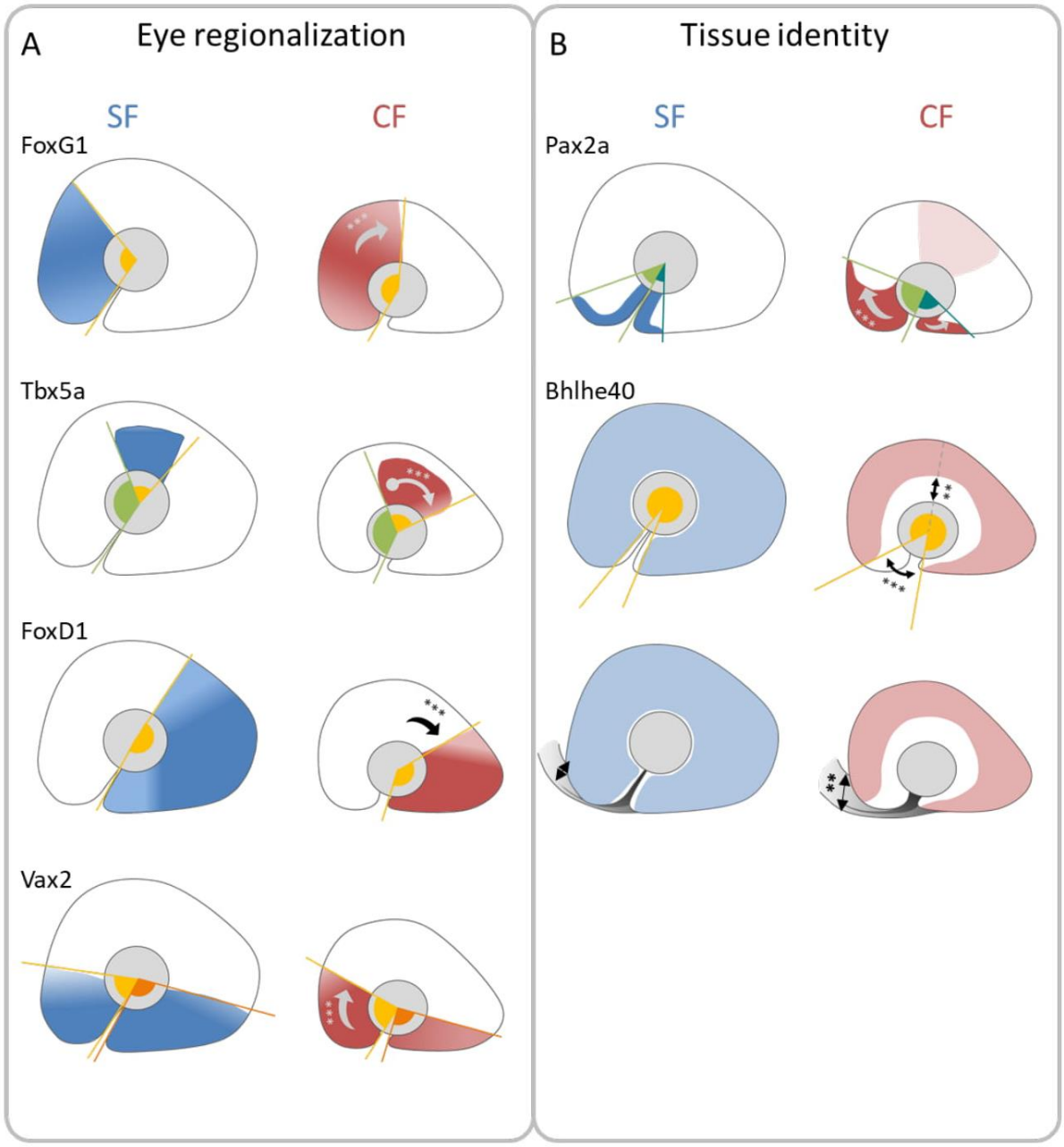

Figure 3: summary diagram of the expression patterns of marker genes of eye quadrants and tissue identity. Expression patterns are represented in blue for surface fish and red for cavefish. Angles measured are represented here. Expression span angles are represented in yellow and orange. The angles measured are between the middle of the choroid fissure and the limit of the expression pattern.

3. Discussion

3.1. Regionalization

Because the ventral quadrant of the cavefish eye was described as reduced and since the expression of the ventralizing morphogen Shh was known to be enlarged in the cavefish, we originally expected a global "ventralization" of the eye quadrants at the expense of the dorsal quadrant which we assumed would be reduced. However this study revealed a quite different story: a shift of marker expression patterns in a fan-opening manner (Figure 3). Indeed, nasal and dorsal quadrants have an increased span at the expense of the temporal and temporo-ventral quadrants.

This observation can lead to several interpretations: looking at the angle quantification one could argue a shift of fate, increasing the nasal identity at the expense of the temporal identity. Alternatively the quantification of the expression surfaces could rather lead to interpret this as a mere reduction of the temporal tissue in the cavefish eye, with a much milder alteration of the nasal eye. This would come as a refinement of the "ventral reduction" previously described in the cavefish. Finally these results could also be interpreted in terms of morphogenesis, as a failure of the different presumptive quadrants to reach their proper position or even a failure of the progenitor cells to enter and populate the eye. These hypotheses are far from being mutually exclusive and the answer could very well lie in a combination of these.

We venture to propose one hypothetical scenario that could account for the observed differences. The increased Hh signalling in cavefish was shown to decrease the size of its optic vesicles (Yamamoto, Stock and Jeffery, 2004) and probably the eye field size (also smaller in the cavefish), which could account for the final smaller eye size. The subsequent early optic vesicle patterning could be roughly conserved as shown by Hernández-Bejarano and colleagues. Of note, a slight increase in *FoxG1* expression was visible in their results, which could be explained not only by the earlier onset of *Fgf8* expression in the anterior neural ridge but also by the increase in size of the olfactory placode of the cavefish which secretes Fgf24 (Hernández-Bejarano *et al.*, 2015; Hinaux *et al.*, 2016). Indeed both these Fgf, along with Fgf3 promote a retinal nasal fate (Picker and Brand, 2005; Picker *et al.*, 2009; Hernández-Bejarano *et al.*, 2015), which could explain a slight expansion of *FoxG1* expression, itself limited or counteracted by the increased Shh expression in cavefish. After the initial evagination and patterning of a reduced optic vesicle, morphogenesis proceeds with the "extended evagination" described by Kwan and colleagues (Kwan *et al.*, 2012), where cells from the medial neural tube continue to enter the optic vesicle to contribute exclusively to the ventro-nasal part of the eye. If this step proceeds normally, it could partially compensate the originally small size of the eye field / optic vesicle, but only in the nasal part while the temporal part would still be fully affected. This would explain the increased angle of *FoxG1* and nasal *Vax2* expression in comparison to the reduced *FoxD1* and temporal *Vax2* territories we observed (Figure 4). It is also worth noting that early Hh signalling can increase *Vax2* expression (before early optic vesicle stage) in *Xenopus*, which could further explain *Vax2* nasal expansion (Wang *et al.*, 2015). Concerning the increase in *Tbx5a* angle of expression toward the temporal quadrant, Fgf signalling has been shown to promote dorsal identity temporally, as demonstrated by the temporal reduction of *Tbx5a* span and its nasal shift in *Fgf8* mutant zebrafish (*Ace*) (Picker and Brand, 2005). In the case of cavefish, either the earlier onset of *Fgf8* expression in the cavefish or the larger olfactory epithelium secreting fgf24 could account for the angle enlargement.

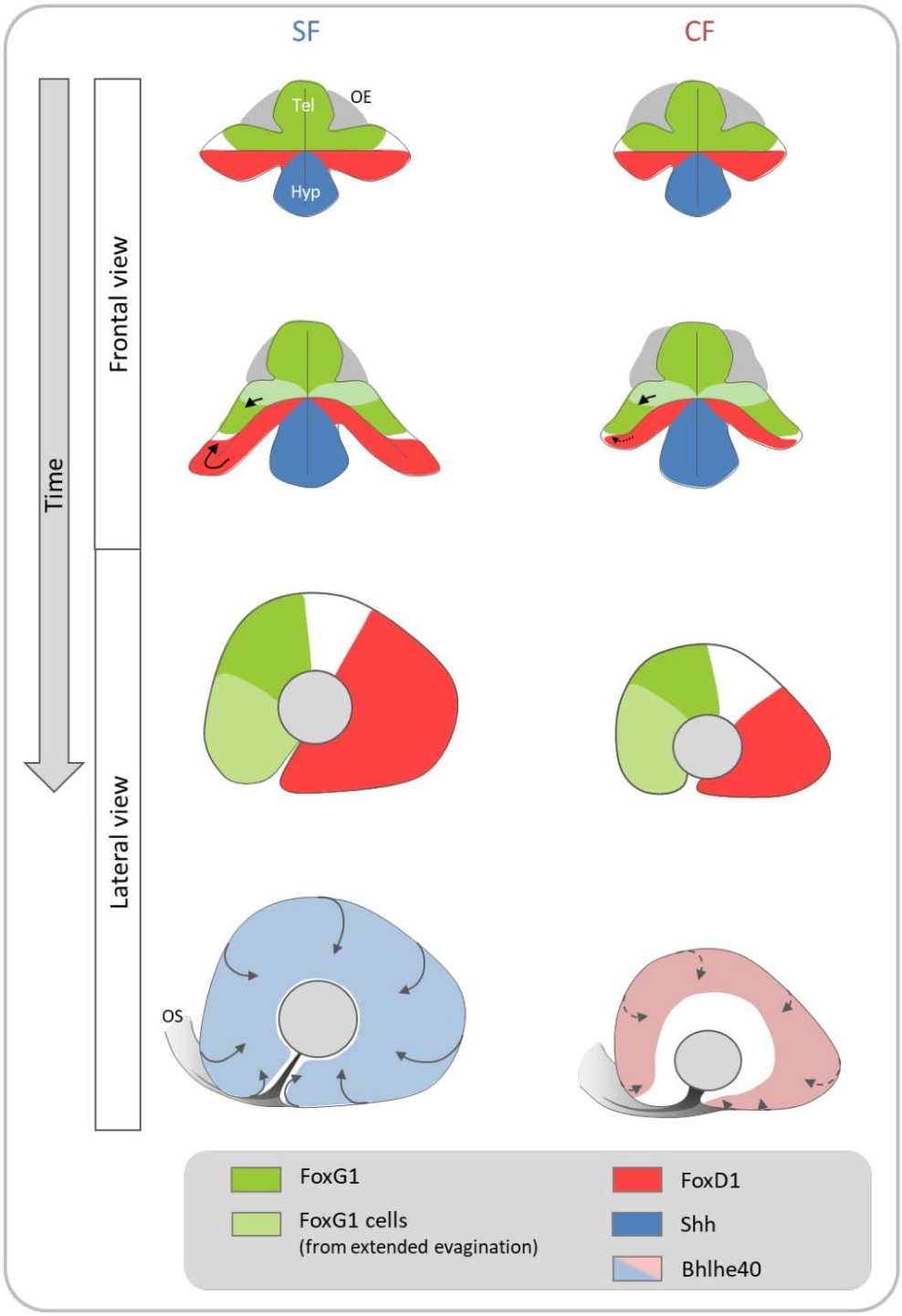

Figure 4: diagram of the hypothetical scenario explaining the lesser decrease in size of the nasal quadrant compared to the temporal quadrant in cavefish.
The small size of the optic vesicles, correctly patterned, explains the decrease in temporal quadrant size. Unaltered extended evagination movements bring new cells into the prospective nasal retina, partially rescuing its size. Finally, the expansion of the RPE to engulf the retina which is concomitant with the rim movement is delayed, leaving the optic stalk wide and optic fissure margins away from each other. OE, olfactory epithelium.

3.2. Tissue identity

It was previously shown that *Pax2a* expression pattern was increased in the cavefish at the expense of the *Pax6*-expressing part of the eye field at neural plate stage (Yamamoto, Stock and Jeffery, 2004). Here we confirm these results and show that *Pax2a* is no longer confined to the optic stalk and optic fissure margins of the cavefish eye but invades the ventral retina and even in a number of cases, the dorsal part of the retina. This phenotype is probably caused by the increase in Shh signalling in the cavefish, as Shh injections in zebrafish embryos or *Ptch1* (a negative regulator of Hh pathway) loss of function in *blowout* mutants cause very similar phenotypes with a larger optic stalk and an invasion of the ventral retina by *Pax2a* expression. Contrarily to *Vax2*, *Pax2a* is expanded in both temporal and ventral directions (Figure 3).

Bhlhe40 expression reveals that the RPE identity is maintained in the cavefish eye. Yet, the expansion and engulfment movement that this tissue is supposed to achieve to reach the rim of the retina, contacting the lens and covering the whole retina seems delayed compared to the surface fish (Figure 3). This could be due to an impaired rim movement, which is the morphogenetic movement that brings the presumptive retina from the ventral optic vesicle leaflet to the more dorsal, lens-facing epithelium by an active migration around the rims of the optic recess (Picker *et al.*, 2009; Heermann *et al.*, 2015; Sidhaye and Norden, 2017)(Figure 4). Potentially, this movement could also be involved in closing up the optic fissure margins as suggested by the presence of a coloboma upon impairment of the rim movement by *BMP4* overexpression in the optic vesicle (Heermann *et al.*, 2015). In that case, impairment of this morphogenetic movement could explain the coloboma phenotype observed in the cavefish. If this movement were delayed but still managed to be completed, then the cavefish coloboma should ultimately close.

4. Material and methods

4.1. Animals

Laboratory stocks of A. mexicanus surface fish and cavefish were obtained in 2004 from the Jeffery laboratory at the University of Maryland. The surface fish were originally collected from San Solomon Spring, Texas and the cavefish are from the Pachón cave in Mexico. Surface fish are kept at 26°C and cavefish at 22°C. Natural spawns are induced after a cold shock (22°C over weekend) and a return to normal temperature for surface fish; cavefish spawns are induced by raising the temperature to 26°C. Embryos destined for *in situ* hybridization were collected after natural spawning, grown at 24°C and staged according to the developmental staging table (Hinaux *et al.*, 2011) and fixed in 4% paraformaldehyde. After progressive dehydration in methanol, they were stored at -20°C.

Animals were treated according to French and European regulations of animals in research. SR' authorization for use of animals in research is 91-116, and Paris Centre-Sud Ethic committee authorization numbers are 2012-52 and 2012-56.

4.2. In situ hybridization

The expression patterns of 6 transcription factors were studied in both surface and cavefish at 36 hpf. FoxD1 cDNAs was available from our cDNA library (FO380710), other cDNAs were cloned for the purpose of this work in pGEMT-Easy (Promega), primers are listed below:

- FoxG1: forward primer CTGACGTTCATGGACCGAGC; reverse primer CAGTCTGCTTCCTGTGGATGT.
- Tbx5a: forward primer GCCTTCATTGCGGTCACTTC; reverse primer CCCTCGTTCCATTCAGGCAT.

- Vax2: forward primer GGGCAAAACATGCGCGTTA; reverse primer CAGTAATCCGGGTCCACTCC.
- Pax2a: forward primer AGCTGCATAACCGAGGCGA; reverse primer CTCCATTAGAGCGAGGGATTCCGA
- Bhlhe40: forward primer : GCACTTTCCCTGCGGATTTC; reverse primer : TGGAGTCTCGTTTGTCCAGC

cDNAs were amplified by PCR, and digoxygenin-labelled riboprobes were synthesized from PCR templates. Embryos were rehydrated by graded series of EtOH/PBS, then for embryos older than 24 hpf, proteinase-K permeabilization at 37°C was performed for 36hpf embryos only (10 µg/ml, 15 min) followed by a post-fixation step. Riboprobes were hybridized for 16 hr at 65°C and embryos were incubated with anti-DIG-AP (Roche, dilution 1/4000) overnight at 4°C. Colorimetric detection with BCIP/NBT (Roche) was used. Mounted embryos were imaged on a Nikon Eclipse E800 microscope equipped with a Nikon DXM 1200 camera running under Nikon ACT-1 software. Brightness and contrast were adjusted using FIJI, some of the images used for illustration purpose were created from an image stack, using the extended depth of field function of Photoshop CS5. Area, distance and angle measurements were performed using FIJI (Schindelin *et al.*, 2012; Schneider, Rasband and Eliceiri, 2012).

5. References

Cechmanek, P. B. and McFarlane, S. (2017) 'Retinal pigment epithelium expansion around the neural retina occurs in two separate phases with distinct mechanisms', *Developmental Dynamics*, 246(8), pp. 598–609. doi: 10.1002/dvdy.24525.

Heermann, S. *et al.* (2015) 'Eye morphogenesis driven by epithelial flow into the optic cup facilitated by modulation of bone morphogenetic protein', *eLife*. eLife Sciences Publications Limited, 4, p. e05216. doi: 10.7554/eLife.05216.

Hernández-Bejarano, M. *et al.* (2015) 'Opposing Shh and Fgf signals initiate nasotemporal patterning of the zebrafish retina', *Development*, 142(22), pp. 3933–3942. doi: 10.1242/dev.125120.

Hinaux, H. *et al.* (2011) 'A developmental staging table for Astyanax mexicanus surface fish and Pachón cavefish.', *Zebrafish*, 8(4), pp. 155–65. doi: 10.1089/zeb.2011.0713.

Hinaux, H. *et al.* (2016) 'Sensory evolution in blind cavefish is driven by early embryonic events during gastrulation and neurulation.', *Development (Cambridge, England)*. Oxford University Press for The Company of Biologists Limited, 143(23), pp. 4521–4532. doi: 10.1242/dev.141291.

Jeffery, W. R. (2009) 'Regressive Evolution in *Astyanax* Cavefish', *Annual Review of Genetics*, 43(1), pp. 25–47. doi: 10.1146/annurev-genet-102108-134216.

Keene, A. C., Yoshizawa, M. and McGaugh, S. E. (2016) *Biology and evolution of the Mexican cavefish*. Available at: https://www.sciencedirect.com/science/book/9780128021484 (Accessed: 2 April 2018).

Kwan, K. M. *et al.* (2012) 'A complex choreography of cell movements shapes the vertebrate eye.', *Development (Cambridge, England)*. Oxford University Press for The Company of Biologists Limited, 139(2), pp. 359–72. doi: 10.1242/dev.071407.

Macdonald, R. *et al.* (1997) 'The Pax protein Noi is required for commissural axon pathway formation in the rostral forebrain', *Development*, 124(12).

Picker, A. *et al.* (2009) 'Dynamic Coupling of Pattern Formation and Morphogenesis in the Developing Vertebrate Retina', *PLoS Biology*. Edited by W. A. Harris. Public Library of Science, 7(10), p. e1000214. doi: 10.1371/journal.pbio.1000214.

Picker, A. and Brand, M. (2005) 'Fgf signals from a novel signaling center determine axial patterning of the

prospective neural retina.', *Development (Cambridge, England)*, 132(22), pp. 4951–62. doi: 10.1242/dev.02071.

Pottin, K., Hinaux, H. and Rétaux, S. (2011) 'Restoring eye size in Astyanax mexicanus blind cavefish embryos through modulation of the Shh and Fgf8 forebrain organising centres.', *Development (Cambridge, England)*, 138(12), pp. 2467–76. doi: 10.1242/dev.054106.

Schindelin, J. *et al.* (2012) 'Fiji: an open-source platform for biological-image analysis.', *Nature methods*, 9(7), pp. 676–82. doi: 10.1038/nmeth.2019.

Schneider, C. A., Rasband, W. S. and Eliceiri, K. W. (2012) 'NIH Image to ImageJ: 25 years of image analysis.', *Nature methods*, 9(7), pp. 671–5. Available at: http://www.ncbi.nlm.nih.gov/pubmed/22930834 (Accessed: 14 May 2018).

Sidhaye, J. and Norden, C. (2017) 'Concerted action of neuroepithelial basal shrinkage and active epithelial migration ensures efficient optic cup morphogenesis', *eLife*. eLife Sciences Publications Limited, 6, p. e22689. doi: 10.7554/eLife.22689.

Take-uchi, M., Clarke, J. D. W. and Wilson, S. W. (2003) 'Hedgehog signalling maintains the optic stalk-retinal interface through the regulation of Vax gene activity.', *Development (Cambridge, England)*. The Company of Biologists Ltd, 130(5), pp. 955–68. doi: 10.1242/DEV.00305.

Wang, X. *et al.* (2015) 'Dorsoventral patterning of the Xenopus eye involves differential temporal changes in the response of optic stalk and retinal progenitors to Hh signalling.', *Neural development*. BioMed Central, 10(1), p. 7. doi: 10.1186/s13064-015-0035-9.

Yamamoto, Y., Stock, D. W. and Jeffery, W. R. (2004) 'Hedgehog signalling controls eye degeneration in blind cavefish.', *Nature*. Nature Publishing Group, 431(7010), pp. 844–7. doi: 10.1038/nature02864.

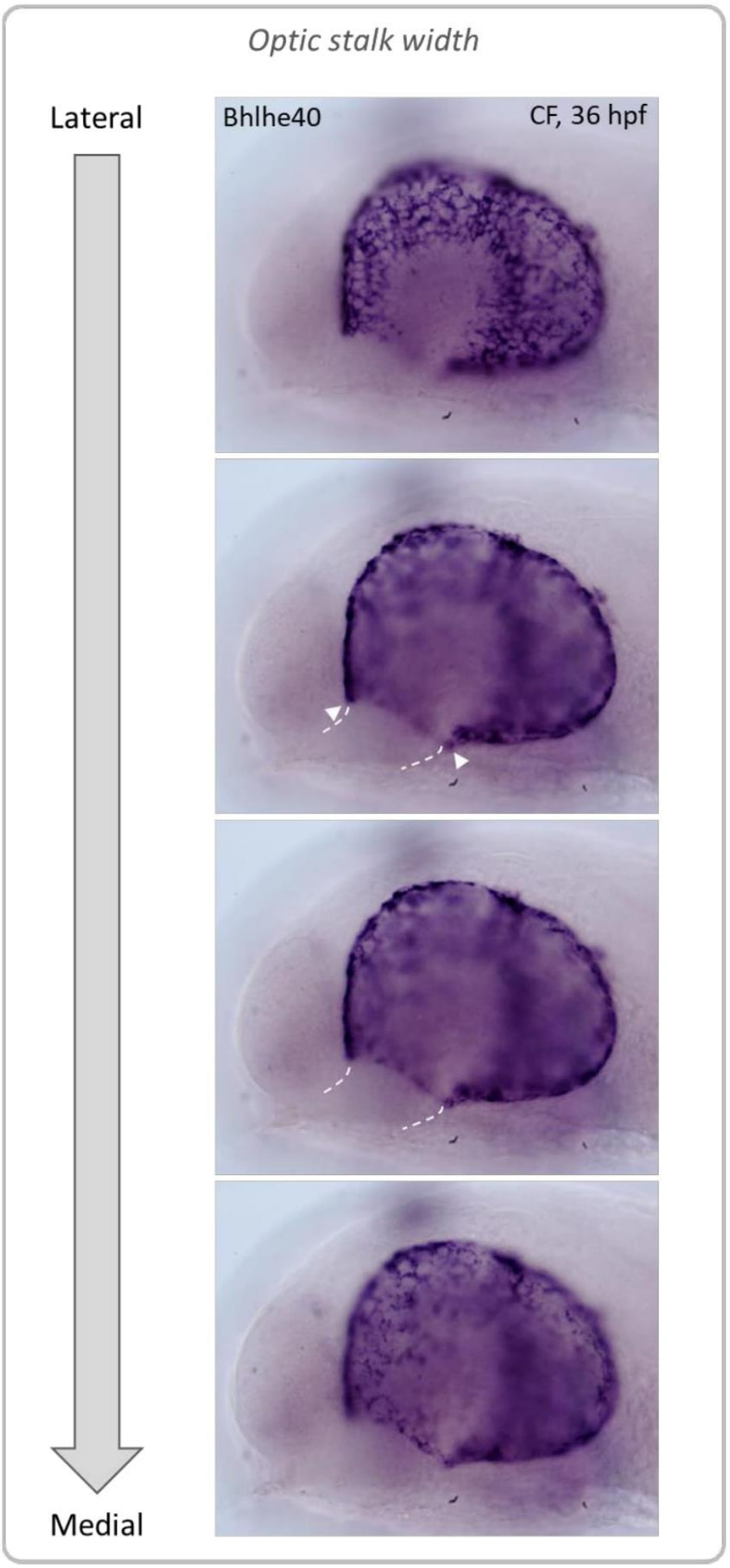

Figure S 1 : Illustration of the gap of *Bhlhe40* staining, which we interpret as the optic stalk width. Different focuses of the same embryo, from lateral to medial. Arrowheads indicate the limits of the staining gap we measured. Doted lines show the exit trajectory of the optic stalk.

2.2. Discussion

The work presented here reveals a morphogenetic defect in the cavefish eye along with a rather unexpected regional identity shift.

Our live imaging analysis suggests that the lens is originally properly located at the middle of the small optic vesicle. The optic cup invagination is correctly initiated as revealed by the curvature of the early optic cup around the lens but fails to proceed. We interpret this result as a correct basal constriction of the lens-facing epithelium, initiating the optic cup curvature but followed by a defective rim movement that fails to complete in proper time the invagination of the optic cup. These results are in agreement with those of the RPE identity showing a delayed engulfment of the retina by this tissue. This slower cell flow is consistent with the previous demonstration by Picker and colleagues that Fgf signalling delays the rim movement, and with the fact that Fgf signalling is enhanced in the cavefish via an earlier onset of Fgf8 expression in the anterior neural ridge and an enlarged olfactory placode (which secretes Fgf24, at least in zebrafish (Picker et al. 2009). This slower rim movement could also contribute to the coloboma phenotype by delaying the juxtaposition of the ventral margins as suggested by the restoration of the cavefish optic fissure closure upon time-specific Fgf signalling inhibition (Pottin et al. 2011).

We also suggest that the extended evagination movement described by Kwan and colleagues (Kwan et al. 2012) proceeds properly as indicated by the elongation of the cavefish optic vesicle/cup over time. As this movement was described to only contribute to the nasal retina, we hypothesize that it could account for the relative increase in nasal quadrant size relative to the temporal quadrant. Under this hypothesis, the small size of the temporal quadrant would be due to the initial small size of the cavefish optic vesicle.

This extended evagination and the consequent elongation of the retina provoke the displacement of a large part of the retinal tissue posterior to the lens, which explains the late ventral position of this lens.

One inconsistency between our two studies concerns the size of the optic stalk which we find to be similar in the live imaging analysis while we find an enlargement in the cavefish by the Bhlhe40 gap measurement. This inconsistency could be due to the different orientation in which these measures were taken, indeed, they are essentially orthogonal to each other: the time lapse analysis could indicate a similar dorso-ventral size of the optic stalk while the RPE gap could point to an increase in the antero-posterior dimension of this structure. Another possibility is that the only cavefish analysed in the time-lapse experiment was not representative. An increased sample size will answer this question.

The morphogenesis results are still very preliminary as only one fish of each morph was analysed (however similar phenotypes have been observed on other acquisitions) and very few parameters were examined. We next want to analyse more embryos, running the analysis in different optic planes, indeed a lateral examination of the time lapses would allow us to visualize other morphogenetic movements such as the pinwheel movement during elongation or the ventral optic fissure margin progression towards each other. It would also be interesting to measure the amount of cells entering the optic vesicle/cup during the extended evagination and to quantify the rim movement.

As more long-term perspectives, we would like to test if the known modified morphogens signalling of the cavefish (Shh and Fgf8) are involved in the rim movement defect by altering them pharmacologically in our transgenic lines during imaging. Such experiments could bring a wider understanding of the role of these morphogens in the morphogenetic movements shaping the eye.

General discussion

In biology, new discoveries are often led by the appearance of new techniques. In the field of development and Evo-Devo, the recent technological explosion of both transgenesis and microscopy techniques has allowed us to finally start watching development in actual living embryos. We are no longer bound to study life on dead samples only (even though this stays very informative), we can now see development happening under our eyes ! This change opened the way to the study of morphogenesis, in particular in model organisms with an external development and a good transparency such as in many fish species. In this context, the cavefish becomes a very interesting model as several of its organs are slightly modified in shape or size and several morphogens signalling modifications have been identified (with probably more to be discovered).

In our case, this project started when we noticed that the optic recess region of the cavefish was enlarged. The connection of this structure with the ventral part of the retina, which was reduced in the cavefish, led us to hypothesize a developmental trade-off between these two structures. Indeed, the eye is no longer under positive selection in the cave environment and ultimately degenerates while the ORR and its neurons remain until adulthood. Our original goal was to test this hypothesis by backtracking the fates and movements of the ventral quadrant cells of the surface fish to their neural plate origin. We were then planning to forward track the cavefish cells originating from the same neural plate region to their final position. However, the difficulty of raising cavefish until adulthood for transgenesis purposes and the live imaging technical challenge prevented us from achieving that goal. Nevertheless, the data collected allowed us to better describe the cavefish eye development and to detect an impairment of the rim movement which seems slower.

The trade-off hypothesis still seems worth investigating since the increase of NPY and Hcrt cells is located in the ventral (according to the neuraxis) ORR/ hypothalamic region which corresponds to the origin of the temporal quadrant. Therefore, neural plate cells which have lost their eye identity could still contribute to these regions. This is further supported by the fate map experiments performed by a former Phd student of the lab who showed that a larger region of the neural plate had a “hypothalamic” fate, in the wide meaning of hypothalamus and ORR combined and as opposed to a ventral retina fate. Refining more precisely the fate of these cells could help us understand whether this loss of the temporal retina offers an indirect advantage to the cavefish, if it is a by-product of another unrelated modification or even just a neutral drift. Indeed, this loss of the temporal retina could be advantageous by leading to an increased number of neurons devoted to another function such as NPY or hypocretin cells. Alternatively this could be simply a “side effect” of some other signalling modifications that were selected for on completely different traits (such as enlarged olfactory epithelium which is induced by Shh and Fgf increased signalling).

Work on the cavefish and other Evo-Devo models really shows us how much can be modified by quite small changes. Indeed, *Shh* expression enlargement seems to be at least partially responsible for both the earlier onset of *Fgf8* and the enlargement of the olfactory epithelia. These modifications lead to an increase in Fgf signalling in turn preventing the correct formation of the ventro-temporal eye, probably delaying the rim movement and at the same time increasing the number of NPY and hypocretin neurons in the ORR/hypothalamus. These fascinating mechanisms allow us to better understand how as little time as 25 000 years in a cave environment can generate such a modified and adapted fish.

References

Affaticati, P. et al., 2015. Identification of the optic recess region as a morphogenetic entity in the zebrafish forebrain. *Scientific Reports*, 5, p.8738. Available at: http://www.ncbi.nlm.nih.gov/pubmed/25736911 [Accessed January 13, 2017].

Ail, D. & Perron, M., 2017. Retinal Degeneration and Regeneration-Lessons From Fishes and Amphibians. *Current pathobiology reports*, 5(1), pp.67–78. Available at: http://www.ncbi.nlm.nih.gov/pubmed/28255526 [Accessed April 9, 2018].

Alsop, D. & Vijayan, M., 2009. The zebrafish stress axis: molecular fallout from the teleost-specific genome duplication event. *General and comparative endocrinology*, 161(1), pp.62–6. Available at: http://linkinghub.elsevier.com/retrieve/pii/S0016648008003560 [Accessed March 8, 2018].

Alunni, A. et al., 2007. Developmental mechanisms for retinal degeneration in the blind cavefishAstyanax mexicanus. *The Journal of Comparative Neurology*, 505(2), pp.221–233. Available at: http://www.ncbi.nlm.nih.gov/pubmed/17853442 [Accessed April 4, 2018].

Alvarez, Y. et al., 2007. Genetic determinants of hyaloid and retinal vasculature in zebrafish. *BMC Developmental Biology*, 7(1), p.114. Available at: http://bmcdevbiol.biomedcentral.com/articles/10.1186/1471-213X-7-114 [Accessed February 27, 2018].

Asai-Coakwell, M. et al., 2007. GDF6, a Novel Locus for a Spectrum of Ocular Developmental Anomalies. *The American Journal of Human Genetics*, 80(2), pp.306–315. Available at: http://www.ncbi.nlm.nih.gov/pubmed/17236135 [Accessed July 19, 2017].

Aspiras, A.C. et al., 2015. Melanocortin 4 receptor mutations contribute to the adaptation of cavefish to nutrient-poor conditions. *Proceedings of the National Academy of Sciences of the United States of America*, 112(31), pp.9668–73. Available at: http://www.ncbi.nlm.nih.gov/pubmed/26170297 [Accessed April 7, 2018].

Avise, J.C. & Selander, R.K., 1972. EVOLUTIONARY GENETICS OF CAVE-DWELLING FISHES OF THE GENUS ASTYANAX. *Evolution; international journal of organic evolution*, 26(1), pp.1–19. Available at: http://doi.wiley.com/10.1111/j.1558-5646.1972.tb00170.x [Accessed March 31, 2018].

Barbieri, A.M. et al., 1999. A homeobox gene, vax2, controls the patterning of the eye dorsoventral axis. *Proceedings of the National Academy of Sciences*, 96(19), pp.10729–10734. Available at: http://www.pnas.org/content/96/19/10729.full [Accessed March 25, 2015].

Barbieri, A.M. et al., 2002. Vax2 inactivation in mouse determines alteration of the eye dorsal-ventral axis, misrouting of the optic fibres and eye coloboma. *Development*, 129(3).

Barsagade, V.G. et al., 2010. Reproductive phase-related variations in cocaine- and amphetamine-regulated transcript (CART) in the olfactory system, forebrain, and pituitary of the female catfish, Clarias batrachus (Linn.). *The Journal of comparative neurology*, 518(13), pp.2503–24. Available at: http://www.ncbi.nlm.nih.gov/pubmed/20503424 [Accessed June 6, 2014].

Beale, A. et al., 2013. Circadian rhythms in Mexican blind cavefish Astyanax mexicanus in the lab and in the field. *Nature Communications*, 4, p.2769. Available at: http://www.nature.com/doifinder/10.1038/ncomms3769 [Accessed April 7, 2018].

Beale, A.D. & Whitmore, D., 2016. Chapter 16 – Daily Rhythms in a Timeless Environment: Circadian Clocks in Astyanax mexicanus. In A. C. Keene, M. Yoshizawa, & S. E. McGaugh, eds. *Biology and Evolution of the Mexican Cavefish*. pp. 309–333.

Beccari, L., Marco-Ferreres, R. & Bovolenta, P., 2013. The logic of gene regulatory networks in early vertebrate forebrain patterning. *Mechanisms of Development*, 130(2–3), pp.95–111. Available at:

http://linkinghub.elsevier.com/retrieve/pii/S0925477312001104 [Accessed March 15, 2018].

Becker, C.G., Meyer, R.L. & Becker, T., 2000. Gradients of ephrin-A2 and ephrin-A5b mRNA during retinotopic regeneration of the optic projection in adult zebrafish. *The Journal of comparative neurology*, 427(3), pp.469–83. Available at: http://www.ncbi.nlm.nih.gov/pubmed/11054707 [Accessed March 11, 2018].

Bedont, J.L., Newman, E.A. & Blackshaw, S., 2015. Patterning, specification, and differentiation in the developing hypothalamus. *Wiley Interdisciplinary Reviews: Developmental Biology*, 4(5), pp.445–468. Available at: http://doi.wiley.com/10.1002/wdev.187 [Accessed March 16, 2018].

Bielen, H. & Houart, C., 2012. BMP Signaling Protects Telencephalic Fate by Repressing Eye Identity and Its Cxcr4-Dependent Morphogenesis. *Developmental Cell*, 23(4), pp.812–822. Available at: https://www.sciencedirect.com/science/article/pii/S1534580712004170 [Accessed April 13, 2018].

Blažek, R., Polačik, M. & Reichard, M., 2013. Rapid growth, early maturation and short generation time in African annual fishes. *EvoDevo*, 4(1), p.24. Available at: http://evodevojournal.biomedcentral.com/articles/10.1186/2041-9139-4-24 [Accessed June 12, 2018].

Bleckmann, H. & Zelick, R., 2009. Lateral line system of fish. *Integrative Zoology*, 4(1), pp.13–25. Available at: http://www.ncbi.nlm.nih.gov/pubmed/21392273 [Accessed April 5, 2018].

Blin, M. et al., 2018. *Developmental evolution and developmental plasticity of the olfactory epithelium and olfactory skills in Mexican cavefish*, Available at: http://www.ncbi.nlm.nih.gov/pubmed/29709597 [Accessed May 11, 2018].

Bradic, M. et al., 2012. Gene flow and population structure in the Mexican blind cavefish complex (Astyanax mexicanus). *BMC evolutionary biology*, 12(1), p.9. Available at: http://www.biomedcentral.com/1471-2148/12/9 [Accessed May 23, 2014].

Brennan, C. et al., 1997. Two Eph receptor tyrosine kinase ligands control axon growth and may be involved in the creation of the retinotectal map in the zebrafish. *Development*, 124(3).

Bulfone, A. et al., 1993. Spatially restricted expression of Dlx-1, Dlx-2 (Tes-1), Gbx-2, and Wnt-3 in the embryonic day 12.5 mouse forebrain defines potential transverse and longitudinal segmental boundaries. *The Journal of neuroscience : the official journal of the Society for Neuroscience*, 13(7), pp.3155–72. Available at: http://www.ncbi.nlm.nih.gov/pubmed/7687285 [Accessed April 12, 2018].

Cai, Z. et al., 2013. Deficient FGF signaling causes optic nerve dysgenesis and ocular coloboma. *Development (Cambridge, England)*, 140(13), pp.2711–23. Available at: http://www.ncbi.nlm.nih.gov/pubmed/11830579 [Accessed March 28, 2018].

Cavodeassi, F., 2018. Dynamic Tissue Rearrangements during Vertebrate Eye Morphogenesis: Insights from Fish Models. *Journal of Developmental Biology*, 6(1), p.4. Available at: http://www.mdpi.com/2221-3759/6/1/4 [Accessed April 11, 2018].

Cavodeassi, F. et al., 2005. Early Stages of Zebrafish Eye Formation Require the Coordinated Activity of Wnt11, Fz5, and the Wnt/β-Catenin Pathway. *Neuron*, 47(1), pp.43–56. Available at: https://www-sciencedirect-com.insb.bib.cnrs.fr/science/article/pii/S0896627305004733 [Accessed March 19, 2018].

Cechmanek, P.B. & McFarlane, S., 2017. Retinal pigment epithelium expansion around the neural retina occurs in two separate phases with distinct mechanisms. *Developmental Dynamics*, 246(8), pp.598–609. Available at: http://doi.wiley.com/10.1002/dvdy.24525 [Accessed February 13, 2018].

Cerdá-Reverter, J.M. et al., 2011. Fish melanocortin system. *European journal of pharmacology*, 660(1), pp.53–60. Available at: http://www.sciencedirect.com/science/article/pii/S0014299910012720 [Accessed March 13, 2014].

Chakraborty, R. & Nei, M., 1974. Dynamics of gene differentiation between incompletely isolated populations of unequal sizes. *Theoretical population biology*, 5(3), pp.460–9. Available at: http://www.ncbi.nlm.nih.gov/pubmed/4460259 [Accessed April 15, 2018].

Chan, J. et al., 2001. Morphogenesis of Prechordal Plate and Notochord Requires Intact Eph/Ephrin B signaling.

, 234(2). Available at: http://www.ncbi.nlm.nih.gov/pubmed/11397014 [Accessed March 14, 2018].

Chuang, J.C. & Raymond, P.A., 2002. Embryonic origin of the eyes in teleost fish. *BioEssays*, 24(6), pp.519–529. Available at: http://doi.wiley.com/10.1002/bies.10097 [Accessed March 16, 2018].

Clarke, J., 2009. Role of polarized cell divisions in zebrafish neural tube formation. *Current Opinion in Neurobiology*, 19(2), pp.134–138. Available at: https://www-sciencedirect-com.insb.bib.cnrs.fr/science/article/pii/S0959438809000403?via%3Dihub [Accessed February 8, 2018].

Cote, R., 2006. Photoreceptor Phosphodiesterase (PDE6). In *Cyclic Nucleotide Phosphodiesterases in Health and Disease*. CRC Press. Available at: http://www.crcnetbase.com/doi/10.1201/9781420020847.ch8 [Accessed April 10, 2018].

Dahm, R. et al., 2007. Development and adult morphology of the eye lens in the zebrafish. *Experimental Eye Research*, 85(1), pp.74–89. Available at: http://www.ncbi.nlm.nih.gov/pubmed/17467692 [Accessed February 20, 2018].

Danesin, C. et al., 2009. Integration of Telencephalic Wnt and Hedgehog Signaling Center Activities by Foxg1. *Developmental Cell*, 16(4), pp.576–587. Available at: https://www-sciencedirect-com.insb.bib.cnrs.fr/science/article/pii/S1534580709000975?_rdoc=1&_fmt=high&_origin=gateway&_docanchor=&md5=b8429449ccfc9c30159a5f9aeaa92ffb#bib17 [Accessed March 20, 2018].

Danesin, C. & Houart, C., 2012. A Fox stops the Wnt: implications for forebrain development and diseases. *Current Opinion in Genetics & Development*, 22(4), pp.323–330. Available at: https://www-sciencedirect-com.insb.bib.cnrs.fr/science/article/pii/S0959437X12000639?via%3Dihub#bib0070 [Accessed March 19, 2018].

DeAngelis, R. et al., 2017. Opposite effects of nonapeptide antagonists on paternal behavior in the teleost fish Amphiprion ocellaris. *Hormones and Behavior*, 90, pp.113–119. Available at: https://www-sciencedirect-com.insb.bib.cnrs.fr/science/article/pii/S0018506X16303348 [Accessed March 1, 2018].

Duboué, E.R. & Keene, A.C., 2016. Chapter 15 – Investigating the Evolution of Sleep in the Mexican Cavefish. In A. C. Keene, M. Yoshizawa, & S. E. McGaugh, eds. *Biology and Evolution of the Mexican Cavefish*. pp. 291–308.

Duboué, E.R.R., Keene, A.C.C. & Borowsky, R.L.L., 2011. Evolutionary convergence on sleep loss in cavefish populations. *Current biology : CB*, 21(8), pp.671–6. Available at: https://www-sciencedirect-com.insb.bib.cnrs.fr/science/article/pii/S0960982211002922?_rdoc=1&_fmt=high&_origin=gateway&_docanchor=&md5=b8429449ccfc9c30159a5f9aeaa92ffb&ccp=y [Accessed June 3, 2014].

Easter, Jr., S.S. & Nicola, G.N., 1996. The Development of Vision in the Zebrafish (Danio rerio). *Developmental Biology*, 180(2), pp.646–663. Available at: http://linkinghub.elsevier.com/retrieve/pii/S0012160696903358 [Accessed February 20, 2018].

Eaton, J.L., Holmqvist, B. & Glasgow, E., 2008. Ontogeny of vasotocin-expressing cells in zebrafish: selective requirement for the transcriptional regulators orthopedia and single-minded 1 in the preoptic area. *Developmental dynamics : an official publication of the American Association of Anatomists*, 237(4), pp.995–1005. Available at: http://www.ncbi.nlm.nih.gov/pubmed/18330923 [Accessed March 25, 2014].

Elbaz, I. et al., 2012. Genetic ablation of hypocretin neurons alters behavioral state transitions in zebrafish. *The Journal of neuroscience : the official journal of the Society for Neuroscience*, 32(37), pp.12961–72. Available at: http://www.ncbi.nlm.nih.gov/pubmed/22973020 [Accessed April 17, 2018].

Elipot, Y. et al., 2014. A mutation in the enzyme monoamine oxidase explains part of the Astyanax cavefish behavioural syndrome. *Nature communications*, 5, p.3647. Available at: http://www.nature.com.gate1.inist.fr/ncomms/2014/140410/ncomms4647/full/ncomms4647.html [Accessed June 3, 2014].

Elipot, Y. et al., 2013. Evolutionary shift from fighting to foraging in blind cavefish through changes in the serotonin network. *Current biology : CB*, 23(1), pp.1–10. Available at: http://www.ncbi.nlm.nih.gov/pubmed/23159600 [Accessed June 3, 2014].

Elliott, W.R., 2016. Chapter 3 – Cave Biodiversity and Ecology of the Sierra de El Abra Region. In A. C. Keene, M. Yoshizawa, & S. E. McGaugh, eds. *Biology and Evolution of the Mexican Cavefish*. pp. 59–76.

England, S.J. et al., 2006. A dynamic fate map of the forebrain shows how vertebrate eyes form and explains two causes of cyclopia. *Development (Cambridge, England)*, 133(23), pp.4613–7. Available at: http://www.ncbi.nlm.nih.gov/pubmed/17079266 [Accessed January 16, 2018].

Espinasa, L. et al., 2017. Contrasting feeding habits of post-larval and adult Astyanax cavefish. *Subterranean Biology*, 21, pp.1–17. Available at: http://subtbiol.pensoft.net/articles.php?id=11046 [Accessed April 2, 2018].

Espinasa, L., Yamamoto, Y. & Jeffery, W.R., 2005. Non-optical releasers for aggressive behavior in blind and blinded Astyanax (Teleostei, Characidae). *Behavioural Processes*, 70(2), pp.144–148. Available at: https://www-sciencedirect-com.insb.bib.cnrs.fr/science/article/pii/S0376635705001531?via%3Dihub#bib9 [Accessed April 6, 2018].

Fischer, A.J., Bosse, J.L. & El-Hodiri, H.M., 2013. The ciliary marginal zone (CMZ) in development and regeneration of the vertebrate eye. *Experimental Eye Research*, 116, pp.199–204. Available at: https://www-sciencedirect-com.insb.bib.cnrs.fr/science/article/pii/S0014483513002571?via%3Dihub [Accessed February 20, 2018].

French, C.R. et al., 2009. Gdf6a is required for the initiation of dorsal–ventral retinal patterning and lens development. *Developmental Biology*, 333(1), pp.37–47. Available at: http://linkinghub.elsevier.com/retrieve/pii/S0012160609009853 [Accessed July 19, 2017].

Fulwiler, C. et al., 1997. Retinal patterning in the zebrafish mutant cyclops. *The Journal of comparative neurology*, 381(4), pp.449–60. Available at: http://www.ncbi.nlm.nih.gov/pubmed/9136802 [Accessed March 28, 2018].

Fumey, J. et al., 2018. Evidence for late Pleistocene origin of Astyanax mexicanus cavefish. *BMC Evolutionary Biology*, 18(1). Available at: https://bmcevolbiol.biomedcentral.com/articles/10.1186/s12862-018-1156-7 [Accessed March 31, 2018].

Furness, A.I., Lee, K. & Reznick, D.N., 2015. Adaptation in a variable environment: Phenotypic plasticity and bet-hedging during egg diapause and hatching in an annual killifish. *Evolution; international journal of organic evolution*, 69(6), pp.1461–1475. Available at: http://doi.wiley.com/10.1111/evo.12669 [Accessed June 12, 2018].

García-Calero, E. et al., 2008. Early mammillary pouch specification in the course of prechordal ventralization of the forebrain tegmentum. *Developmental Biology*, 320(2), pp.366–377. Available at: https://www-sciencedirect-com.insb.bib.cnrs.fr/science/article/pii/S001216060800910X?via%3Dihub [Accessed April 13, 2018].

Genade, T. et al., 2005. Annual fishes of the genus Nothobranchius as a model system for aging research. *Aging Cell*, 4(5), pp.223–233. Available at: http://doi.wiley.com/10.1111/j.1474-9726.2005.00165.x [Accessed June 12, 2018].

Gesto, M. et al., 2014. Arginine vasotocin treatment induces a stress response and exerts a potent anorexigenic effect in rainbow trout, Oncorhynchus mykiss. *Journal of neuroendocrinology*, 26(2), pp.89–99. Available at: http://www.ncbi.nlm.nih.gov/pubmed/24341528 [Accessed April 10, 2014].

Gestri, G. et al., 2018. Cell Behaviors during Closure of the Choroid Fissure in the Developing Eye. *Frontiers in Cellular Neuroscience*, 12, p.42. Available at: http://journal.frontiersin.org/article/10.3389/fncel.2018.00042/full [Accessed March 28, 2018].

Gestri, G., Link, B.A. & Neuhauss, S.C.F., 2012. The visual system of zebrafish and its use to model human ocular diseases. *Developmental neurobiology*, 72(3), pp.302–27. Available at: http://www.ncbi.nlm.nih.gov/pubmed/21595048 [Accessed February 20, 2018].

Gosse, N.J. & Baier, H., 2009. An essential role for Radar (Gdf6a) in inducing dorsal fate in the zebrafish retina. *Proceedings of the National Academy of Sciences of the United States of America*, 106(7), pp.2236–41. Available at: http://www.ncbi.nlm.nih.gov/pubmed/19164594 [Accessed June 13, 2017].

Gramage, E., Li, J. & Hitchcock, P., 2014. The expression and function of midkine in the vertebrate retina. *British Journal of Pharmacology*, 171(4), pp.913–923. Available at: http://doi.wiley.com/10.1111/bph.12495 [Accessed February 21, 2018].

Gregory-Evans, C.Y. et al., 2004. Ocular coloboma: a reassessment in the age of molecular neuroscience. *Journal of Medical Genetics*, 41(12), pp.881–891. Available at: http://www.ncbi.nlm.nih.gov/pubmed/15591273 [Accessed March 28, 2018].

Greiling, T.M.S. & Clark, J.I., 2009. Early lens development in the zebrafish: A three-dimensional time-lapse analysis. *Developmental Dynamics*, 238(9), pp.2254–2265. Available at: http://doi.wiley.com/10.1002/dvdy.21997 [Accessed March 29, 2018].

Gunter, H. & Meyer, A., 2013. Trade-offs in cavefish sensory capacity. *BMC Biology*, 11(1), p.5. Available at: http://bmcbiol.biomedcentral.com/articles/10.1186/1741-7007-11-5 [Accessed June 12, 2018].

Hallonet, M. et al., 1999. Vax1, a novel homeobox-containing gene, directs development of the basal forebrain and visual system. *Genes & development*, 13(23), pp.3106–14. Available at: http://www.ncbi.nlm.nih.gov/pubmed/10601036 [Accessed March 28, 2018].

Hartsock, A. et al., 2014. In vivo analysis of hyaloid vasculature morphogenesis in zebrafish: A role for the lens in maturation and maintenance of the hyaloid. *Developmental Biology*, 394(2), pp.327–339. Available at: https://www.sciencedirect.com/science/article/pii/S0012160614003765 [Accessed January 3, 2018].

Hashiura, T. et al., 2017. Live imaging of primary ocular vasculature formation in zebrafish. *PloS one*, 12(4), p.e0176456. Available at: http://www.ncbi.nlm.nih.gov/pubmed/28445524 [Accessed February 27, 2018].

Hasunuma, I. et al., 2013. Roles of arginine vasotocin receptors in the brain and pituitary of submammalian vertebrates. *International review of cell and molecular biology*, 304, pp.191–225. Available at: http://www.ncbi.nlm.nih.gov/pubmed/23809437 [Accessed March 24, 2014].

Heermann, S. et al., 2015. Eye morphogenesis driven by epithelial flow into the optic cup facilitated by modulation of bone morphogenetic protein. *eLife*, 4, p.e05216. Available at: https://elifesciences.org/articles/05216 [Accessed January 15, 2018].

Heisenberg, C.-P. & Nüsslein-Volhard, C., 1997. The Function ofsilberblickin the Positioning of the Eye Anlage in the Zebrafish Embryo. *Developmental Biology*, 184(1), pp.85–94. Available at: https://www-sciencedirect-com.insb.bib.cnrs.fr/science/article/pii/S0012160697985110?via%3Dihub [Accessed March 28, 2018].

Herget, U. et al., 2014. Molecular neuroanatomy and chemoarchitecture of the neurosecretory preoptic-hypothalamic area in zebrafish larvae. *Journal of Comparative Neurology*, 522(7), pp.1542–1564. Available at: http://doi.wiley.com/10.1002/cne.23480 [Accessed March 1, 2018].

Herget, U. & Ryu, S., 2015. Coexpression analysis of nine neuropeptides in the neurosecretory preoptic area of larval zebrafish. *Frontiers in neuroanatomy*, 9, p.2. Available at: http://www.pubmedcentral.nih.gov/articlerender.fcgi?artid=4325906&tool=pmcentrez&rendertype=abstract [Accessed April 5, 2016].

Hernández-Bejarano, M. et al., 2015. Opposing Shh and Fgf signals initiate nasotemporal patterning of the zebrafish retina. *Development*, 142(22), pp.3933–3942. Available at: http://dev.biologists.org/lookup/doi/10.1242/dev.125120 [Accessed January 2, 2017].

Herrera, E. et al., 2004. Foxd1 is required for proper formation of the optic chiasm. *Development (Cambridge, England)*, 131(22), pp.5727–39. Available at: http://www.ncbi.nlm.nih.gov/pubmed/15509772 [Accessed March 20, 2018].

Hinaux, H. et al., 2017. Lens apoptosis in the Astyanax blind cavefish is not triggered by its small size or defects in morphogenesis H. Escriva, ed. *PLOS ONE*, 12(2), p.e0172302. Available at: http://dx.plos.org/10.1371/journal.pone.0172302 [Accessed April 5, 2018].

Hinaux, H. et al., 2015. Lens defects in Astyanax mexicanus Cavefish: evolution of crystallins and a role for alphaA-crystallin. *Developmental neurobiology*, 75(5), pp.505–21. Available at:

http://doi.wiley.com/10.1002/dneu.22239 [Accessed April 15, 2018].

Hinaux, H. et al., 2016. Sensory evolution in blind cavefish is driven by early embryonic events during gastrulation and neurulation. *Development (Cambridge, England)*, 143(23), pp.4521–4532. Available at: http://www.ncbi.nlm.nih.gov/pubmed/27899509 [Accessed April 5, 2018].

Holly, V.L. et al., 2014. Sfrp1a and Sfrp5 function as positive regulators of Wnt and BMP signaling during early retinal development. *Developmental Biology*, 388(2), pp.192–204. Available at: https://www-sciencedirect-com.insb.bib.cnrs.fr/science/article/pii/S0012160614000402?via%3Dihub [Accessed March 12, 2018].

Horstick, E.J. et al., 2017. Search strategy is regulated by somatostatin signaling and deep brain photoreceptors in zebrafish. *BMC Biology*, 15(1), p.4. Available at: http://bmcbiol.biomedcentral.com/articles/10.1186/s12915-016-0346-2 [Accessed March 1, 2018].

Houart, C. et al., 2002. Establishment of the Telencephalon during Gastrulation by Local Antagonism of Wnt Signaling. *Neuron*, 35(2), pp.255–265. Available at: https://www-sciencedirect-com.insb.bib.cnrs.fr/science/article/pii/S0896627302007511 [Accessed March 19, 2018].

Houart, C., Westerfield, M. & Wilson, S.W., 1998. A small population of anterior cells patterns the forebrain during zebrafish gastrulation. *Nature*, 391(6669), pp.788–92. Available at: http://www.nature.com/articles/35853 [Accessed March 19, 2018].

Hüppop, K., 1987. Food-finding ability in cave fish (Astyanax fasciatus). *International Journal of Speleology*, 16(1/2), pp.59–66. Available at: http://scholarcommons.usf.edu/ijs/vol16/iss1/4 [Accessed June 12, 2014].

Hüppop, K., 2001. How do cave animals cope with the food scarcity in caves ? In H. Wilkens, D. C. Culver, & W. F. Humphreys, eds. *Subterranean ecosystems*. Elsevier, p. 791. Available at: https://books.google.fr/books/about/Subterranean_ecosystems.html?id=4W8VAQAAIAAJ&redir_esc=y [Accessed April 6, 2018].

Ivanovitch, K., Cavodeassi, F. & Wilson, S.W., 2013. Precocious acquisition of neuroepithelial character in the eye field underlies the onset of eye morphogenesis. *Developmental cell*, 27(3), pp.293–305. Available at: http://www.ncbi.nlm.nih.gov/pubmed/24209576 [Accessed November 28, 2017].

Jaggard, J. et al., 2017. The lateral line confers evolutionarily derived sleep loss in the Mexican cavefish. *The Journal of experimental biology*, 220(Pt 2), pp.284–293. Available at: http://www.ncbi.nlm.nih.gov/pubmed/28100806 [Accessed April 7, 2018].

Jaggard, J.B. et al., 2018. Hypocretin underlies the evolution of sleep loss in the Mexican cavefish. *eLife*, 7, p.e32637. Available at: https://elifesciences.org/articles/32637 [Accessed February 7, 2018].

James, A. et al., 2016. The hyaloid vasculature facilitates basement membrane breakdown during choroid fissure closure in the zebrafish eye. *Developmental Biology*, 419(2), pp.262–272. Available at: https://www-sciencedirect-com.insb.bib.cnrs.fr/science/article/pii/S001216061630183X?via%3Dihub [Accessed February 19, 2018].

Jeffery, W. & Martasian, D., 1998. Evolution of Eye Regression in the Cavefish Astyanax : Apoptosis and the Pax-6 Gene. *American Zoologist*, 38(4), pp.685–696. Available at: https://academic.oup.com/icb/article-lookup/doi/10.1093/icb/38.4.685 [Accessed April 3, 2018].

Jeffery, W.R., 2009. Regressive Evolution in *Astyanax* Cavefish. *Annual Review of Genetics*, 43(1), pp.25–47. Available at: http://www.ncbi.nlm.nih.gov/pubmed/19640230 [Accessed April 15, 2018].

Jeffery, W.R., Strickler, A.G. & Yamamoto, Y., 2003. To See or Not to See: Evolution of Eye Degeneration in Mexican Blind Cavefish. *Integrative and Comparative Biology*, 43(4), pp.531–541. Available at: http://icb.oxfordjournals.org/cgi/doi/10.1093/icb/43.4.531 [Accessed June 28, 2016].

Kagawa, N., 2013. Social rank-dependent expression of arginine vasotocin in distinct preoptic regions in male Oryzias latipes. *Journal of fish biology*, 82(1), pp.354–63. Available at: http://www.ncbi.nlm.nih.gov/pubmed/23331157 [Accessed March 25, 2014].

Kapsimali, M. et al., 2004. Inhibition of Wnt/Axin/ -catenin pathway activity promotes ventral CNS midline tissue to adopt hypothalamic rather than floorplate identity. *Development*, 131(23), pp.5923–5933. Available at: http://www.ncbi.nlm.nih.gov/pubmed/15539488 [Accessed March 14, 2018].

Kaufman, R. et al., 2015. Development and origins of zebrafish ocular vasculature. *BMC developmental biology*, 15, p.18. Available at: http://www.ncbi.nlm.nih.gov/pubmed/25888280 [Accessed February 27, 2018].

Kita, E.M., Scott, E.K. & Goodhill, G.J., 2015. Topographic wiring of the retinotectal connection in zebrafish. *Developmental Neurobiology*, 75(6), pp.542–556. Available at: http://doi.wiley.com/10.1002/dneu.22256 [Accessed April 11, 2018].

Koshiba-Takeuchi, K. et al., 2000. Tbx5 and the retinotectum projection. *Science (New York, N.Y.)*, 287(5450), pp.134–7. Available at: http://www.ncbi.nlm.nih.gov/pubmed/10615048 [Accessed December 12, 2017].

Kottelat, M., 2012. Draconectes narinosus, a new genus and species of cave fish from an island of Halong Bay, Vietnam (Teleostei: Nemacheilidae). *Revue suisse de zoologie.*, 119, pp.341–349. Available at: http://www.biodiversitylibrary.org/part/150197 [Accessed April 1, 2018].

Kowalko, J.E., Rohner, N., Linden, T.A., et al., 2013. Convergence in feeding posture occurs through different genetic loci in independently evolved cave populations of Astyanax mexicanus. *Proceedings of the National Academy of Sciences of the United States of America*, 110(42), pp.16933–8. Available at: http://www.pnas.org.gate1.inist.fr/content/110/42/16933.long [Accessed May 27, 2014].

Kowalko, J.E., Rohner, N., Rompani, S.B., et al., 2013. Loss of schooling behavior in cavefish through sight-dependent and sight-independent mechanisms. *Current biology : CB*, 23(19), pp.1874–83. Available at: http://www.ncbi.nlm.nih.gov/pubmed/24035545 [Accessed April 6, 2018].

Kruse-Bend, R. et al., 2012. Extraocular ectoderm triggers dorsal retinal fate during optic vesicle evagination in zebrafish. *Developmental Biology*, 371(1), pp.57–65. Available at: http://www.ncbi.nlm.nih.gov/pubmed/22921921 [Accessed March 22, 2018].

Kwan, K.M. et al., 2012. A complex choreography of cell movements shapes the vertebrate eye. *Development (Cambridge, England)*, 139(2), pp.359–72. Available at: http://www.ncbi.nlm.nih.gov/pubmed/22186726 [Accessed January 4, 2018].

Langecker, T.G., Schmale, H. & Wilkens, H., 1993. Transcription of the opsin gene in degenerate eyes of cave-dwelling Astyanax fasciatus (Teleostei, Characidae) and of its conspecific epigean ancestor during early ontogeny. *Cell and Tissue Research*, 273(1), pp.183–192. Available at: http://link.springer.com/10.1007/BF00304625 [Accessed April 4, 2018].

Lee, J. et al., 2008. Zebrafish blowout provides genetic evidence for Patched1-mediated negative regulation of Hedgehog signaling within the proximal optic vesicle of the vertebrate eye. *Developmental biology*, 319(1), pp.10–22. Available at: http://www.ncbi.nlm.nih.gov/pubmed/18479681 [Accessed May 23, 2016].

Lin, X. et al., 2000. Brain regulation of feeding behavior and food intake in fish. *Comparative Biochemistry and Physiology Part A: Molecular & Integrative Physiology*, 126(4), pp.415–434. Available at: http://www.sciencedirect.com/science/article/pii/S1095643300002300 [Accessed May 21, 2014].

Lowry, C.A. & Moore, F.L., 2006. Regulation of behavioral responses by corticotropin-releasing factor. *General and comparative endocrinology*, 146(1), pp.19–27. Available at: http://apps.webofknowledge.com.gate1.inist.fr/full_record.do?product=WOS&search_mode=GeneralSearch&qid=1&SID=T2MJBmYytCbOOkVxRFI&page=1&doc=10&cacheurlFromRightClick=no [Accessed October 6, 2014].

Lupo, G. et al., 2005. Dorsoventral patterning of the Xenopus eye: a collaboration of Retinoid, Hedgehog and FGF receptor signaling. *Development (Cambridge, England)*, 132(7), pp.1737–48. Available at: http://dev.biologists.org.gate1.inist.fr/content/132/7/1737.long [Accessed February 1, 2016].

Lupo, G. et al., 2011. Retinoic acid receptor signaling regulates choroid fissure closure through independent mechanisms in the ventral optic cup and periocular mesenchyme. *Proceedings of the National Academy of Sciences*, 108(21), pp.8698–8703. Available at:

http://www.pnas.org/cgi/doi/10.1073/pnas.1103802108 [Accessed July 6, 2016].

Macdonald, R. et al., 1995. Midline signalling is required for Pax gene regulation and patterning of the eyes. *Development (Cambridge, England)*, 121(10), pp.3267–78. Available at: http://www.ncbi.nlm.nih.gov/pubmed/7588061 [Accessed March 26, 2018].

Macdonald, R. et al., 1997. The Pax protein Noi is required for commissural axon pathway formation in the rostral forebrain. *Development*, 124(12).

Machluf, Y., Gutnick, A. & Levkowitz, G., 2011. Development of the zebrafish hypothalamus. *Annals of the New York Academy of Sciences*, 1220(1), pp.93–105. Available at: http://doi.wiley.com/10.1111/j.1749-6632.2010.05945.x [Accessed February 28, 2018].

Maeda, R. et al., 2015. Ontogeny of the Saccus Vasculosus, a Seasonal Sensor in Fish. *Endocrinology*, 156(11), pp.4238–4243. Available at: https://academic.oup.com/endo/article-lookup/doi/10.1210/en.2015-1415 [Accessed April 12, 2018].

Mancebo, M.J. et al., 2013. Hypothalamic neuropeptide Y (NPY) gene expression is not affected by central serotonin in the rainbow trout (Oncorhynchus mykiss). *Comparative biochemistry and physiology. Part A, Molecular & integrative physiology*, 166(1), pp.186–90. Available at: http://www.sciencedirect.com/science/article/pii/S1095643313001591 [Accessed October 3, 2014].

Martinez-Morales, J.-R. et al., 2005. Differentiation of the vertebrate retina is coordinated by an FGF signaling center. *Developmental cell*, 8(4), pp.565–74. Available at: http://www.sciencedirect.com/science/article/pii/S1534580705000808 [Accessed March 3, 2015].

Martinez-Morales, J.-R., Cavodeassi, F. & Bovolenta, P., 2017. Coordinated Morphogenetic Mechanisms Shape the Vertebrate Eye. *Frontiers in Neuroscience*, 11, p.721. Available at: http://journal.frontiersin.org/article/10.3389/fnins.2017.00721/full [Accessed January 15, 2018].

Martinez-Morales, J.R. & Wittbrodt, J., 2009. Shaping the vertebrate eye. *Current Opinion in Genetics & Development*, 19(5), pp.511–517. Available at: https://www-sciencedirect-com.insb.bib.cnrs.fr/science/article/pii/S0959437X09001373 [Accessed March 22, 2018].

Martos-Sitcha, J.A. et al., 2013. Vasotocinergic and isotocinergic systems in the gilthead sea bream (Sparus aurata): an osmoregulatory story. *Comparative biochemistry and physiology. Part A, Molecular & integrative physiology*, 166(4), pp.571–81. Available at: http://www.ncbi.nlm.nih.gov/pubmed/24021911 [Accessed June 6, 2014].

Masai, I. et al., 2000. Midline Signals Regulate Retinal Neurogenesis in Zebrafish. *Neuron*, 27(2), pp.251–263. Available at: https://www.sciencedirect.com/science/article/pii/S0896627300000349#FIG1 [Accessed March 19, 2018].

Masai, I. et al., 2003. N-cadherin mediates retinal lamination, maintenance of forebrain compartments and patterning of retinal neurites. *Development (Cambridge, England)*, 130(11), pp.2479–94. Available at: http://www.ncbi.nlm.nih.gov/pubmed/12702661 [Accessed February 19, 2018].

Mathieu, J. et al., 2002. Distinct and cooperative roles for Nodal and Hedgehog signals during hypothalamic development. *Development (Cambridge, England)*, 129(13), pp.3055–65. Available at: http://www.ncbi.nlm.nih.gov/pubmed/12070082 [Accessed March 15, 2018].

Matsuda, K. et al., 2012. Neuroendocrine control of feeding behavior and psychomotor activity by neuropeptideY in fish. *Neuropeptides*, 46(6), pp.275–83. Available at: http://www.sciencedirect.com/science/article/pii/S0143417912001023 [Accessed November 17, 2014].

Mennigen, J.A. et al., 2017. The nonapeptide isotocin in goldfish: Evidence for serotonergic regulation and functional roles in the control of food intake and pituitary hormone release. *General and Comparative Endocrinology*, 254, pp.38–49. Available at: http://www.ncbi.nlm.nih.gov/pubmed/28927876 [Accessed March 1, 2018].

Mennigen, J.A. et al., 2010. Waterborne fluoxetine disrupts feeding and energy metabolism in the goldfish Carassius auratus. *Aquatic toxicology (Amsterdam, Netherlands)*, 100(1), pp.128–37. Available at:

http://www.ncbi.nlm.nih.gov/pubmed/20692053 [Accessed October 3, 2014].

Menuet, A. et al., 2007. Expanded expression of Sonic Hedgehog in Astyanax cavefish: multiple consequences on forebrain development and evolution. *Development (Cambridge, England)*, 134(5), pp.845–55. Available at: http://dev.biologists.org.gate1.inist.fr/content/134/5/845.long [Accessed June 2, 2014].

Miyake, A. et al., 2005. Fgf19 regulated by Hh signaling is required for zebrafish forebrain development. *Developmental Biology*, 288(1), pp.259–275. Available at: https://www-sciencedirect-com.insb.bib.cnrs.fr/science/article/pii/S0012160605006780?via%3Dihub#bib4 [Accessed March 20, 2018].

Moran, D., Softley, R. & Warrant, E.J., 2015. The energetic cost of vision and the evolution of eyeless Mexican cavefish. *Science Advances*, 1(8), pp.e1500363–e1500363. Available at: http://advances.sciencemag.org/cgi/doi/10.1126/sciadv.1500363 [Accessed April 4, 2018].

Nakamachi, T. et al., 2006. Regulation by orexin of feeding behaviour and locomotor activity in the goldfish. *Journal of neuroendocrinology*, 18(4), pp.290–7. Available at: http://www.ncbi.nlm.nih.gov/pubmed/16503924 [Accessed June 6, 2014].

Nakane, Y. et al., 2013. The saccus vasculosus of fish is a sensor of seasonal changes in day length. *Nature Communications*, 4, p.2108. Available at: http://www.nature.com/doifinder/10.1038/ncomms3108 [Accessed April 12, 2018].

Nicolás-Pérez, M. et al., 2016. Analysis of cellular behavior and cytoskeletal dynamics reveal a constriction mechanism driving optic cup morphogenesis. *eLife*, 5, pp.61–79. Available at: http://www.ncbi.nlm.nih.gov/pubmed/27797321 [Accessed March 27, 2017].

Owens, G.L. et al., 2012. In the four-eyed fish (Anableps anableps), the regions of the retina exposed to aquatic and aerial light do not express the same set of opsin genes. *Biology letters*, 8(1), pp.86–9. Available at: http://www.ncbi.nlm.nih.gov/pubmed/21775314 [Accessed May 13, 2018].

De Pedro, N. et al., 1998. Inhibitory effect of serotonin on feeding behavior in goldfish: involvement of CRF. *Peptides*, 19(3), pp.505–11. Available at: http://www.ncbi.nlm.nih.gov/pubmed/9533638 [Accessed June 12, 2014].

Perez, L.N. et al., 2017. Eye development in the four-eyed fish Anableps anableps: cranial and retinal adaptations to simultaneous aerial and aquatic vision. *Proceedings. Biological sciences*, 284(1852), p.20170157. Available at: http://www.ncbi.nlm.nih.gov/pubmed/28381624 [Accessed May 13, 2018].

Pérez Maceira, J.J., Mancebo, M.J. & Aldegunde, M., 2014. The involvement of 5-HT-like receptors in the regulation of food intake in rainbow trout (Oncorhynchus mykiss). *Comparative biochemistry and physiology. Toxicology & pharmacology : CBP*, 161, pp.1–6. Available at: http://www.ncbi.nlm.nih.gov/pubmed/24365333 [Accessed October 2, 2014].

Perron, M. & Harris, W.A., 2000. Retinal stem cells in vertebrates. *BioEssays*, 22(8), pp.685–688. Available at: http://www.ncbi.nlm.nih.gov/pubmed/10918298 [Accessed February 27, 2018].

Picker, A. et al., 2009. Dynamic Coupling of Pattern Formation and Morphogenesis in the Developing Vertebrate Retina W. A. Harris, ed. *PLoS Biology*, 7(10), p.e1000214. Available at: http://dx.plos.org/10.1371/journal.pbio.1000214 [Accessed February 12, 2018].

Picker, A. & Brand, M., 2005. Fgf signals from a novel signaling center determine axial patterning of the prospective neural retina. *Development (Cambridge, England)*, 132(22), pp.4951–62. Available at: http://dev.biologists.org/cgi/doi/10.1242/dev.02071 [Accessed March 12, 2018].

Pillai-Kastoori, L. et al., 2014. Sox11 Is Required to Maintain Proper Levels of Hedgehog Signaling during Vertebrate Ocular Morphogenesis G. S. Barsh, ed. *PLoS Genetics*, 10(7), p.e1004491. Available at: http://dx.plos.org/10.1371/journal.pgen.1004491 [Accessed December 18, 2017].

Pogoda, H.-M. & Hammerschmidt, M., 2007. Molecular genetics of pituitary development in zebrafish. *Seminars in Cell & Developmental Biology*, 18(4), pp.543–558. Available at: https://www-sciencedirect-com.insb.bib.cnrs.fr/science/article/pii/S1084952107000547?via%3Dihub#fig3 [Accessed February 28,

2018].

Pottin, K., Hinaux, H. & Rétaux, S., 2011. Restoring eye size in Astyanax mexicanus blind cavefish embryos through modulation of the Shh and Fgf8 forebrain organising centres. *Development (Cambridge, England)*, 138(12), pp.2467–76. Available at: http://www.ncbi.nlm.nih.gov/pubmed/21610028 [Accessed June 11, 2014].

Poulain, F.E. et al., 2010. Analyzing Retinal Axon Guidance in Zebrafish. *Methods in Cell Biology*, 100, pp.2–26. Available at: https://www-sciencedirect-com.insb.bib.cnrs.fr/science/article/pii/B9780123848925000013?via%3Dihub#f0020 [Accessed March 11, 2018].

Prober, D.A. et al., 2006. Hypocretin/orexin overexpression induces an insomnia-like phenotype in zebrafish. *The Journal of neuroscience : the official journal of the Society for Neuroscience*, 26(51), pp.13400–10. Available at: http://www.ncbi.nlm.nih.gov/pubmed/17182791 [Accessed May 27, 2014].

Protas, M. et al., 2007. Regressive evolution in the Mexican cave tetra, Astyanax mexicanus. *Current biology : CB*, 17(5), pp.452–4. Available at: http://www.ncbi.nlm.nih.gov/pubmed/17306543 [Accessed April 6, 2018].

Protas, M.E. et al., 2006. Genetic analysis of cavefish reveals molecular convergence in the evolution of albinism. *Nature Genetics*, 38(1), pp.107–111. Available at: http://www.ncbi.nlm.nih.gov/pubmed/16341223 [Accessed November 15, 2016].

Puelles, L. & Rubenstein, J.L.R., 2015. A new scenario of hypothalamic organization: rationale of new hypotheses introduced in the updated prosomeric model. *Frontiers in Neuroanatomy*, 9, p.27. Available at: http://www.frontiersin.org/Neuroanatomy/10.3389/fnana.2015.00027/abstract [Accessed March 30, 2018].

Rembold, M. et al., 2006. Individual cell migration serves as the driving force for optic vesicle evagination. *Science (New York, N.Y.)*, 313(5790), pp.1130–4. Available at: http://www.ncbi.nlm.nih.gov/pubmed/16931763 [Accessed February 7, 2018].

Rétaux, S. & Casane, D., 2013. Evolution of eye development in the darkness of caves: adaptation, drift, or both? *EvoDevo*, 4(1), p.26. Available at: http://www.pubmedcentral.nih.gov/articlerender.fcgi?artid=3849642&tool=pmcentrez&rendertype=abstract [Accessed June 2, 2014].

Retaux, S. & Harris, W.A., 1996. Engrailed and retinotectal topography. *Trends in Neurosciences*, 19(12), pp.542–546. Available at: https://www-sciencedirect-com.insb.bib.cnrs.fr/science/article/pii/S016622369610062X?via%3Dihub [Accessed April 10, 2018].

Riddle, M.R. et al., 2018. Insulin resistance in cavefish as an adaptation to a nutrient-limited environment. *Nature*, 555(7698), pp.647–651. Available at: http://www.nature.com/doifinder/10.1038/nature26136 [Accessed April 4, 2018].

Rodríguez-Illamola, A. et al., 2011. Diurnal rhythms in hypothalamic/pituitary AVT synthesis and secretion in rainbow trout: evidence for a circadian regulation. *General and comparative endocrinology*, 170(3), pp.541–9. Available at: http://www.ncbi.nlm.nih.gov/pubmed/21095192 [Accessed March 25, 2014].

Rohner, N., 2016. Chapter 7 – Selection Through Standing Genetic Variation. In A. C. Keene, M. Yoshizawa, & S. E. McGaugh, eds. *Biology and Evolution of the Mexican Cavefish*. pp. 137–152.

Rohner, N. et al., 2013. Cryptic variation in morphological evolution: HSP90 as a capacitor for loss of eyes in cavefish. *Science (New York, N.Y.)*, 342(6164), pp.1372–5. Available at: http://www.ncbi.nlm.nih.gov/pubmed/24337296 [Accessed April 2, 2018].

Romero, A. et al., 2003. One eye but no vision: Cave fish with induced eyes do not respond to light. *Journal of Experimental Zoology*, 300B(1), pp.72–79. Available at: http://doi.wiley.com/10.1002/jez.b.47 [Accessed April 4, 2018].

Rutherford, S.L. & Lindquist, S., 1998. Hsp90 as a capacitor for morphological evolution. *Nature*, 396(6709),

pp.336–342. Available at: http://www.nature.com/articles/24550 [Accessed April 3, 2018].

Saint-Geniez, M. & D'Amore, P.A., 2004. Development and pathology of the hyaloid, choroidal and retinal vasculature. *The International journal of developmental biology*, 48(8–9), pp.1045–58. Available at: http://www.ncbi.nlm.nih.gov/pubmed/15558494 [Accessed February 27, 2018].

Sakurai, T., 2014. Roles of orexins in the regulation of body weight homeostasis. *Obesity research & clinical practice*, 8(5), pp.e414-20. Available at: http://www.sciencedirect.com/science/article/pii/S1871403X13002202 [Accessed November 20, 2014].

Sakuta, H. et al., 2006. Role of Bone Morphogenic Protein 2 in Retinal Patterning and Retinotectal Projection. *Journal of Neuroscience*, 26(42). Available at: http://www.jneurosci.org.insb.bib.cnrs.fr/content/26/42/10868.long [Accessed July 19, 2017].

Sanek, N.A. et al., 2009. Zebrafish zic2a patterns the forebrain through modulation of Hedgehog-activated gene expression. *Development (Cambridge, England)*, 136(22), pp.3791–800. Available at: http://www.ncbi.nlm.nih.gov/pubmed/11493538 [Accessed March 28, 2018].

Schemmel, C., 1980. Studies on the Genetics of Feeding Behaviour in the Cave Fish Astyanax mexicanus f. anoptichthys. *Zeitschrift für Tierpsychologie*, 53(1), pp.9–22. Available at: http://doi.wiley.com/10.1111/j.1439-0310.1980.tb00730.x [Accessed June 13, 2014].

Schulte, D. et al., 1999. Misexpression of the Emx-Related Homeobox Genes cVax and mVax2 Ventralizes the Retina and Perturbs the Retinotectal Map. *Neuron*, 24(3), pp.541–553. Available at: http://linkinghub.elsevier.com/retrieve/pii/S0896627300811113 [Accessed December 12, 2017].

Sedykh, I. et al., 2017. Zebrafish zic2 controls formation of periocular neural crest and choroid fissure morphogenesis. *Developmental Biology*, 429(1), pp.92–104. Available at: https://www-sciencedirect-com.insb.bib.cnrs.fr/science/article/pii/S0012160617301768?via%3Dihub [Accessed March 28, 2018].

Sefc, K.M. et al., 2012. Brood mixing and reduced polyandry in a maternally mouthbrooding cichlid with elevated among-breeder relatedness. *Molecular Ecology*, 21(11), pp.2805–2815. Available at: http://www.ncbi.nlm.nih.gov/pubmed/22493973 [Accessed June 12, 2018].

Sehgal, R. et al., 2008. Ectopic Pax2 expression in chick ventral optic cup phenocopies loss of Pax2 expression. *Developmental biology*, 319(1), pp.23–33. Available at: /pmc/articles/PMC2917900/?report=abstract [Accessed May 23, 2016].

Seth, A. et al., 2006. belladonna/(Ihx2) is required for neural patterning and midline axon guidance in the zebrafish forebrain. *Development (Cambridge, England)*, 133(4), pp.725–35. Available at: http://www.ncbi.nlm.nih.gov/pubmed/16436624 [Accessed March 27, 2018].

Shanmugalingam, S. et al., 2000. Ace/Fgf8 is required for forebrain commissure formation and patterning of the telencephalon. *Development (Cambridge, England)*, 127(12), pp.2549–61. Available at: http://www.ncbi.nlm.nih.gov/pubmed/10821754 [Accessed March 19, 2018].

Sheridan, M.A. & Hagemeister, A.L., 2010. Somatostatin and somatostatin receptors in fish growth. *General and Comparative Endocrinology*, 167(3), pp.360–365. Available at: https://www-sciencedirect-com.insb.bib.cnrs.fr/science/article/pii/S0016648009003359?via%3Dihub [Accessed March 1, 2018].

Sidhaye, J. & Norden, C., 2017. Concerted action of neuroepithelial basal shrinkage and active epithelial migration ensures efficient optic cup morphogenesis. *eLife*, 6, p.e22689. Available at: https://elifesciences.org/articles/22689 [Accessed February 12, 2018].

Simon, V. et al., 2017. Comparing growth in surface and cave morphs of the species Astyanax mexicanus: insights from scales. *EvoDevo*, 8(1), p.23. Available at: https://evodevojournal.biomedcentral.com/articles/10.1186/s13227-017-0086-6 [Accessed April 1, 2018].

Simpson, H.D. et al., 2013. A quantitative analysis of branching, growth cone turning, and directed growth in zebrafish retinotectal axon guidance. *Journal of Comparative Neurology*, 521(6), pp.1409–1429. Available at: http://doi.wiley.com/10.1002/cne.23248 [Accessed March 11, 2018].

Singh, C., Rihel, J. & Prober, D.A., 2017. Neuropeptide Y Regulates Sleep by Modulating Noradrenergic Signaling. *Current Biology*, 27(24), p.3796–3811.e5. Available at: http://www.ncbi.nlm.nih.gov/pubmed/29225025 [Accessed March 8, 2018].

Soules, K.A. & Link, B.A., 2005. Morphogenesis of the anterior segment in the zebrafish eye. *BMC Developmental Biology*, 5(1), p.12. Available at: http://bmcdevbiol.biomedcentral.com/articles/10.1186/1471-213X-5-12 [Accessed February 20, 2018].

Sperry, R.W., 1963. CHEMOAFFINITY IN THE ORDERLY GROWTH OF NERVE FIBER PATTERNS AND CONNECTIONS. *Proceedings of the National Academy of Sciences of the United States of America*, 50(4), pp.703–10. Available at: http://www.ncbi.nlm.nih.gov/pubmed/14077501 [Accessed April 10, 2018].

Stenkamp, D.L., 2015. Development of the Vertebrate Eye and Retina. *Progress in Molecular Biology and Translational Science*, 134, pp.397–414. Available at: https://www-sciencedirect-com.insb.bib.cnrs.fr/science/article/pii/S1877117315001088?via%3Dihub#bb0030 [Accessed February 27, 2018].

Stenkamp, D.L., 2007. Neurogenesis in the fish retina. *International review of cytology*, 259, pp.173–224. Available at: http://www.ncbi.nlm.nih.gov/pubmed/17425942 [Accessed February 20, 2018].

Storm, E.E. et al., 2006. Dose-dependent functions of Fgf8 in regulating telencephalic patterning centers. *Development (Cambridge, England)*, 133(9), pp.1831–44. Available at: http://www.ncbi.nlm.nih.gov/pubmed/12397106 [Accessed March 21, 2018].

Strauss, O., 2005. The Retinal Pigment Epithelium in Visual Function. *Physiological Reviews*, 85(3), pp.845–881. Available at: http://www.physiology.org/doi/10.1152/physrev.00021.2004 [Accessed February 26, 2018].

Strecker, U., Faúndez, V.H. & Wilkens, H., 2004. Phylogeography of surface and cave Astyanax (Teleostei) from Central and North America based on cytochrome b sequence data. *Molecular Phylogenetics and Evolution*, 33(2), pp.469–481. Available at: https://www-sciencedirect-com.insb.bib.cnrs.fr/science/article/pii/S1055790304002246?via%3Dihub [Accessed March 31, 2018].

Strickler, A.G., Yamamoto, Y. & Jeffery, W.R., 2001. Early and late changes in Pax6 expression accompany eye degeneration during cavefish development. *Development genes and evolution*, 211(3), pp.138–44. Available at: http://www.ncbi.nlm.nih.gov/pubmed/11455425 [Accessed April 4, 2018].

Strickler, A.G., Yamamoto, Y. & Jeffery, W.R., 2007. The lens controls cell survival in the retina: Evidence from the blind cavefish Astyanax. *Developmental Biology*, 311(2), pp.512–523. Available at: https://www-sciencedirect-com.insb.bib.cnrs.fr/science/article/pii/S0012160607013140?via%3Dihub [Accessed April 4, 2018].

Sylvester, J.B. et al., 2013. Competing signals drive telencephalon diversity. *Nature Communications*, 4, p.1745. Available at: http://www.nature.com/doifinder/10.1038/ncomms2753 [Accessed March 22, 2018].

Takahashi, H. et al., 2009. Functional mode of FoxD1/CBF2 for the establishment of temporal retinal specificity in the developing chick retina. *Developmental Biology*, 331(2), pp.300–310. Available at: http://www.ncbi.nlm.nih.gov/pubmed/19450575 [Accessed March 12, 2018].

Takahashi, N. et al., 2011. Regulatory mechanism of osteoclastogenesis by RANKL and Wnt signals. *Frontiers in bioscience (Landmark edition)*, 16, pp.21–30. Available at: http://www.ncbi.nlm.nih.gov/pubmed/21196156 [Accessed March 19, 2018].

Take-uchi, M., Clarke, J.D.W. & Wilson, S.W., 2003. Hedgehog signalling maintains the optic stalk-retinal interface through the regulation of Vax gene activity. *Development (Cambridge, England)*, 130(5), pp.955–68. Available at: http://www.ncbi.nlm.nih.gov/pubmed/12538521 [Accessed March 23, 2018].

Tawk, M. et al., 2007. A mirror-symmetric cell division that orchestrates neuroepithelial morphogenesis. *Nature*, 446(7137), pp.797–800. Available at: http://www.nature.com/articles/nature05722 [Accessed February 6, 2018].

Teyke, T., 1990. Morphological Differences in Neuromasts of the Blind Cave Fish <i>Astyanax hubbsi </i>and the Sighted River Fish <i>Astyanax mexicanus</i> *Brain, Behavior and Evolution*,

35(1), pp.23–30. Available at: https://www.karger.com/Article/FullText/115853 [Accessed April 5, 2018].

Thisse, C. & Thisse, B., 2005. High Throughput Expression Analysis of ZF-Models Consortium Clones. *ZFIN Direct Data Submission*. Available at: https://zfin.org/ZDB-PUB-051025-1 [Accessed March 19, 2018].

Veien, E.S. et al., 2008. Canonical Wnt signaling is required for the maintenance of dorsal retinal identity. *Development (Cambridge, England)*, 135(24), pp.4101–11. Available at: http://www.ncbi.nlm.nih.gov/pubmed/19004855 [Accessed March 22, 2018].

Viringipurampeer, I.A. et al., 2012. Pax2 regulates a fadd-dependent molecular switch that drives tissue fusion during eye development. *Human Molecular Genetics*, 21(10), pp.2357–2369. Available at: https://academic.oup.com/hmg/article-lookup/doi/10.1093/hmg/dds056 [Accessed March 27, 2018].

Volkoff, H., 2014. Appetite regulating peptides in red-bellied piranha, Pygocentrus nattereri: Cloning, tissue distribution and effect of fasting on mRNA expression levels. *Peptides*, 56, pp.116–24. Available at: http://www.ncbi.nlm.nih.gov/pubmed/24721336 [Accessed June 4, 2014].

Volkoff, H. et al., 2005. Neuropeptides and the control of food intake in fish. *General and comparative endocrinology*, 142(1–2), pp.3–19. Available at: http://www.sciencedirect.com/science/article/pii/S001664800400317X [Accessed May 1, 2014].

Waddington, C.H., 1953. GENETIC ASSIMILATION OF AN ACQUIRED CHARACTER. *Evolution*, 7(2), pp.118–126. Available at: http://doi.wiley.com/10.1111/j.1558-5646.1953.tb00070.x [Accessed April 3, 2018].

Wagner, H.-J. et al., 2009. A novel vertebrate eye using both refractive and reflective optics. *Current biology : CB*, 19(2), pp.108–14. Available at: http://www.ncbi.nlm.nih.gov/pubmed/19110427 [Accessed May 13, 2018].

Walshe, J. & Mason, I., 2003. Unique and combinatorial functions of Fgf3 and Fgf8 during zebrafish forebrain development. *Development*, 130(18). Available at: http://dev.biologists.org.insb.bib.cnrs.fr/content/130/18/4337.long [Accessed June 14, 2017].

Wang, X. et al., 2015. Dorsoventral patterning of the Xenopus eye involves differential temporal changes in the response of optic stalk and retinal progenitors to Hh signalling. *Neural development*, 10(1), p.7. Available at: http://neuraldevelopment.biomedcentral.com/articles/10.1186/s13064-015-0035-9 [Accessed January 28, 2016].

Weiss, O. et al., 2012. Abnormal vasculature interferes with optic fissure closure in lmo2 mutant zebrafish embryos. *Developmental biology*, 369(2), pp.191–8. Available at: http://linkinghub.elsevier.com/retrieve/pii/S0012160612003624 [Accessed February 19, 2018].

Weitekamp, C.A. et al., 2017. A Role for Oxytocin-Like Receptor in Social Habituation in a Teleost. *Brain, Behavior and Evolution*, 89(3), pp.153–161. Available at: http://www.ncbi.nlm.nih.gov/pubmed/28448987 [Accessed March 1, 2018].

Wen, W. et al., 2015. Sox4 regulates choroid fissure closure by limiting Hedgehog signaling during ocular morphogenesis. *Developmental Biology*, 399(1), pp.139–153. Available at: http://www.sciencedirect.com.insb.bib.cnrs.fr/science/article/pii/S0012160614006678?via%3Dihub#bib58 [Accessed December 18, 2017].

Wilkens, H. & Strecker, U., 2017. *Evolution in the dark : Darwin's loss without selection*, Springer. Available at: https://books.google.fr/books?id=74QlDwAAQBAJ&pg=PA132&lpg=PA132&dq=cavefish+scales&source=bl&ots=jua_Hr2obL&sig=bm-Czxpd6K9XJgJySRIeFdoKWDg&hl=fr&sa=X&ved=0ahUKEwiLyb6l9pnaAhUCI8AKHaHgAPcQ6AEIZTAK#v=onepage&q=cavefish scales&f=false [Accessed April 1, 2018].

Willardsen, M.I. et al., 2009. Temporal regulation of Ath5 gene expression during eye development. *Developmental Biology*, 326(2), pp.471–481. Available at: https://www-sciencedirect-com.insb.bib.cnrs.fr/science/article/pii/S0012160608013250?via%3Dihub [Accessed March 19, 2018].

Windsor, S.P. & McHenry, M.J., 2009. The influence of viscous hydrodynamics on the fish lateral-line system. *Integrative and Comparative Biology*, 49(6), pp.691–701. Available at:

https://academic.oup.com/icb/article-lookup/doi/10.1093/icb/icp084 [Accessed April 15, 2018].

Woods, I.G. et al., 2014. Neuropeptidergic signaling partitions arousal behaviors in zebrafish. *The Journal of neuroscience : the official journal of the Society for Neuroscience*, 34(9), pp.3142–60. Available at: http://www.ncbi.nlm.nih.gov/pubmed/24573274 [Accessed April 17, 2018].

Wu, M.Y. et al., 2011. SNW1 is a critical regulator of spatial BMP activity, neural plate border formation, and neural crest specification in vertebrate embryos. D. L. Stemple, ed. *PLoS biology*, 9(2), p.e1000593. Available at: http://dx.plos.org/10.1371/journal.pbio.1000593 [Accessed March 16, 2018].

Yamamoto, K., Bloch, S. & Vernier, P., 2017. New perspective on the regionalization of the anterior forebrain in *Osteichthyes*. *Development, Growth & Differentiation*, 59(4), pp.175–187. Available at: http://www.ncbi.nlm.nih.gov/pubmed/28470718 [Accessed February 27, 2018].

Yamamoto, Y. et al., 2009. Pleiotropic functions of embryonic sonic hedgehog expression link jaw and taste bud amplification with eye loss during cavefish evolution. *Developmental biology*, 330(1), pp.200–11. Available at: http://www.pubmedcentral.nih.gov/articlerender.fcgi?artid=3592972&tool=pmcentrez&rendertype=abstract [Accessed June 5, 2014].

Yamamoto, Y. & Jeffery, W.R., 2000. Central Role for the Lens in Cave Fish Eye Degeneration. *Science*, 289(5479), pp.631–633. Available at: http://www.ncbi.nlm.nih.gov/pubmed/10915628 [Accessed June 2, 2014].

Yamamoto, Y., Stock, D.W. & Jeffery, W.R., 2004. Hedgehog signalling controls eye degeneration in blind cavefish. *Nature*, 431(7010), pp.844–7. Available at: http://www.nature.com.gate1.inist.fr/nature/journal/v431/n7010/full/nature02864.html [Accessed June 5, 2014].

Yoshizawa, M., 2016. Chapter 13 – The Evolution of Sensory Adaptation in Astyanax mexicanus. In A. C. Keene, M. Yoshizawa, & S. E. McGaugh, eds. *Biology and Evolution of the Mexican Cavefish*. pp. 247–267.

Yoshizawa, M. et al., 2015. Distinct genetic architecture underlies the emergence of sleep loss and prey-seeking behavior in the Mexican cavefish. *BMC Biology*, 13(1), p.15. Available at: http://bmcbiol.biomedcentral.com/articles/10.1186/s12915-015-0119-3 [Accessed April 8, 2018].

Yoshizawa, M. et al., 2010. Evolution of a behavioral shift mediated by superficial neuromasts helps cavefish find food in darkness. *Current biology : CB*, 20(18), pp.1631–6. Available at: http://www.pubmedcentral.nih.gov/articlerender.fcgi?artid=2946428&tool=pmcentrez&rendertype=abstract [Accessed June 6, 2014].

Yoshizawa, M. et al., 2014. The sensitivity of lateral line receptors and their role in the behavior of Mexican blind cavefish (Astyanax mexicanus). *The Journal of experimental biology*, 217(Pt 6), pp.886–95. Available at: http://www.ncbi.nlm.nih.gov/pubmed/24265419 [Accessed April 5, 2018].

Yuasa, J. et al., 1996. Visual projection map specified by topographic expression of transcription factors in the retina. *Nature*, 382(6592), pp.632–635. Available at: http://www.nature.com/doifinder/10.1038/382632a0 [Accessed March 13, 2018].

Zhang, C., Forlano, P.M. & Cone, R.D., 2012. AgRP and POMC neurons are hypophysiotropic and coordinately regulate multiple endocrine axes in a larval teleost. *Cell metabolism*, 15(2), pp.256–64. Available at: http://www.ncbi.nlm.nih.gov/pubmed/22245570 [Accessed March 1, 2018].

Appendix
(articles in co-author)

3. Senory evolution in blind cavefish is driven by early embryonic events during gastruation and neurulation

RESEARCH ARTICLE

Sensory evolution in blind cavefish is driven by early embryonic events during gastrulation and neurulation

Hélène Hinaux, Lucie Devos, Maryline Blin, Yannick Elipot, Jonathan Bibliowicz, Alexandre Alié and Sylvie Rétaux*

ABSTRACT

Natural variations in sensory systems constitute adaptive responses to the environment. Here, we compared sensory placode development in the blind cave-adapted morph and the eyed river-dwelling morph of *Astyanax mexicanus*. Focusing on the lens and olfactory placodes, we found a trade-off between these two sensory components in the two morphs: from neural plate stage onwards, cavefish have larger olfactory placodes and smaller lens placodes. In a search for developmental mechanisms underlying cavefish sensory evolution, we analyzed the roles of Shh, Fgf8 and Bmp4 signaling, which are known to be fundamental in patterning the vertebrate head and are subtly modulated in space and time during cavefish embryogenesis. Modulating these signaling systems at the end of gastrulation shifted the balance toward a larger olfactory derivative. Olfactory tests to assess potential behavioral outcomes of such developmental evolution revealed that *Astyanax* cavefish are able to respond to a 10^5-fold lower concentration of amino acids than their surface-dwelling counterparts. We suggest that similar evolutionary developmental mechanisms may be used throughout vertebrates to drive adaptive sensory specializations according to lifestyle and habitat.

KEY WORDS: Lens placode, Olfactory placode, Trade-off, Complex trait, Signaling, Olfactory skills

INTRODUCTION

Animals rely on their sensory systems to perceive relevant stimuli in their environment. Natural selection favors sensory systems that are adapted to stimuli used for survival and reproduction. In line with this idea, there are numerous examples in the literature of sensory specialization in animals according to their habitat. This concerns both external sensory organs and brain areas that process the sensory information. However, not much is known about how existing sensory systems evolve, particularly in terms of size, to fit a specific environment.

To cite a few examples, diurnal rodents have a larger proportion of cerebral cortex devoted to visual areas than nocturnal rodents, the latter having a larger part of their cortex devoted to somatosensory and auditory areas (Campi and Krubitzer, 2010; Krubitzer et al., 2011). Among cichlid fish in African lakes, the relative size of brain regions in different species varies according to the environment and feeding habits (Pollen et al., 2007). Sensory organs also vary greatly among species. Classical cases include the small eyes but highly developed olfactory epithelium of sharks (Collin, 2012), the vibrissae-like tactile hair covering the otherwise hairless skin of the underground-living naked mole rat (Crish et al., 2003; Park et al., 2003; Sarko et al., 2011) or the variation in the number of lateral line neuromasts in sticklebacks depending on their stream versus marine, or benthic versus limnetic, habitat (Wark and Peichel, 2010).

Of note, the evolution of a particular sensory organ is often discussed with no consideration of the role played by other senses, but recent analyses have revealed co-operations and trade-offs among senses (Nummela et al., 2013). Developmentally, this implies that the control of the size of sensory organs is tightly regulated during embryogenesis and later, and that this regulation is somehow coordinated between the different organs.

In cave animals from all phyla, a striking blind (and de-pigmented) phenotype is repeatedly observed. In the blind cavefish (CF) of the species *Astyanax mexicanus*, which can be advantageously used in developmental comparative analyses because sighted surface fish (SF) of the same species are available (Jeffery, 2008, 2009), the eyes are regressed in adults, but sensory compensations have been reported: CF have more taste buds (chemosensory) (Schemmel, 1967; Varatharasan et al., 2009; Yamamoto et al., 2009) and more head neuromasts (mechanosensory) (Jeffery et al., 2000; Yoshizawa and Jeffery, 2011) than SF. Also consistent with this idea, CF are better at finding food in the dark (Espinasa et al., 2014; Hüppop, 1987) and seem more sensitive to food-related cues than SF (Bibliowicz et al., 2013; Protas et al., 2008). Although the olfactory system (chemosensory) was initially thought to be anatomically and physiologically unchanged in CF (Riedel and Krug, 1997; Schemmel, 1967), later studies found that naris opening is larger in troglomorphic animals (Bibliowicz et al., 2013; Yamamoto et al., 2003), suggesting a possible link between increased food finding capabilities and olfactory specialization. From an evolutionary perspective, these changes in different sensory modules could be either uncoupled or be the result of common selection pressures, acting at developmental and genetic levels (Franz-Odendaal and Hall, 2006; Wilkens, 2010).

Importantly, in *Astyanax* CF the eyes first develop almost normally during embryogenesis before they then degenerate. The triggering event for eye degeneration is lens apoptosis (Alunni et al., 2007; Yamamoto and Jeffery, 2000). The lack of expression of αA-crystallin, a lens differentiation gene (Behrens et al., 1998; Strickler et al., 2007), probably contributes to the apoptotic phenotype in CF (Hinaux et al., 2014; Ma et al., 2014). However, CF eyes are also smaller than SF eyes from embryonic stages onward (Hinaux et al., 2011; Strickler et al., 2001). What are the developmental mechanisms underlying the regulation of sensory organ size in CF? Previous work has shown that increased Shh signaling and heterochronic Fgf8 signaling in CF have pleiotropic effects on neural development: Shh is indirectly responsible for lens apoptosis (Yamamoto et al., 2004) and also impacts the number of taste buds

DECA group, Paris-Saclay Institute of Neuroscience, CNRS, Université Paris Sud, Université Paris-Saclay, Avenue de la terrasse, Gif-sur-Yvette 91198, France.

*Author for correspondence (retaux@inaf.cnrs-gif.fr)

Received 20 June 2016; Accepted 20 October 2016

(Yamamoto et al., 2009), while Shh and Fgf8 influence the relative sizes of the domains of the neural plate and neural tube that are fated to contribute to the retina or to other brain parts (Menuet et al., 2007; Pottin et al., 2011).

Shh and Fgf signaling are also known to affect the development of the placodal region in other vertebrate model species (Bailey et al., 2006; Dutta et al., 2005). The placodes correspond to a region surrounding the neural plate that generates the sensory organs of the head in vertebrates, including the lens, the olfactory epithelium, the otic vesicle and the lateral line (Schlosser, 2006; Streit, 2007, 2008; Torres-Paz and Whitlock, 2014; Whitlock and Westerfield, 2000). Here, we investigated the development of the *Astyanax* CF placodal region, with a particular focus on the lens and olfactory placodes. We report significant differences in patterning between CF and SF embryos and show that Shh, Fgf and Bmp4 modifications contribute to opposite changes in the size of the lens and olfactory placodes in CF. Further comparing olfactory behavior of the two morphs, we uncover outstanding olfactory skills in CF, confirming their functional olfactory specialization.

RESULTS

Early patterning of the placodes

We compared placodal field patterning in Pachón CF and SF embryos at the end of gastrulation/beginning of neurulation (Fig. 1). At 10 hours post fertilization (hpf), the shape and size of the neural plate border domain labeled by *Dlx3b* was similar in SF and CF (Fig. 1A,A′). Inside this *Dlx3b*-positive border, the anterior neural plate markers *Zic1* and *Pax6*, which label the 'eye field' and presumptive forebrain, are prominently expressed (Fig. 1B-C′). At the placodal level, the anteriormost part of the *Pax6*-positive presumptive lens placode territory was lacking in CF embryos, resulting in a smaller lens territory (Fig. 1C-C″). The width (mediolateral extension) of the *Pax6* lens placode domain was similar in SF and CF, consisting of 2-3 cell diameters (Fig. 1C-D′). Examination of the anteriormost placodal region using the *Dlx3b* marker on frontal views also revealed robust differences, with its domain being anteriorly expanded in CF embryos (Fig. 1E-E″, and see below). Thus, early anterior placodal patterning is modified in CF embryos, and the lens placode is reduced in size.

Slightly later, at 12 hpf (end of neurulation) and 16 hpf (mid-somitogenesis), *Dlx3b* expression was progressively reduced to the presumptive olfactory and otic placode and to the adhesive organ or casquette (Fig. 2A-B′, Fig. S1A) (Pottin et al., 2010). The *Dlx3b*-negative ventrolateral head region corresponding to the forming eye vesicle was reduced in CF (Fig. 2A-A″), whereas the *Dlx3b*-positive dorsolateral domain corresponding to the olfactory placode was much larger in CF (Fig. 2B-B″). This was confirmed by the olfactory marker *Eya2* (Fig. 2C-C″).

From 20 hpf onwards, the lens mass was clearly identified using *Pitx3* (Fig. 2D,D′), which is expressed throughout the lens in both SF and CF (Fig. 2F,G), therefore providing a good proxy for lens size. The *Pitx3*-positive lens area was much smaller in CF than in SF embryos (Fig. 2D″).

In parallel, the size of the olfactory epithelium (OE) derived from the olfactory placode was assessed after hatching by Olfactory marker protein (*OMP*) expression (Fig. 2E,E′). The area where

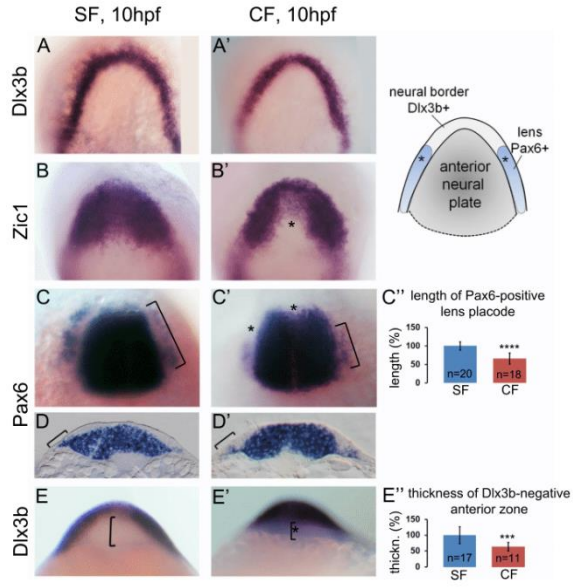

Fig. 1. Early patterning of the anterior placodes and neural plate at 10 hpf. (A-E′) SF (left) and CF (right) embryos after *in situ* hybridization for the indicated genes. (A-C′) Dorsal views, anterior to the top; (D,D′) transverse sections; (E,E′) frontal views. Brackets indicate regions of interest. Asterisks indicate differences between SF and CF. The scheme on the right helps the interpretation of gene expression patterns. (C″,E″) Quantification of gene expression domains in SF and CF for 10 hpf embryos. In this and following figures, numbers in bars indicate the number of embryos used for quantification, and data are mean±s.e.m. ****P<0.0001, ***P<0.001, Mann–Whitney test.

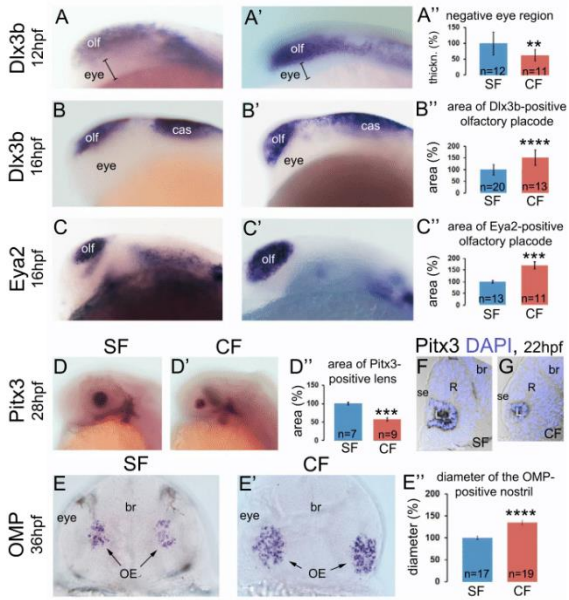

Fig. 2. Late patterning of the anterior placodes. (A-E′) SF (left) and CF (right) embryos showing expression of the indicated genes at the indicated stages. (A-D′) Lateral views, anterior to the left; (E,E′) frontal views. (F,G) Transverse sections through the eyes, with DAPI (blue) nuclear counterstaining. (A″-E″) Quantification of gene expression domains in SF and CF. Measurements were made on lateral (A″-D″) or frontal (E″) views. **P<0.01, ***P<0.001, ****P<0.0001, Mann–Whitney test. br, brain; cas, casquette; L, lens; OE, olfactory epithelium; olf, olfactory placode; R, retina; se, surface ectoderm.

OMP-positive neurons are scattered in a salt and pepper pattern was much larger in CF than in SF (Fig. 2E″), and this difference was maintained at 64 hpf (Fig. S2A).

We also examined the anteriormost derivatives of the placodal field, fated to become the adenohypophysis/pituitary in vertebrates (Dutta et al., 2005). Unfortunately, none of the three *Astyanax* Pitx genes that we cloned was expressed in the pituitary (Fig. S3A-C). We therefore isolated *Lhx3*, a LIM-homeodomain transcription factor considered as an early and specific pituitary marker. *Lhx3* expression starts at ~24 hpf in *Astyanax* (not shown). At 28 hpf, the size of the *Lhx3*-positive domain and the number of *Lhx3*-positive cells were similar in SF and CF (Fig. S1B), suggesting that, anteriorly, only the olfactory and the lens derivatives vary in size between the two morphs. Finally, the posterior otic placode was identical in size in CF and SF according to *Dlx3b* expression (Fig. S1A), suggesting that only the anterior placodes are modified in CF.

Altogether, these patterning data suggest that the olfactory placode and epithelium are continuously enlarged in CF at the expense of a reduction of the lens placode and mass.

A genetic link between lens and olfactory derivative size control in CF?

To test directly a genetic link between the opposite variations in olfactory and lens sizes in CF, we established crosses to generate first (F1) and second (F2) generation hybrids. In 36 hpf F1 hybrids resulting from SF×Pachón CF crosses, the size of the lens (Fig. 3A,A′) and the size of the OE (Fig. 3B,B′) were intermediate between those of a SF and a CF larva of the same age. In 36 hpf F2 hybrids resulting from crosses between two F1 parents, the lens and OE volume were measured concomitantly in single individuals (n=33) on confocal images (Fig. 3C). There was no correlation between lens size and OE size (Fig. 3C′). This suggests that the control of OE size and lens size are complex traits, with a multigenic determinism. These results are in line with previous findings that at least six QTL are involved in the control of lens size (Protas et al., 2007).

Signaling systems and the control of placodal patterning and fate in CF

We next investigated the origins of the modifications of placodal patterning in CF. That differences were observed as early as 10 hpf suggested that they resulted from modifications during gastrulation. Shh hyper-signaling from the notochord and *Fgf8* heterochronic (earlier) expression in the anterior neural ridge are known in CF (Pottin et al., 2011; Yamamoto et al., 2004). In addition, the differences that we observed in the anterior placode region (Fig. 1E,E′) suggested that signaling from the prechordal plate (pcp), an endomesodermal structure with important signaling properties for induction and patterning of the forebrain (Kiecker and Niehrs, 2001), might be affected in CF.

At the end of gastrulation (9.5-10 hpf), the pcp abuts the anterior limit of the embryonic axis, being just rostral to the *Shh*-expressing notochord and just ventral to the *Dlx3b*- and *Fgf8*-expressing anterior neural border (Fig. 4A,B). *Bmp4* expression in the *Astyanax* pcp can be subdivided into the polster (anterior, round in shape, *Shh*-negative) and posterior prechordal plate (ppcp, elongated in shape, *Shh*-positive) domains. *Bmp4* spatiotemporal expression was compared in the two morphs between 9.5 hpf and 11 hpf (Fig. 4A). In SF, *Bmp4* was expressed either in polster only (the majority of embryos) or in polster and ppcp (Fig. 4A-C, Fig. S4A). Conversely, in CF, a majority of embryos showed expression in the ppcp only, and confocal examination confirmed the absence of *Bmp4* expression in the polster for many of them (Fig. 4B). Importantly, the polster, as a structure, is present in CF and the migration of the pcp appears similar in the two morphs as (1) a few CF embryos did show some *Bmp4* staining in the polster (Fig. 4C, Fig. S4A) and (2) the expression of other genes, such as *Pitx1* (Fig. S4C) or the recognized pcp marker *goosecoid* (*Gsc*), was present in SF and CF

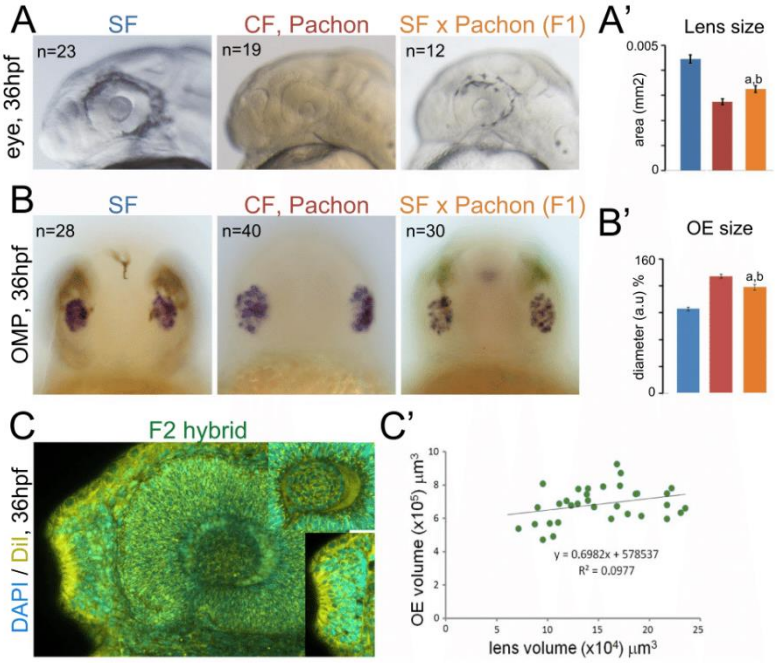

Fig. 3. Lens and OE size in F1 and F2 hybrids. (A,B) Images of the head (A) or after *in situ* hybridization for *OMP* in frontal views (B) of 36 hpf SF, CF and F1 hybrids. (A′) Lens measurements in 36 hpf larvae. a, different from SF (P<0.0001); b, different from CF (P=0.0056). SF and CF lens sizes are also significantly different (P<0.0001). Mann–Whitney tests. SF, blue; CF, red; F1 hybrid, orange. (B′) OE size in the three types of larvae. a, different from SF (P<0.0001); b, different from CF (P=0.0046). SF and CF OEs are also significantly different (P<0.0001). Mann–Whitney tests. (C) Confocal stack and image (inset) of 36 hpf F2 hybrids after DAPI/DiI staining, showing the lens and OE of a single embryo, on which OE and lens volumes were measured. (C′) Correlation plot between OE and lens volume.

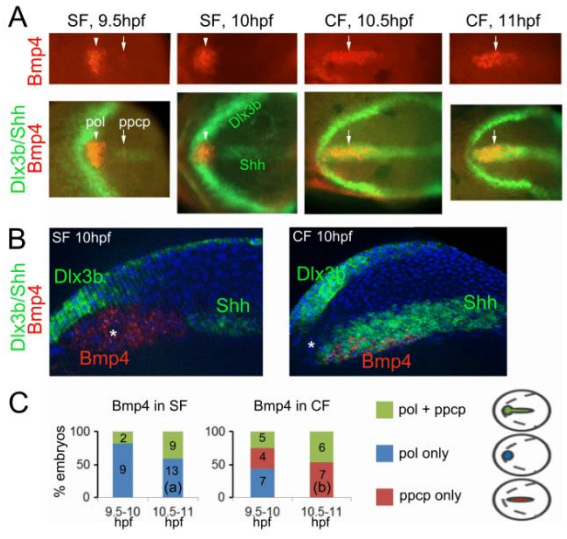

Fig. 4. *Bmp4* expression dynamics in prechordal plate. (A) Expression of *Bmp4* between 9.5 hpf and 11 hpf in SF and CF embryos after triple *in situ* hybridization for *Bmp4* (red), *Dlx3b* (green) and *Shh* (green). Anterior is to the left. (Top) Dorsal views of *Bmp4* expression in the polster (pol, arrowhead) and posterior prechordal plate (ppcp, arrow). (Bottom) Merged images of the entire neural plate. *Dlx3b* labels the neural plate border, and *Shh* is expressed at the ventral midline (ppcp and notochord). (B) Confocal sections through the sagittal plane of 10 hpf SF (left) and CF (right) embryos after triple *in situ* hybridization for *Bmp4* (red), *Dlx3b* (green) and *Shh* (green), showing exclusive or overlapping expression domains between the three genes. Anterior is to the left. Asterisk, polster. (C) Distribution of *Bmp4* pattern types in SF and CF between 9.5 hpf and 11.5 hpf. Color codes match the patterns schematized on the right and numbers in bars give the numbers of embryos examined. The distribution is significantly different between SF and CF at 10.5-11 hpf. a, P=0.0006 for expression in polster only in SF versus CF; b, P=0.00026 for expression in ppcp only in SF versus CF; Fisher's exact test.

with comparable dynamics (Fig. S5). Thus, significant differences in the dynamics of *Bmp4* expression inside the pcp exist between CF and SF (see Fig. 4C legend).

Present and previous results prompted us to investigate whether the multiple changes observed in Shh, Fgf8 and Bmp4 signaling systems are responsible for sensory placode and organ size variations in CF. We designed strategies to assess the influences of Shh and Fgf8, which correspond to quantitative differences in space and time between SF and CF, or the influence of Bmp4, which relates to qualitative differences in expression dynamics inside the pcp between the two morphs.

To test the influence of *Shh* heterotopy and *Fgf8* heterochrony, CF embryos were treated with cyclopamine [an antagonist of the Shh receptor Smoothened (Chen et al., 2002)] or with SU5402 [an antagonist of Fgf receptor signaling (Mohammadi et al., 1997)], respectively, between 6 hpf (shield) and 10 hpf (end of gastrulation), and the sizes of their lens and olfactory placodes were measured at later stages. Cyclopamine (100 µM) resulted in a 19% increase in lens size, as measured at 28 hpf using *Pitx3* as marker (Fig. 5A-A‴). Although significant, the cyclopamine-induced increase in lens size resulted in a lens that was still smaller than in SF. Inhibition of Fgf signaling with 0.5 µM SU5402 had no significant effect on lens size (Fig. 5A‴). By contrast, cyclopamine and SU5402 both induced a significant reduction in the size of the olfactory placode (−25% and −21%, respectively), as measured at 16 hpf using the *Eya2* marker (Fig. 5B-B‴). Notably, the reduction after both treatments in CF resulted in an olfactory placode of identical size to that of SF embryos.

Because the *Bmp4* differences in CF and SF relate to subtle expression dynamics and to the position of the signal within the pcp, their impact was not testable through pharmacological manipulation during a specific time window. An alternative experimental design was used: Bmp4 protein injections were performed at 10 hpf, aiming at anteriorizing or posteriorizing Bmp4 signaling in CF and SF embryos, and thereby mimicking one morph's situation in the other (Fig. 5C). Anterior injections of Bmp4 in CF produced an increase in lens size (+15%; Fig. 5D-D″,F) and a reduction in olfactory placode size (−16%; Fig. 5E-E″,F), suggesting opposite effects of polster Bmp4 signaling on the two sensory derivatives. The CF olfactory placode was also reduced after posterior Bmp4 injection (−16%, Fig. 5E″), suggesting that olfactory derivatives are negatively affected by high levels of Bmp4 signaling at the neural plate stage. Moreover, unlike injections in CF, anterior or posterior injection of Bmp4 in SF did not change lens or olfactory sizes (Fig. 5D″,E″), pointing to the specific lack of Bmp4 in the anterior polster part of the pcp as partly responsible for the small size of the lens in CF, or to the possibility that lens size might already be maximal in SF and therefore cannot be further increased, and that olfactory size might be minimal and cannot be further decreased.

Continued olfactory specialization in juvenile CF

Because an enlargement of the OE in CF may be of functional importance for survival in the dark, we examined whether it remained larger than in SF at juvenile stages. We used the $G_{\alpha olf}$ olfactory marker on 1-month-old larvae, when the OE is not yet folded inside the naris (Hansen et al., 2004; Wekesa and Anholt, 1999) (Fig. 6A,B,D,E). The size of the $G_{\alpha olf}$-positive OE and of the naris opening were significantly larger in CF than in SF (Fig. 6G) (OE, 1.36-fold; naris opening, 1.31-fold; values corrected to body length). Cell counts on sections showed an increased number of cells in the CF OE (Fig. 6H). Labeling of the olfactory projection by insertion of a crystal of lipophilic DiI in the olfactory cup revealed a conserved organization of the olfactory projection onto olfactory bulb glomeruli (Fig. 6C,F). The shape of the OE was consistently round in SF and oval in CF (compare Fig. 6A-F). The olfactory nerve was also longer in CF, which is probably due to the difference in size and shape of the jaw and skull (see also Fig. 7F).

Establishing a sensitive olfactory test

To compare the olfactory skills of 1-month-old juvenile CF and SF (5-6 mm in length), we designed an olfaction assay using amino acids as odorant molecules, in the dark with infrared recordings (Fig. 7A,B, Fig. S6A-C, Movie 1, and see the Materials and Methods). Amino acids are potent feeding cues in teleosts (Byrd and Caprio, 1982; Friedrich and Korsching, 1997) and have been used to test olfactory sensitivity and discrimination (Koide et al., 2009; Lindsay and Vogt, 2004; Vitebsky et al., 2005).

Depending on the fish species and the amino acid, millimolar to nanomolar concentrations trigger neuronal activation in the olfactory system (Dolensek and Valentincic, 2010; Evans and Hara, 1985; Friedrich and Korsching, 1997; Korsching et al., 1997; Vitebsky et al., 2005). We used these concentrations as a starting point. Perfusion of a 10^{-3} M to 10^{-5} M stock of alanine or serine resulted in a strong attractive response (positive preference index score) in both morphs (Fig. 7C,D).

Interestingly, when the test was performed in the light and the quantification of the response was carried out for longer, we

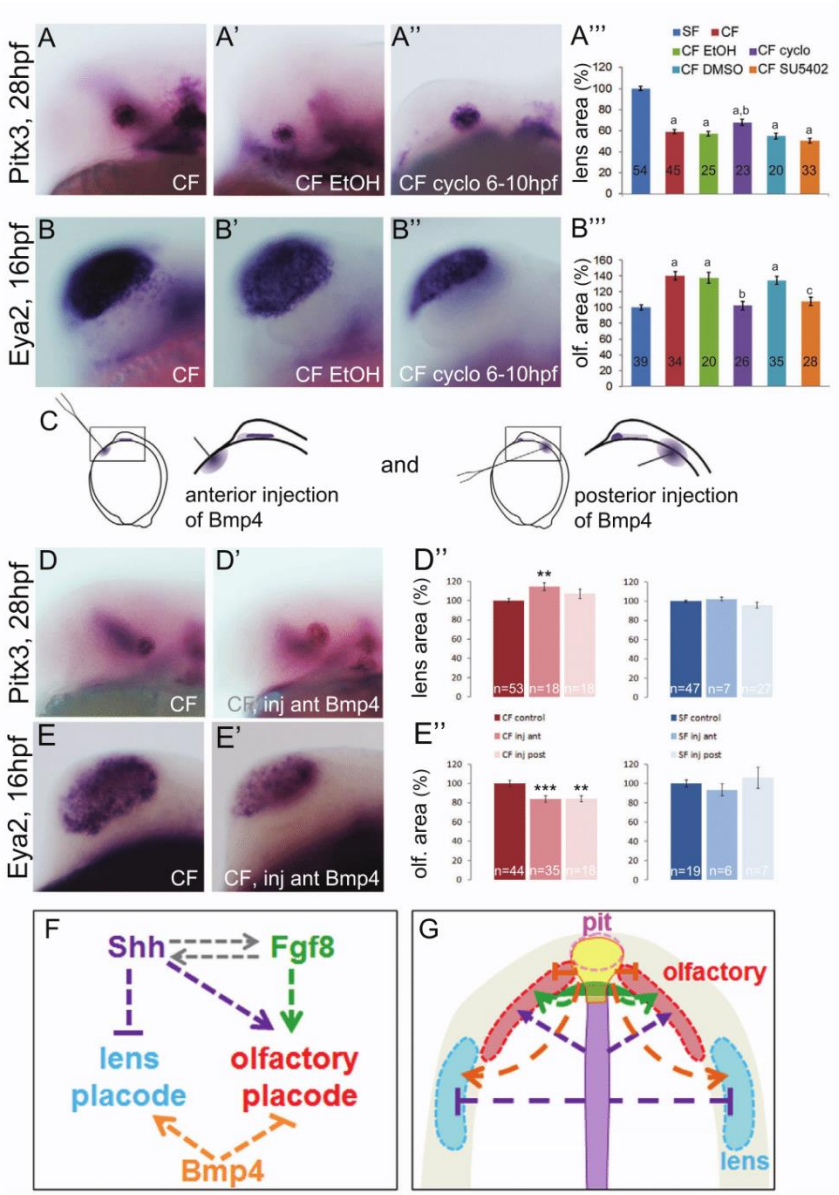

Fig. 5. Impact of early signaling systems on lens and olfactory size. (A-B″) Images of 28 hpf CF embryos showing the *Pitx3*-expressing lens and of 16 hpf CF embryos showing the *Eya2*-expressing olfactory placode, after the indicated treatments. Lateral views, anterior to the left. (A‴) Quantification of lens size according to *Pitx3* expression. Cyclo, 100 µM cyclopamine; SU5402, 0.5 µM SU5402 treatment between 6 hpf and 10 hpf. Ethanol and DMSO (vehicles) had no effect on lens size. Although relatively severely affected for head development (A″), embryos treated with cyclopamine show larger lenses. a, different from SF (P<0.0001); b, different from CF treated with ethanol (P<0.01) and from CF (P<0.05). Mann–Whitney tests. (B‴) Quantification of olfactory placode size according to *Eya2* expression. Ethanol and DMSO had no effect on olfactory placode size. a, different from SF (P<0.0001); b, different from CF treated with ethanol (P<0.001) and from CF (P<0.0001) and not different from SF; c, different from CF treated with DMSO (P<0.001) and from CF (P<0.0001) and not different from SF. Mann–Whitney tests. (C) Experimental design for Bmp4 protein injections at 10 hpf. (Left) Orientations and paths for injecting needles to target the anteriormost region of the head or the more posterior ventral midline. (Right) Magnification of the head region, where the endogenous morph-specific expression pattern of *Bmp4* in the pcp is also depicted by the intensity of purple. (D-E′) Images of 28 hpf CF embryos showing the *Pitx3*-expressing lens and of 16 hpf CF embryos showing the *Eya2*-expressing OE in the indicated conditions. (D″) Quantification of lens size after Bmp4 injections. **P<0.01, Mann–Whitney test. (E″) Quantification of olfactory placode size after Bmp4 injections. **P<0.01, ***P<0.001, Mann–Whitney test. (F) Proposed regulatory network depicting Shh, Fgf8 and Bmp4 signaling effects on lens versus olfactory placode specification and fate. The previously described cross-talk between Shh and Fgf is also indicated (gray; from Pottin et al., 2011).The dotted arrows indicate that effects could be indirect. (G) Signaling network transposed into the embryonic context. In CF embryos, Fgf8 heterochrony and Shh hyper-signaling promote enlargement of the olfactory placode and reduction of the lens placode territory, and the lack of anterior Bmp4 signaling by the polster also contributes to the reduction of the lens domain and the increase of the olfactory domain.

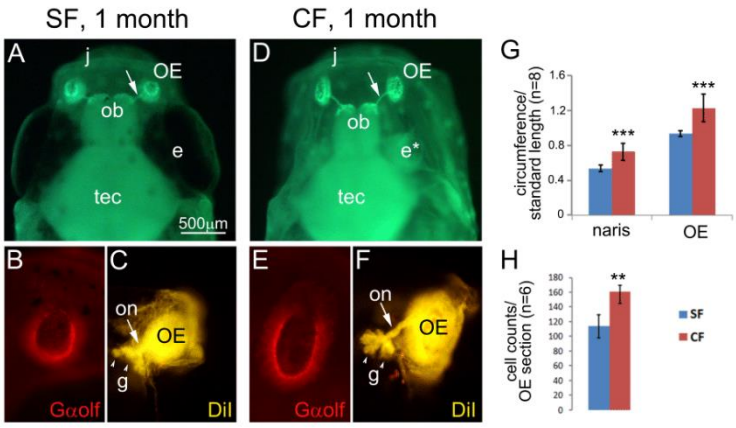

Fig. 6. Organization and size of the olfactory apparatus in juveniles. (A-F) Anatomy of the olfactory apparatus. OE sensory neurons project onto the olfactory bulbs (ob) through the olfactory nerve (on, arrow). (A,B,D,E) $G_{\alpha olf}$ immunofluorescence (green or red) on 1-month-old SF and CF. (A,D) Dorsal views (anterior is up) of the heads; (B,E) high magnification at OE level. (C,F) The olfactory sensory projection after insertion of a crystal of DiI in the olfactory cup of 2-week-old larvae, visualizing olfactory bulb glomeruli (g, arrowheads). Note the differences in OE size and shape (larger and oval in CF) and optic nerve length (longer and thicker in CF). j, jaw; e, eye (asterisk indicates degenerated eye in CF); tec, optic tectum. (G,H) Quantification of OE size (G) and counting of OE cells (H) in 1-month-old SF and CF. Measurements were performed on juveniles of equivalent size and normalized to standard length (G). $G_{\alpha olf}$ was used to measure OE/naris opening circumferences and DAPI-stained sections were used for cell counts. ***P<0.0001, **P<0.01, Mann–Whitney test.

observed that, in contrast to CF, SF were only transiently attracted to the odorant compartment for ~4 min, and then swam randomly in the box (Fig. 7E). We interpret this observation as vision interfering with olfactory-driven behavior: SF can see that no food is present despite the food-related odor, and do not persist in their behavioral response. This confirms the importance of the visual sensory modality in controlling SF behavior, and the accuracy of the behavioral set-up.

Attraction to amino acids is mediated by the OE

In both bony and cartilaginous fish, olfaction is used to localize food sources, breeding partners and predators, as well as for communication and learning, while gustation is primarily involved in feeding, including oral processing and evaluating food palatability through direct contact (Collin, 2012; Derby and Sorensen, 2008). Chemosensory detection of amino acids depends on both gustatory and olfactory sensory modalities (Hara, 1994). In most fish species, the detection threshold of the taste buds is in the micromolar range (Hara, 1994, 2006, 2015), higher than the concentrations used here. However, as CF possess more taste buds than SF on their lips and face (Schemmel, 1967; Varatharasan et al., 2009; Yamamoto et al., 2009), we needed to ascertain that the observed response to amino acids was truly olfactory mediated. We chemically ablated the surface of the OE by application of a Triton X-100 solution onto the naris (Iqbal and Byrd-Jacobs, 2010), which resulted in the disappearance of $G_{\alpha olf}$ immunoreactivity (Fig. 7F). Olfactory responses were measured on bilaterally OE-ablated fish using 10^{-5} M alanine, which induces a strong attraction in both morphs in normal fish (see Fig. 7C). OE-ablated SF and CF did not respond to the odor at any time point (Fig. 7G). Importantly, this lack of attraction was not due to a lack of exploratory behavior (Fig. S6D). Thus, at the concentrations used, the behavioral assay measures olfactory-mediated, but not gustatory-mediated, responses.

CF have a more sensitive olfactory response

To determine and compare the threshold concentrations of amino acid detection of the two morphs, we repeated the experiments at progressively decreasing concentrations. Alanine or serine at 10^{-6} M still resulted in a robust attraction of CF to the amino acid source, whereas SF no longer displayed such attraction (Fig. 8A,B). The result was identical for the two amino acids, and the lack of response in SF was not due to a difference in swimming exploratory behavior (Fig. S7). As expected, SF did not respond to even lower concentrations (10^{-7} M alanine, not shown). To determine the CF discrimination threshold, we further decreased the alanine concentration to 10^{-7} M (not shown), 10^{-9} M, 10^{-10} M and 10^{-11} M. Remarkably, the CF detection threshold was 10^{-10} M (Fig. 7C). Thus, CF are able to respond to 10^5-fold lower concentrations of amino acids than SF.

DISCUSSION

Using *Astyanax* CF as 'natural mutants' we uncovered early developmental origins of natural variations in sensory systems. We discuss our findings in terms of a specific understanding of the developmental mechanisms underlying the CF phenotype, and in terms of a more general understanding of sensory development and evolution in vertebrates.

Specific considerations of CF developmental evolution and phenotype

Adult cavefish are blind. During embryonic and larval development, the two main components of their eyes are affected: the retina is small and lacks a ventral quadrant (Pottin et al., 2011) and the lens undergoes apoptosis, which triggers degeneration of the entire eye (Yamamoto and Jeffery, 2000). Moreover, the CF lens enters apoptosis even if transplanted into an SF optic cup (Yamamoto and Jeffery, 2000), suggesting that CF lens defects could stem from early embryonic events. Here, we show that from the earliest possible stage of lens tracing, using transient expression of *Pax6* at the pan-placodal stage when placodal precursors are still plastic to give rise to several sensory derivatives (Bailey and Streit, 2006; Dutta et al., 2005; Martin and Groves, 2006; Sjödal et al., 2007), the presumptive territory (and hence the number of precursors) of the lens is reduced in CF as compared with SF embryos.

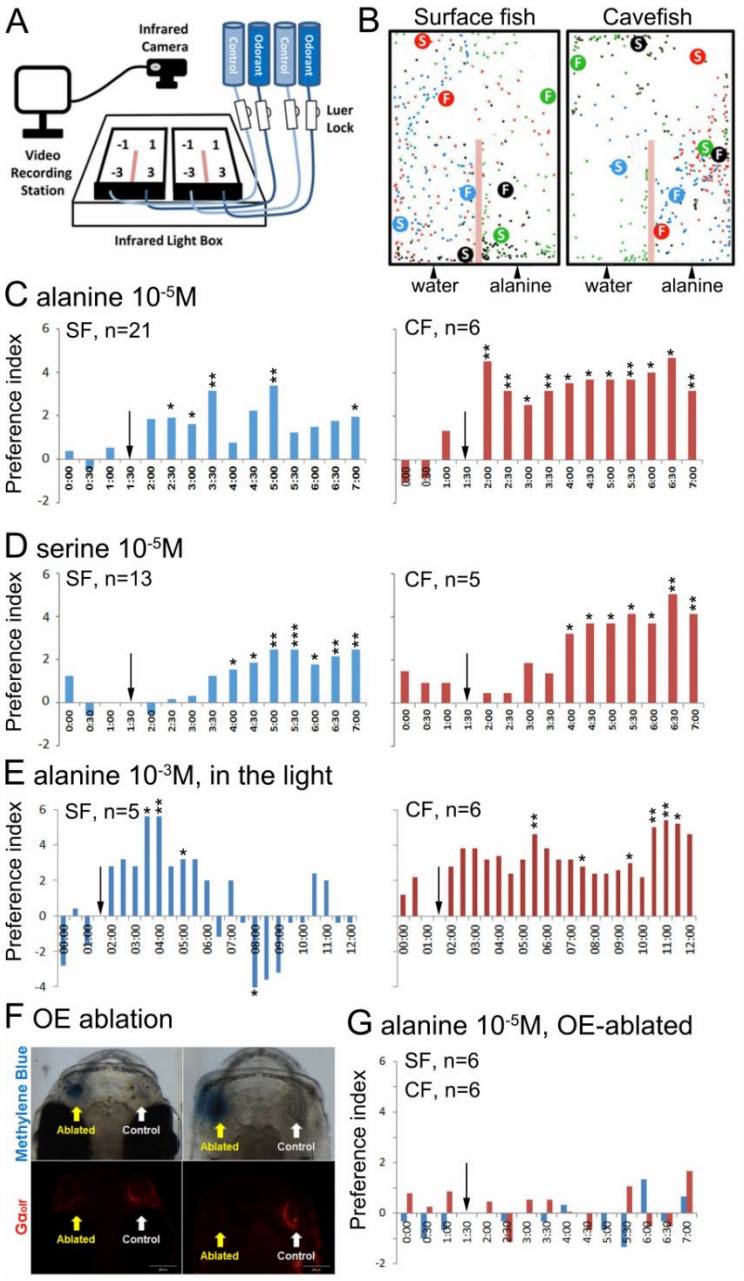

Fig. 7. Olfactory response to amino acids. (A) Behavioral testing set-up. (B) Example of tracking for 1 µM alanine. The position of the four SF (left) or the four CF (right) was noted every 5 s during the test (colored dots). The four different colors follow the four fish in each box, with the start (S) position and the final (F) position indicated for each fish (see also Movie 1). (C,D) Response to 10 µM alanine (C) and 10 µM serine (D). The response to odorant is represented as the preference index as a function of time. Positive values indicate attraction. The arrow indicates the time when the odorant reaches the box. The conditions and number of tests are indicated (*n*=1 corresponds to one test, i.e. the cumulative score of four fish). Asterisks indicate significant response as compared with zero (Mann–Whitney): **P*<0.05, ***P*<0.01, ****P*<0.001. (E) Response to 1 mM alanine in the light during 12 min. (F) Superficial ablation of the OE by Triton X-100 application onto the olfactory cup. Top row illustrates the procedure, with the right side serving as control. Bottom row shows $G_{\alpha olf}$ immunofluorescence (red), which disappears on the ablated side. (G) OE-ablated SF and CF do not respond to 10 µM alanine.

It seems relevant to CF evolution and adaptation that its olfactory placode is enlarged. In the wild, in the Subterráneo cave (and hence a different CF population to the Pachón used here), adult CF have large nostrils and better chemosensory capabilities than non-troglomorphic fish (Bibliowicz et al., 2013). Here, we show that Pachón juveniles also possess large OEs and outstanding olfactory skills, demonstrating a case of parallel developmental and sensory evolution in two independently evolved CF populations (Bradic et al., 2012). Remarkably, only sharks have been reported to present such sensitivity (low response threshold) to amino acids with, for example, 10^{-11} M alanine eliciting electro-olfactogram responses in the hammerhead shark (Tricas et al., 2009). Although we cannot yet conclude that the difference in olfactory skills of CF and SF is entirely attributable to the difference in olfactory organ size, it is tempting to speculate that it at least in part stems from their developmentally controlled olfactory specialization.

In CF, the increase in olfactory placode size parallels the decrease in lens placode size, suggesting a developmental sensory trade-off: (1) in terms of patterning, the presumptive lens placode territory is reduced anteriorly, at a position that corresponds to the presumptive

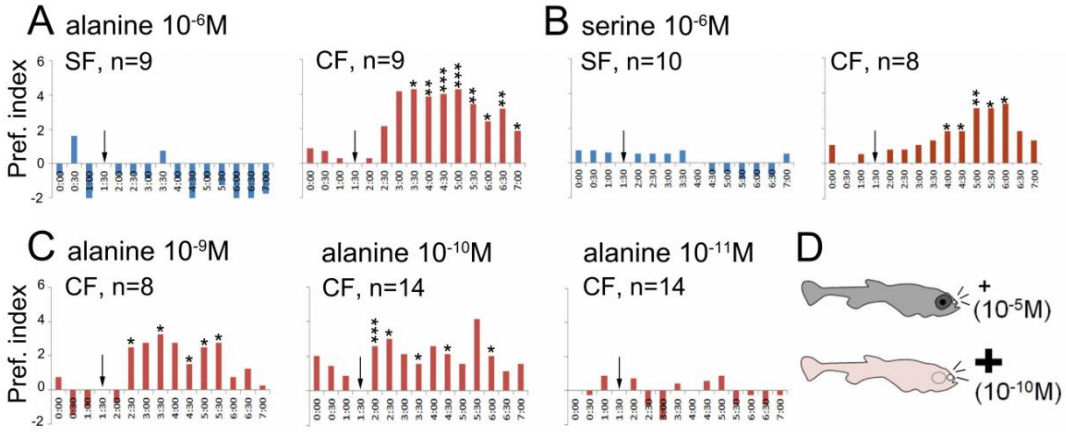

Fig. 8. Olfactory response thresholds in SF and CF. (A-C) Responses of SF and CF to decreasing concentrations of alanine (A,C) and serine (B). CF still respond to 0.1 µM serine (not shown), and therefore CF threshold for this amino acid is at least 0.1 µM. **P*<0.05, ***P*<0.01, ****P*<0.001, Mann–Whitney test. (D) Summary of the differences in olfactory anatomy and skills between SF (top) and CF (bottom).

territory of olfactory precursors according to zebrafish fate maps (Dutta et al., 2005; Toro and Varga, 2007); (2) the experimental manipulation of both Shh and Bmp4 signaling results in concomitant and opposite changes in the size of their lens/olfactory placodes. Together with the case of the gustatory/visual trade-off previously described (Yamamoto et al., 2009), these constitute the only examples to date of a direct link between the development of two sensory organs, involving a pleiotropic effect of these signaling systems, and suggesting indirect selection as an evolutionary driving force underlying the loss of eyes in CF (Jeffery, 2010; Retaux and Casane, 2013). In F2 hybrids, however, we did not observe an inverse correlation between lens and OE size, further suggesting that the developmental trade-off has a multigenic determinism.

We also found that *Bmp4* expression and signaling in the pcp are modified in CF compared with SF embryos (Fig. 4). Although several lines of evidence (*Pitx1* or *Gsc* expression) suggest that there is not a problem with migration of the CF pcp, we cannot exclude differences in cell movements between the two morphs. The dynamics of *Bmp4* expression are altered, whereas the total level of *Bmp4* expression at 10 hpf appears unchanged (Gross et al., 2016). Taking SF as 'wild type' and CF as 'mutant', an interpretation of the expression patterns would be the following: in SF, *Bmp4* is first turned on in the polster before 9.5 hpf and then in the ppcp; in CF, *Bmp4* expression would be turned off prematurely in the polster. Of note, the polster gives rise to the hatching gland, which develops and functions properly in CF [e.g. *Pitx1* expression in Figs S3 and 4; *Agr2* expression (Pottin et al., 2010); hatching time (Hinaux et al., 2011)]. Therefore, the modification in *Bmp4* expression dynamics in CF has no deleterious consequences on polster function, but does influence anterior neural development, as demonstrated by the Bmp4 injection experiments. Coupled with the previously described *Shh* heterotopy in the notochord and ppcp (Pottin et al., 2011; Yamamoto et al., 2004) and to the *Fgf8* heterochrony in the anterior neural territory (Pottin et al., 2011), our data on pcp *Bmp4* expression dynamics substantiate that three major signaling systems and organizer centers that orchestrate forebrain and head morphogenesis are altered in CF. Interestingly, *Bmp4* is found in QTL intervals controlling eye size (Borowsky and Cohen, 2013; Gross et al., 2008; Protas et al., 2007) and craniofacial bone fragmentation (Gross et al., 2016).

General considerations of sensory development and evolution

The data obtained from studies in model organisms on the roles of signaling systems in sensory placode development are sometimes contradictory (reviewed by Saint-Jeannet and Moody, 2014), perhaps owing to the fact that activation of similar combinations of signaling molecules at different time points can result in strikingly different outcomes (Lleras-Forero and Streit, 2012; Sjödal et al., 2007). Here, we studied three signaling systems in two morphs of a single species, and investigated their effects on the specification of regional placodal identity and sensory fate at the end of gastrulation/neural plate stage (Fig. 5F,G). In agreement with a stimulatory role of anterior neural ridge-derived Fgf8 signaling at neural fold stage in olfactory fate in chick (Bailey et al., 2006) and an inhibitory role of Shh in lens fate in zebrafish (Barth and Wilson, 1995; Dutta et al., 2005; Karlstrom et al., 1999; Kondoh et al., 2000; Varga et al., 2001), we found that Fgf8 heterochrony and Shh hyper-signaling at the anterior midline are responsible for the enlargement of the olfactory placode and the reduction of the lens placode territory in CF. Experiments performed in chick (Bailey et al., 2006) and Fgfr expression in zebrafish (ZFIN, *fgfr1a/fgfr1b* expression data) support a potential direct effect of Fgf signaling on the placodal region. Our results on CF, in which the difference with SF in terms of Fgf8 signaling comprises a 1.5 h expression heterochrony at the anterior neural border, points to the importance of the timing of Fgf8 signaling on placodal tissue [of note, *Fgf3* expression is unchanged in CF (Pottin et al., 2011)]. Conversely, Shh signaling effects on the lens and olfactory placode are probably indirect (Dutta et al., 2005), possibly via Fgf8 in the case of the olfactory placode (Pottin et al., 2011).

We also propose that Bmp4, as a signaling molecule secreted from the pcp as a signaling center, may influence placodal cell fate (Fig. 5F,G). This finding is distinct from the well-established early role of Bmp signaling in the specification of the neural plate border region/preplacodal region, which involves Bmp2/4/7 activity from the ventral side of the embryo at late blastula stages and the subsequent inhibition of Bmp signaling from the epidermis by Bmp inhibitors during gastrulation (Ahrens and Schlosser, 2005; Kwon et al., 2010; Nguyen et al., 1998; Reichert et al., 2013; Saint-Jeannet and Moody, 2014). In chick, a direct role for Bmp signaling in

placodal precursor specification at late gastrula stage, as well as a role for the time of Bmp exposure in the decision to follow a lens versus an olfactory fate, have been described (Sjödal et al., 2007). Our comparative approach using CF and SF have revealed a difference in Bmp4 expression dynamics in the pcp. This result and the functional experiments employing local Bmp4 injections at 10 hpf suggest that the timing of Bmp4 signaling from the pcp might be an important cue for lens fate specification, and support a general negative effect of sustained Bmp4 anterior midline signaling on olfactory fate. Our findings are also consistent with *Bmp4*$^{-/-}$ mice having normal olfactory derivatives but lacking lenses, although their placodal progenitors are initially correctly specified (Furuta and Hogan, 1998). Finally, the CF Bmp4 phenotype is not fully penetrant (Fig. 4). This might result from a polymorphism that is not fixed in CF. Yet, all CF have smaller lenses, probably because other pathways (Hh, Fgf, and perhaps others yet to be discovered) still contribute to size control, regardless of the Bmp4 phenotype.

Finally, our results concerning the pituitary are surprising. As Shh signaling is a potent inducer of pituitary fate (Dutta et al., 2005; Herzog et al., 2004; Karlstrom et al., 1999; Kondoh et al., 2000; Treier et al., 2001; Varga et al., 2001), one could expect to find a large adenohypophysis in CF with Shh hyper-signaling (Yamamoto et al., 2004). This was not the case. Indirectly, this suggests that other signaling modifications might compensate for Shh hyper-signaling in CF, and points to a possible negative control of pituitary fate in the placode by Fgf8 from the anterior neural ridge and Bmp4 from the pcp.

Conclusions

None of our experimental treatments led to full 'recovery' of CF lens to a size comparable to that of the SF lens. This is probably due to the fact that both Shh hyper-signaling from the ventral midline and lack of Bmp4 signal from the pcp are responsible for the small lens size in CF (Fig. 5F,G). Conversely, inhibition of either Shh or Fgf signaling in CF resulted in an olfactory placode identical in size to that of SF embryos. This shows the importance of Fgf8 and the associated Fgf8/Shh autoregulatory loop in the control of olfactory fate. These observations illuminate the subtle equilibrium that must exist in space and time between the signaling systems to orchestrate the development of the surrounding sensory epithelium. In model species, manipulation of early signaling systems usually results in 'monstrous' phenotypes. It might thus seem doubtful that morphological evolution is due to modifications at this level. However, we show that subtle changes in the equilibrium between signaling systems at the end of gastrulation can participate in natural morphological evolution, and are part of the developmental evolutionary toolkit. Here, we have deciphered the impact of fine changes in the strength or timing of three signaling pathways emanating from three organizer centers in the developmental evolution of sensory systems in *Astyanax*. As we have studied the CF 'natural mutant', an animal that is viable and adapted to its environment, the early developmental mechanisms that we have uncovered are probably generally applicable and relevant to adaptive sensory evolution and specialization in vertebrates.

MATERIALS AND METHODS

Animals

Laboratory stocks of *A. mexicanus* SF and Pachón CF were obtained in 2004 from the Jeffery laboratory at the University of Maryland and maintained as previously described (Elipot et al., 2014). Embryos were collected after natural spawning, grown at 23°C, staged according to the developmental staging table (Hinaux et al., 2011) and fixed in 4% paraformaldehyde. After progressive dehydration in methanol, they were stored at –20°C.

Animals were treated according to French and European regulations for handling of animals in research. S.R.'s authorization for use of animals in research is 91-116, and Paris Centre-Sud Ethic Committee authorization numbers are 2012-0052 and 2012-0055.

Lens and OE measurements

F1 hybrid larvae were obtained by *in vitro* fertilization of female SF eggs by Pachón male sperm (Elipot et al., 2014). They were photographed at 36 hpf under an Olympus SZX16 stereomicroscope. Measurements were made on the images using ImageJ software (NIH).

F2 larvae were fixed and immediately double stained with DAPI and DiI and imaged under an SP8 confocal microscope (Leica). Lens and OE volumes were measured with Fiji using the MeasureStack plugin.

cDNA cloning

Total RNA from *Astyanax* embryos of various stages (6-36 hpf) was reverse-transcribed using the iScript cDNA synthesis kit (Bio-Rad). Partial cDNA sequences for *Omp* (GenBank ID KP826791.1), *Lhx3* (KP826792.1), *Pitx1* (KP826793.1) and *Pitx2* (KP826794.1) were amplified by PCR (for primers, see the supplementary Materials and Methods) and subcloned in the TOPO-PCR II vector (Invitrogen). *Zic1* (FO290256) and *Eya2* (FO211529) partial cDNAs originate from our cDNA library (Hinaux et al., 2013). Phylogenetic analyses (Figs S8-S12) were conducted to determine orthology relationships. Deuterostomes sequences were retrieved from the Ensembl database based on their annotation, aligned using MAFFT v7.023b (http://mafft.cbrc.jp/alignment/software/) with manual correction. Maximum likelihood analyses were performed using PhyML (Guindon and Gascuel, 2003), with the LG model of amino acid substitution and a BioNJ tree as the input tree. A gamma distribution with four discrete categories was used. The gamma shape parameter and the proportion of invariant sites were optimized during the searches. The statistical significance of the nodes was assessed by bootstrapping (100 replicates). *Shh* (AY661431), *Pax6* (AY651762.1) and *Bmp4* (DQ915173) cDNA were isolated previously.

In situ hybridization

Digoxygenin-labeled riboprobes were synthesized from PCR templates. A protocol for automated whole-mount *in situ* hybridization (Intavis) was used (Deyts et al., 2005). Embryos were photographed *in toto* under a Nikon AZ100 stereomicroscope using agarose wells. Some were embedded in paraffin, sectioned (8 µm) and counterstained, using Prolong Gold anti-fade with DAPI (Invitrogen).

For fluorescent double *in situ* hybridization, Cy3- and FITC-tyramides were prepared and embryos were processed as previously described (Zhou and Vize, 2004; Pottin et al., 2011). Embryos were imaged with either an Olympus SZX16 stereomicroscope, a Zeiss Apotome or a Nikon Eclipse E800 microscope.

Immunohistochemistry

Whole-mount immunofluorescence was performed using $G_{\alpha olf}$ primary antibody (Santa Cruz Biotechnology, sc-383; 1/1000) and Alexa Fluor secondary antibodies (Invitrogen, A-11008 and A-11037; 1/500). Samples were imaged using an Olympus SZX16 microscope. Size measurements were performed on images using ImageJ.

Pharmacological treatments

Manually dechorionated CF embryos were incubated in 100 µM cyclopamine (C-8700, LC Laboratories) or 0.5 µM SU5402 (215543-92-3, Calbiochem) diluted in blue water (Elipot et al., 2014) from 6 to 10 hpf. Controls were incubated in an equivalent concentration of ethanol or DMSO, respectively. They were washed in blue water and fixed at 16 hpf or 28 hpf. To define and ascertain the working concentrations of cyclopamine and SU5402, we checked that hatched larvae have a typical 'comma shape' or tail bud defects, respectively.

Bmp4 protein microinjection

CF and SF embryos at 10 hpf were placed in agarose wells under an Olympus SZX12 stereomicroscope equipped with a micromanipulator.

They were micro-injected with a solution of 0.1 µg/µl Bmp4 protein (R&D Systems), 10% glycerol in Phenol Red/water, either anteriorly to the polster region or under the notochord, posterior to the head. Embryos were photographed under an Olympus SZX16 stereomicroscope and sorted according to the precise region of injection (marked by Phenol Red). They were fixed at 16 hpf or 28 hpf.

Behavioral testing

Four juveniles were placed in each of two behavioral testing boxes positioned on an infrared light source (ViewPoint). They were acclimatized for 2 h in the dark. Perfusion of the amino acid and control solution was initiated simultaneously as recordings started (Dragonfly2 camera, ViewPoint imaging software). A preference index score was calculated for each fish every 30 s, depending on its position relative to the amino acid source: +3 for the quadrant closest to the source, with +1, −1, −3 for the quadrants progressively further from the source (Fig. 7A; supplementary Materials and Methods). This score was then corrected for the position of the fish when the amino acid reached the box at 1.5 min after perfusion opening.

OE ablation

Ablation of the OE was adapted from Iqbal and Byrd-Jacobs (2010). One-month-old fish were anesthetized using 0.1% MS-222 (Sigma) in embryo medium (EM) and chemical ablation of each naris was performed using a solution of 0.05% Methylene Blue, 0.7% Triton X-100 in EM perfused continuously with a micro-injector (Eppendorf, Femtojet) for 90 s. After ablation, fish were allowed to recover for 24 h before being used for behavioral tests or fixed for immunohistochemistry.

Acknowledgements

We thank Stéphane Père and Diane Denis for *Astyanax* care; Laurent Legendre and Victor Simon for obtaining hybrids.

Competing interests

The authors declare no competing or financial interests.

Author contributions

H.H. and S.R. conceived and analyzed embryology experiments; H.H. performed the experiments with help from L.D. and M.B.; S.R., Y.E., J.B. and M.B. conceived and performed the behavior experiments; A.A. performed phylogenetic analyses; S.R. and H.H. wrote the paper.

Funding

This work was supported by Agence Nationale de la Recherche (ANR) grants (ASTYCO and BLINDTEST), a Fondation pour la Recherche Médicale (FRM) grant (Equipe FRM) and Centre National de la Recherche Scientifique (CNR) to S.R. H.H. was supported by Retina France and ANR; Y.B. by ANR and an FRM postdoctoral fellowship; and Y.E. by an FRM Engineer grant.

Data availability

The partial cDNA sequences for Astyanax mexicanus OMP (accession number KP826791.1), *Lhx3* (KP826792.1), *Pitx1* (KP826793.1) and *Pitx2* (KP826794.1) are available at GenBank.

Supplementary information

Supplementary information available online at
http://dev.biologists.org/lookup/doi/10.1242/dev.141291.supplemental

References

Ahrens, K. and Schlosser, G. (2005). Tissues and signals involved in the induction of placodal Six1 expression in Xenopus laevis. *Dev. Biol.* **288**, 40-59.

Alunni, A., Menuet, A., Candal, E., Pénigault, J.-B., Jeffery, W. R. and Rétaux, S. (2007). Developmental mechanisms for retinal degeneration in the blind cavefish Astyanax mexicanus. *J. Comp. Neurol.* **505**, 221-233.

Bailey, A. P. and Streit, A. (2006). Sensory organs: making and breaking the pre-placodal region. *Curr. Top. Dev. Biol.* **72**, 167-204.

Bailey, A. P., Bhattacharyya, S., Bronner-Fraser, M. and Streit, A. (2006). Lens specification is the ground state of all sensory placodes, from which FGF promotes olfactory identity. *Dev. Cell* **11**, 505-517.

Barth, K. A. and Wilson, S. W. (1995). Expression of zebrafish nk2.2 is influenced by sonic hedgehog/vertebrate hedgehog-1 and demarcates a zone of neuronal differentiation in the embryonic forebrain. *Development* **121**, 1755-1768.

Behrens, M., Wilkens, H. and Schmale, H. (1998). Cloning of the alphaA-crystallin genes of a blind cave form and the epigean form of Astyanax fasciatus: a comparative analysis of structure, expression and evolutionary conservation. *Gene* **216**, 319-326.

Bibliowicz, J., Alié, A., Espinasa, L., Yoshizawa, M., Blin, M., Hinaux, H., Legendre, L., Père, S. and Rétaux, S. (2013). Differences in chemosensory response between eyed and eyeless Astyanax mexicanus of the Rio Subterraneo cave. *EvoDevo* **4**, 25.

Borowsky, R. and Cohen, D. (2013). Genomic consequences of ecological speciation in astyanax cavefish. *PLoS ONE* **8**, e79903.

Bradic, M., Beerli, P., García-de León, F. J., Esquivel-Bobadilla, S. and Borowsky, R. L. (2012). Gene flow and population structure in the Mexican blind cavefish complex (Astyanax mexicanus). *BMC Evol. Biol.* **12**, 9.

Byrd, R. P., Jr and Caprio, J. (1982). Comparison of olfactory receptor (EOG) and bulbar (EEG) responses to amino acids in the catfish, Ictalurus punctatus. *Brain Res.* **249**, 73-80.

Campi, K. L. and Krubitzer, L. (2010). Comparative studies of diurnal and nocturnal rodents: differences in lifestyle result in alterations in cortical field size and number. *J. Comp. Neurol.* **518**, 4491-4512.

Chen, J. K., Taipale, J., Cooper, M. K. and Beachy, P. A. (2002). Inhibition of Hedgehog signaling by direct binding of cyclopamine to Smoothened. *Genes Dev.* **16**, 2743-2748.

Collin, S. P. (2012). The neuroecology of cartilaginous fishes: sensory strategies for survival. *Brain Behav. Evol.* **80**, 80-96.

Crish, S. D., Rice, F. L., Park, T. J. and Comer, C. M. (2003). Somatosensory organization and behavior in naked mole-rats I: vibrissa-like body hairs comprise a sensory array that mediates orientation to tactile stimuli. *Brain Behav. Evol.* **62**, 141-151.

Derby, C. D. and Sorensen, P. W. (2008). Neural processing, perception, and behavioral responses to natural chemical stimuli by fish and crustaceans. *J. Chem. Ecol.* **34**, 898-914.

Deyts, C., Candal, E., Joly, J. S. and Bourrat, F. (2005). An automated in situ hybridization screen in the medaka to identify unknown neural genes. *Dev. Dyn.* **3**, 698-708.

Dolensek, J. and Valentincic, T. (2010). Specificities of olfactory receptor neuron responses to amino acids in the black bullhead catfish (Ameiurus melas). *Pflugers Arch.* **459**, 413-425.

Dutta, S., Dietrich, J.-E., Aspöck, G., Burdine, R. D., Schier, A., Westerfield, M. and Varga, Z. M. (2005). pitx3 defines an equivalence domain for lens and anterior pituitary placode. *Development* **132**, 1579-1590.

Elipot, Y., Legendre, L., Père, S., Sohm, F. and Rétaux, S. (2014). Astyanax transgenesis and husbandry: how cavefish enters the lab. *Zebrafish* **11**, 291-299.

Espinasa, L., Bibliowicz, J., Jeffery, W. R. and Retaux, S. (2014). Enhanced prey capture skills in Astyanax cavefish larvae are independent from eye loss. *Evodevo* **5**, 35.

Evans, R. E. and Hara, T. J. (1985). The characteristics of the electro-olfactogram (EOG): its loss and recovery following olfactory nerve section in rainbow trout (Salmo gairdneri). *Brain Res.* **330**, 65-75.

Franz-Odendaal, T. A. and Hall, B. K. (2006). Modularity and sense organs in the blind cavefish, Astyanax mexicanus. *Evol. Dev.* **8**, 94-100.

Friedrich, R. W. and Korsching, S. I. (1997). Combinatorial and chemotopic odorant coding in the zebrafish olfactory bulb visualized by optical imaging. *Neuron* **18**, 737-752.

Furuta, Y. and Hogan, B. L. M. (1998). BMP4 is essential for lens induction in the mouse embryo. *Genes Dev.* **12**, 3764-3775.

Gross, J. B., Protas, M., Conrad, M., Scheid, P. E., Vidal, O., Jeffery, W. R., Borowsky, R. and Tabin, C. J. (2008). Synteny and candidate gene prediction using an anchored linkage map of Astyanax mexicanus. *Proc. Natl. Acad. Sci. USA* **105**, 20106-20111.

Gross, J. B., Stahl, B. A., Powers, A. K. and Carlson, B. M. (2016). Natural bone fragmentation in the blind cave-dwelling fish, Astyanax mexicanus: candidate gene identification through integrative comparative genomics. *Evol. Dev.* **18**, 7-18.

Guindon, S. and Gascuel, O. (2003). A simple, fast, and accurate algorithm to estimate large phylogenies by maximum likelihood. *Syst. Biol.* **52**, 696-704.

Hansen, A., Anderson, K. T. and Finger, T. E. (2004). Differential distribution of olfactory receptor neurons in goldfish: structural and molecular correlates. *J. Comp. Neurol.* **477**, 347-359.

Hara, T. J. (1994). Olfaction and gustation in fish: an overview. *Acta Physiol. Scand.* **152**, 207-217.

Hara, T. J. (2006). Feeding behaviour in some teleosts is triggered by single amino acids primarily through olfaction. *J. Fish Biol.* **68**, 810-825.

Hara, T. J. (2015). Taste in aquatic vertebrates. In *Handbook of Olfaction and Gustation*, Chapter 42, 3rd Edn. (ed. R. L. Doty), pp. 949-958. Chichester: Wiley-Blackwell.

Herzog, W., Sonntag, C., von der Hardt, S., Roehl, H. H., Varga, Z. M. and Hammerschmidt, M. (2004). Fgf3 signaling from the ventral diencephalon is required for early specification and subsequent survival of the zebrafish adenohypophysis. *Development* **131**, 3681-3692.

Hinaux, H., Pottin, K., Chalhoub, H., Père, S., Elipot, Y., Legendre, L. and Rétaux, S. (2011). A developmental staging table for Astyanax mexicanus surface fish and Pachon cavefish. *Zebrafish* **8**, 155-165.
Hinaux, H., Poulain, J., Da Silva, C., Noirot, C., Jeffery, W. R., Casane, D. and Rétaux, S. (2013). De Novo sequencing of Astyanax mexicanus surface fish and Pachon cavefish transcriptomes reveals enrichment of mutations in cavefish putative eye genes. *PLoS ONE* **8**, e53553.
Hinaux, H., Blin, M., Fumey, J., Legendre, L., Heuze, A., Casane, D. and Retaux, S. (2014). Lens defects in Astyanax mexicanus Cavefish: evolution of crystallins and a role for alphaA-crystallin. *Dev. Neurobiol.* **75**, 505-521.
Hüppop, K. (1987). Food-finding ability in cave fish (Astyanax fasciatus). *Int. J. Speleol.* **16**, 59-66.
Iqbal, T. and Byrd-Jacobs, C. (2010). Rapid degeneration and regeneration of the zebrafish olfactory epithelium after Triton X-100 application. *Chem. Senses* **35**, 351-361.
Jeffery, W. R. (2008). Emerging model systems in evo-devo: cavefish and microevolution of development. *Evol. Dev.* **10**, 265-272.
Jeffery, W. R. (2009). Evolution and development in the cavefish Astyanax. *Curr. Top. Dev. Biol.* **86**, 191-221.
Jeffery, W. R. (2010). Pleiotropy and eye degeneration in cavefish. *Heredity (Edin.)* **105**, 495-496.
Jeffery, W. R., Strickler, A. G., Guiney, S., Heyser, D. G. and Tomarev, S. I. (2000). Prox 1 in eye degeneration and sensory organ compensation during development and evolution of the cavefish Astyanax. *Dev. Genes Evol.* **210**, 223-230.
Karlstrom, R. O., Talbot, W. S. and Schier, A. F. (1999). Comparative synteny cloning of zebrafish you-too: mutations in the Hedgehog target gli2 affect ventral forebrain patterning. *Genes Dev.* **13**, 388-393.
Kiecker, C. and Niehrs, C. (2001). The role of prechordal mesendoderm in neural patterning. *Curr. Opin. Neurobiol.* **11**, 27-33.
Koide, T., Miyasaka, N., Morimoto, K., Asakawa, K., Urasaki, A., Kawakami, K. and Yoshihara, Y. (2009). Olfactory neural circuitry for attraction to amino acids revealed by transposon-mediated gene trap approach in zebrafish. *Proc. Natl. Acad. Sci. USA* **106**, 9884-9889.
Kondoh, H., Uchikawa, M., Yoda, H., Takeda, H., Furutani-Seiki, M. and Karlstrom, R. O. (2000). Zebrafish mutations in Gli-mediated hedgehog signaling lead to lens transdifferentiation from the adenohypophysis anlage. *Mech. Dev.* **96**, 165-174.
Korsching, S. I., Argo, S., Campenhausen, H., Friedrich, R. W., Rummrich, A. and Weth, F. (1997). Olfaction in zebrafish: what does a tiny teleost tell us? *Semin. Cell Dev. Biol.* **8**, 181-187.
Krubitzer, L., Campi, K. L. and Cooke, D. F. (2011). All rodents are not the same: a modern synthesis of cortical organization. *Brain Behav. Evol.* **78**, 51-93.
Kwon, H.-J., Bhat, N., Sweet, E. M., Cornell, R. A. and Riley, B. B. (2010). Identification of early requirements for preplacodal ectoderm and sensory organ development. *PLoS Genet.* **6**, e1001133.
Lindsay, S. M. and Vogt, R. G. (2004). Behavioral responses of newly hatched zebrafish (Danio rerio) to amino acid chemostimulants. *Chem. Senses* **29**, 93-100.
Lleras-Forero, L. and Streit, A. (2012). Development of the sensory nervous system in the vertebrate head: the importance of being on time. *Curr. Opin. Genet. Dev.* **22**, 315-322.
Ma, L., Parkhurst, A. and Jeffery, W. R. (2014). The role of a lens survival pathway including sox2 and alphaA-crystallin in the evolution of cavefish eye degeneration. *Evodevo* **5**, 28.
Martin, K. and Groves, A. K. (2006). Competence of cranial ectoderm to respond to Fgf signaling suggests a two-step model of otic placode induction. *Development* **133**, 877-887.
Menuet, A., Alunni, A., Joly, J.-S., Jeffery, W. R. and Retaux, S. (2007). Expanded expression of Sonic Hedgehog in Astyanax cavefish: multiple consequences on forebrain development and evolution. *Development* **134**, 845-855.
Mohammadi, M., McMahon, G., Sun, L., Tang, C., Hirth, P., Yeh, B. K., Hubbard, S. R. and Schlessinger, J. (1997). Structures of the tyrosine kinase domain of fibroblast growth factor receptor in complex with inhibitors. *Science* **276**, 955-960.
Nguyen, V. H., Schmid, B., Trout, J., Connors, S. A., Ekker, M. and Mullins, M. C. (1998). Ventral and lateral regions of the zebrafish gastrula, including the neural crest progenitors, are established by a bmp2b/swirl pathway of genes. *Dev. Biol.* **199**, 93-110.
Nummela, S., Pihlström, H., Puolamäki, K., Fortelius, M., Hemilä, S. and Reuter, T. (2013). Exploring the mammalian sensory space: co-operations and trade-offs among senses. *J. Comp. Physiol. A Neuroethol. Sens. Neural Behav. Physiol.* **199**, 1077-1092.
Park, T. J., Comer, C., Carol, A., Lu, Y., Hong, H. S. and Rice, F. L. (2003). Somatosensory organization and behavior in naked mole-rats: II. Peripheral structures, innervation, and selective lack of neuropeptides associated with thermoregulation and pain. *J. Comp. Neurol.* **465**, 104-120.
Pollen, A. A., Dobberfuhl, A. P., Scace, J., Igulu, M. M., Renn, S. C. P., Shumway, C. A. and Hofmann, H. A. (2007). Environmental complexity and social organization sculpt the brain in Lake Tanganyikan cichlid fish. *Brain Behav. Evol.* **70**, 21-39.
Pottin, K., Hyacinthe, C. and Retaux, S. (2010). Conservation, development, and function of a cement gland-like structure in the fish Astyanax mexicanus. *Proc. Natl. Acad. Sci. USA* **107**, 17256-17261.
Pottin, K., Hinaux, H. and Retaux, S. (2011). Restoring eye size in Astyanax mexicanus blind cavefish embryos through modulation of the Shh and Fgf8 forebrain organising centres. *Development* **138**, 2467-2476.
Protas, M., Conrad, M., Gross, J. B., Tabin, C. and Borowsky, R. (2007). Regressive evolution in the Mexican cave tetra, Astyanax mexicanus. *Curr. Biol.* **17**, 452-454.
Protas, M., Tabansky, I., Conrad, M., Gross, J. B., Vidal, O., Tabin, C. J. and Borowsky, R. (2008). Multi-trait evolution in a cave fish, Astyanax mexicanus. *Evol. Dev.* **10**, 196-209.
Reichert, S., Randall, R. A. and Hill, C. S. (2013). A BMP regulatory network controls ectodermal cell fate decisions at the neural plate border. *Development* **140**, 4435-4444.
Retaux, S. and Casane, D. (2013). Evolution of eye development in the darkness of caves: adaptation, drift, or both? *Evodevo* **4**, 26.
Riedel, G. and Krug, L. (1997). The forebrain of the blind cave fish Astyanax hubbsi (Characidae). II. Projections of the olfactory bulb. *Brain Behav. Evol.* **49**, 39-52.
Saint-Jeannet, J.-P. and Moody, S. A. (2014). Establishing the pre-placodal region and breaking it into placodes with distinct identities. *Dev. Biol.* **389**, 13-27.
Sarko, D. K., Rice, F. L. and Reep, R. L. (2011). Mammalian tactile hair: divergence from a limited distribution. *Ann. N. Y. Acad. Sci.* **1225**, 90-100.
Schemmel, C. (1967). Vergleichende Untersuchungen an den Hautsinnesorganen ober-and unter-irdisch lebender Astyanax-Foramen. *Z. Morph. Tiere.* **61**, 255-316.
Schlosser, G. (2006). Induction and specification of cranial placodes. *Dev. Biol.* **294**, 303-351.
Sjödal, M., Edlund, T. and Gunhaga, L. (2007). Time of exposure to Bmp signals play a key role in the specification of the olfactory and lens placodes ex vivo. *Dev. Cell* **13**, 141-149.
Streit, A. (2007). The preplacodal region: an ectodermal domain with multipotential progenitors that contribute to sense organs and cranial sensory ganglia. *Int. J. Dev. Biol.* **51**, 447-461.
Streit, A. (2008). *The Cranial Sensory Nervous System: Specification of Sensory Progenitors and Placodes*. *StemBook*, doi: 10.3824/stembook.1.31.1.
Strickler, A. G., Yamamoto, Y. and Jeffery, W. R. (2001). Early and late changes in Pax6 expression accompany eye degeneration during cavefish development. *Dev. Genes Evol.* **211**, 138-144.
Strickler, A. G., Byerly, M. S. and Jeffery, W. R. (2007). Lens gene expression analysis reveals downregulation of the anti-apoptotic chaperone alphaA-crystallin during cavefish eye degeneration. *Dev. Genes Evol.* **217**, 771-782.
Toro, S. and Varga, Z. M. (2007). Equivalent progenitor cells in the zebrafish anterior preplacodal field give rise to adenohypophysis, lens, and olfactory placodes. *Semin. Cell Dev. Biol.* **18**, 534-542.
Torres-Paz, J. and Whitlock, K. E. (2014). Olfactory sensory system develops from coordinated movements within the neural plate. *Dev. Dyn.* **243**, 1619-1631.
Treier, M., O'Connell, S., Gleiberman, A., Price, J., Szeto, D. P., Burgess, R., Chuang, P. T., McMahon, A. P. and Rosenfeld, M. G. (2001). Hedgehog signaling is required for pituitary gland development. *Development* **128**, 377-386.
Tricas, T. C., Kajiura, S. M. and Summers, A. P. (2009). Response of the hammerhead shark olfactory epithelium to amino acid stimuli. *J. Comp. Physiol. A Neuroethol. Sens. Neural Behav. Physiol.* **195**, 947-954.
Varatharasan, N., Croll, R. P. and Franz-Odendaal, T. (2009). Taste bud development and patterning in sighted and blind morphs of Astyanax mexicanus. *Dev. Dyn.* **238**, 3056-3064.
Varga, Z. M., Amores, A., Lewis, K. E., Yan, Y. L., Postlethwait, J. H., Eisen, J. S. and Westerfield, M. (2001). Zebrafish smoothened functions in ventral neural tube specification and axon tract formation. *Development* **128**, 3497-3509.
Vitebsky, A., Reyes, R., Sanderson, M. J., Michel, W. C. and Whitlock, K. E. (2005). Isolation and characterization of the laure olfactory behavioral mutant in the zebrafish, Danio rerio. *Dev. Dyn.* **234**, 229-242.
Wark, A. R. and Peichel, C. L. (2010). Lateral line diversity among ecologically divergent threespine stickleback populations. *J. Exp. Biol.* **213**, 108-117.
Wekesa, K. S. and Anholt, R. R. (1999). Differential expression of G proteins in the mouse olfactory system. *Brain Res.* **837**, 117-126.
Whitlock, K. E. and Westerfield, M. (2000). The olfactory placodes of the zebrafish form by convergence of cellular fields at the edge of the neural plate. *Development* **127**, 3645-3653.
Wilkens, H. (2010). Genes, modules and the evolution of cave fish. *Heredity (Edin.)* **105**, 413-422.
Yamamoto, Y. and Jeffery, W. R. (2000). Central role for the lens in cave fish eye degeneration. *Science* **289**, 631-633.
Yamamoto, Y., Espinasa, L., Stock, D. W. and Jeffery, W. R. (2003). Development and evolution of craniofacial patterning is mediated by eye-dependent and -independent processes in the cavefish Astyanax. *Evol. Dev.* **5**, 435-446.
Yamamoto, Y., Stock, D. W. and Jeffery, W. R. (2004). Hedgehog signalling controls eye degeneration in blind cavefish. *Nature* **431**, 844-847.

Yamamoto, Y., Byerly, M. S., Jackman, W. R. and Jeffery, W. R. (2009). Pleiotropic functions of embryonic sonic hedgehog expression link jaw and taste bud amplification with eye loss during cavefish evolution. *Dev. Biol.* **330**, 200-211.

Yoshizawa, M. and Jeffery, W. R. (2011). Evolutionary tuning of an adaptive behavior requires enhancement of the neuromast sensory system. *Commun. Integr. Biol.* **4**, 89-91.

Zhou, X. and Vize, P. D. (2004). Proximo-distal specialization of epithelial transport processes within the Xenopus pronephric kidney tubules. *Dev. Biol.* **271**, 322-338.

4. Neural Development and evolution in Astyanax mexicanus: comparing cavefish and surface fish brains

Neural Development and Evolution in *Astyanax mexicanus*: Comparing Cavefish and Surface Fish Brains

Sylvie Rétaux, Alexandre Alié, Maryline Blin, Lucie Devos, Yannick Elipot and Hélène Hinaux

Development and Evolution of the Forebrain, DECA Group, Neuroscience-Paris Saclay Institute, CNRS avenue de la terrasse, Paris, France

INTRODUCTION

Anybody who visits an *Astyanax* facility hosting surface fish and cavefish in adjacent tanks and who has a good sense of observation will at first have a hard time believing that they truly belong to the same species. Indeed, the two morphs look so different. Usually, the visitor first sees that one is depigmented and albino while the other is nicely colored. Then he rapidly gets a feeling that there is "something wrong" with the head of the cave morph, and he finds that the eyes are missing. These are the two main, obvious morphological differences.

The attentive observer will further compare the two types of fish and he will find much more. He will see that surface morphs swim in the water column and school, while cave morphs have a tendency to occupy the bottom half of the tank, and swim constantly on their own. He will notice that in the surface fish groups, one or two individuals constantly strike at some others, behaving as dominant in the school, and that this does not apply to cave morphs. On the other hand, he will be surprised by how well blind morphs navigate in their tank, almost never bumping on the aquarium walls or into their congeners. If he has the chance to visit the fish facility at feeding time, he will be struck by the fast and furious way the surface fish swim toward food; and he will appreciate the special feeding posture taken by cave morphs, which allows them to clean the food from the bottom of the tanks efficiently within a few minutes. These differences, together with some others that are not obvious at first sight (e.g., reduced sleep/increased wakefulness, attraction to vibrations or olfactory capabilities),

correspond to major behavioral differences between the two *Astyanax* morphs. They correspond to behaviors that can be classified as various types: (1) sensory; (2) motor; and (3) other, more complex and motivated behaviors, which all are governed by various parts of the nervous system.

What are the developmental and evolutionary mechanisms underlying the above-listed changes in the cavefish nervous system and its associated behaviors? Research in the field has mainly explored two directions that will be reviewed here.

First, comparative neurodevelopment and comparative neuroanatomy studies have revealed quantitative variations in the size of specific regions of the brain or in the number or size of specific sensory organs between cave and surface morphs. This type of variation can be coined as "neural specialization," supposedly in adaptation to environmental changes. For example, in the dark, it is probably advantageous to be "olfactory-oriented" to find food and mates, while in a lighted environment, it is important to maintain visual function. Classical cases of such brain evolutionary specialization come, for example, from nocturnal rodents in which the visual cortex is reduced, but the auditory and somato-sensory cortex is expanded (Campi and Krubitzer, 2010; Krubitzer et al., 2011). Among fishes, similar processes are described in cichlid fishes. In African lakes, very closely related cichlid species with distinct ecological specializations have significantly different brains: rock-dwellers (Mbuna) live in complex environments, engage in complex social interactions, and have a large telencephalon; while sand-dwellers (non-Mbuna) live in a simple environment, essentially use visually driven behaviors, and have a large optic tectum and thalamus. Interestingly, it has been shown that differences between Mbuna and non-Mbuna arise early in development, and that boundaries between brain regions, hence the respective sizes of these brain regions, are set up through antagonisms among signaling systems (Sylvester et al., 2010, 2013). In cave *Astyanax* as well, we will see that natural variations in nervous system patterning occur through early signaling modulations.

Second, some recent evidence suggests evolution of "brain neurochemistry" between cave and surface *Astyanax*. Indeed, even subtle changes in neuromodulatory systems are prone to generate significant variations in complex behaviors, such as motivated or social behaviors. This can be achieved if the number of neurons using a given neurotransmitter is changed (a situation that resembles the possibility discussed above, in which the size of a brain region or a neuronal group varies), or if the intensity or amount of neurotransmission is affected at the level of the synthesis, release, reception, modulation, or transduction of the signal. From a neurophysiological point of view, the behavioral syndrome—which is a correlated suite of behavioral phenotypes across multiple situations (Sih et al, 2004), such as those described above—exhibited by cave *Astyanax* clearly evokes the possibility of such disequilibrium in neuromodulatory transmitters.

ADULT BRAIN ANATOMY AND BRAIN NETWORKS

Figure 12.1 presents the comparative anatomy of adult Pachón cavefish and surface fish brains at the macroscopic level. As described by Riedel (1997), the cavefish brain is "slender and elongated." This impression is mainly due to the difference of shape of the telencephalon (trapezoidal in cavefish, ovoid in surface fish) and to the severe reduction in the width and global size of the optic tectum in cavefish (Figure 12.1(A) and (B)).

Concerning the telencephalon, volumetric studies indicate it is enlarged in the Pachón population, but not in other populations, such as Micos or Chica (Peters et al., 1993). The authors of this study hypothesized that telencephalic enlargement was due to the enhancement of the sense of taste, but this should be confirmed by connectivity studies. Qualitative and quantitative observations done in our laboratory in adults and juveniles also suggest that the olfactory bulbs are larger in cavefish (Figure 12.1(A) and (B); Rétaux and Bibliowicz, unpublished). Concerning olfactory connectivity, Riedel and Krug have documented

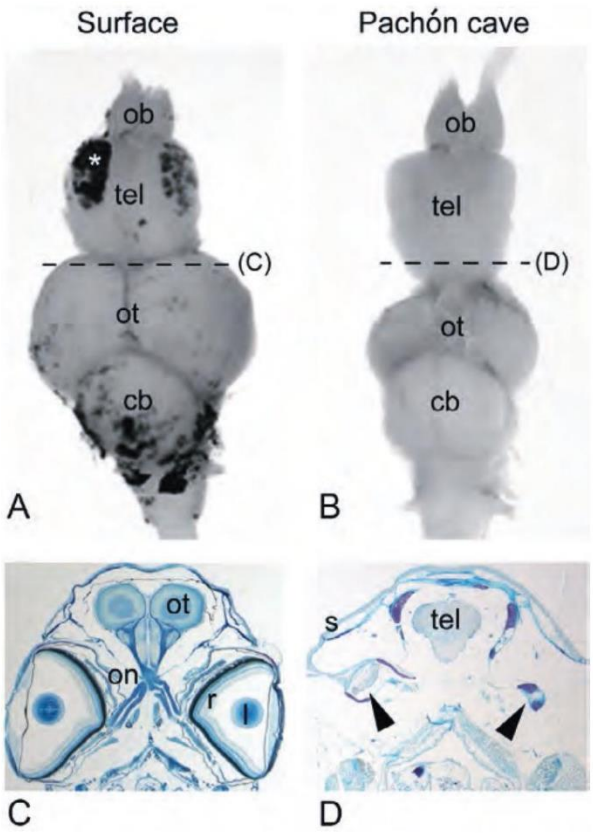

FIGURE 12.1 Comparing adult brains in *Astyanax* surface fish and Pachón cavefish. (A and B) show dorsal views of adult brains after dissection (anterior is up). The two individuals were of identical size (4 cm standard length). The dotted lines indicate the approximate section levels shown in (C) and (D). ob, olfactory bulbs; tel, telencephalon; ot, optic tectum; cb, cerebellum. (C and D) show frontal sections through the head of adult fish, after Klüver and Barrera coloration. The arrowheads on the Pachón picture show degenerated and cystic eye, partially calcified (dark/purple) and covered by skin. r, retina; l, lens; on, optic nerve; ot, optic tectum; s, skin.

that the projections of the olfactory bulb onto the cavefish telencephalon resemble a "simple Bauplan," and they concluded that the telencephalon is not dominated by olfactory inputs (Riedel and Krug, 1997); however, as they only analyzed the cavefish olfactory projections, no comparative surface fish data exists to determine olfactory specialization, or lack thereof, at this level.

At the diencephalic level, the major difference between the two morphs is the absence of eyes in cavefish, and is accompanied by a very severe reduction of the optic nerves (Riedel, 1997; Figure 12.1(C) and (D)). Despite evolution in complete darkness, cavefish have nevertheless conserved their "pineal eye"; the dorsal diencephalic pineal gland (or epiphysis) is structurally intact (Grunewald-Lowenstein, 1956; Herwig, 1976; Langecker et al., 1993; Omura, 1975) and has conserved the ability in larvae to detect light, probably thanks to correct rhodopsin expression (Yoshizawa and Jeffery, 2008). A specific and progressive regression of the regular outer-segment organization of pineal sensory cells nevertheless occurs in 3-, 9-, and 18-month-old cavefish, without affecting other parts of the pineal gland (Herwig, 1976). Interestingly, this regression begins earlier and is more obvious when cavefish are reared in constant darkness than when they are reared in light/dark conditions (Herwig, 1976), and it also occurs in constant light (Omura, 1975). This suggests that part of the degenerative process is attributable to a lack of light-activated neuronal activity.

Caudally, in the mesencephalon, the difference in the size of the optic tectum of the two morphs is striking (Figure 12.1(A) and (B)). This applies to all *Astyanax* cavefish populations examined, including Micos and Chica for which no difference was found with the surface fishes' telencephalon (Peters et al., 1993), or Los Sabinos (our personal observations), and to various extents that seem related to the degree of eye reduction. Logically, tectal hypomorphy has been linked to eye rudimentation (see below). Regarding the connection, as stated above, the optic nerve is greatly reduced, and projections from the retinal cyst are very sparse (Voneida and Sligar, 1976; Figure 12.1(C)). Some residual fibers can be seen in the superficial layers of the medial third of the tectum (as well as in the nucleus opticus hypothalamicus and lateral geniculate nucleus); however, this remnant visual connection is unresponsive to visual cues, and no electrophysiologically detectable signal can be recorded from the optic cyst onto the tectum (Voneida and Fish, 1984). This poses the question of the function of the cavefish "optic" tectum, which does indeed contain efferent pyramidal cells. The only evoked activity that is recordable in the cavefish tectum is generated after somatosensory stimulation (but not lateral line or auditory stimulation, which are invariably evoked in the torus semicircularis), and in a topographical manner (Voneida and Fish, 1984). As it is not unusual to find extravisual modality in the vertebrate tectum, the authors interpreted this finding as a decrease in visual inputs paralleled by an increase in somatic inputs, a situation that is comparable to experimental models following enucleation (e.g., Benedetti, 1992; Chabot et al., 2007; Champoux et al., 2008; Mundinano and Martinez-Millan, 2010). An interesting question would be to know whether the

visual-to-somatic rewiring in cavefish occurs during development as a plasticity phenomenon, in parallel to the progressive degeneration of the eye and the loss of visual innervation, or whether this rewiring is genetically programmed and has already been fixed during evolution in the dark. Comparison with visually deprived surface fish would start answering this question. More generally, cavefish are useful models when studying vision-related and vision-dependent neural plasticity phenomena.

A SPECIAL CASE: DEVELOPMENT AND DEGENERATION OF THE CAVEFISH VISUAL SYSTEM

The genetic mechanisms underlying eye loss in cavefish are reviewed in Chapter 11 of this book (Yamamoto et al.), and the evolutionary forces leading to eye loss have been discussed recently (Rétaux and Casane, 2013). Here, we will only briefly describe the progressive remodeling of the visual system that occurs in cavefish between embryonic and adult stages.

During cavefish early embryogenesis and larval development, an eye is formed from the diencephalic neuroepithelium and its adjacent lens placode. This eye starts forming retinal layers (Alunni et al., 2007) and the proliferative zones of both the retina and the lens are active, although they are smaller than in surface fish larvae (Alunni et al., 2007; Hinaux et al., 2015; Strickler et al., 2002; Figure 12.2(C′) and (D′)). In fact, retinal cells are constantly born and are incorporated into the retina, while concomitantly many retinal cells die by apoptosis. At the end, cell death will win the battle against neurogenesis, and the eye will disappear (Figure 12.1(D)). The initial trigger for eye degeneration in cavefish is thought to be lens apoptosis; transplantation of a surface fish lens into a cavefish optic cup is able to rescue the eye of the cavefish while the reciprocal experiment induces the degeneration of the surface fish eye (Yamamoto and Jeffery, 2000).

The optic tectum, a brain region that derives from the alar plate of the mesencephalon and that constitutes the major retinorecipient structure in the brains of fishes and amphibians, is also patterned and regionalized properly in cavefish. The presumptive optic tectum expresses *Pax6*, *Pax2*, *Engrailed2* in domains of equivalent sizes in the two morphs (Soares et al., 2004; see *Lhx9* in Figure 12.2(A) and (B)). During the first days of development, proliferation is also equivalent in the dorsal mesencephalon of cave and surface larvae (Menuet et al., 2007; Blin and Rétaux, unpublished observations) (see proliferating cell nuclear antigen (PCNA) in Figure 12.2(C) and (D)). When the DiI tracing technique is applied on the initial cavefish retinotectal projection at 36 or 72 h post-fertilization (hpf), it is found that the optic nerve develops from the axons of the first generated retinal ganglion cells, reaches the tectum, and even arborizes on its target (Soares et al., 2004). This may explain why cavefish may be able to see, or at least to have some visual abilities, very transiently, during their first days of life, as suggested by positive electroretinograms and

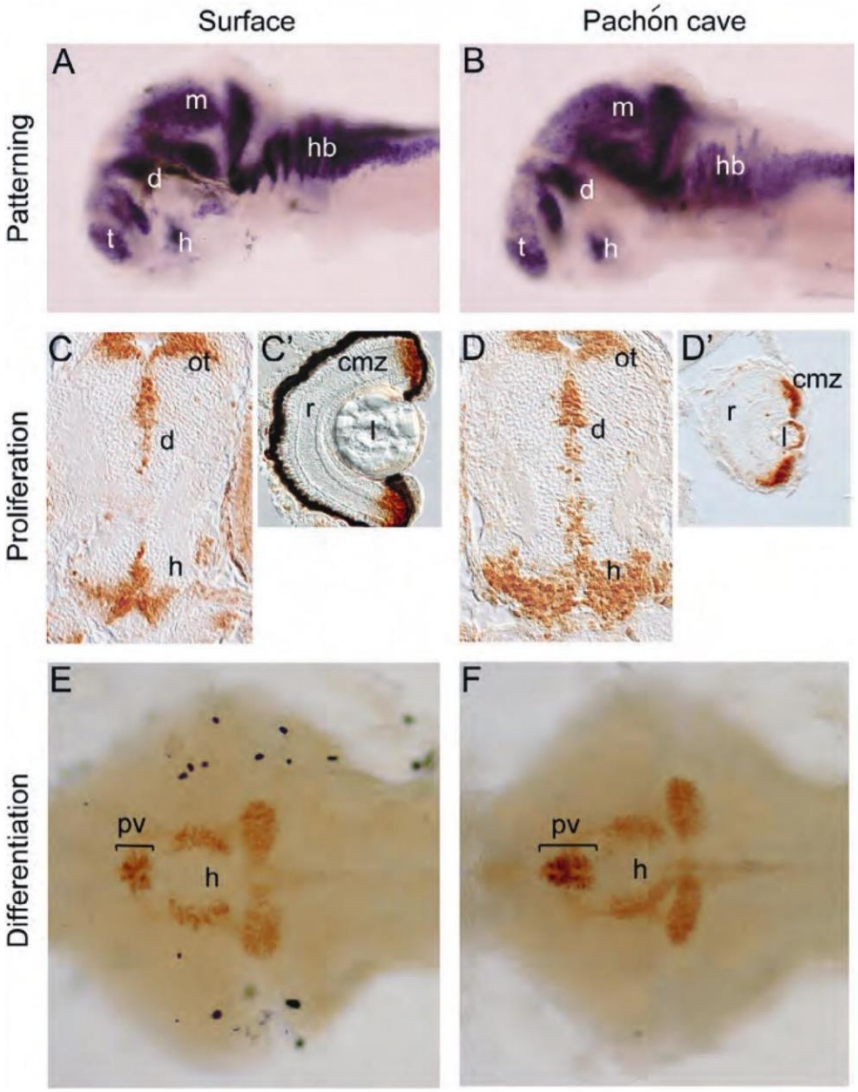

FIGURE 12.2 Comparing larval brain development in *Astyanax* surface fish and Pachón cavefish. (A and B) Patterning of the 36 hpf brain, as observed through the expression of the LIM-homeodomain transcription factor *Lhx9*, *in toto*, on a lateral view. Anterior is left and dorsal is up. t, telencephalon; d, diencephalon; h, hypothalamus; m, midbrain; hb, hindbrain. (CC′ and DD′), proliferation in the 60 hpf larval brain (C and D) and in the 7 dpf eye (C′ and D′), as viewed through PCNA immunohistochemistry on frontal sections. d, diencephalon; h, hypothalamus; ot, optic tectum; r, retina; l, lens; cmz, ciliary marginal zone. (E and F) Differentiated neurons in the hypothalamus (h) and the paraventricular nucleus (pv) at 7 dpf, illustrated here for the serotonergic system on a ventral view of a dissected brain after serotonin immunostaining, *in toto*. Anterior is left.

prey-catching behavior (Daphne Soares, communication at AIM2009); however, as rhodopsin is apparently not expressed in the cavefish retina around these stages (Yoshizawa and Jeffery, 2008), the underlying visual circuit and visual transduction mechanism is therefore unclear and deserves further studies.

As mentioned above, though, the adult cavefish tectum is much reduced in volume (−50%) and contains less neurons (−20%) than in surface fish (Soares et al., 2004). To our knowledge, cell death (by apoptosis, necrosis, or autophagy) has not been investigated in the cavefish optic tectum during the period of

tectal shrinkage. To investigate directly whether tectal regression was a secondary consequence of eye degeneration, the lens transplantation model was used. In lens-transplanted cavefish with a restored eye (on one side only), the size of the corresponding optic nerve and the extant of contralateral tectal innervation are increased; however, the procedure results in only a slight increase in tectal volume (+13%) and tectal neuron number (+8%) (Soares et al., 2004), which hardly compares to the surface fish situation. Importantly, it seems that lens transplantation in cavefish restores the eye as an organ, but does not restore vision-based response, tested in a phototaxis assay (Romero et al., 2003). Thus, in cavefish that received embryonically a surface fish lens, an eye and a retinotectal projection is present (Soares et al., 2004), but this visual system is probably not active or functional. This data strongly suggests that the reduced size of the optic tectum in cavefish is indeed a secondary consequence of eye degeneration, and indicates activity-dependent mechanisms that are probably lacking at the tectal level to maintain the integrity of the structure.

EARLY EMBRYONIC DEVELOPMENT: THE ORIGIN OF CAVEFISH DIFFERENCES?

Fortunately for EvoDevo studies, surface fish and cavefish embryos develop at the same pace, allowing rigorous comparisons of early embryogenesis and larval stages (Hinaux et al., 2011). At the end of gastrulation, at 9.5-10 hpf, Pachón cavefish embryos have a slightly ovoid shape resembling a rugby ball, whereas surface fish embryos exhibit a rounder shape (Hinaux et al., 2011). According to the literature, such a phenotype suggests a slight change in dorsoventral patterning during early embryogenesis (e.g., Barth et al., 1999; Kishimoto et al., 1997; Neave et al., 1997). *Bmp* and *Wnt* signaling molecules and activities have not yet been investigated significantly and in a comparative manner between cavefish and surface fish embryos, but it is well established that Hedgehog expression (Sonic and Tiggy-Winckle) is expanded at the anterior ventral midline during gastrulation (Pottin et al., 2011; Yamamoto et al., 2004; Figure 12.3(A)). Such Hedgehog hypersignaling from the mesoderm in the cavefish gastrula is indirectly responsible, through unknown mechanisms, for lens apoptosis and subsequent eye loss (Yamamoto et al., 2004). As demonstrated by pharmacological manipulations, Hedgehog hypersignaling also affects the precise onset of expression of other signaling molecules such as *Fgf8*, although it does not apparently change *Fgf3* expression (Pottin et al., 2011; Figure 12.3(A)). In fact, Hedgehog heterotopy (expanded expression) and *Fgf8* heterochrony (earlier expression) at the anterior margin of the cavefish neural plate affects the patterning and morphogenesis of its future forebrain. Both the expression patterns of several transcription factors that prefigure the presumptive territories of the retina and other forebrain regions (*Pax6*, *Lhx2/Lhx9*) and the neural plate fate map are slightly modified in cavefish, precisely at midline level where Hedgehog and *Fgf8* signaling are

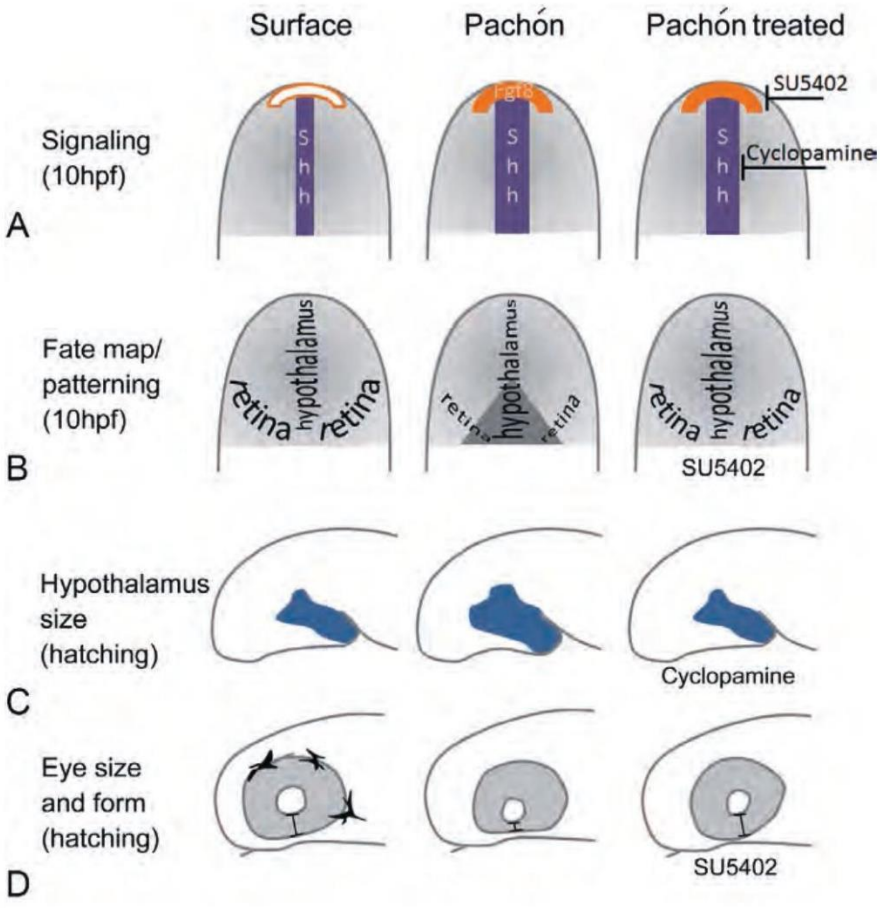

FIGURE 12.3 Comparing the neural plate and embryonic brain morphogenesis in *Astyanax* surface fish and Pachón cavefish. The first and second columns show surface fish and cavefish, respectively. In the third column, the patterning and morphogenetic effects of Hedgehog signaling inhibition by cyclopamine or *FgfR* signaling inhibition by SU5402 on Pachón embryos are depicted and resemble the surface fish phenotype. Schemas are drawn according to experimental evidences from several articles (Menuet et al., 2007; Pottin et al., 2011; Rétaux et al., 2008; Yamamoto et al., 2004). (A) Signaling systems at neural plate stage, schematized on a dorsal view (anterior is up). *Shh* expression (dark/purple at the midline) is larger and *Fgf8* expression (gray/orange at the anterior neural border) is earlier in cavefish. Note: *Fgf8* is not expressed at this early stage in surface fish. (B) Neural fate map and neural plate patterning. The regions of the neural plate fated to become the hypothalamus and the retina are indicated. Several anterior neural plate genes (*Lhx2*, *Lhx9*, *Zic1*, and *Pax6*) show a lack of expression at the cavefish midline (gray). In surface fish embryos, these midline cells are fated to give rise to the ventral quadrant of the retina, which is absent in cavefish. In cavefish, cells located in the equivalent zone of the neural plate (gray triangle) contribute to the hypothalamus or the dorsal retina. (C) Size of the hypothalamus, as labeled by *Nkx2.1a*, on a lateral view of a schematic brain at 24hpf (anterior is left and dorsal is up). (D) Morphology of the eye. Black brackets indicate the ventral quadrant of the retina, strongly reduced in cavefish and restored after SU5402 treatment. Pigment cells on the surface fish eye are drawn.

changed (Pottin et al., 2011; Strickler et al., 2001; Figure 12.3(B)). We have proposed that medial neural plate cells that are normally fated to become the ventral part of the retina instead contribute to the hypothalamus in cavefish (Pottin et al., 2011). At the end of neurulation, the resulting morphology is an eye with a missing ventral quadrant and a forebrain with an enlarged presumptive hypothalamic territory (Figure 12.3(C) and (D)).

Importantly, *Shh* expression is also expanded in Chica and Los Sabinos embryos, and their *Pax6* medial neural plate pattern is modified the same way as in Pachón embryos (Jeffery, 2009; Strickler et al., 2001; Yamamoto et al., 2004). This tells us that similar developmental processes are modulated in independently evolved cavefish populations, and give rise to the same phenotypes. In fact and more generally, in cavefish embryos from all populations examined so far, the eyes first develop and then regress. This observation can even be extended to other cave vertebrates, including mammals, fishes, and amphibians (reviewed in Rétaux and Casane, 2013). Although this could be viewed as a waste of energy for a developing embryo, we have proposed that optic cup morphogenesis corresponds to a developmental constraint and probably cannot be circumvented (Pottin et al., 2011; Rétaux and Casane, 2013). Indeed, from a morphogenetic point of view, the vertebrate forebrain cannot develop properly without undergoing coordinated cell movements that include the initial formation of the visual organ (e.g., England et al., 2006; Rembold et al., 2006).

LARVAL BRAIN DEVELOPMENT: ESTABLISHING SUBTLE DIFFERENCES

During neurulation and after hatching, cavefish continuously display expanded *Shh* expression in all anterior basal forebrain domains (Menuet et al., 2007). In conjunction with the above described consequences of midline-dependent early morphogenetic events, sustained *Shh* hypersignaling affects neuronal patterning in a subtle manner—and to an extent that is developmentally tolerable, viable, and possibly even adaptive. Indeed, the global regionalization of the cavefish brain remains correct and unaffected, as shown by standard expression patterns of all "developmental" genes investigated (see *Lhx9*, e.g., in Figure 12.2(A)).

In the cavefish ventral telencephalon or subpallium, the expression domains of *Shh*, *Nkx2.1b* (a marker of the medial part of the subpallium and the preoptic region) and the *Nkx2.1*-dependent LIM-homeodomain factors *Lhx6* and *Lhx7* (Grigoriou et al., 1998; Sussel et al., 1999) are enlarged (Menuet et al., 2007). This enlargement appears specific to ventral telencephalic neural components under the control of this particular developmental "cascade," as the *Dlx2* or *Nkx2.2* expression domains are unchanged when compared to surface fish. Interestingly, *Nkx2.1b* and *Lhx6* happen to label a population of GABAergic interneurons that migrate tangentially to populate the olfactory bulbs (Menuet et al., 2007), and that we hypothesized to be the equivalent of the mammalian rostral migratory stream (e.g., Lois and Alvarez-Buylla, 1994). As a positive correlation between the abundance of olfactory bulb interneurons and olfactory performance is reported, it is tempting to speculate that the *Shh*-dependent increase in GABA/*Lhx6*/*Nkx2.1b*-positive migratory stream in cavefish could be advantageous for their life in perpetual darkness.

The cavefish hypothalamus, as labeled with *Shh*, with *Nkx2.1a* and *Nkx2.1b* regional markers, with *Lhx6* subterritory marker, or else as assayed

for proliferation (Figure 12.2(B)), appears larger and actively proliferating compared with surface fish (Menuet et al., 2007; Rétaux et al., 2008). Increased proliferation is observed specifically in the hypothalamic and preoptic territories, but not in the more dorsally located diencephalic or mesencephalic regions (Figure 12.2(B)), and a treatment of cavefish embryos with the *Shh*-signaling inhibitor cyclopamine diminishes hypothalamic proliferation and size. This suggests a region-specific, *Shh*-dependent control of proliferation and possibly neurogenesis in the hypothalamus, opening the interesting possibility that this neuroendocrine brain region, which contains many neuronal groups expressing neuromodulatory transmitters, such as monoamines and neuropeptides, has evolved in cavefish.

Is the entire hypothalamus/preoptic region, then, enlarged in cavefish? Or are specific neuronal groups affected, while others are unchanged? Some recent insights came from the comparative analysis of the serotonin neurotransmitter system (Elipot et al., 2013). First, a 4-h heterochrony exists between the appearance of the first serotonin-expressing neurons in the anterior hypothalamus of cavefish (at 18 hpf) and surface fish (at 22 hpf). This may be related to the differences in proliferation/neurogenesis control discussed above. Second, the resulting serotonergic group is larger and contains more cells in cavefish; however, the size of other, more posterior hypothalamic serotonin neuronal groups is identical in cave and surface larvae (Figure 12.2(C)), showing a finely regulated and group-specific regulation of neuron numbers. Third, the size difference in the anterior group is *Shh*-dependent. And finally, this anatomical variation in serotonin circuits seems to translate into behavioral differences, namely an increase in foraging behavior (Elipot et al., 2013).

Much remains to be investigated in a comparative manner on neural patterning, differentiation, and wiring in the larval cavefish brain. But the few aspects that have been investigated so far indicate that we will probably discover discrete, specific, and multiple variations in neuronal patterning in cavefish that result from early embryonic events that change subtle aspects of behavior, and that illustrate the morphogenetic and functional outcomes of developmental evolution and variations.

SENSORY SYSTEMS

The idea of a sensory compensation for absence of vision in animals living in the dark is "classical" and was proposed by early authors, and has been regularly reviewed since (Barr, 1968; Niemiller and Poulson, 2010; Soares and Niemiller, 2013; Wilkens, 1988). Longer appendages in insects and lateral line modifications in fish were often cited. More recently, the idea of sensory modules that would either be developmentally and genetically independent, or that would interact together, and upon which natural selection could act, has been put forward (Franz-Odendaal and Hall, 2006; Wilkens, 2010). Below, we briefly review available data on the developmental evolution of chemosensation

(gustation, olfaction) and mechanosensation (lateral line) systems in *Astyanax*. Of note, although hearing is an important sense for aquatic organisms, differences in auditory capacities have not been reported for cavefishes, including for *Astyanax* (Popper, 1970).

Chemosensory System

A better chemical sense has long been suggested for cave *Astyanax* (Breder and Rasquin, 1943; Humbach, 1960). Strikingly, according to Humbach's observation, blind cavefish would have a sense of taste 300 times more acute for bitter and 2000-4000 times more acute for salty, acid, and sweet substances than *Phoxinus* (a minnow, cyprinid); however, these early studies did not strictly discriminate between olfaction and gustation.

Olfaction is surprisingly poorly studied. A "classical" development of the olfactory organs and their lamellae from ectodermal placodes was described in *Astyanax* (Schemmel, 1967). Quantification of the continuously increasing number of olfactory lamellae in surface fish and the Pachón and Los Sabinos cavefishes throughout their lives shows no significant difference. Schemmel concluded that the olfactory modality cannot be considered as specialized in cavefish. He noted, however, that nasal capsules are more opened and flattened in cavefish, so that lamellae are more exposed. More recently, using *in situ* recordings in the Subterráneo cave, which hosts a hybrid population of mixed troglomorphic and epigean characters, we have found that troglomorphic fish present significantly larger naris size, and this was associated with a strong behavioral response elicited by food extracts (Bibliowicz et al., 2013), opening the possibility that olfactory abilities might have evolved in cave-dwelling *Astyanax*.

Concerning gustation, Schemmel was also the first to describe an increased number of tastebuds in Los Sabinos, and even more in Pachón cavefish (Schemmel, 1967). He reported a several-fold increase in tastebud numbers in adults (Schemmel, 1974). More precisely, three different types of tastebuds are distributed on the lips and oral cavity of both *Astyanax* morphs, but only cavefish harbor some on their lower jaws (Boudriot and Reutter, 2001). Moreover, the nerve fiber plexuses of type II and III tastebuds contain more axons in cavefish (Boudriot and Reutter, 2001), and there are more sensory receptor cells per tastebud in cavefish (Varatharasan et al., 2009). Such an enlarged and predominantly ventrally spread gustatory area on the skin of the head was interpreted as functionally relevant to localize food situated on the bottom, and considered as a compensatory improvement of the sense of taste. Interestingly, Substance P is found in tastebuds of cavefish, but not surface fish or other teleosts (Bensouilah and Denizot, 1991). These authors have proposed that the presence of this neurotransmitter could modulate the threshold of excitability of the taste cells.

In fact, tastebud number amplification in cavefish is already present in the first days post-fertilization (dpf) (Varatharasan et al., 2009; Yamamoto et al.,

2009), and the rate of tastebud development is accelerated in cavefish larvae; the difference with surface fish larvae is small at 5 dpf, but threefold at 22 dpf (Varatharasan et al., 2009). That these differences are detectable only after the onset of eye degeneration and that they increase during the degeneration process suggests a link between gustatory and visual development, a notion that is supported by functional experiments (Yamamoto et al., 2009): (1) *Shh* hypersignaling in the oropharyngeal region of cavefish embryos is responsible for tastebud number amplification; (2) early conditional overexpression of *Shh* in surface fish induces positive effects on later tastebud development and negative effects on eye development in the same embryos; and (3) there is an inverse relationship between eye size and tastebud number in the progeny of crosses between surface and cave *Astyanax*. This constitutes the only example to date of a direct link between the development of two sensory organs involving a pleiotropic effect of *Shh* and suggesting indirect selection as an evolutionary driving force for eye loss in cavefish.

Lateral Line

It has been long known that cavefish (Pachón, Los Sabinos, Chica) possess more free (superficial) neuromasts in the suborbital region of their face, and more fragmentation of infraorbital canal neuromasts than surface fish (Bensouilah and Denizot, 1991; Jeffery et al., 2000; Schemmel, 1967). More recently, Yoshizawa and colleagues (2010, 2012) have reported that neuromasts found at a high density in the suborbital and eye orbit region of cavefish mediate the vibration attraction behavior (VAB). Indeed, cavefish are specifically attracted by vibrations at about 35 Hz at the surface of the water, a behavior that clearly seems advantageous to find food in the dark (Yoshizawa et al., 2010). Of note, the morphology of cavefish sensory receptors also differ; the cupula (hair stereo-cilia covered by gelatinous case) of their free head neuromasts is up to 300 µm in length, compared to about 42 µm in surface fish (Teyke, 1990; see also Varatharasan et al., 2009), and is also larger, as are the neuromasts themselves (Yoshizawa et al., 2010). As the height and diameter of the cupula regulate sensitivity, these large, free neuromasts are twice as sensitive in young adults than smaller ones (Yoshizawa et al., 2014). This could explain why cavefish neuromasts can detect low frequency stimuli (below 50 Hz) in otherwise calm cave pools.

The cavefish VAB-mediating neuromasts develop late, after 2 months of age, when the eye is completely gone (Yoshizawa et al., 2010), which may explain why they invade the cavefish eye orbit region. Moreover, and contrarily to the case of tastebuds discussed above, experimental induction of eye regression in surface fish via Hedgehog overexpression is insufficient to increase the number of orbital neuromasts or to promote the appearance of the VAB (Yoshizawa et al., 2012). It will, therefore, be crucial to understand the developmental mechanisms controlling the timing of head neuromast organogenesis and the

size of individual sensory organs, as well as to determine the neuronal circuits underpinning the VAB. Considering that some cavefish populations (Pachón, Los Sabinos, or Piedras), but not others (Molino), exhibit a strong form of VAB, this system is ideal to investigate the origin of neural and behavioral novelty during evolution.

CAVEFISH BRAIN NEUROCHEMISTRY

The ensemble of cavefish behavioral modifications described in the introduction is sometimes referred to as a "behavioral syndrome," which would appear quite pathological to a clinician, to whom the cavefish condition would probably evoke disorders involving neuromodulatory and aminergic transmission. Actually, we currently know two genes that are important players in these neurotransmitter systems, and which carry mutations in their coding sequence in cavefish: *Oca2* and monoamine oxidase (MAO) (Elipot et al., 2014a; Protas et al., 2006). Moreover, several relevant genes (such as the 14-3-3 protein YWHAE, the glutamate receptor AMPA2 or the cannabinoid receptor CB1) whose expression is altered in cavefish were recently identified through a microarray study (Strickler and Soares, 2011). These genes play roles in neural networks controlling learning, feeding, or addiction, and could therefore underlie some of the cavefish behavioral phenotypes.

Oca2 (ocular and cutaneous albinism-2) is a transmembrane protein involved in the transport of L-tyrosine, the precursor of melanine, into melanosomes. Its mutation in cavefish (Protas et al., 2006) explains the depigmented phenotype that is reviewed in Chapter 8 of this book (Jeffery et al.). But L-tyrosine also happens to be the precursor of dopamine and noradrenalin, two central monoamines, therefore opening the possibility that an expanded L-tyrosine pool is available as a precursor for dopamine in cavefish. In line with this idea, *Oca2* morpholino knockdown in surface fish embryos increases both L-tyrosine and dopamine levels (Bilandžija et al., 2013b), and dopamine and noradrenalin levels are very high in the brains of young adult cavefish when compared with surface fish (Elipot et al., 2014a). Importantly, *Oca2* carries different loss of function mutations in various *Astyanax* cavefish populations (Protas et al., 2006) and more generally, the first step in melanin synthesis is also affected in other cave-dwelling animals, including insects (Bilandžija et al., 2013a), showing striking convergence on a defect in this particular pathway. Of note, the direct link between a large pool of available L-tyrosine due to the *Oca2* deficiency and the high levels of dopamine in the brain of cavefish remains unclear, because the activity of tyrosine hydroxylase, the rate-limiting enzyme of dopamine synthesis, is identical in the brains of surface and cave morphs (Elipot et al., 2014a). An interesting research venue may be offered by the fact that the dopamine synthesis activator gene *YWHAE* is up-regulated in cavefish (Strickler and Soares, 2011). Finally and behaviorally, high noradrenalin levels in cavefish probably play a role in reduced sleep/increased wakefulness, as

suggested by sleep rescue after beta-noradrenergic receptor blockade (Duboue et al., 2012). And high dopamine levels may underlie feeding drive and reward-associated responses (Singh, 2014).

MAO is the serotonin-degrading enzyme. It carries a partial loss-of-function point mutation in Pachón cavefish, leading to very high serotonin levels in the brain (Elipot et al., 2014a). Note that there is only one form of MAO in teleosts, whereas mammals have two. Combined with the larger anterior hypothalamic serotonergic group, this mutation could contribute to the cavefish's persistent foraging behavior (Elipot et al., 2013). The MAO mutation is also likely to explain other cavefish behavioral phenotypes; in surface fish treated with deprenyl, a specific MAO inhibitor, serotonin levels (but not dopamine or noradrenalin) are increased, therefore mimicking the cavefish condition (Elipot et al., 2014a), and both schooling behavior (Kowalko et al., 2013) and hierarchical aggressiveness (Elipot et al., 2013) are lost. The serotonergic raphe nucleus in the hindbrain is probably involved in the loss of aggressiveness. Indeed, low raphe serotonin levels are associated with dominant individuals in surface fish groups, and it is possible to elicit some aggressiveness in cavefish by embryonic manipulations that reduce the size of their raphe serotonergic nucleus (Elipot et al., 2013). On the other hand, the serotonin-dependent brain circuits involved in loss of schooling are unknown, but we have proposed that the lack of collective behaviors in cavefish is probably tightly related to their loss of hierarchical and aggressive behavior (Rétaux and Elipot, 2013 and see also this book, Chapter 17).

In sum, we are at the beginnings of our understanding of cavefish brain neurochemistry, but all the data accumulated so far suggest that the subtle equilibrium and neurotransmission homeostasis present in vertebrate brains are unbalanced in more than a few ways in cavefish. Along the same lines, some "general" neurotransmission genes, such as neuroligin or the neurofilament protein M seem up- or down-regulated in cavefish, respectively, according to cross-species (zebrafish) microarray experiments (Strickler and Jeffery, 2009). Neuroligin is a postsynaptic adhesion molecule thought to control the balance between excitatory and inhibitory synapses (Mackowiak et al., 2014) and NF-M is a cytoskeleton component that regulates axonal growth and homeostasis (Yuan et al., 2012). Therefore, such dysregulations might also have general effects on cavefish neural functions, but their origin and their exact impacts have not yet been investigated.

CONCLUSIONS AND PERSPECTIVES

The *Astyanax* model system is now entering the genome era, with the available Pachón genome (McGaugh et al., 2014) and the exciting possibilities offered by transgenesis and genome-editing techniques (Elipot et al., 2014b; see also Chapter 19 by Burgess et al. in this book). Such progress will render possible many new lines of investigations. Comparative genomics will allow the investigation of *cis*-regulatory aspects in the evolution of gene regulation. Loss and gain

of function experiments in cave and surface morphs will decipher the exact roles and effects of mutations identified in cavefish. With the generation of transgenic fluorescent reporter cavefish and surface fish lines, researchers will be able to compare early cavefish brain morphogenesis and growth by 3D live imaging, or to analyze and manipulate neuronal activity *in vivo*. In other words, the cavefish has become a top model for neuroscience research for investigators interested in brain evolution and morphological, functional, and behavioral adaptation.

ACKNOWLEDGMENTS

Work in the group was supported by ANR grant (Astyco) and (Blindtest) and CNRS. Many thanks to Franck Bourrat for sectioning and coloration of adult *Astyanax* heads, to Stéphane Père, Magalie Bouvet and Diane Denis for taking care of our *Astyanax* colony, and to Laurent Legendre for collaborative help on husbandry methods.

REFERENCES

Alunni, A., et al., 2007. Developmental mechanisms for retinal degeneration in the blind cavefish *Astyanax mexicanus*. J. Comp. Neurol. 505, 221–233.

Barr, T.C., 1968. Cave ecology and the evolution of troglobites. In: Dobzhansky, Th., Hecht, M.K., Steere, W.C. (Eds.), Evolutionary Biology, vol. 2. Plenum Press, New York, pp. 35–101.

Barth, K.A., et al., 1999. Bmp activity establishes a gradient of positional information throughout the entire neural plate. Development 126, 4977–4987.

Benedetti, F., 1992. The development of the somatosensory representation in the superior colliculus of visually deprived mice. Brain Res. Dev. Brain Res. 65, 173–178.

Bensouilah, M., Denizot, J.P., 1991. Taste buds and neuromasts of *Astyanax jordani*: distribution and immunochemical demonstration of co-localized substance P and enkephalins. Eur. J. Neurosci. 3, 407–414.

Bibliowicz, J., et al., 2013. Differences in chemosensory response between eyed and eyeless *Astyanax mexicanus* of the Rio Subterráneo cave. EvoDevo 4, 25.

Bilandžija, H., et al., 2013a. Evolution of albinism in cave planthoppers by a convergent defect in the first step of melanin biosynthesis. Evol. Dev. 14, 196–203.

Bilandžija, H., et al., 2013b. A potential benefit of albinism in *Astyanax* cavefish: downregulation of the *oca2* gene increases tyrosine and catecholamine levels as an alternative to melanin synthesis. PLoS ONE 8, e80823.

Boudriot, F., Reutter, K., 2001. Ultrastructure of the taste buds in the blind cave fish *Astyanax jordani* ("Anoptichthys") and the sighted river fish *Astyanax mexicanus* (Teleostei, Characidae). J. Comp. Neurol. 434, 428–444.

Breder, C.M., Rasquin, P., 1943. Chemical sensory reactions in the Mexican blind characins. Zoologica 28, 169–200.

Campi, K.L., Krubitzer, L., 2010. Comparative studies of diurnal and nocturnal rodents: differences in lifestyle result in alterations in cortical field size and number. J. Comp. Neurol. 518, 4491–4512.

Chabot, N., et al., 2007. Audition differently activates the visual system in neonatally enucleated mice compared with anophthalmic mutants. Eur. J. Neurosci. 26, 2334–2348.

Champoux, F., et al., 2008. Effects of early binocular enucleation on auditory and somatosensory coding in the superior colliculus of the rat. Brain Res. 1191, 84–95.

Duboue, E.R., et al., 2012. β-Adrenergic signaling regulates evolutionarily derived sleep loss in the Mexican cavefish. Brain Behav. Evol. 80 (4), 233–243.

Elipot, Y., et al., 2013. Evolutionary shift from fighting to foraging in blind cavefish through changes in the serotonin network. Curr. Biol. 23 (1), 1–10.

Elipot, Y., et al., 2014a. A mutation in the enzyme monoamine oxidase explains part of the Astyanax cavefish behavioral syndrome. Nat. Commun. 5, 3647.

Elipot, Y., et al., 2014b. *Astyanax* transgenesis and husbandry: how cavefish enters the lab. Zebrafish 11 (4), 291–299.

England, S.J., et al., 2006. A dynamic fate map of the forebrain shows how vertebrate eyes form and explains two causes of cyclopia. Development 133, 4613–4617.

Franz-Odendaal, T.A., Hall, B.K., 2006. Modularity and sense organs in the blind cavefish, *Astyanax mexicanus*. Evol. Dev. 8, 94–100.

Grigoriou, M., et al., 1998. Expression and regulation of *Lhx6* and *Lhx7*, a novel subfamily of LIM homeodomain encoding genes, suggests a role in mammalian head development. Development 125, 2063–2074.

Grunewald-Lowenstein, M., 1956. Influence of light and darkness on the pineal body in *Astyanax mexicanus*. Zoologica 41, 119–128.

Herwig, H.J., 1976. Comparative ultrastructural investigations of the pineal organ of the blind cave fish, *Anoptichthys jordani*, and its ancestor, the eyed river fish, *Astyanax mexicanus*. Cell Tissue Res. 167, 297–324.

Hinaux, H., et al., 2011. A developmental staging table for *Astyanax mexicanus* surface fish and Pachón cavefish. Zebrafish 8, 155–165.

Hinaux, H., et al., 2015. Lens defects in *Astyanax mexicanus* cavefish: focus on crystallin evolution and function. Dev. Neurobiol 75 (5), 505–521.

Humbach, I., 1960. Geruch und Gesmack bei den augenlosen Höhlenfischen *Anoptichthys joedani*, Hubbs und Innes und *Anoptichtys hubbsi*, Alvarez. Naturwissenschaften 47, 551.

Jeffery, W.R., 2009. Regressive evolution in *Astyanax* cavefish. Annu. Rev. Genet. 43, 25–47.

Jeffery, W., et al., 2000. *Prox1* in eye degeneration and sensory organ compensation during development and evolution of the cavefish *Astyanax*. Dev. Genes Evol. 210, 223–230.

Kishimoto, Y., et al., 1997. The molecular nature of zebrafish swirl: BMP2 function is essential during early dorsoventral patterning. Development 124, 4457–4466.

Kowalko, J.E., et al., 2013. Loss of schooling behavior in cavefish through sight-dependent and sight-independent mechanisms. Curr. Biol. 23, 1874–1883.

Krubitzer, L., et al., 2011. All rodents are not the same: a modern synthesis of cortical organization. Brain Behav. Evol. 78, 51–93.

Langecker, T.G., et al., 1993. Transcription of the opsin gene in degenerate eyes of cave-dwelling *Astyanax fasciatus* and its conspecific epigean ancestor during early ontogeny. Cell Tissue Res. 273, 183–192.

Lois, C., Alvarez-Buylla, A., 1994. Long-distance neuronal migration in the adult mammalian brain. Science 264, 1145–1148.

Mackowiak, M., et al., 2014. Neuroligins, synapse balance and neuropsychiatric disorders. Pharmacol. Rep. 66, 830–835.

McGaugh, S.E., et al., 2014. The cavefish genome reveals candidate genes for eye loss. Nat. Commun. 5, 5307.

Menuet, A., et al., 2007. Expanded expression of Sonic Hedgehog in *Astyanax* cavefish: multiple consequences on forebrain development and evolution. Development 134, 845–855.

Mundinano, I.C., Martinez-Millan, L., 2010. Somatosensory cross-modal plasticity in the superior colliculus of visually deafferented rats. Neuroscience 165, 1457–1470.

Neave, B., et al., 1997. A graded response to BMP-4 spatially coordinates patterning of the mesoderm and ectoderm in the zebrafish. Mech. Dev. 62, 183–195.
Niemiller, M.L., Poulson, T.L., 2010. Chapter 7: subterranean fishes of North America: amblyopsidae. In: Trajano, E., Bichuette, M.E., Kapoor, B.G. (Eds.), The Biology of Subterranean Fishes. Science Publishers, Enfield, NH, pp. 1–112.
Omura, Y., 1975. Influence of light and darkness on the ultrastructure of the pineal organ in the blind cave fish, *Astyanax mexicanus*. Cell Tissue Res. 160, 99–112.
Peters, V.N., et al., 1993. Gehirnproportionen und Ausprägungsgrad des Sinnesorgane von *Astyanax mexicanus* (Pisces, Characinidae). Zool. Syst. Evolut. Forsch. 31, 144–159.
Popper, A.N., 1970. Auditory capacities of the Mexican blind cavefish (*Astyanax jordani*) and its eyed ancestor (*Astyanax mexicanus*). Anim. Behav. 18, 552–562.
Pottin, K., et al., 2011. Restoring eye size in *Astyanax mexicanus* blind cavefish embryos through modulation of the Shh and Fgf8 forebrain organising centres. Development 138, 2467–2476.
Protas, M.E., et al., 2006. Genetic analysis of cavefish reveals molecular convergence in the evolution of albinism. Nat. Genet. 38, 107–111.
Rembold, M., et al., 2006. Individual cell migration serves as the driving force for optic vesicle evagination. Science 313, 1130–1134.
Rétaux, S., Casane, D., 2013. Evolution of eye development in the darkness of caves: adaptation, drift, or both? EvoDevo 4, 26.
Rétaux, S., Elipot, Y., 2013. Feed or fight: a behavioral shift in blind cavefish. Commun. Integr. Biol. 6, e23166.
Rétaux, S., et al., 2008. Shh and forebrain evolution in the blind cavefish *Astyanax mexicanus*. Biol. Cell. 100, 139–147.
Riedel, G., 1997. The forebrain of the blind cave fish *Astyanax hubbsi* (Characidae). I. General anatomy of the telencephalon. Brain Behav. Evol. 49, 20–38.
Riedel, G., Krug, L., 1997. The forebrain of the blind cave fish *Astyanax hubbsi* (Characidae). II. Projections of the olfactory bulb. Brain Behav. Evol. 49, 39–52.
Romero, A., et al., 2003. One eye but no vision: cave fish with induced eyes do not respond to light. J. Exp. Zool. B Mol. Dev. Evol. 300, 72–79.
Schemmel, C., 1967. Vergleichende Untersuchungen an den Hautsinnesorganen ober-and unterirdisch lebender *Astyanax*-Foramen. Z. Morph. Tiere. 61, 255–316.
Schemmel, C., 1974. Genetische Untersuchungen zur Evolution des Geschmacksapparates bei cavernicolen Fischen. Z. Zool. Syst. Evolutionforsch. 12, 196–205.
Sih, A., et al., 2004. Behavioral syndromes: an ecological and evolutionary overview. Trends Ecol. Evol. 19, 372–378.
Singh, M., 2014. Mood, food, and obesity. Front. Psychol. 5, 925.
Soares, D., Niemiller, M.L., 2013. Sensory adaptations of fishes to subterranean environments. Bioscience 63, 274–283.
Soares, D., et al., 2004. The lens has a specific influence on optic nerve and tectum development in the blind cavefish *Astyanax*. Dev. Neurosci. 26, 308–317.
Strickler, A.G., Jeffery, W.R., 2009. Differentially expressed genes identified by cross-species microarray in the blind cavefish *Astyanax*. Integr. Zool. 4, 99–109.
Strickler, A.G., Soares, D., 2011. Comparative genetics of the central nervous system in epigean and hypogean *Astyanax mexicanus*. Genetica 139, 383–391.
Strickler, A.G., et al., 2001. Early and late changes in *Pax6* expression accompany eye degeneration during cavefish development. Dev. Genes Evol. 211, 138–144.
Strickler, A.G., et al., 2002. Retinal homeobox genes and the role of cell proliferation in cavefish eye degeneration. Int. J. Dev. Biol. 46, 285–294.

Sussel, L., et al., 1999. Loss *of Nkx2.1* homeobox gene function results in a ventral to dorsal molecular respecification within the basal telencephalon: evidence for a transformation of the pallidum into the striatum. Development 126, 3359–3370.

Sylvester, J.B., et al., 2010. Brain diversity evolves via differences in patterning. Proc. Natl. Acad. Sci. U. S. A. 107, 9718–9723.

Sylvester, J.B., et al., 2013. Competing signals drive telencephalon diversity. Nat. Commun. 4, 1745.

Teyke, T., 1990. Morphological differences in neuromasts of the blind cave fish *Astyanax hubbsi* and the sighted river fish *Astyanax mexicanus*. Brain Behav. Evol. 35, 23–30.

Varatharasan, N., et al., 2009. Taste bud development and patterning in sighted and blind morphs of *Astyanax mexicanus*. Dev. Dyn. 238, 3056–3064.

Voneida, T.J., Fish, S.E., 1984. Central nervous system changes related to the reduction of visual input in a naturally blind fish (*Astyanax hubsi*). Am. Zool. 24, 775–782.

Voneida, T.J., Sligar, C.M., 1976. A comparative neuroanatomic study of retinal projections in two fishes: *Astyanax hubbsi* (the blind cave fish), and *Astyanax mexicanus*. J. Comp. Neurol. 165, 89–105.

Wilkens, H., 1988. Evolution and genetics of epigean and cave *Astyanax fasciatus* (Characidae, Pisces). Support for the neutral mutation theory. In: Hecht, M.K., Wallace, B. (Eds.), Evolutionary Biology, vol. 23. Plenum, New York/London, pp. 271–367.

Wilkens, H., 2010. Genes, modules and the evolution of cave fish. Heredity (Edinb) 105, 413–422.

Yamamoto, Y., Jeffery, W.R., 2000. Central role for the lens in cave fish eye degeneration. Science 289, 631–633.

Yamamoto, Y., et al., 2004. Hedgehog signalling controls eye degeneration in blind cavefish. Nature 431, 844–847.

Yamamoto, Y., et al., 2009. Pleiotropic functions of embryonic sonic hedgehog expression link jaw and taste bud amplification with eye loss during cavefish evolution. Dev. Biol. 330, 200–211.

Yoshizawa, M., Jeffery, W.R., 2008. Shadow response in the blind cavefish *Astyanax* reveals conservation of a functional pineal eye. J. Exp. Biol. 211, 292–299.

Yoshizawa, M., et al., 2010. Evolution of a behavioral shift mediated by superficial neuromasts helps cavefish find food in darkness. Curr. Biol. 20, 1631–1636.

Yoshizawa, M., et al., 2012. Evolution of an adaptive behavior and its sensory receptors promotes eye regression in blind cavefish. BMC Biol. 10, 108.

Yoshizawa, M., et al., 2014. The sensitivity of lateral line receptors and their role in the behavior of Mexican blind cavefish (*Astyanax mexicanus*). J. Exp. Biol. 217, 886–895.

Yuan, A., et al., 2012. Neurofilaments at a glance. J. Cell Sci. 125, 3257–3263.

Résumé en Français

Les métazoaires ont colonisé de nombreux milieux au cours de l'évolution, cette colonisation a été possible grâce à l'apparition de nombreuses caractéristiques. Beaucoup de ces caractéristiques ont émergé grâce à de subtiles et précoces modifications du développement de certains organes. L'étude de ces modifications du développement et de leur effet est souvent appelée l'évolution du développement ou « Evo-Devo ». Notre équipe étudie l'Evo-Devo du cerveau sur un modèle de poisson, Astyanax mexicanus. Cette espèce comporte plusieurs populations dont certaines cavernicoles, aveugles et dépigmentées, vivant dans des grottes mexicaines ; et vivant à la surface, dans des rivières et possédant des yeux normaux. Ces populations présentent de nombreuses différences : comportementales, physiologiques et sensorielles.

Au cours de cette thèse, j'ai participé à une étude concernant les populations de neurones peptidergiques de l'hypothalamus et de la région du récessus optique (ORR) et leur effet sur le comportement de ces poissons. Cependant la majorité de ma thèse concerne le développement de l'œil.

Au cours de l'étude des neurones peptidergiques nous avons comparé le nombre de 9 types de neurones peptidergiques au cours du développement entre les poissons cavernicoles et de surface. Nous avons observé de nombreuses différences entre ces populations de neurones : certains neurones étaient présents en plus grand nombre chez les poissons cavernicoles (hypocrétine (Hcrt), Neuropeptide Y (NPY) et Agouti-related protein), d'autres plus nombreux chez les poissons de surface (Pro-opiomélanocortine A et B, Arginine-Vasotocine) enfin certains en quantité similaire (isotocine) ou présentant des variations transitoires (cocain-and-amphetamine regulated transcript et Melanin-concentrating hormone).

Pour certaines de ces différences, nous avons cherché une cause au niveau des facteurs de transcription, et plus précisément des facteurs Lhx qui sont connu pour leur implication dans la spécification neuronale. Nous avons montré par des doubles hybridations in situ que tous les neurones exprimant Hcrt exprimaient également Lhx9 ; de même, tous les neurones NPY exprimaient Lhx7. Par une approche de « knock-down » et de surexpression de chacun de ces facteurs, nous avons montré que Lhx9 et Lhx7 étaient nécessaires et suffisants pour spécifier les neurones hypocrétine et NPY respectivement. Après quoi, nous avons cherché les causes au niveau des morphogènes. Par des traitements pharmacologiques nous avons montré que des manipulations précoces de la voie Hh modifiaient l'expression de Lhx7 alors que ces traitements ne démontraient aucun impact sur Lhx9. En revanche des traitements modifiant précocement la voie Fgf ou tardivement la voie Hh impactaient le nombre de neurones hypocrétine, démontrant ainsi un effet des Fgf sur l'initiation de la spécification hypocrétine, indépendamment de Lhx9, ainsi qu'un effet de Hh sur la différenciation des cellules hypocrétine. Ainsi, nous avons mis en évidence des effets précoces de signalisations morphogènes ainsi que de certains facteurs de transcription sur les populations de neurones peptidergiques.

Nous avons ensuite cherché à comprendre les effets que pouvaient avoir ces modifications sur le comportement des poissons. Les neuropeptides que nous avons sélectionné ont tous un rôle dans la régulation de la prise alimentaire. Tous les neurones qui étaient plus nombreux chez le poisson cavernicole se trouvent avoir un effet stimulant sur celle-ci alors que les neurones en plus grand nombre chez le poisson de surface ou en quantité égale chez les deux morphotypes sont connus pour leur effet anorexigène. En conséquence, nous avons comparé la prise alimentaire des larves des deux morphes et nous nous attendions à ce que les poissons cavernicoles mangent en plus grande quantité. Cependant, contrairement à nos attentes, les deux morphes mangeaient de façon absolument identique, ce qui fut également démontré après coup chez les adultes par une autre étude (Aspiras *et al.*, 2015). Nous avons également comparé le sommeil chez ces deux morphotypes puisque hypocrétine régule aussi ce comportement et que les poissons cavernicoles dorment moins que les poissons de surface. Pour ce faire, nous avons réalisé un « knock-down » de Lhx9 chez les poissons cavernicoles, celui-ci diminuant durablement le nombre de neurones hypocrétine,

nous avons pu observer l'effet d'une telle diminution sur le comportement des poissons. En effet, après ce traitement, le sommeil des poissons cavernicoles est restauré au niveau des poissons de surface.

Ainsi, notre étude démontre les effets comportementaux que des modifications extrêmement précoces de développement peuvent générer.

La deuxième étude que nous avons menée concerne le développement de l'œil. En effet, si le poisson cavernicole est aveugle et dépourvu d'œil à l'âge adulte, il commence par en développer un qui dégénèrera par la suite. Cet œil embryonnaire présente cependant quelques anomalies : une taille réduite, une rétine souvent ouverte au niveau de la fissure optique et réduite ventralement, un cristallin plus petit et parfois « flottant » ou légèrement détaché de la rétine. Au cours de ma thèse, je me suis penchée sur ces phénotypes rétiniens et ai cherché à les caractériser plus en profondeur, du point de vue des identités tissulaires au sein de la rétine mais aussi du point de vue de la régionalisation. J'ai également cherché à trouver des causes pour ces différences morphologiques par une étude de la morphogénèse de l'œil via une approche d'imagerie 3D live.

Pour mener à bien cette étude de la morphogénèse, il m'a fallu commencer par générer des lignées reportrices marquant mes régions d'intérêt, l'œil et l'ORR chez les deux morphotypes. A cause de la complexité de la région génomique de notre gène d'intérêt, Zic1, nous avons adopté une approche d' « enhancer-trap » ciblé par « Knock-In » grâce à la technologie CRISPR. Après avoir établi nos lignées, Zic1 :GFP, nous avons injecté les œufs transgénique avec de l'ARN H2B-mCherry afin d'obtenir un marquage nucléaire ubiquitaire afin de les imager depuis le stade plaque neurale (10hpf) et jusqu'à un développement avancé de la rétine (environ 30 hpf) . Ces films live nécessitant une bonne résolution spatiale et temporelle ainsi qu'une faible photo-toxicité, nous avons eu recours à la microscopie à feuille de lumière.

Les résultats de cette étude morphogénétique suggèrent que le champ de l'œil est réduit chez le poisson cavernicole, ce qui était déjà connu auparavant, ils suggèrent aussi que le mouvement appelé évagination étendue procède correctement alors que le mouvement d'invagination semble altéré ou retardé. En effet si ce mouvement semble correctement initié, probablement grâce à la constriction basale, il ne parvient pas à continuer à la même vitesse chez le poisson cavernicole que chez le poisson de surface et paraît fortement retardé. Au final, il semblerait que la position très ventrale/proximale du cristallin soit due au fait que ce dernier soit correctement spécifié au milieu de la petite rétine initiale mais qu'à cause de l'évagination étendue qui amène plus de cellules dans la rétine, cette dernière se déplace distalement par rapport au cristallin, faisant apparaitre celui-ci très proximal/ventral. De plus, le retard d'invagination associé à cette évagination étendue fait parfois apparaitre des espaces entre le cristallin et la rétine, expliquant le phénotype de cristallin « flottant ».

D'autre part, l'étude des phénotypes de régionalisation de la rétine, réalisée par hybridation in situ à l'aide de marqueurs des différents quadrants de l'œil révèle une réduction non pas du quadrant ventral dans sa globalité mais plutôt du quadrant temporal alors que les quadrants naso-dorsal semblent préservés.

Concernant l'étude des tissus de l'œil, l'épithélium pigmenté rétinien (RPE) est correctement spécifié mais son recouvrement de la rétine est retardé par rapport au poisson de surface, ce qui est cohérent avec le retard d'invagination de la coupe optique. En revanche l'identité de la tige optique semble étendue nasalement et temporalement, et parfois même dorsalement dans la rétine, indiquant plutôt une modification de la spécification tissulaire.

En conclusion, cette deuxième étude nous a permis de mieux caractériser les phénotypes de rétine du poisson cavernicole en termes de régionalisation et de spécification et indique ainsi une réduction spécifique du quadrant temporal ainsi qu'un élargissement de l'identité « tige optique » dans la rétine. D'autre part, l'étude de la morphogénèse révèle plusieurs modifications du développement, dont une plus petite vésicule optique initiale mais aussi un retard de l'invagination, en cohérence avec de recouvrement de la rétine par le RPE.

université PARIS-SACLAY
ÉCOLE DOCTORALE
Signalisation et réseaux intégratifs en biologie (BIOSIGNE)

Titre : Évolution développementale de la région optique chez le poisson cavernicole aveugle *Astyanax mexicanus*

Mots clés : œil, morphogénèse, poisson cavernicole, hypothalamus, neuropeptides, Evo-Devo

Résumé : L'espèce *Astyanax mexicanus* est composée de deux morphotypes de poissons radicalement différents : le très classique poisson de surface vivant dans des rivières et le poisson cavernicole (CF, cavefish) aveugle et dépigmenté. Ces deux morphotypes diffèrent sur de nombreux aspects, aussi bien en termes de modalités sensorielles, qu'en termes de physiologie ou de comportement. L'approche « Evo-Devo » consiste à tenter de relier des différences développementales précoces à des modifications phénotypiques plus tardives. Dans le cadre de ce travail, nous nous sommes concentrés sur les modifications précoces de l'hypothalamus et de l'œil du CF. Nous montrons que des modifications précoces de signalisation de morphogènes tels que Shh ou Fgf conduisent à une modification de la taille des groupes de neurones peptidergiques au sein de l'hypothalamus, via les facteurs de transcription Lhx, impliqués dans la spécification neuronale. Plus particulièrement, nous montrons l'augmentation de taille des groupes de neurones NPY ainsi qu'hypocretine, qui à son tour provoque une réduction du sommeil chez le CF.
Nous nous sommes aussi intéressés à l'oeil du CF, qui commence par se développer avant de dégénérer. Une réduction du quadrant ventral de la rétine avait été précédemment décrit. Nous rafinons cette description grâce à une étude de la régionalisation de la coupe optique du CF qui suggère une réduction de la rétine temporale plus spécifiquement. Nous proposons également une première description de la morphogénèse de l'oeil du CF grace à l'imagerie live de lignées transgéniques fluorescentes. Cette étude révèle un défaut d'invagination de la coupe optique chez le CF. Globalement, ce travail ouvre la voie vers une meilleure compréhension de l'évolution de la tête du CF.

Title : Developmental evolution of the optic region in the blind cavefish *Astyanax mexicanus*

Keywords : Eye, morphogenesis, cavefish, hypothalamus, neuropeptides, Evo-devo

Abstract : *Astyanax mexicanus* is a fish species comprising two strikingly different morphotypes : the classical river-dwelling surface fish and the blind depigmented cavefish. These two morphs differ in many aspects in terms of sensorial modalities, physiology and behaviour. In the Evo-Devo approach, we try to link early developmental differences to later phenotypic modifications. Here we focus on the early modification of the hypothalamus and the eye of the cavefish. We show that early signalling modification of morphogens such as Shh or Fgfs lead to the modification of neuropeptidergic clusters in the hypothalamus via the neuronal fate-specifying transcription factors Lhx. More particularly, we show an increase in NPY and hypocretin cluster size. In turn, this increased hypocretin cluster size triggers a reduction of sleep in the cavefish larva.
We also examine the embryonic eye of the cavefish which first develops before degenerating. This eye was previously reported to have a reduced ventral retina. We refine this description by studying the regionalisation of the cavefish optic cup and suggest that this reduction concerns more specifically the temporal retina. We also attempt a first description of the cavefish eye morphogenesis by live imaging on fluorescent transgenic lines. This description reveals a defect in the optic cup invagination of the cavefish. Overall, this work started deciphering the developmental evolution of the cavefish head.

Université Paris-Saclay
Espace Technologique / Immeuble Discovery
Route de l'Orme aux Merisiers RD 128 / 91190 Saint-Aubin, France